Design and evaluation of short cationic amphiphilic anticancer peptides with gene delivery potential

By

Roja Hadianamrei

A thesis submitted in partial fulfilment of the requirements for the

degree of Doctor of Philosophy.

The University of Sheffield

Faculty of Engineering

Department of Chemical and Biological Engineering

February 2021

ACKNOWLEDGEMENTS

Thanks to my supervisors, Dr. Xiubo Zhao, and Dr Stephen Brown for their guidance and support throughout this research project.

Thanks to my colleagues Miss Lucie N' Koy and Dr. Silvia Cirillo for their kind technical support.

Special thanks to my dearest friend and colleague Mr. Anas Tomeh for his kind support and for helping me get through the hard times.

Thanks to all my wonderful friends in Sheffield who created unforgettable memories for me.

And finally, thanks to my family whose kind support enabled me to do this PhD.

Table of Contents

List of figures

List of tables

Abstract

In this project three different groups of short cationic amphiphilic peptides were designed and evaluated for their anticancer activity against different cell lines as well as their potential for gene delivery: a series of α-helical peptides with the general formula $C(XXYY)_3$, a series of β-sheet forming peptides with the general formula $(XYXY)_3$, and a series of surfactant-like peptides with the general formula $(X_1X_2)_4K$. Where C is the amino acid cysteine, X represents hydrophobic amino acids (isoleucine and leucine), and Y represents hydrophilic amino acids (arginine and lysine). For surfactant-like peptides, X_1 and X_2 represent the hydrophobic amino acids (isoleucine, alanine, and glycine) and K is the hydrophilic amino acid lysine. These peptides were designed and synthesized for the first time and there is no report of their studies in the literature. Moreover, although peptides with closely related structures have been investigated for their antimicrobial activity, this is the first study on the anticancer activity of such peptides and their potential as non-viral gene vectors. The peptides exhibited varying levels of cytotoxicity against different cell lines which was affected by their composition, their secondary structure, and their hydrophobicity. Among all of the designed peptides the α-helical peptides consisting of isoleucine/leucine and lysine, and the β-sheet forming peptides consisting of isoleucine and lysine, or isoleucine with combination of arginine and lysine, exhibited selective anticancer activity with minimal cytotoxicity in normal human fibroblast cells. All of the designed α-helical peptides delivered the antisense oligodeoxynucelotides (AONs) to the cancer cells more efficiently than fibroblasts, however only the α-helical peptides containing isoleucine were able to deliver the small interfering RNA (siRNA) and induce gene silencing in HCT 116 cancer cells whereas the α-helical peptides containing leucine were unable to release their associated siRNA in the cytoplasm due to strong complexation with siRNA. Among the β-sheet forming peptides, only those containing isoleucine residues were able to form complexes with the AONs and to deliver them to the cancer cells and only $(IKIR)_3$ was able to induce gene silencing in HCT 116 cancer cells. The surfactant-like peptides managed to transfect the HCT 116 with AONs and fluorescently labelled siRNA more efficiently than fibroblasts but did not induce any gene silencing following transfection with functional siRNA due to strong complexation which prevented them from releasing their associated siRNA inside the cells. Overall, the results from this project provide a better understanding of the structure-activity relationship of the short cationic amphiphilic peptides which could be employed for development of more efficient anticancer peptides or peptide-based gene vectors.

Chapter 1: Introduction

This PhD project was aimed at design and evaluation of different series of short cationic amphiphilic peptides with potential anticancer activity and potential application as gene delivery carriers. The peptides were designed based on the structural features required for antimicrobial activity of the short cationic antimicrobial peptides and the features required for nucleic acid complexation and delivery, according to the available literature. The results from this project will be helpful in providing a better understanding of the structural features required for the biological activity of the short cationic amphiphilic peptides in order to optimize the peptide design and develop peptides with improved anticancer and/or gene delivery properties.

The main objectives of this project were:

- Design and synthesis of short cationic amphiphilic peptides with different structures as potential anticancer agents and/or gene delivery vectors
- Systematic variation of the peptide composition and sequence in order to study the structure activity relationship (SAR) of the peptides. Evaluation of the ability of the peptides to deliver nucleic acids (DNA and RNA) to the cancer cells as potential gene carriers
- Evaluation of the ability of the peptides to deliver small interfering RNA (siRNA) to the cancer cells and induce gene silencing as a strategy to inhibit the cancer cell growth and induce apoptosis in cancer cells.
- Evaluation of the ability of the peptides for selective gene delivery to cancer cells (compared to normal non-cancerous cells) in order to determine the safety of gene delivery with these peptides.
- Evaluation of the anticancer activity of the peptides against different cell lines.
- Evaluation of the selectivity of the peptides for cancer cells compared to normal non-cancerous cells in order to determine the safety of the peptides as anticancer agents.

In the following sections in this chapter a thorough review of the available literature on the peptide-based gene delivery will be provided. The next chapters will provide the information regarding the methods used for the experiments and the results obtained from the experiments, as well as concluding remarks and suggestions for future work.

1.1 Background

Gene therapy involves introduction of exogenous genetic material into the cells to modulate or inhibit the expression of a gene, in order to correct a specific inherited or acquired pathological condition [1-10]. In general, four types of nucleic acids are employed for gene therapy: plasmid DNA (pDNA), antisense oligonucleotides (AONs), messenger RNA (mRNA), and RNA interference (RNAi) components including small interfering RNA (siRNA), short hairpin RNA (shRNA) and microRNA (miRNA) [1-3]. The final destination of AONs, siRNA and mRNA is the cytoplasm, whereas pDNA must enter the nucleus to access the transcriptional machinery [1, 3].

Plasmid DNA is widely used to introduce a wild-type transgene into specific cells in which the endogenous gene is either defective or under-expressing, in order to upregulate the synthesis of a deficient protein or to account for a defective or malfunctioning protein [1-2]. mRNA could also be used as an alternative to DNA to induce protein expression [3]. AONs and RNAi on the other hand, target mRNA to inhibit expression of an overexpressing endogenous gene or an oncogene and block the synthesis of the proteins encoded by that gene, but via two different modes of action [1-2, 11].

AONs are 15-30 base single stranded DNA (ssDNA) [1-2, 11] that hybridize to their complementary mRNA in a sequence-specific manner. The resulting AON-mRNA heteroduplex either activates RNaseH which results in mRNA degradation [1-2, 11] or inhibits mRNA maturation by targeting a splicing site on pre-mRNA and modifying the exon content both of which leads to downregulation of the target protein [2, 11]. An alternative to AONs is the splice switching or splice correcting oligonucleotides (SSOs or SCOs). These are RNase H incompetent ONs which prevent or promote the insertion of exons in pre-mRNA through high affinity binding at obligatory splicing sequences [12].

RNAi is a mechanism for post-transcriptional silencing of homologous target genes which involves hybridization of small non-coding double-stranded RNA (dsRNA) molecules with mRNA [13]. RNAi is mediated via three different classes of small dsRNA molecules: miRNA, siRNA and shRNA. miRNAs are endogenously synthesized 20-24 bp non-coding dsRNAs that bind partially to complementary sites on their target mRNA and inhibit its translation via large protein complexes called RNA-induced silencing complex (RISC) [2, 13]. miRNAs do not need to hybridize over their entire sequence to inhibit the translation of the target mRNA. Therefore, a single miRNA is able to down-regulate the expression of a set of mRNAs, which are often related in function [12]. siRNAs are synthetic 19-25 bp dsRNA with a characteristic 2-nucleotide overhang at both 3′ locations which are exogenously introduced into the cells [1-3, 12-13]. Once recognised by RISC, the siRNA unwinds, and its sense strand is degraded by Argo-2. Subsequent hybridization of the antisense strand of siRNA to its complementary mRNA results in cleavage of the mRNA by RISC-associated nuclease and consequently downregulation of the target protein which is encoded by the mRNA [1-3, 12-13]. shRNAs are 25-29 bp dsRNA which contain a loop of 4-23 nucleotides [2]. shRNAs are processed by the Dicer protein (a component of RISC) which remove the loop to produce siRNA and the resulting siRNA follows the rest of the process as described above [2]. The AON and RNAi processes are schematically depicted in Figure 1.

Among the three classes of RNA involved in the RNAi process, siRNA is the most commonly used class for gene therapy [2]. Nevertheless, shRNA delivery has the advantage of continuous expression of shRNA and hence a more stable and longer lasting silencing of the target gene [14]. miRNAs are mostly used as biomarkers and their therapeutic use is still a challenging issue [2]. However, synthetic miRNAs also named “miRNA mimics” [2, 15] can be employed to restore the levels of endogenous miRNAs in an approach known as “miRNA replacement therapy” [2]. This approach is of potential benefit for cancer treatment as under-expression of certain types of tumor-suppressive miRNAs has been associated with many human cancers [15]. Hence, up-regulation of these miRNAs by miRNA replacement therapy could be considered as a new therapeutic strategy for cancer [15]. Currently this approach is under preclinical evaluation for silencing multiple cancer related genes [2].

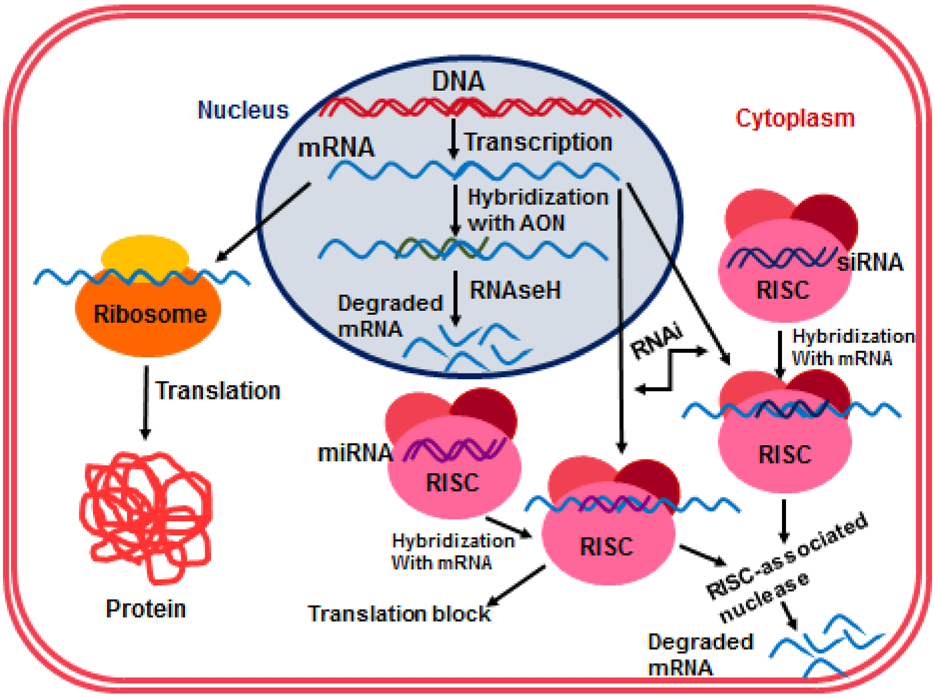

Figure 1- Schematic illustration of different cellular pathways involved in gene expression and silencing. mRNA: messenger RNA; AON: antisense oligonucleotide; miRNA: micro RNA; RISC: RNA induced silencing complex; RNAi: RNA interference; siRNA: Small interfering RNA.

Various types of oligonucleotide analogues and siRNAs with varying intracellular targets and modes of action have been explored for their potential therapeutic effects [10]. However, there are several extracellular as well as intracellular barriers which have to be overcome for efficient delivery of the desired genes to the target cells (Figure 2). Following systemic administration, the therapeutic genes could be subjected to enzymatic degradation [1-2] uptaken by the reticuloendothelial system (RES) [2] or rapidly cleared from the blood circulation by renal filtration [1-2]. At the cellular level gene delivery is hampered by the negative charge of the nucleic acids which diminishes their ability to penetrate into the cells [8-9, 16-18], and their susceptibility to the nuclease enzymes within the cells [1-2, 8, 19]. Although some types of ODNs are able to enter certain types of cells (such as hepatocytes or kidney cells) efficiently in naked form *in vivo*, their bioavailability at their intracellular targets is still limited by poor intracellular trafficking and endosomal entrapment [10]. To overcome these barriers, gene delivery vectors have been used to facilitate the transport of nucleic acids into the cells, protect them from degradation via endosomal escape, enhance bioavailability at the desired intracellular target and provide specific cell targeting [2, 5, 10, 18, 20].

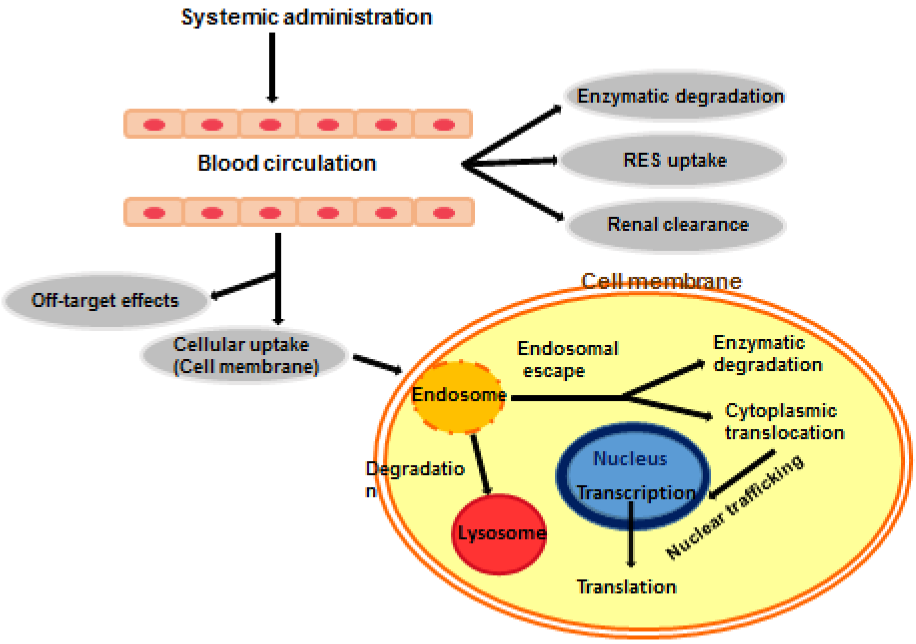

Figure 2- The extracellular and intracellular barriers to gene delivery. RES: reticuloendothelial system.

The gene delivery systems are mainly divided into two categories: viral and non-viral [2, 8, 21-22]. The viral vectors emerged first and account for nearly 70% of the gene therapy clinical trials carried out so far [3]. These vectors which are generally modified viruses such as retroviruses, lentiviruses, adenoviruses and adeno-associated viruses [3] have the advantage of high transfection efficiency [1-3, 6, 8, 18, 21, 23]. However, their immunogenicity, potential oncogenicity and complexity of production have limited their application [1-3, 6, 8, 17, 20, 22] and led to the development of a broad range of non-viral delivery systems as well as physical methods such as electroporation [3, 19, 24], microinjection [8, 24], gene gun [25-27], sonoporation [3] and magnetofection [1, 3] in order to improve the safety of gene delivery. Non-viral vectors have the advantage of lower immunogenicity and lower toxicity [1, 3, 6, 19], are able to deliver larger genetic payloads and are generally easier to synthesize than viral vectors [3]. Nevertheless, these systems are also associated with problems such as low transfection efficiency and low specificity [1, 3, 6, 18]. An account of different gene delivery systems is given in Figure 3.

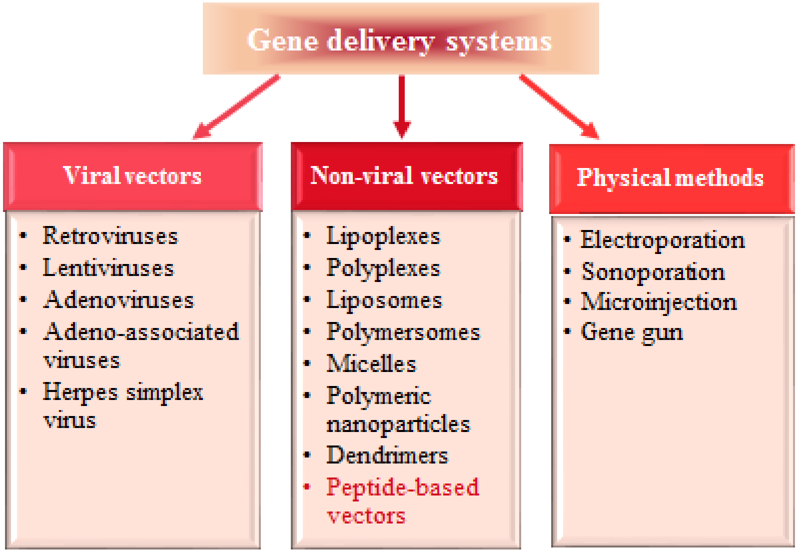

Figure 3- Different types of gene delivery systems.

In order to exert *in vivo* therapeutic effects, the non-viral vectors must be able to condense the gene, protect it from degradation by the serum nucleases, evade detection by the immune system, escape uptake by the reticuloendothelial system (RES), avoid renal clearance, target specific cells, escape the endosomal degradation, release the gene into the cytoplasm and allow for translocation to the nucleus in the case of pDNA [1-3]. The basic principles of non-viral gene delivery are as follows: The electrostatic interactions between the positively charged vectors and negatively charged nucleic acid molecules result in condensation of the large DNA/RNA molecule into small particles and protect them from enzymatic degradation in the external environment. Addition of excess amounts of cationic vectors bestows positive charges on the surface of the particles, and facilitates their cellular uptake via interaction with the negatively charged cell surface. The nucleic acid-vector complexes enter the cells mainly via clathrin/ caveolae -mediated endocytosis, and macropinocytosis [8]. So far, various types of synthetic gene delivery vectors, such as cationic lipids (lipoplexes) [2, 5, 8-9, 22, 28], cationic polymers (polyplexes) [2-3, 7-9, 16, 18, 20-21, 29-30], liposomes [3], polymersomes [3], polymeric micro/ nanoparticles [7], polymeric micelles [7], fibrous scaffolds [7] and dendrimers [3, 8, 20] have been studied. These non-viral delivery systems are usually hydrophilic and positively charged [7].

More recently, peptide-based carriers have been proposed as promising candidates for gene delivery [6, 18, 23]. Synthetic short peptides and self-assembling peptides that specifically bind to oligonucleotides are attractive candidates for new gene delivery systems, because they have low cytotoxicity, are less likely to induce immune responses and are easily degraded in the cells [6, 31]. The resulting peptide-DNA complexes are termed “peptiplex” [16]. Generally, the lysine and arginine residues, which possess positive charges in physiological pH, provide DNA binding [20, 32-34]; whereas the histidine residues provide endosomal escape and thus improve the transfection efficiency [18] due to the “proton sponge effect” [35, 36]. Histidine has a high buffering capacity due to the presence of amine groups which are protonable at acidic pH [35, 37]. Therefore, accumulation of the histidine-rich peptides in the acidic environment of endosomes, change the endosomal pH from acidic to neutral which leads to increased osmolarity, enhanced inflow of water into the endosome and eventually endosomal membrane disruption [35, 36].

Addition of hydrophobic amino acid residues to the peptide vectors promotes the formation of micelle-like nanoparticles, which allows for better complexation of DNA by increasing the local cationic charge density [18]. A typical example of a peptide gene carrier is the polycationic poly-L-lysine (PLL), which is capable of forming complex with DNA through electrostatic interactions between its positively charged amine groups and the negatively charged phosphate groups in the DNA backbone [6, 38]. Although initially emerged as a promising carrier due to its controllable molecular size and shape and potential for chemical modification, its low transfection efficiency and cytotoxicity limited the clinical applications of PLL-based polyplexes [6, 38]. What comes next is a review of the different classes of peptide-based vectors used for gene delivery to provide an insight into the current state of the art in peptide-based gene delivery and the gaps in the available literature.

1.2 Peptide-based gene vectors

1.2.1 Cationic amphiphilic peptides

Various types of cationic amphiphilic peptides of varying lengths and sequences have been designed and studied for their gene delivery potential. These are generally arginine-rich/lysine-rich peptides with one or more hydrophobic amino acids or alkyl/acyl chains. The arginine and lysine residues are positively charged in acidic and neutral pH, thus enabling electrostatic interaction with nucleic acids and the hydrophobic amino acids or alkyl/acyl chains enable interaction with the cell membranes. In most cases the peptides consist of an oligoarginie /oligolysine domain connected to a hydrophobic domain. Nevertheless, in some peptides the arginine and lysine residues are scattered throughout the peptide sequence and there are no separate hydrophobic and hydrophilic domains. What comes next is a summary of the different types of cationic amphiphilic peptides which have been used as gene vectors, an account of which is given in Table 1.

Table 1- different types of cationic amphiphilic peptides used for gene delivery and their associated cargo.

Peptide	Sequence	Cargo	References
LK9	LKKKKKKKKK	pDNA	39
LK15	LKKKKKKKKKKKKKKK	pDNA	39
C12-K6	CH3(CH2)11KKKKKK	pDNA	8
C14-K6	CH3(CH2)13KKKKKK	pDNA	8
C16-K6	CH3(CH2)15KKKKKK	pDNA	8
Chol-K6	Cholestrol-KKKKKK	pDNA	8
PEG17-PLL-CA14	[K(PEG)^{a}K(Cholic acid)^{b}K]n	siRNA	38
PEG17-PLL-CA32	[K(PEG)^{a}K(Cholic acid)^{c}K]n	siRNA	38
Bis(h9)-K-K4	(FLIVIGSII)2KKKKKK	pDNA	16
Bis (h5)-K-K4	(FLIVI)2KKKKKK	pDNA	16
KHV-LHRH^2	KKKKKKKKKKKKH6V8SSQHWSYKLRP	pDNA	18
AK27	AAAAAAAAAAAAHHHHHKKKKKKKKKK	pDNA	42
AK32	AAAAAAAAAAAAHHHHHKKKKKKKKKKKKKKK	pDNA	42
R1V6	RVVVVVV	pDNA, siRNA	6, 40
R2V6	RRVVVVVV	pDNA, siRNA	6, 40
R3V6	RRRVVVVVV	pDNA, siRNA	6, 40
R4V6	RRRRVVVVVV	pDNA, siRNA	6, 40
R3V6-VRBP^1	ATWLPPRRRVVVVVV	pDNA	29
HR15-Chol	HHHHHRRRRRRRRRR-Cholestrol	pDNA	43
HR20-Chol	HHHHHHHHHHRRRRRRRRRR-Cholestrol	pDNA	43
RALA	WEARLARALARALARHLARALARALRACEA	pDNA	22
MAX1	VKVKVKVKV^{D}PPTKVKVKVKV	pDNA	19
MAX8	VKVKVKVKV^{D}PPTKVEVKVKV	pDNA	19
HLT2	VLTKVKTKV^{D}PPTKVEVKVLV	pDNA	19
p5RHH	VLTTGLPALISWIRRRHRRHC	siRNA	43-45

a grafting level=17 %; b grafting level= 14%; c grafting level= 32%.

1.2.1.1 *Peptides with oligolysine domain*

The first report on peptide-based gene vectors was by Dufourcq et al [39] who investigated the ability of short synthetic amphipathic peptides, with known membrane activity, to condense

DNA presuming that the complex can evade the lysosomes. They studied two model peptides with different combinations of lysine and leucine, LK9, LK15, and a 4-5-residue oligolysine as model amphiphilic peptides. The peptide-DNA complexes were probed using ethidium bromide which is an intercalating fluorescent dye. The results revealed that the peptide-DNA complex formation was influenced by the secondary structure of the peptide. Only LK15, which exhibited α-helical structure in solution, allowed for topological changes and consequently condensation of DNA before the charge neutralisation point, whereas the other two peptides were unable to exhibit such effect. Therefore, they suggested the α-helix as “an exquisite structural motif” for the peptide-DNA interaction, which appeared to be electrostatically driven. The resulting peptide-DNA complexes retained significant membrane activity as demonstrated by calcein leakage experiments. The complexes possessed a colloidal character, but it was not clear whether there existed only a DNA mono-molecular condensation or a multimeric aggregation. This study was the first report on short peptide-DNA molecular assembly and demonstrated the ability of short amphiphilic peptides to combine membrane activity and DNA-condensing properties, with potential as non-viral gene carriers [39].

A series of cationic amphiphilic N-phosphoryl oligopeptides composed of a six residue lysine or histidine headgroup and varying lengths of hydrophobic tail (C12-K6, C14-K6, C16-K6, Chol-K6 and C12-H6) was designed by Sun et al and their transfection efficiency for plasmid DNA was evaluated in human embryonic kidney (HEK 293) cells [8]. The transfection efficiency of the lipopeptides was affected by both the length of the N-terminal phosphoryl ester chain and the type of amino acids in the headgroup. The K6-lipopeptides were superior to H6- lipopeptides in terms of DNA binding affinity, ability to condense pDNA and transfection efficiency. Overall, K6-lipopeptide with a hydrophobic chain of twelve carbons (C12-K6) had the highest transfection efficiency among all the lipopeptides, which was comparable to that of poly (ethylene imine) (PEI-25k), a well-defined gene delivery vector, with much lower cytotoxicity [8].

Guo et al [38] introduced a new class of pH-triggered amphiphilic PLLs modified with cholic acid on one side and grafted with poly (ethylene glycol) (PEG) on the other side, via a novel pH sensitive linker (benzoic imine) [38]. This novel structure allows these molecules to form cationic micelles with a hydrophobic core and a hydrophilic surface upon interaction with nucleic acids in aqueous media, with PEG forming a shield around the peptide/nucleic acid complex. The benzoic imine linker is stable at physiological pH but is cleaved at acidic pH of the extracellular environment of tumours, resulting in detachment of the PEG and exposure of the peptide/nucleic acid complex which can then be uptaken by the cancer cells [35].

Two of these peptides, namely PEG17-PLL-CA14 and PEG17-PLL-CA32 (the sequences are provided in Table 1), were evaluated for delivery of siRNA. Both PEG17-PLL-CA14 and PEG17-PLL-CA32 formed nanocomplexes with siRNA, which exhibited a slight positive surface charge at physiological pH and significantly higher positive charges at acidic pH indicating hydrolysis of the linker and PEG cleavage. The PEGylated complexes were stable in serum for up to 48 h. The cellular uptake of PEG17-PLL-CA/Fluorescein-siRNA complexes in PC-3 prostate cancer cells was comparable to the commercial transfection reagent INTERFRin™. The intracellular trafficking study of the PEG17-PLL-CA32/siRNA complexes in mouse TRAMP C1 cells (transgenic prostate adenocarcinoma) revealed the endosomal escape of the complexes with a distribution pattern in the cytoplasm similar to INTERFRin™ /siRNA complexes whereas the non- PEGylated PLL-CA32 was co-localized to lysosomes. Transfection of pGL3 luciferase expressing PC-3 cells with PEG17-PLL-CA32/ GL3 siRNA resulted in 9 fold reduction in gene expression which was similar to that achieved by I INTERFRin™. Moreover, intravenous administration of PEG17-PLL-CA/ VEGF siRNA to TRAMP C1 tumour-bearing mice resulted in 70% reduction in VEGF mRNA levels and 2-fold reduction in tumour size (compared to the controls) which was comparable to the therapeutic effect achieved with the commercial transfection reagent *in vivo* JetPEI™ without any apparent cytotoxicity [38].

Avila et al [16] designed a new class of self-assembling Branched Amphiphilic Peptides Capsules (BAPCs) as a means for gene delivery and evaluated their potential for delivery of double stranded plasmid DNA. An equimolar mixture of two BAPs, bis(h9)-K-K4 and bis(h5)-K-K4 composed of a hydrophilic oligolysine domain (KKKK) and two identical hydrophobic tails (FLIVIGSII and FLIVI respectively) was used for DNA delivery into HeLa cancer cells. The hydrophobic sequences were derived from an internal fragment of the human L-type calcium channel pore-forming segment [16]. Their results indicated that in the presence of double stranded DNA the peptides were unable to form BAPCs. Instead, the peptides either coated the surface of plasmid forming nanofibers (at high peptide to DNA ratio) or condensed the DNA into compact nanoparticles (at low peptide to DNA ratios), with the latter showing much higher transfection efficiency in HeLa cells. Furthermore, the transfection efficiencies of the peptide-DNA complexes were higher than the commercial transfection agent, Lipofectin®. Cellular uptake analysis at low temperature (4 °C) and normal temperature (37 °C) indicated that the uptake occurs via a temperature dependent process such as endocytosis. The peptide/DNA complexes remained inside the cells without being degraded for 48 h and appeared to be localized in the perinuclear area, resulting in EGFP expression in a number of the cells [16]**.**

Another example of cationic amphiphilic peptides is the integrated cationic peptide, K12H6V8SSQHWSYKLRP (KHVLHRH) designed by Tang et al for the targeted delivery of a model gene drug (luciferase-encoding plasmid DNA) to cancer cells [18]. The peptide comprised four functional blocks: a lysine block for DNA binding, a histidine block for endolysosomal release, a hydrophobic valine block to enhance DNA complexation, and luteinizing hormone releasing hormone (LHRH) ligand block as targeting element for cancer cells that overexpress LHRH receptors. The cellular uptake, gene expression and cytotoxicity of this gene delivery system were evaluated in LHRH-receptor-positive human breast cancer cell line MCF-7 and LHRH-receptor-negative human ovarian carcinoma cell line SKOV-3, in comparison to a peptide vector with the same structure but without the LHRH ligand, polyethylenimine (PEI) and naked DNA [18].

Both KHV and KHV-LHRH formed strong complexes with DNA that were less cytotoxic than PEI in both cell lines. The cellular uptake of KHV-DNA and KHV-LHRH-DNA complexes in both cell lines was higher than that of DNA condensed with PEI and much higher that naked DNA which was unable to penetrate the cell lines. The cellular uptake of both peptide-DNA complexes was similar in SKOV-3 cells, whereas in MCF-7 cells the internalization of DNA delivered by KHVLHRH was much higher than that delivered by KHV. These observations indicate the role of the LHRH targeting ligand in enhancing the internalization of DNA in LHRH receptor- positive cells [18]. The DNA delivered by KHV-LHRH was mainly distributed in the perinuclear region and a small portion even entered the nucleus. On the other hand, the DNA delivered by KHV aggregated in the perinuclear region but barely penetrated the nucleus, suggesting the endosomal capture of DNA. Furthermore, the luciferase gene expression was considerably higher in MCF-7 cells treated with KHVLHRH-DNA complexes compared to KHV-DNA complexes which accords with the cellular uptake results. Taken together, the designed integrated cationic peptide vector exhibited high specificity and high transfection efficiency which make it a promising material for targeted gene delivery [18].

A novel class of cationic peptide micelles that self-assembled from an amphiphilic peptide, A12H5Kn (n: 10 or 15 named AK27 and AK32 respectively), were designed by Wiradharma et al [39] as potential gene vectors. The alanine residues were used as the core-forming hydrophobic block and the lysine residues as the DNA binding cationic block. The histidine residues were incorporated to provide endosomal escape. The formation of cationic micelles in aqueous medium enhanced the DNA binding ability and yielded relatively smaller DNA complexes. Although the absolute gene expression efficiency was lower than that mediated by PEI (branched, Mw 25 kDa), the low cytotoxicity of the peptide micelles was a great advantage [41].

1.2.1.2 Peptides with oligoarginine domain

A series of cationic amphiphilic peptides composed of arginines and valines (RV peptides) were designed by Lee et al [6] for carrying plasmid DNA (pDNA) [6]. These peptides consisted of 1-4 arginines as the cationic region and 6 valines as the hydrophobic tail (R1V6, R2V6, R3V6 and R4V6). The transfection efficiency and cytotoxicity of the RV peptides were assessed against poly L-lysine (PLL) as control. The RV peptides formed micelles in aqueous solution and demonstrated higher transfection efficiency and considerably lower cytotoxicity than PLL in HEK293 cells. This enhanced transfection efficiency was supposed to be caused either due to micelle formation or due to the cell penetrating effect imparted by the arginines, as short arginine-rich peptides such as TAT and R9 have been reported to act as cell penetrating peptides. The low cytotoxicity of the RV peptides was attributed to the small number of positive charges in the molecules. Under optimal conditions, the R3V6 peptide was the most efficient RV peptide in HEK293 cells [6]. This study was followed by a complementary study investigating the efficiency of RV peptides (R1V6, R2V6, R3V6 and R4V6) for delivery of siRNA [38]. The siRNA delivery efficiency of the RV peptides was evaluated using firefly- and Renilla luciferase (Rluc)-siRNAs in human embryonic kidney (HEK) 293 cells. Comparison of the silencing efficiencies of different RV peptides complexed with Rluc-siRNA at their optimum conditions revealed that the complexes of Rluc-siRNA with R3V6 at a 1:20 weight ratio had the greatest silencing efficiency among all the RV peptides, which was comparable to that of PEI25k (positive control) [40].

The siRNA delivery efficiency of R3V6 was further confirmed by evaluating the efficiency of R3V6 complexes with siEGFP and siVEGF in silencing the expression of the relevant genes in HEK293 and CT-26 cell lines respectively. The siEGFP-R3V6 peptide complex reduced EGFP expression in HEK293 cells to a lesser extent than the siEGFP-PEI25k complex (positive control), but the siVEGF-R3V6 complex suppressed the VEGF expression similar to that of siVEGF-PEI25k complex in CT-26 cells. However, compared to naked siEGFP /siVEGF and the scramble-siRNA (scr-siRNA)-R3V6 complex which were used as negative controls, both siEGFP-R3V6 and siVEGF-R3V6 had considerably higher silencing efficiency [40]. It was also demonstrated that the fluorescently labelled siRNA-R3V6 peptide complex had higher cellular uptake than the other RV peptide-siRNA complexes and similar levels of cellular association as fluorescently-labeled siRNA-PEI25k complex. The siRNA-R3V6 complexes were non-toxic to HEK293 and CT-26 cells, unlike the siRNA-PEI25k complex. Taken together, this couple of studies suggest RV peptides as safe and efficient delivery carriers for pDNA and siRNA [40].

The gene delivery potential of R3V6 was further studied by linking the vascular endothelial growth factor receptor binding peptide (VRBP) to R3V6 to achieve endothelial-specific delivery of plasmid DNA [29]. The VRBP -R3V6 formed complexes with DNA that protected the DNA from DNase I (nuclease enzyme) for more than 60 min. VRBP-R3V6 achieved approximately 200 folds higher transfection efficiency in endothelial cells compared with R3V6 and even higher transfection efficiency in hypoxic endothelial cells without any apparent cytotoxicity. However, when tested in human embryonic kidney 293 and neuroblastoma N2A cells, VRBP-R3V6 only achieved 10 times higher transfection rate than R3V6, clearly indicating the high specificity of VRBP-R3V6 for endothelial cells [29].

Two cholesterol conjugated amphiphilic oligopeptides, HR15-Chol and HR20-Chol, were designed by Guo et al [42] which were able to self-assemble into cationic micelles in aqueous solution at low concentrations. The formation of micelles increased local charge density, leading to higher DNA binding efficiency than HR15 and HR20 without cholesterol. The micelles induced much higher overall luciferase gene expression than the control peptides in HepG2 human liver carcinoma and HEK293 human embryonic kidney cell lines [42]. Introduction of a histidine residue into the peptide design yielded an increased overall gene expression level, which was further improved by increasing the histidine length from 5 to 10 residues. HR20-Chol micelles induced two times higher luciferase gene expression level in 4T1 mouse breast cancer cells and much higher GFP reporter gene expression in HepG2 human liver carcinoma cells than PEI at their optimal N/P ratios. Moreover, HR20-Chol micelle-DNA complexes were less cytotoxic than PEI/DNA complexes. Hence, these micelles could be a promising carrier for delivery of therapeutic genes [42].

1.2.1.3 Peptides with scattered arginine/lysine residues

Another amphipathic cationic peptide, termed RALA, was designed by McCarthy et al [23] based on the naturally occurring α- helical peptide GALA and evaluated as a carrier for plasmid DNA. The GALA peptide has fusogenic properties; however, it is unable to condense nucleic acids due to its anionic nature. Therefore, the glutamate residues of GALA were replaced with arginin residues in order to improve binding to the negatively charged outer leaflets of membranes and nucleic acids. The RALA peptide formed complexes with plasmid DNA that self-assembled into fusogenic nanoparticles which were stable in the presence of serum [23].

The RALA-DNA nanoparticles demonstrated high transfection efficiencies in NCTC-929 murine fibroblast cells and ZR-75-1 human breast cancer cells and moderate transfection efficiency in PC-3 human prostate cancer cells, which were comparable to that of the commercially available transfection agent Lipofectamine® 2000. Their cytotoxicity towards the named cell lines, on the other hand, was considerably less than Lipofectamine® 2000. Furthermore, evidence of endosomal disruption upon addition of chloroquine, which is a known endosomal disruptor, further confirmed RALA's fusogenic nature. The nanoparticles were detected in the cytosol of PC-3 cells and pDNA was detected in intra-nuclear location. Translation into GFP protein was also clearly evident after 48h [23].

Notably, transfection was reduced following incubation with chlorpromazine and genistein (inhibitors of clathrin and caveolae mediated endocytosis) and methyl-β-cyclodextrin (causing cholesterol depletion) in both ZR-75-1and NCTC-929 cell lines, suggesting clathrin and caveolae mediated endocytosis as the entry pathways for the nanoparticles. RALA-CMV-Red Firefly Luc nanoparticles were found to disperse following injection to C57/BL6 mice, unlike naked DNA which was localized at the site of injection, and gene expression was evident in the lungs and liver following the injection of RALA encapsulated pCMV-Red Firefly Luc. Hence, RALA presents a highly effective gene vector for the systemic delivery of nucleic acids [23].

A series of hydrogel forming cationic self-assembling peptides with different formal charges (namely MAX1, MAX8 and HLT2) were designed by Medina et al [19] and were used to encapsulate an antigen expressing pDNA in order to explore the effect of network charge on the ability of the resulting gel to retain the antigen expressing DNA and to enhance its immuostimulatory effect. The designed pDNA encoded a hybrid protein composed of the melanoma-specific tumor antigen gp100, and the adjuvant high-mobility group binding protein 1 (HMGN1) and was supposed to provoke immune responses against gp100 expressing tumours [19]. All three peptide hydrogels were capable of directly encapsulating and retaining the pDNA with minimal disruption of their rheological properties. The highest pDNA encapsulation efficiency was observed by peptide HLT2, which had a formal charge of +5 at neutral pH. Therefore, this peptide was chosen for the *in vivo* tests. Subcutaneous implantation of pDNA-loaded HLT2 gels into mice resulted in an acute inflammatory response by polymorphonuclear cells at day 7, followed by infiltration of macrophages which led to an enhanced immune response by CD4+/IFNγ+ T cells, and was complemented by the formation of gp100-specific antibodies in day 21. These results clearly show the potential of the designed DNA-loaded self-assembled peptide hydrogels for tumor-specific immunostimulation [19].

Another cationic amphiphilic peptide vector named p5RHH was developed by Hou et al [43] by modifying melittin, a naturally occurring peptide found in bee venom with antimicrobial and cytotoxic activities. Melittin was chemically modified in order to enhance its ability to bind to nucleic acids and reduce its cytotoxic effects without compromising its ability to interact with biological membranes. The resulting peptide was able to deliver anti-GFP siRNA to B16 cells stably expressing GFP-PEST and induce considerable GFP knockdown in these cells even at concentrations as low as 5 nM. p5RHH was also able to deliver a STAT3 specific siRNA to B16-F10 cells resulting in degradation of STAT3 mRNA and subsequent decrease in STAT3 protein expression which led to decreased cell viability within 72 h post-transfection. Moreover, p5RHH/STAT3 siRNA was also capable of inhibiting the angiogenesis in primary Human umbilical vein endothelial cells (HUVECs) as determined by 60% decrease in matrigel tube formation and 50% decrease in transwell cell migration compared to control (p5RHH/ scrambled siRNA). Although p5RHH had lower transfection efficiency than Lipofectamine™ 2000 (IC50 of 50 nM vs 10 nM respectively), it also had markedly lower cytotoxicity which makes it a safer transfection reagent. Transfection of mouse monocyte/macrophage cell line RAW264.7 with p5RHH/ JNK2 siRNA led to a strong decrease in JNK2 protein levels at concentrations as low as 25 nM without cytotoxicity. JNK2 is a known mediator of foam cell formation which is the hallmark of atherosclerotic plaques [43].

p5RHH was also used for delivery of siRNA targeting the p65 subunit of NF-κB, which is involved in various inflammatory disease, in a mouse model of rheumatoid arthritis (RA) [44]. Administration of p5RHH/p65 siRNA nanocomplexes effectively silenced the expression of p65 and a broad array of inflammatory cytokines in the inflamed joints, prevented bone erosions, and preserved cartilage integrity with minimal effects on off-target p65 expression. p5RHH/p65 siRNA treatment rapidly stabilized ankle swelling and significantly suppressed arthritis score, which was maintained for at least10 days [44]. The fluorescently-labelled p5RHH/siRNA nanoparticles were found in the inflamed joints at a substantially higher level than free siRNA, for at least 7 hours after injection and were cleared from the body more slowly than the free siRNA. Although free p65 siRNA also diffused into inflamed tissues, the low level of intracellular accumulation was insufficient to suppress p65 expression. The p5RHH/p65 siRNA nanoparticles did not cause any haematological, renal or hepatic toxicity and did not induce any immune responses *in vivo*. Taken together, these findings demonstrate selective gene silencing by p5RHH/ p65 siRNA *in vivo* with no apparent toxicity [44].

Transfection of ARK1 uterine serous cancer cells and OVCAR8 ovarian cancer cells with p5RHH/ AXL siRNA reduced the expression of AXL and phospho-AXL in both cell lines considerably and decreased their migration and invasion compared to controls (naked AXL siRNA and scrambled siRNA) as determined by matrigel invasion and migration assays [45]. Intravenous or intraperitoneal administration of p5RHH-AXL siRNA nanoparticles to mouse xenographts (NOD/SCID and NU/FOX mice injected with ARK1 and OVCAR8 cells respectively) resulted in fewer intraperitoneal tumor nodules and lower overall tumor mass compared to controls (treated with p5RHH/scrambled siRNA nanoparticles) two weeks post-injection, without causing any apparent toxicities (as determined by haematological and histological tests). Moreover, the levels of AXL mRNA, AXL protein, and markers of metastasis (Matrix metallopeptidase 2 and Matrix metallopeptidase 3) were found to be considerably lower in the tumor tissues of mice treated with p5RHH-AXL siRNA nanoparticles than controls indicating the inhibition of tumor growth and metastasis via AXL knockdown [45].

1.2.2 Non-ionic amphiphilic peptides

The only study on the interaction of a non-ionic self-assembling peptide with oligonucleotides was carried out by Wang et al [4]. They investigated the molecular interaction of a peptide named EAK16-II, with the sequence AEAEAKAKAEAEAKAK, with single- and double-stranded oligodeoxynucleotides (ODNs), namely a guanine hexadecamer (dG16), a cytosine hexadecamer (dC16), and their duplex (dGC16), under various solution conditions. The dG16 and dC16 hexadecamers were chosen as oligonucleotides with same number of nucleotides but different types of base (purine or pyrimidine) to investigate sequence-specificity of the interactions between the self-assembling peptides and the oligonucleotides [4]. EAK16-II bound to ODN molecules within minutes after mixing and formed EAK-ODN complexes that further associated to form EAK-ODN aggregates. The aggregate formation was supposed to be assisted by the inherent self-assembly capability of the peptide. Subsequent binding density function analysis using the ODN fraction in the aggregates and study of the resulting binding isotherms revealed that the binding constant of EAK to ODNs was 2-6 folds higher at pH 4 than pH 7, and that no binding occurred at pH 11 [4].

The observation that the binding constant decreased as EAK became less positively charged suggested the electrostatic interactions between EAK and ODNs as the main driving force for complexation. Nevertheless, hydrogen bonding between EAK and the nucleotides of the ODNs may also be involved, which were supposed to be more efficient in the case of dG16. Furthermore, EAK was found to bind more strongly to single-stranded ODNs compared with double stranded ODNs indicating its preference for single-stranded ODNs. Following the binding studies, the nanoaggregates were further evaluated for the accessibility of the ODNs to the solvent, which is crucial to the stability and efficacy of ODNs during their delivery both *in vitro* and *in vivo*. The ODNs in the aggregates were found to be less accessible to the solvent, suggesting the potential of oligonucleotide encapsulation by EAK16-II [4].

1.2.3 Surfactant-like peptides

Surfactant-like peptides (SLPs), also called lipid-like peptides or peptide surfactants, are amphiphilic peptides consisting of a hydrophilic head and a hydrophobic tail. Generally, the head contains one or two hydrophilic amino acids [43-48] and the tail is composed of four to six hydrophobic amino acids [44, 46, 48-49]. Peptide surfactants with longer tails are rarely designed as increasing the number of hydrophobic residues decreases the overall solubility of the peptide [50, 53].

A short SLP, palmitoyl-GGGAAAKRK, was designed by Mazza et al [54] for delivery of siRNA targeting B-cell lymphoma 2 (Bcl2*) mRNA* to the subthalamic nucleus (STN), as a potential strategy for treatment of neurodegenerative disorders such as Parkinson's disease. The peptide possessed an overall positively charged head group at physiological pH which allowed the complexation with siRNA and the high content of basic amino acid residues was supposed to mimic the structure of cell penetrating peptides. The fluorescently labelled peptide nanofibers (PNFs) were detected within the cytoplasm of the rat primary neurons (extracted from E16 fetal rat brains), indicating the uptake of the PNFs by these neurons. The cell tracking studies using the fluorescently labelled peptide nanofibers (PNFs) revealed the uptake of the PNFs by the rat primary neurons (extracted from E16 fetal rat brains). Furthermore, the fluorescently labelled non-coding siRNA (siNEG-A546) complexed with the fluorescently labelled PNFs was detected in the cytoplasm of the rat primary neurons and SH-SY5Y neuroblastoma cells whereas the naked siNEG-A546 was not internalized. These data suggest the PNF-mediated translocation of the siRNA through the cell membrane [54]. Transfection of SH-SY5Y cells with the PNF/siBCL2 complexes led to significant down regulation of the *BCL2* gene expression manifested by decreased levels of BCL2 protein after 24h compared to untreated cells and cells treated with controls (naked siBCL2, siNEG, PNF: siNEG and PNFs alone). Moreover the induction of apoptosis in the PNF: siBCL2 treated cells was confirmed by TUNEL assay. The induction of apoptosis was sequence-specific as PNF: siNEG did not trigger apoptosis. The *in vivo* experiments with fluorescently labelled PNF: siBCL2 demonstrated the retention siRNA at the site of injection for 48h after stereotactic injection in the rat brain whereas the naked siRNA was cleared from the area of injection shortly after administration. Consequently, the PNF: siBCL2 silenced the expression of *BCL2* and led to ablation of neuronal tissue in the STN in comparison to the non-injected hemisphere and other groups of control-treated animals [54].

More recently, Cao et al [55] designed a series of surfactant-like peptides with the same amino acid composition (IVAGK) but different sequences and evaluated their ability to bind DNA and to self-assemble into virus-mimicking structures, as potential gene delivery vectors. The peptide’s self-assembly and DNA binding properties were greatly influenced by the sequence, as the different sequences resulted in different secondary structures; the conical peptides (G3A3V3I3K3 and K3I3V3A3G3), the dumbbell-shaped peptides (I3V3A3G3K3 and K3G3A3V3I3), and the irregular-shaped peptides (V3G3I3A3K3 and K3A3I3G3V3). The β-sheets forming dumbbell-shaped peptide I3V3A3G3K3 was able to condensate DNA efficiently and form highly stable virus-mimicking supramolecular structures protecting the DNA from enzymatic degradation in two steps: First, electrostatic interactions between the peptide and the DNA, and subsequently self-assembly of the peptide into β-sheet structures as a result of hydrophobic interactions and hydrogen bonding. Thus, the peptide provides a scaffold for ordered arrangement of DNA, in a similar manner to the virus capsid in order to form virus-mimicking supramolecular assemblies. The other three peptides (K3I3V3A3G3, K3G3A3V3I3, and K3A3I3G3V3) were unable to condensate DNA into ordered structures. This was suggested to be due to the different structural features of these peptides compared to I3V3A3G3K3, as in these three peptides the K3 end at the N-terminal is directly connected to the acetyl group, thus inhibiting the electrostatic interaction of the lysine residues with DNA due to steric effect [55].

The peptide-mediated gene transfection was tested by using the GFP reporter gene pEGFP-N2 in human embryonic kidney (HEK293E) cells and compared to Polyethyleneimine (PEI) as the positive control. The I3V3A3G3K3/DNA complexes induced GFP gene expression however, the transfection efficiency was rather low (3.2%) and much lower than PEI (18.3%). the low transfection efficiency of the I3V3A3G3K3/pEGFP-N2 complexes was attributed to the relatively larger polydispersity of these complexes than PEI-DNA complexes. Nevertheless, the fact that even the transfection efficiency of the positive control (PEI) was not high, suggests a technical problem with the applied transfection protocol as HEK293E are not among hard to transfect cells so ideally the transfection efficiency should be higher. On the other hand, the I3V3A3G3K3/DNA complexes exhibited low cytotoxicity towards HEK293E cells which is favourable for gene delivery systems [55].

1.2.4 Peptide amphiphiles

Peptide amphiphiles (PAs) are a class of self-assembling amphiphilic molecules that were first introduced by Matson et al [26]. This class of peptides are generally composed of four domains; Domain I is a hydrophobic moiety, usually an unbranched alkyl group of varying length and composition. Domain II is a β-sheet forming peptide sequence which determines the mechanical properties and gelation kinetics of the PA and also directs the morphology of the self-assembled nanostructures. Domain III consists of one to three charged amino acids to enhance the solubility and further regulate the gelation of the PA. Domain IV, which is not a structural necessity, is a bioactive recognition element which is displayed on the outer surface of the self-assembled nanofibers [26].

Peptide amphiphiles have been investigated as promising tools for non-viral gene delivery. Polyamine groups presented on the surface of the self-assembled nanofibers provide a positive charge at physiological pH that can facilitate uptake of PA-oligonucleotide complexes. Oligonucleotides can be released by degradation of the biodegradable peptide scaffold or by physical release mechanisms governed by diffusion. Cells can uptake nanofibers degraded by proteases and use them in their metabolic pathways showing biocompatibility of PAs [7]. The sequences of the PAs used for gene delivery are provided in Table 2.

Table 2- The sequences of the peptide amphiphiles used for gene delivery and their associated cargo.

Peptide	**Sequence**	**Cargo**	**References**
PA	KGGGAAAK-CO(CH2)14CH3	pDNA	31
MMA-bZip	KDPAALKRAR NTEAARRSRA RKLQRMKQLE-AKLAEIE-K-CO(CH2)10CH3	pDNA	53
RGDGWK-lipopeptide 1	RGDGWK-K-[(CH2)15CH3]2	pDNA	54
Lys-PA	CH3(CH2)11-VVAGK	AON	7
KRSR-PA	CO(CH2)10CH3-PPPP-GKRSR	AON	9
R4-PA	CO(CH2)10CH3-PPPP-RRRR	AON	9
R8-PA	CO(CH2)10CH3-PPPP-KKRRRRRRRR	AON	9
Stearyl-C(LLKK)$_3$C-TAT	CH3(CH2)$_{16}$CO-CLLKKLLKKLLKKCGRKKRRQRRR		55
P-01	GRKKRRQRRR-HHHHHH-KCH3(CH2)$_{16}$-CO-YIGSR	pDNA	56
P-03	GRKKRRQRRR-HHHHHH-KCH3(CH2)$_{16}$-CO-YIGSK	pDNA	56

The first report on the use of PAs for gene delivery was by Guler et al [31] who designed a novel peptide nucleic acid/peptide amphiphile conjugate (PNA-PA) that self-assembled into nanofibers capable of binding to oligonucleotides with high affinity and specificity. The PNA-PA consisted of a β-sheet forming peptide sequence, an alkyl segment and a poly-thymine PNA heptamer. The PNA backbone was used instead of DNA or RNA due to the higher thermal stability of the resulting PNA-DNA or PNA-RNA duplexes and triplexes compared to their DNA-DNA and RNA-RNA counterparts especially at very low ionic strength and compatibility of PNA synthesis with solid-phase peptide synthesis used for PAs. The oligonucleotide attachment point for the PNA recognition unit was provided by branching at one of the lysine residues. The designed PNA-PA molecules were soluble in water at pH 4 and self-assembled into nanofiber gels upon increasing pH to above 7. The self-assembled PNA-PA-DNA system was observed to bind more strongly than the corresponding DNA-DNA duplex [31].

Shortly after, Bitton et al [56] introduced a DNA-binding peptide amphiphile that they termed "MMA-bZip, as it was inspired by the basic Leucine zipper domain (bZIP domain) of the transcription factors. The designed PA consisted of the basic region of GCN4 (general control protein 4 from *Saccharomyces cerevisiae*), a short coiled-coil nucleation sequence, and an alkyl tail connected to a polymerizable methacrylic group. The PAs self-assembled into microstructures with different morphologies such as helical ribbons and tubules, which transformed into lamella upon binding to DNA. The microstructures were supposed to be determined by the specific interaction between the headgroups. Furthermore, the geometry of the self-assembled aggregates could be controlled by adding cosurfactants. However, they suggested that for most practical applications, these assemblies have to be further stabilized through the use of polymerizable hydrophobic tails [56].

A PA-lipopeptide conjugate (RGDGWK-lipopeptide 1) was developed by Samanta et al [57] and was successfully used for in vivo delivery of p53 reporting plasmid DNA to B16F10 tumor bearing mice. The peptide/DNA complexes selectively delivered genes to tumor vasculatures and induced considerable tumor growth inhibition through apoptosis of the tumor endothelial cells [57].

Another cationic PA, Lys-PA, was developed by Bulut et al [7] as a nanofibrous gene delivery system. The designed PA molecules contained a β-sheet forming section composed of hydrophobic amino acid residues and positively charged lysine residues which were able to bind to oligonucleotides and form nanofibers at physiological pH. This peptide was used to deliver Bcl-2 antisense oligodeoxynucleotide (AON), G-3139, to MCF-7 human breast cancer cells and managed to decrease the levels of Bcl-2 mRNA. Bcl-2 protein has a crucial role in mediating apoptosis in several aggressive tumor phenotypes, and its expression inhibition has been shown to induce apoptosis in various types of cancer cells [7]. A few years later, the same group designed a series of self-assembling PAs consisted of an alkyl tail, a proline-rich sequence, and a bioactive unit composed of either a cell penetrating peptide (CPP) sequence

(R4 and R8) or a cell surface proteoglycan binding sequence (KRSR) [9]. The proline residues were incorporated in the PA to confer a spherical shape on the self-assembled structures and the bioactive unit was incorporated to increase the cellular uptake of the system. The designed PA system was evaluated for delivery of G-3129, another Bcl-2 antisense oligonucleotide to MCF-7 cells. The PAs self-assembled into nanospheres decorated with the bioactive peptide sequences on their exterior [9]. KRSR-PA/AON, R4-PA/AON, and R8-PA/AON were more effectively uptaken by the MCF-7 cells than the PAs lacking the bioactive unit which were used as controls. All PA/AON complexes decreased the expression of Bcl-2 gene in MCF-7 cells. The gene silencing observed by KRSR-PA/AON, R8-PA/AON, and their combination was comparable to Lipofectamine®. Increasing the number of arginines in the CPP sequence resulted in enhanced cellular uptake of the oligonucleotides. Interestingly, a mixture of R8-PA and KRSR-PA (molar ratio: 1/3) did not show any superiority to R8-PA in enhancing internalization efficiency, however it reduced the cytotoxicity of R8-PA [9].

Luan et al [58] designed a series of multifunctional peptide amphiphiles consisting of a cationic amphiphilic α-helical antimicrobial peptide, a cell-penetrating segment from HIV-TAT peptide, a stearyl moiety, and cysteine residues, and evaluated their gene delivery potential. The antimicrobial peptide segment was supposed to provide a DNA binding site (via positively charged amino acids such as lysine and arginine) as well as endo-lysosomal escape due to its membrane disrupting property. The stearyl moieties were supposed to promote the antimicrobial peptide segment to form α-helical conformation by providing an intramolecular hydrophobic environment which would be of benefit for DNA binding and cellular uptake. The TAT segment was embedded into the peptide structure to provide additional DNA binding site and also enhance the cellular uptake. TAT peptide is able to bind to and condense DNA using electrostatic interactions and to translocate it across plasma membranes via endocytosis. The problem with TAT peptide-mediated endocytosis is that generally the peptide/DNA complexes are localized to endosomes, and eventually degraded in lysosomes. Thus, efficient TAT-peptide mediated gene transfection requires peptides that are capable of endosomal escape. The endosomal escape of the peptide/DNA complexes can be enhanced through hydrophobic modification of the peptide such as stearylation which provides a hydrophobic intramolecular environment thus promoting the formation of α-helical conformation which results in enhanced DNA binding ability and cellular uptake. The incorporation of cysteine residues into peptides can also increase the α-helical content. The presence of cysteine residues also increases the probability of crosslinking via formation of disulphide bonds in acidic endosomes or lysosomes, thus improving the stability of the peptide/DNA complexes [58].

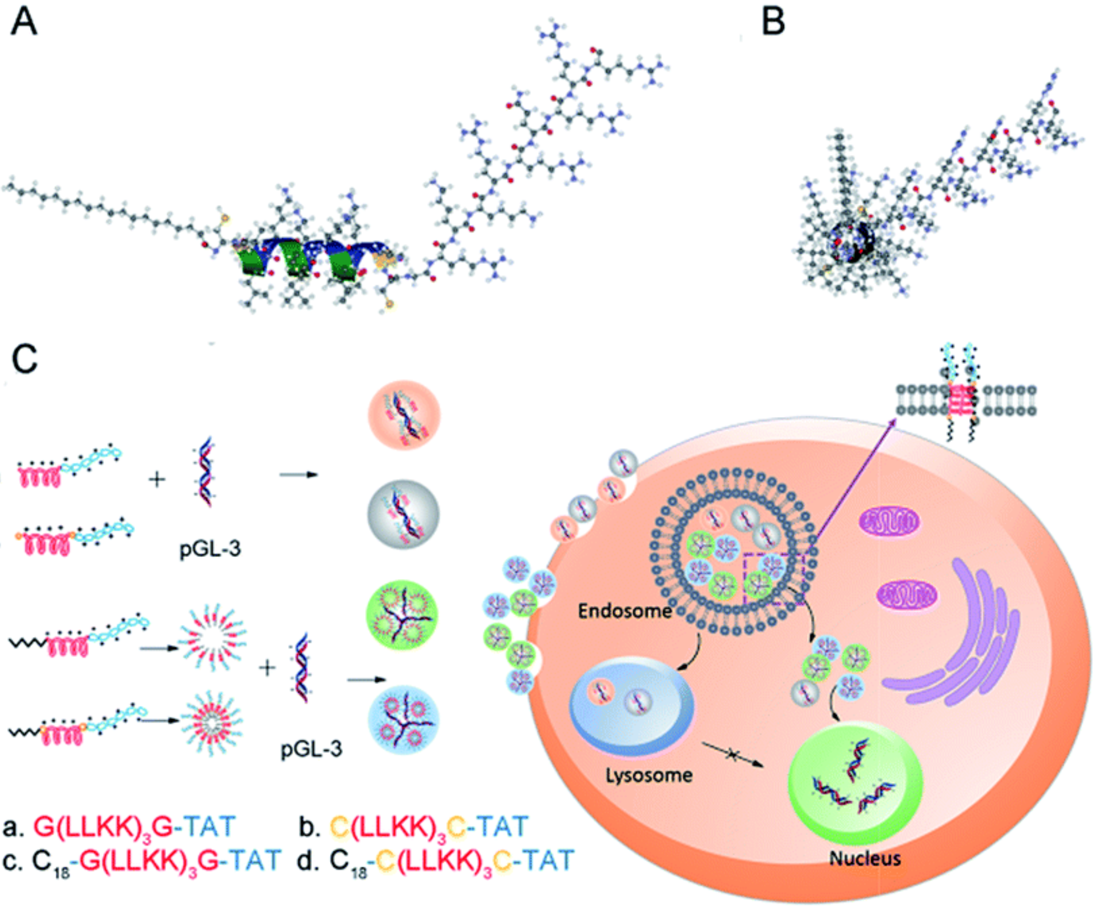

Figure 4- (A) A structural representation of C_{18}-C(LLKK)$_3$C-TAT shows the α-helical backbone of (LLKK)$_3$ and the distribution of TAT and cysteine residues. (B) A representation of the side chain orientations for the main helical backbone. (C) A schematic illustration of the plasmid DNA condensation and gene delivery mediated by each of the TAT peptide-based gene vectors. Reproduced from reference 58 with permission from The Royal Society of Chemistry.

The peptides were evaluated for luciferase gene transfection in 293T and NIH-3T3 cells at different N/P ratios, compared with Lipo2000. Addition of the functional moieties (TAT, stearyl, and Cysteine) increased the transfection efficiency of the peptide vectors to a great extent in both cell lines in a very similar manner and N/P ratio of 4 was found to be optimal for luciferase gene expression by all the peptides. Among all of the peptides, C18-C(LLKK)$_3$C-TAT, exhibited the highest transfection efficiency in both cell lines which was comparable to Lipofectamine 2000 which was used as the positive control. No significant cytotoxicity was observed in either cell line for any of the peptide/DNA complexes. Moreover, the cellular uptake of YOYO-1-labeled plasmid DNA complexed with each peptide at the optimal N/P ratio of 4 was also assessed in 293T and NIH-3T3 cells. As it was expected, the stearylated peptides exhibited higher cellular uptake levels than their non-stearylated counterparts. In a similar manner, increasing the length of the cationic peptide segment either by fusing TAT and antimicrobial peptide together, or by linking them via a disulfide bond resulted in higher cellular uptake. This was suggested to be due to more efficient condensation of the DNA into nanoparticles with favourable size and zeta potential by these peptides. The highest level of fluorescence from YOYO-1-labeled plasmid was achieved by C18-C(LLKK)3C-TAT and C(LLKK)3CTAT which was considerably higher than that of Lipofectamine 2000. The peptide/plasmid complexes were found to be uptaken mainly via caveolin-mediated endocytosis, and partially via clathrin-mediated endocytosis and micropinocytosis, depending on the size of the complexes. It was suggested that the complexes with the size of 60-120 nm are mainly internalized via clathrin-mediated endocytosis, the complexes with sizes ranging from 120 to 500 nm are mainly internalized via caveolin-mediated endocytosis, and the larger particles are uptaken via macropinocytosis [58].

Building on to their previous work, more recently the same research group designed a new series of multifunctional peptides keeping the TAT peptide as the DNA binding element and the stearyl moiety to promote the α-helical structure but replacing the antimicrobial peptide with six continuous histidine residues which would provide a proton sponge effect and serve as endolysosomal membrane-disrupting segment [59]. In addition, they introduced a laminin receptor-targeting segment (YIGSR) to the peptide molecule to enhance specific cell targeting. Two of the designed peptide vectors (P-01 and P-03) demonstrated high transfection efficiencies for delivery of pGL3 luciferase reporter DNA to B16F10 and 293T cells which were considerably higher than Lipofectamine 2000 at N/P ratio of 6, which was found to be the best N/P ratio for the peptide/DNA complexes. It was suggested that the optimum peptide-DNA binding and the most stable self-assembled structures are formed at this N/P ratio thus resulting in the highest transfection efficiency. The presence of the stearyl moiety was found to be crucial for gene delivery with these vectors as the peptide lacking this segment showed very low transfection efficiency. The targeting segment (YIGSR) was also found to have an essential role in increasing the transfection efficiency as the peptides that either lack this segment or have it replaced with a disordered sequence showed very poor transfection efficiencies. Furthermore, changes to peptide sequence which resulted in reduced helicity of the peptide adversely affected the transfection efficiency of the resulting peptides [59].

No significant cytotoxicity was observed for peptide/DNA complexes with different N/P ratios in neither of the two cell lines. Only P-03/DNA complex exhibited low levels of cytotoxicity against the B16F10 cells at N/P ratio of 8, which was significantly lower than Lipofectamine 2000. In addition to the in vitro transfection studies, the transfection efficiency of the peptide vectors was also studied in vitro using pIRES2-EGFP plasmid encoding green fluorescent protein (GFP) and luciferase reporter gene pGL3 in zebrafish. The P-01/pIRES2-EGFP complex was able to induce considerably higher expression of GFP in zebrafish than the naked plasmid which was used as the negative control. In the same way, the P-01/pGL3 complex exhibited higher luminescence than the naked plasmid [59].

Similar to their previous study, the cellular uptake of the peptides complexed with YOYO-1-labelled plasmid DNA (at N/P ratio of 6) was studied using FACS and confocal microscopy. P-01 displayed higher cell penetration efficiency, P-03 displayed almost the same ability to deliver DNA as P-01 in 293T cells and slightly lower ability than P-01 in B16F10 cells. Both P-01 and P-03 have advantages over Lipofectamine 2000 in entering cells, which may be a key factor in determining their transfection efficiency. The other peptides showed poor cellular further confirming that the α-helical conformation of the peptide, the position of the TAT peptide derived segment in the peptide sequence, and the presence of the YIGSR laminin receptor targeting segment all play roles in the cellular uptake and consequently the transfection efficiency of the peptide vectors. The primary cellular entry pathway of the Peptide/DNA complex was found to be endocytosis. The same cellular entry pathways (endocytosis and macropinocytosis) were suggested for these peptide/DNA complexes based on their particle size [59].

1.2.5 Bola amphiphilic peptides

Zhang et al [21] designed two self-assembling Bola amphiphilic peptides with dual ligands (RGD as targeting moiety and R8 as cell penetrating sequence) and evaluated their potential for cancer cell targeted gene delivery. The efficiency of the designed peptides, P1 and P2 (with sequences RGD-ADDA-RRRRRRRR and RGD-AHX-RRRRRRRR respectively), to deliver pGL-3 luciferase reporter gene was assessed in human cervical carcinoma (HeLa) cells which overexpress αvβ3 and αvβ5 integrins on their surface and also in human embryonic kidney (HEK 293T) cells which don't express the integrins, in comparison to P3 (with sequence RGD-RRRRRRRR) which has the same number of arginines and the targeting moiety but lacks the bola-like structure. Both P1 and P2 were able to fully condense the DNA even at low w/w ratios in a much more effective manner than P3 indicating the importance of bola-like structure for enhanced DNA-binding ability. This was attributed to the presence of a hydrophobic linker in the peptide molecule which results in closer architecture and increased charge density of the resulting nanoparticles. Despite the different DNA binding affinities, all three peptides were able to protect plasmid DNA from hydrolysis by DNase I at different w/w ratios. P1 exhibited the highest transfection efficiency in both cell lines among all peptides, which was slightly lower than PEI which was used as positive control. The cancer cell specific delivery of pGL3 was confirmed by considerably higher amount of P1/pDNA complexes in HeLa cells, which were mainly accumulated in the prenuclear area and the nucleus, compared to HEK 293 T cells. None of the peptide vectors exhibited any obvious cytotoxicity against either cell lines even at high concentrations. Thus, the designed bola amphiphilic peptides represent efficient and safe vectors for cancer targeted gene delivery [21].

1.2.6 Peptide dendrimers

Kokil et al. [60] designed a series of asymmetric peptide dendrimers, with varying charge densities and different head groups (arginine or lysine) as nucleic acid vectors. In addition, a subset of these dendritic peptides was constructed by conjugation of the side arms with cholic acid/decanoic acid to investigate the effect of lipid conjugation on the cellular uptake of the dendrimers. The dendrimers were found to self-assemble into micelles at micromolar concentrations. The ability of the dendrimers to deliver nucleic acids to the cells was evaluated using different types of nucleic acids in different cell lines. Of all the constructed dendrimers, only the lipidated dendrimers D7, D9, and D12 were successful in delivering their cargo to the cells, indicating the essential role of the lipid conjugation in enhancing the cellular uptake of the peptide dendrimers. D7 was able to deliver FITC-labelled siRNA to the H-4-II-E hepatocytes, D9 was able to deliver FITC-labelled siRNA and pEGFP plasmid DNA to the hepatocytes and FAM-ssDNA to myotubes and DAOY cells. D12 was also able to deliver FAM-ssDNA to myotubes and DAOY cells. However, the delivery efficiency of the dendrimer-nucleic acid complexes was only measured in the case of FITC-labelled siRNA, indicating high efficiency for D9 (comparable to lipofectamine 2000 which was used as the positive control) and very low efficiency for D7 and in all other cases the transfection was only assessed using fluorescence microscopy images. Hence conjugation with cholic acid has a stronger effect on the cellular uptake of the dendrimers compared to decanoic acid [60].

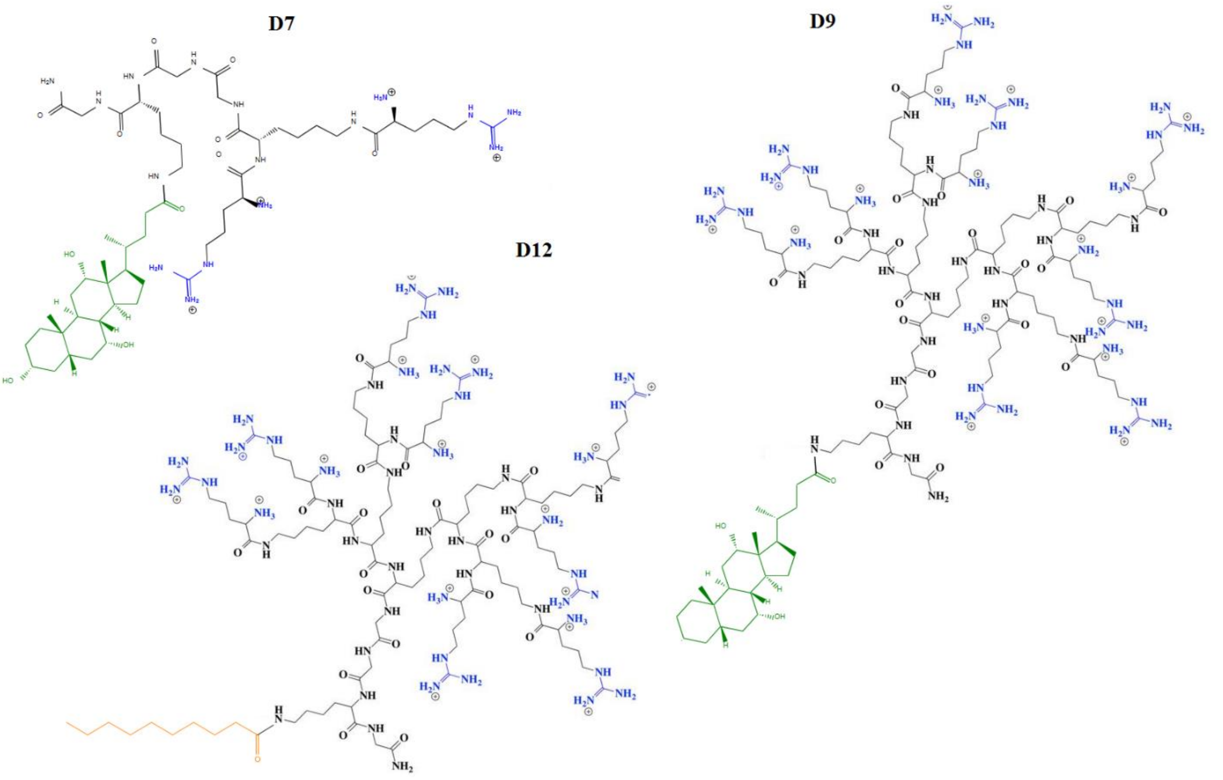

Figure 5- Chemical structure of the lipidated peptide dendrimers. Reproduced from reference 60 with modifications, Creative Commons Attribution 4.0 International License accessible at http://creativecommons.org/licenses/by/4.0/.

1.2.7 Cell penetrating peptides

Cell-penetrating peptides (CPPs), formerly known as protein transduction domains, are a heterogeneous group of peptides that possess one common feature: membrane translocation ability [8-9, 17, 61-64]. CPPs are generally short cationic or amphiphilic peptides (less than 30 amino acids in length) [8-9, 56-57, 65-68] containing highly basic amino acids such as arginine and lysine [16, 62, 68]. The first CPP to be discovered was TAT peptide which is the basic domain of the transactivating transcriptional activator protein of human immunodeficiency syndrome virus type 1 (HIV-1 TAT protein) [12, 61-62, 69, 70], the shortest amino acid sequence which enables the cell penetration and promotes the viral gene expression [62, 69]. Another CPP which was discovered shortly after, is Penetratin which was derived from Antennapedia homeodomain, a transcription factor of *Drosophilia melanogaster* [12, 61, 62, 71,72] that naturally enters nerve cells and regulates neural morphogenesis [62, 72]. Penetratin was among the first CPPs to be used for delivery of nucleic acids to the cells based on its enhanced cellular uptake property. Penetratin was successfully used to deliver anti GL2 firefly luciferase siRNA to CHO-AA8-Luc Tet-Off cells stably expressing luciferase and to deliver anti GFP siRNA to C166-GFP and EOMA-GFP cells stably expressing GFP and induced higher level of gene silencing which was retained for longer duration of time compared to Lipofectamine™2000 in all the tested cell lines [73]. Over the past two decades, several other CPPs with different sequences have been discovered and many more chimeric and synthetic CPPs have been developed by modifying the naturally occurring CPPs, merging the sequences from different CPPs, or through rational design [62, 63]. CPPs present a new class of peptide-based gene vectors as many of them are found to be capable of forming complex with nucleic acids and transporting them across the cell membrane owing to their potential to cross biological membranes [12, 57, 64].

CPPs penetrate into the cells by different mechanisms that are independent but can occur simultaneously, based on their structure and physicochemical properties. Short, cationic, arginine-rich CPPs interact with the cell membrane through electrostatic interaction between the positively charged amino acids and the negatively charged proteoglycans, and subsequently increase the permeability of the cell membrane through a receptor-independent pathway, which results in the uptake of the peptide and any associated cargo via endocytosis [62, 74-75]. Based on the physicochemical properties of the peptide, and its associated cargo, the CPP-nucleic acid conjugates can enter the cells via single or multiple endocytic pathways [76]. Apart from endocytosis, CPPs can penetrate the cells through alternative energy-independent pathways such as direct translocation (pore formation, inverted micelle formation, carpet-like model and the membrane-thinning model) [62, 63,77], or adaptive translocation (anion scavenging with charge neutralization or CPP inversion using transmembrane potential) in the case of arginine rich CPPs [62, 74]. In addition to these general receptor-independent mechanisms, some CPPs can enter the cells by specific receptor-mediated cellular entry pathways such as scavenger receptor-mediated uptake [78].

CPPs can be designed with predetermined structures and can be easily modified with different chemical entities. Moreover, CPPs can be combined with other gene delivery systems which further broadens their applications in gene delivery [79]. Due to their unique biological properties as well as biocompatibility and ease of synthesis, in the last two decades there has been rapid development in the application of CPPs either as gene vectors or for functionalization of other types of gene vectors [8, 17, 61]. What comes next is a summary of different types of CPP-mediated gene delivery systems, an account of which is given in Table 3.

Table 3- the sequences of the cell penetrating peptides used for gene delivery and their associated nucleic acids.

Peptide name	**Peptide sequence**	**Cargo**	**Reference**
Penetratin	RQIKIWFQNRRMKWKK	siRNA	73
TAT	GRKKRRQRRR	pDNA	68, 70,80
TAT-LK15	RKKRRQRRRGGGKLLKLLLKLLLKLLK	pDNA, siRNA, shRNA	70, 14
TAT-R3V6	GRKKRRQRRRRRRVVVVVV	pDNA	30
TAT-PV	GRKKRRQRRRPKKKRKV	pDNA	80
MPG-8	GALFLGWLGAAGSTMGAPKKKRKV	siRNA	93
CADY	GLWRALWRLLRSLWRLLWRAS-NH2	siRNA	94-96
Transportan	GWTLNSAGYLLGKINLKALAALAKKIL	siRNA	57, 65,73
Transportan 10	AGYLLGKINLKALAALAKKIL	pDNA, SCO	84-85
PepFect 6	CH3(CH2)$_{16}$-CO-AGYLLGKINLKALAALAKKIL-(QN[1])4	siRNA	79
PepFect 14	CH3(CH2)$_{16}$-CO-AGYLLGKLLOOLAAAALOOLL	SCO, pDNA	86, 89
PepFect 15	CH3(CH2)$_{16}$-CO-AGYLLGKLLOOLAAAALOOLL-(QN[1])4	SCO	87
PF14-O	CH3(CH2)$_{16}$-CO-AGYLLGKLLOOLAOOALOOLL	pDNA	89
PF14-E	CH3(CH2)$_{16}$-CO-AGYLLGKLLEOLAAAALOOLL	pDNA	89
C22-PF14	CH3(CH2)$_{16}$-CO-AGYLLGKLLOOLAAAALOOLL	pDNA	89
C22-PF14-O	CH3(CH2)$_{16}$-CO-AGYLLGKLLOOLAOOALOOLL	pDNA	89
PEG-MMP-Pepfect14	CH3(CH2)$_{16}$-CO-AGYLLGKLLOOLAAAALOOLL-(CH2)5CO-PLGLAG-PEG	pDNA	88
PepFect 51	CH3(CH2)$_{16}$-CO-WLKLWKKWLKLWTFFYGGSRGKRNNFKTEEY	siRNA	90
NickFect 51	CH3(CH2)$_{16}$-CO-AGYLLG(δ-NH)-OINLKALAALAKKIL	pDNA, siRNA, SCO	91
NickFect 53	CH3(CH2)$_{16}$-CO-AGYLLG(α-NH)-OINLKALAALAKKIL	pDNA, siRNA, SCO	91
NickFect 55	CH3(CH2)$_{16}$-CO-AGYLLG(δ-NH)-OINLKALAALAKAIL	pDNA	92
NickFect 61	CH3(CH2)$_{16}$-CO-AGYLLG(ε-NH)-KINLKALAALAKKIL	pDNA, siRNA, SCO	91
Hph1	YARVRRRGPRR	-	94
Hph1–Hph1–dsRBD	MGSSHHHHHHSSGLVPRGSHMASAGSYARVRRRGPRRGHYARVRRRGPRRRRSLQPWFFMEELNTYRQKQGVVLKYQELPNSGPPHDRRFTFQVIIDGREFPEGEGRSKKEAKNAAAKLAVEILNKEEFE LRRQACGRTRAPPPPPLRSGC	siRNA	97
WRAP1	LLWRLWRLLWRLWRLL	siRNA	98
WRAP5	LLRLLRWWWRLLRLL	siRNA	98
Oligoarginine	(R)n , n= 6-15	siRNA	17, 32, 62
rPOA	[C-(D-R9)-C]n, n=2-4	pDNA, siRNA	81-82
Stearyl-polyarginine	CH3(CH2)$_{16}$-CO-[R-NH(CH2)5CO-R]4	SCO	83
Oligolysine	(K)n , n= 6-15		65

[1] Trifluoromethylquinoline

1.2.7.1 TAT and TAT-derived peptides

A fusion protein obtained by covalently linking Tat peptide to the membrane lytic peptide, LK15 (TAT–LK15) was used to condense pEGFPLuc plasmid DNA and its transfection efficiency in human colorectal adenocarcinoma HT29 and human fibrosarcoma HT1080 cells was compared to TAT and LK15 peptides [70]. All of the three peptides were able to form complexes with DNA, but only the TAT-LK15-DNA complexes were considerably uptaken by the cells. Attachment of LK15 to TAT resulted in smaller DNA complexes with higher charge density, significantly improved the physiochemical properties of the complexes, and enhanced the transfection efficiency and gene expression in human colorectal adenocarcinoma HT29 cells and human fibrosarcoma HT1080 cells compared to TAT or LK15 alone. However, the transfection efficiency of the TAT-LK15/DNA complexes was lower than that of commercial transfection reagents such as PEI and lipofectin®. The TAT-LK15/DNA complexes did not exhibit significant cytotoxicity against HT29 cells *in vitro*.

The enhanced transfection efficiency of the TAT-LK15/DNA compared with TAT or LK15 was supposed to be mainly due to the increased cellular uptake of the complexes. To validate this assumption, the membrane destabilizing ability of TAT-LK15 peptide was tested by liposome leakage assay compared to LK15 as positive control and Tat as negative control. The TAT-LK15 induced calcein release from liposomes in a manner similar to LK15. Complexation with DNA reduced the membrane lytic activity of the TAT-LK15 the extent of which was directly proportional to the charge ratio; nevertheless, at the optimum charge ratio of 3:1 which was used for transfection, the complexes retained considerable residual lytic activity thus providing evidence for cell penetration ability of the TAT-LK15/DNA complexes [70].

Consequently, the cellular penetration and transfection efficiency of the peptide-DNA complexes was evaluated in HT29 multicellular tumour spheroids (MCTS) as a mimic of tumours. Consistent with the transfection studies in monolayer cells, the transfection efficiency of TAT-LK15/DNA complexes was considerably higher than TAT/DNA complexes. However, the level of EGFP expression in MCTS was lower than monolayer cells and was confined to the edge of the spheroids thus indicating the failure of Tat–LK15/DNA complexes to penetrate deep into the MCTS. This was further confirmed by tracking the distribution of fluorescein-labelled plasmid (pDsRed2-1) complexed with TAT and TAT-LK15 peptides in spheroids, showing high levels of fluorescence at the spheroids' rim, which decreased rapidly with increased depth [70].

Following this study TAT-LK15 was used to deliver shRNA and siRNA targeting the BCR-ABL oncoprotein in K562 chronic myeloid leukemia cells and was shown to effectively transfect cells without considerable cytotoxicity. TAT-LK15/siRNA complexes induced at least 70% silencing at 48 h post-transfection with a maximum reduction between 5 and 10 µg of siRNA. However, gene silencing was transient and could not be observed after 48 h. On the other hand, TAT-LK15/shRNA complexes induced a more stable gene silencing, which continued for up to 8 days post-transfection and was much higher than that achieved by Lipofectamine®/shRNA plasmid complex (85% vs. 40% respectively) [14].

Another example of a peptide vector based on TAT is a peptide system composed of TAT, the A domain of the nuclear protein High mobility group box 1 (HMGB1) and R3V6 as a delivery system for plasmid DNA containing heme oxygenease-1 (HO-1) gene [30]. HMGB1A was supposed to be capable of delivering DNA into the cells due to its positive charge and its ability to form complexes with DNA. It was presumed that subsequent expression of HO-1 would result in anti-inflammatory response, which would be further intensified by the synergistic anti-inflammatory effect of HMGB1A [30]. TAT-linked HMGB1A was produced by recombinant DNA technology, and after complexation with DNA, the complex was coated with R3V6. The DNA-TAT-HMGB1A-R3V6 complex had higher transfection efficiency than the DNA- PLL, DNA-R3V6, and DNA-TAT-HMGB1A complexes in RAW 264.7 cells and reduced the TNF-α and IL-6 levels in RAW 264.7 cells activated by lipopolysaccharides (antigens from gram negative bacteria) indicating the anti-inflammatory effect of the complex [30].

Yi et al [80], introduced two different kinds of nuclear localization signals (NLS), PKKKRKV (PV) and HMGB1, to a TAT-based gene delivery system, in an attempt to achieve high nuclear transfection. The combination of cell penetrating peptides and nuclear localization signals has been recently suggested as a promising strategy to improve cellular uptake as well as nuclear accumulation. Three types of peptide/DNA complexes were formed; TAT-PV/DNA, in which the NLS was covalently fused to TAT, TAT/DNA/PV and TAT/DNA/HMGB1 which were formed by electrostatic conjugation of the NLS with TAT/DNA complex. The transfection efficiency of the peptide/DNA complexes was evaluated in Human cervical carcinoma (HeLa) and African green monkey kidney (Cos7) cell lines using pGL-3 plasmids containing luciferase reporter gene. The cellular uptake/nuclear accumulation studies were performed using the same plasmid labelled with the green, fluorescent tag YOYO-1. The TAT/DNA complex was used as control. In addition, trans-cyclohexane-1,2-diol

(TCHD) was added to the cell culture medium to further enhance the nuclear accumulation of the TAT peptide [80].

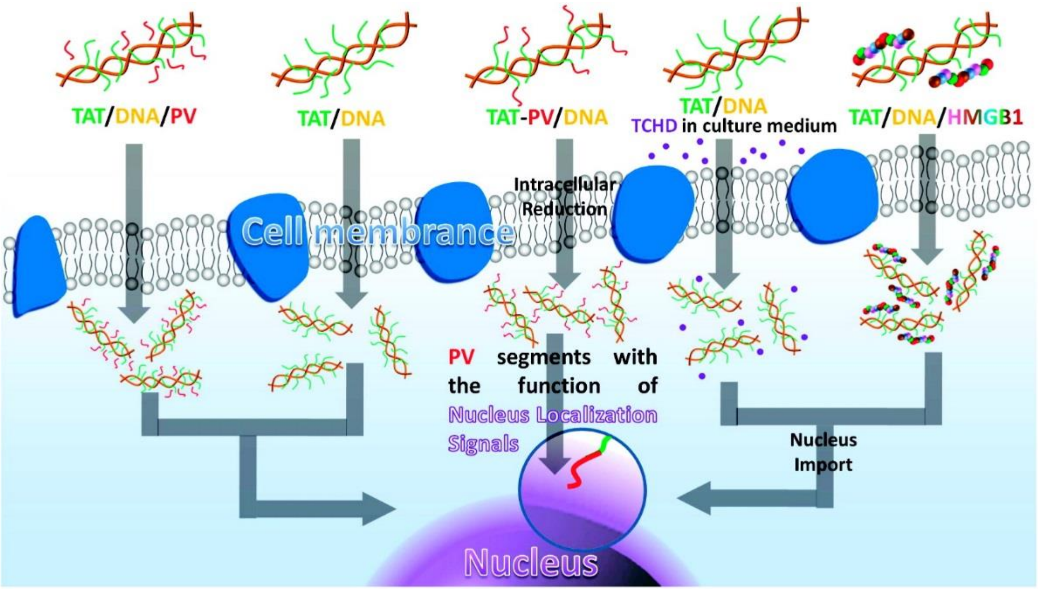

Figure 6- Gene delivery mediated by different TAT Peptide-based gene vectors, including TAT/DNA, TAT-PV/DNA, TAT/DNA/PV, TAT/DNA/HMGB1, and TAT/DNA with TCHD in DMEM medium. Reprinted with permission from reference 80. Copyright (2012) American Chemical Society.

Addition of TCHD increased the gene expression achieved by TAT/DNA complexes by 2 fold in both cell lines. TAT-PV/DNA complexes induced 200 fold higher luciferase reporter gene expression than TAT/DNA complexes in both cell lines at the optimum N/P ratio of 15. However, introduction of PV to the gene delivery system through electrostatic interaction did not have any significant effect on gene expression, which was supposed to be due to the instability of the TAT/DNA/PV ternary complexes and the low contribution of the noncovalently bound NLS to the nuclear localization. In the same way, the TAT/DNA/HMGB1 complex increased the gene expression by 3 folds compared to TAT/DNA which was considerably lower than the covalently conjugated TAT-PV/DNA further confirming that the covalent binding/fusion of the NLS to the CPP has a greater effect on enhanced nucleofection. Moreover, the TAT-PV/DNA complex exhibited high accumulation of the YOYO-1 labelled plasmid in the nucleus in both cell lines whereas the nuclear accumulation of the plasmid was very low in the case of the TAT/DNA/HMGB1 and TAT/DNA in the presence of TCHD, and no plasmid was detected in the case of TAT/DNA/PV and TAT/DNA in the absence of TCHD. These data clearly indicate that introduction of nuclear localization signals to the TAT-peptide based vector via covalent binding enhances the gene delivery efficiency. None of the complexes exhibited any apparent cytotoxicities neither in HeLa nor in Cos7 cell lines even at high N/P ratios [80].

1.2.7.2 Oligoarginines and poly arginines

Oligoarginines are synthetic CPPs [9, 17, 21, 32, 58] which were designed using the active motif of TAT as a guide [32] and short-chain oligolysines which were introduced as a less toxic alternative to oligoarginines [20]. It has been suggested that a minimum of six to eight cationic amino acids in the peptide chain is required to compact DNA into structures that are active in receptor-mediated gene delivery [20]. The first study on the use of peptide-based carriers for siRNA delivery was by law et al [32], who investigated the physicochemical properties of complexes formed between R9, a CPP derived from the HIV 1 Tat protein, and a connective tissue growth factor (CTGF) encoding siRNA. R9 readily formed complexes with siRNA, as a result of decreased surface charge at increasing peptide concentration. Negligible peak shifts in UV and CD spectra indicated lack of significant structural changes in siRNA. Furthermore, the salt dissociation experiment showed that R9 bound to siRNA through noncovalent interactions. The highest binding ratio of R9 to siRNA was found to be 10.3:1 according to UV/vis spectra and CD and 39.1:1according to DLS (corresponding to charge ratios of 2.2:1 (+/-) and 8.4:1, respectively). The observed difference in binding ratio was assigned to the difference in signal contribution between absorption and light scattering [32].

A few years later, Kim et al [17] introduced a short arginine peptide (R15) as vector for siRNA delivery. The peptide formed stable complexes with siRNA at a charge ratio of 3:1 and delivered siRNA into COS-7 cells *in vitro*, resulting in efficient gene silencing. The intracellular tracking of the peptide-siRNA complexes in live cells demonstrated the accumulation of siRNA in the perinuclear region 24h after transfection, confirming that siRNA was targeted to the perinuclear region to interact with RNA-induced silencing complex (RISC). These data were further confirmed by effective down-regulation of HER-2 mRNA and significant tumor growth inhibition after intratumoral administration of HER-2-specific siRNA-R9 complexes in SKOV-3 mouse xenografts. The designed delivery system proved to be nontoxic due to lack of body weight change in the mice during treatment [17].

Based on the body of literature on the DNA-binding and cell penetrating properties of the oligoarginines Won et al [81] synthesized a reducible poly(oligo-d-arginine) (rPOA) peptide as a potential pulmonary gene delivery system. The peptide was composed of C-(D-R9)-C repeating unit forming disulfide bonds between terminal cysteinyl-thiol groups of short peptides. The transfection studies were carried out in three different cell lines: HEK 293 (human embryonic kidney), H9c2 (Norway rat myoblasts), and L2 (Norway rat lung epithelial cells) using pGL3 luciferase encoding plasmid DNA. D-R9 and PEI were used as controls. rPOA and PEI induced considerable luciferase gene expression in all the three cell lines in a

DNA dose-dependent manner, whereas D-R9 induced very low gene expression in all the three cell lines. rPOA exhibited higher transfection efficiency (similar to PEI) in HEK 293 and L2 cells in comparison to H9c2 cells. Furthermore, the level of luciferase gene expression in L2 cells was reduced by nearly 25 times when the cells were transfected with the rPOA//DNA complexes in the presence of buthionine-sulfoximine (BSO) which inhibits production of glutathione in the cytosol, further confirming the effect of the disulfide bond reduction on the gene delivery efficiency of the peptide vector. On the other hand, the rPOA//DNA complexes showed significantly lower cytotoxicity towards L2 cells than PEI/DNA complexes making them favourable gene vector candidates. In addition to *in vitro* transfection, the rPOA//DNA complexes induced stable gene expression in the lungs of the mice following intratracheal injection, which was maintained for up to 7 days without any toxicities. At the optimal transfection conditions, the rPOA//DNA complexes induced 20 folds and 100 folds higher luciferase expression than PEI/DNA complexes and naked DNA respectively [81].

The rPOA was also successfully used to for delivery of siRNA both *in vitro* and *in vivo* [82]. The cellular trafficking studies using fluorescently labeled luciferase-targeted siRNA (siLuc) in squamous cell carcinoma (SCC) cells, revealed the rapid cellular uptake of the peptide-siRNA complexes (30 min), followed by rapid localization of the siRNA in the cytoplasm (1-2 hours). This was suggested to be due to dissociation of the siRNA/ rPOA complex and rapid release of the siRNA to the cytosol in response to intracellular glutathione. The cytoplasm-sensitive siRNA delivery of rPOA was further confirmed by measuring the secretion level of VEGF after transfection of the SCC cells with siRNA against vascular endothelial growth factor (siVEGF) in the presence or absence of buthionine- sulfoximine. The siVEGF/rPOA complex decreased the level of VEGF protein and VEGF mRNA by 50% and 70% respectively in the absence of BSO, which was much higher than siVEGF/PEI (positive control). However, in the presence of BSO, the levels of VEGF were reduced by only 20% with siVEGF/rPOA, clearly demonstrating the important role of the glutathione and the disulfide bond reduction in the controlled release of the siRNA into the cytoplasm. The transfection efficiency of the siVEGF/rPOA was further investigated in mice using a subcutaneous tumor model, owing to the angiogenic property of VEGF which is essential for tumor growth. The siVEGF/rPOA reduced the intratumoral levels of VEGF two folds and induced tumor suppression in the treated animals whereas the naked siRNA and the rPOA/scrambled siRNA complex which were used as controls failed to do so [82].

Lehto et al [83] investigated the transfection efficiency of a N-terminal stearylated polyarginine, stearyl-$(RxR)_4$, consisting of 6-aminohexanoic acid spacer between the Arginine residues for delivery of plasmids and splice-correcting oligonucleotides (SCOs) in comparison with unmodified $(RxR)_4$, and stearylated R9. The commercial transfection reagent Lipofectamine™ 2000 was used as the positive control. Unmodified $(RxR)_4$ formed complexes with plasmid DNA, however it exhibited poor transfection efficiency indicating its low cellular uptake. On the other hand, stearyl-$(RxR)_4$ efficiently delivered pGL3 luciferase expressing plasmid to several cell lines including Chinese hamster ovary (CHO), baby hamster kidney (BHK21) and human embryonic kidney (HEK293) cells, and induced significantly higher luciferase gene expression than non-stearylated $(RxR)_4$ and stearylated R9. The transfection efficiency of stearyl-$(RxR)_4$ was lower than with Lipofectamine™ 2000, however it was considerably less toxic. Moreover, Transfection of CHO cells with EGFP expressing plasmid revealed that stearyl-$(RxR)_4$/plasmid complexes transfected uniformly most of the cell population whereas, despite higher per-cell transfection efficiency Lipofectamine™ 2000/plasmid complexes did not seem to reach the whole cell population. Stearyl-$(RxR)_4$ also promoted significant splice correction in HeLa pLuc 705 cells when complexed with 2′-OMe SCOs whereas unmodified $(RxR)_4$ and stearyl-R9 failed to do so. the cellular uptake study using Cy5-labeled 2′-OMe SCOs revealed that In the same manner as plasmid transfection, the stearyl-(RxR)4/2′-OMe SCO complexes transfected almost 100% of the cell population whereas Lipofectamine/SCO complexes failed to do so in spite of higher splice correction efficiency [83].

1.2.7.3 Transportan and its derivatives

Transportan (TP) is a chimeric CPP, which has 12 amino acids from the neuropeptide galanin fused with 14 amino acids from the wasp venom mastoparan [61]. Transportan has been successfully used to deliver siRNA and induce gene silencing in COS7 cells stably expressing pGL2 firefly luciferase reporter gene [73]. TP-siRNA complexes also managed to reduce the level of luciferase expression considerably in CHO cells stably expressing luciferase (CHO-AA8-Luc) more efficiently than Lipofectamine® 2000. Furthermore, the reduction in luciferase levels achieved by TP-siRNA complexes initiated 24 h after transfection and lasted for 3 days whereas the lipofectamine-induced gene silencing started 48 hours post-transfection and only lasted for 1 day. The high transfection efficiency of transportan was further confirmed by transfecting C166-GFP and EOMA-GFP cells stably expressing GFP with transportan-GFP si-RNA complexes [73].

A derivative of transportan, named transportan10 (TP10), which is also a novel chloroquine analogue was developed by Mäe et al [84] and its cell penetration efficiency was enhanced by adding a stearyl moiety to the N-terminal. The peptide efficiently delivered 2′-OMe RNA splice correcting oligonucleotides to luciferase expressing HeLa pLuc 705 cells and promoted splice correction at a level comparable to Lipofectamine® 2000, without causing any cytotoxicity. The unmodified TP10 exhibited considerably lower transfection efficiency than stearyl-TP10 which clearly indicates the effect of N-terminal stearylation on enhancing the cell penetration and gene delivery efficiency of the peptide [84]. Stearyl-TP10, was also used for delivery of plasmid DNA, both *in vitro* and *in vivo* [85]. The peptide formed complexes with luciferase encoding plasmid DNA (pGL3) which exhibited high transfection efficiency even in presence of serum, and induced high levels of luciferase gene expression, comparable to Lipofectamine™ 2000, in different cell lines including U2OS (human osteosarcoma), U87(human primary glioblastoma), and HEK293 cells without any cytotoxic effects. Using the enhanced green fluorescent protein (EGFP)-encoding plasmid it was observed that the stearyl-TP10/pDNA complexes managed to transfect the entire cell population, even at high cell confluency, whereas, Lipofectamine™ 2000 could not reach all of the cells. Furthermore, stearyl-TP10/plasmid nanoparticles induced considerable luciferase expression 24 hours after intramuscular or intradermal administration to mice, without causing any toxicities or immune responses. Nevertheless, the naked plasmid also induced significant luciferase expression although the expression levels were less than peptide/pDNA complexes [85]. Based on the promising results showing efficient gene delivery by TP10, several other derivatives of TP10 were designed either by chemical modification of the peptide sequence or by conjugation of TP10 sequence to other functional peptide sequences. These TP10-derived peptide vectors can be classified into two main groups with the general names of Pepfects and Nickfects.

1.2.7.3.1 PepFects

The first of these TP10-derivatives, PepFect 6 (PF6) was developed by covalently introducing pH titratable trifluoromethylquinoline moieties into stearyl-TP10 to facilitate endosomal escape [79]. PF6 was able to induce significant siRNA-mediated gene silencing at low concentrations of siRNA in a dose-dependent manner which was markedly higher than that of Lipofectamine in various adherent cell-lines including luciferase-stable embryonic kidney (HEK) and human osteosarcoma (U2OS) cells as well as the more refractory HepG2 hepatoma cell-line and the response was well-preserved in serum. Treating stably EGFP expressing CHO cells with PF6/siRNA in the presence of serum, resulted in gene silencing in entire cell populations within 48 h, which was persistent over 5 days. Repeating the same treatments every third day gave a complete RNAi response for at least 8 days. PF6 showed minimal cytotoxicity *in vitro* and did not provoke any inflammatory responses when systemically administered to mice. *In vivo* administration of PF6/siRNA to mice at a 1 mg/kg dose resulted in significant reduction in HPRT1 expression in kidneys, liver and lungs after 72 h without any apparent acute toxicity, as confirmed by histopathological examinations, whereas controls treated did not show any reduction in HPRT1 levels. These results were further confirmed by reduced expression of luciferase over 2 weeks in mice expressing luciferase in the liver after treatment with 1 mg/kg of PF6/luc-siRNA. On the contrary, naked luc-siRNA was unable to induce any RNAi response [79].

Another peptide of this series, PepFect14 (PF14), was used to efficiently deliver splice-correcting oligonucleotides (SCOs) to HeLa pLuc705 cells as well as mdx mouse myotubes which is a model of Duchenne’s muscular dystrophy and induce splice-correction at higher rates than Lipofectamine® 2000 without any cytotoxic effects [86]. Modification of PepFect14 with endosomolytic trifluoromethylquinoline moieties gave rise to a new CPP named PepFect15, which was able to deliver Cy5-labeled SCOs as well as anti-microRNAs targeting miRNA into HeLa pLuc705 cells more efficiently than Pep-Fect14 and Lipofectamine® 2000 at their respective optimal molar ratios and to induce splice correction in a dose dependent manner. This was the first report on peptide- mediated anti-microRNA delivery. In addition, it was shown that the PepFect15/SCO complexes were largely internalized through scavenger receptor class A (SCARA) mediated endocytosis [87].

A novel tumor-activatable gene delivery system was developed by Veiman et al [88] by conjugation of PF14 to PEG via a tumor-responsive linker, matrix metalloproteinase 2 (MMP2).

They used PEG as a shield to inactivate PF14, assuming that the PEGylated PF14 would form core-shell nanoparticles when complexed with DNA, with the peptide-DNA complex in the core and the PEG oriented as an outer shell. Thus, the peptide-DNA complex will not be in contact with the blood until it reaches the specific tissues in which the cell penetration activity of the peptide can be restored via enzymatic cleavage of PEG resulting in higher cellular uptake and gene expression. A comparison between different chain lengths of PEG (PEG600, PEG1000 and PEG2000) revealed that the most condensed and most stable peptide-DNA complexes are formed when PF14 is functionalized with PEG2000 [88].

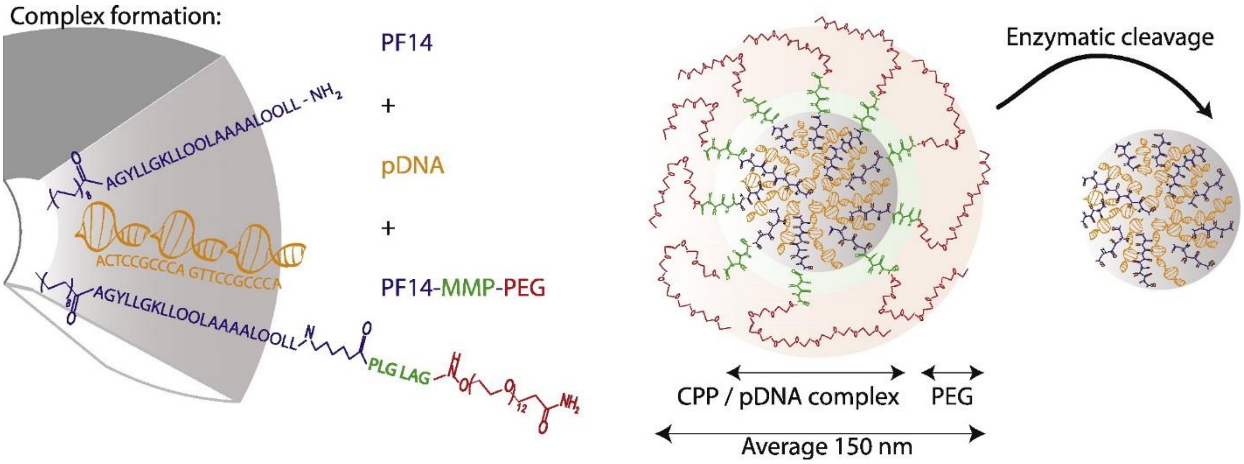

Figure 7- Schematic construction principle of the tumour-targeted peptide/pDNA complex. The peptide vector is made by C-terminal modification of PF14 with PEG using an MMP2-sensitive peptide linker. Hypothetically, the core of the complex consists of PF14 and DNA and PEG orients itself as an outer shell providing a neutral shield that inhibits transfection. Cleavage of the outer shell by a tumour-specific MMP2 generates the active particle which is able to transfect the cells. Reprinted from reference 88, Copyright © 2015 Veiman et al.

Transfection of CHO cells with the serum treated peptide-pDNA complexes revealed lower stability and transfection efficiency compared to PF14/pDNA complexes. Intravenous administration of the peptide-pDNA complexes to mice further confirmed the inhibitory effect of PEGylation on the transfection as the luciferase gene expression in the lungs was largely decreased by increasing the PEG content of the peptide-pLuc DNA complexes. In addition, PEGylation altered the biodistribution and pharmacokinetics of the peptide-pDNA complexes compared to unmodified PF14. The PF14/pDNA complexes had higher accumulation in the lungs whereas the PEGylated peptide/pDNA complexes had lower accumulation in the lungs but higher distribution in other tissues such as spleen and heart. The PEGylated complexes had lower elimination rate and higher circulation half-life than PF14 which was supposed to be due to lower contact with blood serum elements, and reduced accumulation in the lungs [88].

The potential of the functionalized PF14 to induce tumour-specific gene expression *in vivo* was evaluated in mouse Xenografts bearing subcutaneous tumors from human glioblastoma cell line U87. Despite their high *in vitro* transfection efficiency, PF14/pDNA complexes were unable to trigger significant gene expression in tumors. This was supposed to be in part due to the high clearance rate and low circulation time of the complexes and in part due to the high uptake and accumulation of the complexes in the lung tissue (as very high level of gene expression was observed in the lungs). On the other hand, even 10% PEGylation rate induced significant gene expression in tumors, which was up to 7-fold higher than the control, and very low gene expression in the lungs, as a result of higher accumulation of the particles in the tumour tissue compared to the lungs [88].

The tumor specificity of the complexes was further increased by introducing a tumor-specific cleavable linker, MMP2 between PEG and PF14. PEG moieties with different molecular weights were covalently attached to the C-terminal of PF14 via an MMP2-cleavable sequence (PEGylation rate of 50%) and the ability of the resulting multifunctional peptides to deliver the pDNA to the cancer cells was assessed in U87 and Neuro2a cells. The peptide-pDNA complexes were unable to induce any gene expression in U87 and Neuro2a cells unless they were pre-incubated with MMP enzyme prior to transfection in which case they induced high levels of gene expression comparable to the unmodified PF14, without any cytotoxicity. These findings clearly indicate the effect of MMP2 activation on transfection efficiency. In vivo administration of the above-mentioned complexes to Neuro2a tumor bearing mice resulted in increased gene expression in the tumor tissue and decreased gene expression in the lungs. Moreover, increasing the PEGylation rate up to 70% allowed for specific gene expression in the tumor without affecting the gene expression levels in other organs [88].

Following on this study, they further tried to improve the transfection efficiency and specificity of PF14 by modifying the charge and the fatty acid moiety [89]. They developed PF14 analogues with increased and decreased net charge by replacing the amino acids in the original peptide sequence with more basic or more acidic amino acids. PF6, which is a well-established siRNA vector and commercial PEI-based reagent jetPEI were also used as positive controls. The charge-modified peptides were able to bind and condense pDNA both in the presence and absence of serum, and the size and zeta potential of the complexes were not significantly different from PF14. PF14-O which has the highest charge among all the peptides had the highest transfection efficiency in CHO cells which was even higher than PF6 and jetPEI. When administered to mice C22-PF14 and PF14-O were the most efficient vectors for pLuc plasmid DNA and highly induced luciferase gene expression in the liver, with minimal gene expression in the lungs as opposing to PF14 which induced higher gene expression in the lungs. Applying both modifications at the same time, resulted in C22-PF14-O peptide with even higher liver specific gene delivery efficiency showing the synergistic effect of charge and fatty acid modification on the liver specific gene delivery efficiency [89].

Another series of gene vectors derived from PF14 were [90] developed by conjugating the cell penetrating peptide sequence from either PF14 or Pepfect28 and a glioma homing peptide

(ANG, BTX, CooP, or EPRNEEK) in an attempt to achieve targeted gene delivery to glioma cells. Among all of the resulting peptides only PF51, which consisted of PF28 and ANG, managed to deliver siRNA and induce high level of luciferase gene silencing in U87 MG-luc2 cells (which stably expressed luciferase). Covalent conjugation of the glioma targeting peptide to PF14 adversely affected its transfection efficiency. On the contrary, when the targeting peptide was modified with hexaglutamate and noncovalently conjugated to PF14, the resulting peptide-siRNA complexes exhibited considerable gene silencing efficiency in U87 MG-luc2 cells. The highest gene silencing efficiency was achieved when PF14 was noncovalently conjugated with modified ANG, at a peptide to siRNA molar ratio of 1 and siRNA concentration of 25 nM. In contrast to the U87 MG-luc2 cells, HeLa-luc cells, were less transfected by the same peptides indicating the successful glioma-targeted delivery of the siRNA using the peptide vectors [90].

1.2.7.3.2 NickFects

The second group of TP10 derivatives, NickFects, were produced by chemical modification of the lysine residue Lys7, which is the linker between the galanin motif and the mastoparan motif [91]. Replacing the Lys7 with Ornithine, produced NickFect 53 (NF53). NickFect 61 (NF61) was produced by conjugating the two peptide motifs via the ε-NH2 group of Lys7 instead of α-NH2 which is normally used. Finally, NickFect 51 (NF51) was produced by replacing the Lys7 with Ornithine and then binding it to the Glycine residue number 6 (Gly6) via δ-NH2 group. NickFects formed complexes with plasmid DNA, splice correcting oligonucleotides and siRNA in the size range of 60–160 nm which were stable in the presence of serum. The peptides delivered pGL3 luciferase encoding plasmid to CHO cells with high efficiency which was several orders of magnitude higher than stearyl-TP10 in the absence of serum. NF51 which showed the highest transfection efficiency among all the peptides was further used for delivery of pGL3 plasmid DNA to various other normal and cell lines including U2OS, U87, HEK, mouse embryonic fibroblast (MEF), Jurkat and A20 and managed to transfect all the cell lines efficiently and induce high levels of luciferase gene expression which was comparable to Lipofectamine™ 2000 in the case of U2OS, U87, Jurkat and A20 cells. In a similar manner, NF51 complexed with EGFP encoding plasmid transfected CHO, U87, and U2OS cell with 80% efficiency and 45% efficiency in the absence and presence of serum respectively. NF51 also managed to deliver SCO to Hela pLuc705 cells and induce splice-correction which was 4-5 times higher than stearyl-TP10 and even higher than Lipofectamine™ 2000 both in the absence and presence of serum. The NF51/SCO complexes were internalized within 4 h after transfection and were translocated to the nuclei in 24 h, and they were found to be capable of endosomal escape. NF53 and NF61 also managed to deliver SCO to the cells but with lower efficiency than NF53, stearyl-TP10 and Lipofectamine™ 2000. NickFects also delivered anti EGFP siRNA to CHO cells stably expressing EGFP and induced gene silencing at a level higher than Lipofectamine™ 2000 and Lipofectamine™ RNAiMAX in serum-free medium and similar to Lipofectamine™ 2000 in the presence of serum. Moreover, NF51/siRNA complexes successfully transfected the entire cell population whereas a considerable proportion of the cells was not transfected by Lipofectamine™ 2000 [91].

Replacing one of the lysine residues in the mastoparan motif of NF51 with alanine produced NF55 which had lower net positive charge and higher α-helicity than the parent peptide [92]. NF55 formed stable complexes with plasmid DNA pLuc2 which were resistant to protease degradation and exhibited two times higher transfection efficiency than the NF51 in HeLa and U87-MG cells. Intravenous Administration of NF55/Cy5-labled pDNA complexes to tumor bearing mice revealed accumulation of the pDNA in the tumor tissue 3 h post-injection and accumulation in the bladder and renal tissue after 24 h. Administration of the NF55/ pLuc2 complexes to mice induced same level of gene expression in liver, 5 times higher gene expression in cerebellum and two times lower gene expression in the lungs compared to the commercial transfection reagents JetPEI and Turbofect, and much higher gene expression in liver and cerebellum than the parent peptide, NF51. Due to high levels of gene expression in the brain, the *in vivo* gene expression efficiency of the NF55/pDNA complexes was further evaluated using a mouse model of intracranial brain tumor. The NF55/ pLuc2 complexes induced 45 fold higher gene expression in tumor-containing striatum; nevertheless, similarly high gene expression was also detected in unaffected brain regions and lungs indicating that NF55 provides brain tissue-specific gene delivery, but not tumor-specific gene delivery. To improve the tumor-specificity of NF55, a PEGylated analogue (NF552) was produced by C-terminal conjugation to PEG2000. Addition of 20% NF552 to NF55 increased the tumour accumulation 3 times and decreased the lung accumulation 38 times compared to the NF55 alone in a subcutaneous tumor model. The NF55/pDNA complexes elevated the level of liver enzymes 24 h post-injection, however they did not cause any pathological changes to the liver tissue, nor did they induce any pathological changes to the lung tissue indicating the biocompatibility and safety of NF55 as a gene vector [92].

1.2.7.4 Miscellaneous CPPs

1.2.7.4.1 MPG-8

MPG-8 is an amphipathic peptide designed by Crombez et al [93], which was shown to transfect cancer cells with siRNA targeting cyclin B1 both *in vitro and in vivo.* Subnanomolar concentrations of Cyc-B1 siRNA complexed to MPG-8 significantly inhibited proliferation of PC3, MCF7 and SKBr3-HER2 cancer cell lines, but had only a moderate effect on HS68 fibroblasts. Local intra-tumoral administration of MPG-8/siRNA to human prostate carcinoma cell PC3-xenografted mice resulted in considerable tumour growth inhibition after 50 days. Functionalization of MPG-8 with cholesterol significantly improved the tissue distribution and stability of the associated siRNA *in vivo* and inhibited tumour growth upon systemic injection without triggering any non-specific inflammatory response [93].

1.2.7.4.2 CADY

CADY is a secondary amphipathic oligopeptide designed by Crombez et al [94], containing aromatic tryptophan and cationic arginine residues which enables it to adopt a helical conformation within cell membranes, with charged residues on one side and tryptophan residues that favour cellular uptake, on the other side. CADY was shown to form stable complexes with siRNA, and to deliver it effectively to a wide variety of cell lines, including suspension and primary cell lines. CADY-siRNA complexes were uptaken very rapidly (within 30 min) and the transfection efficiency was directly related to the molar ratio of CADY/siRNA with optimal results obtained at the molar ratio of 80/1. CADY/siRNA complexes promoted knockdown of GADPH mRNA in U2OS cells the extent of which was directly proportional to the siRNA concentration. The maximal mRNA silencing (95%) was obtained at 20 nmol/l siRNA concentration. By contrary, GAPDH protein reduction was inversely proportional to siRNA concentrations and a complete knockdown of the target protein was obtained at 10 nmol/l siRNA concentration. CADY-mediated delivery of siRNA-targeting p53 into mammalian cells gave rise to 97% knockdown of p53 protein after 48 and 72 hours, and after 5 days 60% reduction in p53 protein levels was maintained indicating stability of CADY/siRNA complexes within cells. Even more, CADY was able to deliver siRNA into difficult to transfect cell lines such as THP1 and primary HUVEC and 3T3C cell lines and to induce considerable GADPH knockdown both at the mRNA and protein level without any toxicity [94].

CADY was also used to deliver siRNA targeting a housekeeping gene (GAPDH) to mouse embryonic stem cells (mES) and T lymphocytes (Jurkat T), both recognized as challenging to transfect cell lines [95]. The CADY peptides were monomeric in solution but upon contact with siRNA rapidly self-assembled into stable nanoparticles with a “raspberry”-like “core shell” organization exposing the Arg and Lys residues on the surface. Applying the CADY-siRNA nanoparticles in serum-containing medium resulted in significant knockdown of the GAPDH target gene and reduced the GAPDH-mRNA level substantially, with no significant toxicity [95]. Further studies revealed that CADY/siRNA complexes are mainly internalized by direct translocation through the membrane but not the endosomal pathway. CADY/siRNA complexes induce a transient cell membrane perturbation, which is rapidly restored by cell membrane fluidity, followed by rapid translocation of the complex to the cytoplasm, without compromising membrane integrity or cell viability [96].

1.2.7.4.3 Hph1

A fusion protein (Hph1–Hph1–dsRBD) composed of two CPP molecules and a double-stranded RNA binding domain (dsRBD), was designed by Li et al [97] for siRNA delivery. The calcium-condensed effects were assessed on GAPDH and green fluorescent protein (GFP) genes *in vitro*, followed by in vivo evaluations in a mouse heart transplantation model. Almost 100% of the HeLa cells treated with the Hph1–Hph1– dsRBD/FAM-siRNA complex were shown to be FAM-siRNA positive, in contrast to the cells treated with naked FAM-siRNA. The Hph1–Hph1–dsRBD/anti-GFP siRNA (siGFP) complex induced GFP gene silencing in HeLa cells after 48 h, the extent of which was directly proportional to peptide/siRNA molar ratio, with nearly complete knock down at the molar ratio of 60:1. Moreover, 48 h after treatment of HeLa cells with Hph1–Hph1–dsRBD/anti-GAPDH siRNA complex at the molar ratio of 30:1, the GAPDH mRNA level was reduced to 30% of the initial level (prior to treatment). These results were further confirmed by western blot analysis which demonstrated decreased level of GAPDH protein in HeLa cells after treatment with Hph1–Hph1–dsRBD/anti-GAPDH siRNA complex [97].

The GFP gene silencing effect of the protein-siRNA complex was also affected by the presence of calcium in the medium during the condensation step. The calcium-condensed effects considerably increased the cellular uptake of the protein-siRNA complexes and their GFP gene silencing effects. When the condensation was carried out at calcium concentration between 23.1 mM and 69.2 mM, the GFP gene was silenced in a calcium concentration-dependent manner with the maximum knock down (94%) being achieved at 69.2 mM calcium concentration. However, at concentrations below or above this range, the gene-silencing tendency of the complex was drastically decreased suggesting that a certain amount of calcium might compensate or reinforce the function of protein-siRNA complexes. The Hph1-Hph1-dsRBD was able to deliver FAM-labelled siRNA to the heart transplant tissue efficiently and to distribute it throughout the tissue in a mouse model in a manner similar to CPP-EGFP whereas the naked FAM-siRNA could not get into the heart tissue. The peptide exhibited very low cytotoxicity and did not suppress the cell proliferation [97].

1.2.7.4.4 WRAP

Konate et al. [98] developed a new family of CPPs consisting of short tryptophan- and arginine-rich amphipathic Peptides (WRAP) and evaluated their efficiency in siRNA delivery. The peptides consisted of tryptophan residues with different distributions (either scattered all along the sequence or clustered in one domain of the sequence) and the same number of arginine residues in order to keep the same content of positive charges. Except WRAP3, the rest of the peptides had random structures in solution but underwent conformational change and adopted alpha helical conformation when complexed to siRNA. In the case of WRAP3, the secondary structure could not be determined due to the absence of asymmetric carbon in glycine residues representing 50% of the sequence which resulted in very low circular dichroism signal [98].

The transfection and gene silencing efficiency of the different WRAP/siRNA complexes was evaluated in various cell lines including U87 (human primary glioblastoma), KB (human keratin-forming tumor), MCF7 (human breast adenocarcinoma), HuH7 (human hepatocellular carcinoma), MDA-MB-231 (human metastatic breast adenocarcinoma), HT29 (human colon adenocarcinoma), Neuro2a (mouse neuroblastoma), CMT93 (mouse rectal carcinoma), and RM1 (mouse prostate carcinoma) cell lines. All of the cell lines were stably expressing the FLuc/NLuc reporter genes and were therefore transfected with the anti-luciferase siRNA. The peptides WRAP1 and WRAP5 were able to induce high levels of gene silencing (50-80%) in all of the tested cell lines when complexed to siRNA in a dose-dependent manner [98].

Although the transfection efficiency of the peptide-siRNA complexes was less than RNAiMAX which was used as the positive control, their cytotoxicity was also much lower thus suggesting a safer and more biocompatible gene delivery system. Moreover, the peptides were able to induce considerable gene silencing (60%) in U87 cells even in the presence of serum. The peptide-siRNA complexes were internalized by U87 cells very rapidly (IC50 of internalized siRNA were 240 s and 185 s for WRAP1 and WRAP5 respectively) and luciferase gene silencing was observable after 5 min of incubation. WRAP1- and WRAP5 were also complexed with siRNA against the cyclin dependent kinase 4 (CDK4), which is known to be overexpressed in glioblastoma, and their gene silencing efficiency was evaluated in U87 cells. The peptide-siRNA complexes reduced the CDK4 protein levels by up to 80% in a dose-dependent manner [98].

1.3 Antimicrobial and anticancer peptides

Naturally occurring antimicrobial peptides (AMPs) with activity against a wide range of bacteria have been isolated from different organisms including eukaryotic microorganisms, plants and animals [99-106]. Some of these AMPs also exhibit anticancer activity via cell membrane disruption [99 ,101, 107-111]. Most of the AMPs and anticancer peptides (ACPs) exert their antimicrobial or anticancer effect by interacting with the lipid bilayer of cell membrane and increasing the membrane permeability which final leads to membrane rupture or perforation and brings about the cell death [99, 100, 103-106, 112]. The antimicrobial action of the AMPs starts with electrostatic interaction between the positively charged moieties in the peptide and the negatively charged heads of the phospholipids in the bacterial cell membrane followed by insertion of the hydrophobic regions of the peptide into the phospholipid bilayer. This process could be associated with conformational changes in the peptide from random structures to α-helical or β-sheet structure [99, 104, 105].

Due to the more negative surface charges of the bacterial cell membranes compared to the mammalian cell membranes, cationic AMPs have higher affinity for bacterial cells than mammalian cells which bestows selective antimicrobial effect upon them with minimal toxicity in the host mammalian cells which is an advantage of these peptides over other groups of antibiotics which inhibit the formation of bacterial cell wall or protein biosynthesis [99, 100, 105, 106]. Similar to bacterial cell membranes, the cancer cell membranes are also more negatively charged than normal human cell membranes due to the higher composition of negatively charged molecules such as phosphatidylserine, O-glycosylated mucin, sialilated gangliosides, and heparan sulphates [103, 115, 116] which results in higher selectivity of the ACPs for the cancer cells than normal mammalian cells.

Despite the structural diversity of the AMPs, they have some common features which are supposed to be essential for their antimicrobial/anticancer activity. These features include positive net charge, amphiphilicity, and high abundance of glycine, lysine, arginine and leucine [99,103-105]. Although the naturally occurring AMPs have considerable antibacterial and anticancer activity, they have some disadvantages such as poor bioavailability, potential immunogenicity, and high production costs. To overcome these problems, more research has been directed towards development of synthetic antimicrobial/anticancer peptides using the active motif of the naturally occurring AMPs/ACPs as a guide [99, 103, 107]. Over the past two decades a variety of synthetic AMPs/ACPs have been developed by modifying the sequences of the naturally occurring AMPs either by shortening the peptide sequence using minimalist de novo design strategy or by replacing the amino acids with other types of amino acids or with D-amino acids or fluorinated amino acids [99, 102, 103, 106, 107, 112, 114-116]. Furthermore, terminal modifications such as N-terminal acetylation, and C-terminal amidation, have also been used to improve the biological activity of the AMPs and ACPs [107, 112, 117-119].

1.4 Design principles for the short cationic amphiphilic peptides

In this research project we designed three series of short cationic amphiphilic peptides for potential applications as gene carriers or anticancer peptides based on the basic characteristics required for such biological activities according to the available literature on the peptide-based gene carriers and AMPs/ACPs. A series of α-helical cationic amphiphilic peptides with the general formula $C(XXYY)_3$, where C is amino acid cysteine, X represents hydrophobic amino acids (isoleucine or leucine) and Y represents cationic amino acids (arginine or lysine) were designed based on the structural features of a series of synthetic α-helical cationic amphiphilic peptides with proven antimicrobial and anticancer activities as follows [99, 101, 112]:

1- Combination of arginine/lysine with Isoleucine/leucine in tetrads has high propensity of α-helix formation.
2- N-terminal cysteine strengthens the α-helix.
3- Combination of cationic amino acid residues (arginine and lysine) and hydrophobic amino acid residues (isoleucine and leucine) enables interaction with cancer cell membranes.
4- C-terminal amidation enhances the antimicrobial/anticancer activity of the peptide.
5- Cationic amino acids (arginine and lysine) provide a binding site for nucleic acids and hydrophobic domain enables penetration into the cell membrane.

A series of β-sheet forming peptides with the general formula $(XYYX)_3$, where X represents the hydrophobic amino acids (isoleucine and leucine) and Y represents cationic amino acids (arginine and lysine) were designed based on the basic features observed in the naturally occurring β-sheet forming AMPs including the following [120-123]:

1- amphipathic dyad repeats occur commonly in β-sheet forming AMPs.
2- Isoleucine and leucine have strong β -sheet folding propensities.
3- A combination of hydrophobic amino acids and cationic amino acids (arginine or lysine) enables interaction with cancer cell membranes.
4- C-terminal amidation enhances the antimicrobial/anticancer activity of the peptide.
5- Cationic amino acids (arginine and lysine) provide a binding site for nucleic acids and hydrophobic domain enables penetration into the cell membrane.

A series of surfactant-like peptides with the general formula $(X_1X_2)_4K$ where K is amino acid lysine, X_1 and X_2 represent hydrophobic amino acids (isoleucine, alanine and glycine) were designed assuming that lysine provides a binding site for DNA/RNA and the hydrophobic tail allows for cell penetration.

1.5 Conclusion

The development of nanostructured gene delivery systems with specifically tailored and finely tunable physicochemical and biological properties for efficient, targeted gene delivery is a new era in molecular medicine. Ideally, such gene delivery systems should be able to complex with and condense the DNA/RNA molecules, selectively deliver them to the target cells with high efficiency and release them at considerable rates without compromising their biological activity. The clinical translation of such gene delivery strategies would be expression/inhibition of specific genes in specific target tissues resulting in the desired therapeutic effect with minimal off-target effects. Various materials such as natural or synthetic polymers and lipids have been used for the development of nanosized non-viral gene delivery systems with varying advantages. More recently, peptides have attracted attention as new biomaterials for gene delivery. The biocompatibility and versatility of peptides make them ideal candidates for gene delivery. Moreover, biologically active peptide vectors can be produced via incorporation of the functional sequences from bioactive peptides into the synthetic peptides. Enhanced cellular uptake through incorporation of cell penetrating peptide sequences and tumor tissue targeting through incorporation of biological recognition elements into the peptide structure, are examples of biologically active peptide-based gene vectors. Nevertheless, despite the vast body of literature on peptide-mediated gene delivery, except few cases, most of the currently developed peptide-based gene vectors are still not comparable to commercially available lipid-based transfection agents and viral gene vectors in terms of transfection efficiency which has limited their therapeutic use. Hence, there is still much room for further development of peptide-based gene vectors with improved transfection efficiency and higher specificity through rational design and structure activity relationship studies.

1.6 References

1. Y. Zhang, A. Satterlee, L. Huang, *In vivo* gene delivery by nonviral vectors: Overcoming hurdles? *Mol. Ther.*, 20 (2012): 1298-1304.
2. H. Yin, R. L. Kanasty, A.A. Eltoukhy, A. J. Vegas, J. R. Dorkin, D. G. Anderson. Non-viral vectors for gene-based therapy. *Nat. rev. genet.*, 15 (2014): 541-555.
3. C. H. Jones, C. K. Chen, A. Ravikrishnan, S. Rane, B. A. Pfeifer. Overcoming nonviral gene delivery barriers: Perspective and future. *Mol. Pharmaceutics*, 10 (2013): 4082-4098.

4. M. Wang, M. Law, J. Duhamel, P. Chen. Interaction of a self-assembling peptide with oligonucleotides: Complexation and aggregation. *Biophysical J.*, 93 (2007): 2477-2490.
5. M. Damen, J. Aarbiou, S. F.M. van Dongen, R. M. Buijs-Offerman, P. P. Spijkers, M. van den Heuvel, K. Kvashnina, R. J.M. Nolte, B. J. Scholte, M. C. Feiters. Delivery of DNA and siRNA by novel gemini-like amphiphilic peptides. *J. Control. Release,* 145 (2010): 33-39.
6. D. W. Ryu, H. A. Kim, H. Song, S. Kim, M. Lee, Amphiphilic peptides with arginines and valines for the delivery of plasmid DNA. *J. Cell. Biochem.,* 112 (2011):1458-1466.
7. S. Bulut, T. S. Erkal, S. Toksoz, A. B. Tekinay, T. Tekinay, M. O. Guler. Slow release and delivery of antisense oligonucleotide drug by self-assembled peptide amphiphile nanofibers. *Biomacromolecules,* 12 (2011):3007-3014.
8. Y. Sun, L. Chen, F. Sun, X. Tian, S. Z. Luo. New amphiphilic N-phosphoryl oligopeptides designed for gene delivery. *Int. J. Pharm.*, 468 (2014): 83-90.
9. D. Mumcuoglu, M. Sardan, T. Tekinay, M. O. Guler, A. B. Tekinay. Oligonucleotide delivery with cell surface binding and cell penetrating peptide amphiphile nanospheres. *Mol. Pharmaceutics,* 12 (2015): 1584-1591.
10. P. Järver, T. Coursindel, S.E. L Andaloussi, C. Godfrey, M. JA Wood, M. J Gait. Peptide-mediated cell and *in vivo* delivery of antisense oligonucleotides and siRNA. *Mol. Ther. Nucleic Acids*, 1(2011):e27.
11. J. H.P. Chan, S. Lim, W. S. Fred Wong, antisense oligonucleotides: From design to therapeutic application. *Clin. Exp. Pharmacol. Physiol.,* 33(2006):533-540.
12. P. Boisguérin, S. Deshayes , M.l J. Gait, L. O'Donovan, C. Godfrey, et al. Delivery of therapeutic oligonucleotides with cell penetrating peptides. *Adv. Drug Deliv. Rev.,* 87 (2015): 52-67.
13. G. Ozcan, B.Ozpolat, R. L. Coleman, A. K. Sood, G. Lopez-Berestein, Preclinical and clinical development of siRNA-based therapeutics. Adv. Drug Deliv. Rev., 87 (2015): 108-119.
14. Y. Arthanari, A. Pluen, R. Rajendran, H. Aojula, C. Demonacos, Delivery of therapeutic shRNA and siRNA by Tat fusion peptide targeting bcr-abl fusion gene in Chronic Myeloid Leukemia cells. *J. Controlled Release*. 145 (2010): 272-280.

15. H. Wang, Y. Jianga, H. Peng, Y. Chen, P. Zhub, Y. Huang, Recent progress in microRNA delivery for cancer therapy by non-viral synthetic vectors. *Adv. Drug Deliv. Rev.,* 81 (2015): 142-160.
16. L. A. Avila, L. RMM Aps, P. Sukthankar, N. Ploscariu, S. Gudlur, et al. Branched amphiphilic cationic oligopeptides form peptiplexes with DNA: A study of their biophysical properties and transfection efficiency. *Mol. Pharmaceutics,* 12 (2015):706-715.
17. S. W. Kim, N. Y. Kim, Y. B. Choi, S. H. Park, J. M. Yang, S. Shin. RNA interference *in vitro* and *in vivo* using an arginine peptide/siRNA complex system. *J. Control. Release*, 143 (2010): 335-343.
18. Q. Tang, B. Cao, H. Wu, G. Cheng. Selective gene delivery to cancer cells using an integrated cationic amphiphilic peptide. *Langmuir*, 28 (2012):16126-16132.
19. S. H. Medina, S. Li, O.M. Z. Howard, M. Dunlap, A. Trivett , J. P. Schneider, J. J. Oppenheim. Enhanced immunostimulatory effects of DNA-encapsulated peptide hydrogels. *Biomaterials*, 53 (2015): 545-553.
20. G. N. Goparaju, P. K. Gupta. Design of amphiphilic oligopeptides as models for fine tuning peptide assembly with plasmid DNA. *Drug Discoveries Ther.,* 8(2014):165-172.
21. J. X. Chen, X. D. Xu, S. Yang, J. Yang, R. X. Zhuo, X. Z. Zhang. Self-assembled BolA-like amphiphilic peptides as viral-mimetic gene vectors for cancer cell targeted gene delivery. *Macromol. Biosci.,* 13 (2013,): 84-92.
22. S. M. Standley, D. J. Toft, H. Cheng, S. Soukasene, J. Chen, S. M. Raja, V. Band, H. Band, V. L. Cryns, S. I. Stupp. Induction of cancer cell death by self-assembling nanostructures incorporating a cytotoxic peptide. *Cancer Res*., 70(2010): 3020-3026.
23. H. O. McCarthy, J. McCaffrey, C. M. McCrudden , A. Zholobenko, A. A. Ali, et al. Development and characterization of self-assembling nanoparticles using a bio-inspired amphipathic peptide for gene delivery. *J. Control. Release*, 189 (2014): 141-149.
24. D. Yoshida, K. Kim, I. Takumi, F. Yamaguchi, K. Adachi, A. Teramoto. A transfection method for short interfering RNA with the lipid-like self-assembling nanotube, A6K. *Med. Mol. Morphol.*, 46 (2013):86-91.
25. X. Zhao, S. Zhang. Designer self-assembling peptide materials. *Macromol. Biosci.*, 7(2007):13–22.

26. J. B. Matson, R. H. Zha, S. I. Stupp. Peptide self-assembly for crafting functional biological materials. *Curr. Opin. Solid State Mater. Sci.,* 15 (2011): 225-235.
27. Y. Loo, S. Zhang, C. A.E. Hauser. From short peptides to nanofibers to macromolecular assemblies in biomedicine. *Biotechnol. Adv*., 30 (2012): 593-603.
28. M.E. Padin-Iruegas, Y. Misao, M.E. Davis, V.F.M. Segers, G. Esposito, T. Tokunou, K. Urbanek , T. Hosoda, M. Rota, P. Anversa, A. Leri, R.T. Lee, J. Kajstura. Cardiac progenitor cells and biotinylated IGF-1 nanofibers improve endogenous and exogenous myocardial regenration after infarction. *Circulation*, 120 (2009):876-887.
29. D.W. Ryu, H.A. Kim, S. Kim, M. Lee. VEGF receptor binding peptide-linked amphiphilic peptide with arginines and valines for endothelial cell-specific gene delivery. *J Drug Target.*, 20(2012):574-581.
30. B. Kim, J.H. Song, M. Lee. Combination of TAT-HMGB1A and R3V6 amphiphilic peptide for plasmid DNA delivery with anti-inflammatory effect. *J Drug Target.*, 22(2014):739-47.
31. M. O. Guler, J. K. Pokorski, D. H. Appella, S. I. Stupp. Enhanced oligonucleotide binding to self-assembled nanofibers. *Bioconjugate Chem*., 16(2005): 501-503.
32. M. Law, M. Jafari, P. Chen. Physicochemical characterization of SiRNA-peptide complexes. *Biotechnol. Prog.,* 24 (2008): 957-963.
33. D. Lejeune, N. Delsaux , B. Charloteaux, A. Thomas, R. Brasseur. Protein-nucleic acid recognition: Statistical analysis of atomic interactions and influence of DNA structure. Proteins, 61 (2005):258-271.
34. S.D.D.T.A. Jones, N.M. Luscombe, H.M. Berman, J.M. Thornton. Protein-RNA interactions: a structural analysis. Nucleic Acids Res., 29 (2001):943-954.
35. M. Zhao, L. Liang, K. Ziyao, F. Siliang, M. Qingbin, and L. Keliang. "Histidine-enriched multifunctional peptide vectors with enhanced cellular uptake and endosomal escape for gene delivery." *J. Mater. Chem. B,* 5 (2016): 74-84.
36. P. Midoux, C. Pichon, J. J. Yaouanc, and P. A. Jaffres. chemical` vectors for gene delivery: a current review on polymers, peptides and lipids containing histidine or imidazole as nucleic acids carriers. *Br. J. Pharmacol.,* 157 (2009): 166-178.
37. C. Pichon, C. Goncalves, and P. Midoux. Histidine-Rich Peptides and Polymers for Nucleic Acids Delivery. *Adv. Drug Delivery Rev.,* 53 (2001): 75-94.
38. J. Guo, W. P. Cheng, J. Gu, C. Ding, X. Quc, et al. Systemic delivery of therapeutic small interfering RNA using a pH-triggered amphiphilic poly-L-lysine nanocarrier to suppress prostate cancer growth in mice. *Eur. J. Pharm. Sci.,* 45 (2012): 521-532.

39. J. Dufourcq, W. Neri, N. Henry-Toulmeè. Molecular assembling of DNA with amphipathic peptides. *FEBS Lett.*, 421 (1998): 7-11.
40. D. W. Ryu, H. A. Kim, J. H. Ryu, D. Y. Lee, M. Lee. Amphiphilic peptides with arginine and valine residues as siRNA Carriers. *J. Cell. Biochem.,* 113 (2012):619-628.
41. N. Wiradharma, M. Khan, Y. W. Tong, S. Wang, Y.Y. Yang. Self-assembled cationic peptide nanoparticles capable of inducing efficient gene expression in vitro. *Adv. Funct. Mater.,* 18 (2008) :943-951.
42. X. D. Guo, F. Tandiono, N. Wiradharma, D. Khor, C. G. Tan, et al. Cationic micelles self-assembled from cholesterol-conjugated oligopeptides as an efficient gene delivery vector. Biomaterials, 29 (2008): 4838-4846.
43. K. K. Hou, H. Pan, G. M. Lanza, S. A. Wickline. Melittin derived peptides for nanoparticle based siRNA transfection. *Biomaterials,* 34 (2013): 3110-3119.
44. H. F. Zhou, H. Yan, H.Pan, K. K. Hou, A. Akk, et al. Peptide-siRNA nanocomplexes targeting NF-κB subunit p65 suppress nascent experimental arthritis. *J. Clin. Invest.,* 124 (2014):4363-4374.
45. K. A. Mills, J. M. Quinn, S. T. Roach, M. Palisoul, M. Nguyen, et al. p5RHH nanoparticle-mediated delivery of AXL siRNA inhibits metastasis of ovarian and uterine cancer cells in mouse xenografts. *Sci. Rep.*, 9 (2019):1-10
46. S. Zhang, D. M. Marini, W. Hwang, S. Santoso. Design of nanostructured biological materials through self-assembly of peptides and proteins. *Curr. Opin. Chem. Biol.*, 6 (2002):865-871.
47. S. Zhang, X. Zhao. Design of molecular biological materials using peptide motifs. *J. Mater. Chem.*, 14 (2004):2082-2086.
48. A. Dehsorkhi, V. Castelletto, I. W. Hamley. Self-assembling amphiphilic peptides. *J. Pept. Sci.,* 20 (2014): 453-467.
49. C. Tang, F. Qiu, X. Zhao. Molecular design and applications of self-assembling surfactant-like peptides. *J. Nanomater*., 2013, doi:10.1155/2013/469261.
50. Y. Yang, U. Khoe, X. Wang, A. Horii, H. Yokoi, S. Zhang. Designer self-assembling peptide nanomaterials. *Nano Today,* 4(2009): 193-210.
51. J.R. Lu, X.B. Zhao, M. Yaseen. Biomimetic amphiphiles: Biosurfactants. *Curr. Opin. Colloid Interface Sci.*, 12 (2007): 60-67.
52. S. Zhang. Fabrication of novel biomaterials through molecular self-assembly. *Nat. Biotech.*, 21(2003): 1171-1178.

53. S. Zhang. Lipid-like Self-Assembling Peptides. *Acc. Chem. Res*., 45 (2012): 2142–2150.
54. M. Mazza, M. Hadjidemetriou, I. de Lazaro, C.Bussy, K. Kostarelos. Peptide nanofiber complexes with siRNA for deep brain gene silencing by stereotactic neurosurgery. *ACS Nano.*, 9(2015):1137-1149.
55. M. Cao, Y. Wang, W. Zhao, R. Qi, Y. Han, et al. Peptide-induced DNA condensation into virus-mimicking nanostructures. *ACS Appl. Mater. Interfaces*, 10 (2018): 24349-24360.
56. R. Bitton, J. Schmidt, M. Biesalski, R.Tu, M. Tirrell, H. Bianco-Peled. Self-assembly of model DNA-binding peptide amphiphiles. *Langmuir***,** 21 (2005): 11888-11895.
57. S. Samanta, R. Sistla, A. Chaudhuri. The use of RGDGWK-lipopeptide to selectively deliver genes to mouse tumor vasculature and its complexation with p53 to inhibit tumor growth. *Biomaterials*, 31 (2010): 1787-1797.
58. L. Luan, Q. Meng, L. Xu, Z. Meng, H. Yan et al. Peptide amphiphiles with multifunctional fragments promoting cellular uptake and endosomal escape as efficient gene vectors. *J. Mater. Chem. B*, 3 (2015):1068-1078.
59. Z. Meng, Z. Kang, C. Sun, S.Yang, B. Zhao, et al. Enhanced gene transfection efficiency by use of peptide vectors containing laminin receptor-targeting sequence YIGSR. *Nanoscale*, 10 (2018): 1215-1227.
60. G. R. Kokil, R. N. Veedu, B. Tri Le, G. A. Ramm , H.S. Parekh. Self-assembling asymmetric peptide-dendrimer micelles - a platform for effective and versatile in vitro nucleic acid delivery. *Sci. Rep.*, 8(2018):1-16.
61. M. Mäe, Ülo Langel. Cell-penetrating peptides as vectors for peptide, protein and oligonucleotide delivery. *Curr. Opin. Pharmacol.*, 6 (2006): 509-514.
62. M. Rizzuti, M. Nizzardo, C. Zanetta, A. Ramirez, S. Corti. Therapeutic applications of the cell- penetrating HIV-1 Tat peptide. *Drug Discovery Today*, 20 (2015): 77-85.
63. J.P. Richard et al. Cell-penetrating peptides. A re-evaluation of the mechanism of cellular uptake. *J. Biol. Chem.*, 278 (2003):585-590.
64. C.Bechara, S. Sagan. Cell-penetrating peptides: 20 years later, where do we stand? *FEBS Lett.*, 587 (2013): 1693-1702.
65. T. Lehto, K. Kurrikoff, Ü.Langel. Cell-penetrating peptides for the delivery of nucleic acids. *Expert Opin. Drug Delivery,* 9 (2012): 823-836.
66. E. Koren, V.P. Torchilin. Cell-penetrating peptides: breaking through to the other side. Trends Mol. Med., 18(2012): 385-393.

67. F. Milletti. Cell-penetrating peptides: classes, origin, and current landscape. *Drug Discovery Today*, 17 (2012): 850-860.
68. I. Nakase et al. Cell-penetrating peptides (CPPs) as a vector for the delivery of siRNAs into cells. *Mol. Biosyst.*, 9 (2013): 855-861.
69. A.D Frankel, C.O. Pabo. Cellular uptake of the tat protein from human immunodeficiency virus. *Cell*, 55 (1988): 1189-1193.
70. A. F. Saleh 1, H. Aojula, Y. Arthanari, S. Offerman, M. Alkotaji, A. Pluen. Improved Tat-mediated plasmid DNA transfer by fusion to LK15 peptide. *J. Controlled Release*, 143 (2010): 233-242.
71. D. Derossi, A.H. Joliot, G. Chassaing, A. Prochiantz. The third helix of the antennapedia homeodomain translocates through biological membranes. *J. Biol. Chem.*, 269 (1994):10444-10450.
72. Joliot, A. et al. Antennapedia homeobox peptide regulates neural morphogenesis. *Proc. Natl. Acad. Sci. U. S. A.*, 88 (1991):1864-1868.
73. A. Muratovska, M. R. Eccles. Conjugate for efficient delivery of short interfering RNA (siRNA) into mammalian cells. *FEBS Letters*, 558 (2004): 63-68.
74. C. Foged, H.M. Nielsen. Cell-penetrating peptides for drug delivery across membrane barriers. *Expert Opin. Drug. Deliv.*, 5 (2008): 105-117.
75. D. Derossi et al. Cell internalization of the third helix of the Antennapedia homeodomain is receptor-independent. *J. Biol. Chem.*, 271 (1996): 18188-18193.
76. G. Tünnemann. Cargo-dependent mode of uptake and bioavailability of TAT-containing proteins and peptides in living cells. *FASEB J.*, 20 (2006): 1775-1784.
77. F. Madani et al. Mechanisms of cellular uptake of cell-penetrating peptides. *J. Biophys.* 2011: 1-10.
78. K. Ezzat et al. Scavenger receptor-mediated uptake of cell-penetrating peptide nanocomplexes with oligonucleotides. *FASEB J.*, 26 (2012): 1172-1180.
79. S. E. L. Andaloussi, T. Lehto, I. Maäger, K. Rosenthal-Aizman, I. I. Oprea, et al. Design of a peptide-based vector, PepFect6, for efficient delivery of siRNA in cell culture and systemically in vivo. *Nucleic Acids Res.*, 39 (2011): 3972-3987.
80. W. J. Yi, J. Yang, C. Li, H. Y. Wang, C..W. Liu, et al. Enhanced Nuclear Import and Transfection Efficiency of TAT Peptide-Based Gene Delivery Systems Modified by Additional Nuclear Localization Signals. *Bioconjugate Chem.*, 23 (2012): 125-134.

81. Y.W. Won, H. A. Kim, M. Lee, Y.H. Kim. Reducible Poly(oligo-d-arginine) for enhanced gene expression in mouse lung by intratracheal injection. Mol. Ther., 18 (2010): 734-742.
82. Y.W. Won, S. M. Yoon, K. M. Lee, Y.H. Kim. Poly(oligo-D-arginine) with internal disulfide linkages as a cytoplasm-sensitive carrier for siRNA delivery. Mol. Ther., 19 (2011): 372-380.
83. T. Lehto, R. Abes, N. Oskolkov, J. Suhorutšenko, D. Maria. Copolovici et al. Delivery of nucleic acids with a stearylated (RxR) 4 peptide using a non-covalent co-incubation strategy. J. Controlled Release, 141 (2010): 42-51.
84. M. Mäe, S. E. L. Andaloussi, P.Lundin, N. Oskolkov, H. J. Johansson, et al., A stearylated CPP for delivery of splice correcting oligonucleotides using a non-covalent co-incubation strategy. *J. Controlled Release*, 134 (2009): 221-227.
85. T. Lehto, O. E. Simonson, I. Mäger, K. Ezzat, H. Sork et al. A Peptide-based vector for efficient gene transfer in vitro and in vivo. *Mol. Ther.*, 19 (2011):1457-1467.
86. K. Ezzat1, S. E. L. Andaloussi, E. M. Zaghloul, T. Lehto, S. Lindberg et al. PepFect 14, A novel cell-penetrating peptide for oligonucleotide delivery in solution and as solid formulation. *Nucleic Acids Res.*, 39 (2011): 5284-5298.
87. S. Lindberg, A. Muñoz-Alarcona, H. Helmforsa, D. Mosqueiraa, D. Gyllborga, et al. PepFect15, a novel endosomolytic cell-penetrating peptide for oligonucleotide delivery via scavenger receptors. *Int. J. Pharm*., 441 (2013): 242-247.
88. K. L. Veiman, K. Künnapuu, T. Lehto, K. Kiisholts, K. Pärn et al. PEG shielded MMP sensitive CPPs for efficient and tumor specific gene delivery in vivo. *J. Controlled Release*, 209 (2015): 238-247.
89. K. Kurrikoff, K. L. Veiman, K. Künnapuu, E. M. Peets, T. Lehto et al. Effective in vivo gene delivery with reduced toxicity, achieved by charge and fatty acid -modified cell penetrating peptide. *Sci Rep,* 7(2017):17056.
90. A. Srimanee, M. Arvanitidou, K. Kim, M. Hällbrink, Ü. Langel. Cell-penetrating peptides for siRNA delivery to glioblastomas. *Peptides,* 104 (2018): 62-69.
91. P. Arukuusk, L. Pärnaste, N. Oskolkov, D. M. Copolovici, H. Margus et al. New generation of efficient peptide-based vectors, NickFects, for the delivery of nucleic acids. *Biochim. Biophys. Acta*, 1828 (2013): 1365-1373.
92. K. Freimann, P. Arukuusk, K. Kurrikoff, L. D. Ferreira Vasconcelos, K. L. Veiman et al. Optimization of in vivo DNA delivery with NickFect peptide vectors. *J. Controlled Release,* 241 (2016): 135-143.

93. L. Crombez, M. Catherine Morris, S. Dufort, G. Aldrian-Herrada, Q. Nguyen et al. Targeting cyclin B1 through peptide-based delivery of siRNA prevents tumour growth. *Nucleic Acids Res.,* 37(2009): 4559-4569.
94. L. Crombez, G. Aldrian-Herrada, K. Konate, Q. N Nguyen, G. K McMaster, et al. A new potent secondary amphipathic cell–penetrating peptide for siRNA delivery into mammalian cells. *Mol. Ther.,* 17 (2009): 95-103.
95. S. Deshayes , K. Konate , A. Rydström , L. Crombez ,C. Godefroy, et al. Self-assembling peptide-based nanoparticles for siRNA Delivery in primary cell lines. *Small,* 8(2012): 2184-2188.
96. A. Rydström, S. Deshayes, K. Konate, L. Crombez, Kärt Padari, et al. Direct Translocation as major cellular uptake for CADY self-assembling peptide-based nanoparticles. , *PLoS One*, 6 (2011): e25924-e25924.
97. H. Li, X. Zheng, V. Koren, Y. K.Vashist, T. Y. Tsui. Highly efficient delivery of siRNA to a heart transplant model by a novel cell penetrating peptide-dsRNA binding domain. *Int. J. Pharm.*, 469 (2014): 206-213.
98. K. Konate, M. Dussot, G. Aldrian, A. Vaissière, V. Viguier et al. Peptide-based nanoparticles to rapidly and efficiently “wrap ’n roll” siRNA into cells. *Bioconjugate Chem.,* 30 (2019): 592-603.
99. H. Gong, J. Zhang, X. Hu, et al. Hydrophobic control of the bioactivity and cytotoxicity of de novo-designed antimicrobial peptides. *ACS Appl. Mater. Interfaces,* 11 (2019): 34609-34620.
100. D. Ciumac, R.A. Campbell, L. A. Clifton, et al. Influence of acyl chain saturation on the membrane-binding activity of a short antimicrobial peptide. *ACS Omega*, 2 (2017): 7482-7492.
101. C. Chen, J. Hu, P. Zeng, et al. Molecular mechanisms of anticancer action and cell selectivity of short α-helical peptides. *Biomaterials*, 35 (2014): 1552-1561.
102. J. Hu, C. Chen, S. Zhang, et al. Designed antimicrobial and antitumor peptides with high selectivity. *Biomacromolecules,* 12 (2011): 3839-3843.
103. N. Wiradharma, U. Khoe, C.A.E. Hauser, et al. Synthetic cationic amphiphilic α-helical peptides as antimicrobial agents. *Biomaterials*, 32 (2011): 2204-2212.
104. M. Majerowicz, A.J. Waring, S. Wen, and F. Bringezu. Interaction of the antimicrobial peptide Dicynthaurin with membrane phospholipids at the air−liquid interface. *J. Phys. Chem. B*, 111 (2007): 3813-3821

105. Imranpasha and B. Kumar. Kinetics of interaction between antimicrobial peptide nisin and Langmuir monolayers of DPPC and DPPG molecules. *Phys. Rev. E*, 100 (2019): 032404-1-032404-7

106. Z.Y. Ong, S.J. Gao, and Y.Y. Yang. Short synthetic β-sheet forming peptide amphiphiles as broad spectrum antimicrobials with antibiofilm and endotoxin neutralizing capabilities. Adv. Funct. Mater., 23 (2013): 3682-3692.

107. C. Chen, C. Yang, Y. Chen, et al. Surface physical activity and hydrophobicity of designed helical peptide amphiphiles control their bioactivity and cell selectivity. *ACS Appl. Mater. Interfaces*, 8 (2016): 26501-26510.

108. D. Gaspar, A. S. Veiga, and M. A. Castanho. From antimicrobial to anticancer peptides. A review. *Front. Microbiol.*, 4 (2013): 1-16.

109. D. W. Hoskin, and A. Ramamoorthy. Studies on anticancer activities of antimicrobial peptides. *Biochim. Biophys. Acta, Biomembr.*, 1778 (2008): 357-375.

110. S. Riedl, D. Zweytick, and K. Lohner. Membrane-active host defense peptides-challenges and perspectives for the development of novel anticancer drugs. *Chem. Phys. Lipids,* 164 (2011): 766-781.

111. N. Papo, and Y. Shai. Host defense peptides as new weapons in cancer treatment. Cell. Mol. Life Sci., 62 (2005): 784-790.

112. C. Chen, Y. Chen, C. Yang, et al. High selective performance of designed antibacterial and anticancer peptide amphiphiles. *ACS Appl. Mater. Interfaces, 7* (2015): 17346-17355.

113. H. Sato and J. B. Feix. Peptide-membrane interactions and mechanisms of membrane destruction by amphipathic alpha-helical antimicrobial peptides. *Biochim Biophys Acta,* 1758 (2006) :1245-1256.

114. S. Rotem, and A. Mor. Antimicrobial peptide mimics for improved therapeutic properties. *Biochim. Biophys. Acta, Biomembr.,* 1788 (2009): 1582-1592.

115. C.D. Fjell, J. A. Hiss, R. E. Hancock, and G. Schneider. Designing antimicrobial peptides: form follows function. *Nat. Rev. Drug Discovery,* 11 (2011): 37-51.

116. Y. Shai. From innate immunity to de novo designed antimicrobial peptides. *Curr. Pharm. Des.,* 8 (2002): 715-725.

117. A. Braunstein, N. Papo, and Y. Shai. In vitro activity and potency of an intravenously injected antimicrobial peptide and its DL amino acid analog in mice infected with bacteria. *Antimicrob. Agents Chemother.*, 48 (2004): 3127-3129.

118. Z. Y. Ong, N. Wiradharma, and Y. Y. Yang. Strategies employed in the design and optimization of synthetic antimicrobial peptide amphiphiles with enhanced therapeutic potentials. *Adv. Drug Delivery Rev.,* 78 (2014): 28-45.
119. Z.Y. Ong, J. Cheng, Y. Huang, et al. Effect of stereochemistry, chain length and sequence pattern on antimicrobial properties of short synthetic β-sheet forming peptide amphiphiles. *Biomaterials,* 35 (2014): 1315-1325.
120. D. Minor and P. Kim. Measurement of the β-sheet-forming propensities of amino acids. Nature 367 (1994): 660-663.
121. W.C. Wimley. Toward genomic identification of β-barrel membrane proteins: Composition and architecture of known structures. *Protein Sci.,* 11 (2002): 301-312.
122. C. K. Smith, J. M. Withka and L. Regan. A thermodynamic scale for the beta-sheet forming tendencies of the amino acids. *Biochemistry,* 33(1994): 5510-5517.
123. K. H. Mayo, E. Ilyina and H. Park. A recipe for designing water-soluble, beta-sheet-forming peptides. *Protein Sci.,* 5(1996):1301-15.

Chapter 2: Materials and methods

2.1 Peptide synthesis

Three different series of short cationic amphiphilic peptides were designed and synthesized: a series of α-helical peptides (with the sequences CIIKKIIKKIIKK-NH2, CLLKKLLKKLLKK-NH2, CIIRRIIRRIIRR-NH2, CLLRRLLRRLLRR-NH2, CIIKKIIKKIIKKII-NH2, Lc-propargylglycine-IIKKIIKKIIKKI-NH2), a series of β-sheet forming peptides (with the sequences IKIKIKIKIKIK-NH2, LKLKLKLKLKLK-NH2, LRLRLRLRLRLR-NH2, IKIRIKIRIKIR-NH2, IRIKIRIKIRIK-NH2, LKLRLKLRLKLR-NH2, LRLKLRLKLRLK-NH2) and a series of surfactant-like peptides (with the sequences IAIAIAIAK-NH2, IGIGIGIGK-NH2, AGAGAGAGK-NH2). The α-helical and β-sheet forming peptides were synthesized by GL Biochem (Shanghai) Ltd. upon order and were supplied at 98-99% purity. The surfactant-like peptides were synthesized from L-amino acids by Fmoc solid phase synthesis using a CEM Liberty microwave peptide synthesizer and amidated at C-terminal using a Rink-amide MBHA resin (0.83 mM/g) coupled with Fmoc-Lys (Boc)-OH, then deprotected and coupled with Fmoc-Ala-OH. The N-terminal amino acid was capped using acetic anhydride before cleavage from the resin. The peptides were purified by centrifugation at 10000 rpm for 20 minutes at 4 °C, and precipitation of the supernatant with cold ether. The purification step was repeated 8 times to increase the purity of the peptides. The final product was dissolved in Milli-Q water and lyophilized for 2 days. Finally, the purity of peptides was measured by reverse-phase high performance liquid chromatography (RP-HPLC) and MALDI-TOF mass spectrometry.

2.2 Preparation of peptide solutions

The peptide solutions were prepared by dissolving the peptide powder in deionized Milli-Q water at room temperature and their pH was adjusted to 6-6.5 using sodium hydroxide (0.1M) and hydrochloric acid (0.1M) solutions in order to get as close as possible to the physiological pH while maintaining the pH under the isoelectric point for arginine and lysine to allow for protonation of these amino acid residues in the peptides. The peptide solutions were stored at 4-8 °C and warmed up to the room temperature prior to use in experiments.

2.3 Liquid chromatography-Mass spectrometry (LC-MS)

LC-MS was used to verify the peptide sequence and molecular weight. A 55-minute data dependent acquisition (DDA) method was set up on the QExactive HF (Thermo Fisher™). The full MS scan from m/z= 375-1500 was acquired in the Orbitrap at a resolution of 120,000 in profile mode. Subsequent fragmentation was Top 2 in the HCD cell, with detection of ions in the Orbitrap using centroid mode, with a resolution of 30,000. The following MS method parameters were used for MS1: Automatic Gain Control (AGC) target 3e6 with a maximum injection time (IT) of 60 ms and MS2: AGC target 1e5, IT of 60 ms and isolation window 2 Da. The intensity threshold was 2e3, normalized collision energy 27, charge exclusion was set to unassigned, 1, exclude isotopes was on, apex trigger deactivated. The peptide match was set to preferred with dynamic exclusion of 20 seconds. The LC mobile phase consisted of two buffers: Buffer A consisting of 0.1% v/v Formic acid in water and Buffer B consisting of 80% v/v Acetonitrile and 20% v/v Formic acid in water (0.1%). The runs started with 97% of buffer A and 3% of buffer B. The proportion of buffer B was increased to 50% B at mins, 90% at 32 mins and finally decreased to 3% at 37 mins.

2.4 Reverse phase high performance liquid chromatography (RP-HPLC)

The purity of the peptide samples was checked by reverse phase high performance liquid chromatography (RP-HPLC) using Waters 2695 HPLC system, with Waters 2487 UV/Visible detector set at the wavelength of 205 nm, and Xbridge C18 column (4.6 x 250mm). All measurements were carried out for 25 min with a mobile phase consisting of Acetonitrile and Trifluoroacetic acid (TFA) in water (0.1% V/V), with a gradient of Acetonitrile from 5 to 95% over 20 mins at a flow rate of 1 ml/min.

2.5 Circular dichroism (CD) spectroscopy

The secondary structure of the peptide was determined by CD spectroscopy using a Jasco J-810 spectropolarimeter and a quartz cell of 1 cm path length and the peptide concentration was fixed at 10 µM. The samples were scanned at the wavelength of 190-240 nm and a scanning speed of 100 nm/min. The CD measurements were performed on peptides dissolved in DI water, Phosphate buffer (PB) solution (pH= 7.4), SDS micelles (SDS concentration of 25 mM), and small unilamellar vesicles (SUV)s made of two different types of phospholipids, DPPC and DPPG. Each sample was scanned three times and the data were expressed as the average of the three measurements. The mean residual molar ellipticity was calculated using the following equation:

Equation 2.1. $$\theta_M = \frac{\theta obs}{10} \cdot \frac{M_{RW}}{c.l}$$

Where Θ_M is residue molar ellipticity (deg.cm^2.dmol^{-1}), Θ_{obs} is the observed ellipticity at a given wavelength (mdeg), M_{RW} is residue molecular weight obtained by dividing the molecular weight of the peptide by the number of amino acid residues, c is the peptide concentration (mg/ml) and l is the path length of the cell (cm) [1-3].

2.6 Preparation of the phospholipid SUVs and SLS micelles

The DPPC and DPPG SUVs were prepared by thin film hydration method. The lipids were dissolved in chloroform at a concentration of 2 mg/ml, then the solvent was evaporated under vacuum using a rotary evaporator (Heidolph Instruments GmbH & CO). The resulting thin lipid film was rehydrated with Phosphate buffer (pH=7.4) and then brough to the desired size by extrusion using Avanti mini-Extruder (Avanti Polar Lipids, USA) containing a polycarbonate membrane with a pore size of 200 nm. The size and zeta potential of the SUVs was measured by Dynamic light scattering (DLS) using ZetaPALS zeta potential analyzer, Brookhaven instruments corporation, and reported as the average of 6 scans.

2.7 Surface pressure measurement

The surface pressure measurements were preformed using a Langmuir trough (NIMA technology Ltd, Coventry, UK), with a 3 ml built-in Teflon trough and a Wilhelmy plate attached to the pressure sensor. The trough was filled with 3 ml of Phosphate buffer (pH=7.4), the peptide solution was injected underneath the buffer surface using a Hamilton microsyringe and the changes to the surface pressure at the air-water interface was recorded as a function of time for 2 h [4]. The changes to surface pressure in lipid monolayers was studied using two different types of phospholipid monolayers, DPPC and DPPG. The lipids were dissolved in chloroform (0.5 mg/ml) and spread at the air-buffer interface using a Hamilton microsyringe. After allowing 20 min for the solvent to evaporate and the lipid monolayer to equilibrate, the peptide solution was injected underneath the monolayer into the subphase with a final concentration of 20 µM and the changes to the surface pressure was monitored as a function of time for 2 h. The initial pressure of the lipid monolayer was set to 28 mN/m corresponding to the average cell membrane resting pressure [5-7]. All the measurements were performed in triplicate and the values were reported as the average of the three runs.

2.8 Peptide-nucleic acid complexation

The peptide-nucleic acid complexation was assessed by measuring the changes to the zeta potential of the Antisense oligonucleotide or siRNA following incubation with peptide solution. The zeta potential was measured by ZetaPALS zeta potential analyzer (Brookhaven instruments corporation) which calculates the zeta potential based on the electrophoretic mobility of the particles using the Smoluchowski method [8].

2.9 Culture of human cells

Four different human cell lines were used to carry out the experiments: HCT 116 colorectal carcinoma cells, HeLa cervical cancer cells, MDA-MB-231 metastatic breast cancer cells, and human dermal fibroblast cells (HDFs). HCT 116 cells were derived from colorectal carcinoma in an adult male and have a mutation in codon 13 of the ras proto-oncogene [9]. HeLa cells were derived from cervical adenocarcinoma in an adult female and contain human papilloma virus [10]. MDA-MB-231 cells were derived from the metastatic site in an adult female with breast cancer [11]. Human dermal primary fibroblasts are derived from human skin.

All cells were cultured in Dulbecco's Modified Eagle Medium (DMEM) with high glucose and L-glutamine, without Sodium Pyruvate and HEPES (GIBCO®, Thermo Fisher Technologies, Cat. No. 11965092) in 75 cm^2 flasks (cell culture treated, blue filtered cap, Nunc™, Cat. No. 156499) and kept in incubator (MCO-20AIC, Sanyo) at 37 °C under 5% CO2 and 95% humidity. The medium was enriched with 10% foetal bovine serum (FBS, Sigma-Aldrich®, Cat. No. F9665) and 1% antibiotic (100 U/ml penicillin and 100 µg/ml streptomycin, GIBCO®, Thermo Fisher Scientific, Cat. No. 15140122). The cell culture and all the experiments were carried out under laminar flow hood (Esco Airstream® Class II Biological Safety Cabinet) to ensure sterile conditions. The cells were regularly sub-cultured at 70-80% confluence.

In order to passage the cells, the medium was removed from the flasks, and the cells were washed with 5-10 ml of 37 °C phosphate buffered saline (PBS, pH 7.2, without CaCl2 and MgCl2 ions, GIBCO®, Thermo Fisher Scientific, Cat. No. 10010023) to remove any residual medium. Subsequently, the cells were immersed in 1-2 ml of Trypsin-EDTA (0.05% GIBCO®, Thermo Fisher Scientific, Cat. No. 25300104) and incubated for 3-5 min at 37 °C to allow for detachment of the cells from the surface of the flask. The cells were then resuspended in 6-12 ml of DMEM (depending on the cell line and the confluence required in the new flasks) and 1-2 ml of this final cell suspension was transferred to a new flask containing 10 ml of pre-warmed 37 °C DMEM.

The initial batch of cells were prepared from the cryopreserved frozen cells which were stored under liquid nitrogen. The cryovial containing the cells was warmed for 1-2 min in the 37 °C water bath, then carried under the laminar flow hood (after sterilizing the outside of the vial with 70% ethanol) and its content was transferred to a 15 ml falcon tube (BD Falcon™, Cat. No. 352096) containing 9 ml of 37 °C DMEM and centrifuged at 200 × g for 5 minutes to allow for precipitation of the cells. Subsequently, the supernatant was gently removed, avoiding aspiration of the cells, the cell pellet was resuspended in 2 ml of DMEM and transferred to a

T-25 flask (cell culture treated, blue 49 vent/close cap, Nunc™, Cat. No. 156499) and kept in the incubator. After the 2 days the cells were trypsinized and transferred to a T-75 flask.

2.10 Preparation of multiwell plates for high throughput experiments

For the transfection and cytotoxicity experiments, the cells were cultured in 96 well plates (Grenier Bio One, Cat No. 655088) or 384 well plates (Perkin Elmer, Cat No. 6007460) which allow for high throughput experiments. The cells were seeded at a density of 4000-6000 cells/well in 96 well plates and 800-1000 cells/well in 384 well plates depending on the type of cell and type of experiment. In order to prepare the plates, the cells were trypsinized following the same protocol used for passaging the cells, and then resuspended in excess amount of medium. To calculate the required dilution for the cell suspension to give the required seeding density in the plates, the concentration of the cell suspension was measured using an automated cell counter device Countess® II Automated Cell Counter, Life Technologies, Thermo Fisher Scientific). 10 µL of the cell suspension was mixed with 10 µL of trypan blue dye (0.4%, Invitrogen™, Thermo Fisher Scientific) and spread on a Countess® Cell Counting Chamber Slide (Invitrogen™, Thermo Fisher Scientific, Cat. No. C10313). The slide was then inserted into the cell counter device which measured the number of cells per mL of the suspension. The cell suspension was then diluted to the required concentration using excess amount of medium and then seeded into the plates using an automated liquid dispenser device (Multidrop Combi, Thermo Fisher Scientific) to ensure the homogenous dispersion of the cells in different wells throughout the plate and minimize the pipetting errors associated with the use of multichannel pipettes. The plates were incubated at 37 °C overnight to allow for attachment of the cells and used for experiments the next day.

2.11 Fixing and staining of the cells

2.11.1 Fixing of the cells

In order to prepare the cells for microscopy, the cells were fixed with paraformaldehyde and then stained using different fluorescent probes. The medium was removed, the cells were washed twice with PBS to remove any residual media and then immersed in 3.7% formaldehyde (prepared from the 37% Formaldehyde, CAS No. 50-00-0, Sigma-Aldrich®, by dilution with PBS) for 15-20 min at room temperature. Subsequently formaldehyde was removed, and the cells were washed twice with PBS and then subjected to staining.

2.11.2 Staining with Hoechst 33342

Hoechst 33342 (Thermo Fisher Scientific, Cat. No. 62249) was used for staining the nuclei at a concentration of 2 µg/ml. The cells were immersed in 100 µL/well of Hoechst 33342 solution for 96 well plates and 30 µL/well for 384 well plates and incubated at room temperature for 20 min, in the dark. Subsequently, Hoechst 33342 solution was removed, the cells were washed twice with PBS and then either subjected to further staining with other fluorescent stains or re-immersed in PBS and imaged with microscope. Hoechst 33342 is a cell-permeable blue, fluorescent stain which is used for fixed- and live-cell staining of DNA and nuclei [12]. It binds to the minor groove of double-stranded DNA, with a preference for adenine-thymine (A-T) rich regions [12-13]. Hoechst is excited by ultraviolet light at 350 nm and emits blue fluorescence at 460 to 490 nm [12-13].

2.11.3 Staining with Phalloidin

In order to stain the cytoplasm, Alexa fluor™ 488 Phalloidin (Thermo Fisher Scientific, Cat. No. A12379) or Alexa Fluor™ 568 phalloidin (Thermo Fisher Scientific, Cat. No. A12380) were used as follows: briefly, the cells which were previously fixed with formaldehyde were permeabilized using 0.01% triton™ X-100 (Sigma-Aldrich, CAS No. 0009002931) for 2-3 min, washed twice with PBS and immersed in 100 µL of Alexa Fluor® 568 phalloidin or Alexa fluor® 488 Phalloidin at a concentration of 150-200 nMol/L for 20 minutes at room temperature, in the dark. Subsequently, the phalloidin solution was removed, the cells were washed twice with PBS and then re-immersed in PBS and imaged with the microscope. Alexa Fluor™ 568 phalloidin and Alexa fluor® 488 Phalloidin consist of a high-affinity filamentous actin (F-actin) probe (phalloidin) conjugated to either Alexa Fluor™ 568 or Alexa fluor® 488 fluorescent dye. The conjugate selectively stains F-actin filaments and emits strong red or green fluorescence at 600 nm and 518 nm respectively [14-15].

2.12 Mitochondrial damage test

The ability of the cationic amphiphilic peptides to induce damage to mitochondria was assessed by studying the changes to the morphology and distribution pattern of the mitochondria within the cells using the mitochondrial probe MitoTracker® Red CMXRos (Thermo Fisher Scientific, Cat. No. M7512) and studying the mitochondrial membrane depolarization using JC-1 mitochondrial probe (Invitrogen™) following manufacturer’s protocols. Following treatment with the cationic amphiphilic peptides, MitoTracker® Red CMXRos at the concentration of 200-250 nMol/L in FBS-free DMEM was added to the cells and incubated at 37 °C for 30 min. after the incubation time, the cells were washed twice with PBS, fixed with 3.7% formaldehyde, re-immersed in 100 µL of PBS and imaged with high content microscope. For JC-1 staining the cells were cultured in 96 well plates at a seeding density of 4000 cells/well and allowed to grow overnight. The peptide solutions were added to the cells with a final concentration of 40 µM and incubated for 72 h. Subsequently, the cells were stained with JC-1 (Invitrogen™) following the manufacturer's protocol as follows; the cells were washed with PBS once, then prewarmed (37 ˚C) fresh media containing JC-1 (10 µg/ml) was added to the cells (100 µl/ well) and incubated at 37 ˚C for 15 min. Then the media containing the stain was removed, the cells were washed with PBS once and the wells were filled with PBS (100 µl/well) and imaged with the high content microscope using the CY3 and FITC filters.

2.13 High content microscopy

The high content fluorescent automated wide field microscope (ImageXpress® Micro System) was used to capture images of the cells following AON/siRNA transfection and following incubation with peptide solutions. The images were then processed or subjected to analysis using MetaXpress® software 5.3.01 (Molecular Devices).

2.14 Confocal laser scanning microscopy (CLSM)

The subcellular localization of the peptide-AON or peptide-siRNA complexes (in the case of surfactant-like peptides) was evaluated using confocal laser scanning microscope (CLSM, Nikon Instruments Europe B.V.) and the data were analysed with NIS Element software. The cells were cultured in a glass bottom dish (35 mm, high, Ibidi, Cat. No. 81156), transfected with the peptide-AON or peptide-siRNA complexes for 24 h, the fixed with 3.7% formaldehyde solution in PBS, and stained with Hoechst 333432 and Alexa fluor™ 488 Phalloidin /Alexa Fluor™ 568 phalloidin following the protocols described in Section 11.2-11.3.

2.15 MTT assay

The MTT cell viability assay was used to evaluate the cytotoxicity of the cationic amphiphilic peptides in HCT 116, HeLa, MDA-MB-231 and HDF cells. MTT assay is based on the ability of viable cells to convert the water soluble MTT dye (3-(4,5-thiazol-2-yl)-2,5-diphenyltetrazolium bromide) into the water insoluble formazan dye by NAD(P)H-dependent cellular oxidoreductase enzymes. The quantity of formazan is directly proportional to the number of viable cells, therefore, measuring the photometric absorbance of the formazan dissolved in DMSO gives a measure of the number of viable cells [16-17].

The MTT solution (5mg/ml) was prepared by dissolving required amount of MTT in DI water and then filtered through syringe filters with a pore size of 0.22 µm prior to being used for experiments. The MTT solution was kept at -20 °C and protected from light. Sodium chromate (2M/L) was used as positive control and deionized water was used as negative control in all cases. To measure the cytotoxicity of the cationic amphiphilic peptides, the cells were cultured in 96 well plates (clear, flat bottom, Corning, Cat. No. 3596), treated with different concentrations of the cationic amphiphilic peptides (1-20 µMol/L in the case of α-helical and β-sheet forming peptides and 1-100 µMol/L in the case of surfactant-like peptides) and incubated at 37 °C for 24-120 h depending on the type of peptides. Subsequently, MTT solution (5mg/ml) was added to the cells (20 µL/well) and incubated at 37 °C for 4 h after which the culture medium was removed and replaced with DMSO (100 µL/well). The plates were shaken on the shaker at low speed at room temperature for 15 min to allow for complete dissolution of the formazan dye in DMSO and then the absorbance of formazan was measured at one of its absorption maxima (590 nm) using microplate reader (Varioskan Flash™, Thermo Fisher Scientific). 2 mMol/L Sodium chromate tetrahydrate solution (CAS number: 10034-82-91, Sigma-Aldrich®) which is known to be cytotoxic was used as positive control and untreated cells were considered as negative control. The relative cell viability was calculated as the ratio of the formazan absorbance in the treatment wells to the untreated controls. Each experiment was repeated as 3 technical replicates and 2-3 biological replicates and the values of cell viability were reported as the average of the 6-9 replicates.

2.16 Cell proliferation test

The cell proliferation test was performed on HCT 116 cells following treatment with different concentrations (1-20 µMol/L) of the cationic amphiphilic peptides in order to measure the antiproliferative activity of the peptides. The cells were cultured in 96 well plates as described in Section 10 and incubated with the peptides for 72 h. Then the cells were fixed and stained with Hoechst 33342 as described in Section 11.2. The plates were imaged with high content microscope and the total number of cells in each well was counted using the MetaXpress® software by applying appropriate algorithms. The number of cells in the wells treated with different concentrations of the cationic amphiphilic peptides were compared to the untreated control wells. All experiments were performed in replicates and the data were reported as the average of 6 replicates (2 biological replicates and 3 technical replicates).

2.17 Transfection with antisense oligodeoxynucelotides (AONs)

The ability of the cationic amphiphilic peptides to deliver AONs to the cells was measured using FAM-labelled c-Myc AON. 6-FAM (6-Carboxyfluorescein or Spiro(isobenzofuran-1(3H),9'-(9H) xanthene)-6-carboxylic acid, 3',6'-dihydroxy-3-oxo) is a green, fluorescent dye with excitation ad emission maxima of 495 nm and 517 nm respectively [18]. The c-Myc solution was stored at -20 °C and protected from light. The stock solution was diluted to the required concentrations with antibiotic-free DMEM and used immediately. The peptide solutions were mixed with the AON solution at different N/P ratios (1-5), and left to form complex at room temperature for 30-40 min. the N/P ratio is the molar ratio between the positively charged nitrogen atoms (from the amine groups) in the peptide or polymer to the negatively charged phosphate groups in the DNA/RNA which is preferred to the molar ratio in the transfection studies. The amount of AON was kept constant at 0.1 µg/well and the amount of peptide was varied based on the N/P ratio. The peptide-AON complexes were then added to the cells (20 µl of the solution added to 80 µL of the cells in culture medium in 96 well plates or 100 µl of the transfection complex to 900 µL of the cells in culture medium in 35 mm petri dishes) and incubated at 37 °C for 24 h. The cells were then fixed, stained with Hoechst and imaged with the high content or CLSM microscope. The lipid-based commercial transfection reagent Oligofectamine ™ (Invitrogen™, Life Technologies, Cat. No. 12252011) was used as positive control in all of the AON transfection experiments.

2.18 Transfection with siRNA

The ability of the cationic amphiphilic peptides to deliver small interfering RNA (siRNA) to the cells was measured using the fluorescently labelled siRNA, siGLO™ red (Dharmacon, Cat. No. D-001630-02-05) and the functional siRNAs, Epithelial Cell Transforming 2 (ECT2) and Ubiquitin B (UBB). The scrambled non-targeting siRNA was used as control. The functional and non-targeting siRNAs were from the On Target-Plus Dharmacon siRNA collection. The siRNA stock solutions were diluted with serum-free and antibiotic-free DMEM to give a final concentration of 25-30 nMol/L per well. The cationic amphiphilic peptide solutions were mixed with the siGLO™ solution at N/P ratio of 1-5, with the final concentration of siGLO™ between 30-50 nMol/L, left to complex at room temperature for 30-40 min and then added to the cells cultured in antibiotic-free DMEM (20 µL per well in 96 well plates) and incubated for 24-72 h. The ECT2 and UBB siRNA solutions were mixed with the cationic amphiphilic peptide solutions at N/P ratio of 5 and allowed to form complexes for 30-40 min at room temperature. The transfection complexes were then added to the cells cultured in antibiotic-free DMEM (10 µL per well in 384 well plates for ECT2 and UBB), left on the bench at room temperature for 30-40 min and then incubated at 37 °C for 72 h to allow for the gene silencing to take place. 24 h after transfection, the cells were supplemented with equal volume of DMEM containing 2% antibiotic. At the end of the experiment the cells were fixed, stained with Hoechst 33432 and imaged with high content microscope. The lipid based commercial transfection reagent DharmaFECT™ 1 (DF1) (Dharmacon, Cat. No.T-2001-02) was used as the positive control in all cases. The transfection/gene silencing experiments with ECT2 siRNA and UBB siRNA was performed in duplicates (two biological and two technical replicates) and the data were reported as the average of the 4 replicates.

2.19 Analysis of the data

The statistical analysis of the quantitative data was performed using Microsoft® Excel 2016. All data were expressed as Mean ± standard Error (SE) in graphs and compared using Student's t-test at 95% confidence interval ($\alpha = 0.05$) and values of $p < 0.05$ were considered as denoting a statistically significant difference in all cases. The microscopic images were analyzed using MetaXpress® software 5.3.01 (Molecular Devices) and further processed with Fiji Image J to adjust the brightness and contrast and add the scale bars.

2.20 References

1. N. Wiradharma, U. Khoe, C.A.E. Hauser, et al. Synthetic cationic amphiphilic α-helical peptides as antimicrobial agents. *Biomaterials*, 32 (2011): 2204-2212.
2. Z.Y. Ong, S.J. Gao, and Y.Y. Yang. Short synthetic β-sheet forming peptide amphiphiles as broad spectrum antimicrobials with antibiofilm and endotoxin neutralizing capabilities. Adv. Funct. Mater., 23 (2013): 3682-3692.
3. Z.Y. Ong, J. Cheng, Y. Huang, et al. Effect of stereochemistry, chain length and sequence pattern on antimicrobial properties of short synthetic β-sheet forming peptide amphiphiles. *Biomaterials*, 35 (2014): 1315-1325.
4. H. Gong, J. Zhang, X. Hu, et al. Hydrophobic control of the bioactivity and cytotoxicity of de novo-designed antimicrobial peptides. *ACS Appl. Mater. Interfaces*, 11 (2019): 34609-34620.
5. C. Chen, Y. Chen, C. Yang, et al. High selective performance of designed antibacterial and anticancer peptide amphiphiles. *ACS Appl. Mater. Interfaces*, *7* (2015): 17346-17355.
6. D. Ciumac, R.A. Campbell, L. A. Clifton, et al. Influence of acyl chain saturation on the membrane-binding activity of a short antimicrobial peptide. *ACS Omega*, 2 (2017): 7482-7492.
7. C. Chen, J. Hu, P. Zeng, et al. Molecular mechanisms of anticancer action and cell selectivity of short α-helical peptides. *Biomaterials*, 35 (2014): 1552-1561.
8. V. K. Paruchuri, A. V. Nguyen, and J. D. Miller. Zeta-potentials of self-assembled surface micelles of ionic surfactants adsorbed at hydrophobic graphite surfaces, *Colloids Surf. A, Physicochem. Eng. Asp.*, 250 (2004): 519-526.

9. http://www.lgcstandards-atcc.org/products/all/CCL-247.aspx?geo_country=gb, accessed on 28/08/2019.
10. http://www.lgcstandards-atcc.org/products/all/HTB-26.aspx?geo_country=gb, accessed on 28/08/2019.
11. http://www.lgcstandards-atcc.org/products/all/CCL-2.aspx?geo_country=gb, accessed on 28/08/2019.
12. https://www.thermofisher.com/order/catalog/product/62249, accessed 11/08/2016.
13. J. Portugal and M. J. Waring. Assignment of DNA binding sites for 4′,6-diamidine-2-phenylindole and bisbenzimide (Hoechst 33258). A comparative footprinting study. *BBA- Gene Structure and Expression*, 949 (1988): 158-168.
14. https://www.thermofisher.com/order/catalog/product/A12380?ICID=search-product, accessed on 11/08/2016.
15. https://www.thermofisher.com/order/catalog/product/A12379, accessed on 11/08/2016.
16. T. Mosmann. Rapid colorimetric assay for cellular growth and survival: Application to proliferation and cytotoxicity assays. J. *Immunol. Methods*, 65 (1983): 55-63.
17. M. V. Berridge, P. M. Herst, and A. S. Tan. Tetrazolium dyes as tools in cell biology: New insights into their cellular reduction. *Biotechnol. Annu. Rev.*, 11(2005): 127-152.
18. https://www.thermofisher.com/order/catalog/product/C1360?uk&en#/C1360?uk&en

Chapter 3: biological activity of α-helical cationic amphiphilic peptides

3.1 Background and aims

This chapter includes the results from the evaluation of a series of short cationic amphiphilic peptides with α-helical secondary structure for their ability to deliver nucleic acids to the cancer cells as well as their cytotoxicity against normal and cancer cells. The peptides were designed based on the structural features of the α-helical cationic antimicrobial peptides assuming that the same structural features might enable the peptide to interact with the cancer cells as both cancer cell membranes and bacterial cell membranes are more negatively charged than normal mammalian cell membranes [1-6]. It was also hypothesized that the positively charged peptides would be able to form complexes with the nucleic acids via electrostatic interactions with the negatively charged phosphate groups on the backbone of the nucleic acids and to compress them into nano-sized structures. Due to the amphiphilic nature of the peptides, it was supposed that the peptides would be able to penetrate into the cell membrane via interaction with the membrane phospholipids and to transfer their associated nucleic acid cargo across the cell membrane [7-17].

The aims of this chapter are:

- Designing a new series of cationic amphiphilic peptides with α-helical secondary structure based on the structural features of the antimicrobial and anticancer peptides and evaluating their potential anticancer activity as well as their ability to deliver genes to the cancer cells.
- Evaluating the selectivity of the designed cationic amphiphilic peptides for the cancer cells compared to the normal cells in order to develop tools for selective anticancer therapy.
- Studying the structure-activity relationship of the designed cationic amphiphilic peptides in order to optimize the biological activity of the peptides through rational design.

3.2 Experimental

3.2.1 Cytotoxicity tests

The anticancer activity of the cationic amphiphilic peptides was measured in terms of their ability to interfere with cell viability, i.e., the metabolic/enzymatic activity of the cells, and also their ability to interfere with cell proliferation and was compared to the normal non-cancerous cells in order to determine any selective cytotoxicity against cancer cells. The cytotoxicity of the peptides was assessed in three different cancer cell lines, HCT 116, MDA 231-MB and HeLa as well as human dermal fibroblasts (HDFs) as a model for non-cancerous cells.

The ability of the cationic amphiphilic peptides to interfere with the metabolic/enzymatic activity of the cells was assessed using the standard MTT test. The cells were treated with peptide solutions with concentrations ranging from 1 µM to 20 µM, incubated for 24-72 h at 37 °C and then subjected to MTT assay as described in chapter 2The morphology and distribution of the mitochondria was studied using the mitochondrial probe Mitotracker™ following incubation of the cells with cationic amphiphilic peptides at concentration of 20 µM as described in chapter 2 after 72 h the mitochondria were stained using mitochondrial probe MitoTracker® Red following the protocol described in chapter 2 and imaged with high content microscope. The effect of the cationic amphiphilic peptides on the cell proliferation was measured by counting the total number of cells following incubation with different concentrations of the peptide solutions (1-20 µM). The data were normalized against untreated controls and reported as mean ± SE.

3.2.2 Transfection tests

The ability of the cationic amphiphilic peptides to form complexes with the nucleic acids and to deliver them to the cells was assessed using cMyc- antisense oligonucleotide (cMyc-AON) and small interfering RNA (siRNA) against ECT2 and UBB genes both in cancer cell lines (HCT 116 and HeLa) and in human dermal fibroblasts (HDFs) following the transfection protocols described in chapter 2 Section 11. The scrambled non-targeting siRNA (NT siRNA) was used as a control to assess the net-effect of the ECT2 and UBB gene silencing on the cell proliferation without including the cell death caused by siRNA induced toxicity.

3.3 Results & discussion

3.3.1 Structure of the peptides

The sequences of the designed α-helical cationic amphiphilic oligopeptides are provided in Table 3.1 using the standard one letter codes for amino acids. The peptides consist of 13-15 amino acids, are amidated at the C-terminal and unmodified at the N-terminal except II-14 which is modified with an alkyne group in the N-terminal.

Table 3.1. The sequences of the designed α-helical cationic amphiphilic peptides.

Peptide name	Peptide sequence
IIKK	CIIKKIIKKIIKK-NH2
LLKK	CLLKKLLKKLLKK-NH2
IIRR	CIIRRIIRRIIRR-NH2
LLRR	CLLRRLLRRLLRR-NH2
CI-15	CIIKKIIKKIIKKII-NH2
II-14	LC-Propragyl-GIIKKIIKKIIKKII-NH2

3.3.2 Cell viability/metabolic activity

The ability of the α-helical cationic amphiphilic peptides to interfere with the metabolic activity of the cells as determined by MTT assay is presented in Figures 3.1-3.4. Reduction of MTT by NADH-dependent and NADPH-dependent oxidoreductase enzymes is an indicative of the cellular metabolic activity [18-19]. The values of half maximal inhibitory concentration (IC_{50}) of the peptides in different cell lines, as derived from the concentration-response curves (Figures S1-S24 in the supplemental data), are presented in Table 3.2. The values of IC_{50} for each replicate were calculated using the regression equation for each plot and reported as the average ± SD of the 6 replicates.

Table 3.2. Values of half maximal inhibitory concentration (IC_{50}) of the cationic amphiphilic peptides in different cell lines as determined by MTT assay.

Peptide	IC_{50} (µM)			
	HCT	HeLa	MDA-MB-231	HDF
IIKK	28.8 ± 6.3	46.5 ± 4.6	>100	>100
LLKK	22.6 ± 1.7	82.6 ± 8.7	>100	>100
IIRR	>100	>100	51.5 ± 10.1	21.9 ± 2.5
LLRR	15.6 ± 1	26.7 ± 1.3	38 ± 9.5	23.9 ± 4.8
CI-15	7.7 ± 0.2	2.7 ± 0.5	>100	83 ± 4.8
II-14	13.6 ± 0.2	16.6 ± 0.8	>100	80.8 ± 8.4

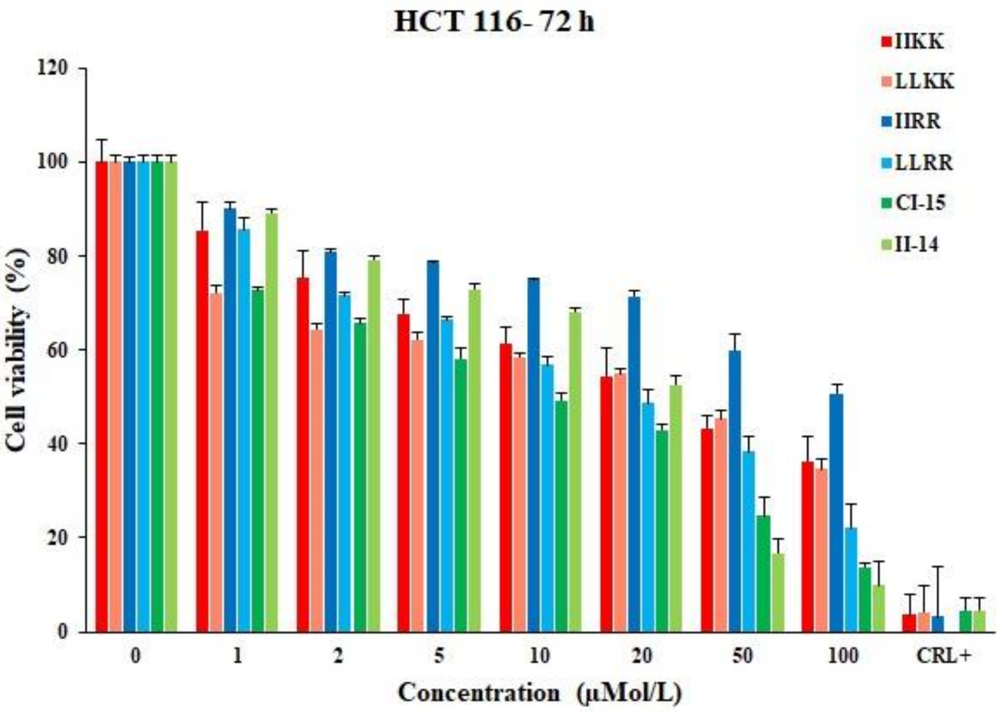

Figure 3.1. Viability of HCT 116 cells after incubation with different concentrations of the cationic amphiphilic peptides for 72 h as determined by MTT test. All data were normalized against untreated controls and reported as Mean ± SE (n = 6). Sodium chromate (2 mMol/L) was used as positive control (CRL+).

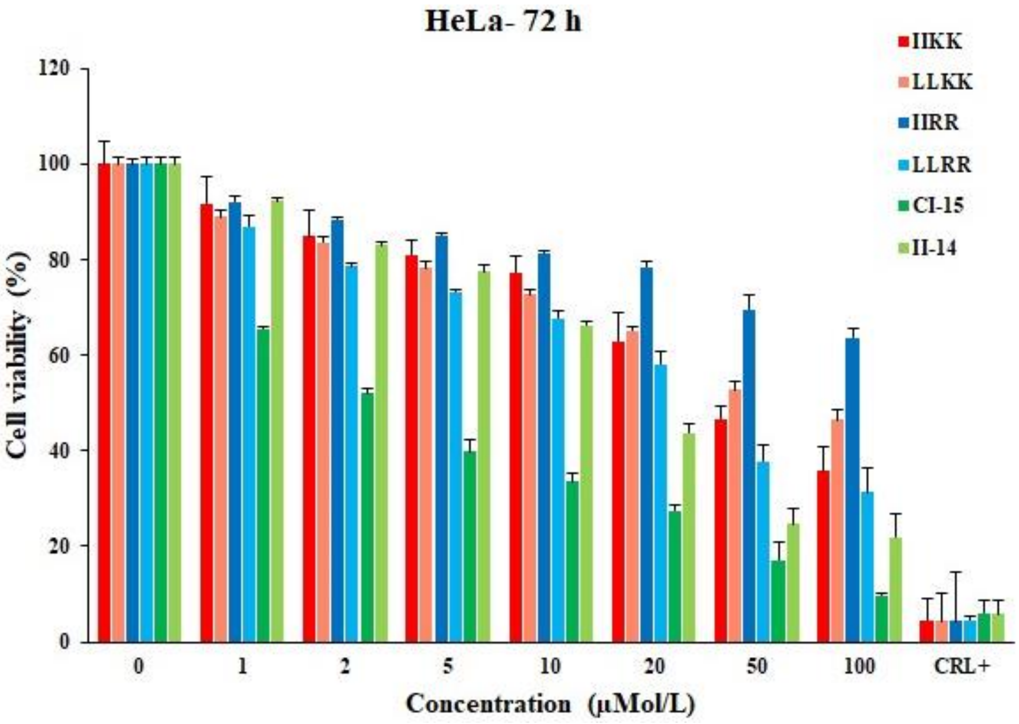

Figure 3.2. Viability of HeLa cells after incubation with different concentrations of the cationic amphiphilic peptides for 72 h as determined by MTT test. All data were normalized against untreated controls and reported as Mean ± SE (n = 6). Sodium chromate (2 mMol/L) was used as positive control (CRL+).

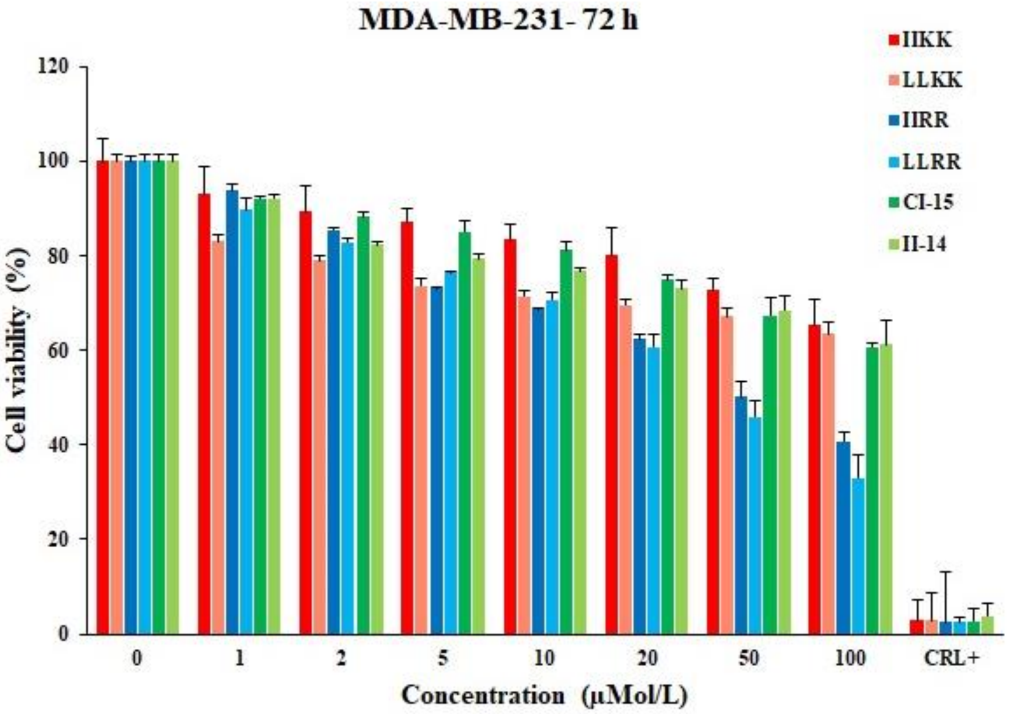

Figure 3.3. Viability of MDA-MB-231 cells after incubation with different concentrations of the cationic amphiphilic peptides for 72 h as determined by MTT test. All data were normalized against untreated controls and reported as Mean ± SE (n = 6). Sodium chromate (2 mMol/L) was used as positive control (CRL+).

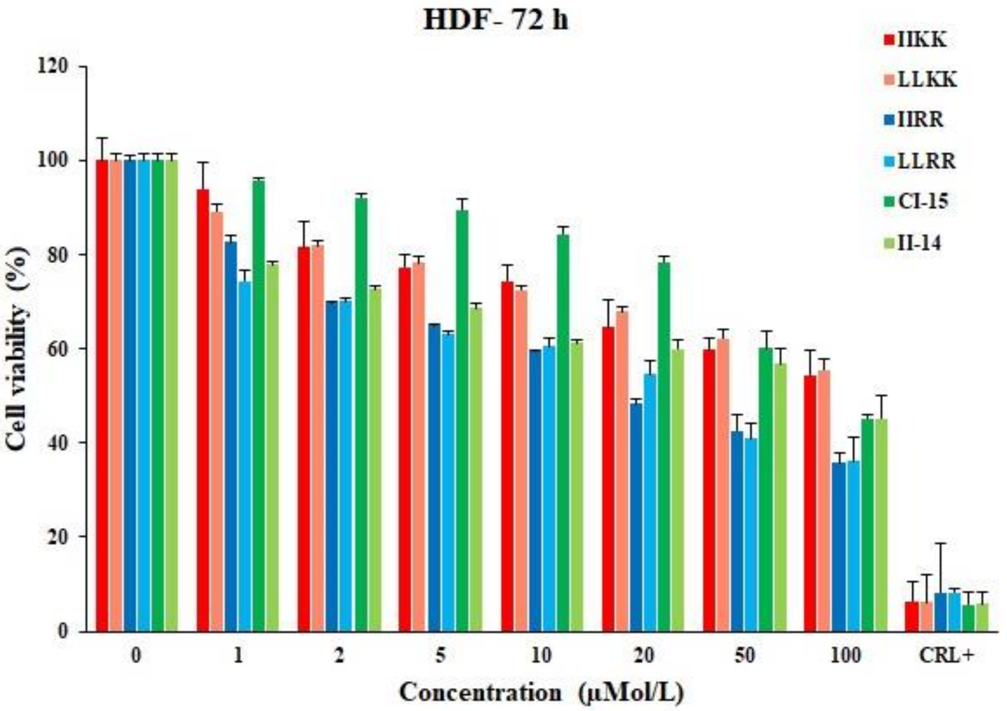

Figure 3.4. Viability of human dermal fibroblast (HDF) cells after incubation with different concentrations of the cationic amphiphilic peptides for 72 h as determined by MTT test. All data were normalized against untreated controls and reported as Mean ± SE (n = 6). Sodium chromate (2 mMol/L) was used as positive control (CRL+).

As it could be observed in Figure 3.1, all of the peptides except IIRR showed some level of toxicity towards HCT 116 cells as indicated by their ability to reduce the cell viability to some extent. As it could be inferred from Table 3.2 and Figure 3.1, CI-15 and II-14 possess the lowest values of IC_{50} (7.7 ± 0.2 µM, and 13.6 ± 0.2 µM respectively) and highest level of growth inhibition (86.2 ± 0.3 % and 90 ± 0.9 % respectively) in HCT 116 cells indicating higher potency and efficacy of these peptides compared to the rest of the peptides. Although considerable differences were observed between the IC_{50} values of the rest of the peptides in this group, there were no significant differences between their maximal growth inhibition with the exception of IIRR which was not toxic to HCT 116 cells in the experimental range of concentration. Thus, changing the composition and/or length of the peptides affects their potency as anticancer agents more than their efficacy.

In a similar manner to HCT 116, IIRR did not exhibit any toxic effect in HeLa cells even at the highest experimental concentrations (Figure 3.3) and the other peptides showed varying levels of toxicity against HeLa cells with CI-15 and II-14 having the lowest values of IC_{50} (2.7 ± 0.5 µM, 16.6 ± 0.8 µM respectively) and highest level of growth inhibition (90.4 ± 0.2 % and 78.2 ± 0.8 % respectively). However, some of the peptides which exhibited considerable cytotoxicity against HCT 116 (IIKK and LLKK) showed very weak toxicity against HeLa indicating the higher selectivity of these peptides for HCT 116.

On the other hand, MDA-MB-231 showed a quite different response to the α-helical cationic amphiphilic peptides compared to the other two cancer cell lines (Figure 3.3). IIRR which was not toxic to HCT 116 and HeLa exhibited some level of toxicity in MDA-MB-231 whereas the peptides which were highly toxic to the other two cell lines such as CI-15 and II-14 were not toxic to MDA-MB-231 cells. In general, only the peptides consisting of arginine residues (IIRR and LLRR) were toxic to MDA-MB-231 whereas the peptides containing lysine residues were not toxic to these cells. The cytotoxicity trend in HDFs was also similar to MDA-MB-231. IIRR and LLRR were toxic to HDFs whereas the other peptides had very low toxicity in these cells. Thus, the lysine containing peptides possessed selective cytotoxicity against cancer cells (except MDA-MB-231) with minimal toxicity in HDFs which indicates selective anticancer activity.

As it could be inferred from the above-mentioned data, combination of lysine and isoleucine made the peptide more toxic towards cancer cells than fibroblasts, whereas combination of lysine and leucine made the peptide selectively toxic towards HCT 116 and combination of arginine and isoleucine diminished the anticancer activity but made the peptide toxic to fibroblasts. Increasing the length of the isoleucine and lysine containing peptides increased their toxicity towards HCT 116 and HeLa but did not affect their toxicity against MDA 231-MB and HDF. Moreover, replacing the N-terminal cysteine of these peptides with glycine decreased the potency of the peptide in HCT 116 and HeLa.

In order to determine the initiation time for the cytotoxic activity of the peptides, additional MTT tests were performed 24 h after incubation of the cells with the cationic amphiphilic peptides which were found to be cytotoxic against each cell line in order to detect any cytotoxic effects within the first 24 h. The peptides which did not show any cytotoxicity in certain cell lines after 72 h were excluded from further experiments. The results are depicted in Figures 3.5-3.8.

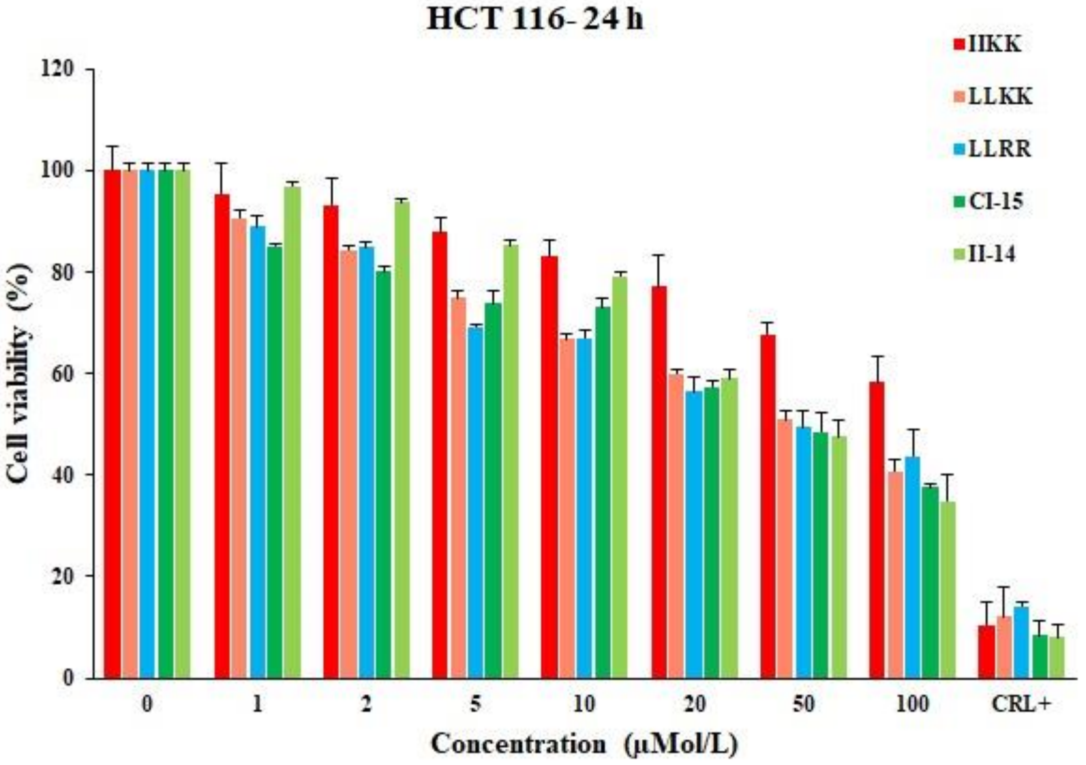

Figure 3.5. Viability of HCT 116 cells after incubation with different concentrations of the cationic amphiphilic peptides for 24 h as determined by MTT test. All data were normalized against untreated controls and reported as Mean ± SE (n = 6). Sodium chromate (2 mMol/L) was used as positive control (CRL+).

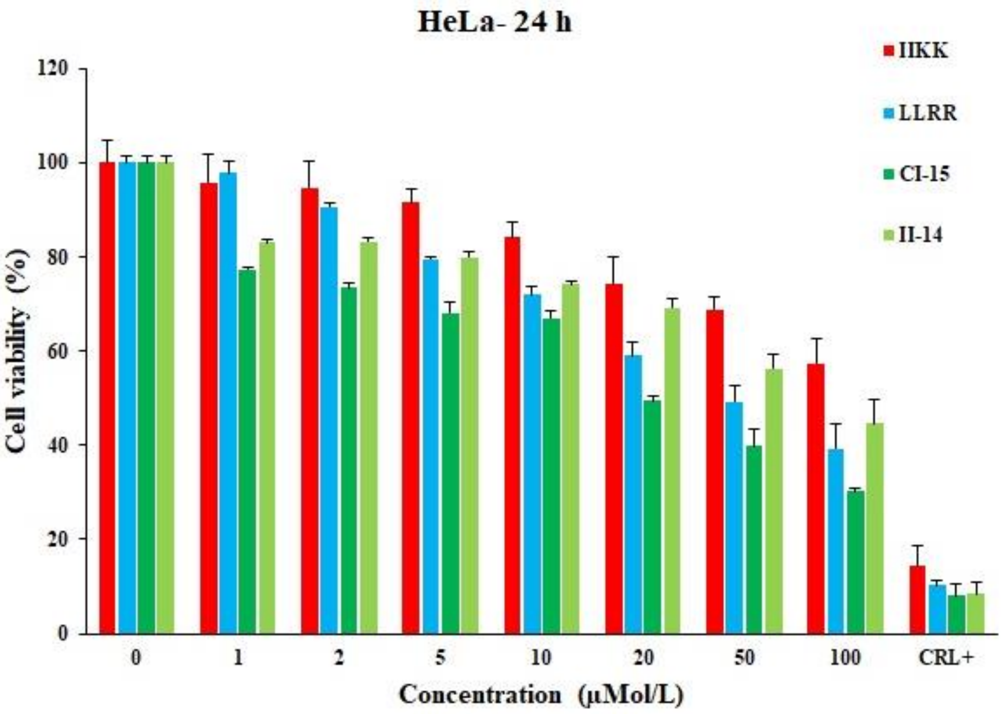

Figure 3.6. Viability of HeLa cells after incubation with different concentrations of the cationic amphiphilic peptides for 24 h as determined by MTT test. All data were normalized against untreated controls and reported as Mean ± SE (n = 6). Sodium chromate (2 mMol/L) was used as positive control (CRL+).

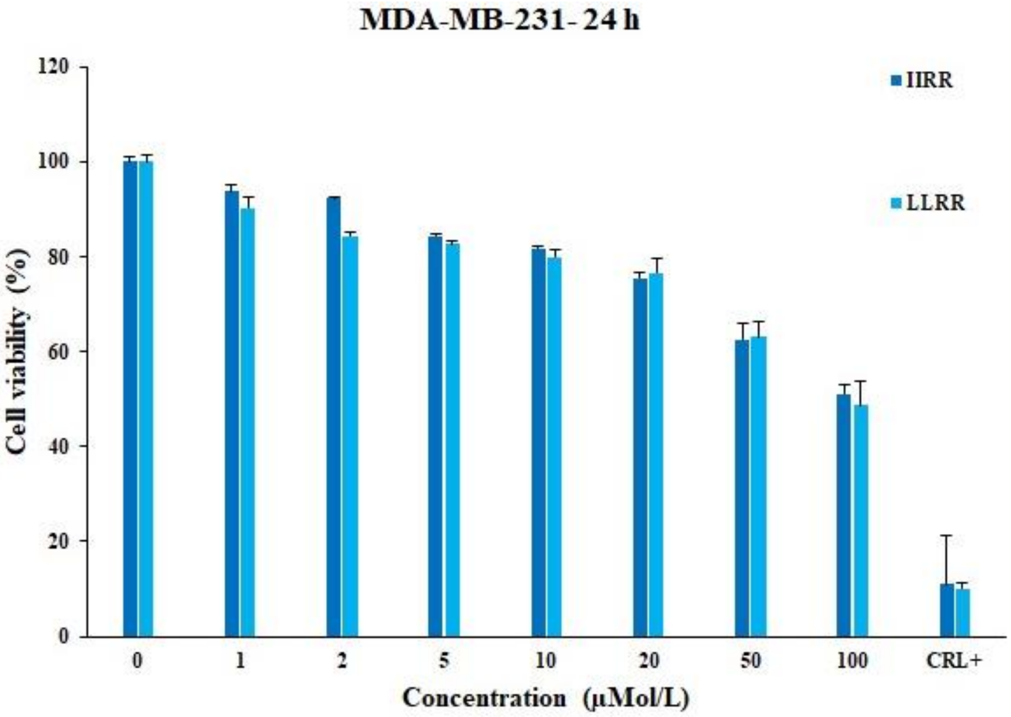

Figure 3.7. Viability of MDA-MB-231 cells after incubation with different concentrations of the cationic amphiphilic peptides for 24 h as determined by MTT test. All data were normalized against untreated controls and reported as Mean ± SE (n = 6). Sodium chromate (2 mMol/L) was used as positive control (CRL+).

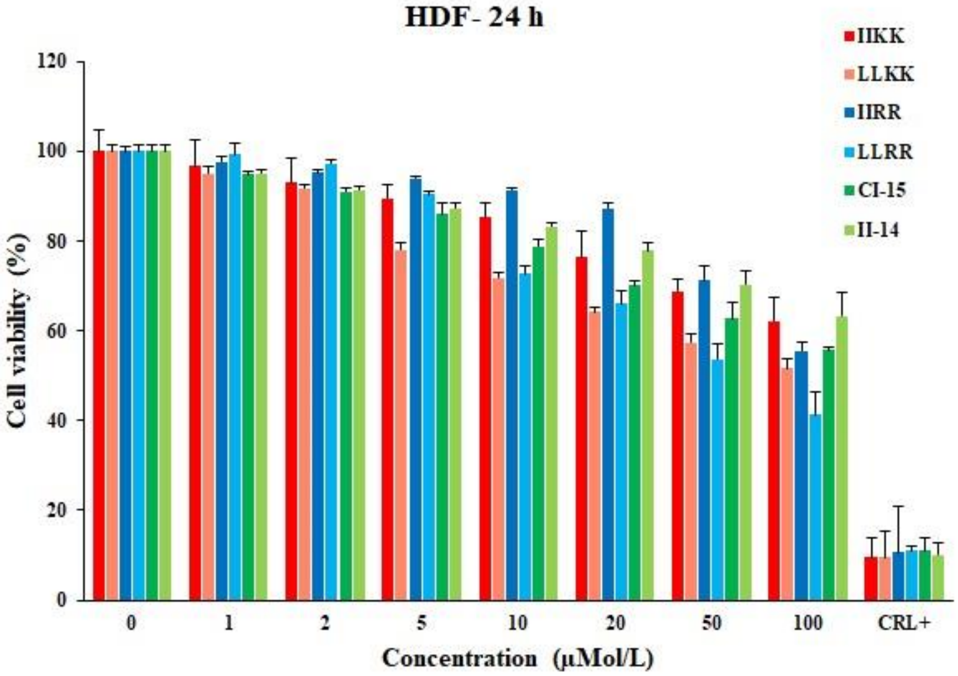

Figure 3.8. Viability of human dermal fibroblast (HDF) cells after incubation with different concentrations of the cationic amphiphilic peptides for 24 h as determined by MTT test. All data were normalized against untreated controls and reported as Mean ± SE (n = 6). Sodium chromate (2 mMol/L) was used as positive control (CRL+).

As it could be observed in Figures 3.5-3.6, IIKK induced minimal reduction in the cell viability in 24 h whereas the rest of the cationic amphiphilic peptides reduced the cell viability considerably after 24 h. Hence, the cytotoxic effect of the cationic amphiphilic peptides in HCT 116 and HeLa initiates within the first 24 h and further increases until 72 h except IIKK which has a slower initiation of action indicating longer course of cytotoxicity for this peptide compared to the other peptides which suggests different modes of interaction of these peptides with the cancer cells. In MDA-MB-231 cells IIRR and LLRR caused a slight decrease in the cell viability within 24 h (figure 3.7). However, the extent of the cytotoxic effect was considerably less than the cytotoxicity after 72 h incubation suggesting that the cytotoxic effect of these peptides starts within 24 h and increases over time. In HDF cells, in a similar fashion to HCT 116 and HeLa, IIKK and IIRR did not reduce the cell viability significantly within 24 h, whereas the cytotoxicity of LLKK, LLRR and CI-15 initiated within 24 h and further increased over time until 72 h (Figure 3.8). Taken together, it could be inferred from these observations that the cationic amphiphilic peptides differ in the initiation of their cytotoxic action. IIKK and IIRR appear to exert a late cytotoxic effect which takes place more slowly than the other peptides whereas the rest of the peptides exhibit an early initiation of cytotoxic action starting in less than 24 h and further increasing over time until 72 h.

To conclude, the most toxic peptides against cancer cells with low level of toxicity against fibroblasts were the peptides consisting of isoleucine and lysine. Nevertheless, MDA 231-MB showed a different behaviour than HCT 116 and HeLa and was only responsive to treatment with the cationic amphiphilic peptides consisting of arginine and isoleucine or leucine. The observed difference in the behaviour of the MDA 231-MB cells compared to HCT 116 and Hela could be due to the different structural features of the MDA 231-MB cells from the other two cancer cell lines such as the difference in the expression of the cell surface receptors which are responsible for internalization of the peptides. Another possible reason for the observed difference could be the difference in the cellular entry pathways for the peptides in different cancer cell lines or the difference in the cellular pathways which are responsible for the cellular damage caused by the peptides. However, unravelling the biological differences between the MDA 231-MB cells and HCT 116/HeLa which would lead to different response to the treatment with the cationic amphiphilic peptides is beyond the scope of this study and could be subject to further study.

3.3.3 Mitochondrial damage

As discussed in Section 2.1, the MTT assay indicated reduction in the metabolic activity of the cells following treatment with the cationic amphiphilic peptides. To further investigate the effect of the cationic amphiphilic peptides on the cell metabolism, the cells were studied for the mitochondrial health as mitochondria play a key role in cellular metabolism [20-21]. The mitochondrial health was measured by the mitochondrial morphology & distribution pattern within the cells after treatment with the cationic amphiphilic peptides as compared to the normal phenotype in the untreated controls. Each cell line was incubated with the cationic amphiphilic peptides which were found to be toxic against that cell line (based on the MTT test), after 72 h the mitochondria were stained using mitochondrial probe MitoTracker® Red following the protocol described in Section 2.12 and the cells were imaged with high content microscope. Figures 3.9-3-11 show the HCT 116, HeLa and MDA 231-MB cells stained with MitoTracker® Red.

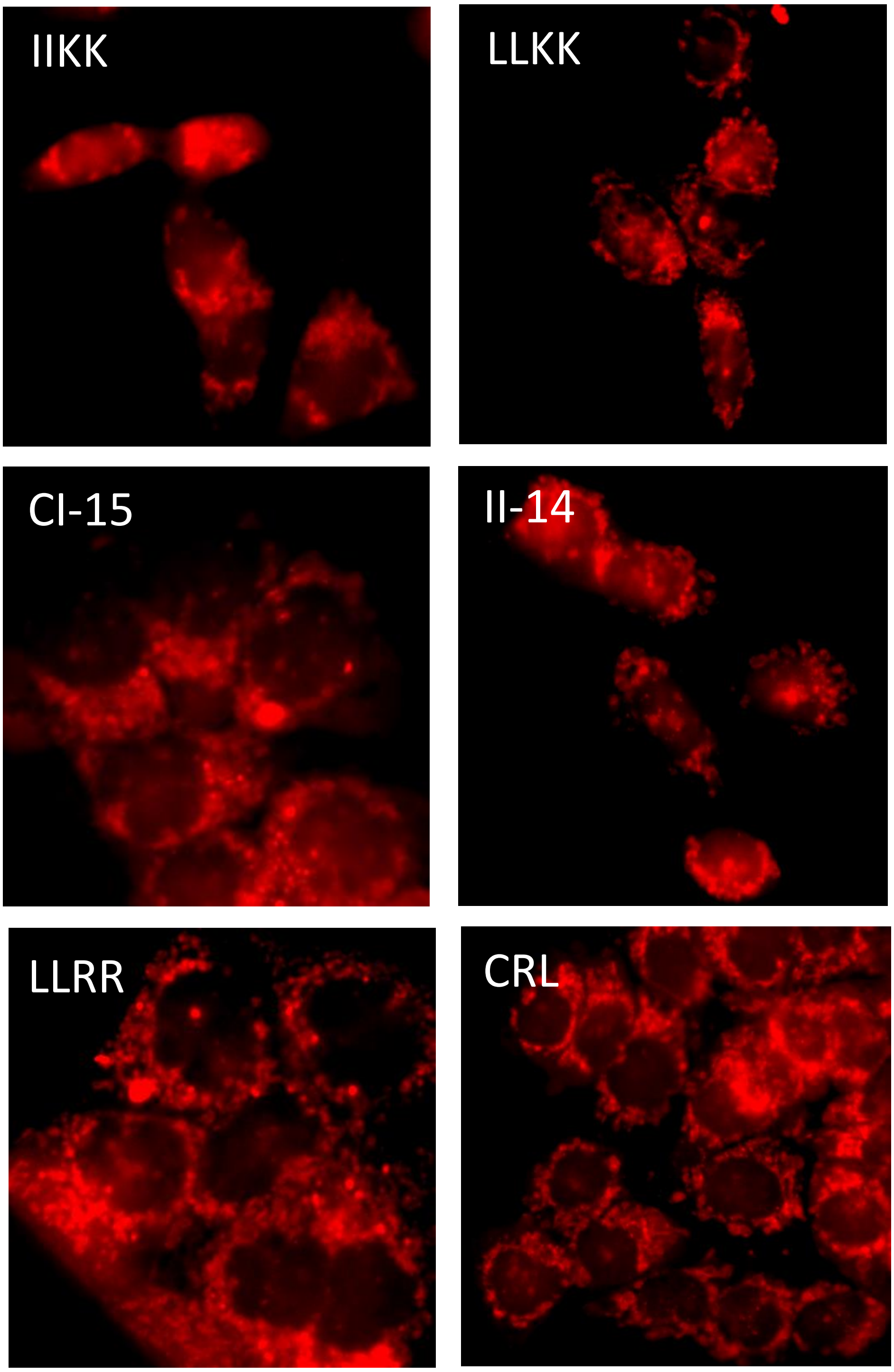

Figure 3.9. The morphology and distribution pattern of the mitochondria in HCT 116 cells incubated with cationic amphiphilic peptides for 72 h. The mitochondria were stained with MitoTracker® Red, ×40 magnification.

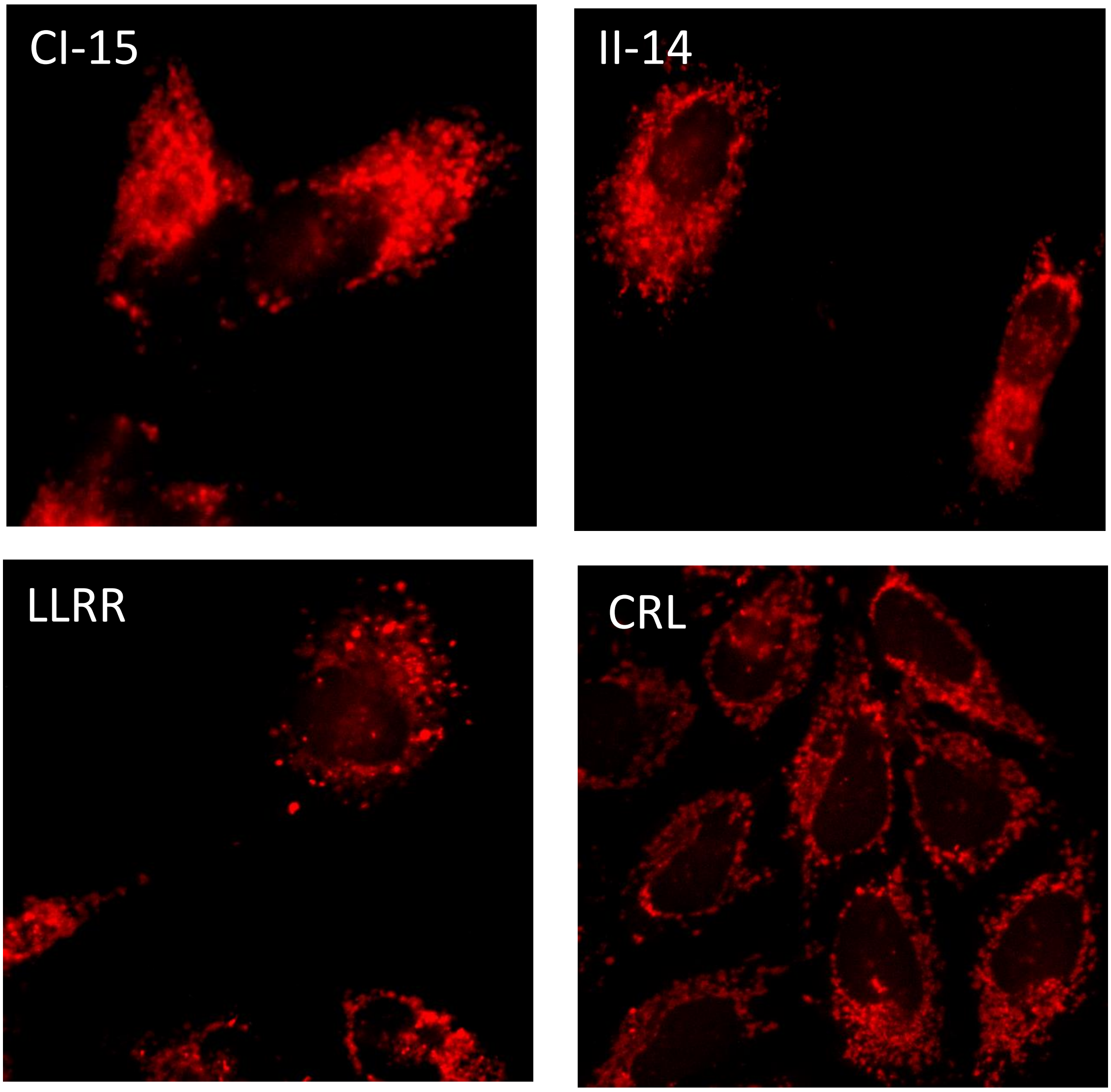

Figure 3.10. The morphology and distribution pattern of the mitochondria in HeLa cells incubated with cationic amphiphilic peptides for 72 h. The mitochondria were stained with MitoTracker® Red, ×40 magnification.

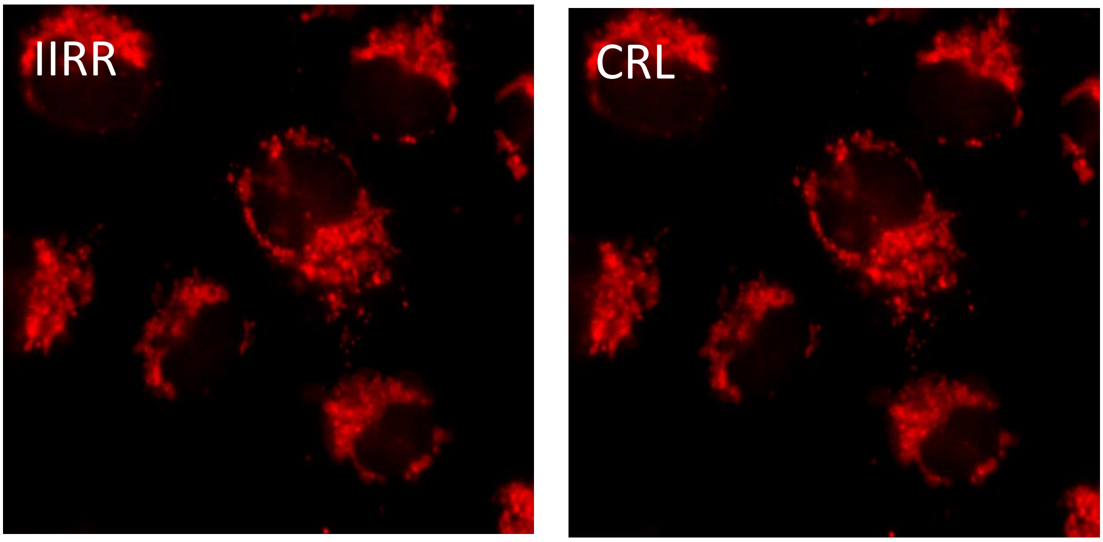

Figure 3.11. The morphology and distribution pattern of the mitochondria in MDA-MB-23 cells incubated with cationic amphiphilic peptides for 72 h. The mitochondria were stained with MitoTracker® Red, ×40 magnification.

As it could be observed in Figure 3.9, treatment of the HCT 116 cells with CI-15, II-14, IIKK, LLKK and LLRR resulted in significant changes to the shape and distribution pattern of the mitochondria compared to the normal phenotype in untreated controls. Unlike the healthy controls in which the mitochondria were evenly distributed around the nuclei in a ring-shaped conformation, in cells treated with CI-15 and LLRR, the mitochondria formed clumps which were more localized to one side of the cytoplasm and the higher accumulation of the mitotracker in these organelles gave rise to brighter, more intense fluorescence signal which is another indicator of the damaged mitochondria. In a similar fashion, treating the cells with II-14, IIKK, and LLKK resulted in big clumps of mitochondria localized more to one side of the cytoplasm. Moreover, the cells were smaller in size and more elongated in shape compared to the untreated healthy controls which clearly indicates that the cells are not healthy. In a similar manner, incubating HeLa cells with CI-15, II-14 and LLRR resulted in elongated cells with the mitochondria clumped together and migrated to one side of the cells and more intense fluorescence signal emitted from these mitochondria than the healthy mitochondria in the untreated control cells as is evident from Figure 3.10 Similar morphological changes were observed in MDA 231-MB cells treated with IIRR which was the only cationic amphiphilic peptide showing cytotoxicity in these cells (Figure 3.11).

To further confirm the mitochondrial damage caused by the cationic amphiphilic peptides, the HCT 116 colorectal cancer cells and the HDF cells were treated with the α-helical cationic amphiphilic peptides for 72 h and then stained with JC-1 which is a mitochondrial membrane potential indicator. JC-1 is membrane permeant and its accumulation in the mitochondria depends on the mitochondrial membrane potential. Accumulation of the JC-1 in the healthy mitochondria results in red fluorescence from the JC-1 aggregates [22-23]. Damage to the mitochondria leads to depolarization of the mitochondrial membrane, which is a distinctive feature of the early stages of apoptosis. This results in reduced accumulation of JC-1 in the mitochondria, which is indicated by a shift from red fluorescence to green fluorescence which is mainly from JC-1 monomers [24-25]. For this experiment, only the α-helical cationic amphiphilic peptides with higher anticancer activity and higher selectivity for cancer cells were selected and the peptides with poor anticancer activity and/or the peptides which were equally toxic to cancer cells and normal cells were not included. As it could be observed in Figures 3.12-3.13, treatment of the HCT 116 colorectal cancer cells with the peptides results in mitochondrial damage as denoted by higher proportion of green fluorescence than red fluorescence whereas in the untreated controls the healthy mitochondria are indicated by red fluorescence. In the human dermal fibroblasts on the other hand, the red to green fluorescence ratio was in favour of the healthy mitochondria which is consistent with the lower cytotoxicity of these peptides in HDFs than cancer cells.

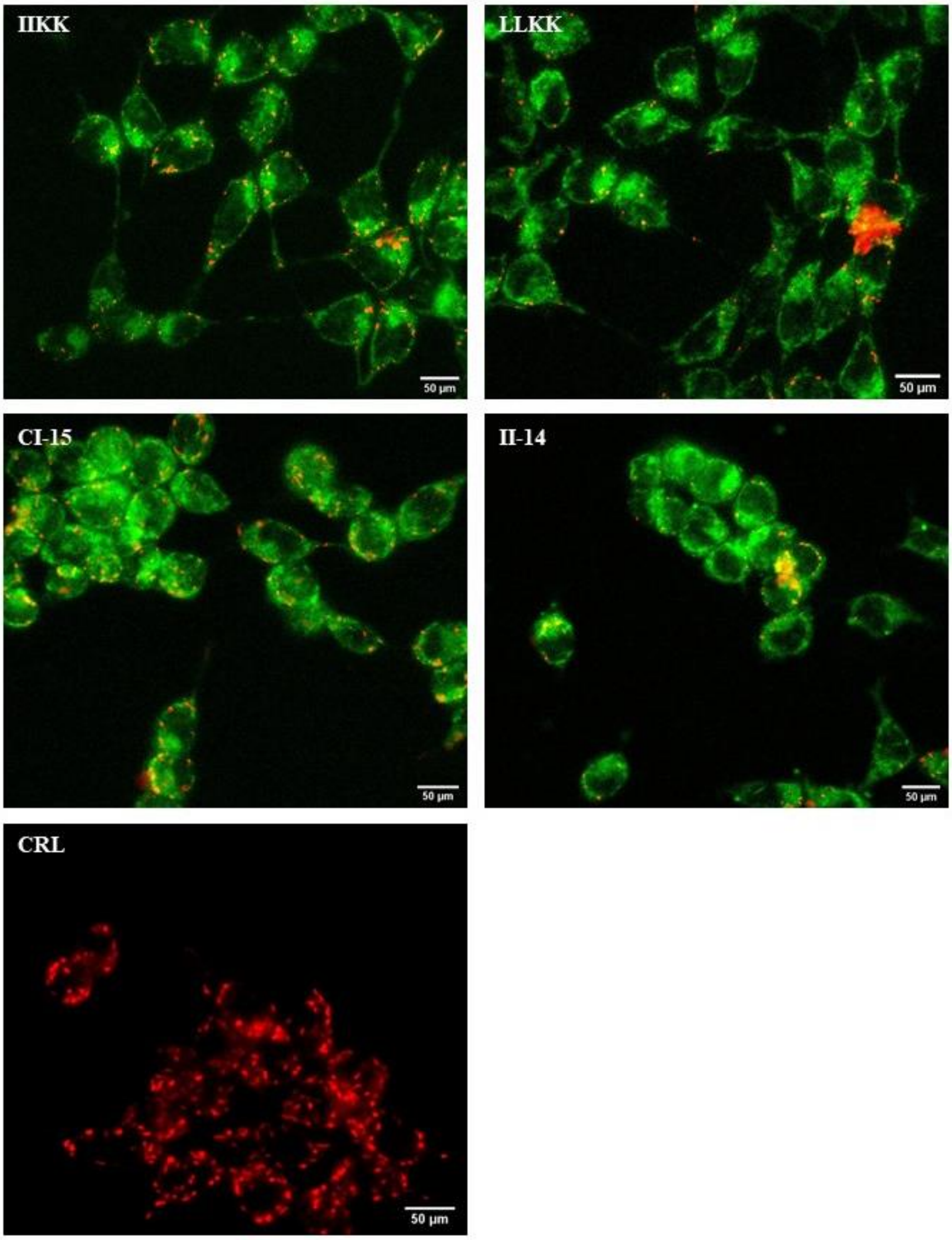

Figure 3.12. High content images of HCT 116 colorectal cancer cells stained with JC-1 after incubation with α-helical cationic amphiphilic peptides for 72 h. The green colour indicates damaged mitochondria in pre-apoptotic cells and red colour indicates the healthy mitochondria. 40 × magnification, scale bar: 50 µm.

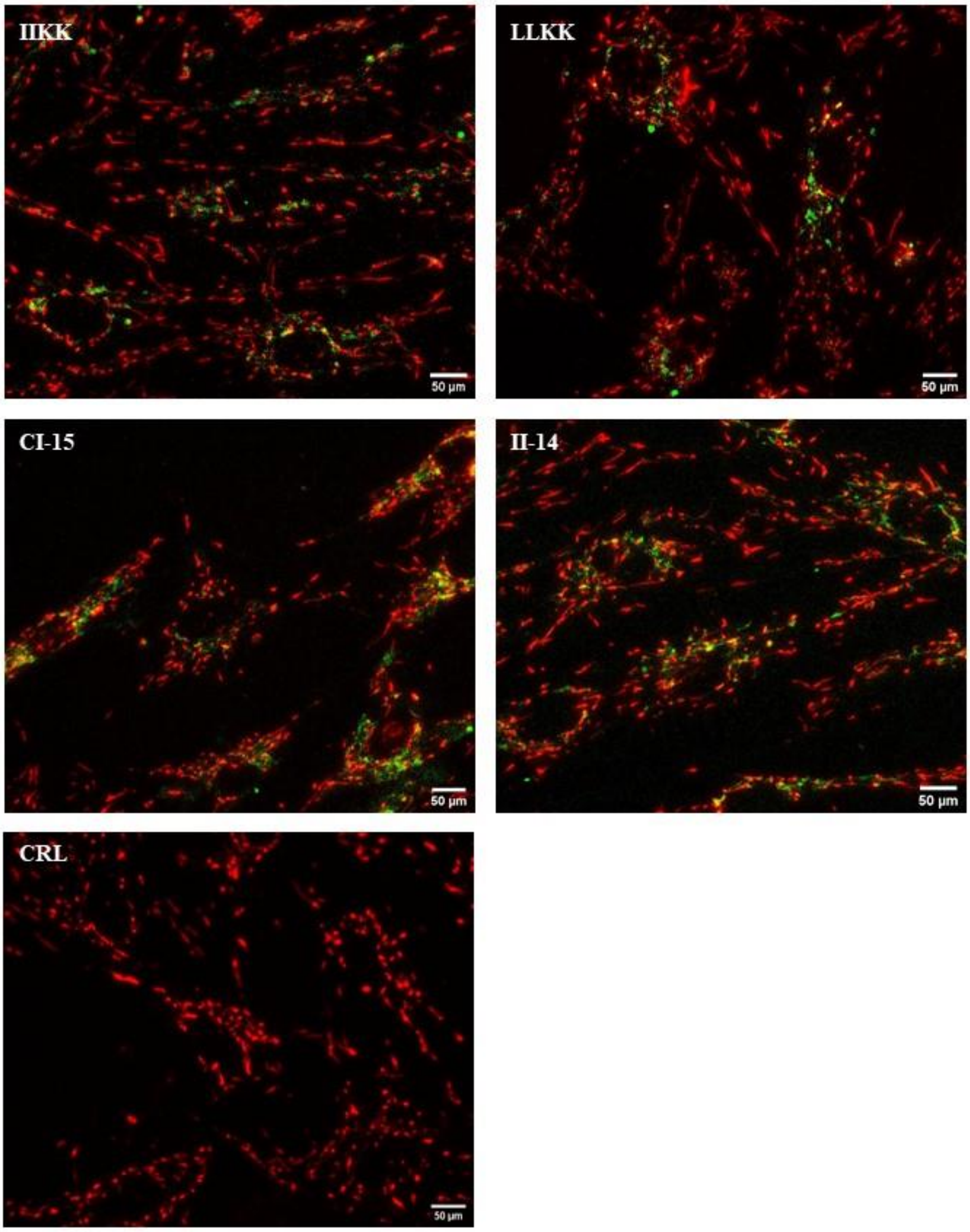

Figure 3.13. High content images of human dermal fibroblast cells stained with JC-1 after incubation with α-helical cationic amphiphilic peptides for 72 h. The green colour indicates damaged mitochondria in pre-apoptotic cells and red colour indicates the healthy mitochondria. 40 × magnification, scale bar: 50 µm.

3.3.4 Cell proliferation

The ability of the cationic amphiphilic peptides to inhibit the cell proliferation in HCT 116 cells is depicted in Figures 3.14-3.15.

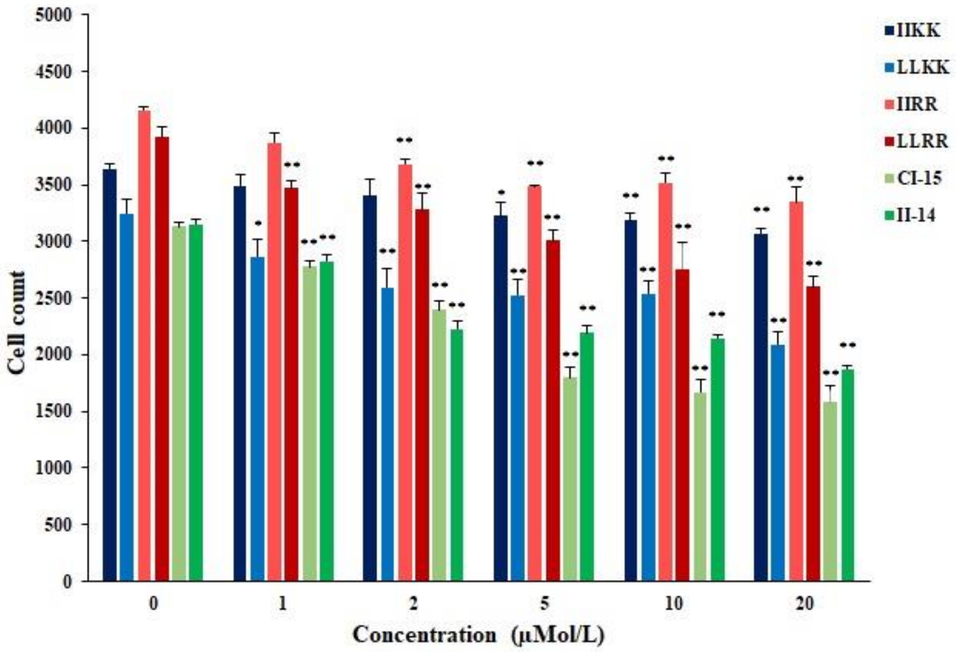

Figure 3.14. Average cell counts of HCT 116 cells incubated with different concentrations of cationic amphiphilic peptides for 72 h. The data were reported as Mean ± SE (n = 6). * indicates values of $p < 0.05$ and ** indicates values of $p < 0.005$ as compared to the controls.

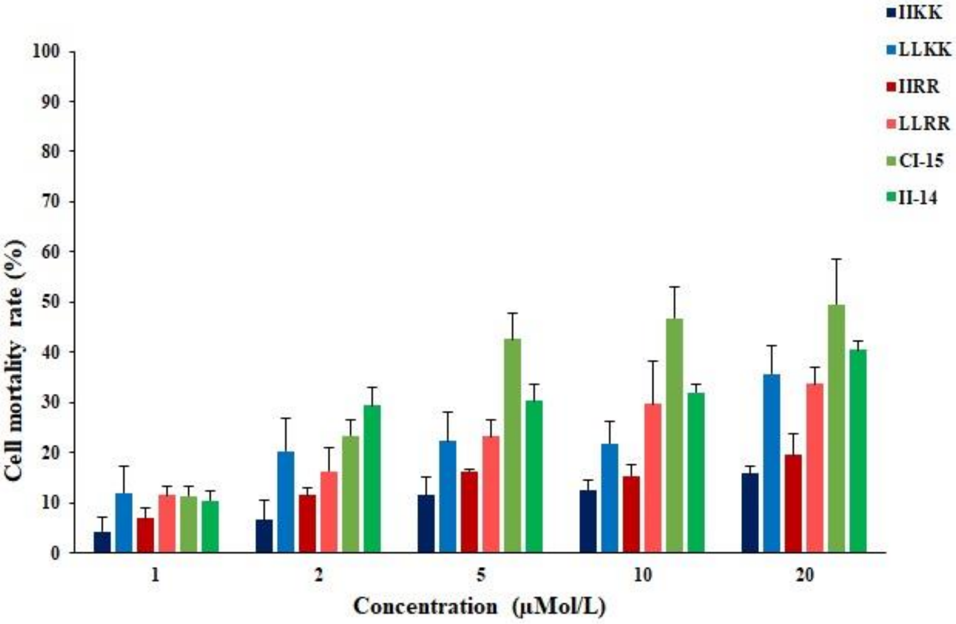

Figure 3.15. Mortality rates of HCT 116 cell incubated with different concentrations of cationic amphiphilic peptides for 72 h. All data were normalized against untreated controls and reported as Mean ± SE (n = 6).

As it could be observed LLKK, LLRR, CI-15 and II-14 reduced the cell number considerably compared to the controls indicating the antiproliferative effect of these peptides whereas IIKK and IIRR did not reduce the cell count considerably suggesting cytostatic effect for these peptides without any antiproliferative or apoptotic activity. It could be inferred from these data that among the peptides with 13 amino acid residues, the peptides containing leucine exert their cytotoxic effect by avoiding the cell proliferation whereas the peptides containing isoleucine reduce the metabolic activity of the cells without inhibiting the cell proliferation or inducing apoptosis. This might be due to the different special orientation of the isoleucine and leucine in the peptide chain which could affect the exposure of these lipophilic residues and their availability for interaction with the phospholipids in the cell membrane. On the other hand, increasing the length of the isoleucine and lysine containing peptide by adding one or two isoleucine residues bestows strong antiproliferative activity on the peptide. This might be due to the change in the hydrophilic/lipophilic balance of the peptide resulting in stronger interaction with or greater penetration into the cell membrane; or due to change in the peptide folding resulting in higher exposure and better interaction of the isoleucine residues with the cell membrane. However, there is lack of experimental evidence to support any of these assumptions and unravelling the biological and/or biochemical basis for the observed difference in the biological effects of the cationic amphiphilic peptides remains subject to future studies.

3.3.5 Transfection with AONs

Figures 3.16-3.21 show HCT 116 cells transfected with different cationic amphiphilic peptides complexed with FITC-labelled cMyc- AON at different N/P ratios as described in Section 2.17. cMyc belongs to a family of proto-oncogenes encoding nuclear phosphoproteins that play a key role in cell proliferation and apoptosis [26]. The intensity of the green fluorescence is proportional to the amount of the AON within the cells which is an indicator of the successful transfection.

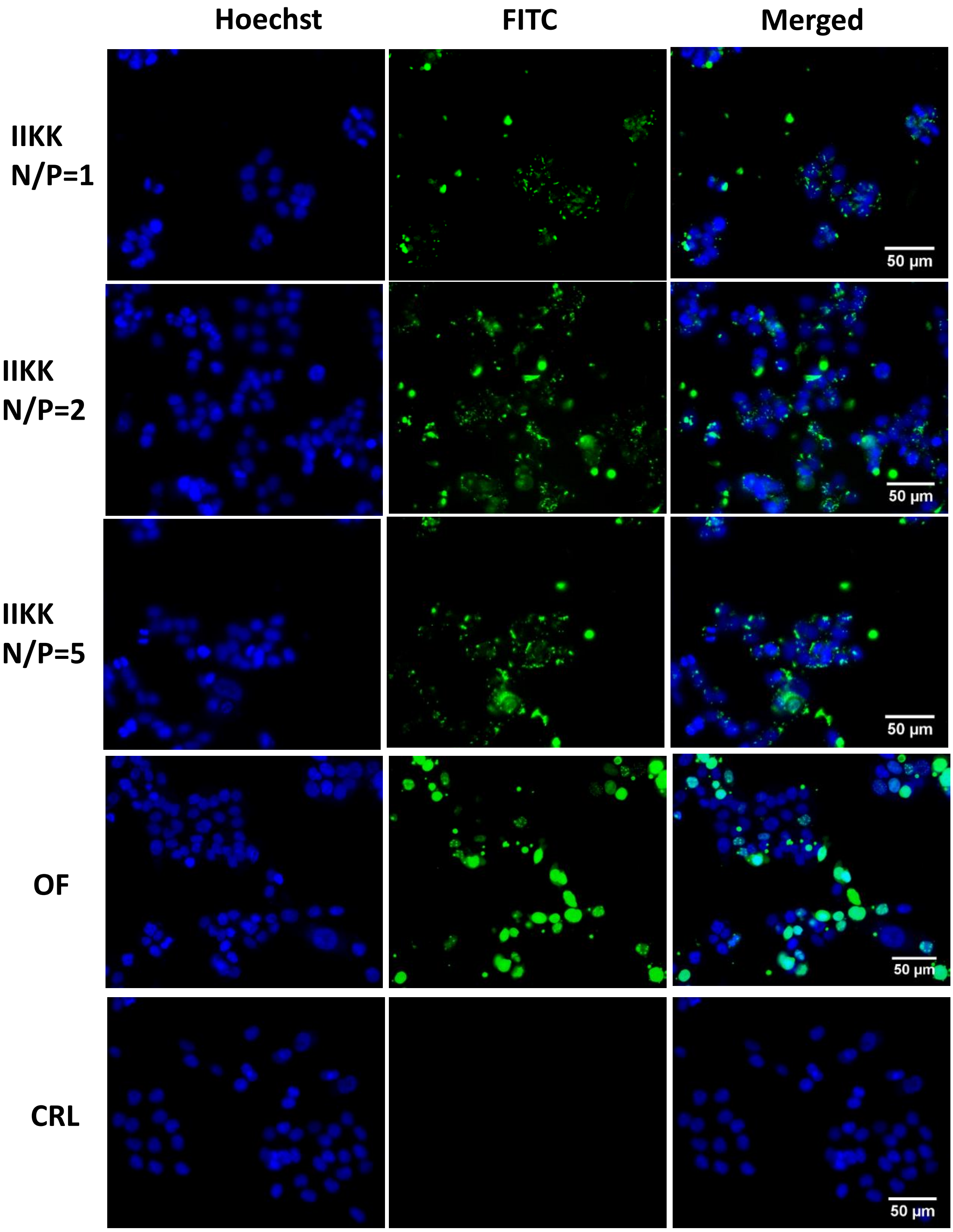

Figure 3.16. High content images of HCT 116 cells transfected with FITC-labelled c-Myc AON using IIKK at different N/P ratios. Oligofectamine™ (OF) was used as positive control and naked c-Myc AON was used as negative control. The nuclei were stained with Hoechst 33342, ×20 magnification.

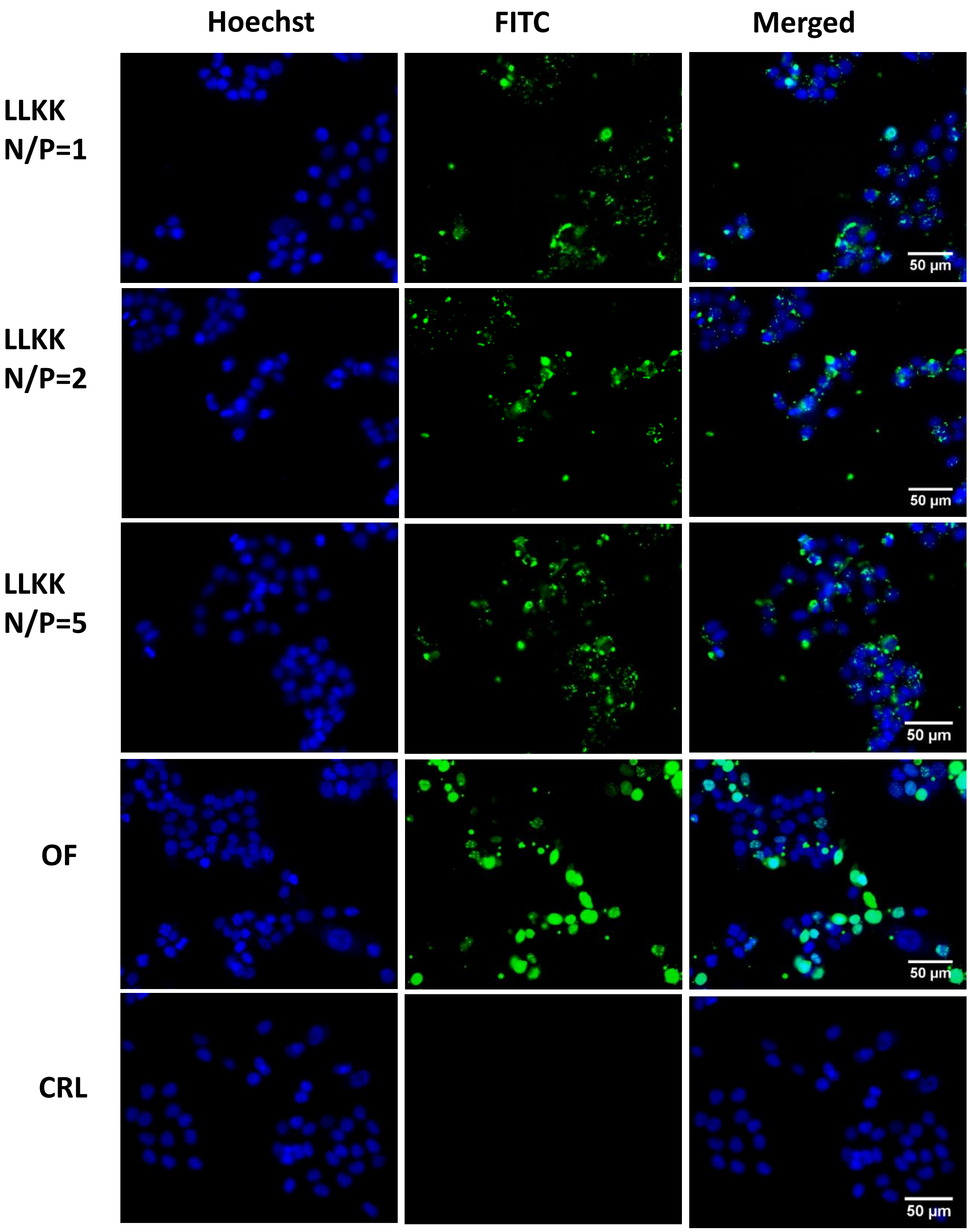

Figure 3.17. High content images of HCT 116 cells transfected with FITC-labelled c-Myc AON using LLKK at different N/P ratios. Oligofectamine™ (OF) was used as positive control and naked c-Myc AON was used as negative control. The nuclei were stained with Hoechst 33342, ×20 magnification.

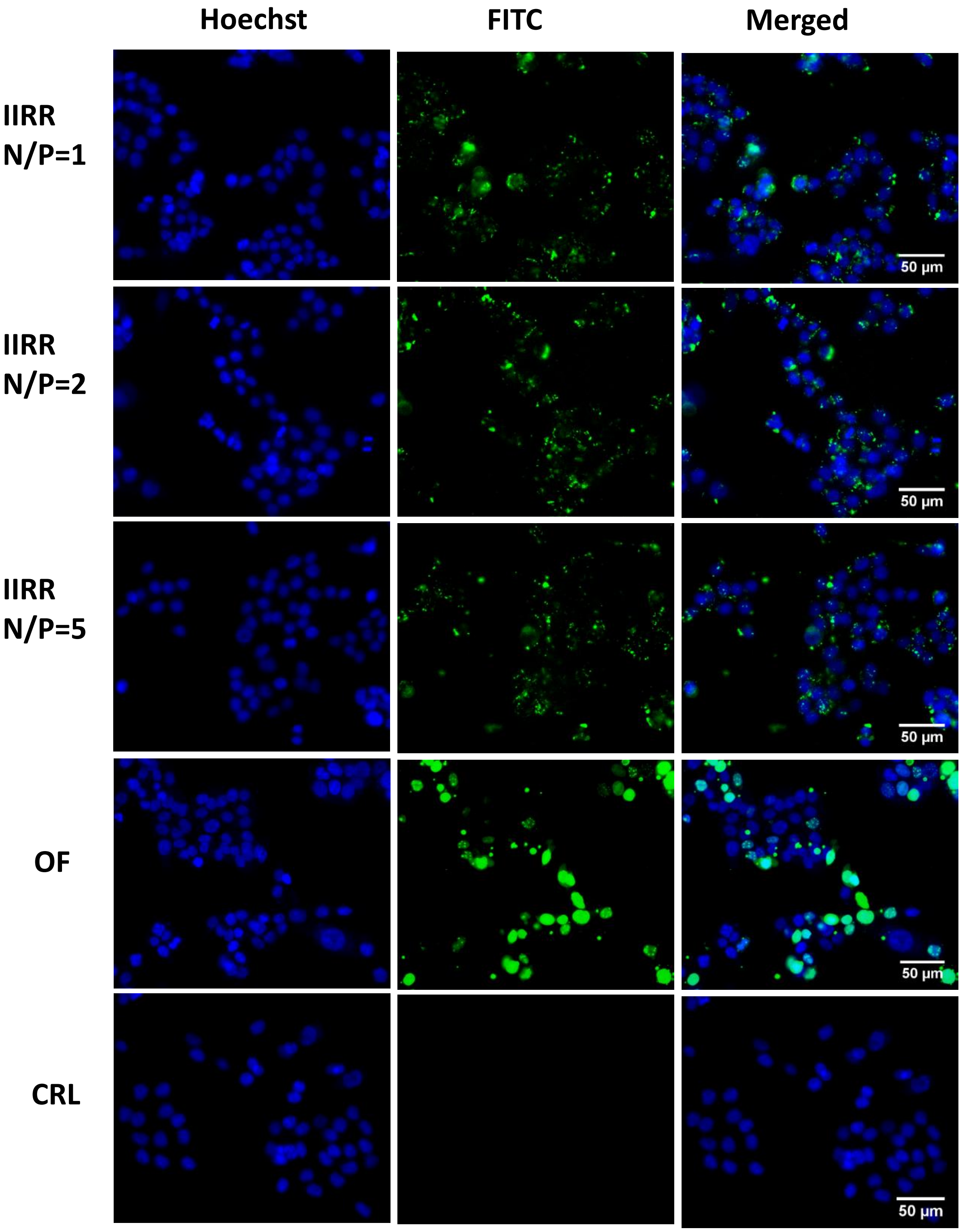

Figure 3.18. High content images of HCT 116 cells transfected with FITC-labelled c-Myc AON using IIRR at different N/P ratios. Oligofectamine™ (OF) was used as positive control and naked c-Myc AON was used as negative control. The nuclei were stained with Hoechst 33342, ×20 magnification.

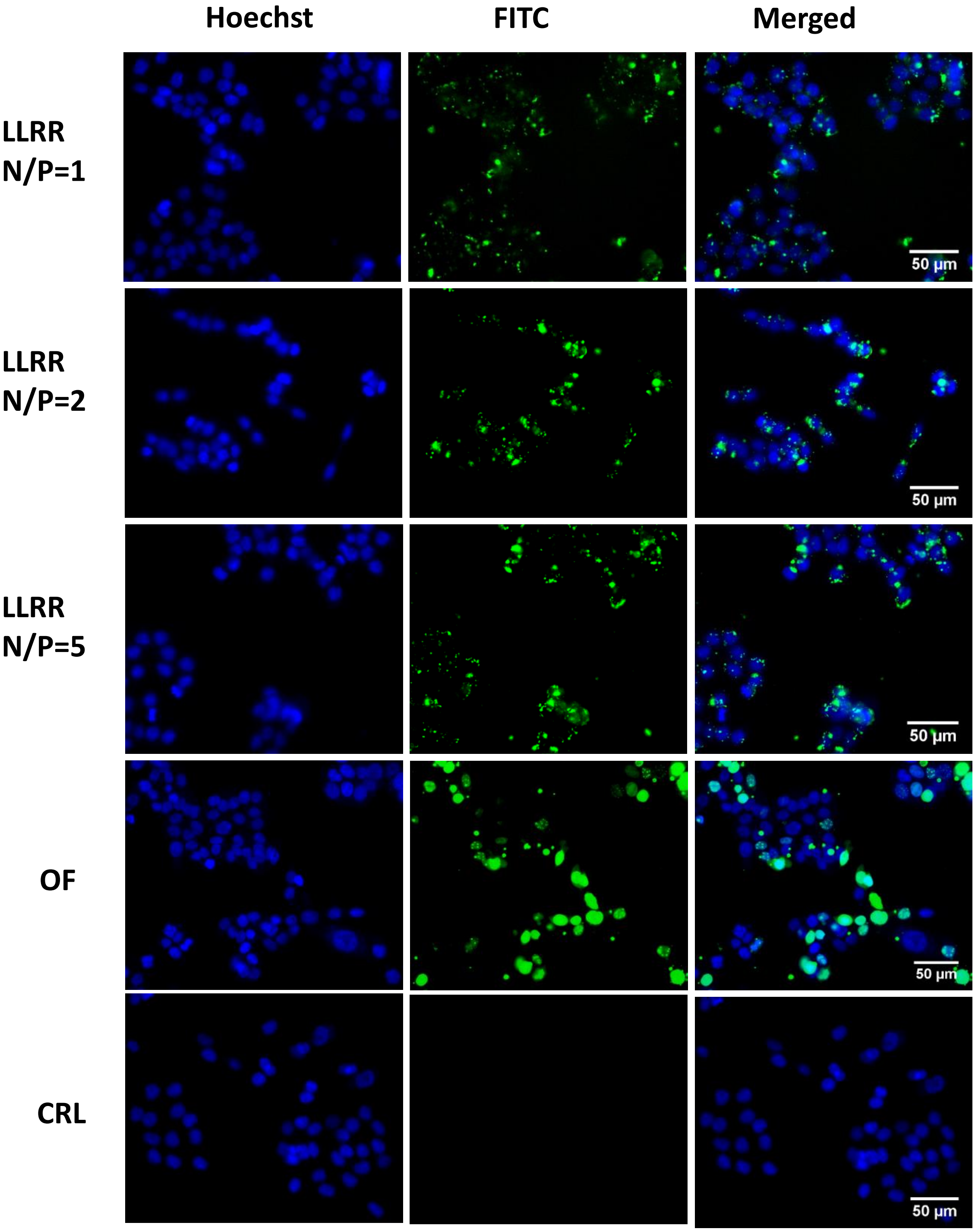

Figure 3.19. High content images of HCT 116 cells transfected with FITC-labelled c-Myc AON using LLRR at different N/P ratios. Oligofectamine™ (OF) was used as positive control and naked c-Myc AON was used as negative control. The nuclei were stained with Hoechst 33342, ×20 magnification.

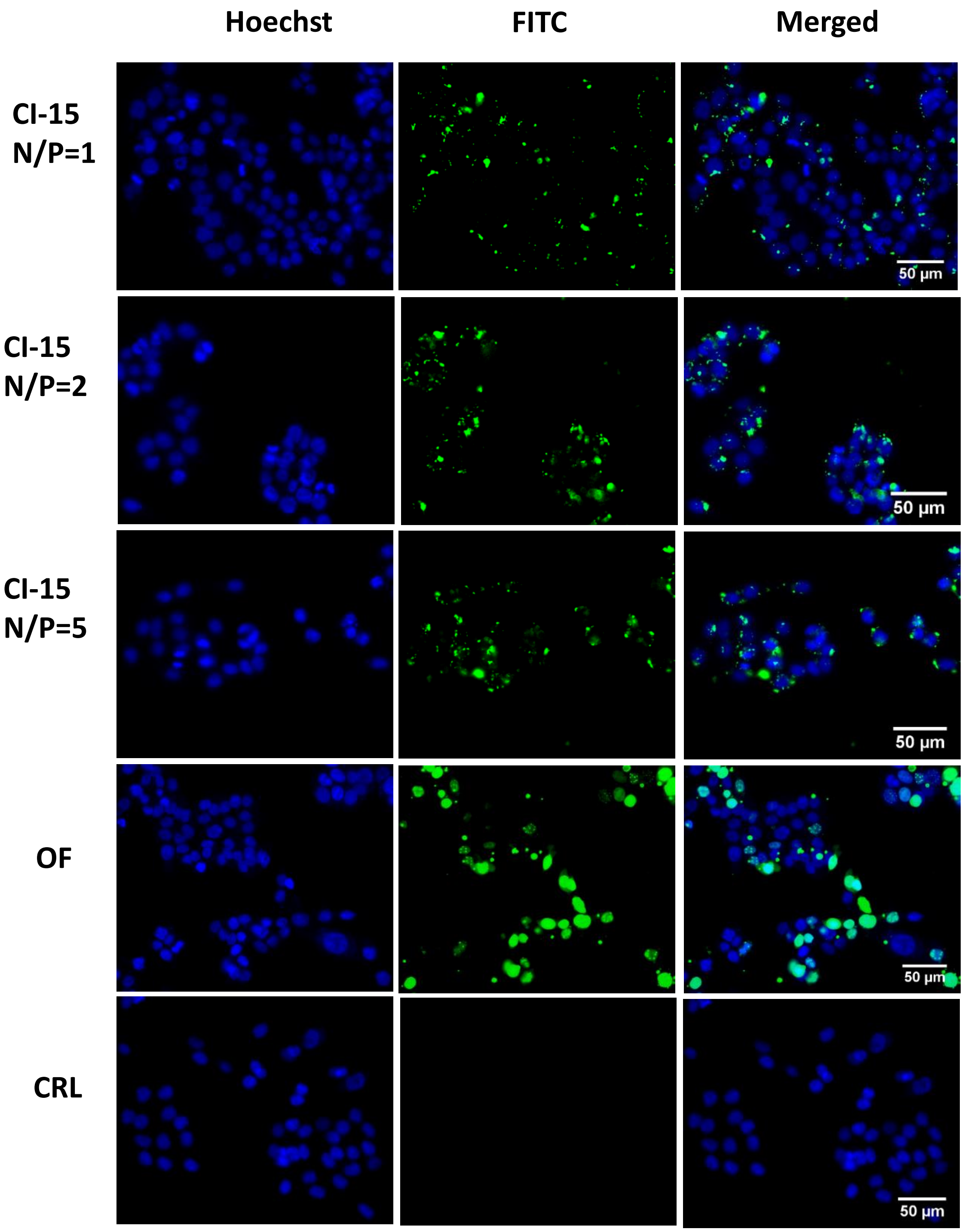

Figure 3.20. High content images of HCT 116 cells transfected with FITC-labelled c-Myc AON using CI-15 at different N/P ratios. Oligofectamine™ (OF) was used as positive control and naked c-Myc AON was used as negative control. The nuclei were stained with Hoechst 33342, ×20 magnification.

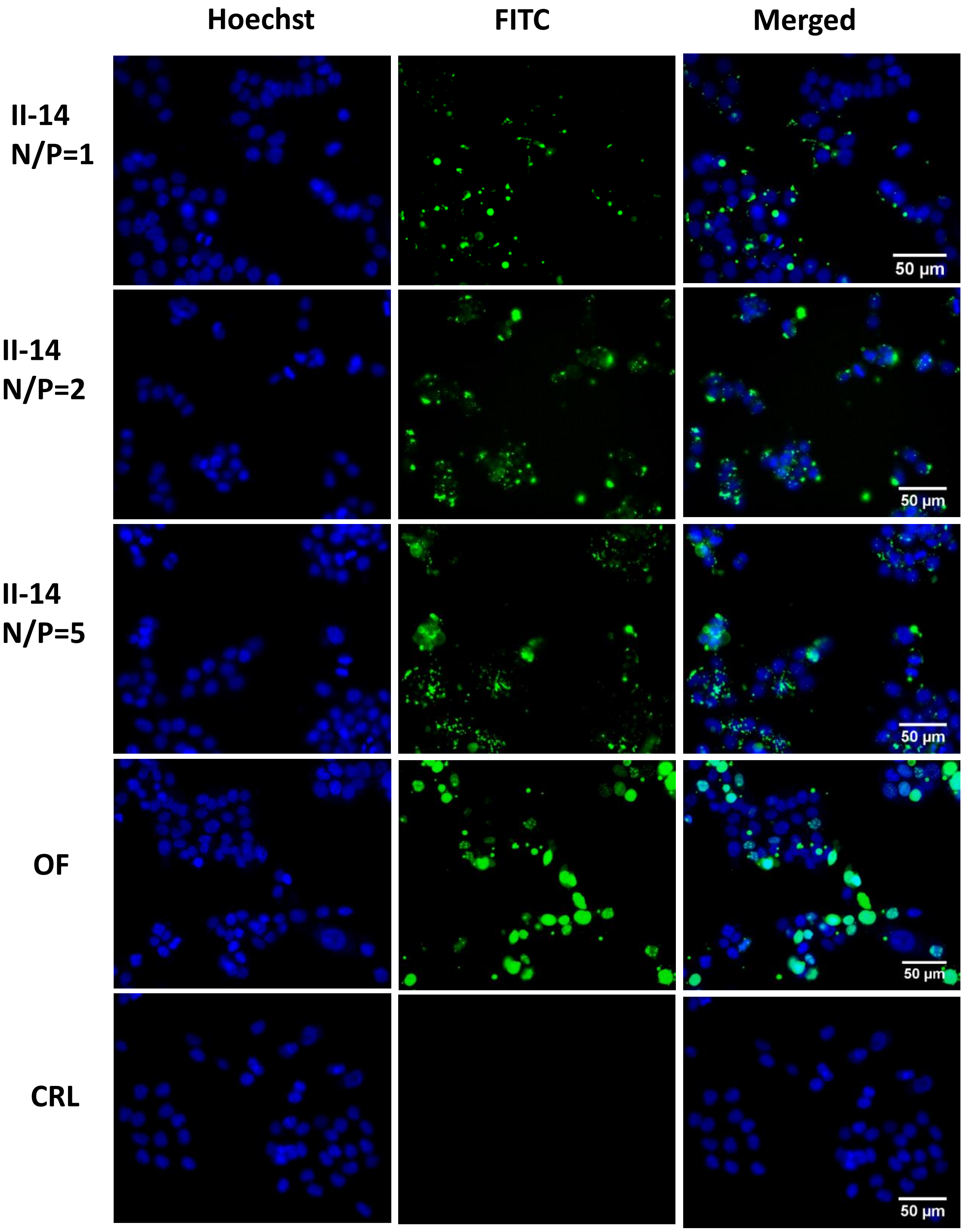

Figure 3.21. High content images of HCT 116 cells transfected with FITC-labelled c-Myc AON using II-14 at different N/P ratios. Oligofectamine™ (OF) was used as positive control and naked c-Myc AON was used as negative control. The nuclei were stained with Hoechst 33342, ×20 magnification.

As it could be observed, all of the peptides were able to transfect the HCT 116 cells successfully at all of the tested N/P ratios whereas the naked AONs were unable to enter the cells; nevertheless, increasing the peptide to nucleic acid ratio (N/P ratio) resulted in higher cellular uptake of the AONs. Moreover, at lower N/P ratios, the peptide-AON complexes appeared as small dots localized to one region of the perinuclear area whereas at higher N/P ratios larger complexes were formed which covered the entire perinuclear area. The transfection efficiency of the peptides (the proportion of the cells in the population which were successfully transfected) was comparable to the commercial transfection reagent Oligofectamine™ which was used as the positive control. However, the Oligofectamine™ delivered the AONs to the nuclei whereas the peptides delivered the AONs to the perinuclear area.

Figures 3.22-3.27 show HeLa cells transfected with different cationic amphiphilic peptides complexed with FITC-labelled cMyc- AON at different N/P ratios. As it could be observed the cationic amphiphilic peptides transfected Hela cells successfully, with the level of cellular uptake being directly proportional to the peptide to nucleic acid ratio. However, the cellular uptake of the peptide-AON complexes was lower than HCT 116 cells and the complexes were more distributed within the cytoplasm. Transfection of HDF cells with the peptide-AON complexes resulted in very low level of transfection at N/P ratios less than 5 and only at N/P ratio of 5 efficient transfection was achieved (Figures 3.28-3.33) and the peptide-AON complexes were distributed within the cytoplasm.

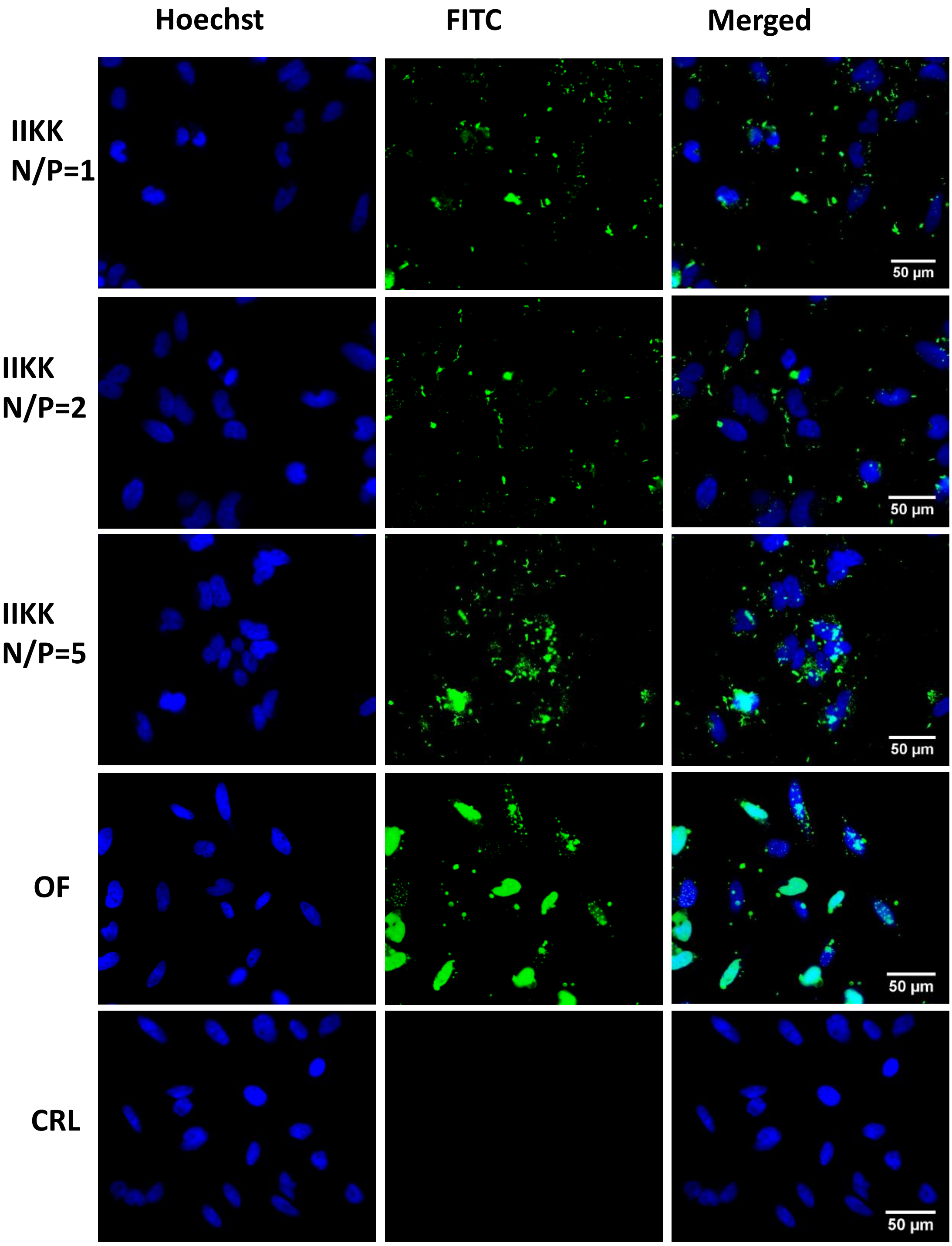

Figure 3.22. High content images of HeLa cells transfected with FITC-labelled c-Myc AON using IIKK at different N/P ratios. Oligofectamine™ (OF) was used as positive control and naked c-Myc AON was used as negative control. The nuclei were stained with Hoechst 33342, ×20 magnification.

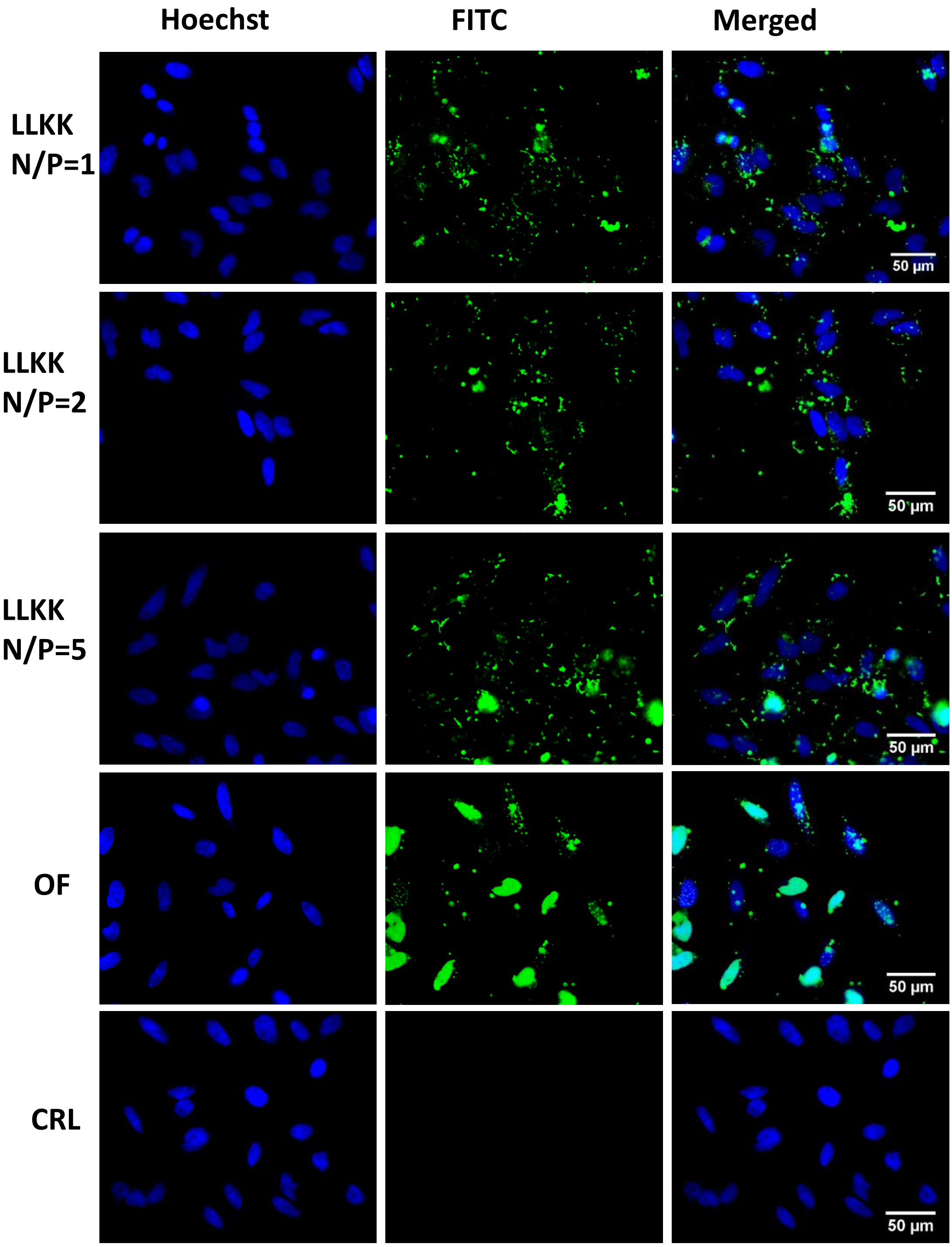

Figure 3.23. High content images of HeLa cells transfected with FITC-labelled c-Myc AON using LLKK at different N/P ratios. Oligofectamine™ (OF) was used as positive control and naked c-Myc AON was used as negative control. The nuclei were stained with Hoechst 33342, ×20 magnification.

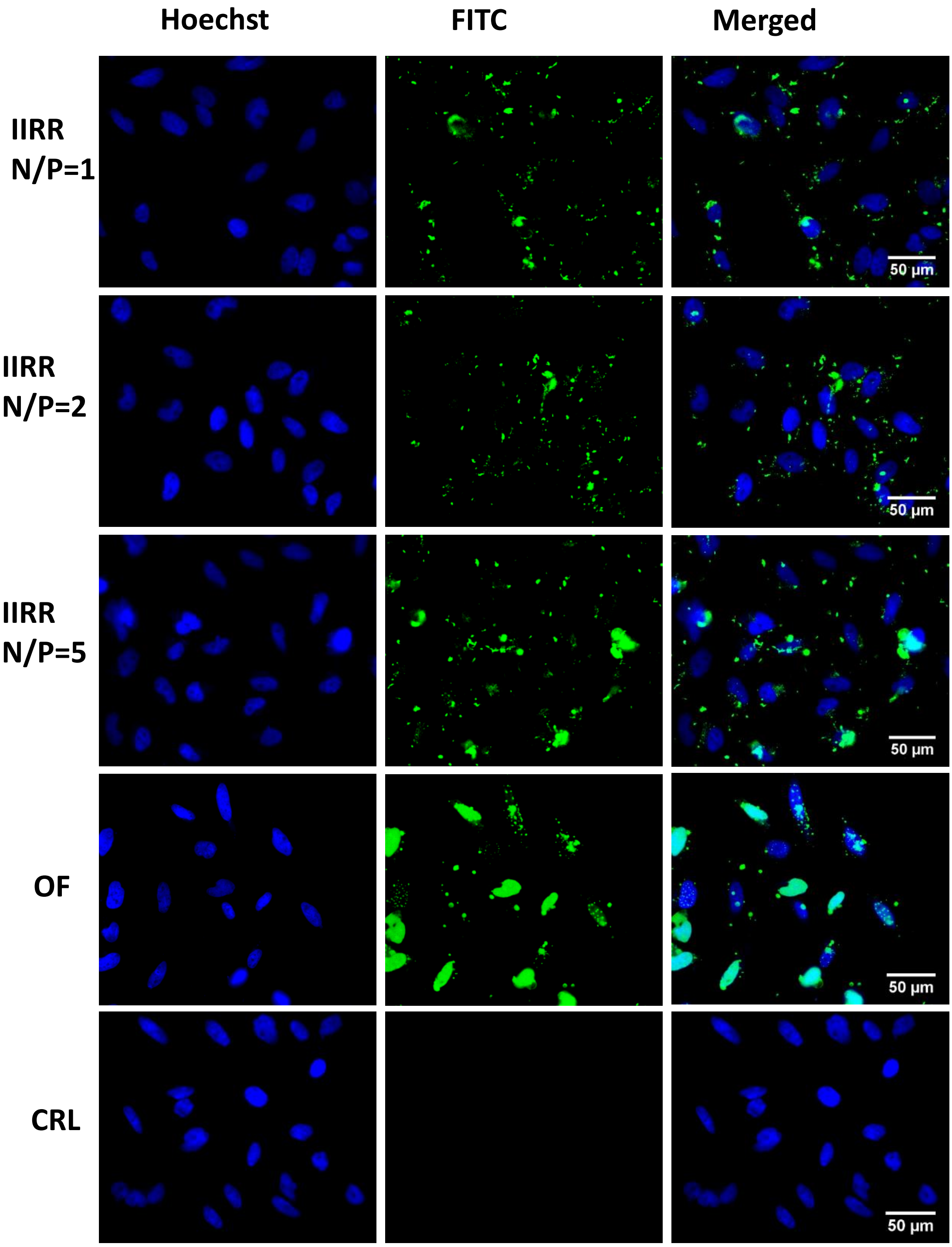

Figure 3.24. High content images of HeLa cells transfected with FITC-labelled c-Myc AON using IIRR at different N/P ratios. Oligofectamine™ (OF) was used as positive control and naked c-Myc AON was used as negative control. The nuclei were stained with Hoechst 33342, ×20 magnification.

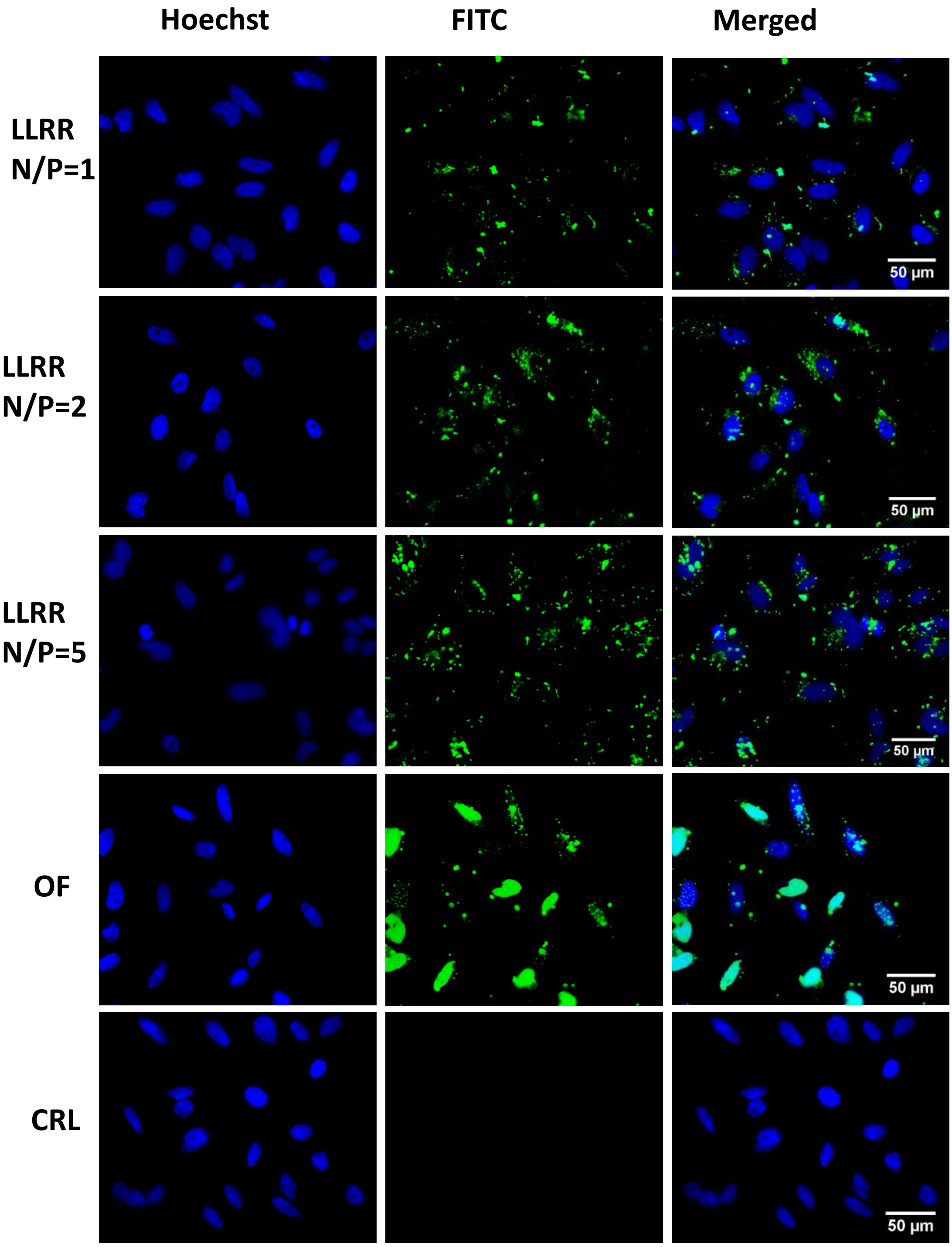

Figure 3.25. High content images of HeLa cells transfected with FITC-labelled c-Myc AON using LLRR at different N/P ratios. Oligofectamine™ (OF) was used as positive control and naked c-Myc AON was used as negative control. The nuclei were stained with Hoechst 33342, ×20 magnification.

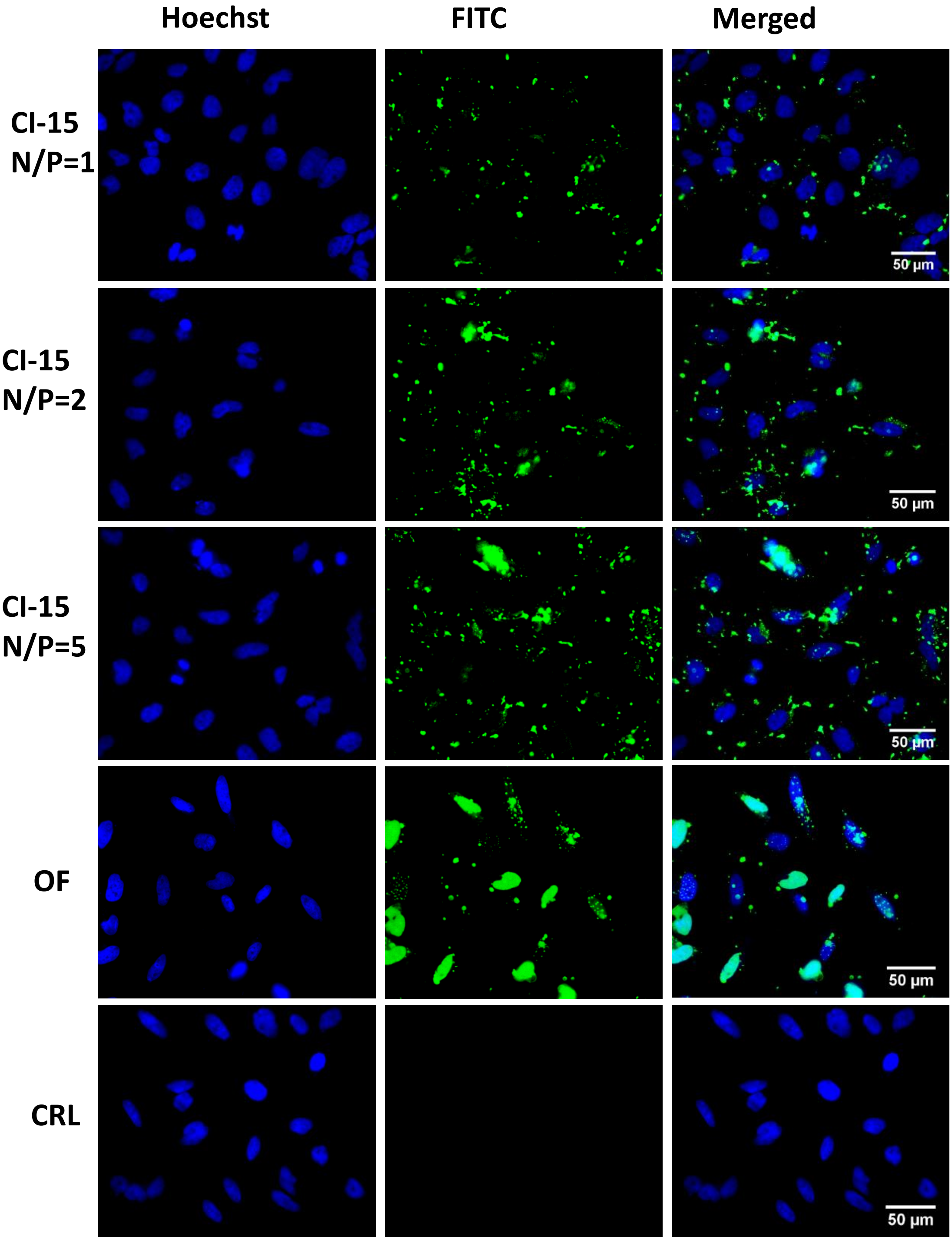

Figure 3.26. High content images of HeLa cells transfected with FITC-labelled c-Myc AON using CI-15 at different N/P ratios. Oligofectamine™ (OF) was used as positive control and naked c-Myc AON was used as negative control. The nuclei were stained with Hoechst 33342, ×20 magnification.

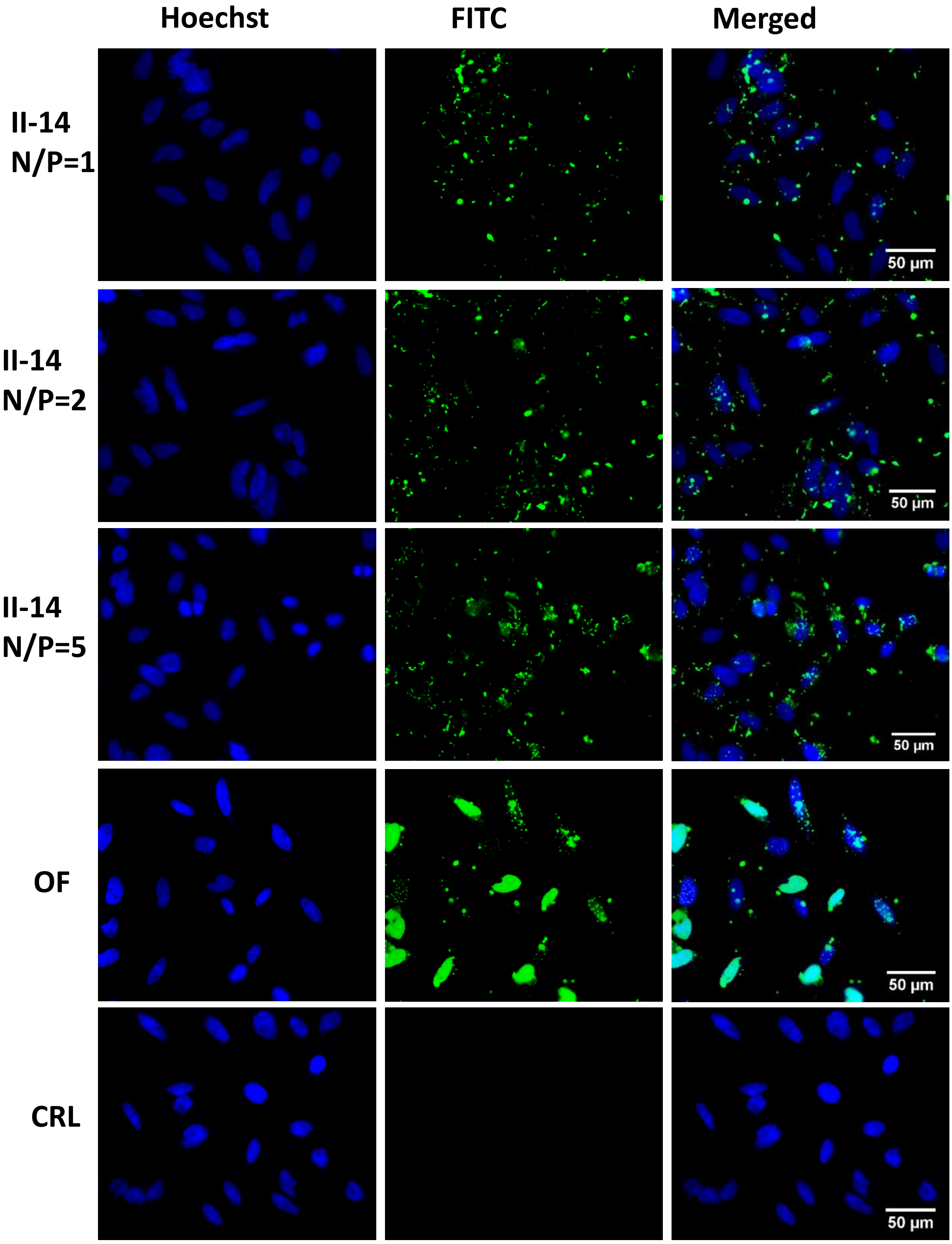

Figure 3.27. High content images of HeLa cells transfected with FITC-labelled c-Myc AON using II-14 at different N/P ratios. Oligofectamine™ (OF) was used as positive control and naked c-Myc AON was used as negative control. The nuclei were stained with Hoechst 33342, ×20 magnification.

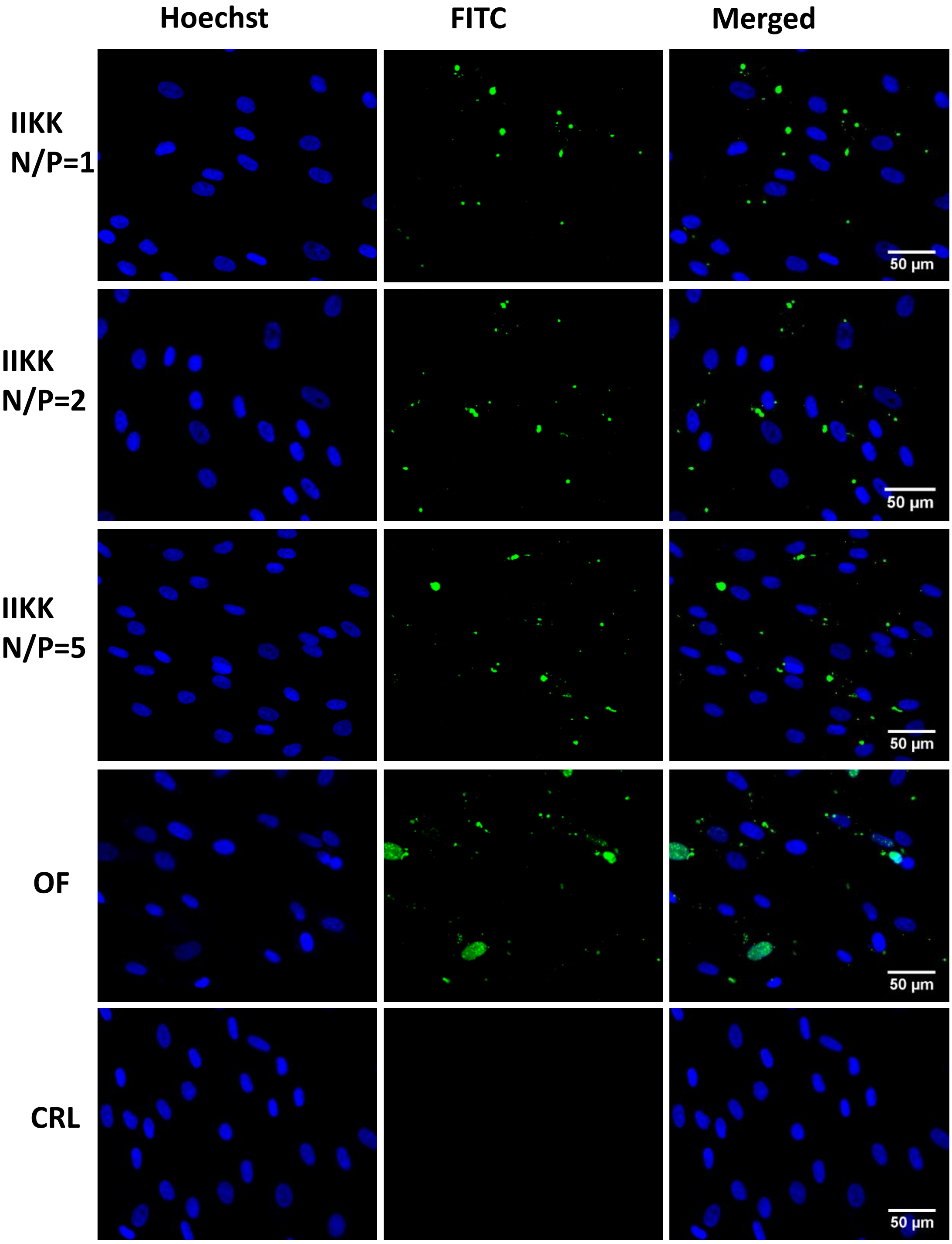

Figure 3.28. High content images of HDF cells transfected with FITC-labelled c-Myc AON using IIKK at different N/P ratios. Oligofectamine™ (OF) was used as positive control and naked c-Myc AON was used as negative control. The nuclei were stained with Hoechst 33342, ×20 magnification.

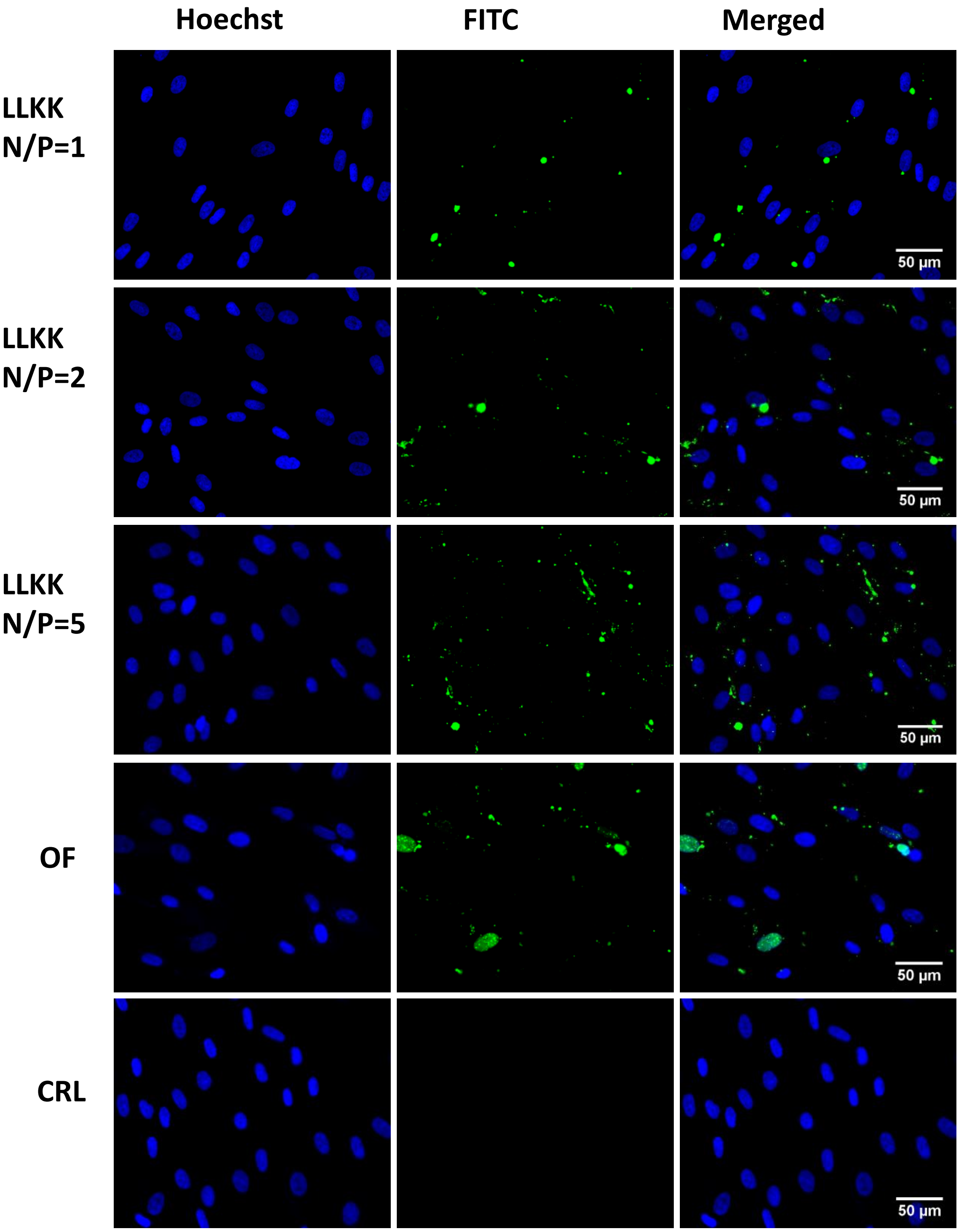

Figure 3.29. High content images of HDF cells transfected with FITC-labelled c-Myc AON using LLKK at different N/P ratios. Oligofectamine™ (OF) was used as positive control and naked c-Myc AON was used as negative control. The nuclei were stained with Hoechst 33342, ×20 magnification.

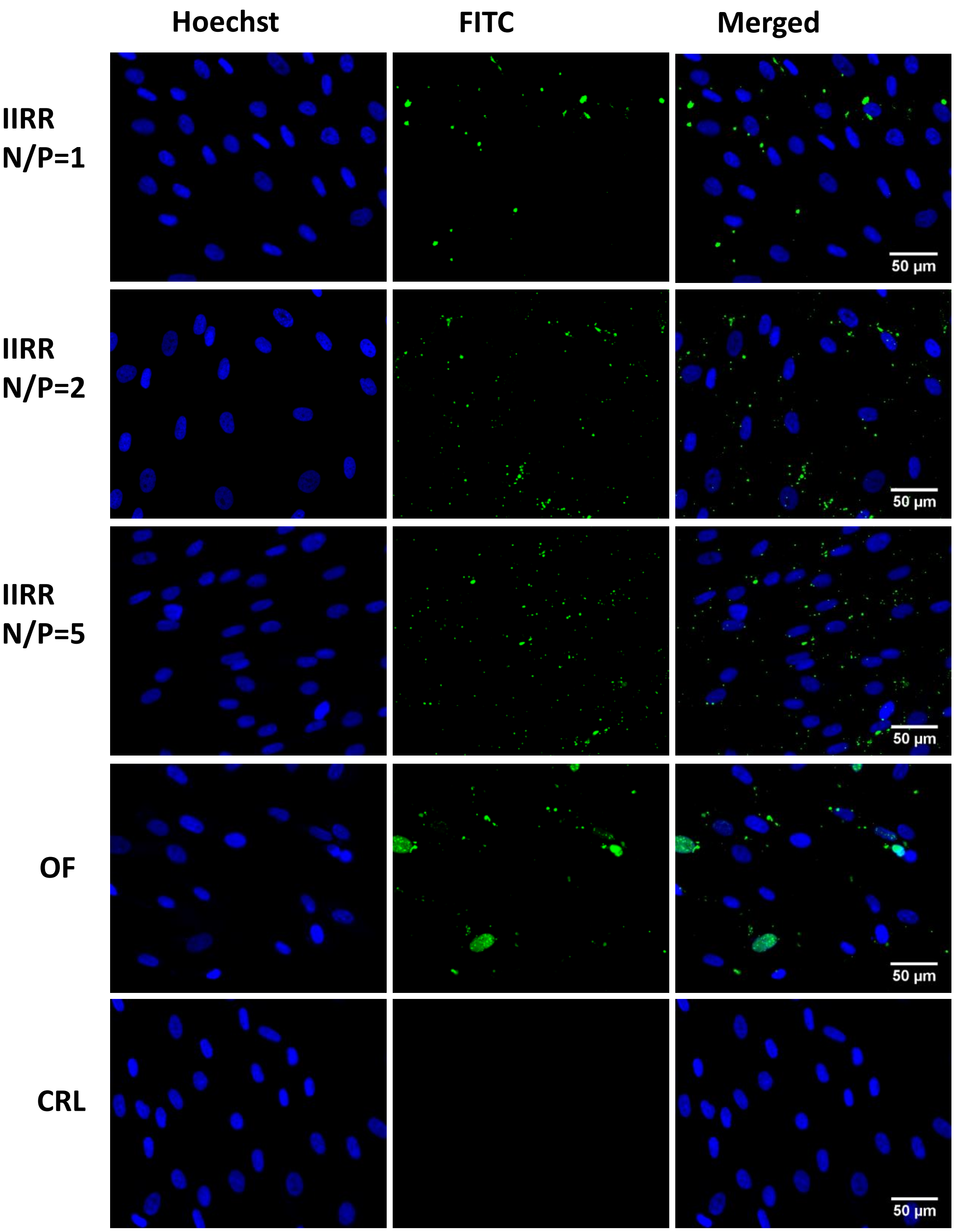

Figure 3.30. High content images of HDF cells transfected with FITC-labelled c-Myc AON using IIRR at different N/P ratios. Oligofectamine™ (OF) was used as positive control and naked c-Myc AON was used as negative control. The nuclei were stained with Hoechst 33342, ×20 magnification.

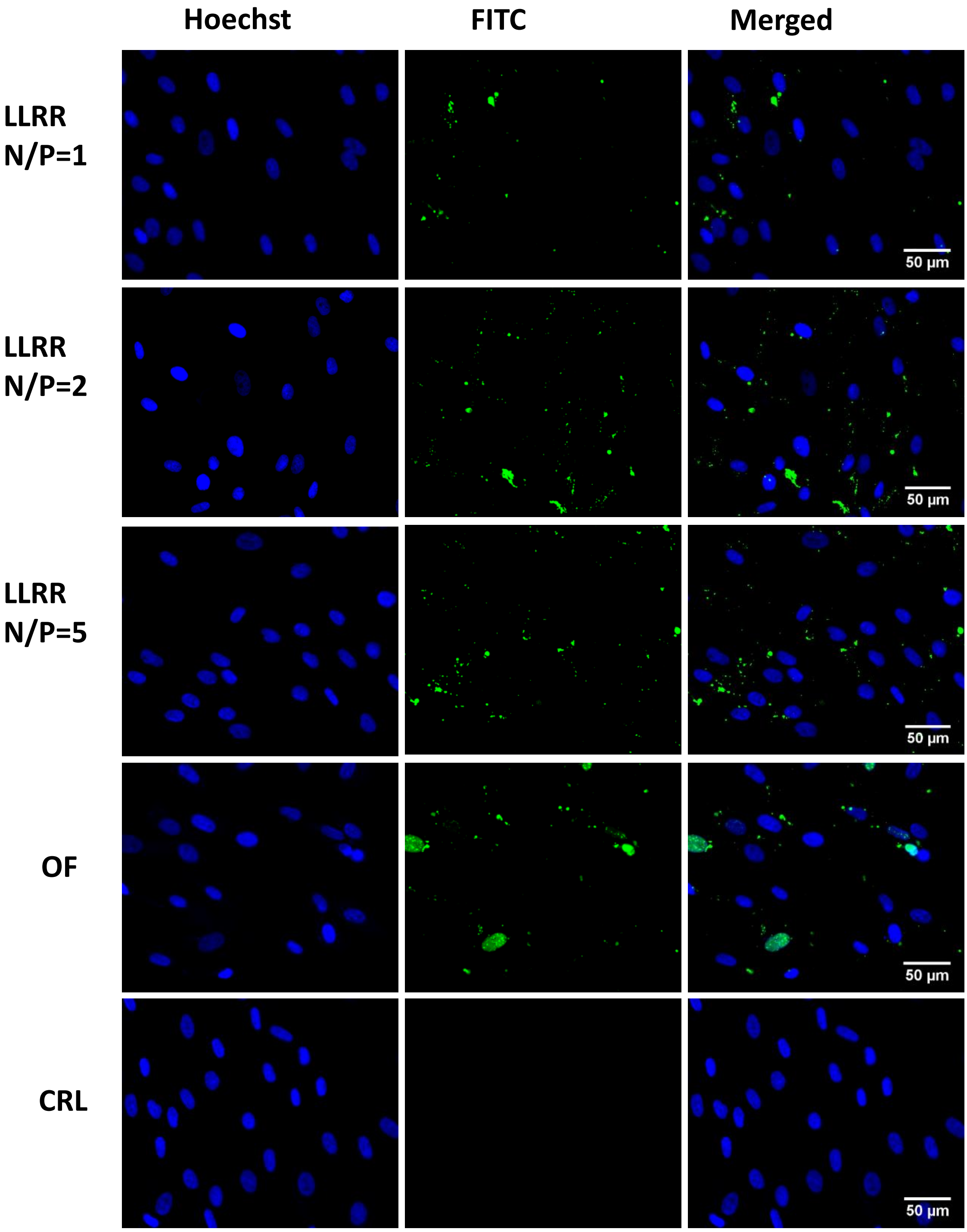

Figure 3.31. High content images of HDF cells transfected with FITC-labelled c-Myc AON using LLRR at different N/P ratios. Oligofectamine™ (OF) was used as positive control and naked c-Myc AON was used as negative control. The nuclei were stained with Hoechst 33342, ×20 magnification.

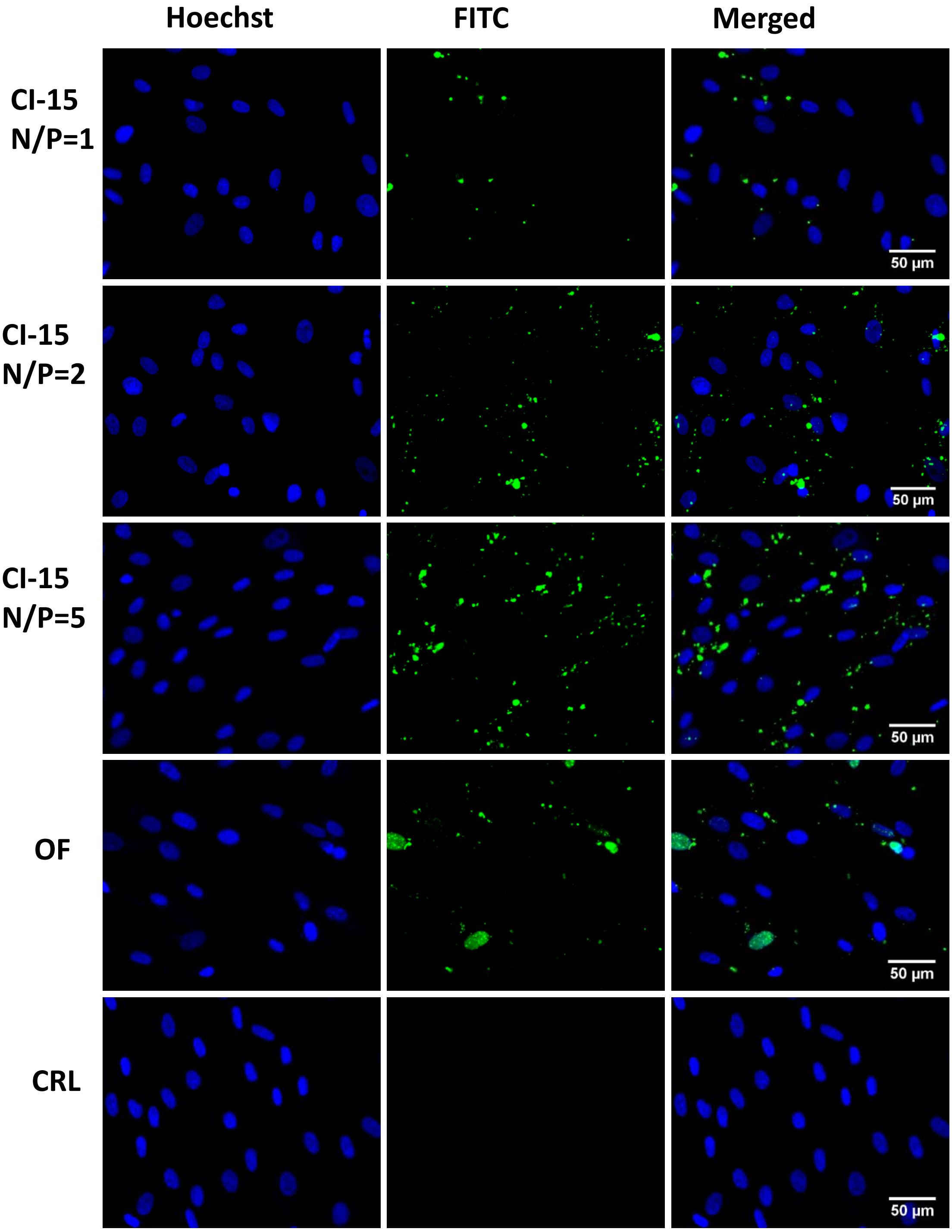

Figure 3.32. High content images of HDF cells transfected with FITC-labelled c-Myc AON using CI-15 at different N/P ratios. Oligofectamine™ (OF) was used as positive control and naked c-Myc AON was used as negative control. The nuclei were stained with Hoechst 33342, ×20 magnification.

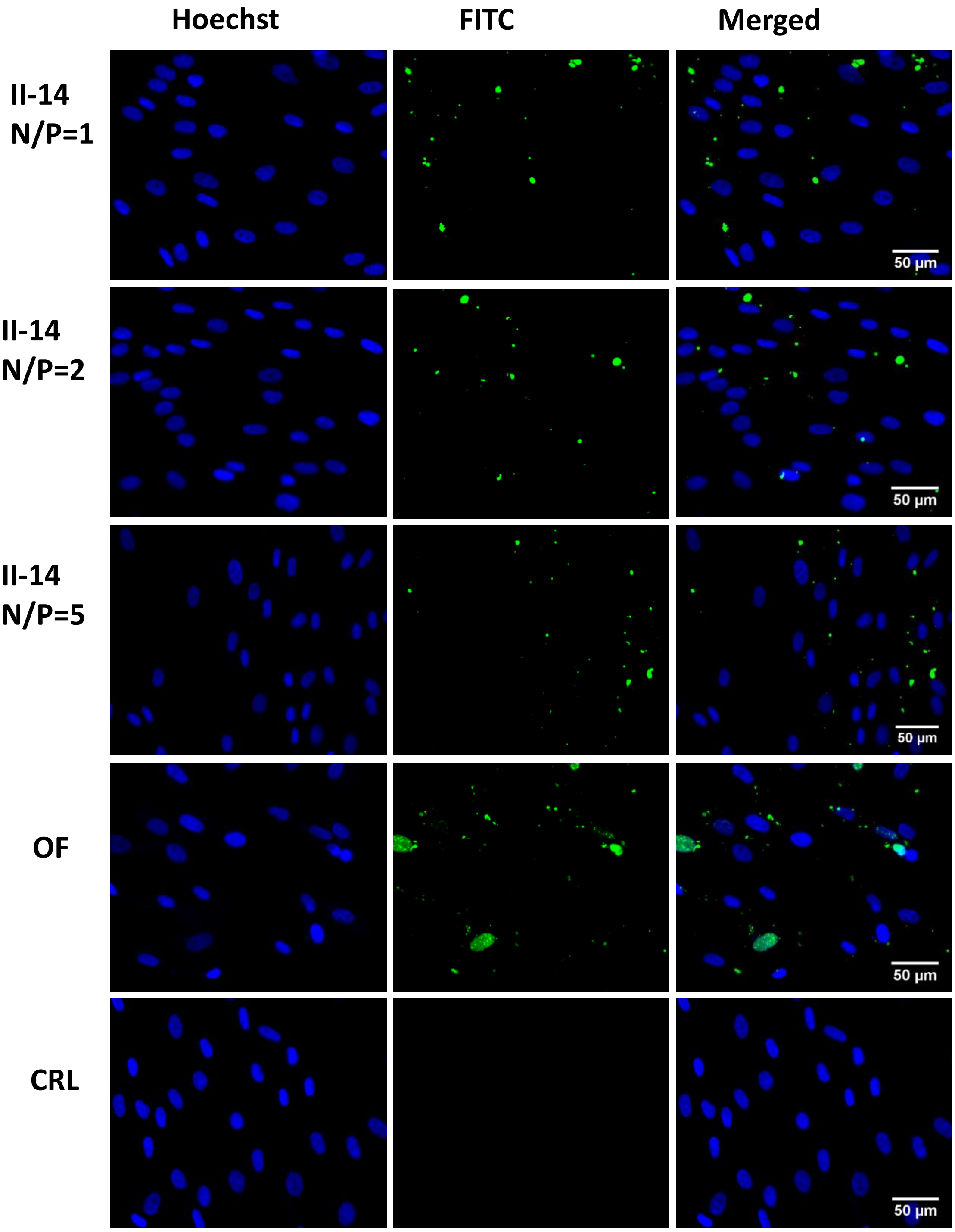

Figure 3.33. High content images of HDF cells transfected with FITC-labelled c-Myc AON using II-14 at different N/P ratios. Oligofectamine™ (OF) was used as positive control and naked c-Myc AON was used as negative control. The nuclei were stained with Hoechst 33342, ×20 magnification.

The higher cellular uptake of the peptide-AON complexes by the cancer cells compared to the normal cells suggests some degree of selectivity for cancer cells. This could be due to the more effective interaction of the peptides with the cancer cell membranes compared to the normal cell membranes as the cancer cells are supposed to be more negatively charged than normal cells as a result of higher content of polysaccharides attached to their outer leaflet and could therefore interact more strongly with the positively charged amphiphilic peptides. Other possible contributing factors could be the higher metabolic activity of the cancer cells compared to the normal cells necessitating the higher uptake of the nutrients from the extracellular environment or the higher expression of the cell surface receptors which are involved in the cellular entry of the peptide-AON complexes. Nevertheless, since the exact cellular uptake mechanisms and entry pathways of the peptides are not studied here, there is no data available to support any of the above-mentioned assumptions.

3.3.6 Transfection with siRNA

Following successful transfection of the cancer cells with peptide-AON complexes, the ability of the cationic amphiphilic peptides to deliver siRNA to the cells was assessed using two different types of siRNA targeting the ECT2 and the UBB genes, following the protocol described in chapter 2 Section 12. Both ECT2 and UBB are involved in the cell proliferation and silencing these genes with siRNA is known induce apoptosis in the cells. Since these genes are more highly expressed in cancer cells than non-cancerous cells, they serve as good targets for cancer treatment [27-28].

In order to verify the ability of the ECT2-siRNA and the UBB-siRNA to induce apoptosis in the cancer cells used in this study, HCT 116 cells were first transfected with ECT2-siRNA and UBB-siRNA using the commercial transfection reagent Dharmafect1™ and after 72 h incubation the total number of cells were counted and compared to the untreated control cells (Figure 3.34). As it could be observed both ECT2-siRNA and UBB-siRNA managed to reduce the number of cells considerably compared to the control. Although the scrambled non-targeting siRNA also reduced the number of cells significantly compared to the control, the extent of decrease in cell number induced by the ECT2 and UBB siRNA was several folds higher than the scrambled siRNA. The observed reduction in the cell number achieved by the non-targeting siRNA is supposed to be in part due to the cytotoxic effect of the transfection reagent itself as the lipid based transfection reagents are shown to have high cytotoxicity in various cell lines, which is the main reason they are not considered for clinical applications and are only used for investigational purposes.

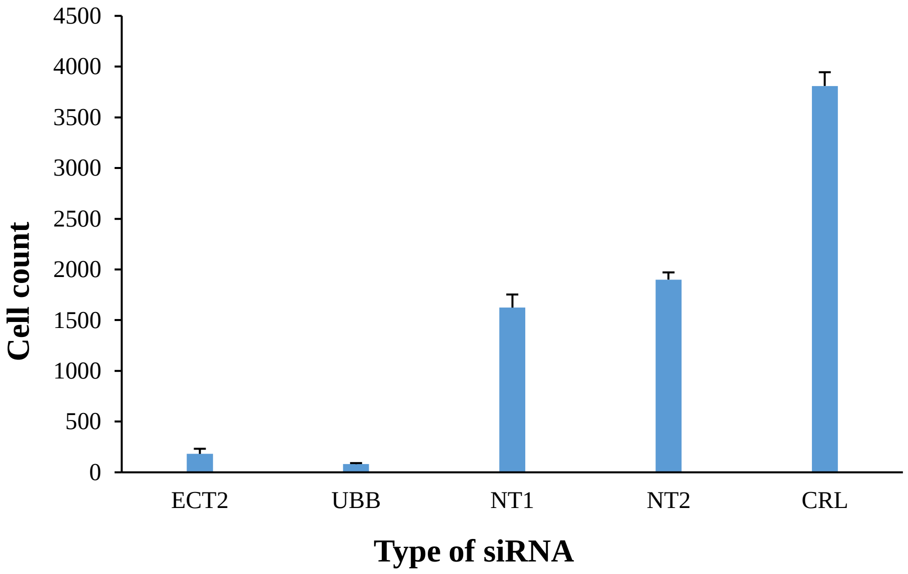

Figure 3.34. Reduction in the number of HCT 116 cells as a result of transfection with ECT2-siRNA and UBB-siRNA using Dharmafect1™. Scrambled non-targeting siRNA (NT1 and NT2) were used for comparison.

Figures 3.35-3.38 illustrate the efficiency of the cationic amphiphilic peptides for delivering ECT2-siRNA and UBB-siRNA to HCT 116 cells. Successful transfection results in silencing of ECT2 and UBB genes which leads to reduction in the number of cells compared to the untreated controls.

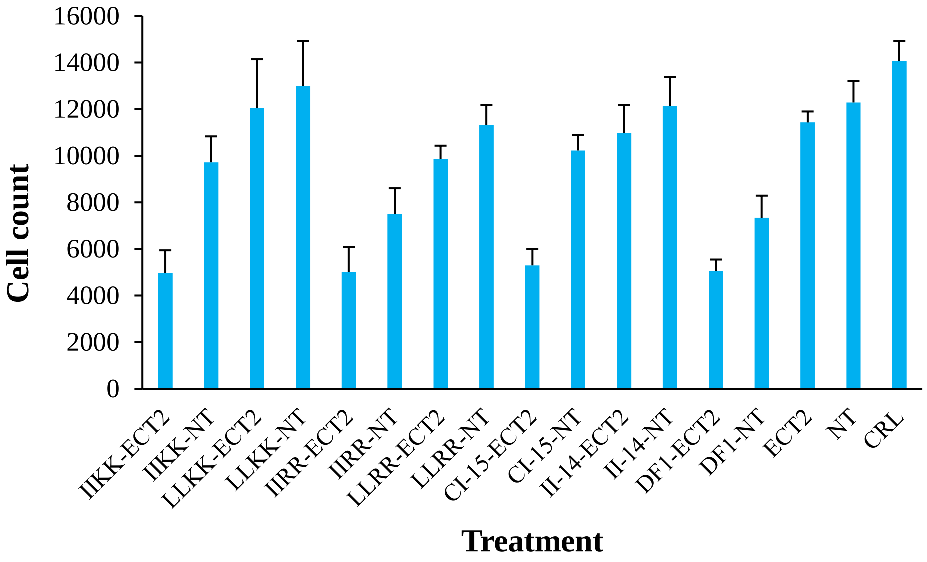

Figure 3.35. Reduction in the number of HCT 116 cells following transfection with ECT2-siRNA and scrambled non-targeting siRNA using the cationic amphiphilic peptides. Dharmafect1™ was used as positive control.

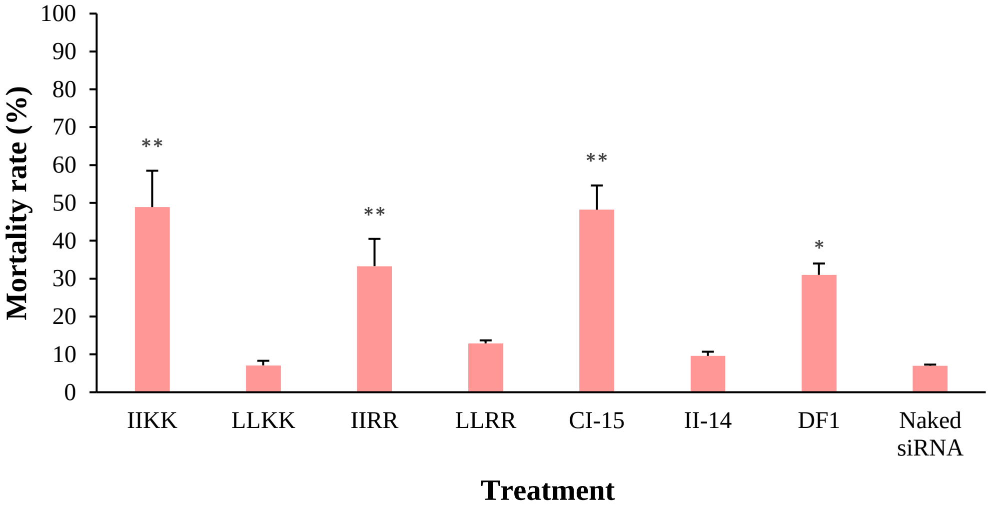

Figure 3.36. ECT2 gene silencing in HCT 116 cells transfected with ECT2-siRNA using the cationic amphiphilic peptides. The data were normalized against non-targeting siRNA. Dharmafect1™ was used as positive control. * indicates values of $p < 0.05$ and ** indicates values of $p < 0.005$ as compared to naked siRNA.

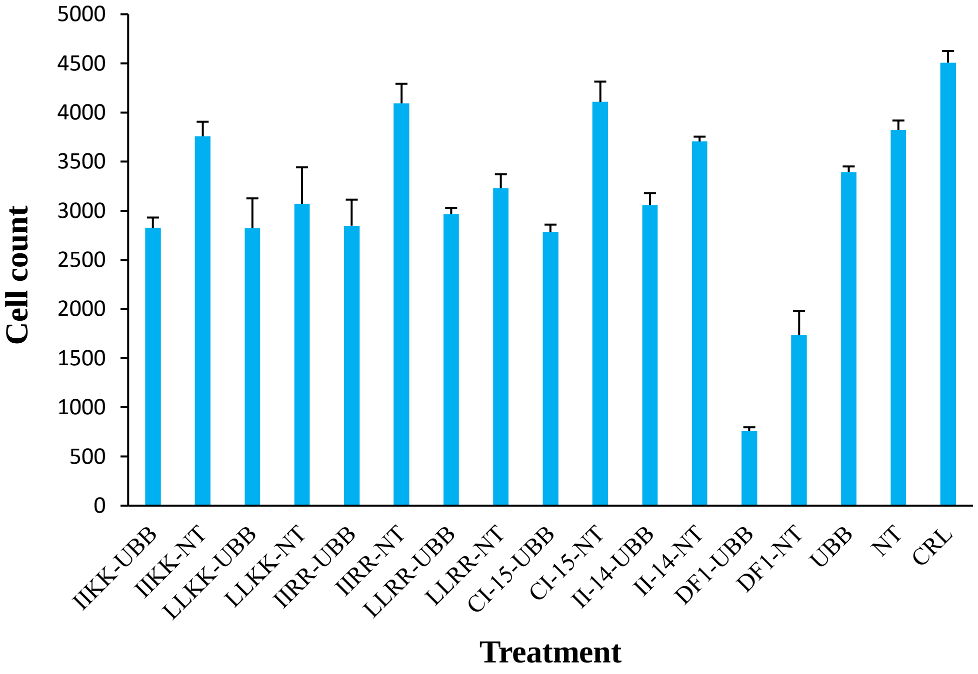

Figure 3.37. Reduction in the number of HCT 116 cells following transfection with UBB-siRNA and scrambled non-targeting siRNA using the cationic amphiphilic peptides. Dharmafect1™ was used as positive control.

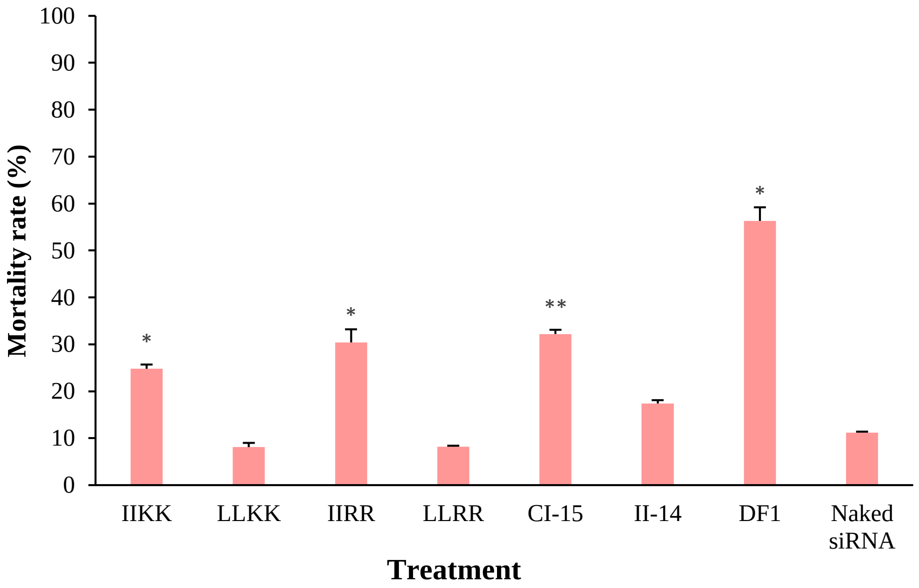

Figure 3.38. UBB gene silencing in HCT 116 cells transfected with UBB-siRNA using the cationic amphiphilic peptides. The data were normalized against non-targeting siRNA. Dharmafect1™ was used as positive control. * indicates values of $p < 0.05$ and ** indicates values of $p < 0.005$ as compared to naked siRNA.

Comparing the average cell counts in the HCT 116 cells transfected with ECT2 siRNA using the cationic amphiphilic peptides with untreated controls showed significant reduction in the cell number when the cells were transfected using IIKK, IIRR and CI-15 which was comparable to Dharmafect1™, whereas transfection with LLRR, LLKK and II-14 did not reduce the cell number significantly compared to the control. Nevertheless, transfection of the HCT 116 cells with the scrambled non-targeting siRNA using IIKK, IIRR, CI-15 and Dharmafect1™ also induced significant decrease in cell number compared to the controls, although it was much lower than the cells transfected with ECT2.

It could be inferred from these data that transfecting the HCT 116 Cells with siRNA using IIKK, IIRR, CI-15 and Dharmafect1™ induced some level of reduction in the cell number regardless of the type of siRNA which is obviously not resulting from the gene silencing induced by the siRNA and is most likely due to the general cytotoxicity caused by the transfection complex. This is supposed be either due to the partial cell membrane disruption caused by the peptides during cellular entry or due to the general effects of siRNA on the cellular machinery and enzymes which are involved in their function and metabolism. Hence, to decouple the antiproliferative/apoptotic effect from the general cytotoxic effect caused by transfection, and determine the net gene silencing effect, the mortality rates in the cells transfected with ECT2 siRNA were normalized against the non-targeting siRNA and then compared to the naked siRNA as the negative control.

As it could be observed, IIKK, LLKK and CI-15 induced considerable gene silencing (presented as mortality rate) compared to the naked siRNA which was even higher than Dharmafect1™ which was used as the positive control. A similar trend was observed following transfection of HCT 116 cells with UBB siRNA using the cationic amphiphilic peptides. Nonetheless, IIKK and CI-15 induced higher mortality in HCT 116 cells when complexed with ECT2 siRNA compared to UBB siRNA, whereas Dharmafect1™ induced higher mortality when complexed with UBB siRNA.

Transfection of HDF cells with ECT2 siRNA complexed with cationic amphiphilic peptides resulted in higher mortality rate with IIKK, IIRR and CI-15 compared to the naked siRNA which was comparable to or higher than Dharmafect1™ whereas the other peptides failed to induce any significant gene silencing in these cells (Figures 3.39-3.40). However, the gene silencing induced by these peptides and also by Dharmafect1™ was considerably lower than HCT 116 which is supposed to be in part due to the lower expression of ECT2 in these cells compared to cancer cells in general and HCT 116 in particular and in part as a result of lower cellular uptake of the peptide-siRNA complexes by HDFs than HCT 116 in the same way as c-Myc AON transfection.

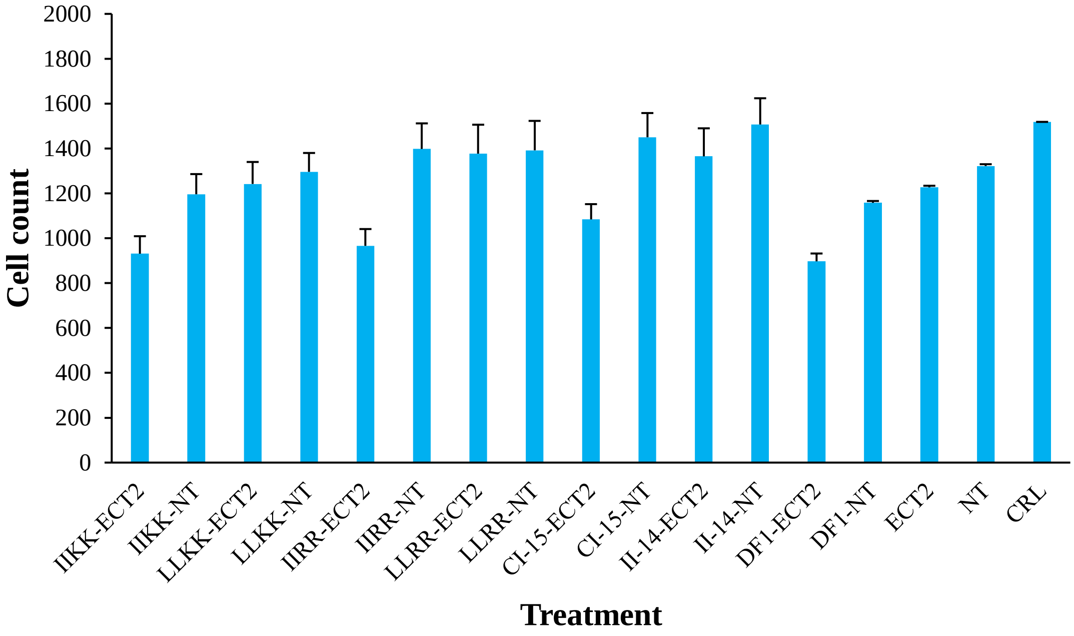

Figure 3.39. Reduction in the number of HDF cells following transfection with ECT2-siRNA and scrambled non-targeting siRNA using the cationic amphiphilic peptides. Dharmafect1™ was used as positive control.

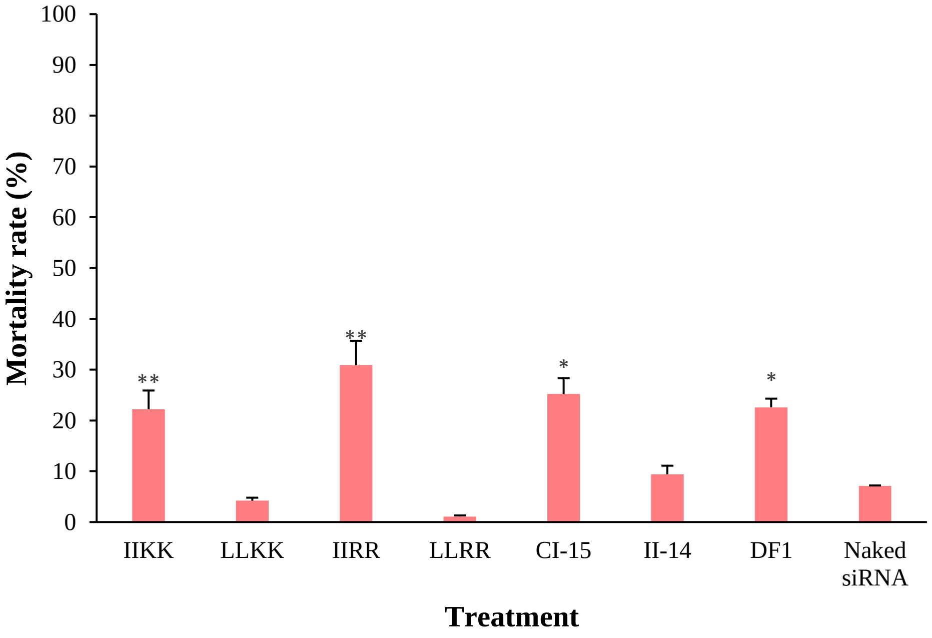

Figure 3.40. ECT2 gene silencing in HDF cells transfected with UBB-siRNA using the cationic amphiphilic peptides. The data were normalized against non-targeting siRNA. Dharmafect1™ was used as positive control. * indicates values of $p < 0.05$ and ** indicates values of $p < 0.005$ as compared to naked siRNA.

Considering all the above-mentioned data, it could be concluded that the cationic amphiphilic peptides containing Isoleucine in their hydrophobic domain were capable of delivering siRNA to both HCT 116 colorectal cancer cells and normal fibroblast cells and inducing gene silencing in these cells whereas peptides with leucine residues as their hydrophobic amino acids, were not able to induce any gene silencing in neither of the two cell lines. Furthermore, replacing the cysteine in the N-terminal of the isoleucine-rich peptide CI-15 with LC-Propargylglycine, diminished the transfection efficiency of the resulting peptide, II-14 suggesting the importance of the N-terminal cysteine for efficient gene delivery.

The low transfection efficiency of these peptides could be caused by poor electrostatic interaction between the peptide and siRNA resulting in weak complex formation or contrastingly, by very strong complexation between the peptide and the siRNA which would prevent dissociation of the siRNA from the peptide within the cytosol and thus prevent the siRNA from accessing the cellular machinery required for its biological action. Although the complexation and successful delivery of cMyc AONs to the cells (Section 3.5) indicates the ability of the peptides for complexation with nucleic acids there is still possibility of different affinity of the peptides for siRNA compared to AONs due to the structural differences between the two types of nucleic acids as AONs are single stranded DNA whereas siRNA are double stranded RNA. To investigate the two suggested possibilities, the complexation of the peptides with siRNA and AONs were studied by measuring the changes to the zeta potential of the nucleic acids following incubation with the cationic amphiphilic α-helical peptides at different N/P ratios. Change of the zeta potential from the negative values for the nucleic acids to the neutral or positive values is indicative of complex formation between the peptide and the nucleic acid and the magnitude of the positive zeta potential is proportional to the strength of the resulting peptide-nucleic acid complexes [29-31].

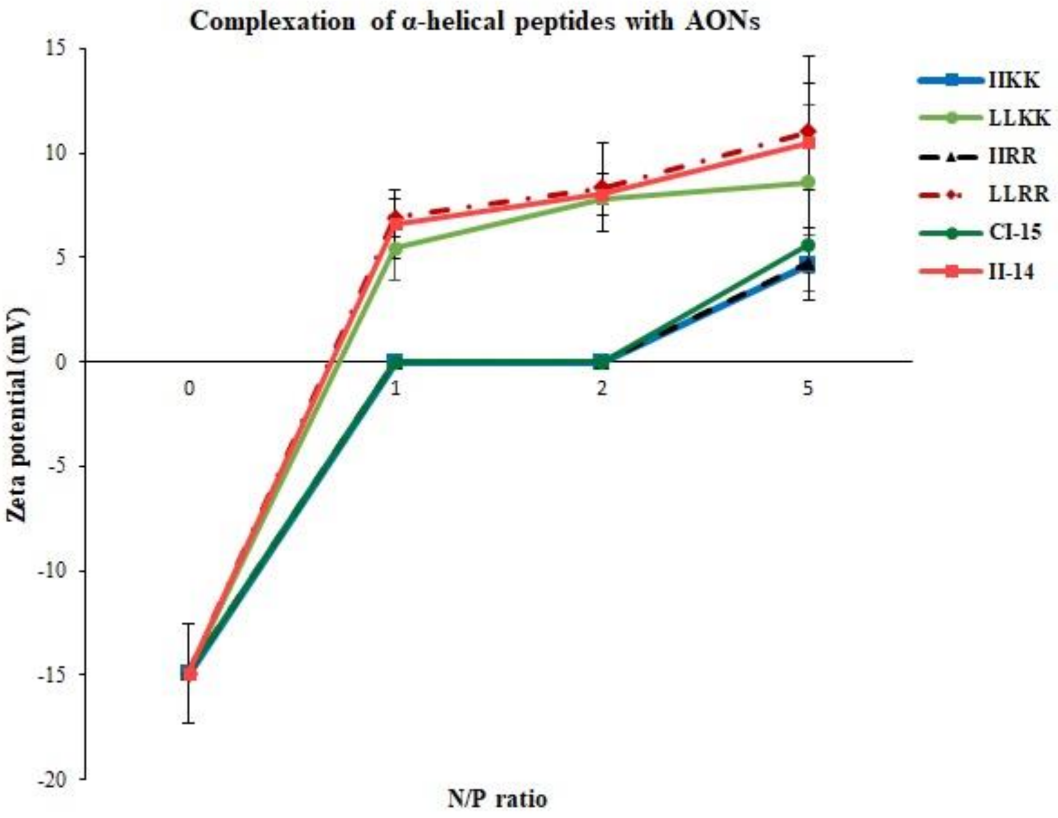

Figure 3.41. Changes to the zeta potential of the cMyc Antisense oligonucleotides (AONs) following complexation with cationic amphiphilic α-helical peptides at different N/P ratios. Values at N/P = 0 indicate the zeta potential of the naked AON. The data are reported as the average of three measurements.

As it could be observed in Figure 3.41, all of the cationic amphiphilic α-helical peptides formed complexes with AONs even and changed the values of zeta potential to near neutral or positive in all the N/P ratios indicating complex formation which is consistent with the results from transfection studies (Section 3.5). The values of zeta potential increased with increasing the N/P ratio from 1 to 5 which indicates stronger complexation due to increased peptide concentration. As it could be observed, there is a clear distinction between the peptides which were capable of inducing gene silencing in the cells (IIKK, IIRR, CI-15) and those which were unable to do so (LLKK, LLRR, II-14) in terms of the values of zeta potential and the former group show considerably lower zeta potential than the latter. This suggests the stronger complexation between the leucine-rich peptides and II-14 which is in favour of the assumption that the observed lack of gene silencing by these peptides is due to strong complexation with siRNA which does not allow for release of the siRNA inside the cells. To further confirm this, the complexation of the peptides with siRNA at the same N/P ratio which was used for the gene silencing (N/P =5) was studied as presented in Figure 3.42. A similar trend was observed for peptide-siRNA complexation and the order of increase in the zeta potential was similar to that observed for peptide-AON complexation further indicating stronger complex formation as the likely reason for lack of gene silencing.

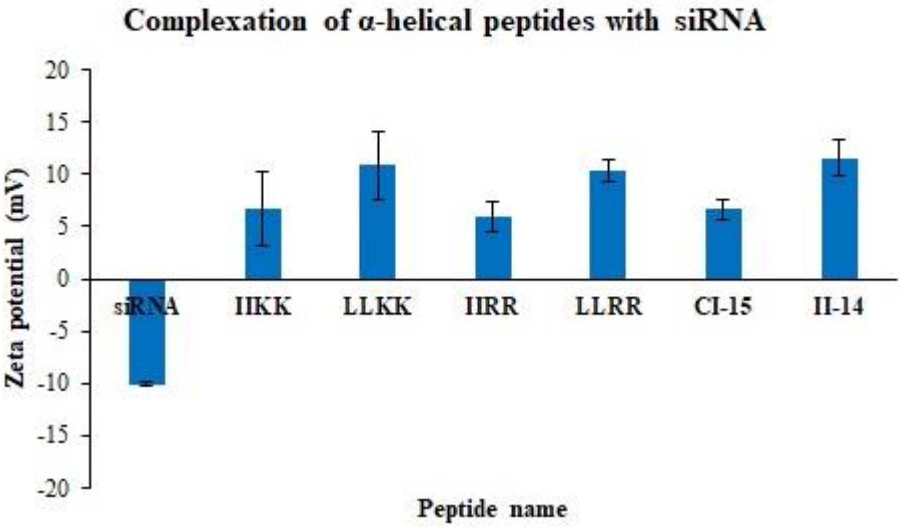

Figure 3.42. Changes to the zeta potential of the siGLO™ red siRNA following complexation with cationic amphiphilic α-helical peptides at the N/P ratio of 5.

3.4 Conclusion

A series of α-helical cationic amphiphilic peptides were rationally designed based on the structural requirements for antimicrobial and anticancer peptides and were evaluated for their anticancer activity as well as their gene delivery potential. The peptides exhibited varying levels of toxicity in different cell lines suggesting some level of selectivity. Peptides containing lysine showed higher toxicity towards cancer cells than fibroblasts which indicates selective anticancer activity. Increasing the chain length of these peptides by adding one or two isoleucine residues increased their toxicity towards HCT 116 and HeLa, whereas replacing isoleucine with leucine made the peptide selectively toxic against HCT 116. On the other hand, peptides containing arginine had higher toxicity in fibroblasts and MDA 231-MB than HCT 116 and HeLa. In general, MDA 231-MB cells appeared to be less responsive to the cationic amphiphilic peptides than the other cancer cell lines.

The cytotoxic peptides decreased the metabolic activity of the cells by damaging the mitochondria which was evident from the changes to the morphology and distribution pattern of the mitochondria and also mitochondrial membrane depolarization in the cells treated with these peptides compared to the normal phenotype in the untreated control cells. The peptides composed of leucine with either arginine or lysine exhibited antiproliferative effect and decreased the number of cells whereas their isoleucine containing counterparts did not reduce the number of the cells and mainly exerted their toxic effect via damaging the cells and decreasing their metabolic activity without actually killing the cells. However, increasing the chain length of the isoleucine containing peptides by adding one or two isoleucine residues, bestowed antiproliferative activity on the resulting peptides.

All of the designed cationic amphiphilic peptides were able to bind to the cMyc- AON and to deliver it to the cancer cells in a concentration-dependent manner, i.e., increased cellular uptake of the peptide-AON complexes by increasing the peptide to AON ratio. On the other hand, the transfection efficiency in fibroblasts was much lower than the cancer cells and higher concentrations of the peptides were required for efficient delivery of the AONs to these cells, which suggests the cationic amphiphilic peptides as gene vectors with higher selectivity for cancer cells compare to normal noncancerous cells. Among all of the cationic amphiphilic peptides, the peptides consisting of isoleucine residues in their hydrophobic domain delivered ECT2-siRNA and UBB-siRNA to HCT116 cells efficiently, and ECT2-siRNA to HDF cells with lower efficiency, whereas their leucine containing counterparts failed to do so. Also, replacing the N-terminal cysteine with LC-Propargylglycine resulted in low transfection efficiency suggesting the importance of the N-terminal cysteine for successful gene delivery. The higher gene delivery efficiency of the above named cationic amphiphilic peptides in HCT 116 colorectal cancer cells compared to the normal fibroblast cells shows some level of selective gene delivery to cancer cells which is desirable for a gene delivery system as it would minimize the adverse effects associated with gene therapy.

3.5 References

1. N. Wiradharma, U. Khoe, C. A.E. Hauser, et al. Synthetic cationic amphiphilic α-helical peptides as antimicrobial agents. *Biomaterials*, 32 (2011): 2204-2212.
2. J.S. Khara, Y. Wang, X.Y. Ke, et al. Anti-mycobacterial activities of synthetic cationic a-helical peptides and their synergism with rifampicin. *Biomaterials*, 35 (2014): 2032-2038.
3. P. Wanga, Y. H. Nan, S.T. Yang, et al. Cell selectivity and anti-inflammatory activity of a Leu/Lys-rich α-helical model antimicrobial peptide and its diastereomeric peptides. *Peptides*, 31 (2010): 1251-1261.

4. J. Hu, C. Chen, S. Zhang et al. Designed Antimicrobial and Antitumor Peptides with High Selectivity. *Biomacromolecules*, 12 (2011): 3839-3843.
5. Z. Jiang, A.I. Vasil, L. Gera, Rational design of α-Helical antimicrobial peptides to target gram-negative pathogens, acinetobacter baumannii and pseudomonas aeruginosa: Utilization of charge, ’specificity determinants,’ total hydrophobicity, hydrophobe type and location as design parameters to improve the therapeutic ratio. *Chem Biol Drug Des.,* 77(2011): 225-240.
6. L. A. Avila, L. RMM Aps, P. Sukthankar, N. Ploscariu, S. Gudlur, et al. Branched amphiphilic cationic oligopeptides form peptiplexes with DNA: A study of their biophysical properties and transfection efficiency. *Mol. Pharmaceutics*, 12 (2015):706-715.
7. G. N. Goparaju, P. K. Gupta. Design of amphiphilic oligopeptides as models for fine tuning peptide assembly with plasmid DNA. *Drug Discoveries Ther.*, 8(2014):165-172.
8. H. O. McCarthy, J. McCaffrey, C. M. McCrudden , A. Zholobenko, A. A. Ali, et al. Development and characterization of self-assembling nanoparticles using a bio-inspired amphipathic peptide for gene delivery. *J. Control. Release*, 189 (2014): 141-149.
9. M. Law, M. Jafari, P. Chen. Physicochemical characterization of SiRNA-peptide complexes. *Biotechnol. Prog.,* 24 (2008): 957-963.
10. D. Lejeune, N. Delsaux , B. Charloteaux, A. Thomas, R. Brasseur. Protein-nucleic acid recognition: Statistical analysis of atomic interactions and influence of DNA structure. Proteins, 61 (2005):258-271.
11. S.D.D.T.A. Jones, N.M. Luscombe, H.M. Berman, J.M. Thornton. Protein-RNA interactions: a structural analysis. Nucleic Acids Res., 29 (2001):943-954.
12. J. Guo, W. P. Cheng, J. Gu, C. Ding, X. Quc, et al. Systemic delivery of therapeutic small interfering RNA using a pH-triggered amphiphilic poly-L-lysine nanocarrier to suppress prostate cancer growth in mice. *Eur. J. Pharm. Sci.*, 45 (2012): 521-532.
13. J. Dufourcq, W. Neri, N. Henry-Toulmeè. Molecular assembling of DNA with amphipathic peptides. *FEBS Lett.*, 421 (1998): 7-11.
14. K. K. Hou, H. Pan, G. M. Lanza, S. A. Wickline. Melittin derived peptides for nanoparticle based siRNA transfection. *Biomaterials,* 34 (2013): 3110-3119.
15. H. F. Zhou, H. Yan, H.Pan, K. K. Hou, A. Akk, et al. Peptide-siRNA nanocomplexes targeting NF-κB subunit p65 suppress nascent experimental arthritis. *J. Clin. Invest.,* 124 (2014):4363-4374.

16. K. A. Mills, J. M. Quinn, S. T. Roach, M. Palisoul, M. Nguyen, et al. p5RHH nanoparticle-mediated delivery of AXL siRNA inhibits metastasis of ovarian and uterine cancer cells in mouse xenografts. *Sci. Rep.*, 9 (2019):1-10
17. Sittampalam GS, Coussens NP, Nelson H, et al., editors. Assay Guidance Manual [Internet]. Bethesda (MD): Eli Lilly & Company and the National Center for Advancing Translational Sciences; 2004.
18. T. Mosmann. Rapid colorimetric assay for cellular growth and survival: Application to proliferation and cytotoxicity assays. J. *Immunol. Methods*, 65 (1983): 55-63.
19. M. V. Berridge, P. M. Herst, and A. S. Tan. Tetrazolium dyes as tools in cell biology: New insights into their cellular reduction. *Biotechnol. Annu. Rev.*, 11(2005): 127-152.
20. D. Voet, J. G. Voet, C. W. Pratt. Fundamentals of Biochemistry (2nd ed.), 2006, John Wiley and Sons, Inc. pp. 547, 556.
21. R. Moreno-Sánchez, S. Rodríguez-Enríquez, A. Marín-Hernández, E. Saavedra. Energy metabolism in tumor cells. *FEBS J.*, 274 (2007): 1393-1418.
22. S T Smiley, M Reers, C Mottola-Hartshorn, M Lin, A Chen, T W Smith, G D Steele, L B Chen. Intracellular heterogeneity in mitochondrial membrane potentials revealed by a J-aggregate-forming lipophilic cation JC-1. *PNAS*, 88 (1991): 3671-3675.
23. M. Reers, T. W. Smith, and L. B. Chen. J-aggregate formation of a carbocyanine as a quantitative fluorescent indicator of membrane potential. *Biochemistry,* 30 (1991): 4480-4486.
24. M. Mancini, B. O. Anderson, E. Caldwell, et al. Mitochondrial proliferation and paradoxical membrane depolarization during terminal differentiation and apoptosis in a human colon carcinoma cell line. *J Cell Biol.*, 138 (1997): 449-69.
25. G. V. Kulkarni, W. Lee, A. Seth, and C. A. McCulloch. Role of mitochondrial membrane potential in concanavalin A-induced apoptosis in human fibroblasts. *Exp. Cell Res.*, 245(1998): 170-178.
26. https://www.genecards.org/cgi-bin/carddisp.pl?gene=MYC, accessed on 20/08/2019.
27. https://www.genecards.org/cgi-bin/carddisp.pl?gene=ECT2, accessed on 20/08/2019.
28. https://www.genecards.org/cgi-bin/carddisp.pl?gene=UBB, accessed on 20/08/2019.
29. M. Li, S. Schlesiger, S. K. Knauer, and C. Schmuck, Introduction of a tailor made anion receptor into the side chain of small peptides allows fine-tuning the thermodynamic signature of peptide-DNA binding. *Org. Biomol. Chem.*, 2016, 14 (2016): 8800-8803.

30. J. Coles, A. Esposito, H. T. Chuah, and I. Toth. The synthesis and characterization of lipophilic peptide-based carriers for gene delivery. *Tetrahedron*, 66 (2010): 5435-5441.
31. G. Québatte, E. Kitas, and J. Seelig. riDOM, a Cell-Penetrating Peptide. Interaction with DNA and Heparan Sulfate. *J. Phys. Chem. B,* 117 (2013): 10807-10817.

Chapter 4: biological activity of β-sheet forming peptides

4.1 Background and aims

This chapter includes the results from the evaluation of a series of short cationic amphiphilic peptides with β-sheet βsecondary structure for their ability to deliver nucleic acids to the cancer cells as well as their cytotoxicity against normal and cancer cells. The peptides were designed based on the structural features of the β-sheet forming cationic antimicrobial peptides assuming that the same structural features might enable the peptide to interact with the cancer cells as both cancer cell membranes and bacterial cell membranes are more negatively charged than normal mammalian cell membranes [1-3]. It was also assumed that the positively charged peptides containing arginine and lysine would be able to form complexes with the nucleic acids via electrostatic interactions with the negatively charged phosphate groups on the backbone of the nucleic acids and to compress them into nano-sized structures. the peptides were also supposed to interact with the cell membrane due to their amphiphilic nature and to transfer their associated nucleic acid cargo to the cells [4-14].

The aims of this chapter are:

- Designing a new series of cationic amphiphilic oligopeptides with β-sheet secondary structures based on the structural features of the antimicrobial and anticancer peptides and evaluating their potential anticancer activity as well as their ability to deliver genes to the cancer cells.
- Evaluating the selectivity of the designed cationic amphiphilic peptides for the cancer cells as compared to the normal cells in order to develop tools for selective anticancer therapy.
- Studying the structure-activity relationship of the designed cationic amphiphilic peptides in order to optimize the biological activity of the peptides through rational design.

4.2 Experimental

4.2.1 Cytotoxicity tests

The ability of the cationic amphiphilic peptides to interfere with the metabolic/enzymatic activity of the cells was assessed using the standard MTT test. The cells were treated with peptide solutions with concentrations ranging from 1 μM to 20 μM, incubated for 24-72 h at 37 °C and then subjected to MTT assay as described in chapter 2. The morphology and distribution of the mitochondria was studied using the mitochondrial probe Mitotracker™ following incubation of the cells with cationic amphiphilic peptides at concentration of 20 μM as described in chapter 2. After 72 h the mitochondria were stained using mitochondrial probe MitoTracker® Red following the protocol described in chapter 2 and imaged with high content microscope. The effect of the cationic amphiphilic peptides on the cell proliferation was measured by counting the total number of cells following incubation with different concentrations of the peptide solutions (1-20 µM). The data were normalized against untreated controls and reported as mean ± SE.

4.2.2 Transfection tests

The ability of the cationic amphiphilic peptides to form complexes with the nucleic acids and to deliver them to the cells was assessed using cMyc- antisense oligonucleotide (cMyc-AON) and small interfering RNA (siRNA) against ECT2 and UBB genes both in cancer cell lines (HCT 116 and HeLa) and in human dermal fibroblasts (HDFs) following the transfection protocols described in chapter 2. The scrambled non-targeting siRNA (NT siRNA) was used as a control to assess the net-effect of the ECT2 and UBB gene silencing on the cell proliferation without including the cell death caused by siRNA induced toxicity.

4.3 Results & discussion

4.3.1 Peptide structures

The sequences of the designed cationic amphiphilic oligopeptides are provided in Table 4.1 using the standard one letter codes for amino acids. The peptides consist of 12 amino acids, are amidated at the C-terminal and unmodified at the N-terminal.

Table 4.1. Sequences of the designed beta sheet-forming cationic amphiphilic oligopeptides.

Peptide name	Peptide sequence
IKIK	IKIKIKIKIKIK-NH2
LKLK	LKLKLKLKLKLK-NH2
LRLR	LRLRLRLRLRLR-NH2
IKIR	IKIRIKIRIKIR-NH2
IRIK	IRIKIRIKIRIK-NH2
LKLR	LKLRLKLRLKLR-NH2
LRLK	LRLKLRLKLRLK-NH2

4.3.2 Cell viability/metabolic activity

The ability of the cationic amphiphilic peptides to interfere with the metabolic activity of the cells as determined by MTT assay is depicted in Figures 4.1-4.4. Reduction of MTT by NADH-dependent and NADPH-dependent oxidoreductase enzymes is an indicative of the cellular metabolic activity [15-16]. The values of half maximal inhibitory concentration (IC_{50}) of the peptides in different cell lines, as derived from the concentration-response curves (figures S25-S52 in the supplemental data), are presented in Table 4.2. The values of IC_{50} for each replicate were calculated using the regression equation for each plot and reported as the average ± standard deviation of the 6 replicates.

Table 4.2. Values of half maximal inhibitory concentration (IC50) of the cationic amphiphilic peptides in different cell lines as determined by MTT assay. All data are reported as the Mean ± SD of 6 repeats.

Peptide	**IC_{50} in different cell lines**			
	HCT 116	**HeLa**	**MDA-MB-231**	**HDF**
IKIK	32.7 ± 4.5	8.9 ± 2.1	10.9 ± 0.5	4.4 ± 0.3
LKLK	14.5 ± 1.3	17.7 ± 6.5	> 40	> 40
LRLR	31.8 ± 2.9	> 40	34.1 ± 1.2	22.7 ± 2.4
IKIR	30.1 ± 5.2	15.5 ± 1.2	> 40	34.5 ± 0.9
IRIK	20.9 ± 2	14.5 ± 2.3	> 40	38.6 ± 0.2
LKLR	> 40	> 40	11.4 ± 1.2	24.1 ± 0.7
LRLK	> 40	> 40	14.1 ± 1.1	22.5 ± 1.4

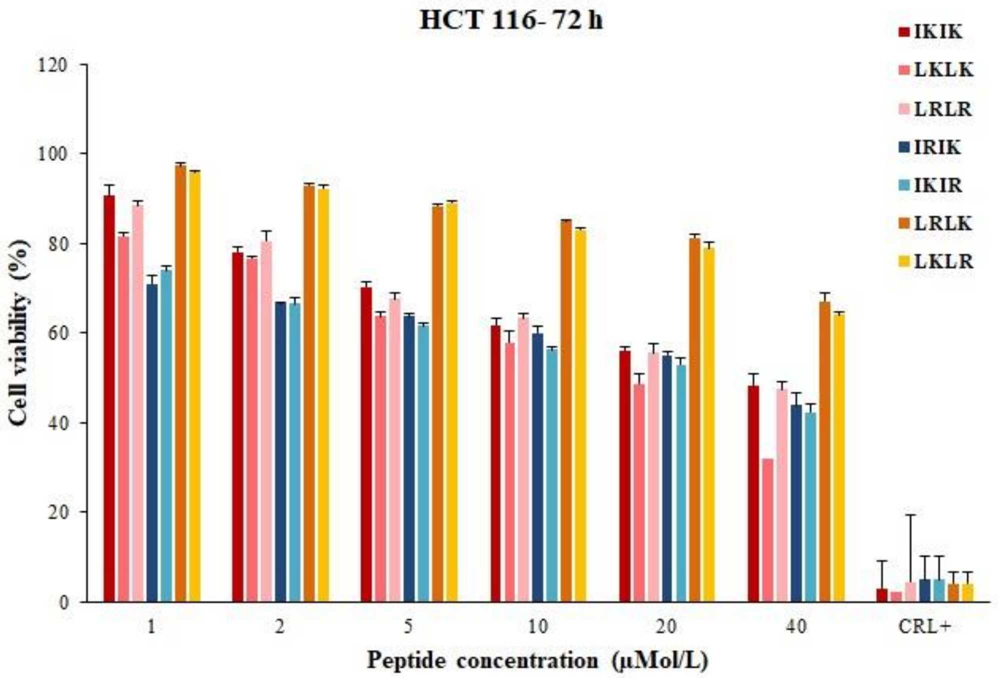

Figure 4.1. Viability of HCT 116 cells after incubation with different concentrations of the cationic amphiphilic peptides for 72 h as determined by MTT test. All data were normalized against untreated controls and reported as Mean ± SE (n = 6). Sodium chromate (2 mMol/L) was used as positive control (CRL+).

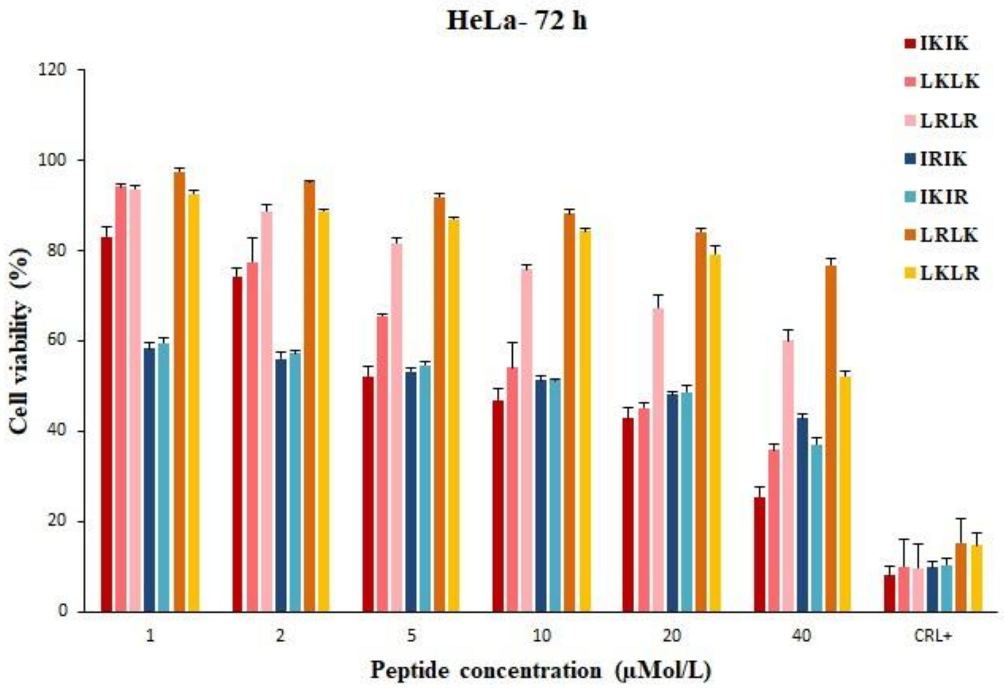

Figure 4.2. Viability of HeLa cells after incubation with different concentrations of the cationic amphiphilic peptides for 72 h as determined by MTT test. All data were normalized against untreated controls and reported as Mean ± SE (n = 6). Sodium chromate (2 mMol/L) was used as positive control (CRL+).

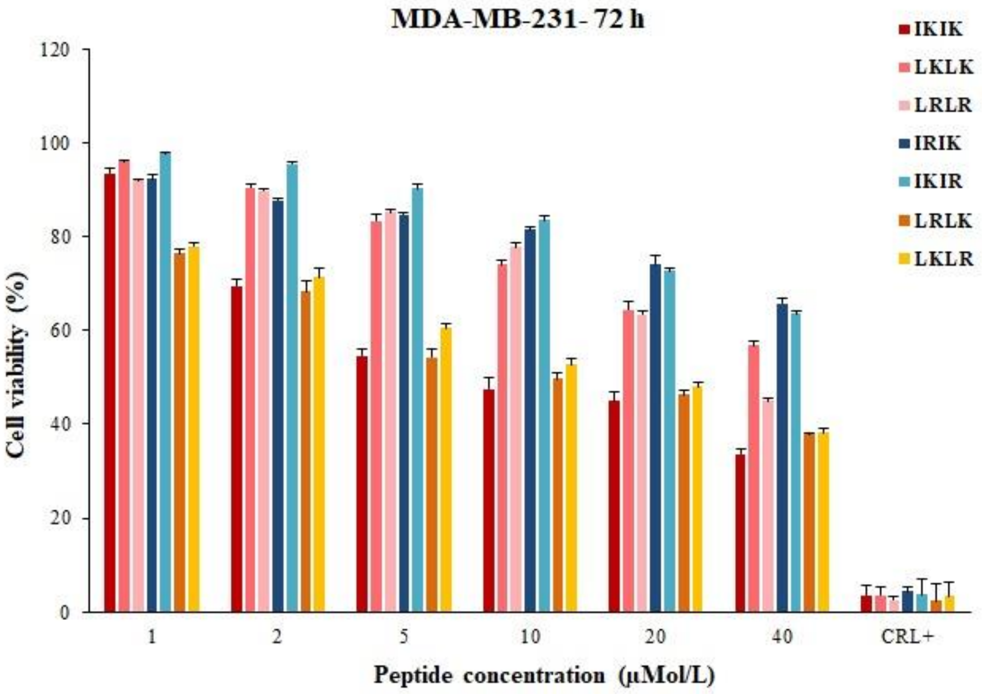

Figure 4.3. Viability of MDA-MB-231 cells after incubation with different concentrations of the cationic amphiphilic peptides for 72 h as determined by MTT test. All data were normalized against untreated controls and reported as Mean ± SE (n = 6). Sodium chromate (2 mMol/L) was used as positive control (CRL+).

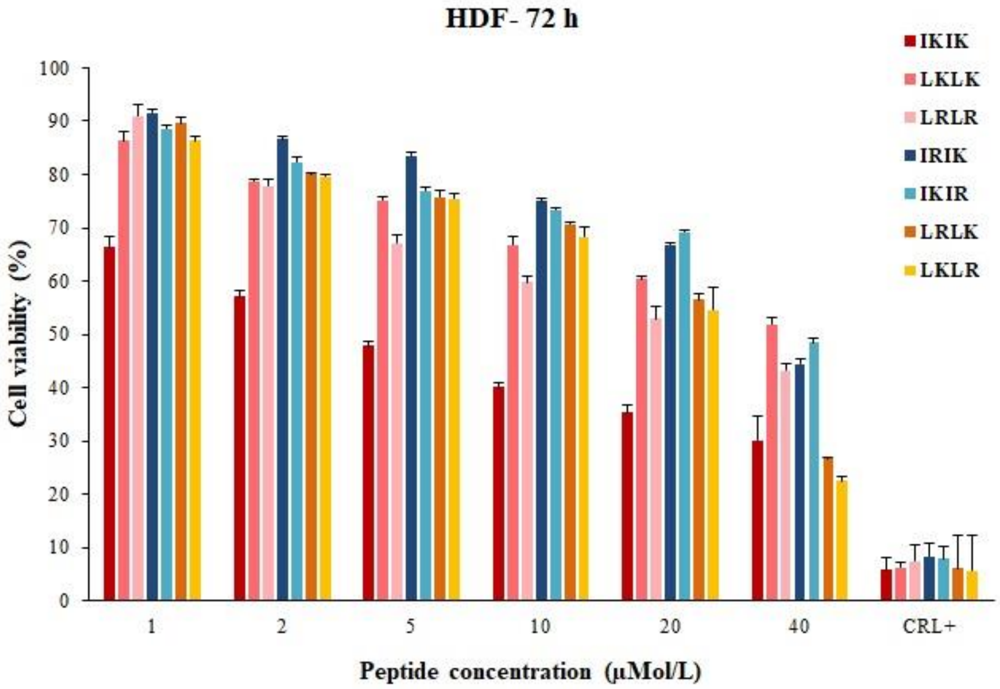

Figure 4.4. Viability of HDF cells after incubation with different concentrations of the cationic amphiphilic peptides for 72 h as determined by MTT test. All data were normalized against untreated controls and reported as Mean ± SE (n = 6). Sodium chromate (2 mMol/L) was used as positive control (CRL+).

As it could be inferred from these Figures, LKLK was the most toxic peptide in HCT 116, with highest efficacy and potency in the experimental concentration range (IC_{50} = 14.5 ± 1.3 µM and 68.1 ± 2.1 % growth inhibition). Replacing leucine with isoleucine reduced the potency and efficacy of the resulting peptide, IKIK, considerably (IC_{50} = 32.7 ± 4.5 µM and 51.7 ± 3.3 % growth inhibition). In a similar manner, replacing arginine with lysine reduced the potency and efficacy of the resulting peptide, LRLR, significantly (IC_{50} = 31.8 ± 2.9 µM and 52.5 ± 0.8 % growth inhibition). IKIR and IRIK showed considerable toxicity in HCT 116 cells whereas their leucine containing analogues, LKLR and LRLK did not show any toxicity against HCT 116 in the experimental range of concentration. Thus, replacing isoleucine with leucine in the peptides with mixed arginine and lysine residues diminishes their cytotoxicity against HCT 116.

In HeLa cells, on the other hand, IKIK was the most toxic peptide (IC_{50} = 8.9 ± 2.1 µM and 74.4 ± 1.4 % growth inhibition). LKLK, IRIK, and IKIR were also highly toxic to HeLa cells but there was not significant difference between them. LRLR, LRLK, and LKLR did not show any considerable toxicity in HeLa. Thus, combination of leucine and arginine diminishes the anticancer activity in HeLa cells.

In MDA-MB-231, on the contrary, except IKIK which was highly toxic (IC_{50} =10.9 ± 0.5, 66.1 ± 1.4 % growth inhibition), the rest of the isoleucine containing peptides and also LKLK were not toxic whereas the leucine and arginine containing peptides (LRLR, LRLK, and LKLR), which had weak toxicity or no toxicity against HCT 116 and HeLa, appeared to be highly toxic. The trend of cytotoxicity in HDFs was also similar to MDA-MB-231. IKIK had the highest toxicity (IC_{50} = 4.4 ± 0.3 and 70 ± 3.1 % growth inhibition), in HDFs followed by the arginine and leucine containing peptides whereas LKLK, IRIK and IKIR had very weak toxicity.

As it could be inferred from the above data, the β-sheet forming cationic amphiphilic peptides showed different cytotoxicity patterns in different cell lines. IKIK showed high cytotoxicity against all the tested cell lines with higher toxicity in HDFs than cancer cells which is a disadvantage for an anticancer peptide. Replacing the isoleucine residues in IKIK with leucine residues, diminished the toxicity of the resulting peptide, LKLK, in MDA-MB-231 and HDF and made it more selectively toxic to HCT 116 and HeLa. In the same way, replacing half of the lysine residues in IKIK with arginine, diminished the cytotoxicity of the resulting peptides (IKIR and IRIK) against MDA-MB-231 and HDF while maintaining their cytotoxicity against HCT 116 and HeLa. On the other hand, replacing half or all the lysine residues in LKLK with arginine made the resulting peptides more toxic to HDF and MDA 231-MB than HCT 116 and HeLa. These results suggest LKLK, IKIR and IRIK as selective anticancer peptides with minimal cytotoxic effect in normal cells.

In order to determine any cytotoxic effects within the first 24 h, additional MTT tests were performed with the cationic amphiphilic peptides which were found to be cytotoxic against each cell line, excluding the peptides which did not show any cytotoxicity in certain cell lines after 72 h, the results of which are depicted in Figures 4.5-4.8.

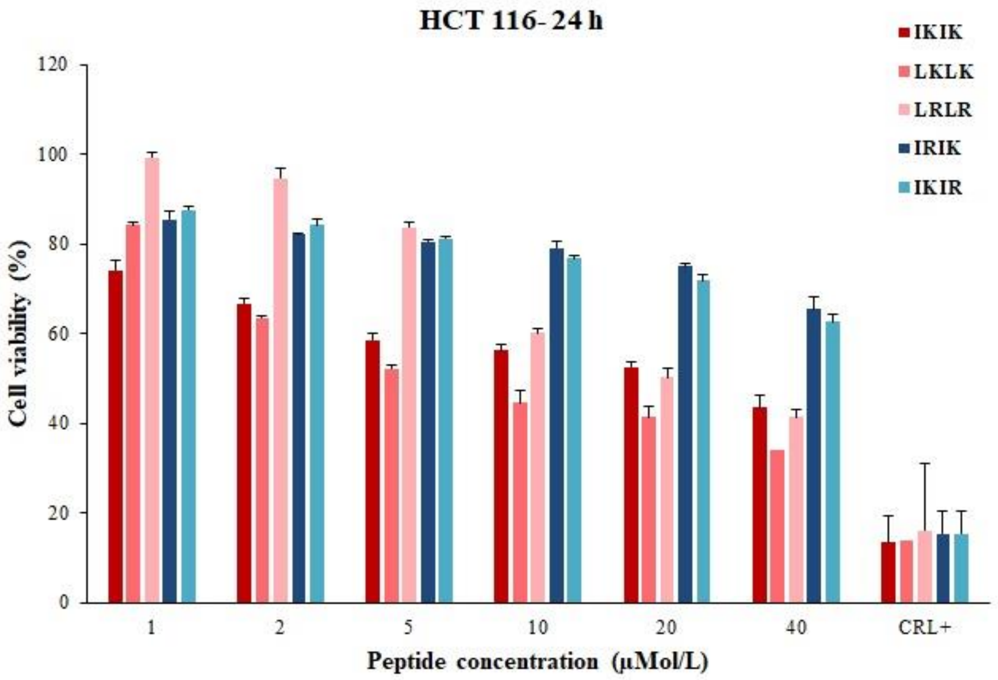

Figure 4.5. Viability of HCT 116 cells after incubation with different concentrations of the cationic amphiphilic peptides for 24 h as determined by MTT test. All data were normalized against untreated controls and reported as Mean ± SE (n = 6). Sodium chromate (2 mMol/L) was used as positive control (CRL+).

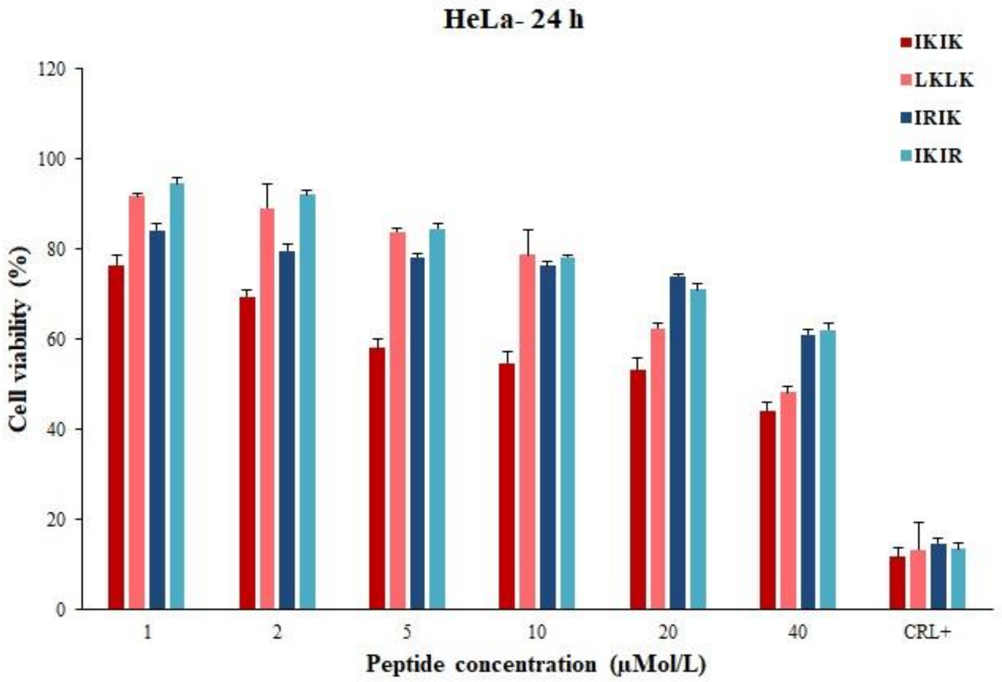

Figure 4.6. Viability of HeLa cells after incubation with different concentrations of the cationic amphiphilic peptides for 24 h as determined by MTT test. All data were normalized against untreated controls and reported as Mean ± SE (n = 6). Sodium chromate (2 mMol/L) was used as positive control (CRL+).

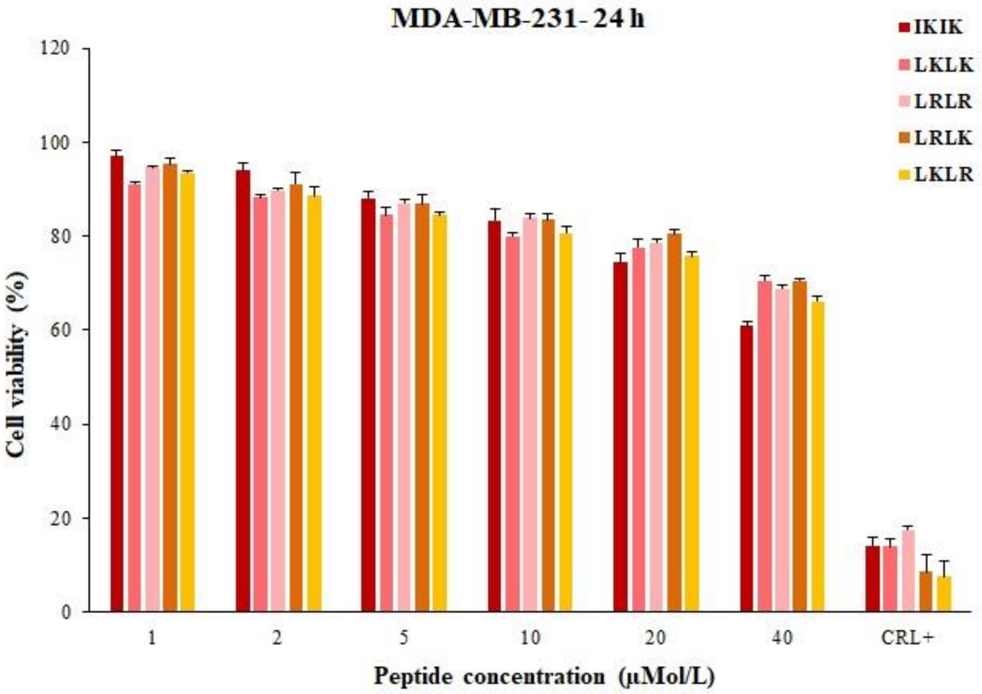

Figure 4.7. Viability of MDA-MB-231 cells after incubation with different concentrations of the cationic amphiphilic peptides for 24 h as determined by MTT test. All data were normalized against untreated controls and reported as Mean ± SE (n = 6). Sodium chromate (2 mMol/L) was used as positive control (CRL+).

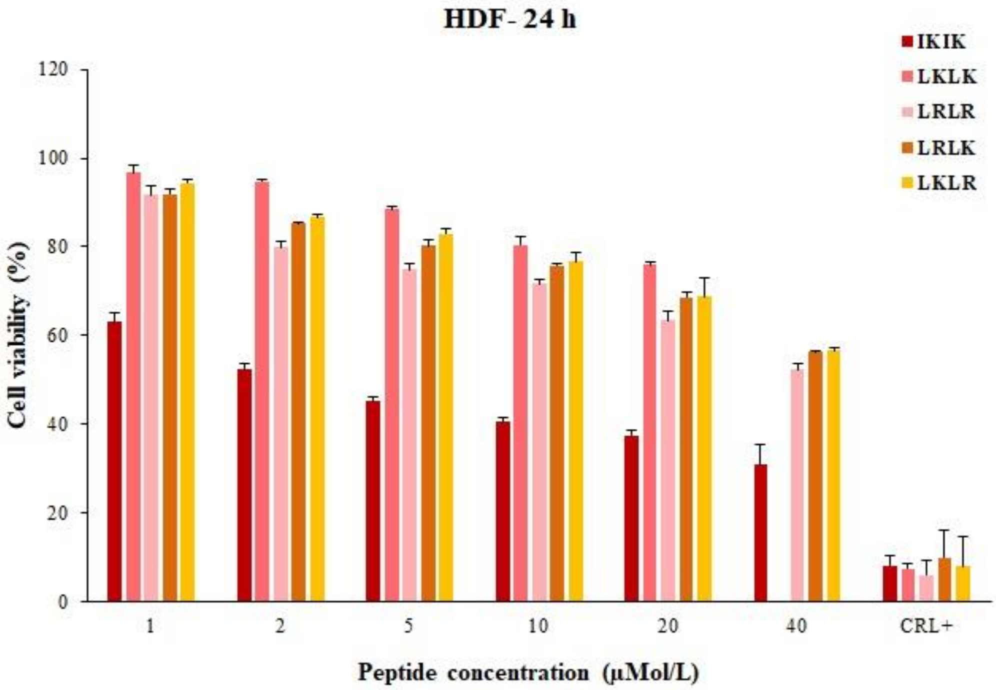

Figure 4.8. Viability of HDF cells after incubation with different concentrations of the cationic amphiphilic peptides for 24 h as determined by MTT test. All data were normalized against untreated controls and reported as Mean ± SE (n = 6). Sodium chromate (2 mMol/L) was used as positive control (CRL+).

As it could be observed among the cationic amphiphilic peptides which exhibited cytotoxicity against HCT 116 cells, IKIK, LKLK and LRLR caused a considerable decrease in the cell viability within 24 h which was comparable to the cytotoxic effect achieved in 72 h. IKIR and IRIK on the other hand induced less decrease in cell viability than the other peptides and to their own growth inhibition after 72 h. These observations indicate that the cytotoxic action of IKIK, LKLK and LRLR initiates early and reaches its maximum within 24 h whereas IKIR and IRIK require more time to reach their maximum cytotoxic effect. Similarly, in Hela cells IKIK showed considerable cytotoxicity in 24 h, whereas IKIR and IRIK and LKLK decreased the cell viability significantly but to a lesser extent than the effect observed after 72 h.

In MDA-MB-231, all of the tested cationic amphiphilic peptides (IKIK, LKLK, LRLR, LRLK and LKLR) caused a minimal decrease in the cell viability in 24 h which was markedly lower than the effect achieved after 72 h suggesting a longer course of cytotoxic action for these peptides in MDA-MB-231 cells. Similar to HCT 116 and HeLa, in HDF cells IKIK induced considerable reduction in cell viability within 24 h the extent of which was comparable to that induced in 72 h. LRLK, LKLR, LRLR and LKLK also decreased the cell viability significantly compared to the controls indicating an early initiation of action for these peptides, although the extent of the cytotoxic effect was lower than that achieved in 72 h.

Considering all the above, it could be concluded that the β-sheet forming cationic amphiphilic peptides consisting of either arginine or lysine residues in their hydrophilic domain have an early initiation and a fast course of cytotoxic action which completes in 24 h whereas the β-sheet forming cationic amphiphilic peptides consisting of a mixture of arginine and lysine residues in their hydrophobic domain have a longer course of action which requires 72 h to induce a strong cytotoxic effect. Nevertheless, MDA-MB-231 does not follow the general trend observed in other cell lines and in these cells all the peptides exert a slow and prolonged cytotoxic effect.

4.3.3 Mitochondrial damage

As discussed in Section 3.2, the MTT assay indicated reduction in the metabolic activity of the cells following treatment with the beta sheet-forming cationic amphiphilic peptides. To further investigate the effect of the peptides on the cell metabolism, the morphology & distribution pattern of the mitochondria within the cells was studied after treating the cells with the cytotoxic peptides and was compared to the normal phenotype in the untreated controls. Each cell line was incubated with the peptides which were found to be toxic against that cell line (based on the MTT test). Figures 4.9-4.11 show the HCT 116, HeLa and MDA 231-MB cells stained with MitoTracker® Red.

As it could be observed, in HCT 116 cells incubated with IKIK and LKLK the mitochondria are more shifted towards one side of the cells and are spread over a larger area of the cytoplasm compared to the untreated controls. Also, the higher fluorescence intensity in some areas of the cytoplasm indicates accumulation of the mitochondria in these areas as large formations which is a sign of hyperactivity of the mitochondria in response to a stimulating or notorious factor. Incubation of HCT 116 cells with LRLR, IKIR and IRIK on the other hand resulted in smaller than usual cells with large blocks of mitochondria appearing in different areas of the cytoplasm which indicates damage to the cells. Similar effects were observed in HeLa cells following incubation with IKIK, LKLK, IKIR and IRIK and in MDA 231-MB cells following incubation with IKIK, LRLR, LKLR and LRLK suggesting the changes to the distribution and activity of the mitochondria as a result of exposure to the cytotoxic peptides.

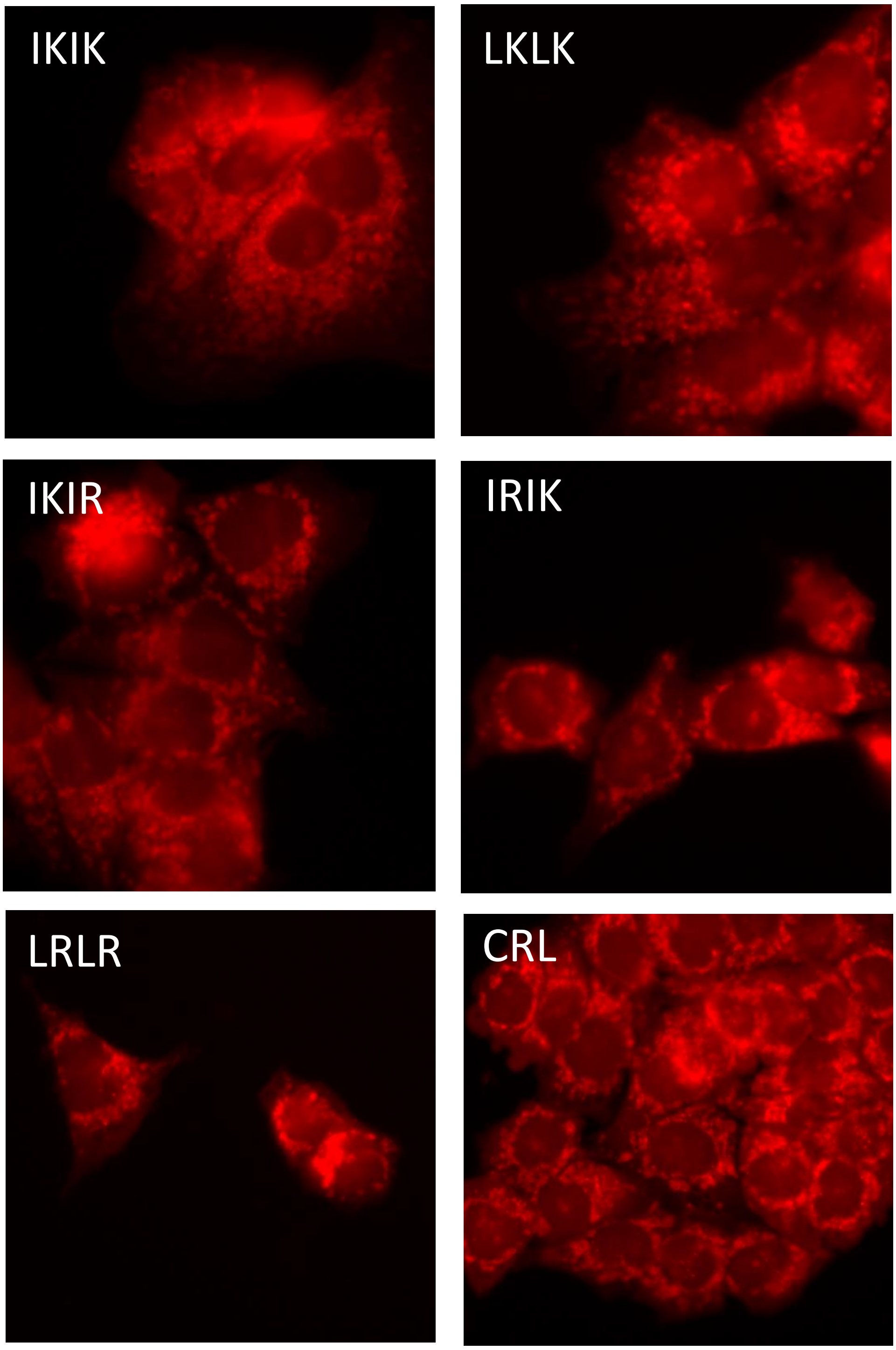

Figure 4.9. The morphology and distribution pattern of the mitochondria in HCT 116 cells incubated with cationic amphiphilic peptides for 72 h. The mitochondria were stained with MitoTracker® Red, ×40 magnification.

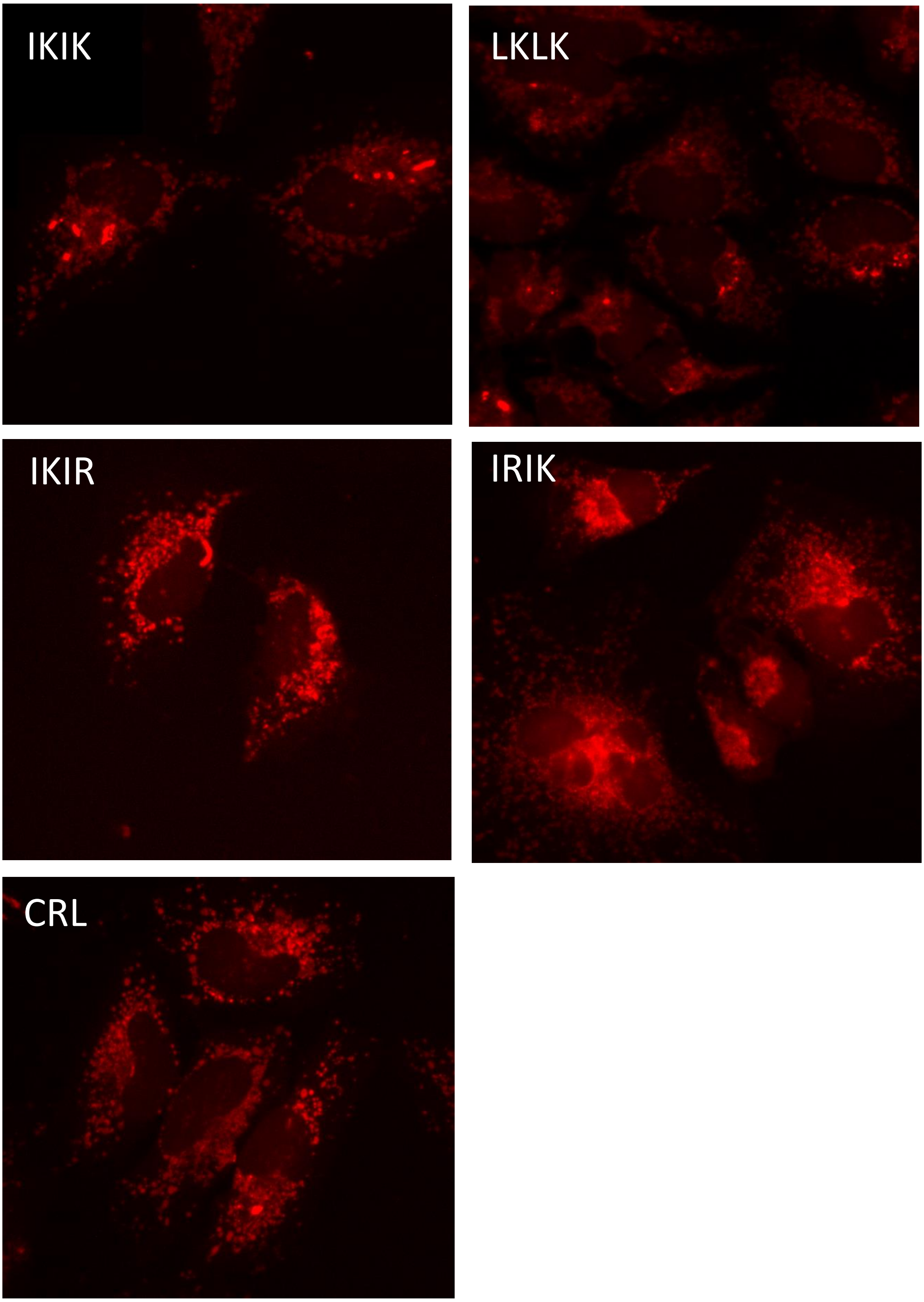

Figure 4.10. The morphology and distribution pattern of the mitochondria in HeLa cells incubated with cationic amphiphilic peptides for 72 h. The mitochondria were stained with MitoTracker® Red, ×40 magnification.

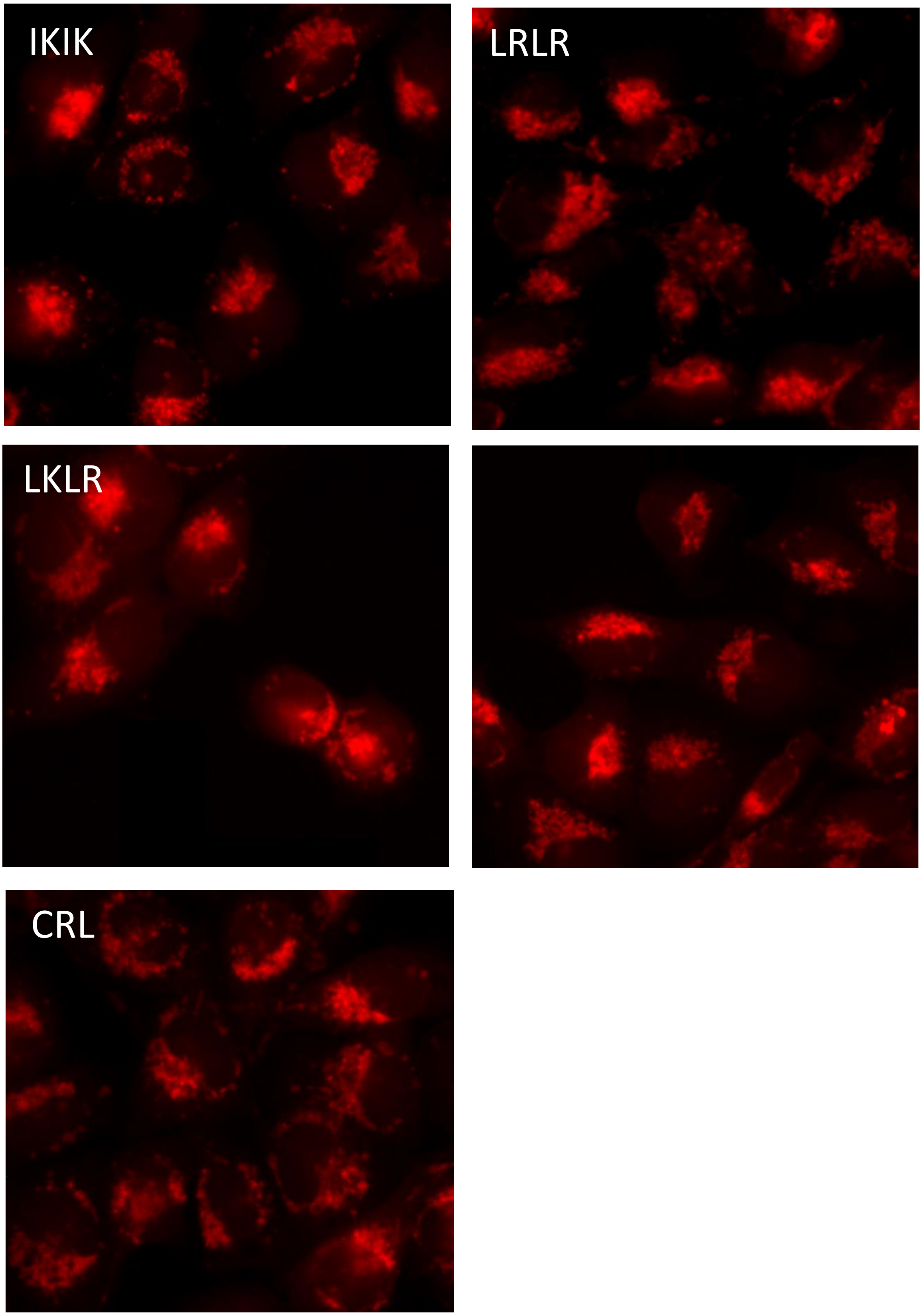

Figure 4.11. The morphology and distribution pattern of the mitochondria in MDA-MB-231 cells incubated with cationic amphiphilic peptides for 72 h. The mitochondria were stained with MitoTracker® Red, ×40 magnification.

To further confirm the mitochondrial damage caused by the β-sheet forming cationic amphiphilic peptides, the HCT 116 colorectal cancer cells and HDF cells were stained with JC-1 mitochondrial stain following treatment with the peptides. For this experiment, only the β-sheet forming cationic amphiphilic peptides with high anticancer activity and higher selectivity for cancer cells than HDFs were tested and the peptides which were equally toxic to cancer cells and fibroblasts were not included. As it could be observed in figures 4.12-4.13, the higher ratio of green fluorescence to red fluorescence in the HCT 116 cells treated with IRIK, IKIR, and LKLK indicates the great extent of the mitochondrial damage caused by these peptides as compared to the untreated controls which showed mainly red fluorescence from healthy mitochondria. On the contrary, in the HDFs the peptides showed higher proportion of red to green fluorescence indicating less damage to mitochondria which agrees with their lower toxicity in HDFs.

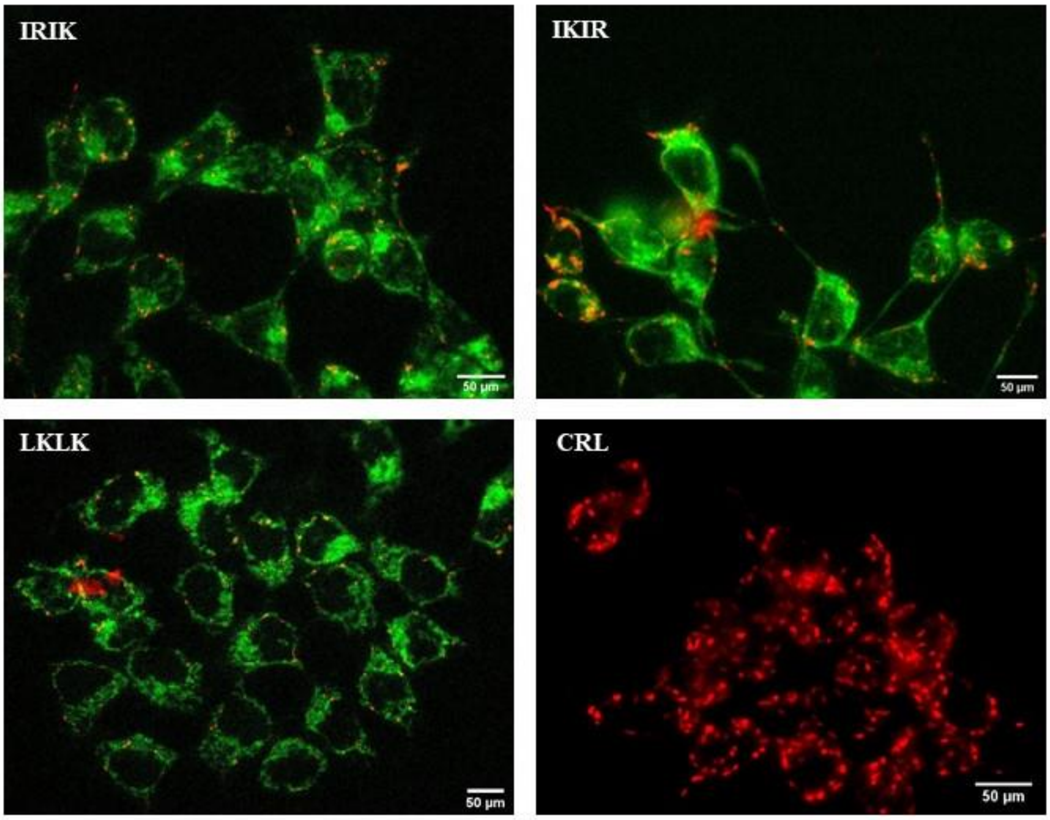

Figure 4.12. High content images of HCT 116 colorectal cancer cells stained with JC-1 after incubation with β-sheet forming cationic amphiphilic peptides for 72 h. The green colour indicates damaged mitochondria in pre-apoptotic cells and red colour indicates the healthy mitochondria. 40 × magnification, scale bar: 50 µm.

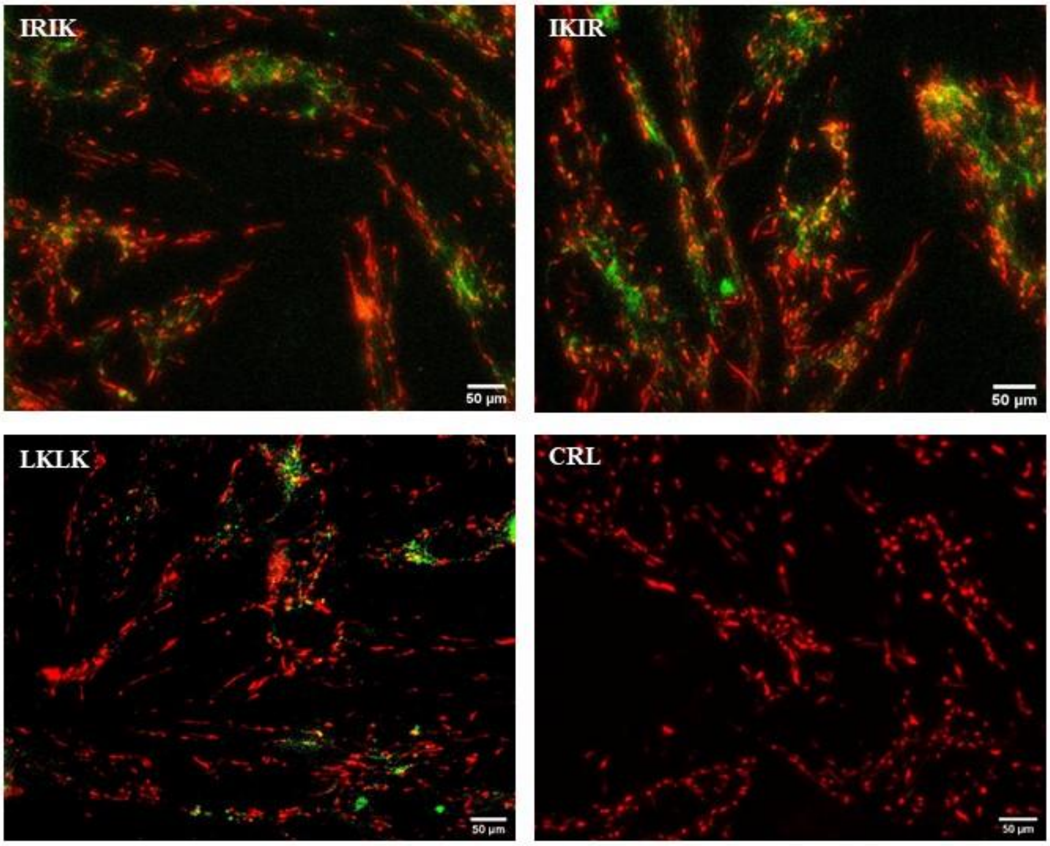

Figure 4.13. High content images of human dermal fibroblast cells stained with JC-1 after incubation with β-sheet forming cationic amphiphilic peptides for 72 h. The green colour indicates damaged mitochondria in pre-apoptotic cells and red colour indicates the healthy mitochondria. 40 × magnification, scale bar: 50 µm.

4.3.4 Cell proliferation

The ability of the β-sheet forming cationic amphiphilic peptides to inhibit the cell proliferation in HCT 116 cells is presented in Figures 4.14-4.15. As it could be observed incubating the HCT 116 cells with the cytotoxic peptides, IKIK, LKLK, IKIR and IRIK, caused a slight decrease in the number of cells in a concentration dependent manner suggesting some level of antiproliferative activity. Nevertheless, the low extent of the observed growth inhibitory effect suggests that the strong cytotoxic effect exerted by these peptides is mainly via reduction of the metabolic activity of the cells and the antiproliferative effect has a minor contribution to the overall cytotoxicity.

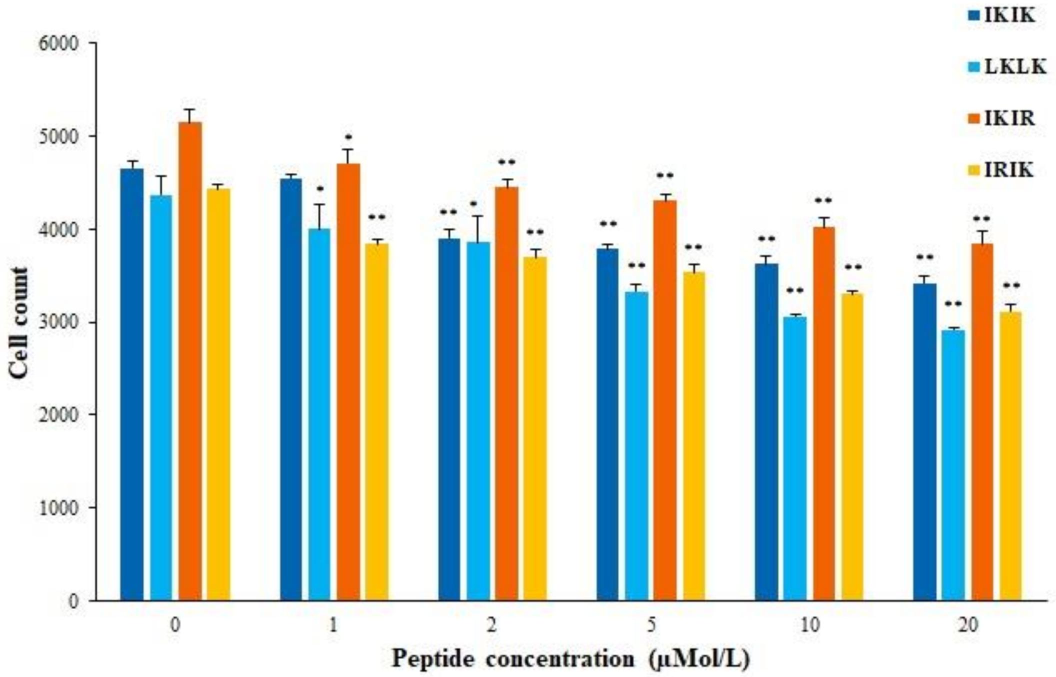

Figure 4.14. Average cell counts of HCT 116 cells incubated with different concentrations of cationic amphiphilic peptides for 72 h. The data were reported as Mean ± SE (n = 6). * indicates values of $p < 0.05$ and ** indicates values of $p < 0.005$ as compared to the controls.

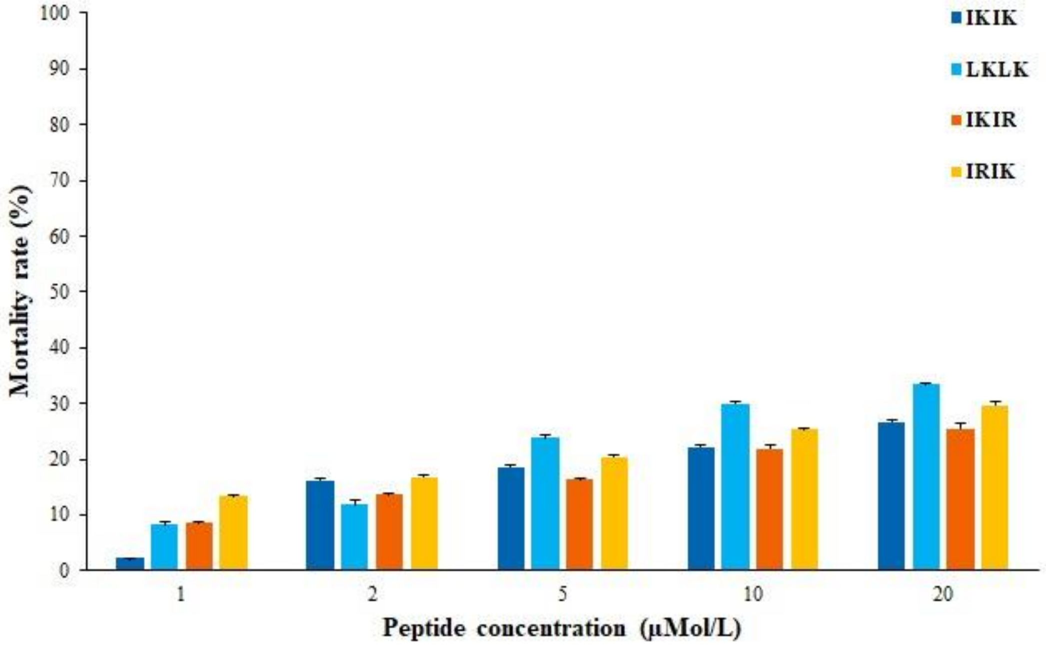

Figure 4.15. Mortality rates of HCT 116 cell incubated with different concentrations of cationic amphiphilic peptides for 72 h. All data were normalized against untreated controls and reported as Mean ± SE (n = 6).

4.3.5 Transfection with AONs

Figures 4.16- 4.22 show the HCT 116 cells transfected with FITC-labelled cMyc- AON using the cationic amphiphilic peptides at different N/P ratios as described in chapter 2. The intensity of the green fluorescence is proportional to the amount of the AON within the cells which is an indicator of the successful transfection.

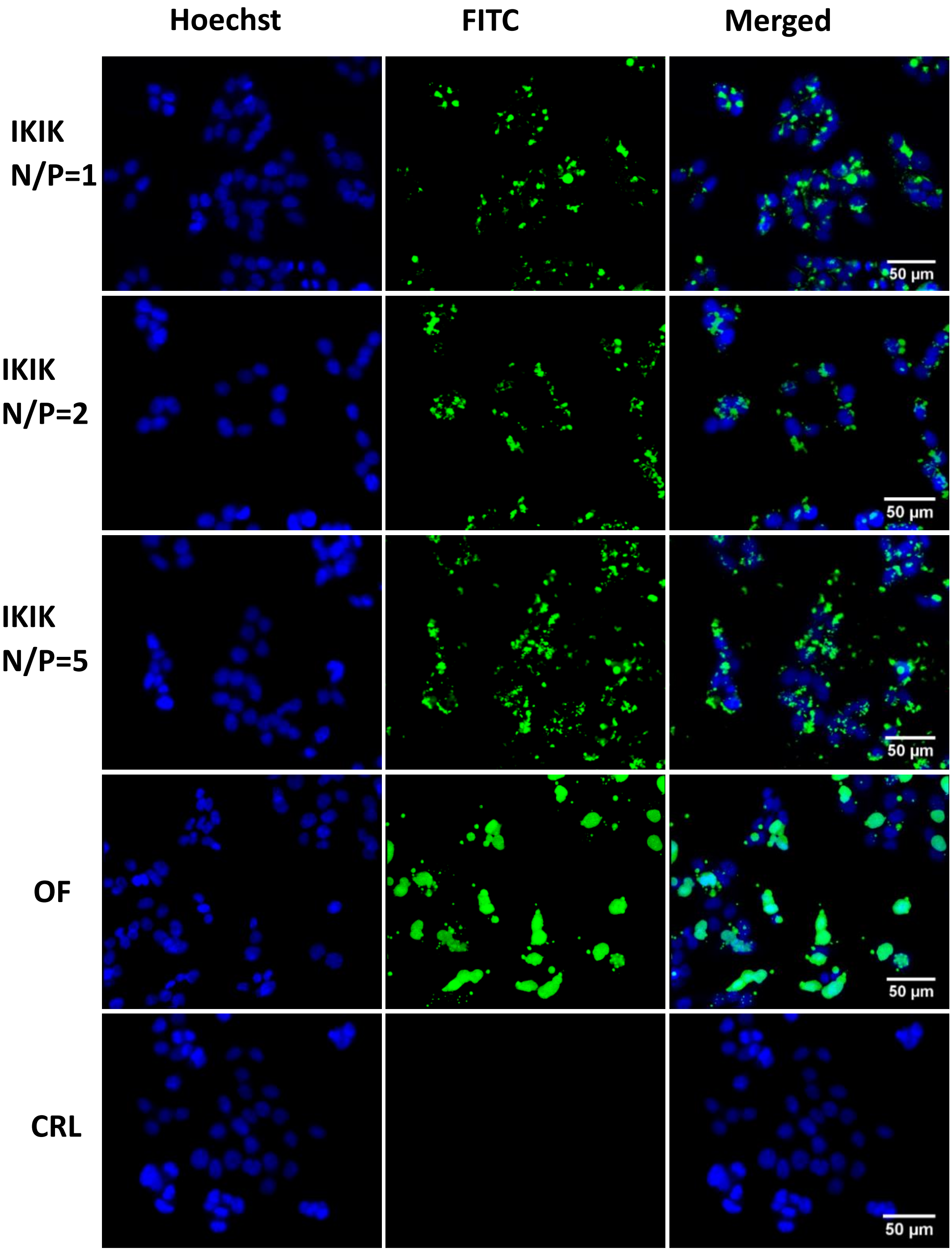

Figure 4.16. High content images of HCT 116 cells transfected with FITC-labelled c-Myc AON using IKIK at different N/P ratios. Oligofectamine™ (OF) was used as positive control and naked c-Myc AON was used as negative control. The nuclei were stained with Hoechst 33342, ×20 magnification.

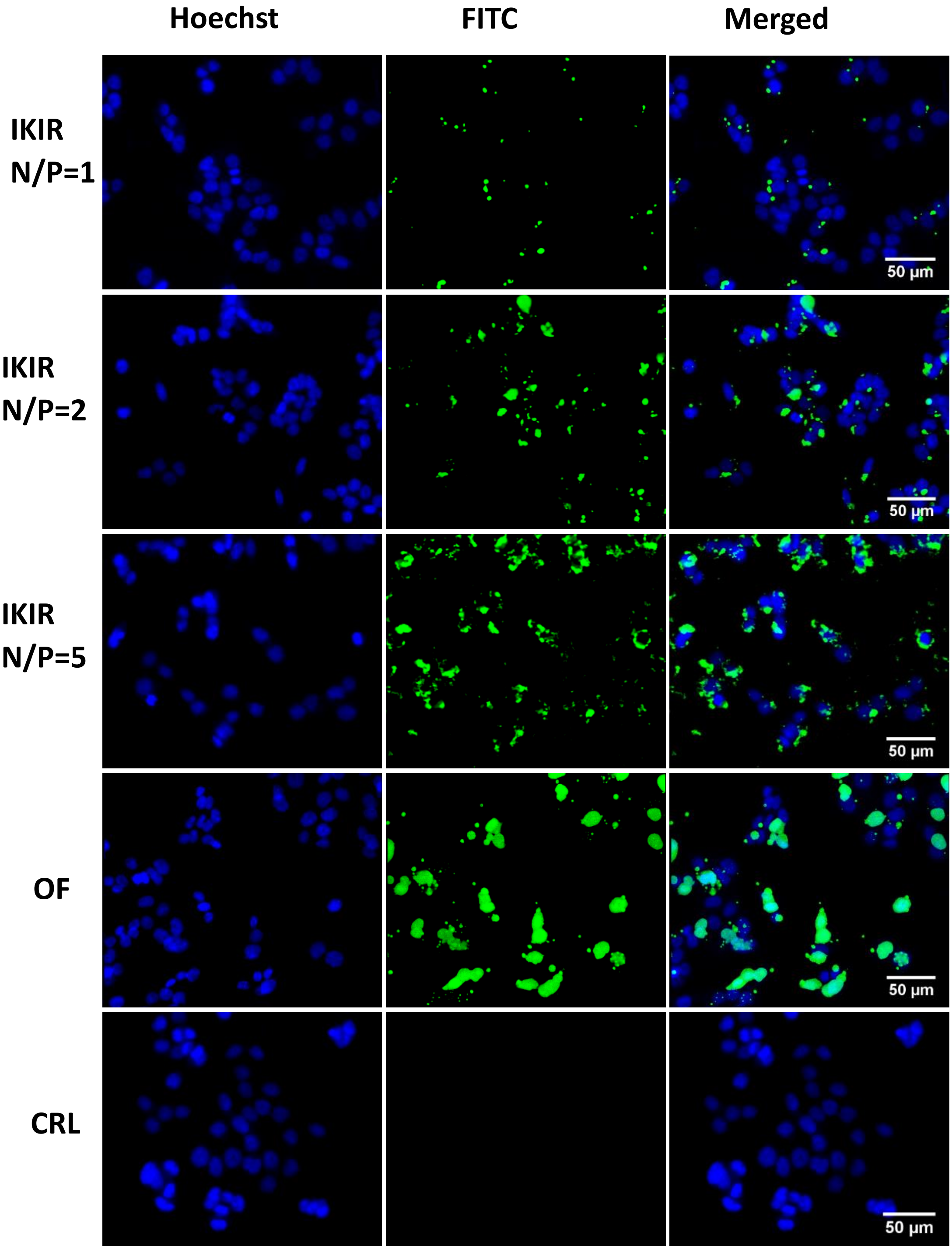

Figure 4.17. High content images of HCT 116 cells transfected with FITC-labelled c-Myc AON using IKIR at different N/P ratios. Oligofectamine™ (OF) was used as positive control and naked c-Myc AON was used as negative control. The nuclei were stained with Hoechst 33342, ×20 magnification.

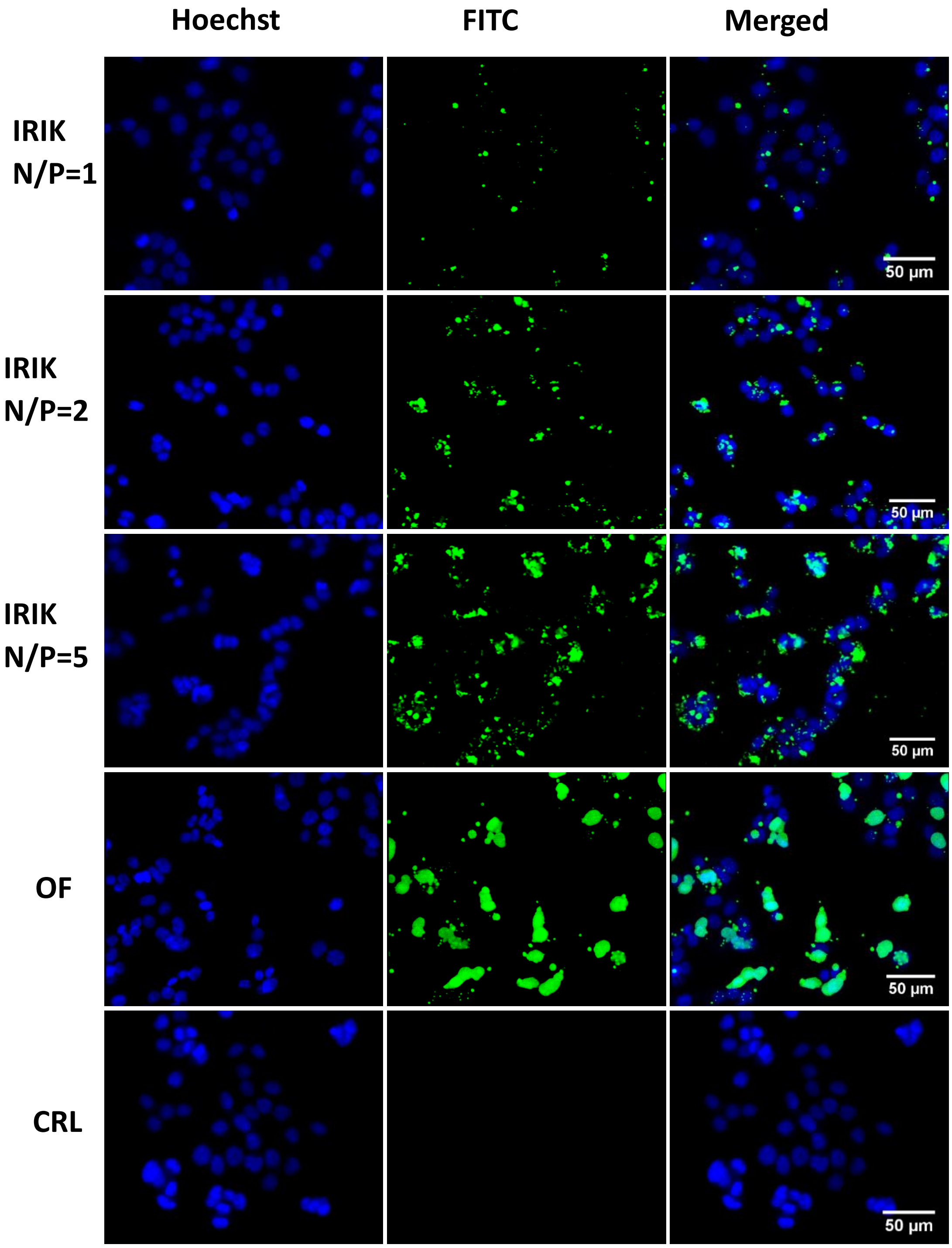

Figure 4.18. High content images of HCT 116 cells transfected with FITC-labelled c-Myc AON using IRIK at different N/P ratios. Oligofectamine™ (OF) was used as positive control and naked c-Myc AON was used as negative control. The nuclei were stained with Hoechst 33342, ×20 magnification.

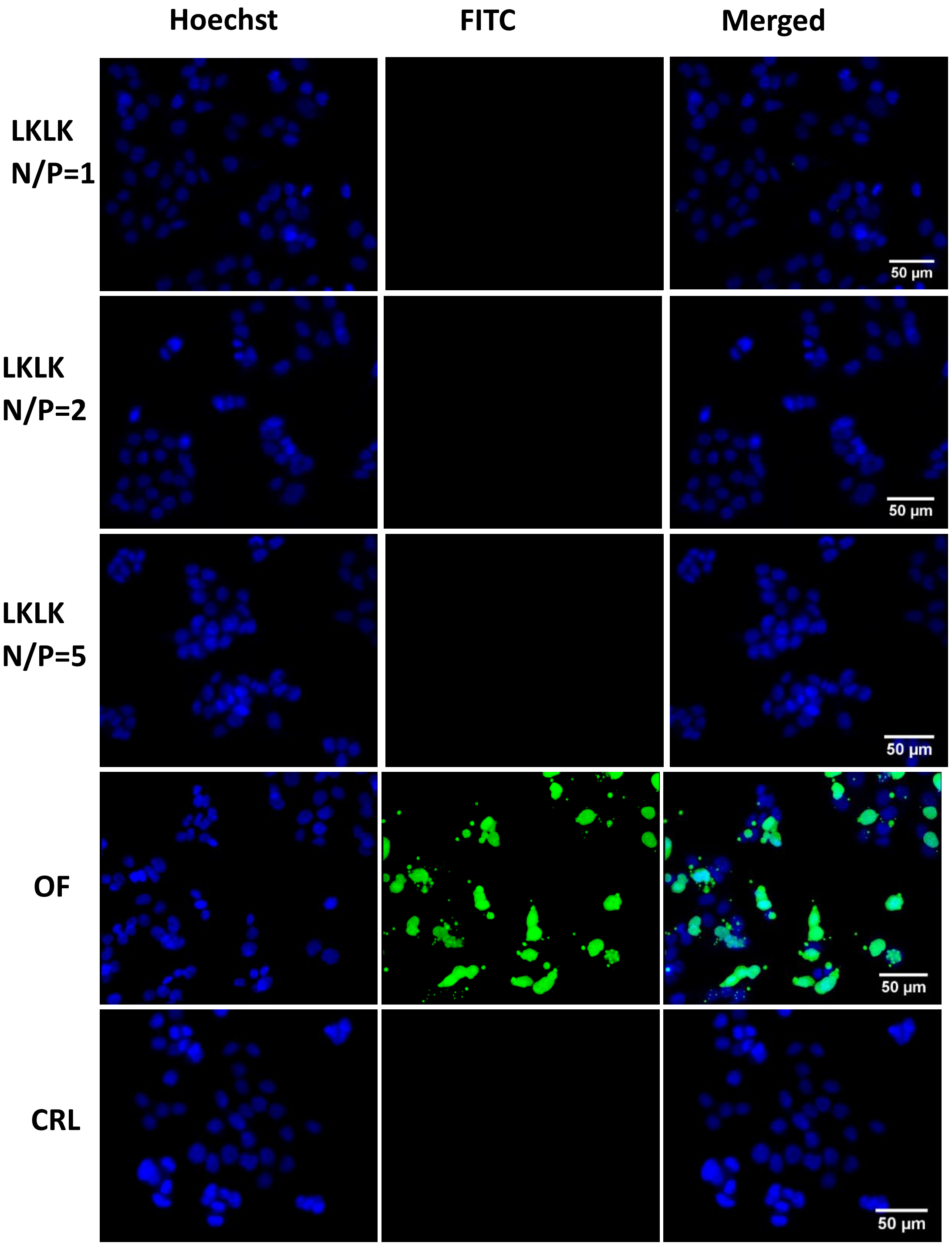

Figure 4.19. High content images of HCT 116 cells transfected with FITC-labelled c-Myc AON using LKLK at different N/P ratios. Oligofectamine™ (OF) was used as positive control and naked c-Myc AON was used as negative control. The nuclei were stained with Hoechst 33342, ×20 magnification.

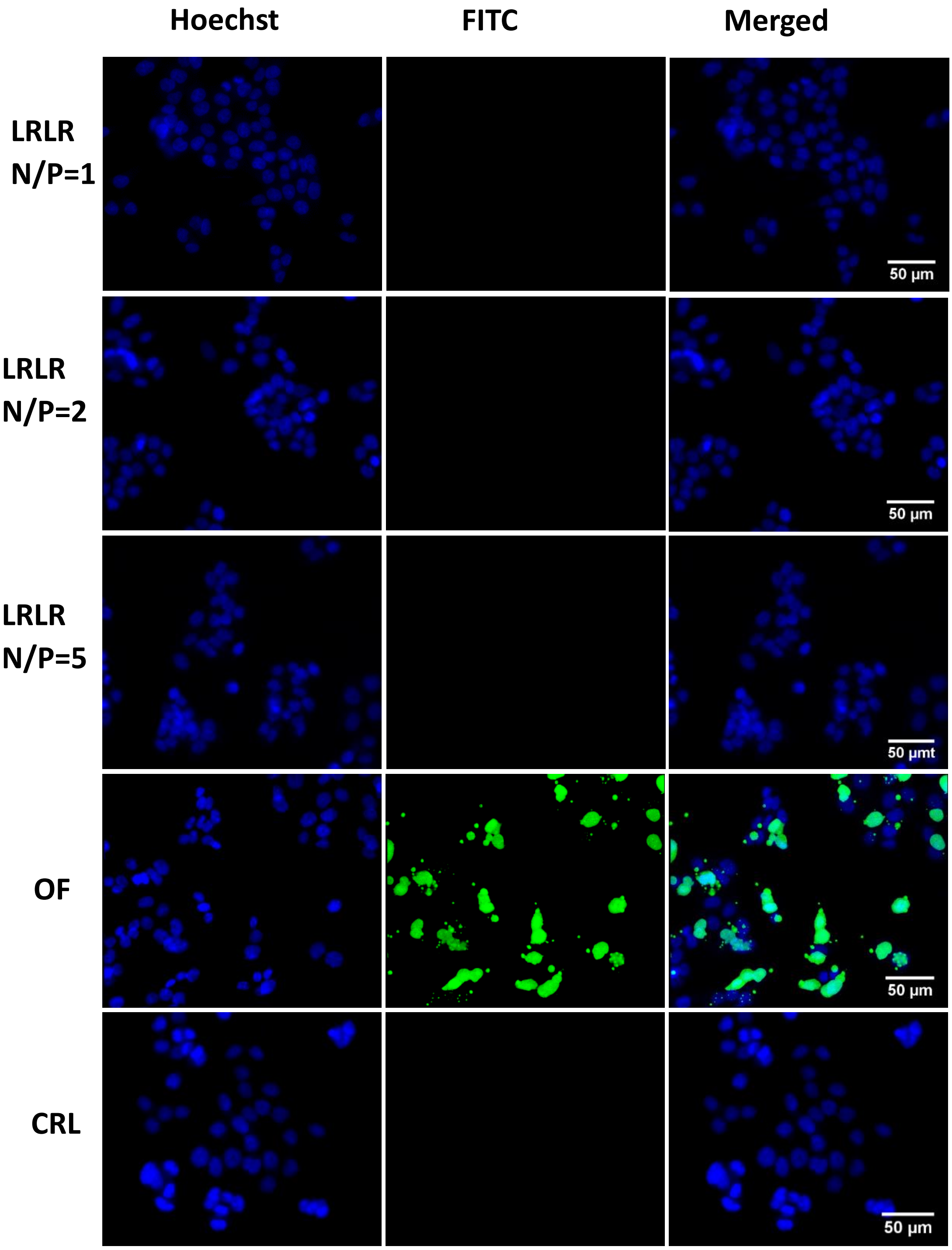

Figure 4.20. High content images of HCT 116 cells transfected with FITC-labelled c-Myc AON using LRLR at different N/P ratios. Oligofectamine™ (OF) was used as positive control and naked c-Myc AON was used as negative control. The nuclei were stained with Hoechst 33342, ×20 magnification.

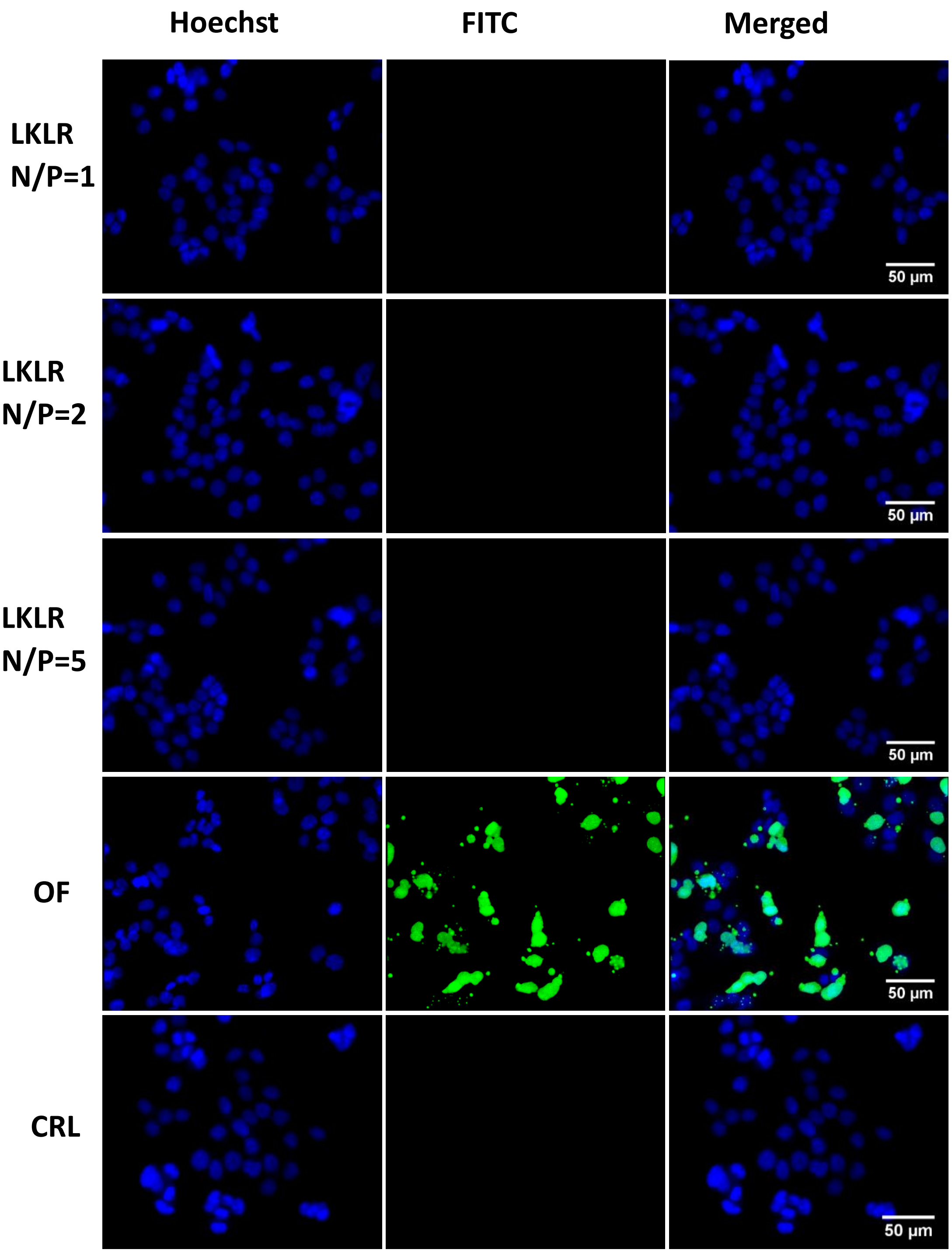

Figure 4.21. High content images of HCT 116 cells transfected with FITC-labelled c-Myc AON using LKLR at different N/P ratios. Oligofectamine™ (OF) was used as positive control and naked c-Myc AON was used as negative control. The nuclei were stained with Hoechst 33342, ×20 magnification.

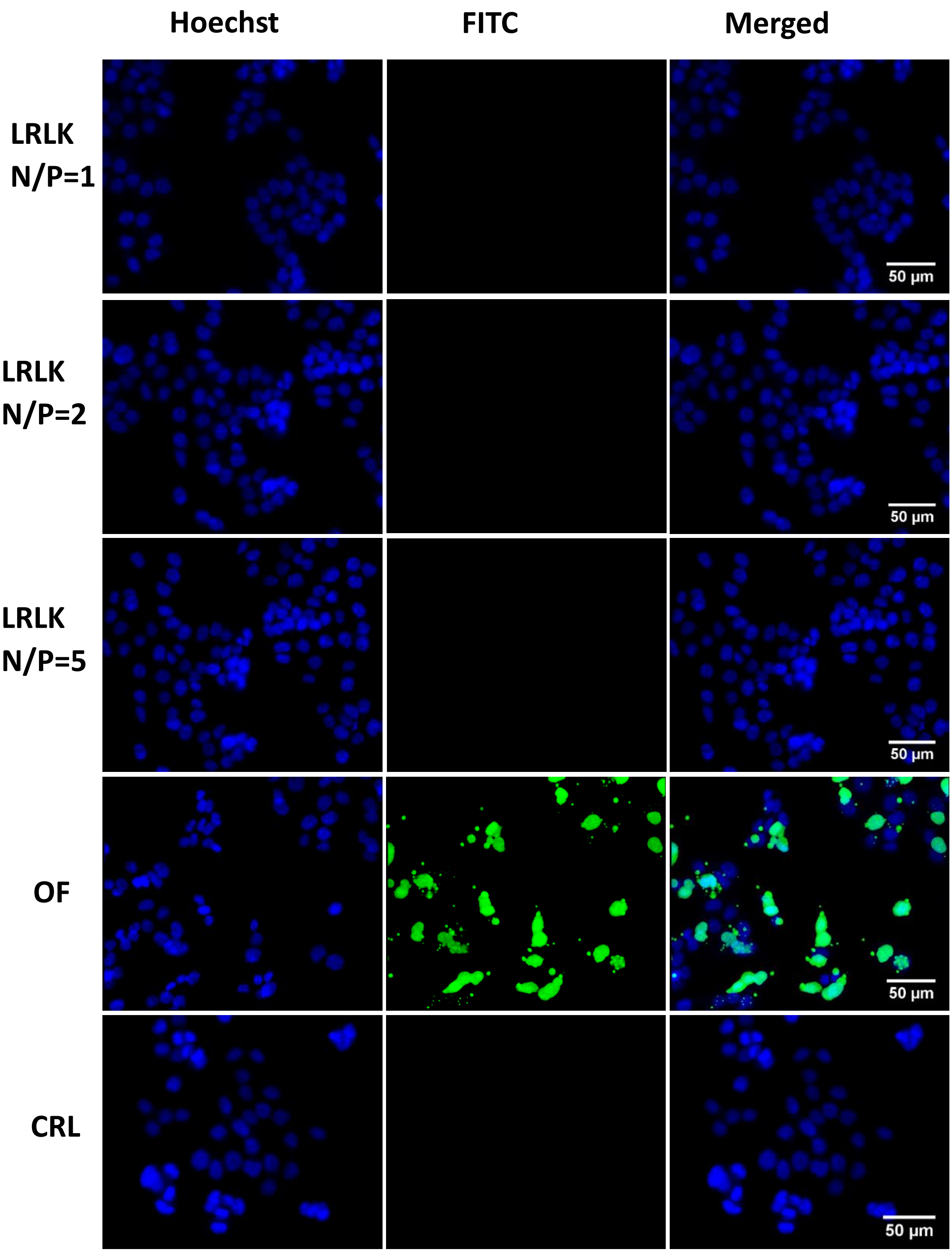

Figure 4.22. High content images of HCT 116 cells transfected with FITC-labelled c-Myc AON using LRLK at different N/P ratios. Oligofectamine™ (OF) was used as positive control and naked c-Myc AON was used as negative control. The nuclei were stained with Hoechst 33342, ×20 magnification.

As it could be observed, only the peptides composed of isoleucine residues were able to deliver the AONs to the HCT 116 cells whereas the peptides composed of leucine residues were unable to deliver any associated AONs to the cells. Increasing the ratio of the peptide to AON, resulted in higher cellular uptake as indicated by the higher fluorescence intensity. Moreover, at higher peptide to AON ratios the peptides formed larger complexes with AONs which covered the entire perinuclear area whereas lower peptide to AON ratios formed smaller peptide-AON complexes which were localized to one side of the perinuclear area.

Based on these observations, the peptides which successfully transfected the HCT 116 cells with c-Myc AON were further evaluated for their transfection efficiency in HeLa and HDF cells, the results of which are demonstrated in Figures 4.23-4.28. As it could be observed, a similar trend was found in HeLa cells, nevertheless, due to the larger size of these cells compared to HCT 116, the peptide-AON complexes were distributed over a larger area around the nuclei. Moreover, higher cellular uptake was achieved with low peptide to AON ratios in HeLa cells compared to HCT 116 cells. In HDF cells on the other hand, efficient transfection was only achieved with IKIK, IKIR and IRIK at N/P ratios above 2 whereas at ratio of 1, except for IKIK, very low amounts of AON were delivered to the cells. Unlike the perinuclear localization pattern observed in HCT 116 and HeLa, in HDFs the peptide-AON complexes were distributed throughout the cytoplasm. As it could be conferred from the above data, the cationic amphiphilic peptides consisting of isoleucine and lysine and/or arginine were able to deliver the cMyc-AON to both cancer cells and normal fibroblasts with concentration-dependent efficiency, whereas replacing isoleucine with leucine diminished the ability of the cationic amphiphilic peptides to deliver cMyc-AON to the cells.

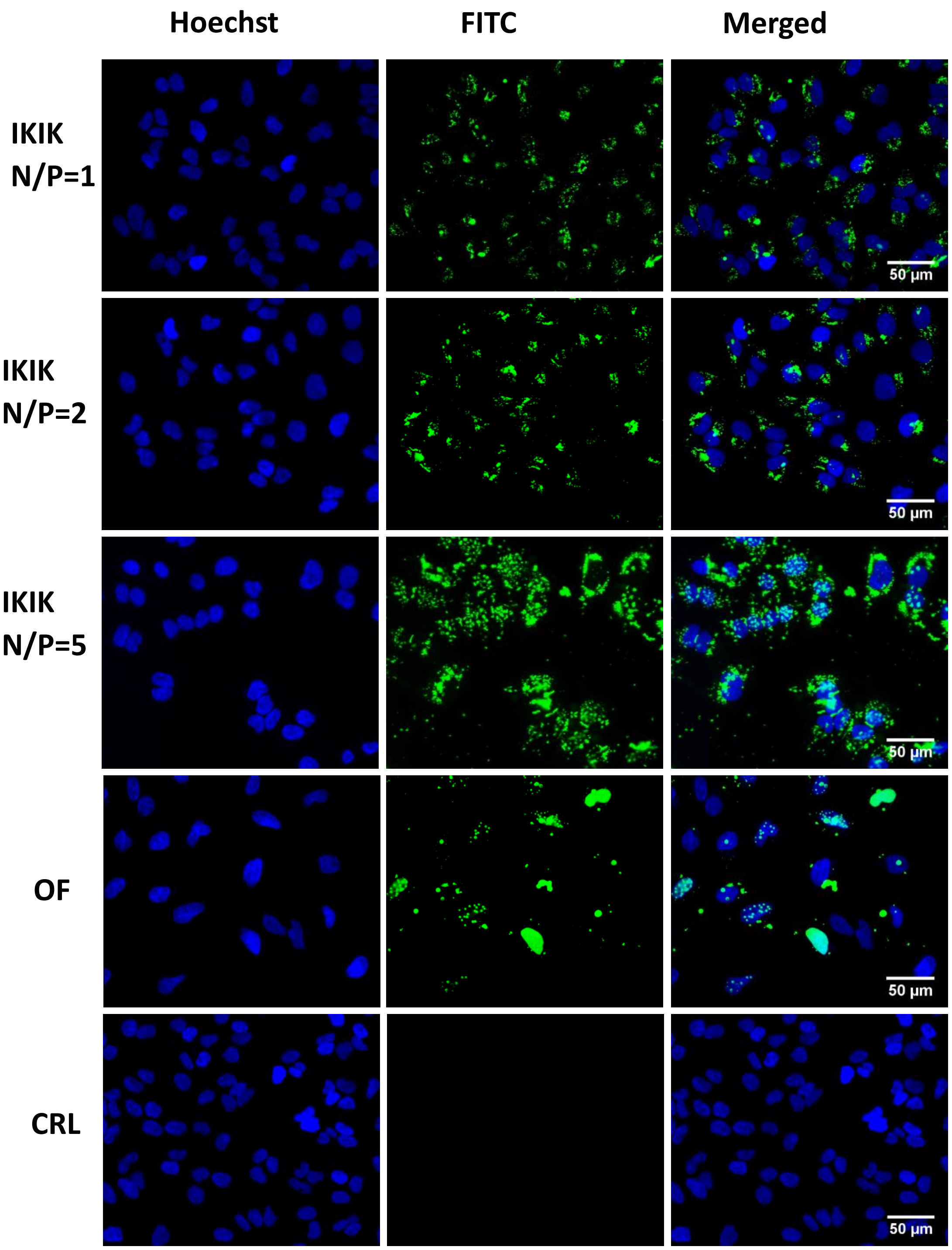

Figure 4.23. High content images of HeLa cells transfected with FITC-labelled c-Myc AON using IKIK at different N/P ratios. Oligofectamine™ (OF) was used as positive control and naked c-Myc AON was used as negative control. The nuclei were stained with Hoechst 33342, ×20 magnification.

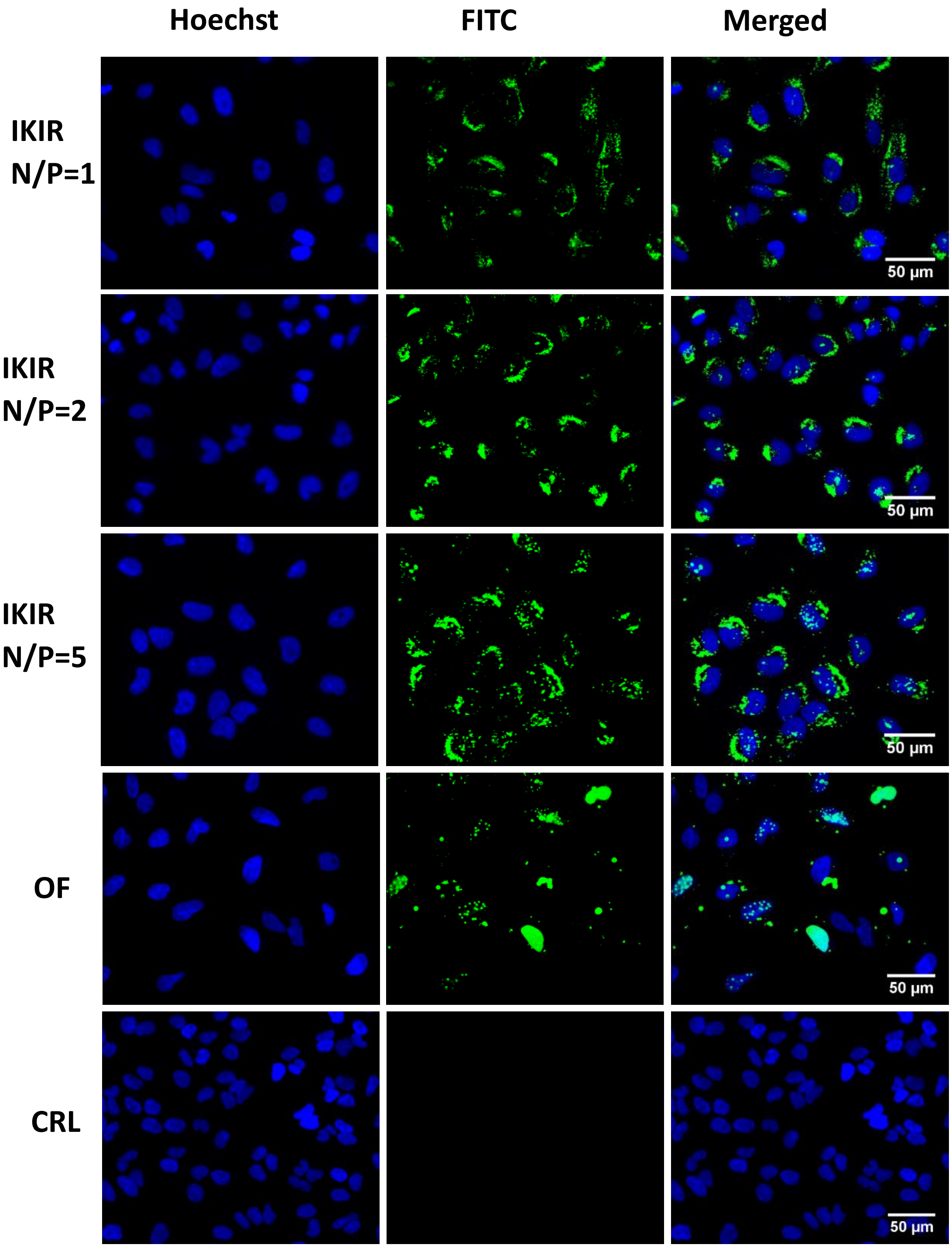

Figure 4.24. High content images of HeLa cells transfected with FITC-labelled c-Myc AON using IKIR at different N/P ratios. Oligofectamine™ (OF) was used as positive control and naked c-Myc AON was used as negative control. The nuclei were stained with Hoechst 33342, ×20 magnification.

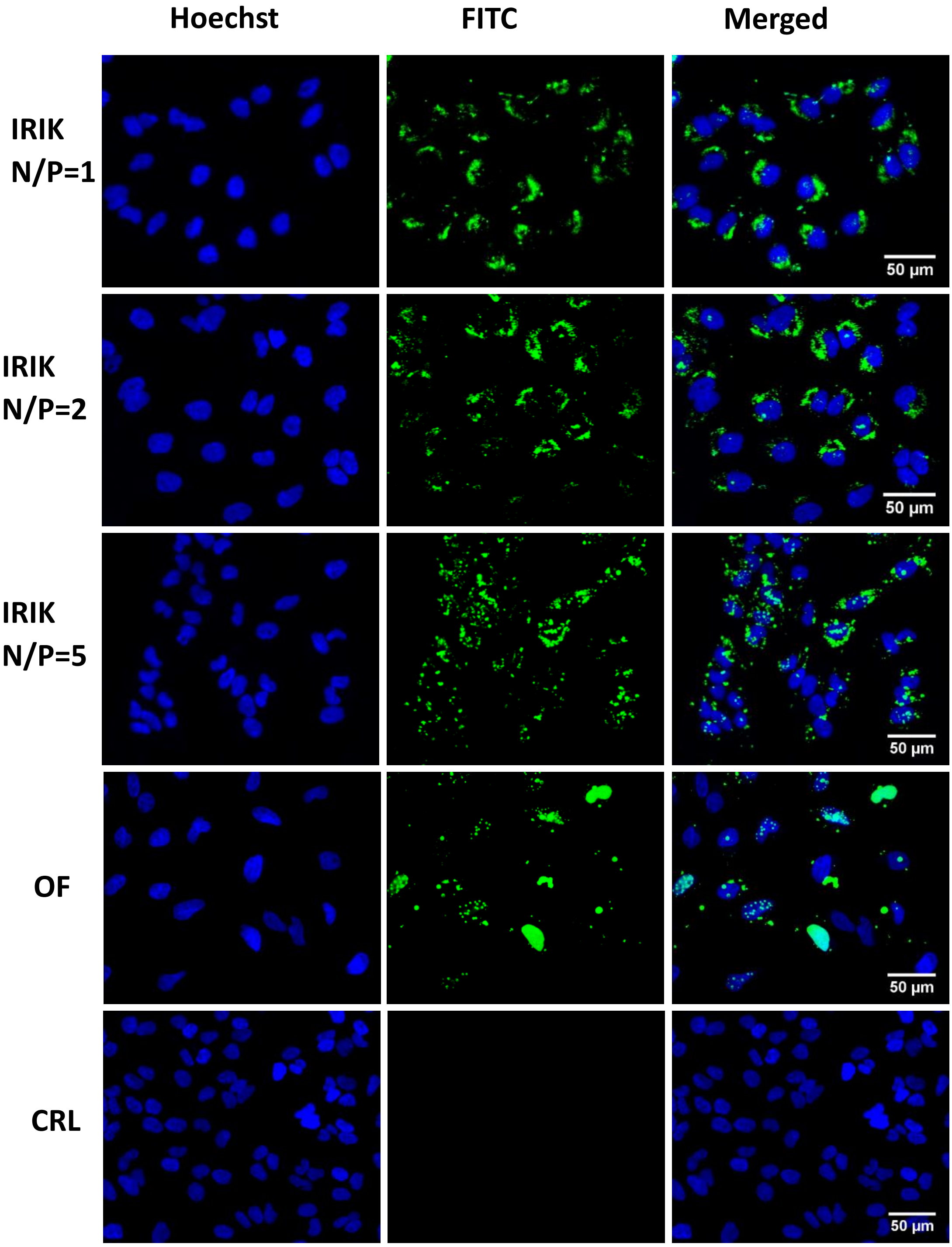

Figure 4.25. High content images of HeLa cells transfected with FITC-labelled c-Myc AON using IRIK at different N/P ratios. Oligofectamine™ (OF) was used as positive control and naked c-Myc AON was used as negative control. The nuclei were stained with Hoechst 33342, ×20 magnification.

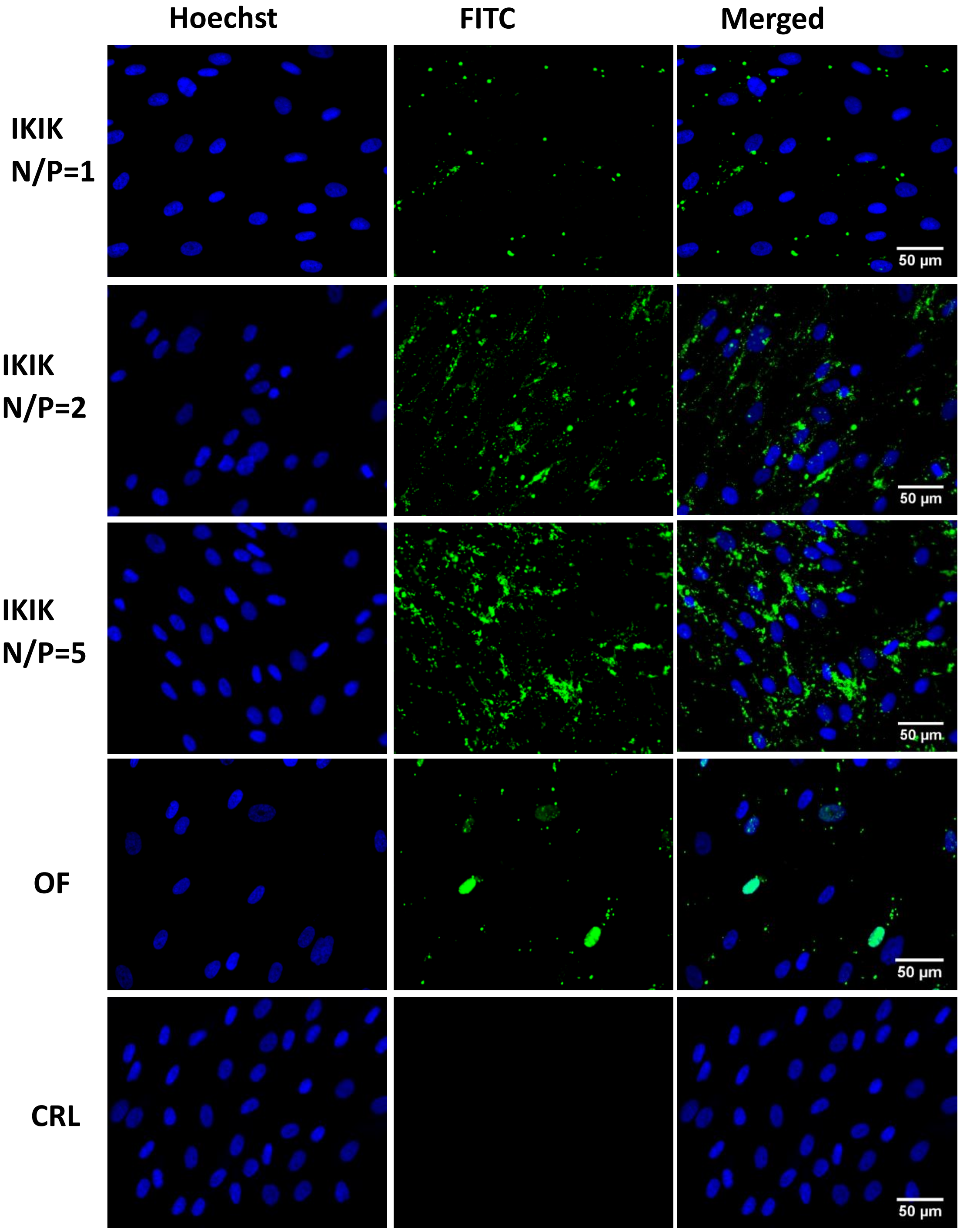

Figure 4.26. High content images of HDF cells transfected with FITC-labelled c-Myc AON using IKIK at different N/P ratios. Oligofectamine™ (OF) was used as positive control and naked c-Myc AON was used as negative control. The nuclei were stained with Hoechst 33342, ×20 magnification.

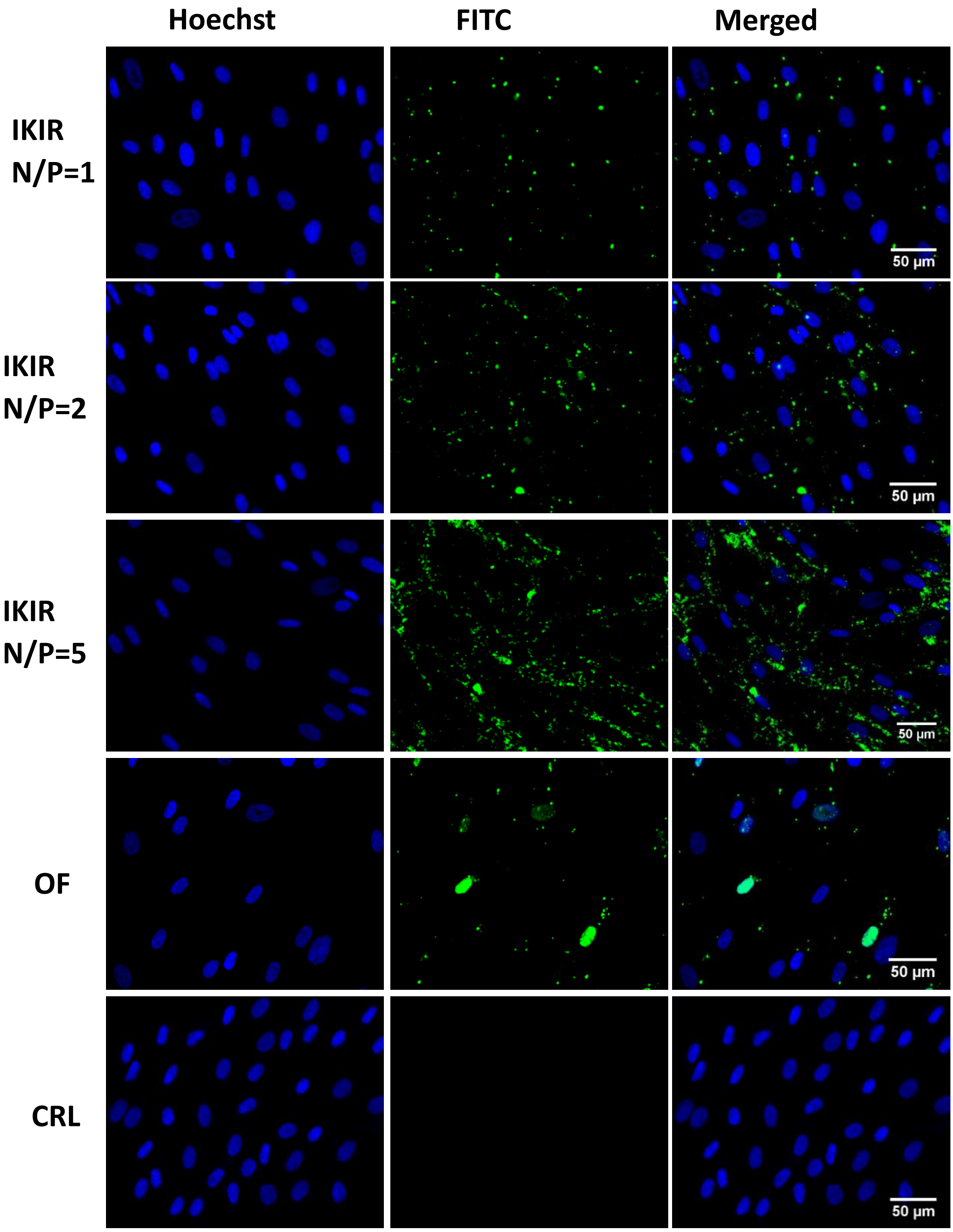

Figure 4.27. High content images of HDF cells transfected with FITC-labelled c-Myc AON using IKIR at different N/P ratios. Oligofectamine™ (OF) was used as positive control and naked c-Myc AON was used as negative control. The nuclei were stained with Hoechst 33342, ×20 magnification.

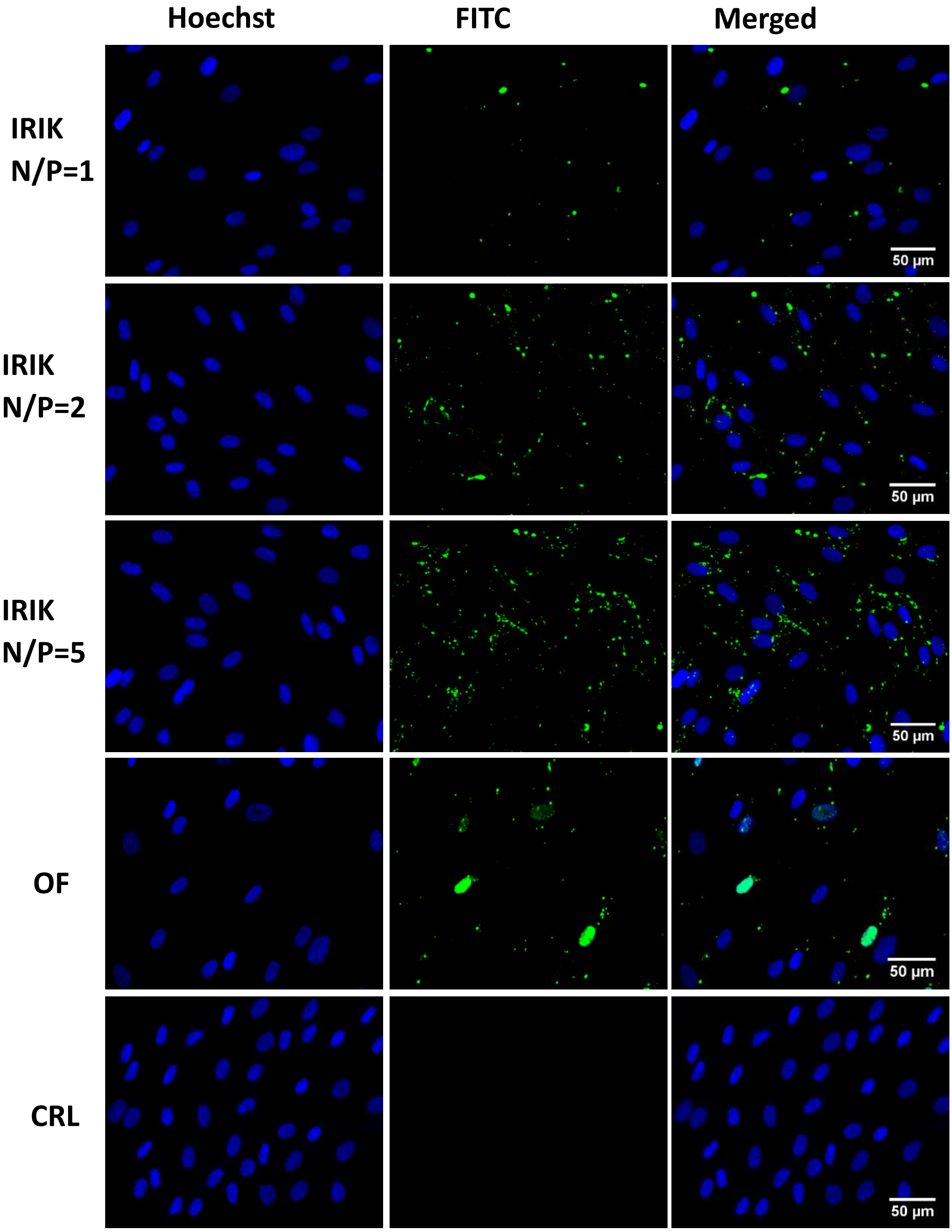

Figure 4.28. High content images of HDF cells transfected with FITC-labelled c-Myc AON using IRIK at different N/P ratios. Oligofectamine™ (OF) was used as positive control and naked c-Myc AON was used as negative control. The nuclei were stained with Hoechst 33342, ×20 magnification.

In order to unravel the reason for lack of transfection by the leucine rich peptides the complexation of peptides with cMyc AON was studied by measuring the changes to the zeta potential of the AONs following incubation with the peptides at different N/P ratios. Complexation with the peptide results in a change in the zeta potential from negative values to near neutral or positive the extent of which is indicative of the strength of the peptide-AON complexation [17-19].

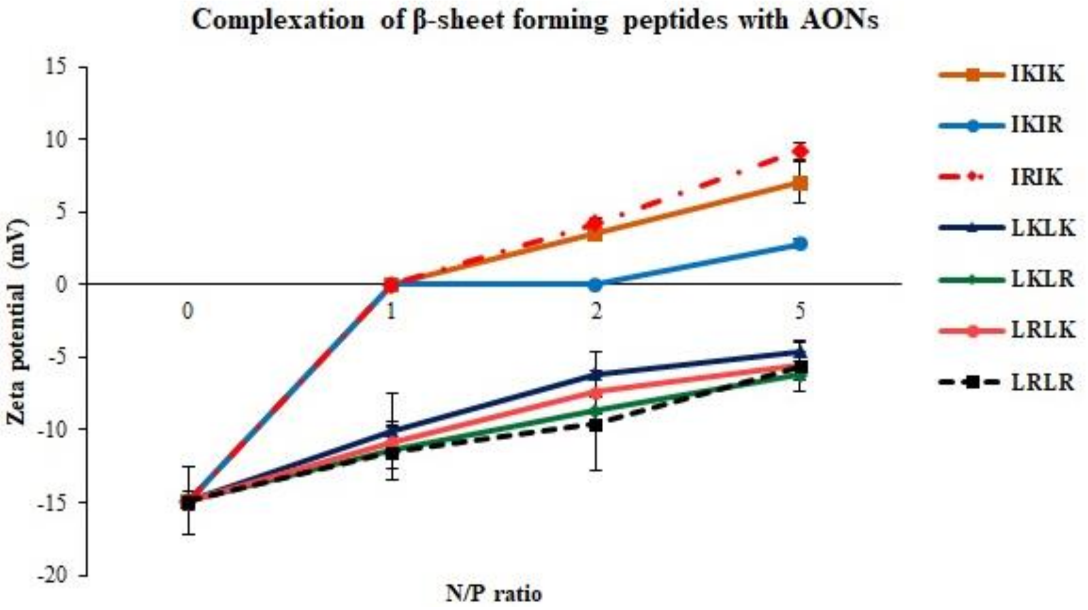

Figure 4.29. Changes to the zeta potential of the cMyc antisense oligonucleotides (AONs) following incubation with cationic amphiphilic β-sheet forming peptides at different N/P ratios. The values at N/P = 0 indicate the zeta potential of the naked AON. The data are reported as the average of three measurements.

As it could be observed in Figure 4.29, the peptides consisting of isoleucine residues increased the values of zeta potential of the naked AON from negative to neutral or positive indicating peptide-AON complexation whereas the peptides consisting of leucine residues where unable to do so indicating poor complexation between these peptides and the AONs. Although these peptides decrease the negative value of the zeta potential to some extent the values are still far from neutral. Hence, lack of transfection with these peptides is due to poor complexation of the peptides with AON.

4.3.6 Transfection with siRNA

Following transfection of the cancer cells with the cationic amphiphilic peptide-AON complexes, the peptides which successfully delivered cMyc AON to the cells (IKIK, IKIR, and IRIK) were tested for their ability to deliver siRNA to the cells using two different types of siRNA targeting the ECT2 and the UBB genes, following the protocol described in chapter 2.

Both ECT2 and UBB are involved in the cell proliferation and silencing these genes with siRNA is known induce apoptosis in the cells. Since these genes are more highly expressed in cancer cells than non-cancerous cells, they serve as good targets for cancer treatment [20-21]. Figures 4.30-4.33 illustrate the transfection efficiency of the peptide-siRNA complexes in HCT 116 cells. As mentioned earlier, successful transfection results in silencing of ECT2 and UBB genes and consequently reduction in the number of cells compared to the untreated controls.

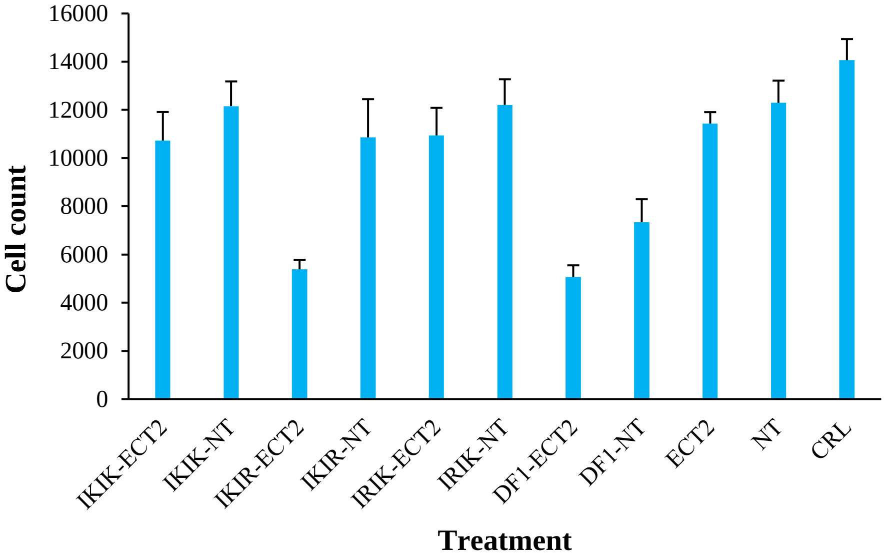

Figure 4.30. Reduction in the number of HCT 116 cells following transfection with ECT2-siRNA and scrambled non-targeting siRNA using the cationic amphiphilic peptides. Dharmafect1™ was used as positive control.

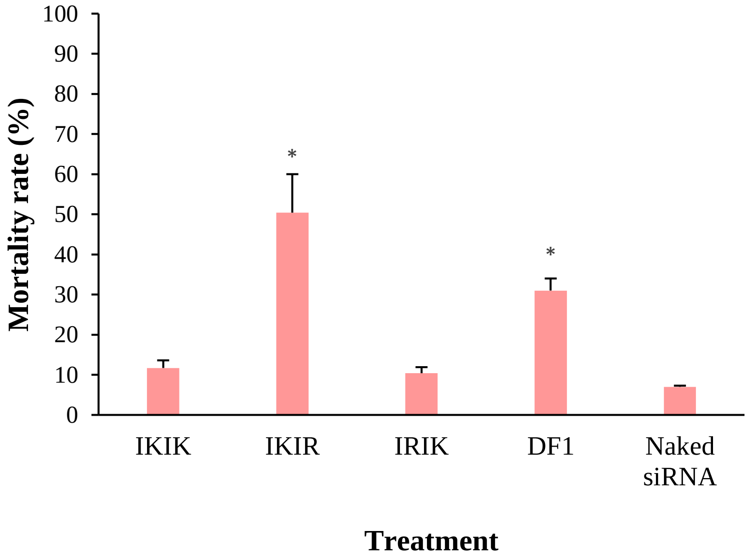

Figure 4.31. ECT2 gene silencing in HCT 116 cells transfected with ECT2-siRNA using the cationic amphiphilic peptides. The data were normalized against non-targeting siRNA. Dharmafect1™ was used as positive control. * indicates values of $p < 0.05$ as compared to naked siRNA.

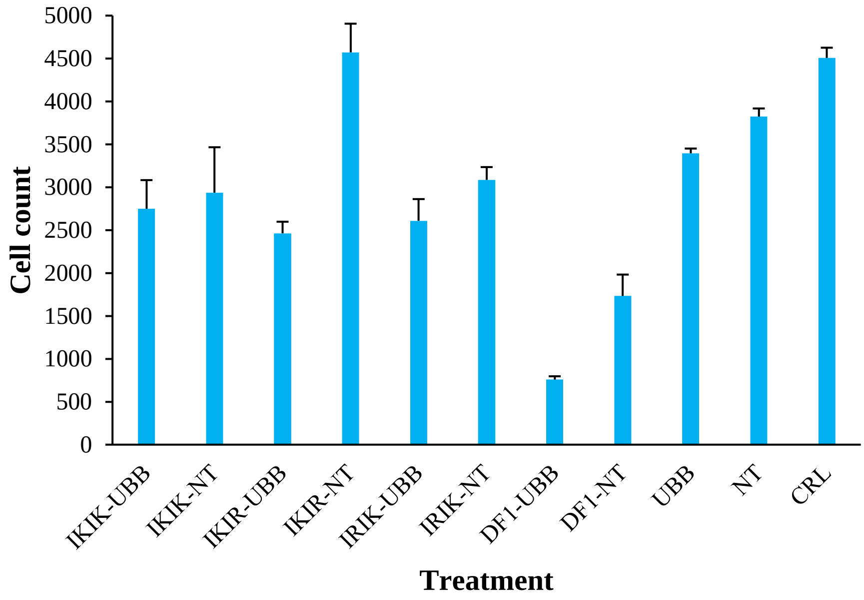

Figure 4.32. Reduction in the number of HCT 116 cells following transfection with UBB-siRNA and scrambled non-targeting siRNA using the cationic amphiphilic peptides. Dharmafect1™ was used as positive control.

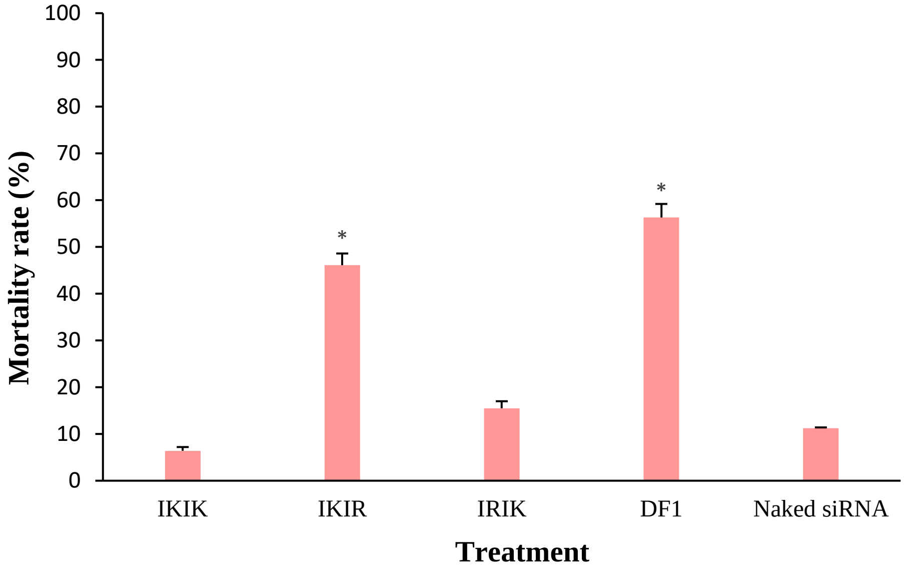

Figure 4.33. UBB gene silencing in HCT 116 cells transfected with UBB-siRNA using the cationic amphiphilic peptides. The data were normalized against non-targeting siRNA. Dharmafect1™ was used as positive control. * indicates values of $p < 0.05$ as compared to naked siRNA.

As it could be observed transfection with IKIR-ECT2 siRNA complexes resulted in a significant decrease in the number of HCT 116 cells compared to the untreated controls ($p = 0.0005$) which was comparable to Dharmafect1™ whereas IKIK and IRIK did not reduce the number of cells significantly ($p_1 = 0.18$, $p_2 = 0.16$ respectively). Nevertheless, transfection of

HCT 116 cells with IKIR complexed with scrambled non-targeting siRNA also induced a slight decrease in the total number of cells compared to the controls which was not comparable to IKIR-ECT2 siRNA but still significant. Therefore, as mentioned earlier in the previous chapters, to decouple the antiproliferative/apoptotic effect from the general cytotoxic effect caused by transfection, and determine the net gene silencing effect, the mortality rates in the cells transfected with ECT2 siRNA were normalized against the non-targeting siRNA and then compared to the naked siRNA as the negative control.

Transfection of HCT 116 cells with IKIR-ECT2 siRNA resulted in 50.4% mortality compared to the controls transfected with naked ECT2 siRNA clearly indicating successful gene silencing by the IKIR-ECT2 siRNA complex which was markedly higher than Dharmafect1™ (p value). Although Dharmafect1™ had a higher apparent transfection efficiency for ECT2 siRNA than IKIR, it also induced significant mortality when used for delivery of non-targeting siRNA, indicating that the observed cell mortality following Dharmafect1™-ECT2 siRNA transfection is in part caused by the general cytotoxicity of Dharmafect1™ as a lipid-based transfection reagent and in part by the silencing of ECT2 gene. Thus, after normalizing the apparent mortalities against general cytotoxicity of the complexes, the net gene silencing effect achieved by IKIR-ECT2 was higher than Dharmafect1™-ECT2. On the other hand, neither IKIK nor IRIK did not induce any significant gene silencing and did not cause significant mortality in the cells compared to the naked ECT2 siRNA ($p_1 = 0.38$, $p_2 = 0.39$ respectively). In a similar fashion, transfection of HCT 116 cells with IKIR-UBB siRNA induced considerable gene silencing in these cells which was slightly less than Dharmafect1™-UBB (46.1% vs. 56.3%) whereas IKIK-UBB and IRIK-UBB failed to induce any significant gene silencing as compared to the control (6.4 % and 15.5% mortality rate, $p_1 = 0.3$, $p_2 = 0.47$ respectively).

IKIR-ECT2 also induced significantly higher mortality in HDF cells than naked siRNA and untreated controls whereas IKIK, IRIK and Dharmafect1™ did not induce any significant mortality in these cells (Figures 4.34-4.35). Furthermore, the mortality rate of HDF cells transfected with IKIR-ECT2 was considerably lower than HCT 116 cells transfected with the same transfection complex. This might be due to lower expression of ECT2 gene in HDFs compared to HCT 116 resulting in lower responsiveness of these cells to ECT2 gene silencing or due to the lower uptake of the peptide-siRNA complexes by HDFs compared to cancer cells.

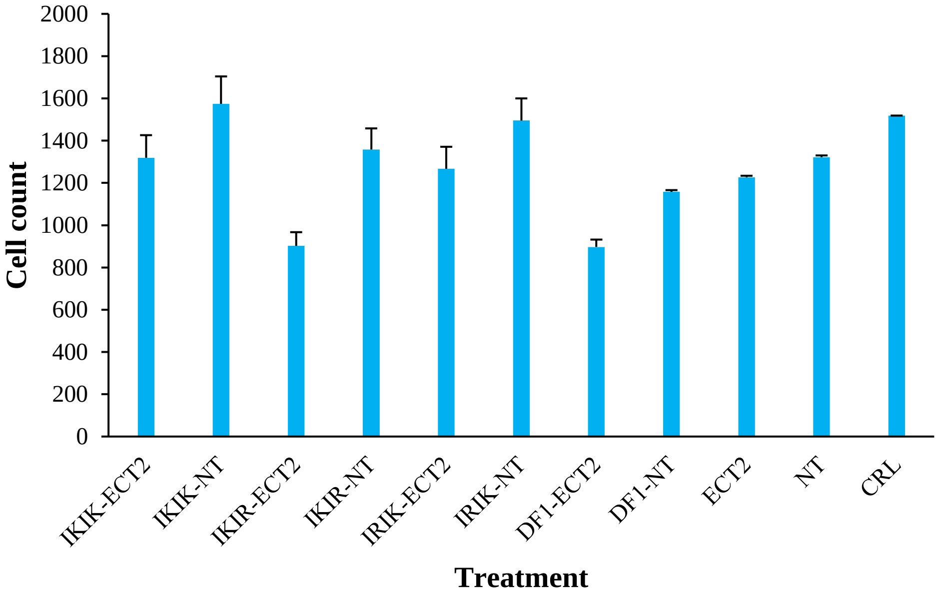

Figure 4.34. Reduction in the number of HDF cells following transfection with ECT2-siRNA and scrambled non-targeting siRNA using the cationic amphiphilic peptides. Dharmafect1™ was used as positive control.

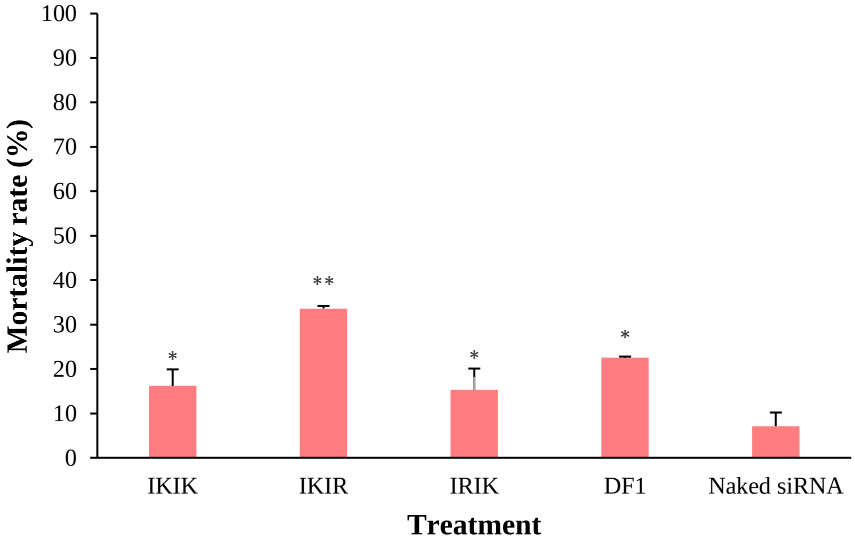

Figure 4.35. ECT2 gene silencing in HDF cells transfected with ECT2-siRNA using the cationic amphiphilic peptides. The data were normalized against non-targeting siRNA. Dharmafect1™ was used as positive control. * indicates values of $p < 0.05$ and ** indicates values of $p < 0.005$ as compared to naked siRNA.

As it could be inferred from these data, despite the similar amino acid composition of IKIR and IRIK, changing the repeat pattern of the hydrophobic and hydrophilic amino acid residues in the peptide sequence results in different transfection efficiencies. Although all the three peptides were able to penetrate the cell membrane and enter the cells (as evidenced by successful delivery of cMyc AON to the HCT 116 cells), only IKIR induced successful gene silencing following siRNA transfection. This might be due to the stronger complexation between the peptide and siRNA in the case of IRIK and IKIK compared to IKIR which prevents the siRNA from release within the cytosol and thus prevents it from accessing the RNAi machinery and exerting its silencing effect as according to the results from complexation with AONs (Figure 4.27) IRIK and IKIK formed the strongest complexes with AONs among all of the peptides in this group as indicated by greater increase values of zeta potential. Nevertheless, to confirm that similar electrostatic interactions occur between the peptide and siRNA, the changes to the zeta potential of these three peptides upon complexation with siRNA at the N/P ratio of 5 which was used for transfection/gene silencing was measured. As it could be inferred from Figure 4.36, a similar trend was observed for peptide-siRNA complexation and higher values of zeta potential were achieved by IRIK and IKIK indicating stronger complexation than IKIR.

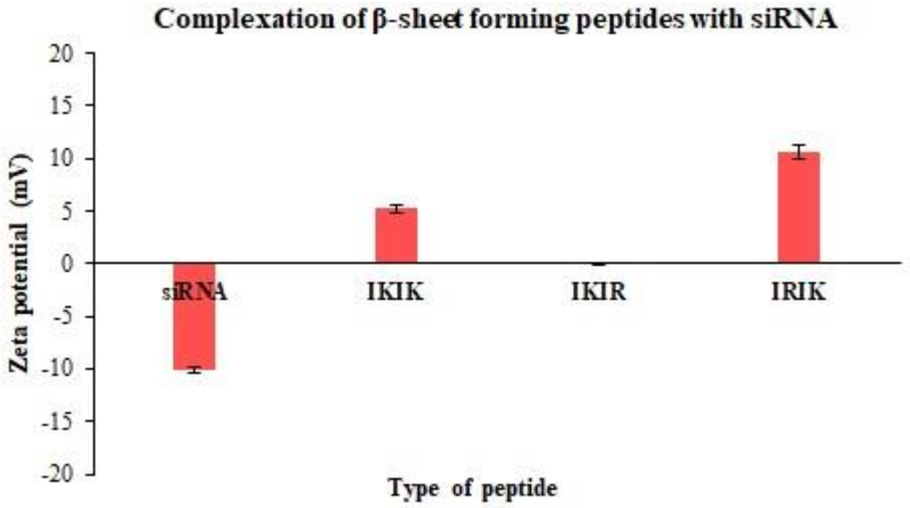

Figure 4.36. Changes to the zeta potential of the siGLO™ red siRNA following complexation with the cationic amphiphilic β-sheet forming peptides at the N/P ratio of 5. The data are reported as the average of three measurements.

4.4 Conclusion

A series of β-sheet forming cationic amphiphilic peptides were rationally designed based on the structural requirements for antimicrobial and anticancer peptides and were evaluated for their anticancer activity as well as their gene delivery potential. The peptides showed different cytotoxicity patterns in different cell lines. IKIK showed high cytotoxicity in HCT 116, HeLa, MDA-MB-231 and HDF. Replacing half of the lysine residues in IKIK with arginine, diminished the cytotoxicity of the resulting peptides against MDA-MB-231 and HDF and made the peptide selectively toxic against HCT 116 and HeLa. In a similar manner, replacing the isoleucine residues in IKIK with leucine residues preserved the cytotoxicity of the peptide (LKLK) against HCT 116 and HeLa but reduced its cytotoxicity against HDF and MDA-MB-231. On the contrary, replacing the lysine residues in LKLK with arginine residues diminished the toxicity of peptide (LRLR) against HeLa and increased its toxicity in HDF and MDA-MB-231. Replacing half of the lysine residues with arginine made the resulting peptides more selectively toxic to MDA 231-MB and HDF. Overall, LKLK, IKIR and IRIK were found to be more selectively toxic to HCT 116 and HeLa with minimal toxicity against fibroblasts suggesting these cationic amphiphilic peptides as selective anticancer peptides. Cell proliferation studies in HCT 116 revealed weak antiproliferative effect of the β-sheet forming cationic amphiphilic peptides suggesting that the cytotoxicity of these peptides is mainly caused by reduction of the cellular metabolic activity and antiproliferative effect has only a minor contribution to the overall cytotoxicity of the peptides. The peptides were shown to exert their anticancer effect by damaging the mitochondria as it was evidenced by changes to the morphology of mitochondria and mitochondrial membrane depolarization following treatment with these peptides.

The cationic amphiphilic peptides containing isoleucine residues in their hydrophobic domain were able to deliver the cMyc-AON to both cancer cells and normal fibroblasts in a concentration-dependent manner whereas the peptides containing leucine in their hydrophobic domain failed to so. Transfection of HCT 116 cells with IKIR-ECT2 siRNA and IKIR-UBB siRNA resulted in considerable gene silencing in these cells which was comparable to the commercial transfection reagent Dharmafect1™ whereas IKIK-siRNA and IRIK-siRNA complexes failed to induce any significant gene silencing in HCT 116 cells. IKIR-ECT2 also induced gene silencing in HDF cells but at a lower level than HCT 116 cells which suggests this peptide as a candidate for gene delivery to cancer cells with low adverse effects in normal cells.

4.5 References

1. Z. Y. Ong, S. J. Gao, and Y. Y.Yang. Short synthetic β -sheet forming peptide amphiphiles as broad spectrum antimicrobials with antibiofilm and endotoxin neutralizing capabilities. *Adv. Funct. Mater.*, 23 (2013): 3682-3692.
2. Z. Y. Ong, J. Cheng, Y. Huang, et al. Effect of stereochemistry, chain length and sequence pattern on antimicrobial properties of short synthetic β-sheet forming peptide amphiphiles. *Biomaterials*, 35 (2014):1315-1325.
3. H. Wu, Z.Y. Ong, S. Liu, et al. Synthetic β-sheet forming peptide amphiphiles for treatment of fungal keratitis. *Biomaterials*, 43 (2015): 44-49.
4. L. A. Avila, L. RMM Aps, P. Sukthankar, N. Ploscariu, S. Gudlur, et al. Branched amphiphilic cationic oligopeptides form peptiplexes with DNA: A study of their biophysical properties and transfection efficiency. Mol. Pharmaceutics, 12 (2015):706-715.
5. G. N. Goparaju, P. K. Gupta. Design of amphiphilic oligopeptides as models for fine tuning peptide assembly with plasmid DNA. Drug Discoveries Ther., 8(2014):165-172.
6. H. O. McCarthy, J. McCaffrey, C. M. McCrudden, A. Zholobenko, A. A. Ali, et al. Development and characterization of self-assembling nanoparticles using a bio-inspired amphipathic peptide for gene delivery. J. Control. Release, 189 (2014): 141-149.
7. M. Law, M. Jafari, P. Chen. Physicochemical characterization of SiRNA-peptide complexes. Biotechnol. Prog., 24 (2008): 957-963.
8. D. Lejeune, N. Delsaux , B. Charloteaux, A. Thomas, R. Brasseur. Protein-nucleic acid recognition: Statistical analysis of atomic interactions and influence of DNA structure. Proteins, 61 (2005):258-271.
9. S.D.D.T.A. Jones, N.M. Luscombe, H.M. Berman, J.M. Thornton. Protein-RNA interactions: a structural analysis. Nucleic Acids Res., 29 (2001):943-954.
10. J. Guo, W. P. Cheng, J. Gu, C. Ding, X. Quc, et al. Systemic delivery of therapeutic small interfering RNA using a pH-triggered amphiphilic poly-L-lysine nanocarrier to suppress prostate cancer growth in mice. Eur. J. Pharm. Sci., 45 (2012): 521-532.
11. J. Dufourcq, W. Neri, N. Henry-Toulmeè. Molecular assembling of DNA with amphipathic peptides. FEBS Lett., 421 (1998): 7-11.
12. K. K. Hou, H. Pan, G. M. Lanza, S. A. Wickline. Melittin derived peptides for nanoparticle based siRNA transfection. Biomaterials, 34 (2013): 3110-3119.

13. H. F. Zhou, H. Yan, H.Pan, K. K. Hou, A. Akk, et al. Peptide-siRNA nanocomplexes targeting NF-κB subunit p65 suppress nascent experimental arthritis. J. Clin. Invest., 124 (2014):4363-4374.
14. K. A. Mills, J. M. Quinn, S. T. Roach, M. Palisoul, M. Nguyen, et al. p5RHH nanoparticle-mediated delivery of AXL siRNA inhibits metastasis of ovarian and uterine cancer cells in mouse xenografts. Sci. Rep., 9 (2019):1-10
15. T. Mosmann. Rapid colorimetric assay for cellular growth and survival: Application to proliferation and cytotoxicity assays. J. *Immunol. Methods*, 65 (1983): 55-63.
16. M. V. Berridge, P. M. Herst, and A. S. Tan. Tetrazolium dyes as tools in cell biology: New insights into their cellular reduction. *Biotechnol. Annu. Rev.*, 11(2005): 127-152.
17. M. Li, S. Schlesiger, S. K. Knauer, and C. Schmuck, Introduction of a tailor made anion receptor into the side chain of small peptides allows fine-tuning the thermodynamic signature of peptide-DNA binding. *Org. Biomol. Chem.*, 2016, 14 (2016): 8800-8803.
18. J. Coles, A. Esposito, H. T. Chuah, and I. Toth. The synthesis and characterization of lipophilic peptide-based carriers for gene delivery. *Tetrahedron*, 66 (2010): 5435-5441.
19. G. Québatte, E. Kitas, and J. Seelig. riDOM, a Cell-Penetrating Peptide. Interaction with DNA and Heparan Sulfate. *J. Phys. Chem. B*, 117 (2013): 10807-10817.
20. https://www.genecards.org/cgi-bin/carddisp.pl?gene=ECT2, accessed on 20/08/2019.
21. https://www.genecards.org/cgi-bin/carddisp.pl?gene=UBB, accessed on 20/08/2019.

Chapter 5: biological activity of surfactant-like peptides

5.1 Background and aims

Synthetic or naturally derived short peptides that specifically bind to oligonucleotides are attractive candidates for novel gene delivery systems, because they have low cytotoxicity, are less likely to induce immune responses and are easily degraded in the cells [1-2]. The resulting peptide-nucleic acid complexes, facilitate translocation across the cell membrane, provide better endosomal escape and protect the nucleic acids from enzymatic degradation thus resulting in enhanced transfection efficiency [3]. To date, various types of peptides have been tried for gene delivery to different types of cells among which cationic amphiphilic peptides have shown greater promise as gene vectors and have therefore received more attention for such applications over the past decade [4-21].

Despite the considerable body of research on the use of amphiphilic peptides for delivery of pDNA and siRNA, only few of these peptides have shown high levels of transfection efficiency, especially in the case of siRNA delivery systems. In addition, only a few of these peptide vectors were selective towards specific types of cells [5, 11, 21], whereas the other peptides were more likely to transfect every type of cells without any preference. Hence, there is still much room for development of more efficient and more selective peptide-based gene vectors.

Here in, we report the design and evaluation of a series of cationic amphiphilic peptides with the general formula $(X_1X_2)4K$, where X_1 and X_2 are hydrophobic amino acids (I, A and G), in an attempt to develop a new highly efficient and non-toxic peptide-based gene delivery system with potential applications in cancer treatment. This series consists of two peptides: $(IA)_4K$ and $(IG)_4K$, with the amino acid sequences IAIAIAIAK-NH2 and IGIGIGIGK-NH2 respectively. The peptides were rationally designed based on the generally known principles that the lysine residues, which are positively charged in physiological pH, provide nucleic acid binding [7, 14-16] and the hydrophobic amino acid residues promote the spontaneous peptide self-assembly into nanoparticles, which allows for better complexation with nucleic acids by increasing the local cationic charge density [5].

5.2 Experimental

5.2.1 Transfection studies

The gene delivery efficiency of the peptides was evaluated in HCT 116 colorectal cancer cells and human dermal fibroblast (HDF) cells. The initial proof of concept transfection studies were carried out using two fluorescently labelled transfection indicators; c-Myc antisense oligonucleotide labelled with 6-FAM and siGLO™ red transfection indicator. Peptide/c-Myc or peptide/siGLO™ complexes of varying N/P ratios were prepared as described in Sections 2.17-2.18. Following addition of the transfection complex to the cells, the cells were incubated at 37 °C for 24-72h. Commercially available transfection reagents, Oligofectamine™ and DharmaFECT1™ were used as positive controls and the naked c-Myc or siGLO were used as negative control in all experiments. At the end of the incubation period, the cells were fixed using 3.7% formaldehyde, stained with fluorescent dyes (Hoechst 33342 for the nuclei and Alexa fluor® 568 Phalloidin or Alexa fluor® 488 Phalloidin for the cytoplasm) following the protocols described in Section 2.11.3 and imaged using high content fluorescent microscope. The intracellular localization of the peptide-cMyc or peptide- siGLO™ complexes in HCT and HDF cells was further evaluated by confocal laser scanning microscope (CLSM).

5.2.2 Cytotoxicity studies

The cytotoxicity of the peptides in HCT 116 and HDF cells was tested *in vitro* by MTT assay following the protocol described in Section 2.15. The cells were treated with peptide solutions of different concentrations ranging from 0.1 µM/L to 10 µM/L and incubated at 37 °C for 24-120 h and then subjected to MTT assay.

5.3 Results and discussion

5.3.1 Transfection with AONs

The high content microscope images of HCT 116 colorectal cancer cells transfected with $(IA)_4$K-c-Myc complexes and $(IG)_4$K-c-Myc complexes of N/P ratios ranging from 0.5 to 3 after 24 h and 72 h incubation are depicted in Figures 5.1-5.3. As it could be observed, both peptides were able to deliver their associated c-Myc to the cells at all of the tested N/P ratios after 24 h incubation to a higher extent compared with the commercial transfection reagent (Oligofectamine™) whereas the negative controls (i.e., naked c-Myc) where unable to get into the cells. Moreover, the c-Myc was still retained within the cells after 72 h which suggests a stable transfection. The transfection pattern was similar for both peptides. At lower N/P ratios (0.5, 1) the green fluorescence from FAM was mainly observed at the perinuclear area which indicates the localization of the c-Myc in the perinuclear area. On the other hand, at N/P ratios greater than 1, the peptide-c-Myc complexes are observed as large clumps around the nuclei, part of which appears to be at a different focal plane from the nuclei which suggests that the peptide-c-Myc complexes may be partially outside the cells on the outer cell membrane.

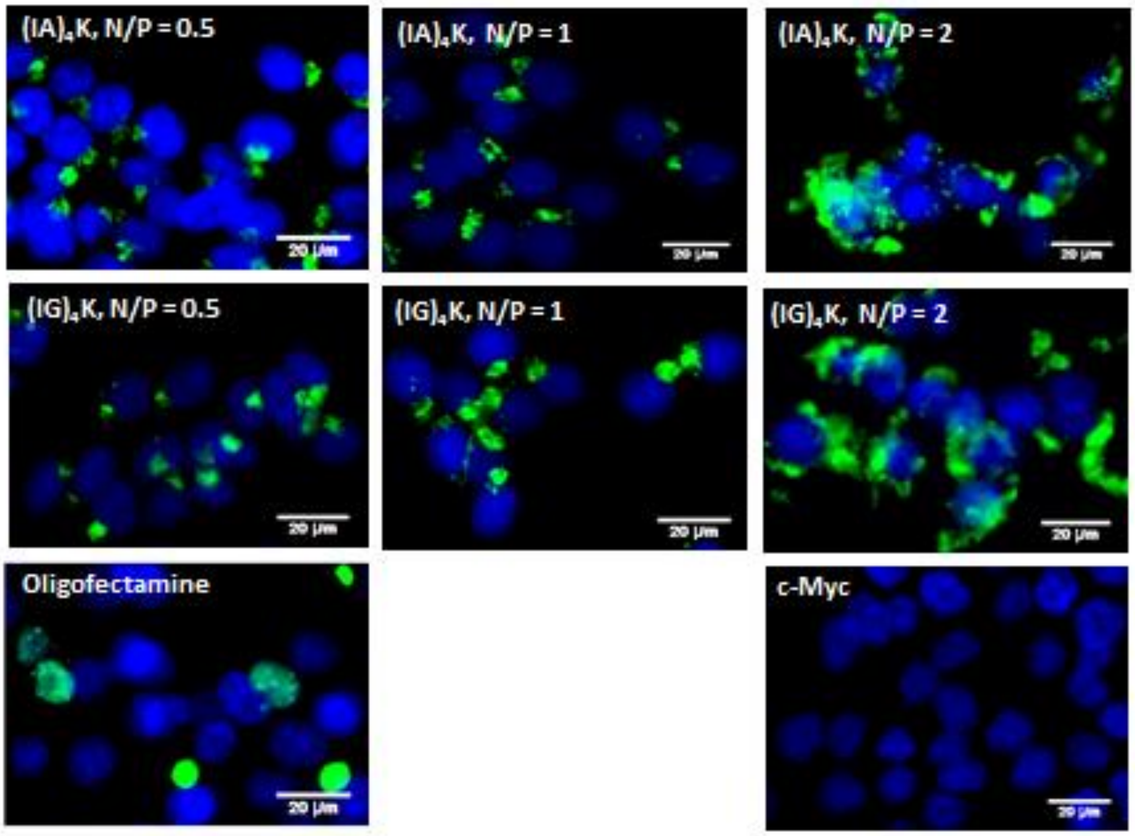

Figure 5.1. High content images of HCT 116 cells 24 h after transfection with $(IA)_4K$-cMyc and $(IG)_4K$-c-Myc complexes of various N/P ratios. The nuclei are stained with Hoechst 33342 (blue) and c-Myc is labelled with FAM (green). Oligofectamine™ was used as positive control and naked c-Myc was used as negative control. ×20 magnification, scale bar = 20 µm.

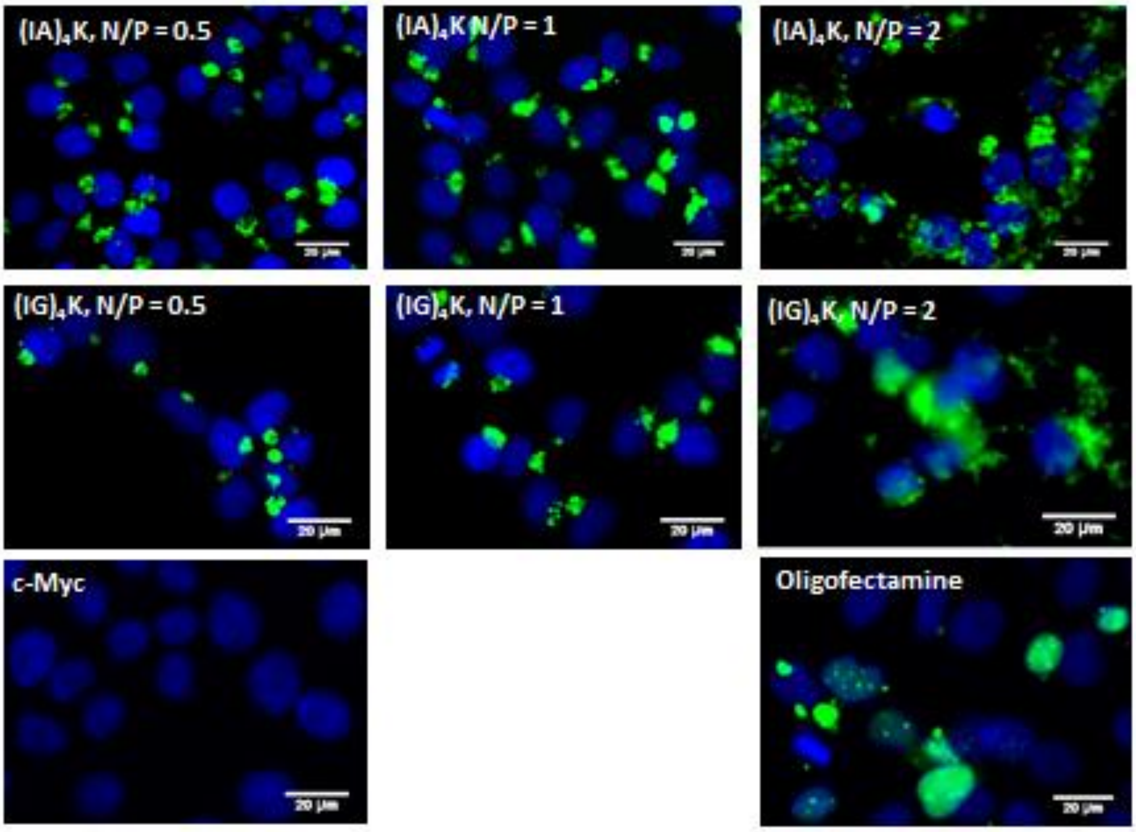

Figure 5.2. High content images of HCT 116 cells 72 h after transfection with (IA)$_4$K-cMyc and (IG)$_4$K-c-Myc complexes of various N/P ratios. The nuclei are stained with Hoechst 33342 (blue) and c-Myc is labelled with FAM (green). Oligofectamine™ was used as positive control and naked c-Myc was used as negative control. ×20 magnification, scale bar = 20 µm.

To confirm the presence of the peptide-c-Myc complexes inside the cells, the cells were also imaged with CLSM 24 h after transfection with (IG)$_4$K-c-Myc complexes. CLSM has the ability to create Z-stacks, which allows for detecting only the fluorescence produced very close to the focal plane and eliminating the out of focus signals coming from the areas away from the focal plane. As a result, the CLSM images show only the objects which are at the same focal plane (i.e. at the same depth within the specimen) and the areas away from the focal plane are removed from resulting images. Thus, any objects observed within a confocal image are by default supposed to be located at the same focal plane within the specimen [22-23]. It is evident from the CLSM images, that the (IG)$_4$K-c-Myc complexes at N/P ratio of 1 and 2 are inside the cells, and mainly localized in the perinuclear area. These images provide further evidence that the peptides are able to deliver their associated AONs to the cancer cells.

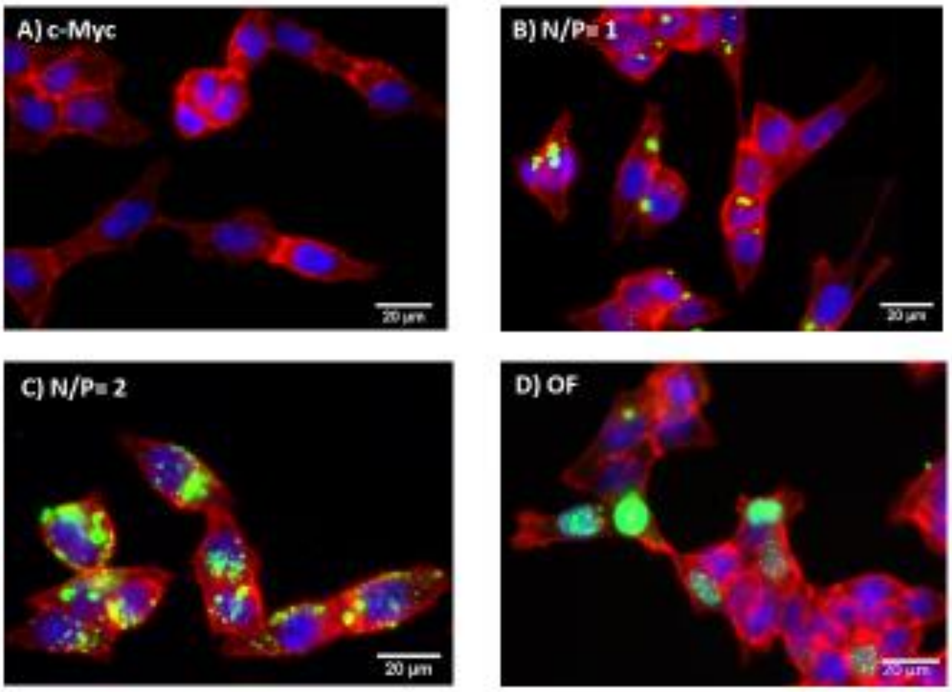

Figure 5.3. High content microscope images of HCT 116 cells transfected with $(IG)_4K$-c-Myc complexes after 24 h. The cytoplasm is stained with Alexafluor®568-Phalloidin (red), the nuclei are stained with Hoechst 33342 (blue) and c-Myc is labelled with FAM (green). Oligofectamine™ was used as positive control and naked c-Myc was used as negative control. ×40 magnification, Scale bar = 20 µm.

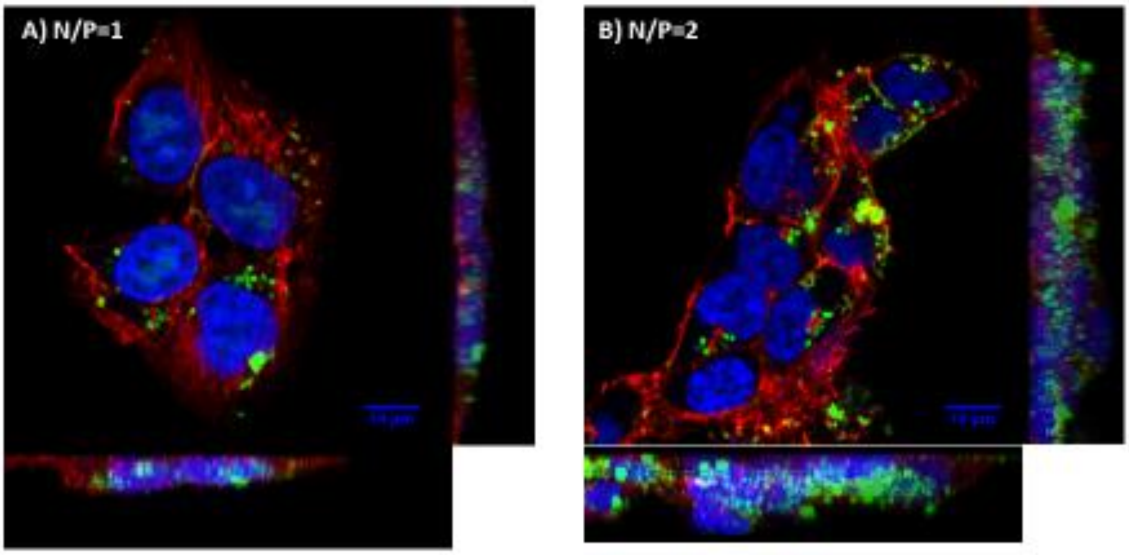

Figure 5.4. CLSM images of HCT116 cells transfected with $(IG)_4K$-c-Myc complexes after 24 h. The cytoplasm is stained with Alexafluor®568-Phalloidin (red), the nuclei are stained with Hoechst 33342 (blue) and c-Myc is labelled with FAM (green). ×40 magnification, Scale bar = 10 µm.

In order to assess the selectivity of the peptide-AON complexes for cancer cells versus normal cells, the transfection studies with $(IA)_4K$-c-Myc and $(IG)_4K$-c-Myc complexes were carried out in Human dermal fibroblast (HDF) cells under similar experimental conditions as HCT 116 cells, the results of which are depicted in Figures 5.5-5.7. As it could be observed in these images, both $(IA)_4K$ and $(IG)_4K$ were able to transfect the HDF cells with c-Myc but unlike HCT 116, in HDF cells the peptide-c-Myc complexes are scattered all over the cytoplasm. In a similar fashion to HCT 116 cells, at N/P ratio of 2, a proportion of the complexes appear to be attached to the outer cell membrane. These observations were further confirmed and supported by CLSM images of HDFs transfected with $(IG)_4K$-cMyc complexes (Figure 5.8).

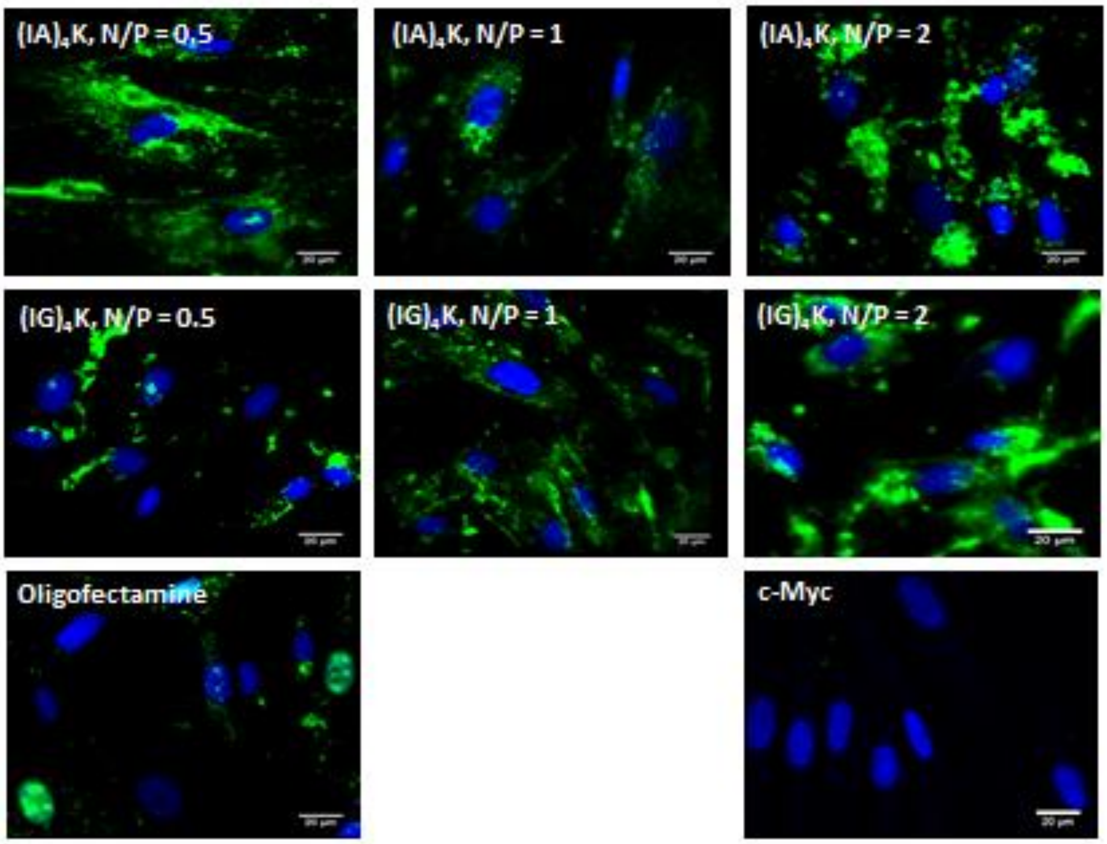

Figure 5.5. High content images of HDF cells 24 h after transfection with $(IA)_4K$-c-Myc and $(IG)_4K$-c-Myc complexes of various N/P ratios. The nuclei are stained with Hoechst 33342 (blue) and c-Myc is labelled with FAM (green). Oligofectamine™ was used as positive control and naked c-Myc was used as negative control. ×20 magnification, scale bar = 20 µm.

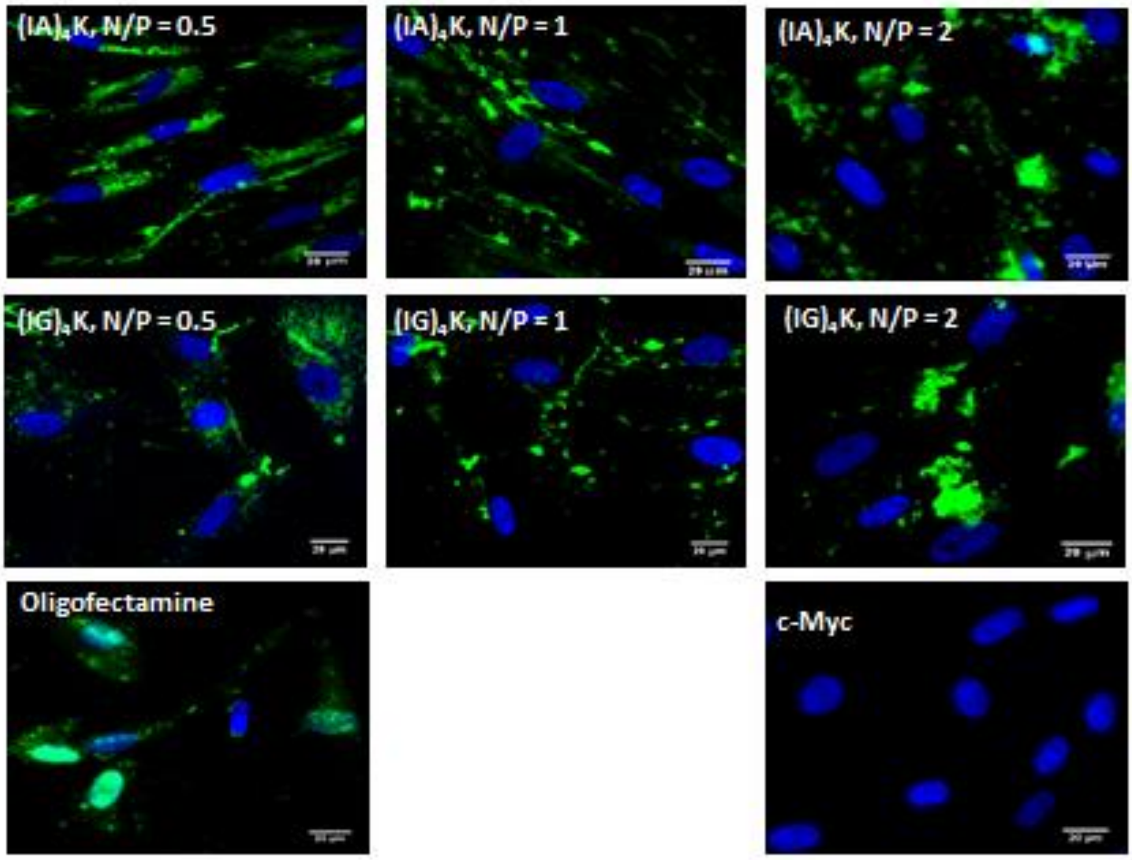

Figure 5.6. High content images of HDF cells 24 h after transfection with $(IA)_4$K-c-Myc and $(IG)_4$K-c-Myc complexes of various N/P ratios. The nuclei are stained with Hoechst 33342 (blue) and c-Myc is labelled with FAM (green). Oligofectamine™ was used as positive control and naked c-Myc was used as negative control. ×20 magnification, scale bar = 20 µm.

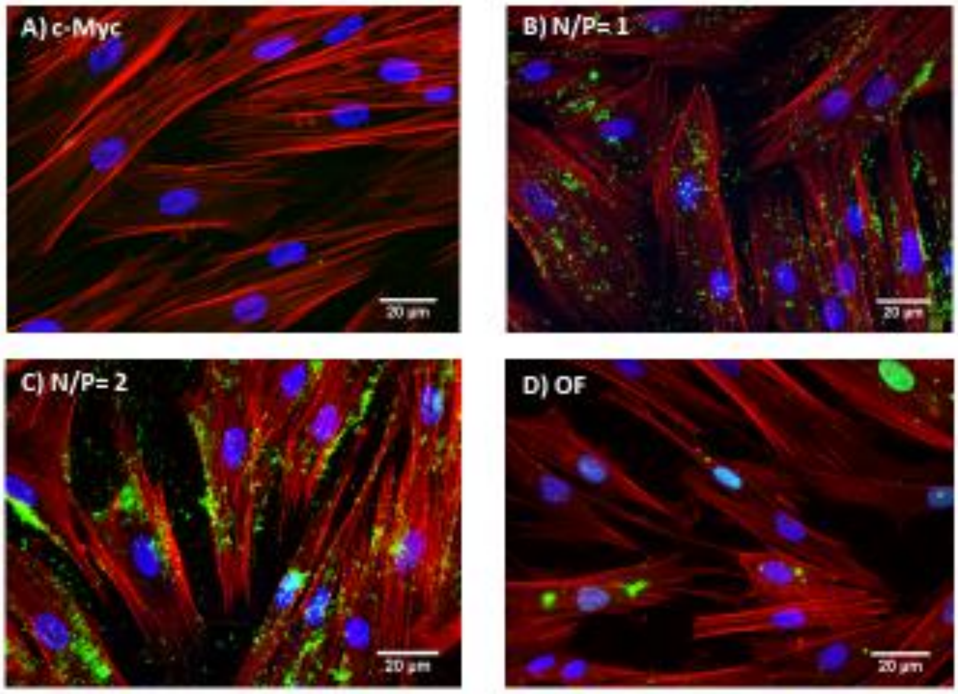

Figure 5.7. High content microscope images of HDF cells transfected with $(IG)_4K$-c-Myc complexes after 24 h. The cytoplasm is stained with Alexafluor®568-Phalloidin (red), the nuclei are stained with Hoechst 33342 (blue) and c-Myc is labelled with FAM (green). Oligofectamine was used as positive control and naked c-Myc was used as negative control. ×20 magnification, scale bar = 20 µm.

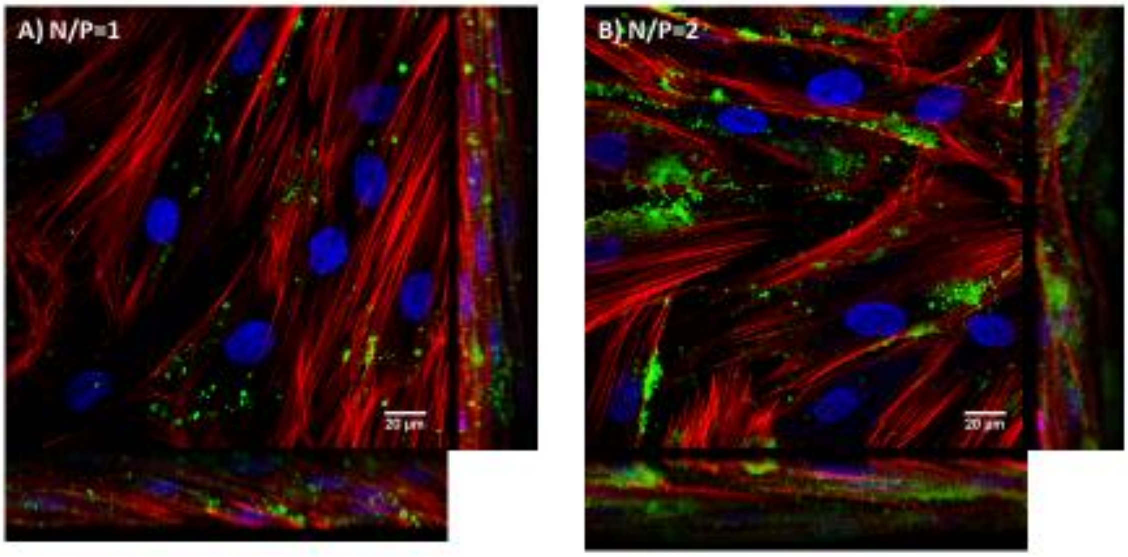

Figure 5.8. CLSM images of HDF cells transfected with $(IG)_4K$-c-Myc complexes after 24 h. The cytoplasm is stained with Alexafluor®568-Phalloidin (red), the nuclei are stained with Hoechst 33342 (blue) and c-Myc is labelled with FAM (green). Oligofectamine was used as positive control and naked c-Myc was used as negative control. ×40 magnification, scale bar = 20 µm.

5.3.2 Transfection with siRNA

Following successful transfection of HCT116 and HDF cells with peptide-c-Myc complexes, the peptides were tested for their ability to bind to and transfer siRNA to the cells. For this purpose, a fluorescently labelled siRNA, siGLO™ red was used as transfection indicator and the cells were treated with peptide-siRNA complexes under the experimental conditions described in Section 2.18. The high content microscope images of the HCT 116 cells and HDF cells transfected with $(IA)_4K$- siGLO™ and $(IG)_4K$- siGLO™ complexes of different N/P ratios for 24-72h are depicted in Figures 5.9-5.12.

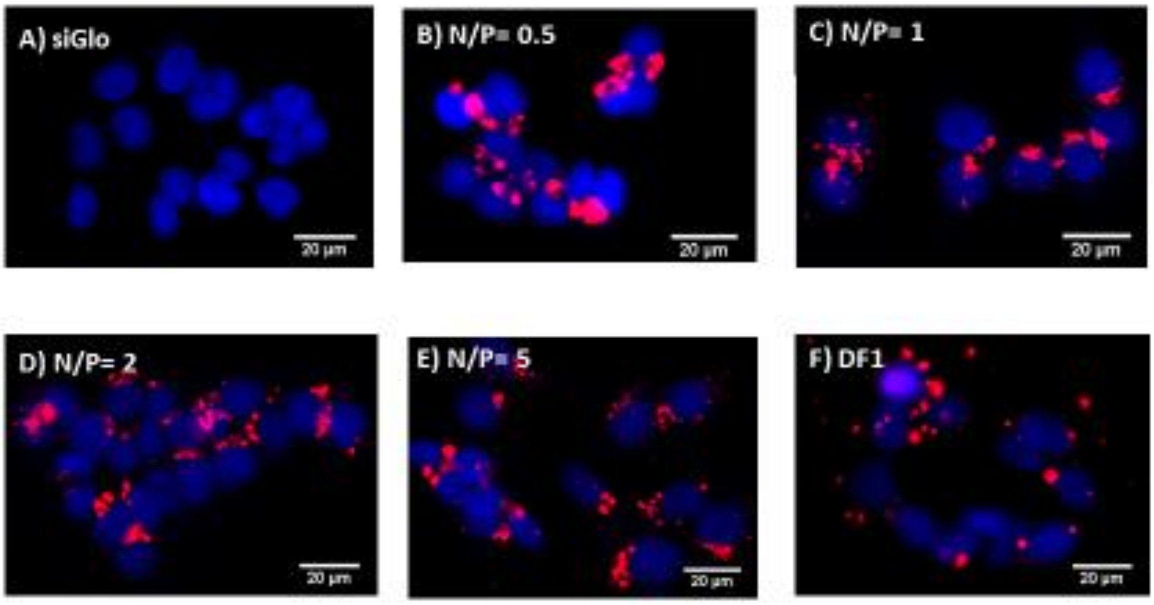

Figure 5.9. High content images of HCT 116 cells 24 h after transfection with $(IA)_4K$-siGLO red complexes. The nuclei are stained with Hoechst 33342 (blue), and siGLO™ is labelled with cy3 (red). ×20 magnification, scale bar = 20 µm.

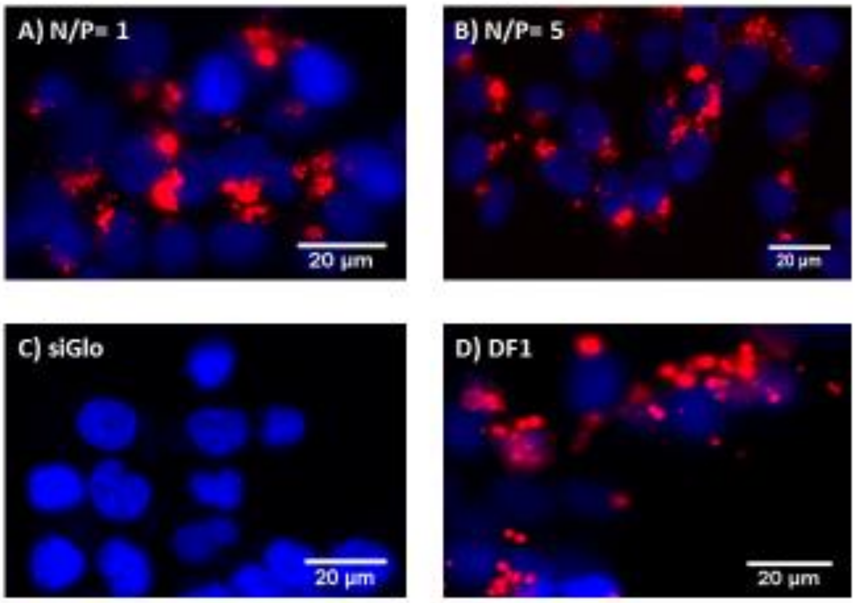

Figure 5.10. High content images of HCT 116 cells 72 h after transfection with $(IA)_4K$-siGLO red complexes. The nuclei are stained with Hoechst 33342 (blue), and siGLO™ is labelled with cy3 (red). ×20 magnification, scale bar = 20 µm

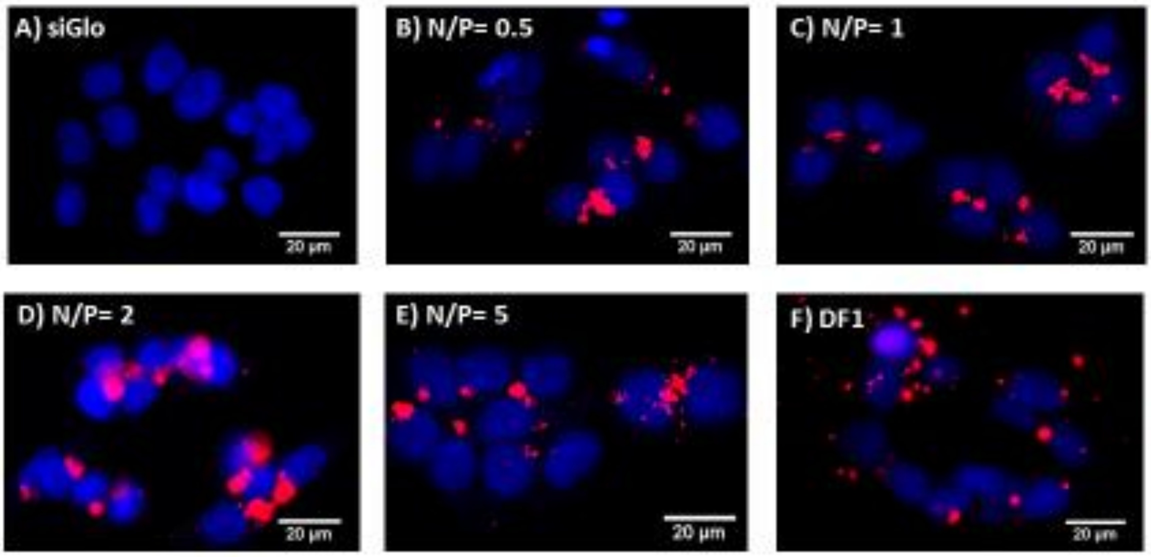

Figure 5.11. High content images of HCT 116 cells 24 h after transfection with $(IG)_4K$-siGLO red complexes. The nuclei are stained with Hoechst 33342 (blue), and siGLO™ is labelled with cy3 (red). ×20 magnification, scale bar = 20 µm

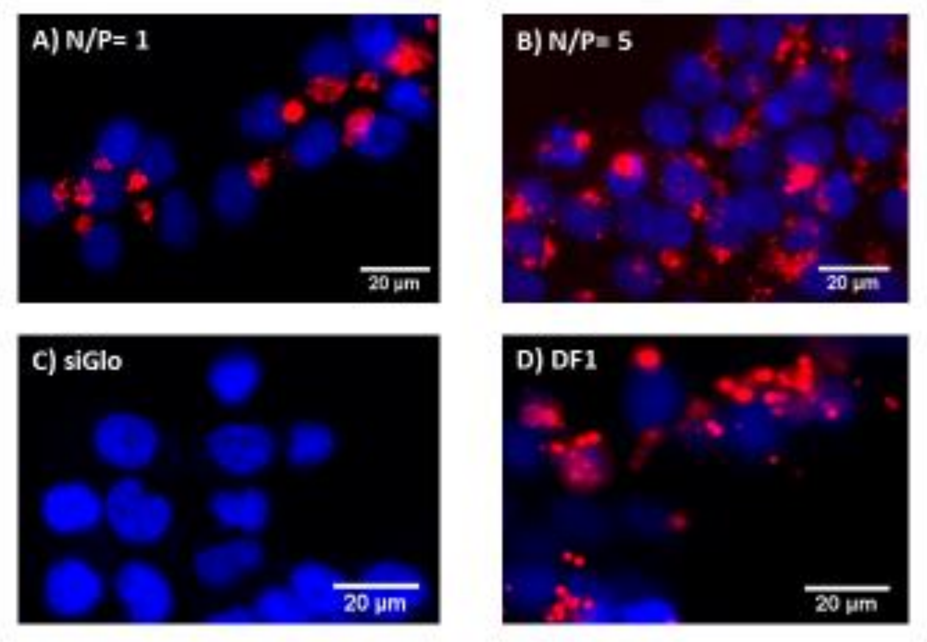

Figure 5.12. High content images of HCT 116 cells 72 h after transfection with $(IG)_4$K-siGLO red complexes. The nuclei are stained with Hoechst 33342 (blue), and siGLO™ is labelled with cy3 (red). ×20 magnification, scale bar = 20 µm

Similar to what observed for c-Myc AON, the images demonstrate the presence of siGLO™ in the perinuclear area of the HCT 116 cells 24 h after transfection with $(IA)_4$K- siGLO™ and $(IG)_4$K- siGLO™ complexes, the extent of which is comparable to the commercial transfection reagent (DharmaFECT™1), whereas the negative controls (naked siGLO™) were not uptaken by the cells. The presence of the peptide- siGLO™ complexes in the cells after 72 h indicates a stable transfection. However, unlike the pattern observed for c-Myc AON, increasing the N/P ratio does not change the morphology and distribution pattern of the peptide- siGLO™ complexes even up to N/P ratio of 5.

The observed difference in transfection pattern between c-Myc and siGLO™ might be due to the different structural properties of the two transfection indicators as c-Myc AON is a single-stranded oligodeoxyribonucleic acid whereas siGLO™ is a double-stranded oligoribonucleic acid as the two do not differ significantly in length. A closer look at the images, reveals that after 72 hours the peptide- siGLO™ complexes are not localized in one point anymore and are slightly scattered around the nuclei. No explanation for this observation could be given at this point and further analysis is required to unveil the potential causes of this observation. These data were further confirmed by the CLSM images which clearly demonstrate the presence of $(IG)_4$K- siGLO™ complexes in the cytoplasm of the HCT 116 cells 24 h after transfection (Figure 5.13).

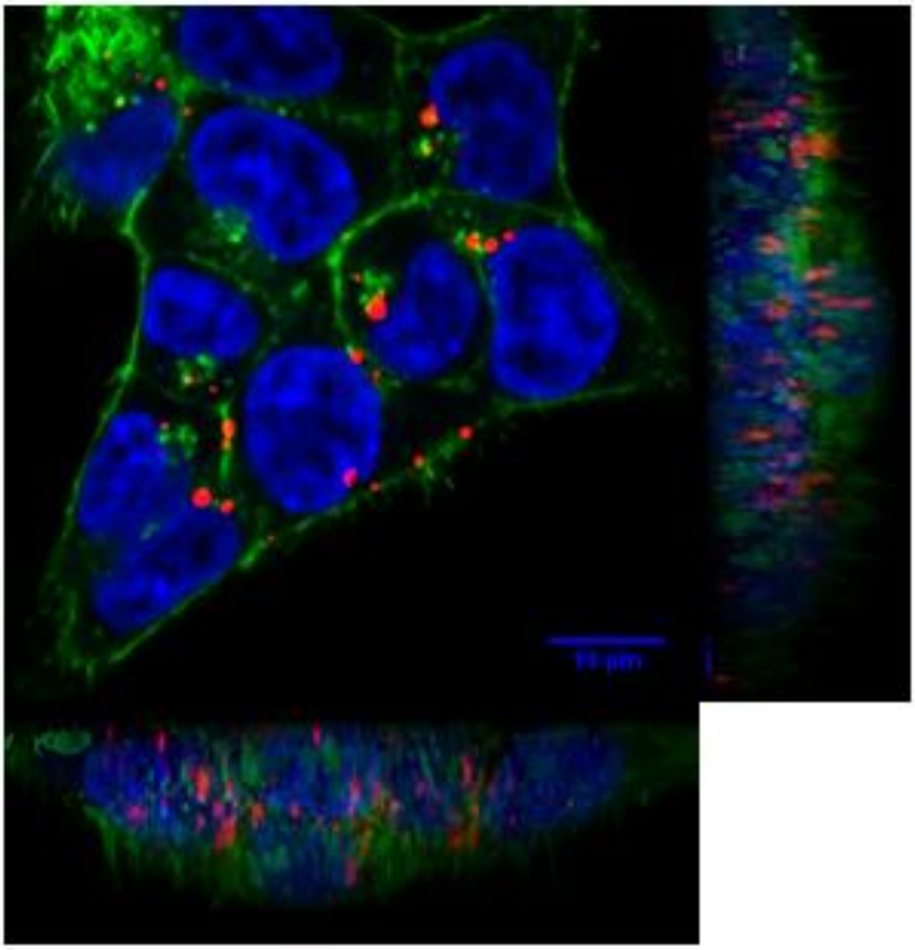

Figure 5.13. CLSM image of HCT116 cells 24 h after transfection with $(IG)_4K$ siGLO red complexes (N/P=1). The nuclei are stained with Hoechst 33342 (blue), cytoplasm is stained with Alexafluor®488-Phalloidin (green), and siGLO™ is labelled with cy3 (red).

The transfection studies with $(IA)_4K$- siGLO™ and $(IG)_4K$- siGLO™ complexes in HDF cells indicates that the complexes are uptaken by the cells 24 h after transfection and are still retained within the cells after 72 h (Figures 5.14-5.17). Similar to what observed for peptide-AON complexes in HDFs, the peptide- siGLO™ complexes are scattered throughout the cytoplasm of the HDFs. On the other hand, similar to HCT 116 cells increasing the N/P ratio does not affect the morphology or distribution pattern of the peptide- siGLO™ complexes but after 72 h the complexes appear to be more widely spread over the cytoplasm. The presence of the peptide- siGLO™ complexes inside the cells, and not at the cell boundaries or cell membrane, was further confirmed by the CLSM images which clearly demonstrate the $(IG)_4K$-siGLO™ complexes in the cytoplasm of HDF cells 24h after transfection (Figure 5.18).

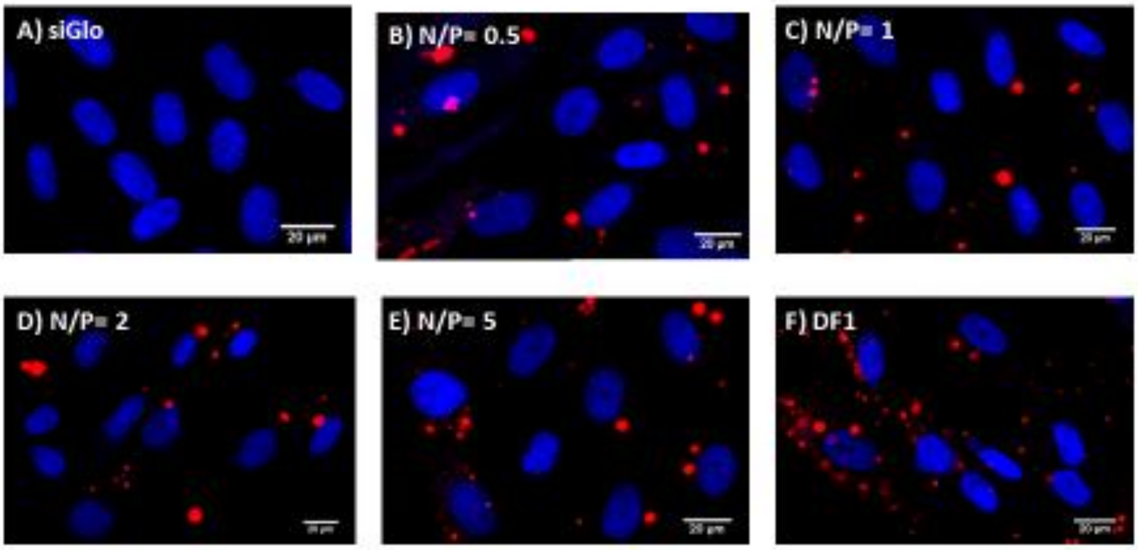

Figure 5.14. High content images of HDF cells 24 h after transfection with (IA)$_4$K-siGLO red complexes. The nuclei are stained with Hoechst 33342 (blue), and siGLO™ is labelled with cy3 (red). ×20 magnification, scale bar = 20 µm

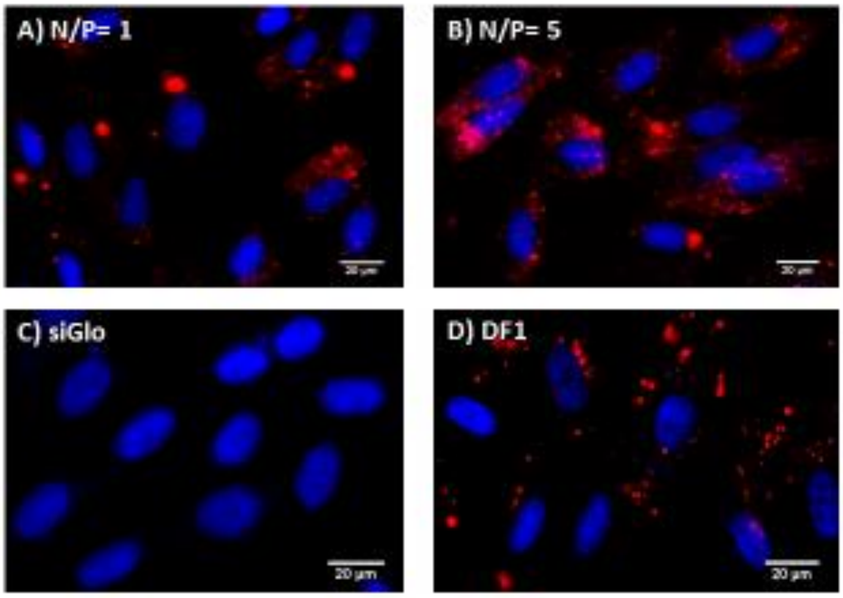

Figure 5.15. High content images of HDF cells 72 h after transfection with (IA)$_4$K-siGLO red complexes. The nuclei are stained with Hoechst 33342 (blue), and siGLO™ is labelled with cy3 (red). ×20 magnification, scale bar = 20 µm

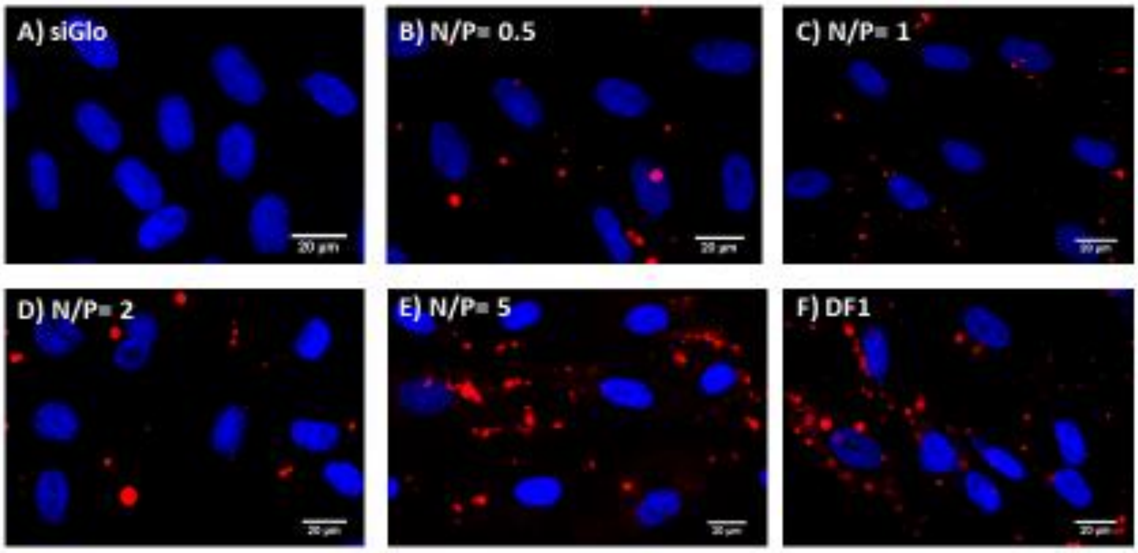

Figure 5.16. High content images of HDF cells 24 h after transfection with $(IG)_4K$-siGLO red complexes. The nuclei are stained with Hoechst 33342 (blue), and siGLO™ is labelled with cy3 (red). ×20 magnification, scale bar = 20 µm

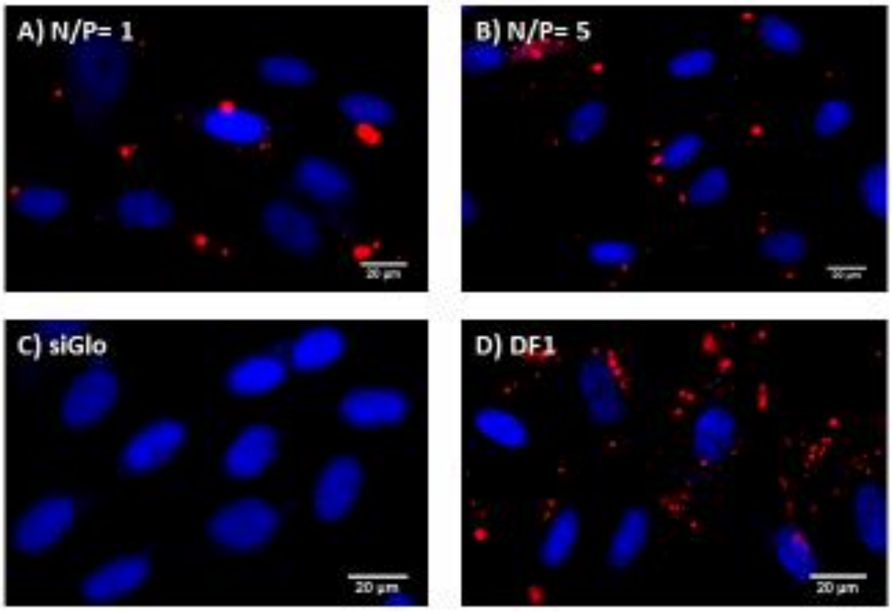

Figure 5.17. High content images of HDF cells 72 h after transfection with $(IG)_4K$-siGLO red complexes. The nuclei are stained with Hoechst 33342 (blue), and siGLO™ is labelled with cy3 (red). ×20 magnification, scale bar = 20 µm

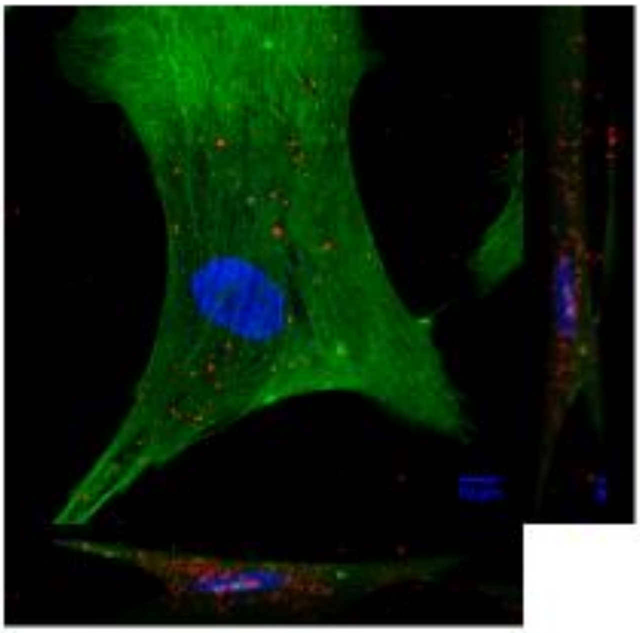

Figure 5.18. CLSM image of a HDF cell 24 h after transfection with $(IG)_4K$ siGLO red complexes (N/P=1). The nuclei are stained with Hoechst 33342 (blue), cytoplasm is stained with Alexafluor®488-Phalloidin (green), and siGLO™ is labelled with cy3 (red).

Following successful transfection of the HCT 116 cells with siGLO™, the ability of the peptide-siRNA complexes to induce gene silencing was tested using anti-PLK1 (Polo like kinase 1) siRNA following the protocol explained in Section 2.18. PLK1 is a serine/threonine kinase which plays a key role in regulating the cell cycle during mitosis and its inhibition results in cell proliferation inhibition and apoptosis [24]. PLK1 is overexpressed in many tumours and is associated with carcinogenesis. Therefore, it represents a promising target for anticancer therapy. Silencing of PLK1 gene results in down regulation of PLK1 enzyme which inhibits the cell proliferation and eventually brings about apoptosis [25-26]. Surprisingly, the peptide-siRNA complexes did not induce any gene silencing as compared to the negative controls whereas Dharmafect1™-siRNA complex (positive control) induced considerable gene silencing (Figure 5.19). Considering the fact that the peptides could transfer the siRNA to the cells but could not result in gene silencing it can be assumed that either the peptides remain attached to the siRNA and cannot release their cargo inside the cytoplasm or the peptide-siRNA complexes are entrapped inside one of the intracellular organelles and therefore the siRNA cannot reach the cellular machinery in order to exert its silencing effect. In order to investigate the reason for the observed lack of gene silencing by the peptide-siRNA complexes, the changes to the zeta potential of the AONs and the siRNA upon complexation with the surfactant-like peptides were studied and used as a measure of the strength of the peptide-nucleic acid complex. As it could be observed in Figures 5.20-5.21, the values of zeta potential for both AONs and siRNA changed from negative to positive upon complexation with the peptides the extent of which increased with increasing the N/P ratio. The large positive values of zeta potential indicate formation of strong complexes between the peptides and the siRNA which is in favour of the first assumption.

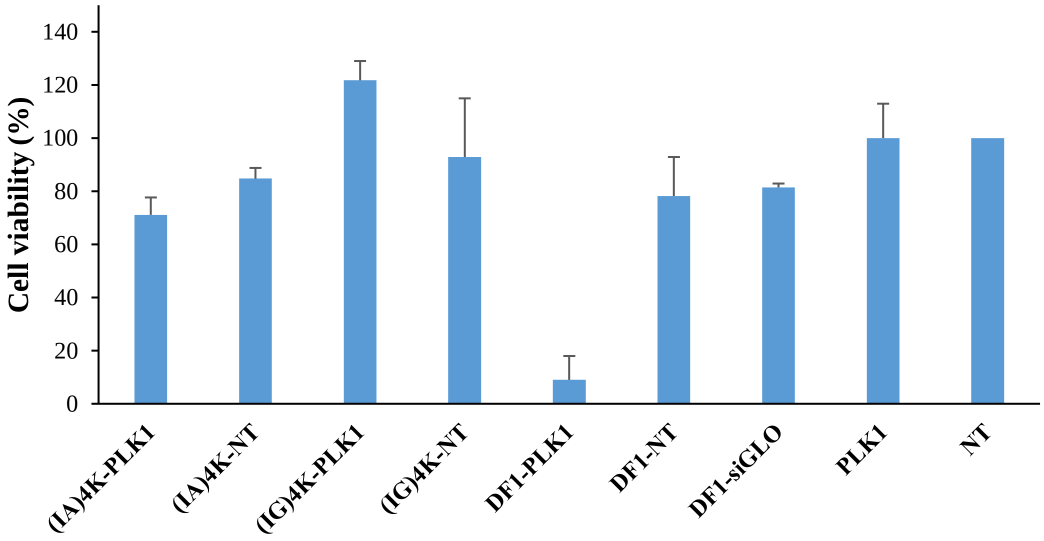

Figure 5.19. Transfection of HCT 116 cells with PLK1 siRNA using $(IA)_4K$ and $(IG)_4K$ cel. Scrambled non-targeting siRNA (NT) was used as control and DharmaFECT™1 (DF1) was used as positive control. The data are reported as Mean ± SD (n = 6).

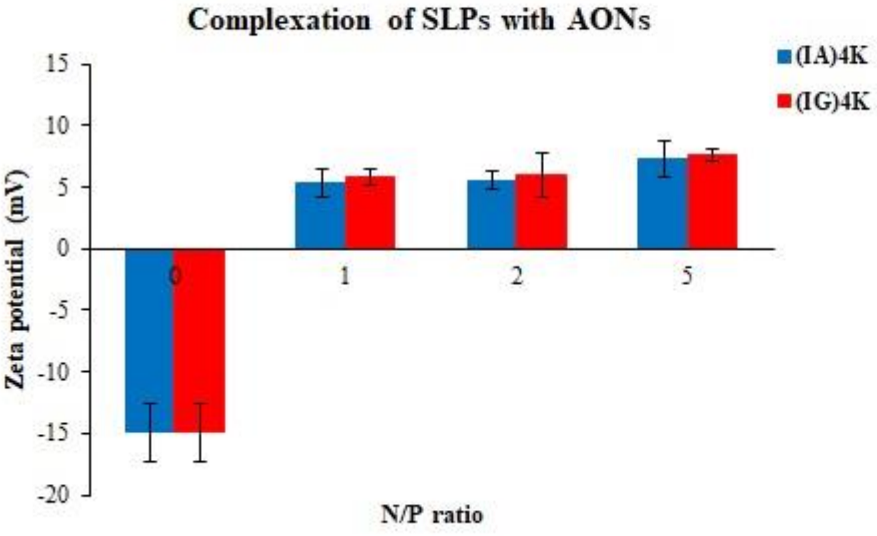

Figure 5.20. Changes to the zeta potential of c-Myc antisense oligonucleotides (AONs) upon complexation with surfactant-like peptides at different N/P ratios. N/P = 0 indicates the zeta potential of the naked c-Myc AON. The data are reported as the average of three measurements.

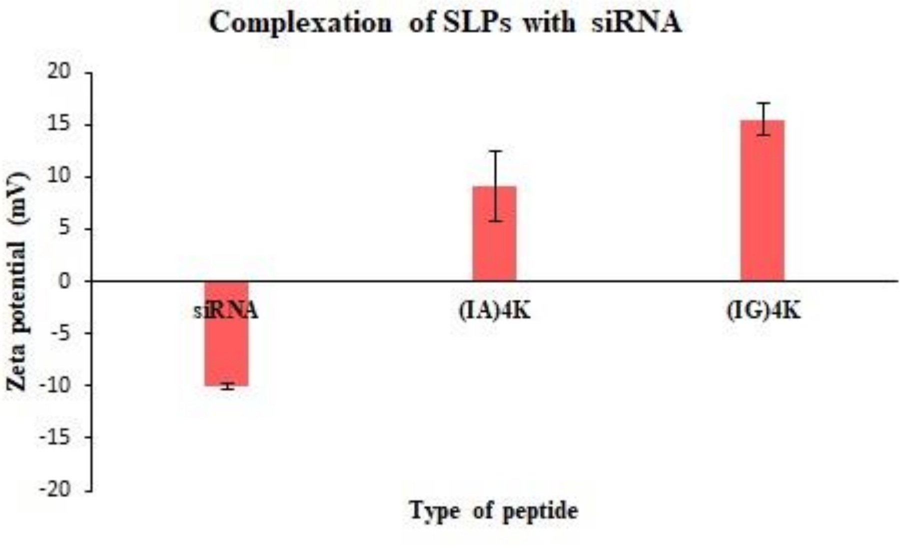

Figure 5.21. Changes to the zeta potential of siGLO™ red siRNA upon complexation with surfactant-like peptides at N/P ratio of 5. The data are reported as the average of three measurements.

5.3.3 Cytotoxicity

In addition to complexation with nucleic acids and transferring them to the cells, lack of toxicity is another necessary criterion for any gene delivery system. Therefore, the peptides were subjected to cytotoxicity tests in HCT 116 and HDF cells using the MTT cell viability assay. The results from the cytotoxicity tests in HCT116 and HDF cells are depicted in figures 5.22-5.23. As it could be observed, the viability values of the cells treated with $(IA)_4K$ and $(IG)_4K$ solutions are relatively high and, in most cases, comparable or even higher than the negative control which indicates lack of cytotoxicity towards HCT 116 and HDF cells for these peptides at the concentration range studied in these experiments (1-10 µM) even after 3 days. Need not say that due to the minor variations in the cell seeding number among different wells in the plates, the final cell count in the wells after the designated incubation time would differ to some degree, therefore it is plausible to observe a higher cell count and therefore a greater absorbance for the test wells compared to the control.

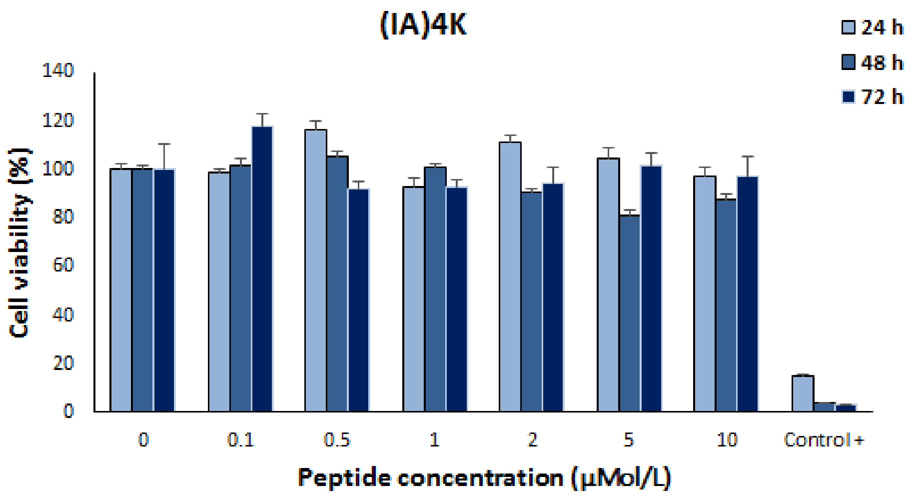

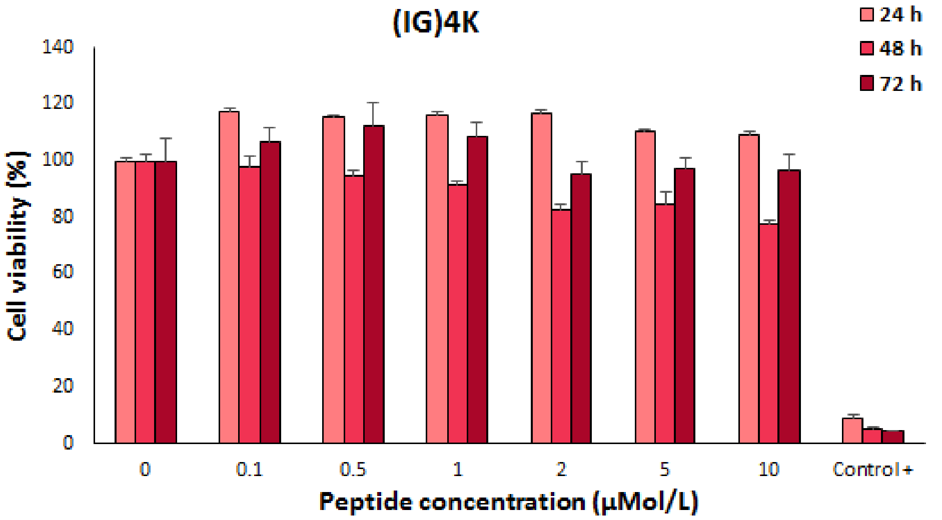

Figure 5.22. Cytotoxicity of $(IA)_4K$ and $(IG)_4K$ in HCT 116 colorectal cancer cells as determined by MTT assay. Sodium chromate (2 mMol/L) was used as positive control in all cases. All data are reported as Mean ± SE (n=9).

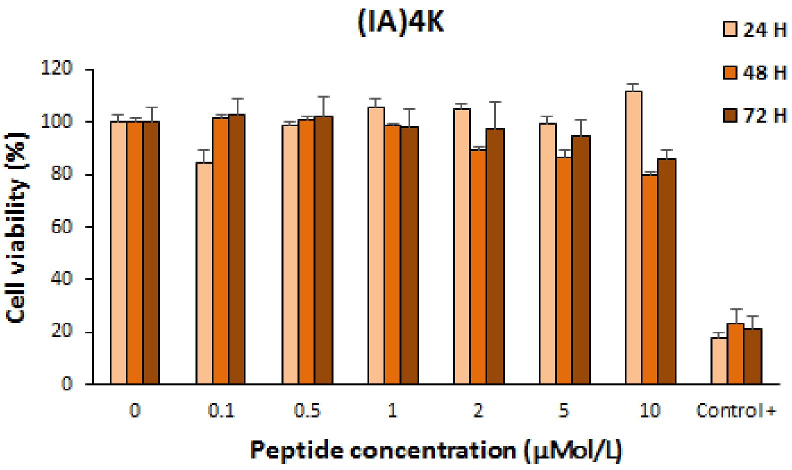

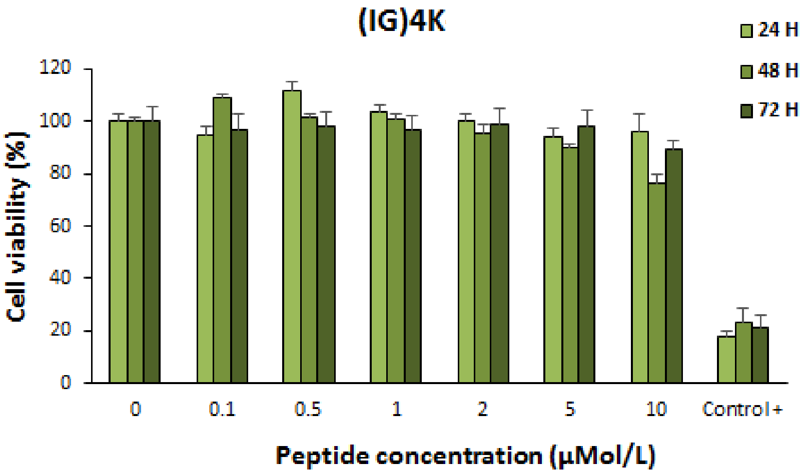

Figure 5.23. Cytotoxicity of $(IA)_4K$ and $(IG)_4K$ in HDF cells as determined by MTT assay. Sodium chromate (2 mMol/L) was used as positive control in all cases. All data are reported as Mean ± SE (n=9).

5.4 Conclusion

Taking into account all of the transfection data in HCT 116 and HDF cells, it could be concluded that (IA)4K and (IG)4K were capable of binding to AONs and siRNA and to deliver their associated nucleic acids to the human cells with relatively high efficiency. However, these peptides did not show any selectivity for cancer cells over normal cells, which is not favourable if these peptides are considered for gene delivery to treat cancer because it raises concerns over the adverse effects of these cancer therapeutics. On the other hand, the ability of these peptides to transfect both normal cells and cancer cells with high efficiency suggests their potential application as general transfection reagent either for delivery of genes to normal cells to correct a genetic disorder or for investigational use. Since these peptides show minimal levels of cytoxicity in HCT 116 cells even at high concentrations and after long exposure times (up to 5 days), they could be regarded as a safe transfection reagent which is an advantage for these peptides over the commercially available transfection reagents such as Oligofectamine™, Lipofectamine™, Effectene™, and Dharmafect™1 which are generally highly toxic to the cells at concentrations used for systemic gene delivery. The current results clearly demonstrate the ability of the studied peptides to deliver AON and siRNA to the normal and cancer cells. Nevertheless, due to the strong complexation between the peptides and the nucleic acids, they were unable to release their cargo inside the cell which resulted in lack of functionality of the associated nucleic acids (PLK1 siRNA).

5.5 References

1. D. W. Ryu, H. A. Kim, H. Song, S. Kim, M. Lee, Amphiphilic peptides with arginines and valines for the delivery of plasmid DNA. *J. Cell. Biochem.,* 112 (2011):1458-1466.
2. S.D.D.T.A. Jones, N.M. Luscombe, H.M. Berman, J.M. Thornton. Protein-RNA interactions: a structural analysis. *Nucleic Acids Res.*, 29 (2001):943-954.
3. P. Järver, T. Coursindel, S.E. L Andaloussi, C. Godfrey, M. JA Wood, M. J Gait. Peptide-mediated cell and *in vivo* delivery of antisense oligonucleotides and siRNA. *Mol. Ther. Nucleic Acids*, 1(2011): e27.
4. L. A. Avila, L. RMM Aps, P. Sukthankar, N. Ploscariu, S. Gudlur, et al. Branched amphiphilic cationic oligopeptides form peptiplexes with DNA: A study of their biophysical properties and transfection efficiency. *Mol. Pharmaceutics,* 12 (2015):706-715.
5. Q. Tang, B. Cao, H. Wu, G. Cheng. Selective gene delivery to cancer cells using an integrated cationic amphiphilic peptide. *Langmuir,* 28 (2012):16126-16132.
6. S. H. Medina, S. Li, O.M. Z. Howard, M. Dunlap, A. Trivett , J. P. Schneider, J. J. Oppenheim. Enhanced immunostimulatory effects of DNA-encapsulated peptide hydrogels. *Biomaterials,* 53 (2015): 545-553.
7. G. N. Goparaju, P. K. Gupta. Design of amphiphilic oligopeptides as models for fine tuning peptide assembly with plasmid DNA. *Drug Discoveries Ther.,* 8(2014):165-172.
8. S. M. Standley, D. J. Toft, H. Cheng, S. Soukasene, J. Chen, S. M. Raja, V. Band, H. Band, V. L. Cryns, S. I. Stupp. Induction of cancer cell death by self-assembling nanostructures incorporating a cytotoxic peptide. *Cancer Res.*, 70(2010): 3020-3026.

9. H. O. McCarthy, J. McCaffrey, C. M. McCrudden , A. Zholobenko, A. A. Ali, et al. Development and characterization of self-assembling nanoparticles using a bio-inspired amphipathic peptide for gene delivery. *J. Control. Release*, 189 (2014): 141-149.
10. D. Yoshida, K. Kim, I. Takumi, F. Yamaguchi, K. Adachi, A. Teramoto. A transfection method for short interfering RNA with the lipid-like self-assembling nanotube, A6K. *Med. Mol. Morphol.*, 46 (2013):86-91.
11. D.W. Ryu, H.A. Kim, S. Kim, M. Lee. VEGF receptor binding peptide-linked amphiphilic peptide with arginines and valines for endothelial cell-specific gene delivery. *J Drug Target.*, 20(2012):574-581.
12. B. Kim, J.H. Song, M. Lee. Combination of TAT-HMGB1A and R3V6 amphiphilic peptide for plasmid DNA delivery with anti-inflammatory effect. *J Drug Target.*, 22(2014):739-47.
13. S.D.D.T.A. Jones, N.M. Luscombe, H.M. Berman, J.M. Thornton. Protein-RNA interactions: a structural analysis. *Nucleic Acids Res.*, 29 (2001):943-954.
14. J. Guo, W. P. Cheng, J. Gu, C. Ding, X. Quc, et al. Systemic delivery of therapeutic small interfering RNA using a pH-triggered amphiphilic poly-L-lysine nanocarrier to suppress prostate cancer growth in mice. *Eur. J. Pharm. Sci.*, 45 (2012): 521-532.
15. N. Venkatesan, B. H. Kim, Peptide conjugates of oligonucleotides: Synthesis and applications. *Chem. Rev.*, 106 (2006): 3712-3761.
16. J. Dufourcq, W. Neri, N. Henry-Toulmeè. Molecular assembling of DNA with amphipathic peptides. *FEBS Lett.*, 421 (1998): 7-11.
17. D. W. Ryu, H. A. Kim, J. H. Ryu, D. Y. Lee, M. Lee. Amphiphilic peptides with arginine and valine residues as siRNA Carriers. *J. Cell. Biochem.*, 113 (2012):619-628.
18. P. Sukthankar, L. A. Avila, S. K. Whitaker, T. Iwamoto, A. Morgenstern, C. Apostolidis, K. Liud, R. P. Hanzlikd, E. Dadachova, J.M. Tomicha. Branched amphiphilic peptide capsules: Cellular uptake and retention of encapsulated solutes. *Biochim. Biophys. Acta,* 1838(2014): 2296-2305.
19. N. Wiradharma, M. Khan, Y. W. Tong, S. Wang, Y.Y. Yang. Self-assembled cationic peptide nanoparticles capable of inducing efficient gene expression in vitro. *Adv. Funct. Mater.*, 18 (2008) :943-951.

20. X. D. Guo, F. Tandiono, N. Wiradharma, D. Khor, C. G. Tan, et al. Cationic micelles self-assembled from cholesterol-conjugated oligopeptides as an efficient gene delivery vector. *Biomaterials,* 29 (2008): 4838-4846.
21. H. F. Zhou, H. Yan, H.Pan, K. K. Hou, A. Akk, et al. Peptide-siRNA nanocomplexes targeting NF-κB subunit p65 suppress nascent experimental arthritis. *J. Clin. Invest.*, 124 (2014):4363-4374.
22. J. B. Pawley (editor). Handbook of Biological Confocal Microscopy (3rd ed., 2006). Berlin: Springer.
23. http://www.olympusmicro.com/primer/techniques/confocal/confocalintro.html, accessed on 16/09/2016
24. F. A. Barr, H. H.W. Silljé, and E. A. Nigg. Polo-like kinases and the orchestration of cell division. *Nat. Rev. Mol. Cell Biol.*, 5 (2004): 429-441.
25. X. Liu, M. Lei, and R.L. Erikson. Normal cells, but not cancer cells, survive severe Plk1 depletion, *Mol Cell Biol,* 26 (2006): 2093-2108.
26. K. Strebhardt, and A. Ullrich, Targeting polo-like kinase 1 for cancer therapy, *Nat Rev Cancer*, 6 (2006): 321-330.

Chapter 6: Physicochemical and biophysical characterization of the cationic amphiphilic peptides

6.1 Background and aims

In the previous chapters three different series of cationic amphiphilic peptides with different structures have been introduced and their biological activities in terms of anticancer effect and gene delivery potential have been discussed. In this chapter the physicochemical properties of the peptides are characterized to verify the peptide sequences, measure the purity of the synthesized peptide samples, and confirm the predicted secondary structures of the peptides. Furthermore, the interaction of the peptides with lipid monolayers and bilayers (i.e., unilamellar lipid vesicles) are studied in order to provide a biophysical basis for the observed biological activities. The unilamellar phospholipid vesicles and the phospholipid monolayers have been widely used as models for cell membrane with the former mimicking the phospholipid bilayer of the cell membrane and the latter mimicking the outer leaflet of the cell membrane [1-16]. The changes to the conformation of the peptides upon contact with the phospholipid vesicles can be used to predict their conformational changes upon interaction with the cell membrane. The changes to the surface pressure at the air/water interface following contact of the peptides with the phospholipid monolayers can be used as an indicator of the penetration/insertion of the peptide into the lipid monolayer the extent of which is proportional to the extent of interaction between the peptide and the lipid monolayer and corresponds to the membrane-ruptive effect of the peptide [1-8, 12,13]. Different types of phospholipids with different charges (i.e., negative or zwitter ionic) can be used to create lipid monolayers and bilayers with surface charges similar to the cancer cell membranes or normal human cell membranes as it has been reported that the cancer cell membranes are more negatively charged than normal human cell membranes [5, 17, 18].

The aims of this chapter are:

- Verifying the sequence and purity of the synthesized cationic amphiphilic peptide samples.
- Determining the secondary structure of the designed peptides in order to confirm the α-helical or β-sheet conformation in the aqueous solution and upon contact with curved lipid bilayers (unilamellar phospholipid vesicles) as a mimic of cell membrane.
- Investigating the interaction of the peptides with lipid monolayers as a mimic of cell membrane outer leaflet

- Studying the correlation between the physicochemical properties of the cationic amphiphilic peptides and their biological activity as obtained from the cell-based assays.

6.2 Experimental

6.2.1 Sequence and purity check

In order to verify the sequences and the purities of the synthesized cationic amphiphilic peptides, the peptides were subjected to RP-HPLC and LC-MS analysis as described in detail in Sections 2.3-2.4.

6.2.2 Preparation of small unilamellar lipid vesicles (SUVs) and SDS micelles

The phospholipid SUVs with different surface charges were prepared from DPPC and DPPG following the procedure described in Section 2.6 and mixed with the cationic amphiphilic peptide solutions in order to study the conformational changes of the peptides upon interaction with lipid bilayers. The sodium lauryl sulphate (SDS) micelles were prepared by dissolving SDS in DI water at the concentration of 25 mM which is above its critical micelle concentration (CMC) value. The particle size and zeta potential of the SUVs and micelles were determined by Dynamic light scattering (DLS) as described in Section 2.6.

6.2.3 Determination of the peptide secondary structure

The secondary structure of the peptides in aqueous media (i.e., DI water and phosphate buffer at physiological pH (7.4)) and their conformational changes upon contact with SDS micelles and small unilamellar phospholipid vesicles were studied by Circular dichroism spectroscopy as described in Section 2.5.

6.2.4 Changes to the surface pressure at the air/water interface and interaction with phospholipid monolayers

The changes to the water surface pressure upon injection of the cationic amphiphilic peptide solutions and the changes to the surface pressure at the air/water interface upon contact of the cationic amphiphilic peptides with the DPPC and DPPG lipid monolayers were studied using Langmuir trough as described in detail in Section 2.7. The concentrations of the peptides used for these experiments were chosen based on the values of IC_{50} for the peptides as determined by cell-based assays.

6.3 Results & discussion

6.3.1 Sequence and purity check using LC-MS and RP-HPLC

The LC-MS spectra and RP-HPLC chromatograms of the cationic amphiphilic α-helical peptides are provided in Figures 6.1-6.6. A full account of the peaks in the RP-HPLC chromatogram and the corresponding areas and heights are provided in Tables S1-S15 in the supplemental data. The purity of the peptides was calculated by using the ratio of the abundance (peak intensity) of the ions corresponding to the peptide molecular mass (both for the peptide monomers and peptide dimers in the case of the peptides which existed as dimers in the solution) to the total ion abundance and reported as percentage in Tables 6.1,6.3, and 6.5.

The molecular weights of the α-helical peptides as measured by LC-MS and the predicted molecular weights calculated by the software are presented in Table 6.1. The peptide sequences were checked using the m/z values corresponding to the 2^+ and 3^+ ions. As it could be observed the ions corresponding to the designed peptide sequences were detected Nevertheless, in some cases ions with greater charges (4^+-7^+) and molecular masses corresponding to the peptide or the peptide dimer were also detected as presented in Table 6.1. In the case of IIKK and LLKK, the m/z values corresponding to the peptide sequence/molecular weight were not found but instead the 6+ and 7+ ions corresponding to the dimer of the peptides were detected (Figures 6.5-6.6). This suggests that these two peptides may exist as dimers in the solution. For the rest of the α-helical peptides both the ions corresponding to the monomers and dimers were detected. The presence of peptide dimers instead of monomers in the case of IIKK and LLKK could have contributed to the higher IC_{50} values of these peptides compared to the rest of the α-helical peptides. Also, it could have contributed to the higher helical content of these two peptides compared to their arginine-rich counter parts (IIRR and LLRR) as it is discussed in section 6.3.3.

In all cases the spectra also consisted of other ions which could be generated either by the peptide breakdown along the amide bonds during the ionization, or by the impurities in the sample. The m/z values and corresponding molecular masses of these impurities are also provided in Table 6.1. The values of molecular weight for the peptides as measured by the LC-MS based on the 2+ and 3+ ions (6+ and 7+ ions in the case of IIKK and LLKK) were very close to the values calculated using the software showing the accuracy of the LC-MS measurements (Table 6.2).

The RP-HPLC chromatograms of the peptides also show major peaks corresponding to the peptides and other smaller peaks indicating impurities. In the case of CI-15, the two peaks with very close RT in RP-HPLC appear to be the monomer and the dimer of the peptide based on the LC-MS spectrum. Also, the LC-MS spectrum of II-14 shows two peaks with close retention times both of which appear as one large peak in RP-HPLC chromatogram. The retention times for the ions corresponding to the peptides in LC-MS were higher than the retention times for the major peaks in RP-HPLC due to the different dimensions of the LC columns in the two devices and the different compositions of the mobile phases. However, the order of increase in the retention times of the peptides were very similar. One exception was II-14 which had higher

RP-HPLC retention time than most of the other α-helical peptides but in LC-MS its RT was less than the other α-helical peptides. This might be due to the fact that this peptide was analyzed by LC-MS using the same composition but a different gradient of the solvents in the mobile phase compared to the other peptides in this group to improve the separation and resolution as the first attempt to analyse this peptide using the same conditions as the rest of the peptides did not yield good results. The purity of the peptides was measured by calculating the ratio of the abundance (peak intensity) of the ions corresponding to the peptide mass to the total ion abundance (both for the peptide monomers and peptide dimers in the case of the peptides which existed as dimers in the solution) and presented in Table 6.1.

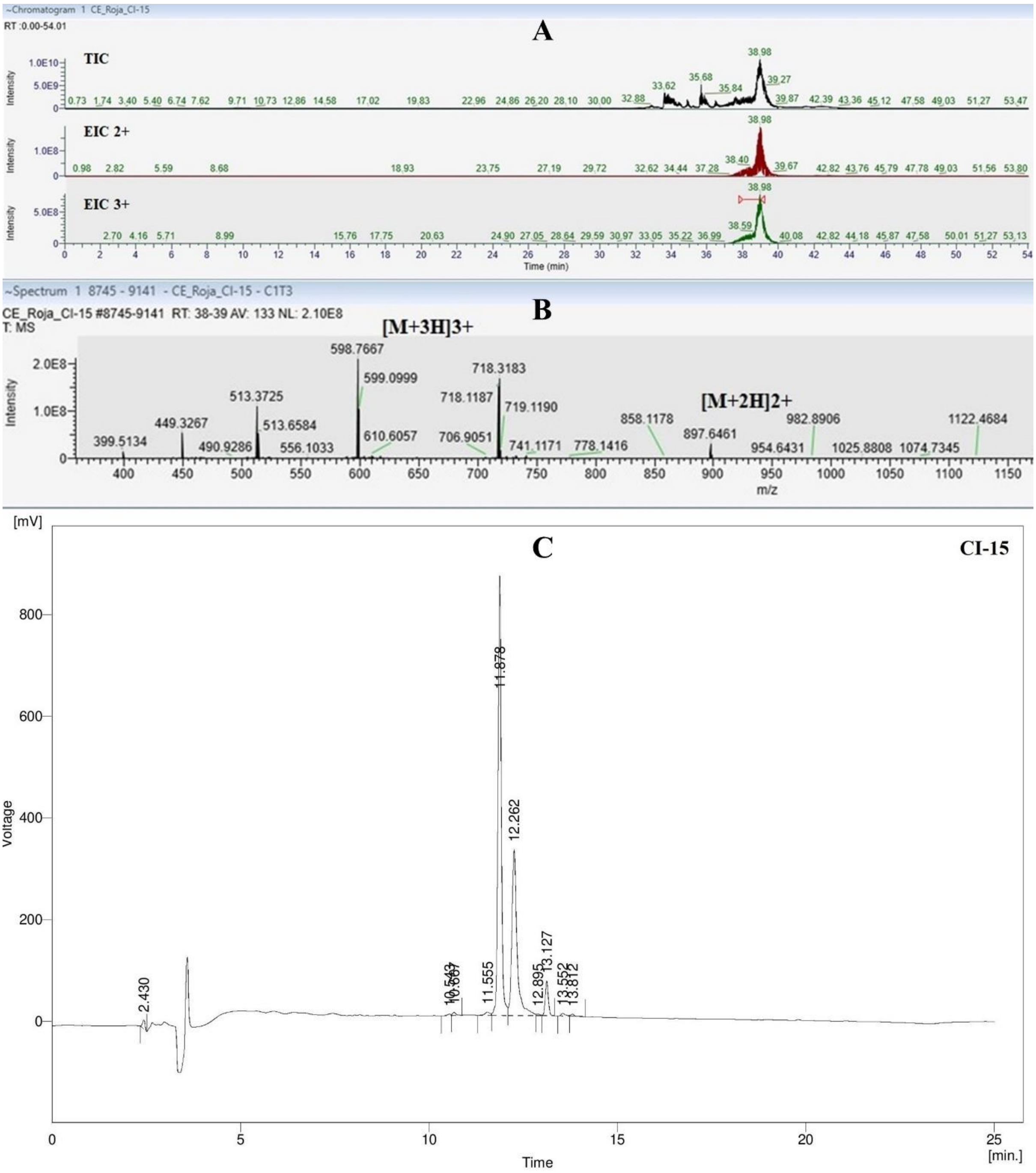

Figure 6.1. LC chromatogram (A), MS spectrum (B) and RP-HPLC chromatogram (C) of CI-15. TIC: total ion chromatogram; EIC: Extracted ion chromatogram; [M+2H]2+ and [M+3H]3+ denote the 2+ and 3+ ions corresponding to the designed peptide sequence.

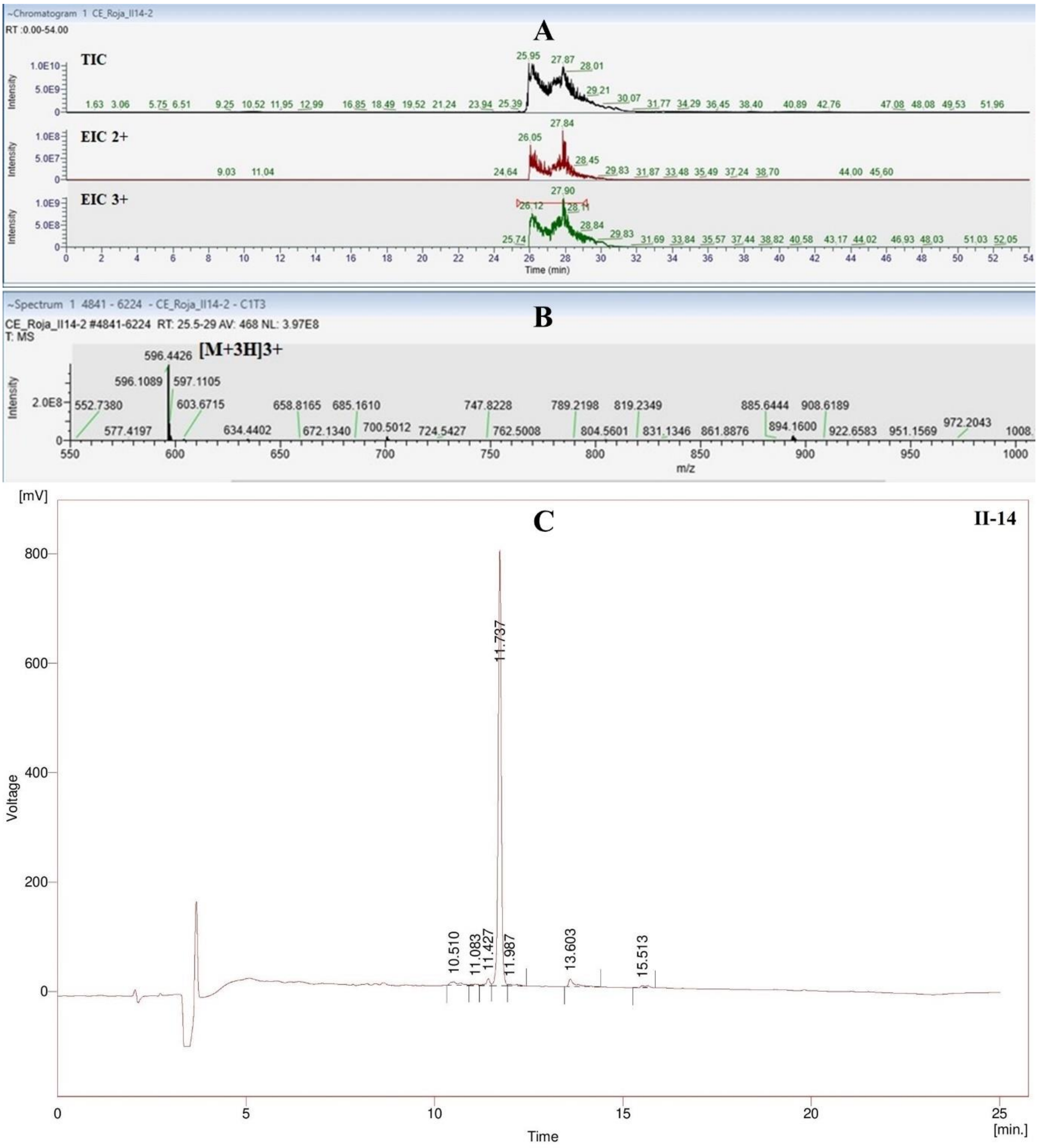

Figure 6.2. LC chromatogram (A), MS spectrum (B) and RP-HPLC chromatogram (C) of II-14. TIC: total ion chromatogram; EIC: Extracted ion chromatogram; [M+3H]3+ denote the 3+ ion corresponding to the designed peptide sequence.

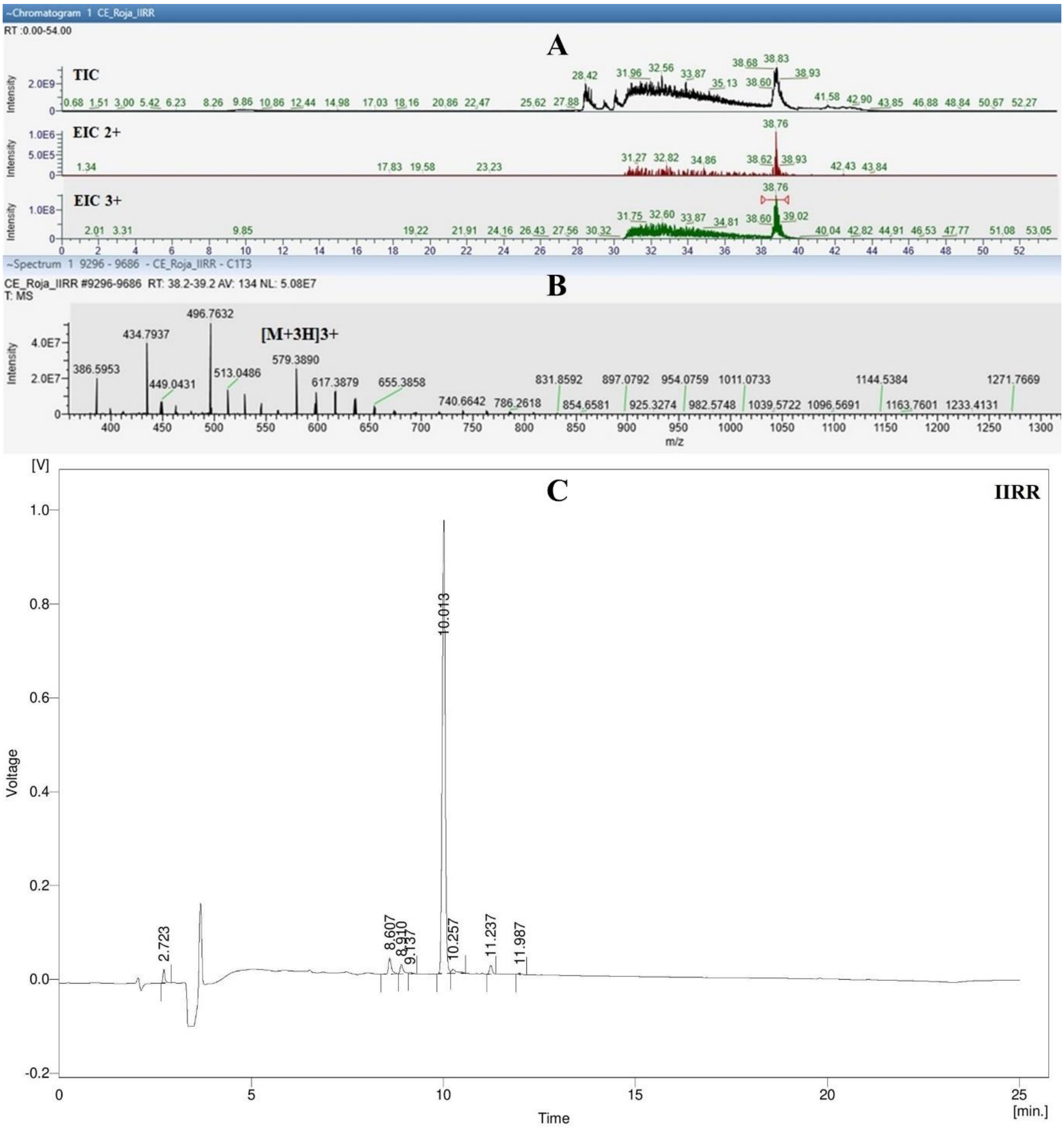

Figure 6.3. LC chromatogram (A), MS spectrum (B) and RP-HPLC chromatogram (C) of IIRR. TIC: total ion chromatogram; EIC: Extracted ion chromatogram; [M+3H]3+ denote the 3+ ion corresponding to the designed peptide sequence.

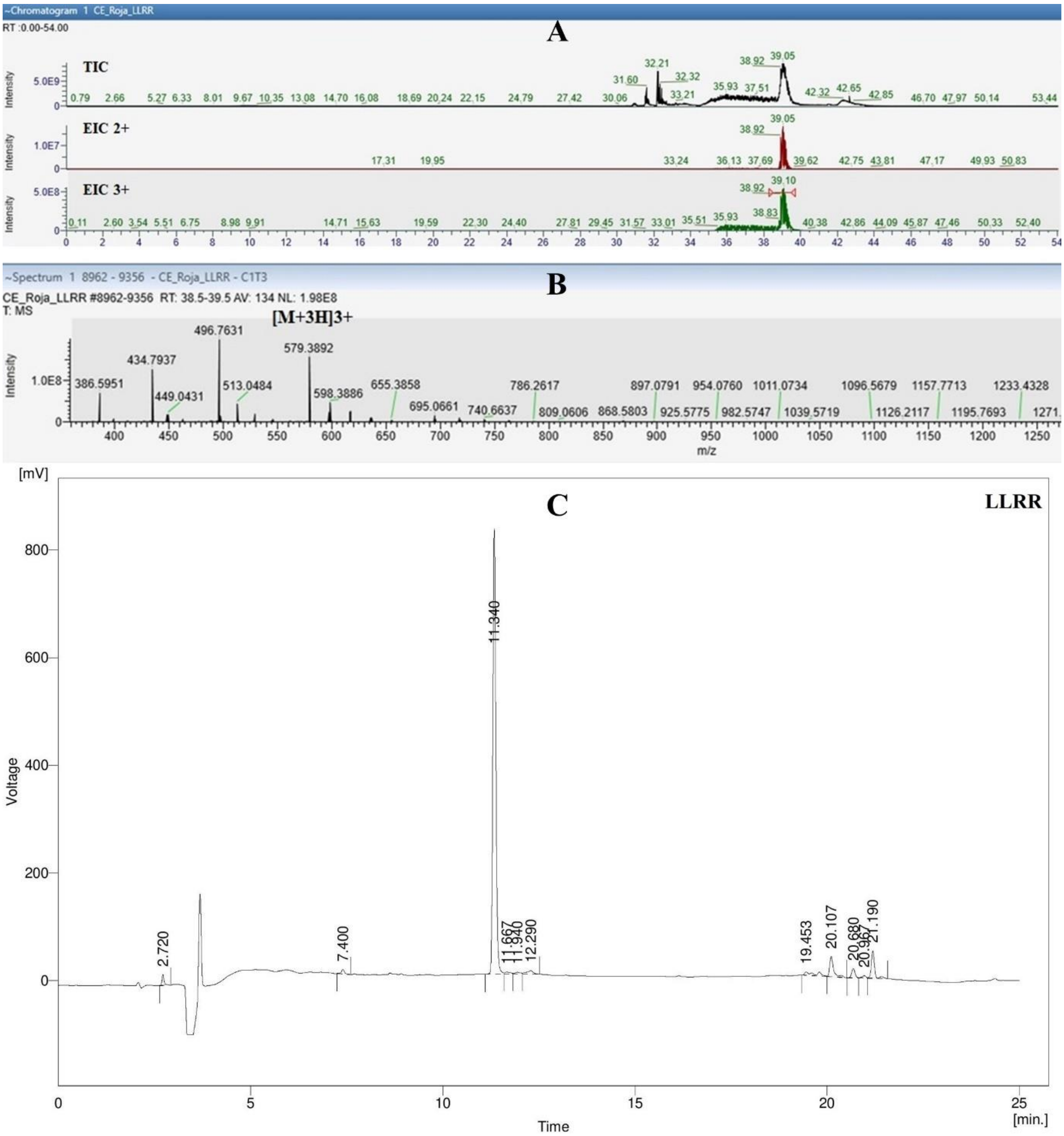

Figure 6.4. LC chromatogram (A), MS spectrum (B) and RP-HPLC chromatogram (C) of LLRR. TIC: total ion chromatogram; EIC: Extracted ion chromatogram; [M+3H]3+ denote the 3+ ion corresponding to the designed peptide sequence.

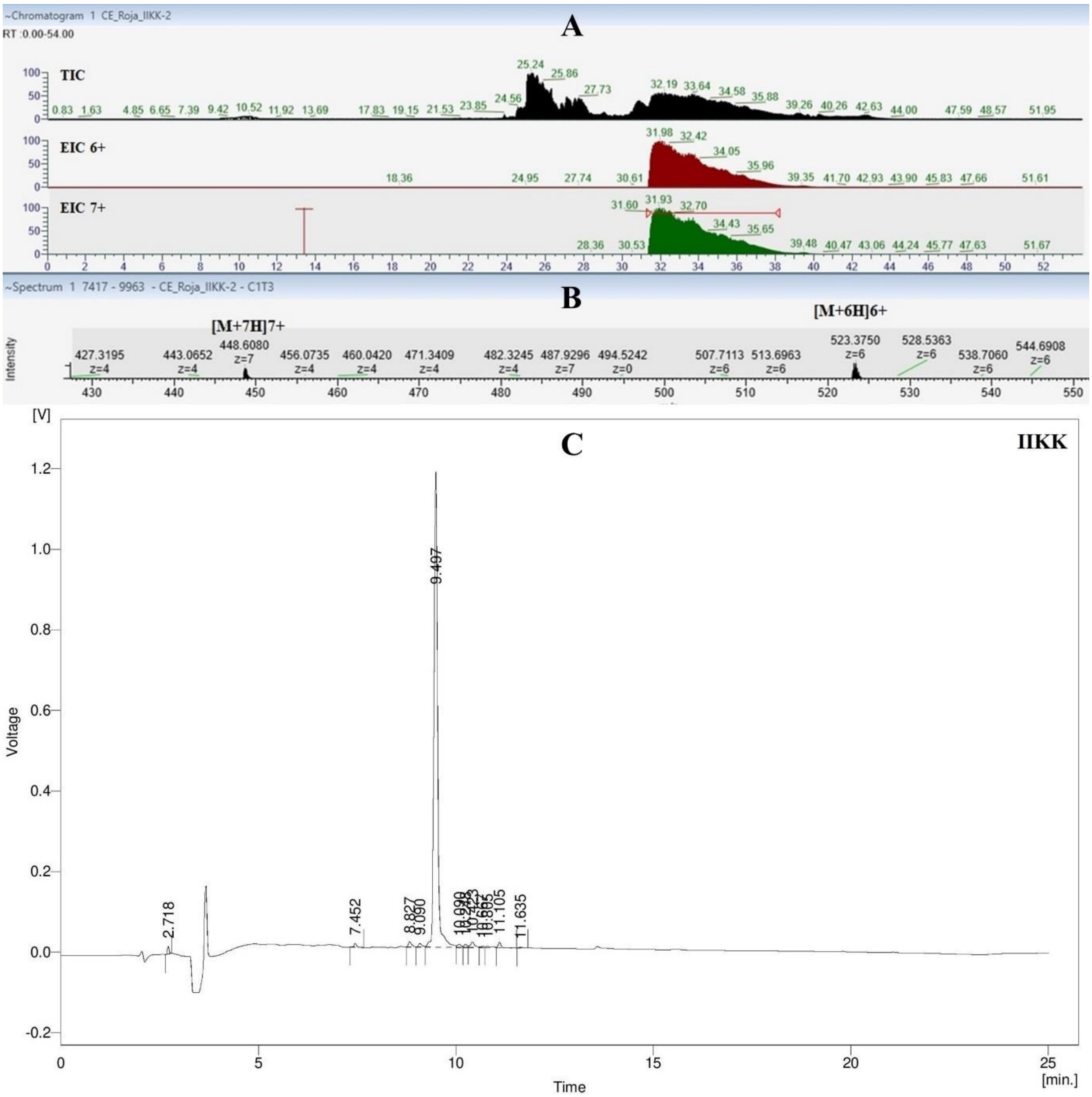

Figure 6.5. LC chromatogram (A), MS spectrum (B) and RP-HPLC chromatogram (C) of IIKK. TIC: total ion chromatogram; EIC: Extracted ion chromatogram; [M+6H]6+ and [M+7H]7+denote the 6+ and 7+ ions corresponding to the dimer of the peptide sequence.

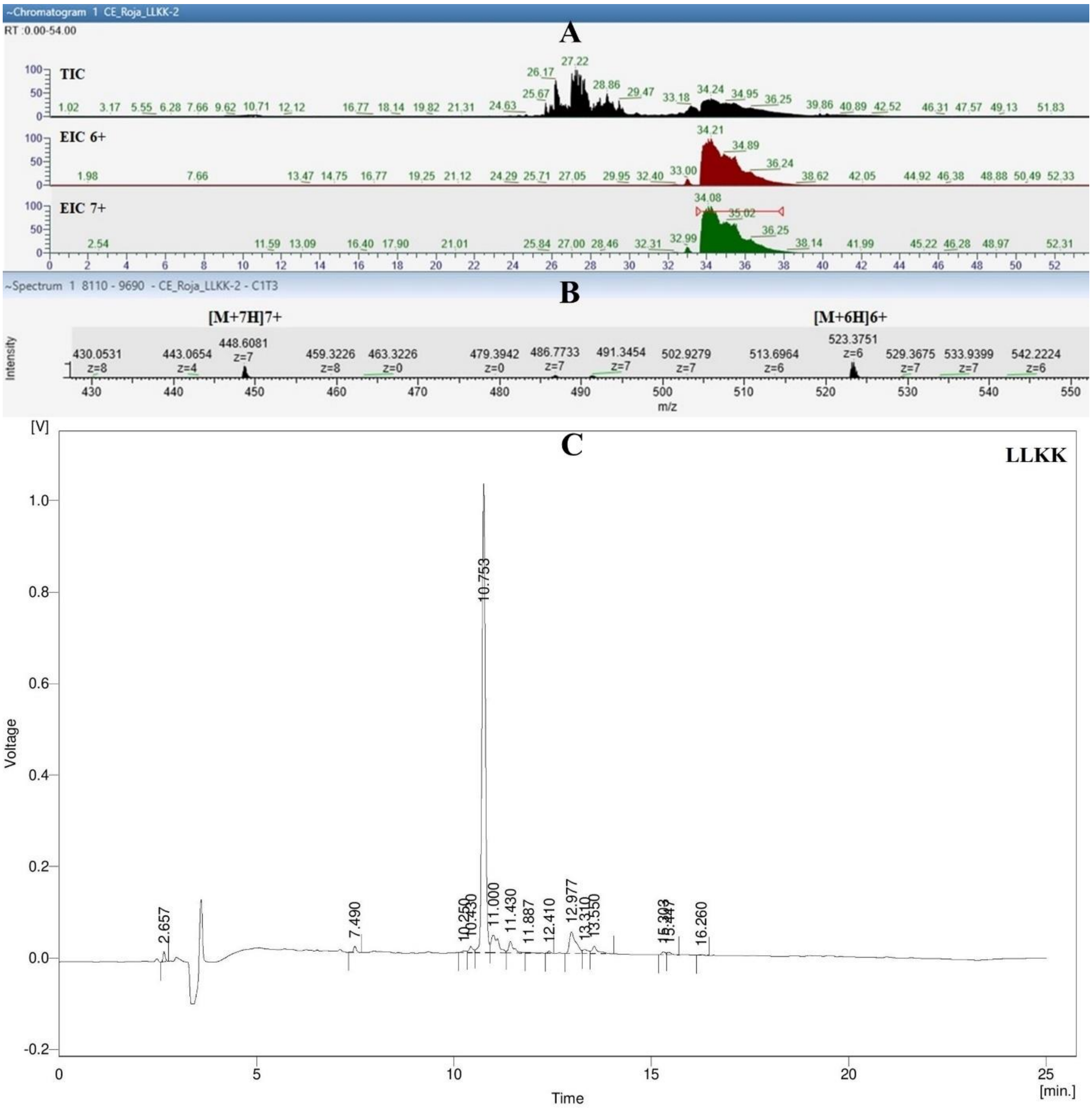

Figure 6.6. LC chromatogram (A), MS spectrum (B) and RP-HPLC chromatogram (C) of LLKK. TIC: total ion chromatogram; EIC: Extracted ion chromatogram; [M+6H]$^{6+}$ and [M+7H]$^{7+}$denote the 6+ and 7+ ions corresponding to the dimer of the peptide sequence.

Table 6.1. The m/z values, Retention times and molecular masses of the main peaks in the LC-MS TIC of the α-helical cationic amphiphilic peptides and their purities as measured by LC-MS.

Peptide	RT (min)	m/z	Charge	Molecular mass	Compound	Purity (%)
IIKK	25.2	404.28	4+	1613.12	Impurity	77.5
	27.7	392.78	8+	3134.27	IIKK dimer	
	32	523.37	6+	3134.25	IIKK dimer	
	32	448.61	7+	3133.26	IIKK dimer	
LLKK	26.2	402.61	4+	1606.44	Impurity	70.3
	27.2	404.28	4+	1613.12	Impurity	
	28.9	392.78	8+	3134.27	LLKK dimer	
	34.1	448.61	7+	3133.26	LLKK dimer	
	34.2	523.37	6+	3134.25	LLKK dimer	
IIRR	28.4	442.79	4+	1767.17	Impurity	78.9
	31.9	496.76	7+	3470.34	IIRR dimer	
	32.5	434.79	8+	3470.35	IIRR dimer	
	33.9	496.62	7+	3469.34	IIRR dimer	
	38.8	579.39	3+	1735.17	IIRR	
LLRR	31.6	442.79	4+	1767.17	Impurity	74.9
	32.2	446.79	4+	1783.16	Impurity	
	35.9	496.76	7+	3470.34	LLRR dimer	
	39	434.79	4+	1735.16	LLRR	
	39.1	579.39	3+	1735.17	LLRR	
CI-15	33.6	457.57	4+	1826.3	Impurity	86.5
	35.7	461.57	4+	1842.3	Impurity	
	38.9	598.77	3+	1793.30	CI-15	
	38.9	897.65	2+	1793.30	CI-15	
	39.3	718.32	5+	3586.59	CI-15 dimer	
	39.3	513.37	7+	5856.61	CI-15 dimer	
II-14	25.9	447.58	4+	1786.33	II-14	94.5
	25.9	400.78	4+	1599.2	Impurity	
	25.9	475.85	4+	1899.28	Impurity	
	26	894.16	2+	1786.32	II-14	
	27.9	596.44	3+	1786.33	II-14	

Table 6.2. The calculated molecular weights of the cationic amphiphilic β-sheet forming peptides, the molecular weights measured by LC-MS, RP-HPLC retention times (RT) and peak areas. The molecular weights were calculated using the software available at www.pepcalc.com.

Peptide	MW (calculated)	MW (measured)	RP-HPLC RT (min)	Peak area (%)
IIKK	1568.16	1566.63	9.5	92.8
LLKK	1568.16	1566.63	10.8	75.9
IIRR	1736.24	1735.17	10	89.2
LLRR	1736.24	1735.17	11.3	79.6
CI-15	1794.47	1793.28	11.9	58.1
II-14	1786.38	1786.32	11.7	89.5

The LC-MS spectra and RP-HPLC chromatograms of the β-sheet forming cationic amphiphilic peptides are presented in Figures 6.7-6.13. The peptide sequences were checked using the m/z values corresponding to the 2+ and 3+ ions. As it could be inferred from Table 6.3, the ions corresponding to the designed peptide sequences were detected however in most cases the spectra also consisted of other ions which could be either from the shorter peptide sequences or from the impurities in the sample. The molecular masses of the ions corresponding to the peptides and the main impurities and the purity (%) of the peptides as calculated from LC-MS TIC are presented in table 6.3. In general, the purity of the peptides was low and even lower than the purities of the α-helical peptides. The low purity of the peptides indicates that the observed biological activities (cytotoxicities) may be in part caused by the impurities in the sample. Also, assuming that the cytotoxicities are merely caused by the peptides and not by any other substances in the samples, the low purity of the peptide samples could result in higher concentrations needed to achieve significant cytotoxicity leading to higher IC_{50} values especially in the case of peptides with lower purity. Therefore, it will cast doubt on the reliability of the IC_{50} values calculated using these peptide samples.

Both the TIC and the RP-HPLC chromatogram show two large peaks one of which corresponds to the peptide and the other corresponding to the other molecules based on the molecular masses. The retention times of the peaks corresponding to the peptides in LC-MS and RP-HPLC were different due to the differences in the dimensions of the stationary phase in the two devices and the difference in the composition of the mobile phases used for the LC-MS and RP-HPLC analyses. However, the order of increase in the retention times were similar, with the exception of LKLK which had higher retention time than IKIK in RP-HPLC but similar retention times in LC-MS.

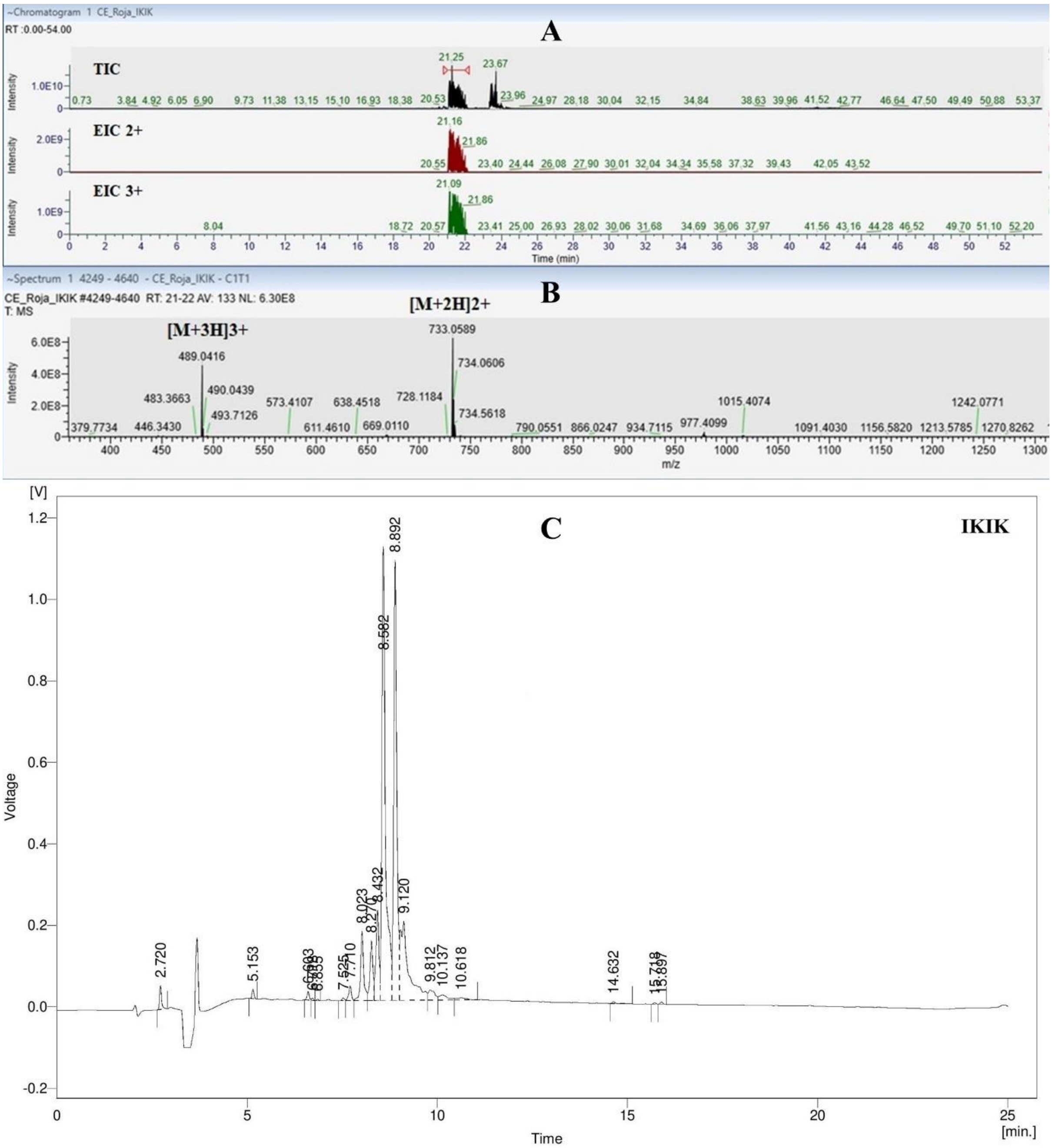

Figure 6.7. LC chromatogram (Al), MS spectrum (B) and RP-HPLC chromatogram (C) of IKIK. TIC: total ion chromatogram; EIC: Extracted ion chromatogram; $[M+2H]^{2+}$ and $[M+3H]^{3+}$ denote the 2+ and 3+ ions corresponding to the designed peptide sequence.

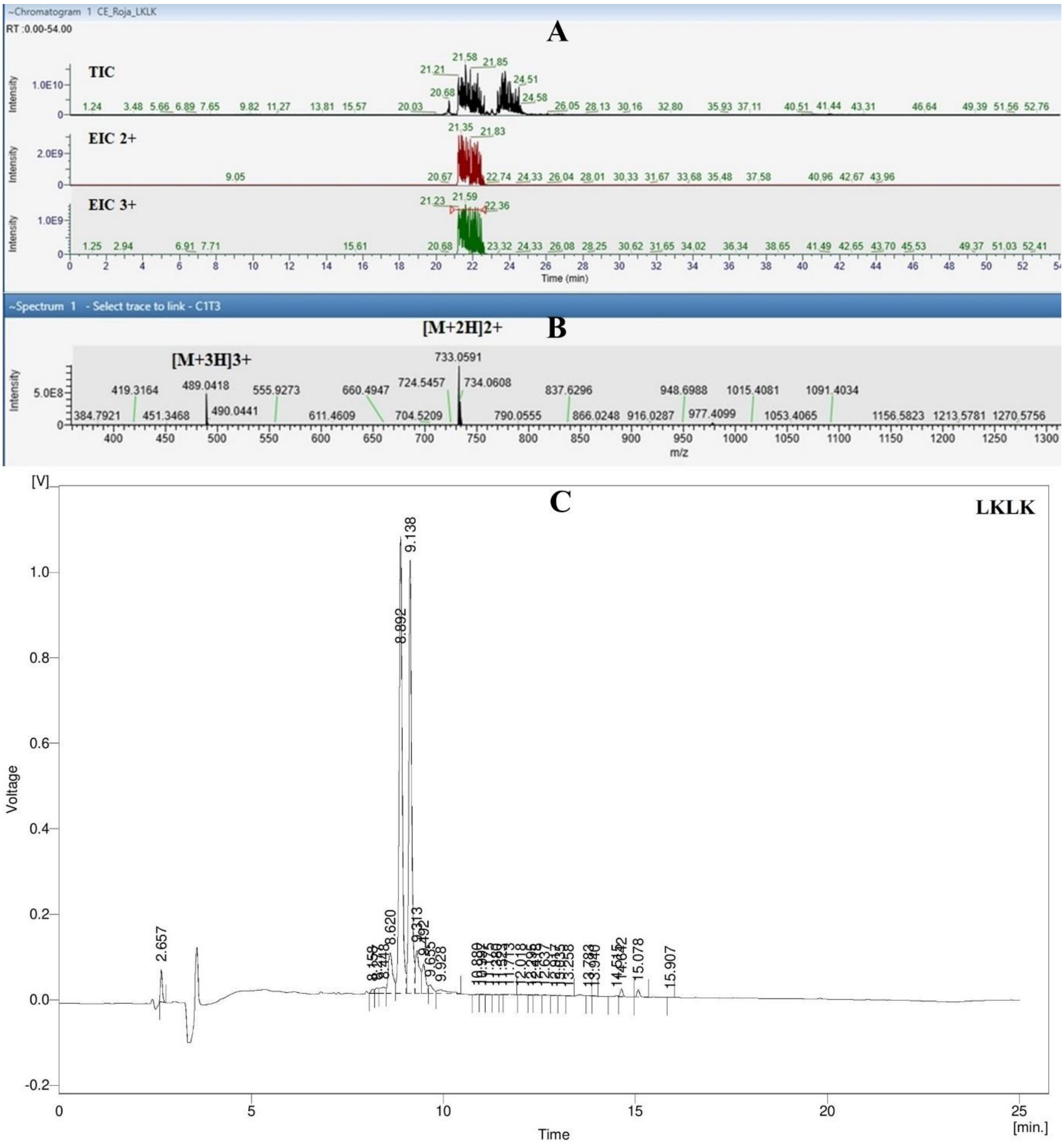

Figure 6.8. LC chromatogram (Al), MS spectrum (B) and RP-HPLC chromatogram (C) of LKLK. TIC: total ion chromatogram; EIC: Extracted ion chromatogram; $[M+2H]^{2+}$ and $[M+3H]^{3+}$ denote the 2+ and 3+ ions corresponding to the designed peptide sequence.

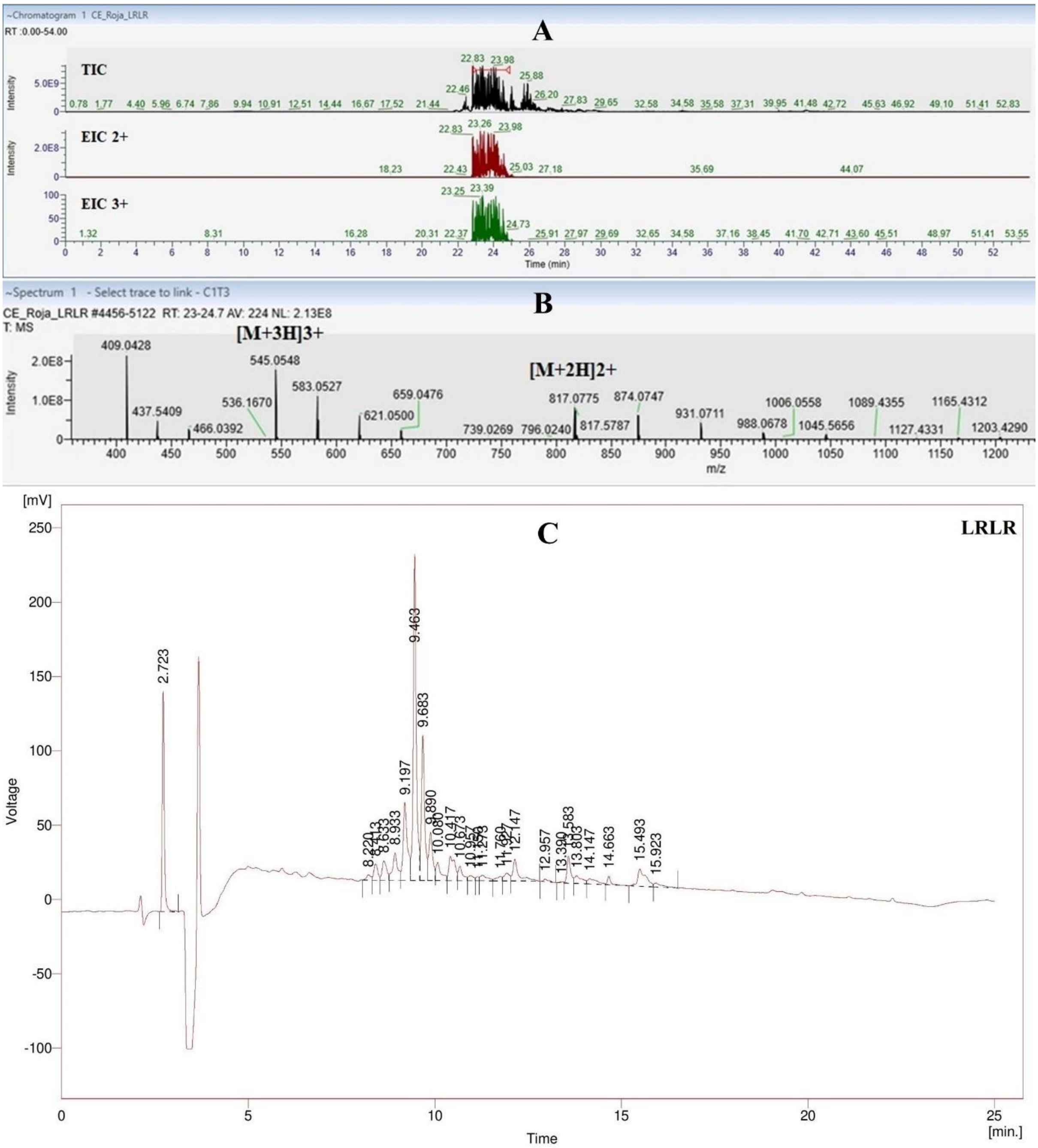

Figure 6.9. LC chromatogram (Al), MS spectrum (B) and RP-HPLC chromatogram (C) of LRLR. TIC: total ion chromatogram; EIC: Extracted ion chromatogram; $[M+2H]^{2+}$ and $[M+3H]^{3+}$ denote the 2+ and 3+ ions corresponding to the designed peptide sequence.

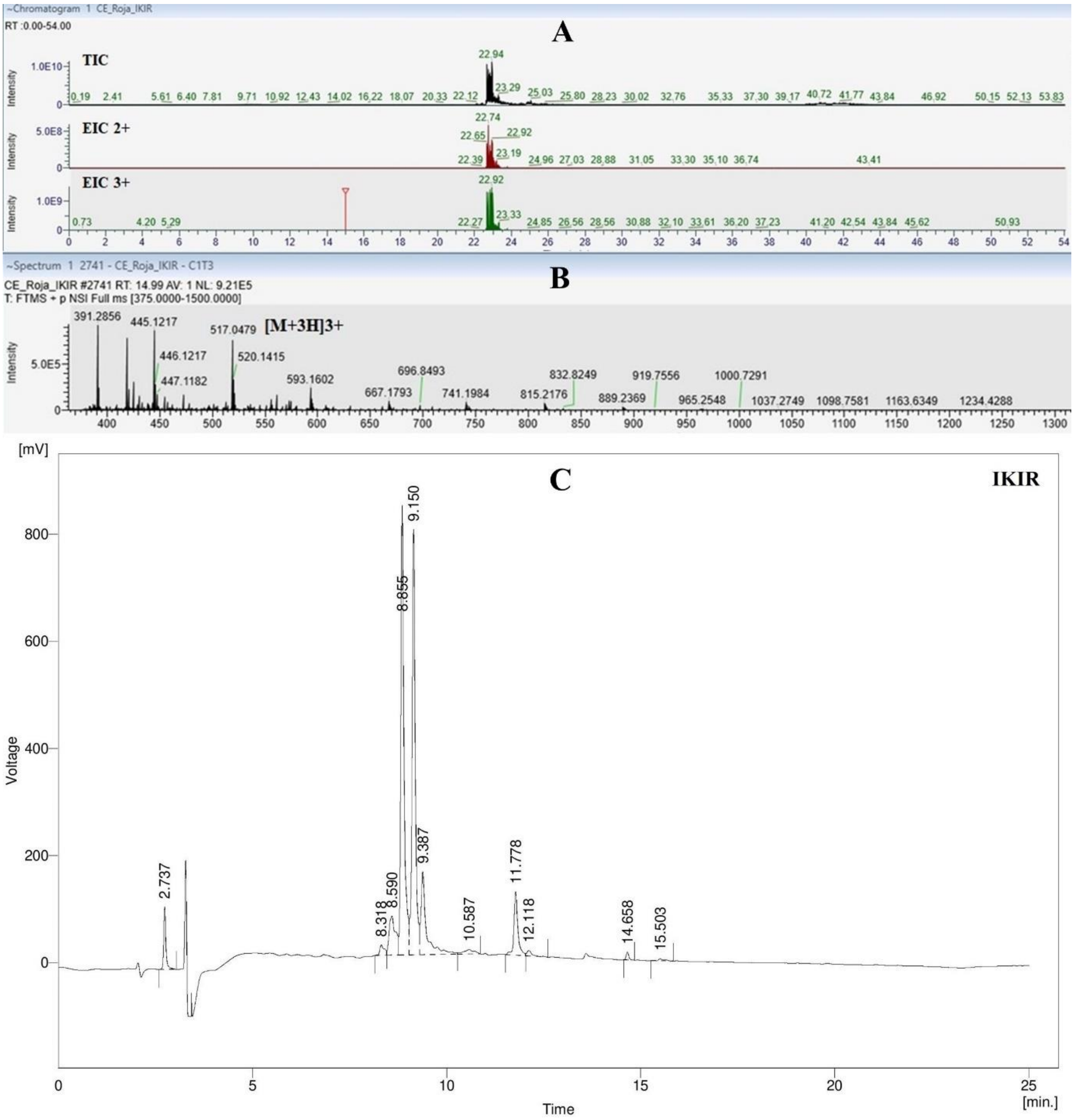

Figure 6.10. LC chromatogram (Al), MS spectrum (B) and RP-HPLC chromatogram (C) of IKIR. TIC: total ion chromatogram; EIC: Extracted ion chromatogram; $[M+3H]^{3+}$ denote the 3+ ion corresponding to the designed peptide sequence.

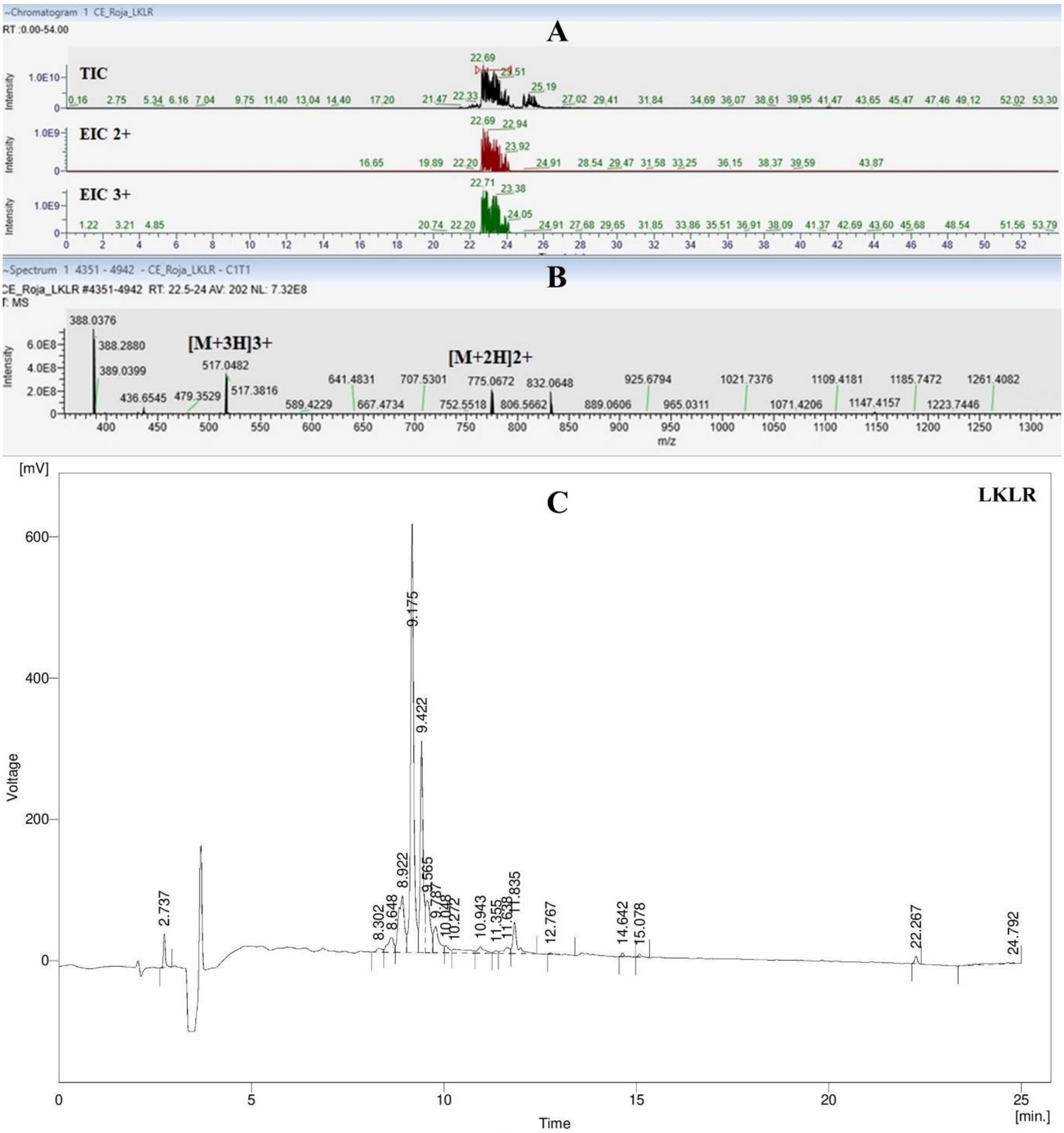

Figure 6.11. LC chromatogram (Al), MS spectrum (B) and RP-HPLC chromatogram (C) of LKLR. TIC: total ion chromatogram; EIC: Extracted ion chromatogram; $[M+2H]^{2+}$ and $[M+3H]^{3+}$ denote the 2+ and 3+ ions corresponding to the designed peptide sequence.

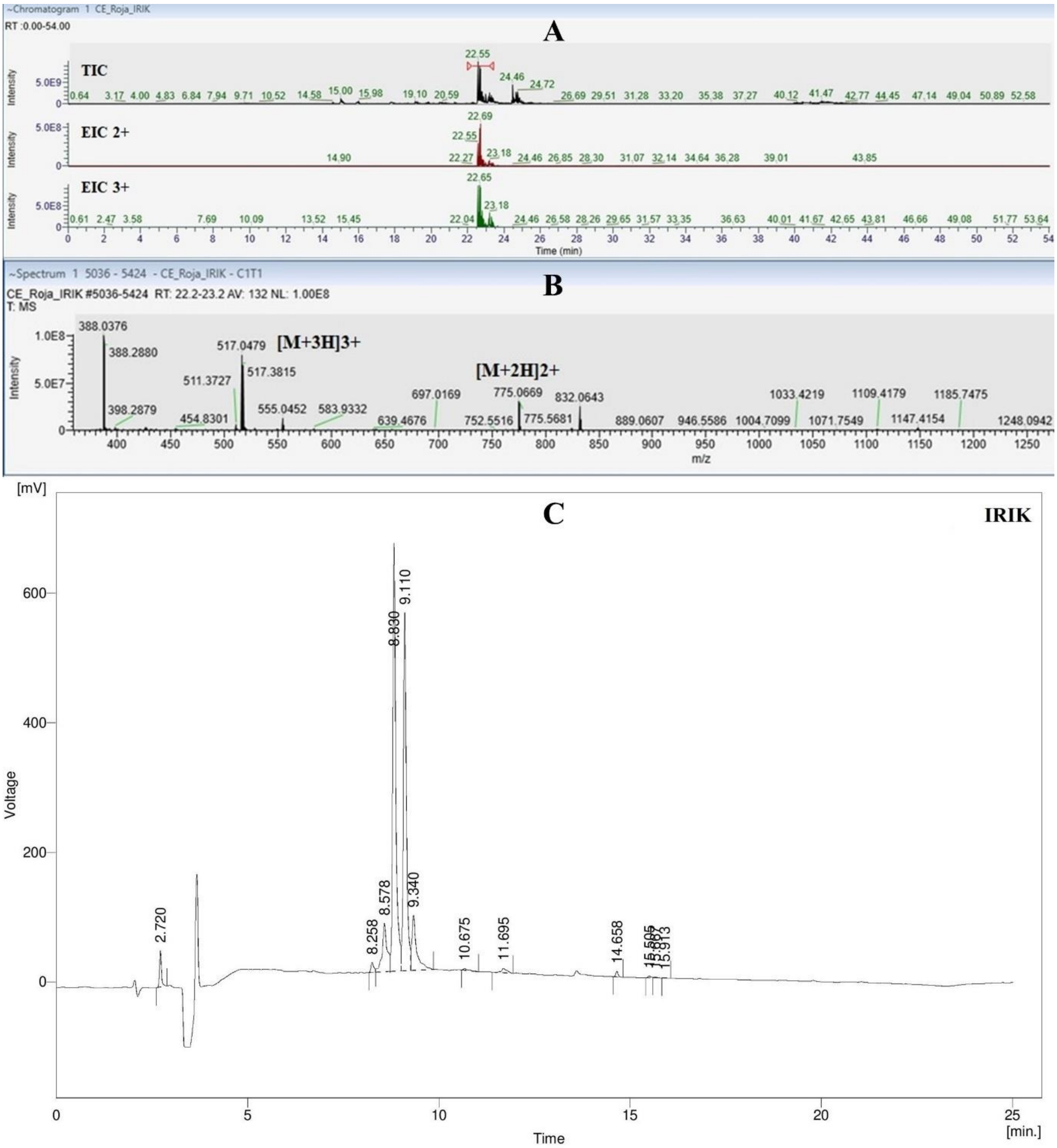

Figure 6.12. LC chromatogram (Al), MS spectrum (B) and RP-HPLC chromatogram (C) of IRIK. TIC: total ion chromatogram; EIC: Extracted ion chromatogram; [M+2H]2+ and [M+3H]3+ denote the 2+ and 3+ ions corresponding to the designed peptide sequence.

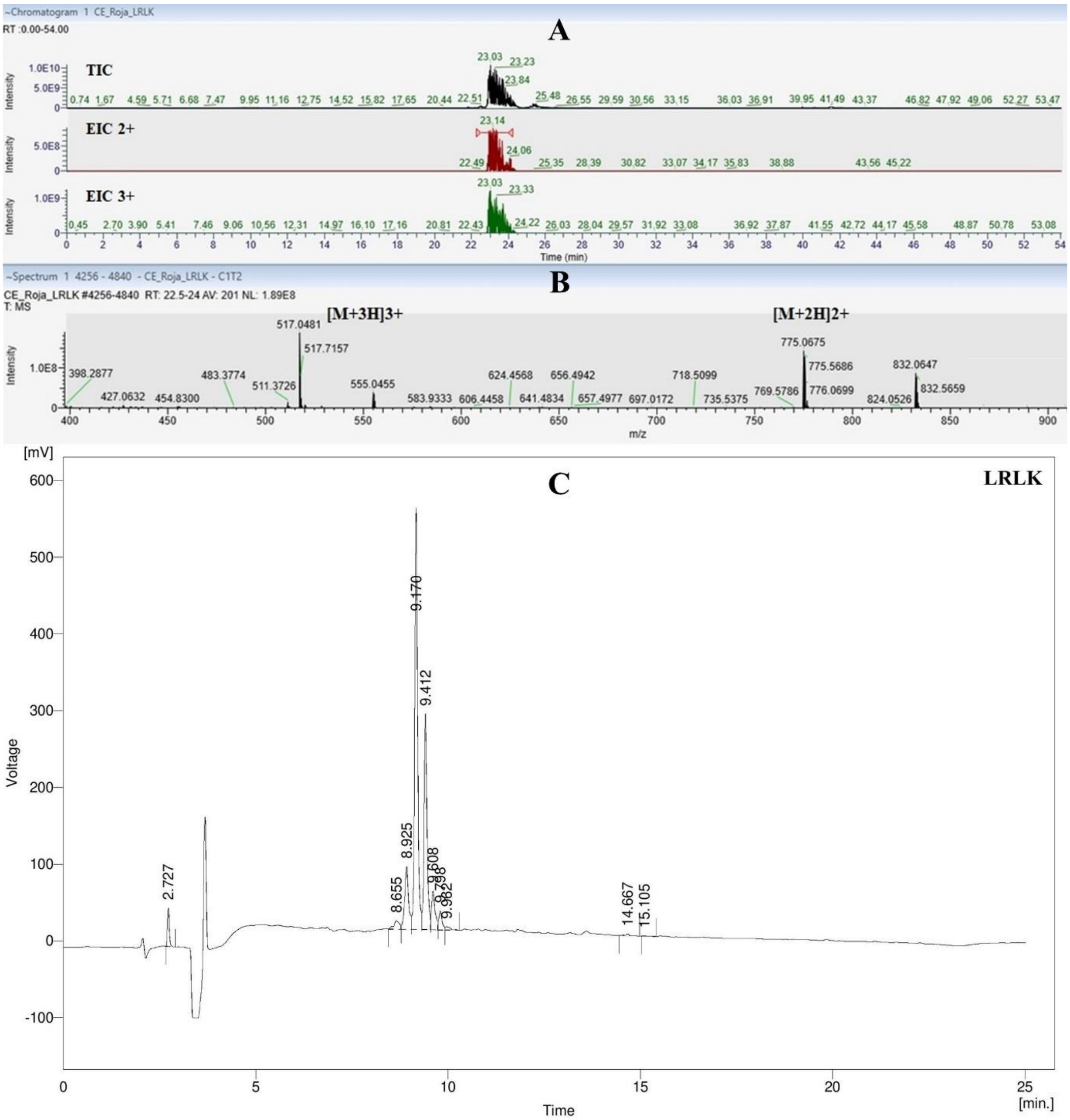

Figure 6.13. LC chromatogram (Al), MS spectrum (B) and RP-HPLC chromatogram (C) of LRLK. TIC: total ion chromatogram; EIC: Extracted ion chromatogram; [M+2H]2+ and [M+3H]3+ denote the 2+ and 3+ ions corresponding to the designed peptide sequence.

Table 6.3. The m/z values, Retention times and molecular masses of the main peaks in the LC-MS TIC of the β-sheet forming cationic amphiphilic peptides and their purities as measured by LC-MS.

Peptide	RT (min)	m/z	Charge	Molecular mass	Compound	Purity (%)
IKIK	21.1	489.042	3+	1464.12	IKIK	60.3
	21.2	733.059	2+	1464.12	IKIK	
	23.4	814.59	2+	1627.18	Impurity	
	23.6	404.79	4+	1627.16	Impurity	
LKLK	21.6	489.042	3+	1464.12	LKLK	56.7
	21.8	733.059	2+	1464.12	LKLK	
	23.7	814.59	2+	1627.18	Impurity	
	23.8	404.79	4+	1627.16	Impurity	
IKIR	22.9	517.05	3+	1548.14	IKIR	57.7
	22.9	775.07	2+	1548.14	IKIR	
	23.2	388.04	4+	1548.16	IKIR	
	25	428.80	4+	1711.2	Impurity	
	25	429.05	4+	1712.2	Impurity	
IRIK	22.6	517.05	3+	1548.14	IRIK	58.2
	22.6	775.07	2+	1548.14	IRIK	
	23	388.04	4+	1548.16	IRIK	
	24.5	428.80	4+	1711.2	Impurity	
	24.5	429.05	4+	1712.2	Impurity	
LKLR	22.7	517.05	3+	1548.14	LKLR	69.7
	22.7	775.07	2+	1548.14	LKLR	
	23.5	388.04	4+	1548.16	LKLR	
	25.2	428.80	4+	1711.2	Impurity	
	25.2	429.05	4+	1712.2	Impurity	
LRLK	23.2	517.05	3+	1548.14	LRLK	78.1
	23.2	775.07	2+	1548.14	LRLK	
	23.8	388.04	4+	1548.16	LRLK	
	25.5	428.80	4+	1711.2	Impurity	
	25.5	429.05	4+	1712.2	Impurity	
LRLR	23.5	545.05	3+	1632.16	LRLR	59.5
	24.2	817.08	2+	1632.16	LRLR	
	24.2	409.4	4+	1632.16	LRLR	
	26.3	450.06	4+	1796.24	Impurity	

Table 6.4. The calculated molecular weights of the cationic amphiphilic β-sheet forming peptides, the molecular weights measured by LC-MS, RP-HPLC retention times and peak areas. The molecular weights were calculated using the software available at www.pepcalc.com.

Peptide	MW (calculated)	MW (measured)	RP-HPLC RT (min)	Peak area (%)
IKIK	1465.01	1464.12	8.6	65
LKLK	1465.01	1464.12	8.9	77.8
LRLR	1633.09	1632.15	9.5	38.7
IKIR	1549.05	1548.15	8.8	69.3
IRIK	1549.05	1548.15	8.8	78.6
LKLR	1549.05	1548.15	9.2	59.7
LRLK	1549.05	1548.15	9.2	75.7

The LC-MS spectra of the surfactant-like peptides are provided in Figures 6.14-6.15. The sequences were checked based on the m/z values for 1+ and 2+ ions corresponding to the designed peptide sequences. Nevertheless, presence of other ions in the spectra indicates impurities. Based on the molecular masses of the major impurities, they are likely to be peptides with different sequences containing addition amino acid residues which could be produced as the by-products of the peptide synthesis (Table 6.5). The calculated molecular weights of the peptides were very close to the values of molecular weight measured by LC-MS as it is evident from Table 6.6. The RP-HPLC chromatograms of the two surfactant-like peptides were in accordance with their LC-MS spectra and showed several peaks corresponding to the impurities. Comparison of the retention times of the major peaks for the two peptides indicates greater hydrophobicity for $(IA)_4K$ which is due to the greater hydrophobicity of the Alanine residues than Glycine residues. As it could be observed in Table 6.5 the purity of these peptides was very low and lower than the other two groups of peptides which raises concerns about the validity of the biological data obtained from these peptides. Therefore, the observed biological activity of these peptides (the ability of the peptides to deliver nucleic acids to the cells) may be affected by the presence of these impurities as they may also exert some biological activity which can add to the observed biological activity of the peptides.

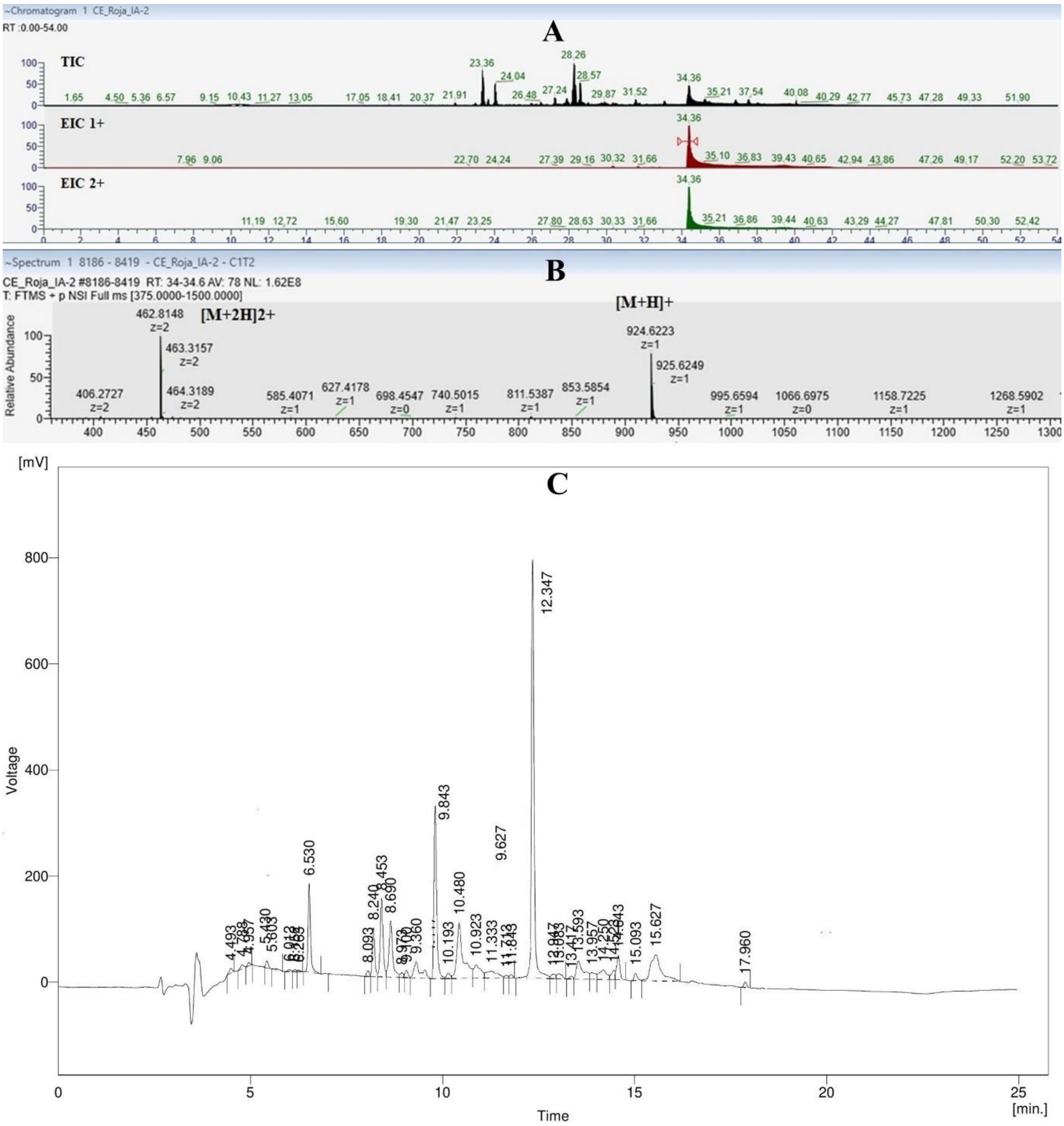

Figure 6.14. LC chromatogram (A), MS spectrum (B) and RP-HPLC chromatogram (C) of (IA)4K. TIC: total ion chromatogram; EIC: Extracted ion chromatogram; [M+H]+ and [M+2H]2+ denote the 1+ and 2+ ions corresponding to the designed peptide sequence.

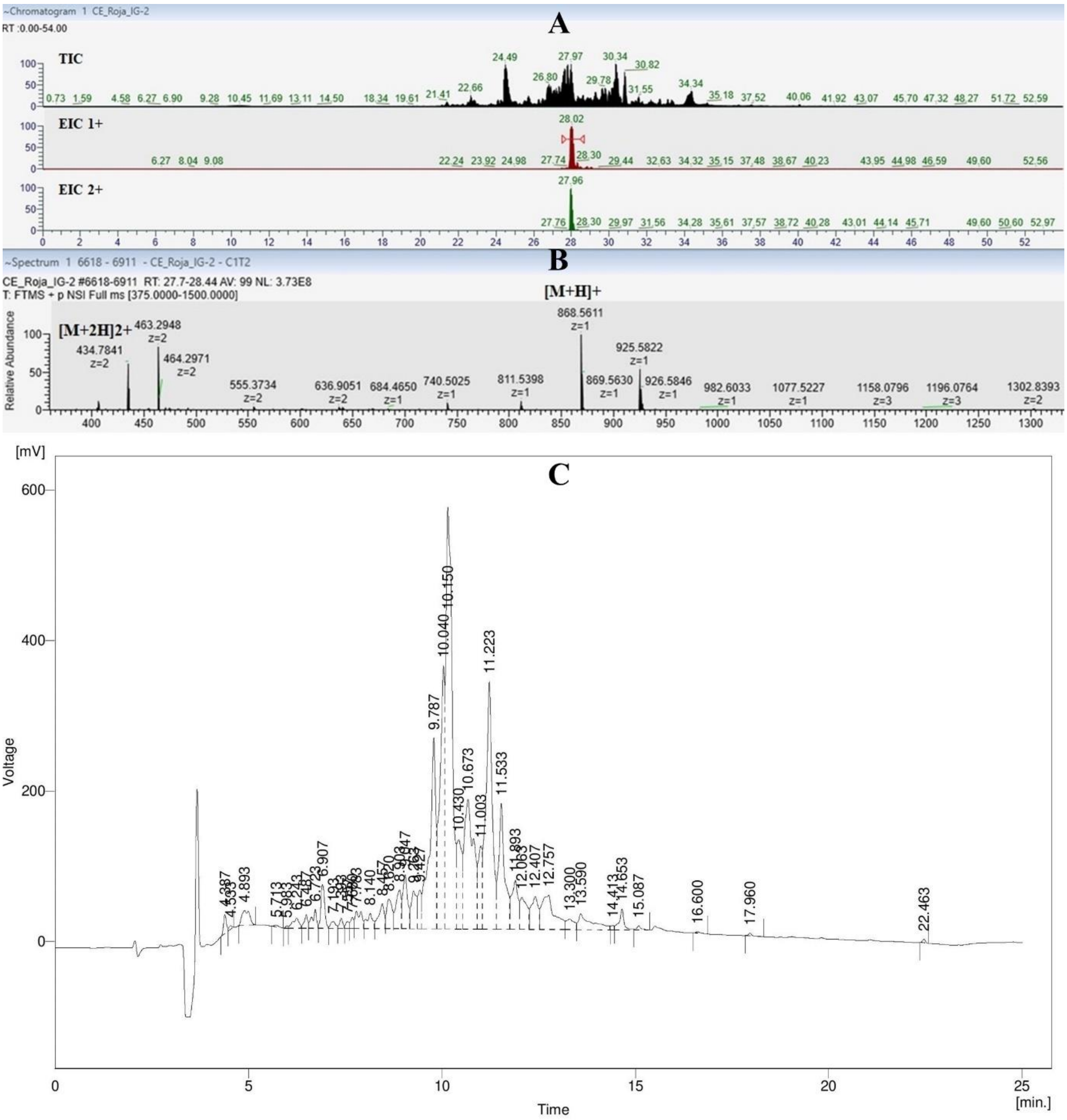

Figure 6.15. LC chromatogram (A), MS spectrum (B) and RP-HPLC chromatogram of (IG)4K. TIC: total ion chromatogram; EIC: Extracted ion chromatogram; [M+H]+ and [M+2H]2+ denote the 1+ and 2+ ions corresponding to the designed peptide sequence.

Table 6.5. The m/z values, Retention times and molecular masses of the main peaks in the LC-MS TIC of the surfactant-like peptides and their purities as measured by LC-MS.

Peptide	RT (min)	m/z	Charge	Molecular mass	Compound	Purity (%)
$(IA)_4K$	23.4	627.42	1+	626.42	Impurity	33.6
	28.3	811.54	1+	810.54	Impurity	
	28.3	406.27	2+	810.54	Impurity	
	34.4	924.62	1+	923.62	(IA)4K	
	34.4	462.81	2+	923.62	(IA)4K	
$(IG)_4K$	24.5	498.83	2+	995.66	Impurity	21.8
	26.8	555.37	2+	1108.74	Impurity	
	28	868.56	1+	867.56	(IG)4K	
	28	434.78	2+	867.56	(IG)4K	
	30.3	491.3261	2+	980.65	Impurity	

Table 6.6. The calculated molecular weights of the surfactant-like peptides, the molecular weights measured by LC-MS, RP-HPLC retention times and peak areas. The molecular weights were calculated using the software available at www.pepcalc.com.

Peptide	MW (calculated)	MW (measured)	RP-HPLC RT (min)	Peak area (%)
$(IA)_4K$	924.18	923.62	8.6	55
$(IG)_4K$	868.01	868.56	8.9	20.2

6.3.2 Relationship between peptide hydrophobicity and anticancer activity

The RP-HPLC retention times can be used as a measure of the hydrophobicity of the peptides as in RP-HPLC the stationary phase is nonpolar and the mobile phase is polar, therefore the less polar peptides with greater hydrophobicity spend more time in the stationary phase than the polar/hydrophilic peptides resulting in longer retention times [2, 19-21]. As it could be observed in Table 6.2, the order of increase in the retention times (hydrophobicity) of α-helical peptides is as follows:

IIKK < IIRR < LLKK < LLRR < II-14 < CI-15

It could be inferred from this data that replacing the lysine residues with arginine increases the hydrophobicity of the peptide. In a similar manner, replacing isoleucine with leucine increases the hydrophobicity of the peptide. Nevertheless, it appears that the effect of changing the hydrophobic amino acid residues (i.e., replacing isoleucine with leucine) on the overall hydrophobicity of the peptide is significantly greater than the effect of changing the hydrophilic amino acid residues (i.e., replacing lysine with arginine). Changing the hydrophobic amino acids results in 1.3 min increase in the retention time of LLKK and LLRR compare to IIKK and IIRR respectively whereas changing the hydrophilic amino acids increases the retention time only by 0.5 mins (30 sec). Increasing the length of the peptide chain from 13 amino acids in IIKK to 15 amino acids in CI-15 and II-14 increases the retention time of the peptides considerably (2.4 min and 2.2 min respectively) due to addition of two hydrophobic amino acid residues (isoleucine). However, replacing the cysteine residue in CI-15 with LC-propargylglycine in II-14 does not alter the hydrophobicity of the peptide significantly. Comparison of the hydrophobicity of the α-helical peptides with their anticancer activity revealed that the more hydrophobic peptides had stronger anticancer activity than the less hydrophobic peptides (Figure 6.16). The only exception was IIRR which was more hydrophobic than IIKK but had weaker anticancer activity. The off trend behaviour of IIRR which results from its unexpectedly poor anticancer activity could either be as a result of its poor interaction with the cancer cell membrane or resulting from its poor interaction with the mitochondrial membrane in cancer cells. Hence, the anticancer activity of these peptides is not only governed by their hydrophobicity and other factors such as secondary structure also appear to contribute to their apparent cytotoxicity as it is discussed in Section 6.3.3.

On the other hand, there was not a direct relationship between the toxicity of the peptides in HDF and their hydrophobicity (Figure 6.17). Nevertheless, among the peptides which contained lysine residues, increased hydrophobicity led to increased toxicity in HDF cells. Therefore, it could be concluded that the cytotoxicity of the lysine rich α-helical peptides in HDF cells is influenced by their hydrophobicities while in arginine rich peptides such correlation does not exist.

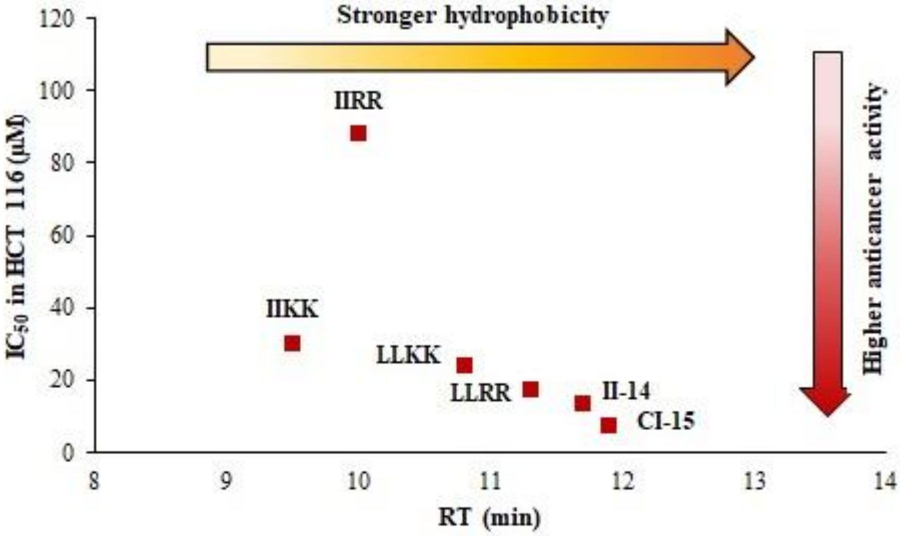

Figure 6.16. Relationship between the hydrophobicity of the α-helical cationic amphiphilic peptides as measured by their RP-HPLC retention time (RT) and their anticancer activity in HCT 116.

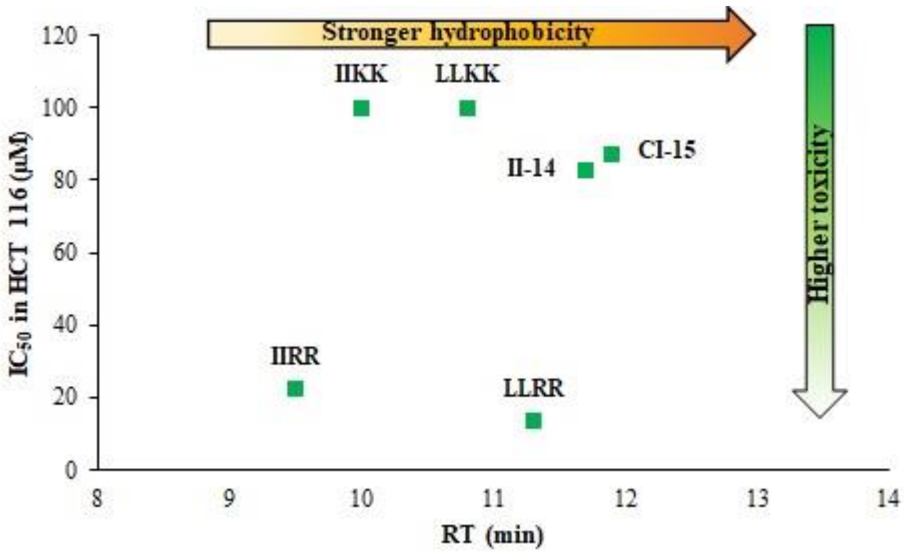

Figure 6.17. Relationship between the hydrophobicity of the α-helical cationic amphiphilic peptides as measured by their RP-HPLC retention time (RT) and their anticancer activity in HDF cells.

The order of increase in the RP-HPLC retention times (hydrophobicities) of the β-sheet forming peptides is as follows (Table 6.4):

IKIK < IKIR = IRIK < LKLK < LKLR= LRLK < LRLR

As it could be inferred from these data, replacing isoleucine residues with leucine residues and replacing lysine residues with arginine residues results in increased hydrophobicity of the peptides, similar to the trend observed for the α-helical peptides. However, unlike the α-helical peptides in which the hydrophobic amino acid residues had a greater role in determining the overall hydrophobicity of the peptide, in β-sheet forming peptides the effect of changing the hydrophilic amino acid residues on the overall hydrophobicity of the peptide molecule is higher than changing the hydrophobic amino acid residues. For example, replacing all the isoleucine residues in IKIK with leucine residues results in LKLK which shows 0.3 mins increase in retention time whereas replacing all the lysine residues in LKLK with arginine residues results in LRLR which has 0.6 mins increase in the retention time.

A closer look at the retention times for these two groups of peptides reveals that the extent of increase in the retention time resulting from replacing lysine residues with arginine residues in β-sheet forming peptides is similar to the α-helical peptides (0.6 min vs. 0.5 min respectively) whereas replacing isoleucine with leucine has far weaker effect on the overall hydrophobicity of the β-sheet forming peptides than α-helical peptides (0.3 min vs. 1.3 min respectively). As a result, except IKIK and LRLR which have completely different combination of amino acids, for the rest of the peptides the difference between the retention times is not significant and in the case of peptides with same amino acid combination but different sequence (i.e., IKIR and

IRIK or LKLR and LRLK) the retention times are the same. Unlike the α-helical peptides, there was no direct relationship between the hydrophobicity of the β-sheet forming peptides and their anticancer activity (Figure 6.18) although LKLR, LRLK and LRLR which had higher hydrophobicities than the rest of the peptides showed poor anticancer activity. Hence, the anticancer activity of β-sheet forming peptides is less influenced by their hydrophobicity than the α-helical peptides. However, since the purity of this group of peptides was very low, it is not clear if the observed anticancer activities are merely resulting from the peptides or are partially caused by the other impurities in the peptide solutions. Therefore, it is possible that lack of correlation between the hydrophobicity and the anticancer activity of the peptides is due to the presence of other molecules in the peptide solution which may also possess cytotoxicity. Similar to HCT 116, in HDF cells also there was no direct correlation between the hydrophobicity of the β-sheet peptides and their anticancer activity (Figure 6.19). However, in contrary to the trend in HCT 116, in HDF cells the peptides with highest hydrophobicities (LKLR, LRLK, and LRLR) exhibited lower cytotoxicity than the other peptides, except IKIK which was highly toxic to HDFs.

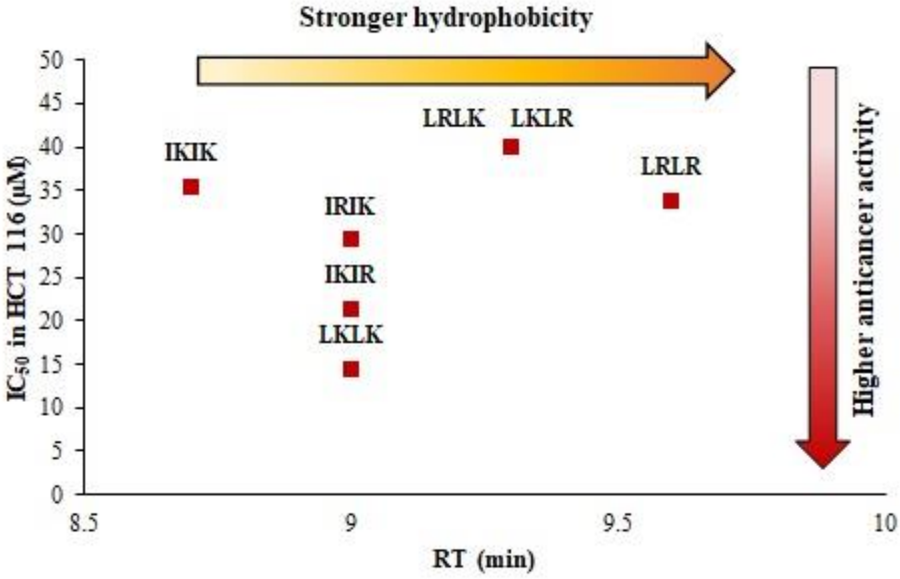

Figure 6.18. Relationship between the hydrophobicity of the β-sheet forming cationic amphiphilic peptides as measured by their RP-HPLC retention time (RT) and their anticancer activity in HCT 116 cells.

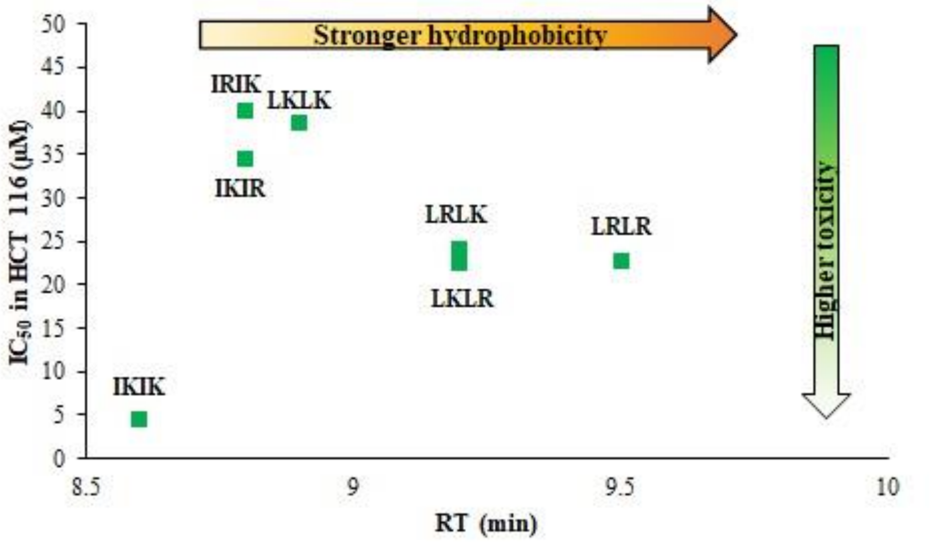

Figure 6.19. Relationship between the hydrophobicity of the β-sheet forming cationic amphiphilic peptides as measured by their RP-HPLC retention time (RT) and their anticancer activity in HDF cells.

6.3.3 Secondary structure of the peptides

The secondary structure of the designed cationic amphiphilic peptides in aqueous solution (DI water and phosphate buffer) and their conformational changes upon interaction with curved surfaces were determined by CD spectroscopy. Three types of curved surfaces were used in these experiments to provide anionic and neutral environments in order to mimic the cancer cell and normal cell membranes:

1- Zwitter ionic (neutral) DPPC SUVs with an average particle size of 165 ± 5 nm as a mimic of normal mammalian cell membrane.
2- Anionic DPPG SUVs with an average particle size of 153.6 ± 24.6 nm as a mimic of cancer cell membranes.
3- Anionic SDS micelles with an average particle size of 143.8 ± 22.9 nm as a mimic of cancer cell membranes.

The CD spectra of the α-helical peptides in different experimental conditions are presented in Figures 6.20-6.24. As it could be observed the peptides had random coil structure in the aqueous media (Water and PB) as denoted by a negative peak at 198-200 nm [1-3, 11, 12]. This is supposed to be due to the strong intermolecular hydrogen bonding between the peptides and the water molecules as well as the electrostatic repulsion between the adjacent positively charged arginine/lysine residues [2, 9].

However, all of the peptides adopted α-helical structures in anionic environments, SDS micelles and DPPG SUVs, denoted by a positive peak at 193 nm and negative peaks at 208 nm and 220-222 nm [1-3, 10, 11] which is indicative of conformational change due to the interaction of the positively charged amphiphilic peptides with the negatively charged SDS micelles and/or negatively charged DPPG SUVs. This results in the polar surface of the α-helix interacting with the hydrophilic heads and the nonpolar surface interacting with the hydrophobic tails of the DPPG/SDS molecules [2]. On the other hand, the peptides adopted weak α-helical structures in the zwitter ionic DPPC SUVs which indicates a weak interaction between the cationic amphiphilic peptides and the zwitter ionic phospholipid bilayers. This could be due to the affinity to the membrane bilayer by hydrophobicity as ideally the peptides are expected to have non-ordered or random structures in DPPC SUVs. Also, the CD spectra in DPPC SUVs had lower quality than the spectra in DPPG SUVs and SDS micelles indicating the need for optimization of measurements in DPPC SUVs.

These results are in accordance with the results reported for other types of short cationic amphiphilic α-helical antimicrobial/anticancer peptides and cell penetrating peptides in the literature. For example, Hu et al [9] introduced a class of short cationic amphiphilic peptides, with the general formula $G(IIKK)_n$ I-NH2 (n=1-4) with selective antimicrobial and anticancer activity. The peptides were unfolded in water and in DPPC SUVs but folded into α-helical structure in DPPG SUVs [9]. The most efficient peptide from this series, $G(IIKK)_3$I-NH2, named as G3, was further modified to achieve higher antimicrobial/anticancer activity and higher selectivity. A series of G3 derivatives were developed by Chen et al [2] by changing the N-terminal and C-terminal amino acids. The resulting peptides, $(IIKK)_3$, $G(IIKK)_3$, and $(IIKK)_3$I, had random coil structure in DI water but adopted α-helical structures in SDS micelles [2]. Gong et al [1] reported similar results for another group of G3 derivatives including $G(ILKK)_3$L, $G(IVKK)_3$I, $G(IVKO)_3$I, and $IK(KKII)_2$KI, showing unfolded random coil structure in Tris-HCl buffer but α-helical conformation in SDS micelles and DPPG SUVs [1]. Similarly, several different types of cell penetrating peptides including CADY, MAP, EB1 and TP10 have been reported to have unfolded random coil structure in aqueous solution and in neutral phospholipid vesicles (DOPC), and to fold into α-helix in negatively charged phospholipid vesicles (DOPG) [11].

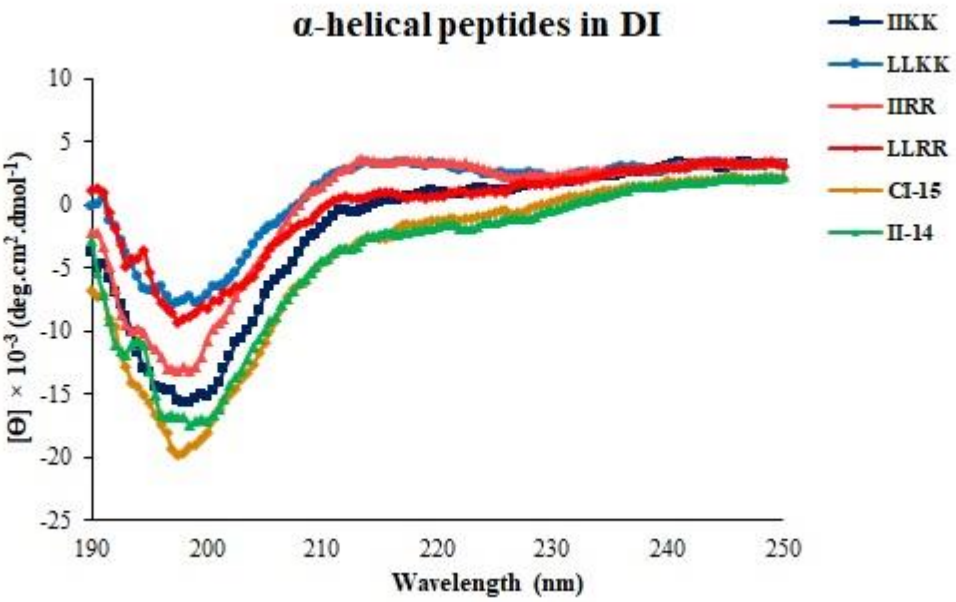

Figure 6.20. CD spectra of the α-helical cationic amphiphilic peptides in DI water. The data are presented as average of three repeats.

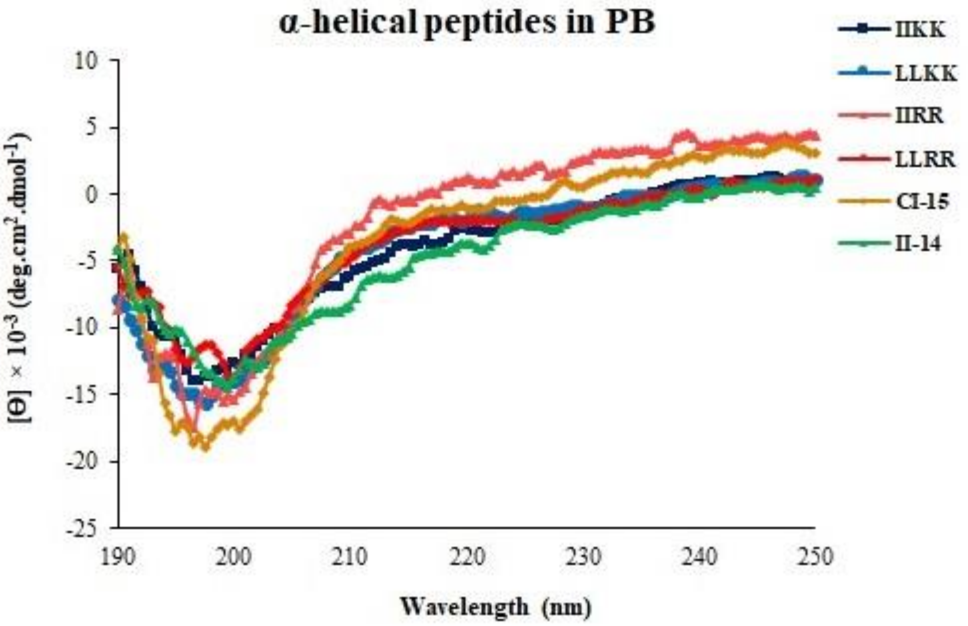

Figure 6.21. CD spectra of the α-helical cationic amphiphilic peptides in phosphate buffer (PB) pH=7.4. The data are presented as average of three repeats.

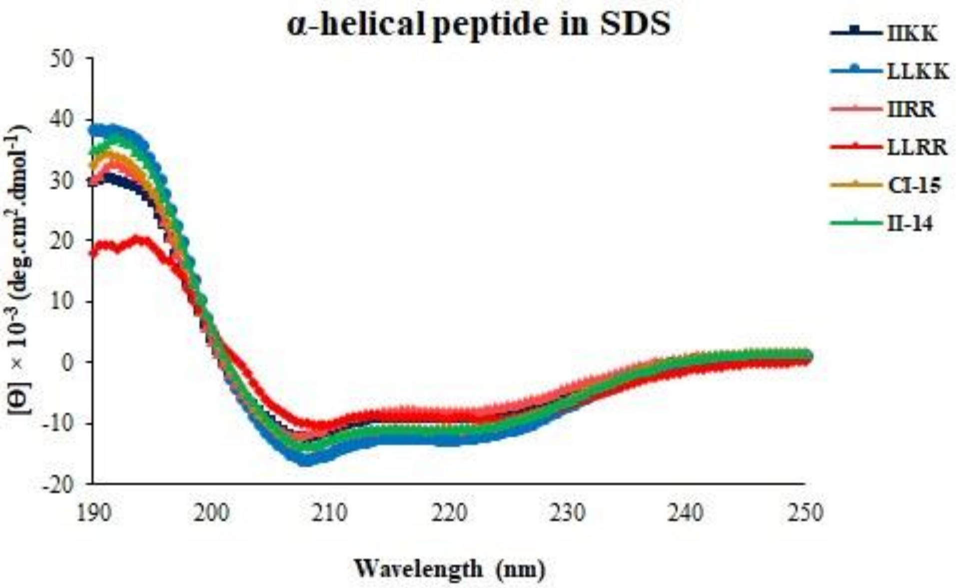

Figure 6.22. CD spectra of the α-helical cationic amphiphilic peptides in SDS micelles. The data are presented as average of three repeats.

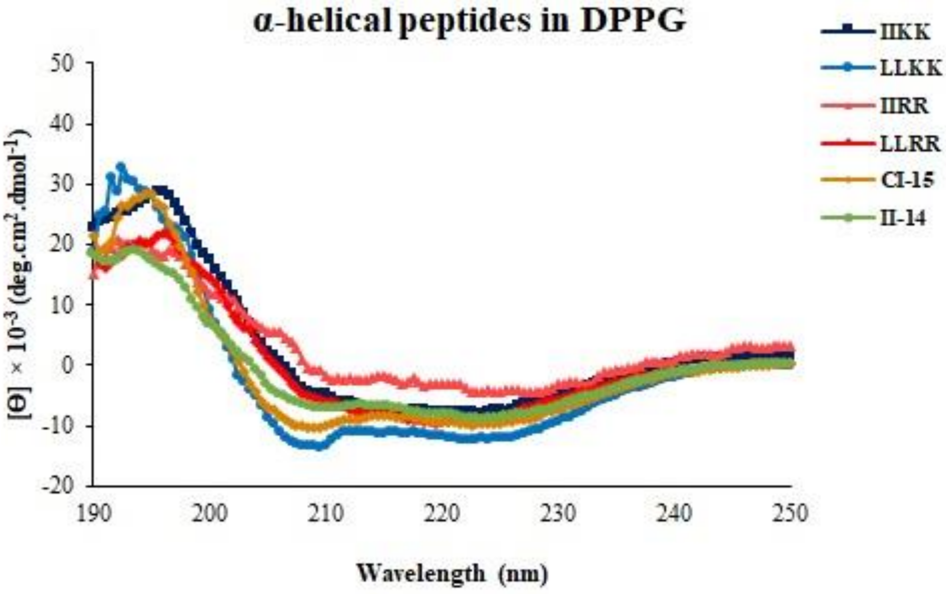

Figure 6.23. CD spectra of the α-helical cationic amphiphilic peptides in DPPG SUVs. The data are presented as average of three repeats.

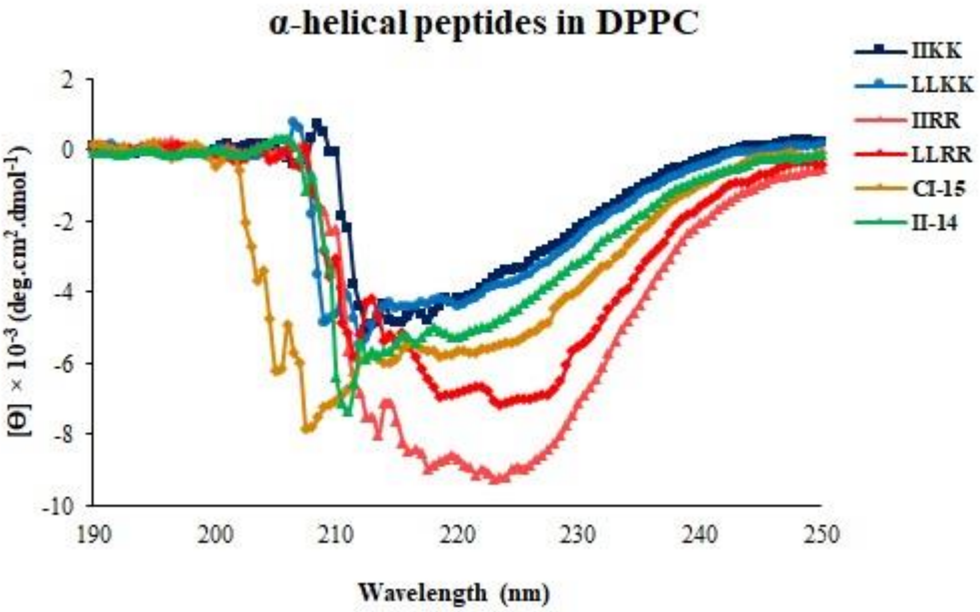

Figure 6.24. CD spectra of the α-helical cationic amphiphilic peptides in DPPC SUVs. The data are presented as average of three repeats.

In order to compare the degree of helicity of the peptides, the mean residue molar ellipticity at 220-222 nm was used as a measure of helicity [1-3, 10]. Among all peptides, CI-15 and II-14 exhibited the highest helicity in DPPG SUVs which indicates the effect of the C-terminal Isoleucine on the α-helix formation which is in accordance with the results reported by Chen et al [3]. Nevertheless, II-14 has lower helicity than CI-15 which is supposed to be due to the presence of LC-Propargylglycine instead of Cysteine in N-terminal which disfavours the helical formation. Similar findings have been reported by Chen et al suggesting that the presence of glycine residue at the N-terminal decreases the helical content of the G3 derivatives [3].

There was a good correlation between the helical content of the peptides in DPPG and DPPC SUVs and their cytotoxicity against normal cells and cancer cells respectively as depicted in Figures 6.25-6.26. The peptides with higher degree of helicity in DPPG SUVs exhibited higher anticancer activity whereas the peptides with lower degree of helicity in DPPG SUVs lacked strong anticancer activity. The degree of helicity in DPPC SUVs on the other hand, corresponds to the toxicity of the peptides in fibroblasts. The peptides which showed high helical content in DPPG SUVs and low helical content in DPPC SUVs (IIKK, LLKK, II-14, and CI-15) possess selective anticancer activity. On the contrary, IIRR which has high toxicity against

HDFs and poor anticancer activity, has highest degree of helicity in DPPC SUVs and lowest degree of helicity in DPPG SUVs.

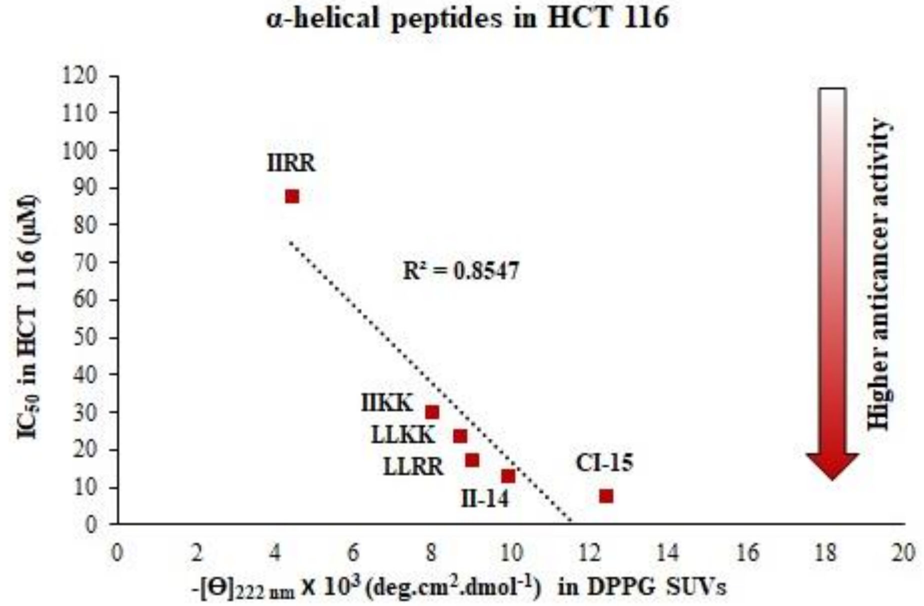

Figure 6.25. Relationship between the helicity of the cationic amphiphilic peptides in DPPG SUVs and their anticancer activity against HCT 116 colorectal cancer cells. (R^2: correlation coefficient).

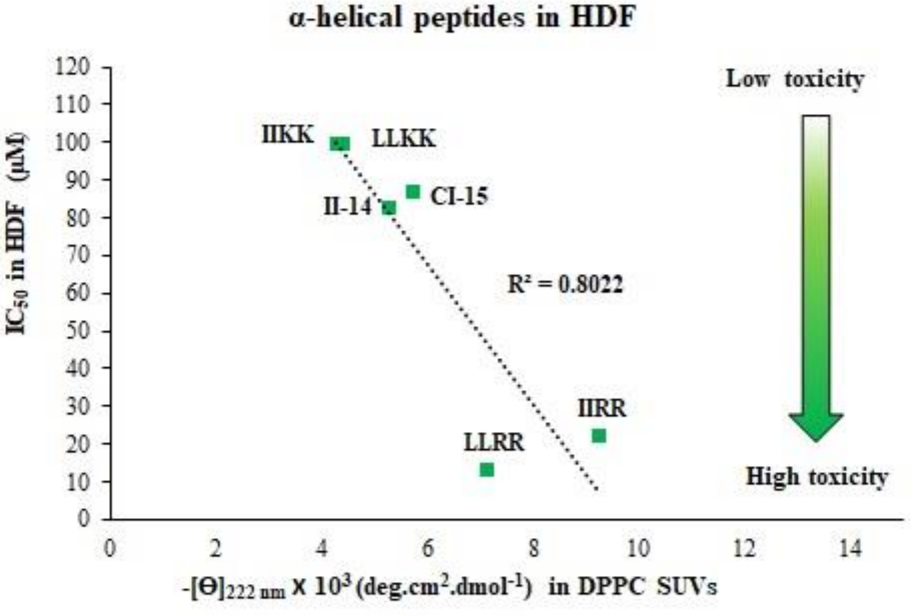

Figure 6.26. Relationship between the helicity of the cationic amphiphilic peptides in DPPC SUVs and their toxicity in normal cells (HDFs). It should be noted that the values of IC_{50} for IIKK and LLKK were higher than 100 µM and were edited as 100 µM for clarity. (R^2 : correlation coefficient)

The CD spectra of the β-sheet forming cationic amphiphilic peptides in different experimental conditions are presented in Figures 6.27-6.31. As it could be observed, except IKIR and IRK, which formed β-sheet in aqueous solution (DI water and phosphate buffer), the rest of the peptides exhibited unfolded random coil structure as indicated by a negative peak at near 198-200 nm [11,14,15]. This is supposed to be because of the electrostatic repulsion between the positively charged arginine/lysine residues [14]. However, in anionic environments (SDS micelles and DPPG SUVs) all peptides formed β-sheet structures denoted by a positive peak at 197-200 nm and a negative peak at 217-218 nm [14-16] due to the interaction between the positively charged peptides and the negatively charged SDS/DPPG headgroups followed by interaction of the hydrophobic residues with the hydrophobic tail of the SDS/DPPG [14, 16]. Considering the low purity of the peptide samples, the observed conformational change into β-sheet indicates that the impurities in the sample did not affect the secondary structure of the peptides in anionic hydrophobic surfaces which is in favour of the correlation between the secondary peptide structures and their observed biological activities.

In DPPC SUVs on the other hand, most of the peptides showed a combination of random coil structure and partial β-sheet structure, showing a positive peak at 194-200 nm and a negative peak at 200-205 nm with the exception of IKIR and IRIK which exhibited a weak β-sheet conformation with a positive peak at 198-200 nm and a negative peak at 219 nm. These data suggest a weak interaction between the cationic amphiphilic peptides and the zwitter ionic DPPC lipid vesicles. One possible explanation could be that some of the peptide molecules have partially penetrated into the lipid bilayer forming partial β-sheet structures whereas the remaining peptide molecules are still in the unfolded random coil conformation in the aqueous phase (the SUVs were suspended in PB). Therefore, the spectra show both the absorption maximum for the β-sheet and the absorption minimum for the random coil. Another explanation could be presence of both structures in the peptide molecule as is commonly observed in some larger peptides and proteins with some α-helical or β-sheet segments and some segments which have random coil structure.

These findings are in accordance with the results from other studies with similar cationic amphiphilic β-sheet forming antimicrobial peptides. For example, Ong et al [14] designed a class of short cationic antimicrobial peptides with the general formula $(X_1Y_1X_2Y_2)_n$ (n=2-3, X_1 and X_2 : Val, Ileu, Phe, Trp; Y_1 and Y_2: Arg or Lys). All of the designed peptides had random coil structure in water, but they transformed into β-sheet structure in SDS micelles [14]. Similar observations have been reported for some of the cell penetrating peptides including Penetratin, MPG, and M918 which had random coil structure in water and neutral DOPC phospholipid vesicles but folded into β-sheet conformation in anionic DOPG phospholipid vesicles [11].

In order to compare the degree of β-sheet formation between different cationic amphiphilic peptides, the values of mean residue molar ellipticity at 197-200 nm were used as a measure of the β-sheet content [16]. As it could be observed, IKIR and IRIK have the highest tendency for forming β-sheet structures both in neutral and anionic environments among all peptides in this group. This suggests that the presence of isoleucine residues is more favourable for β-sheet formation than leucine residues. Moreover, the combination of lysine and arginine seems to lead to higher tendency for β-sheet conformation than either arginine or lysine as IKIK which consists of isoleucine and lysine does not form β-sheet structure in aqueous solution.

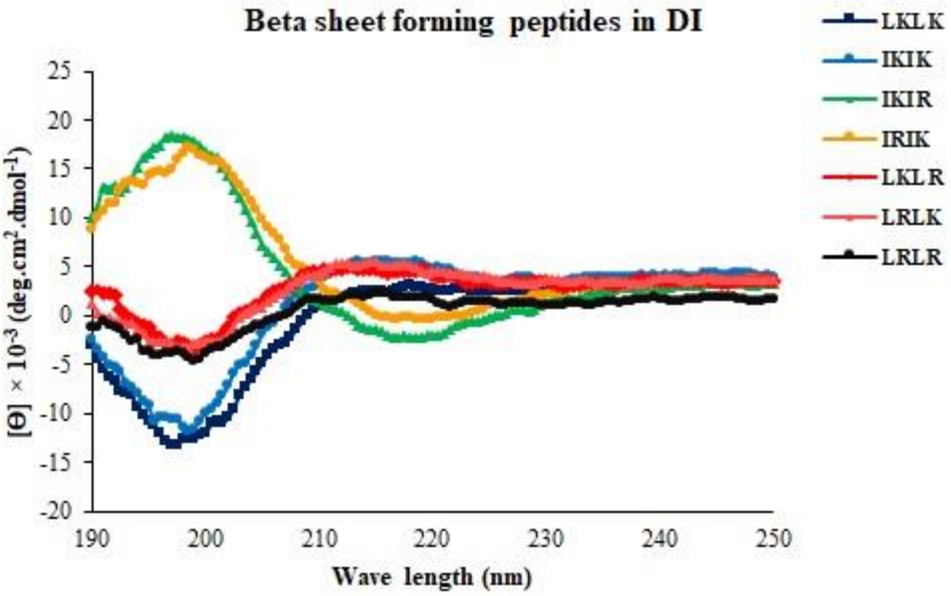

Figure 6.27. CD spectra of the β-sheet forming cationic amphiphilic peptides in DI water. The data are presented as average of three replicates.

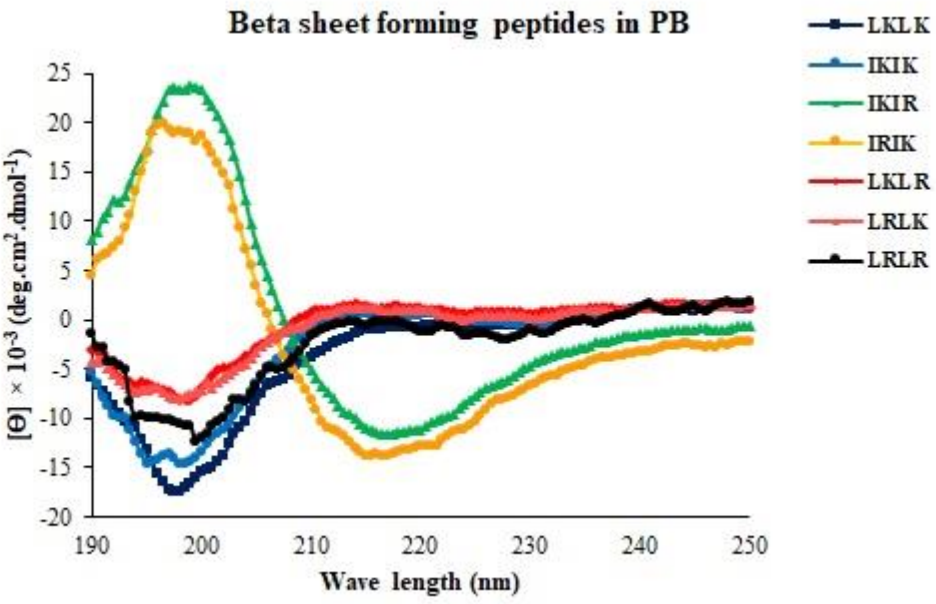

Figure 6.28. CD spectra of the β-sheet forming cationic amphiphilic peptides in phosphate buffer (PB) pH=7.4. The data are presented as average of three repeats.

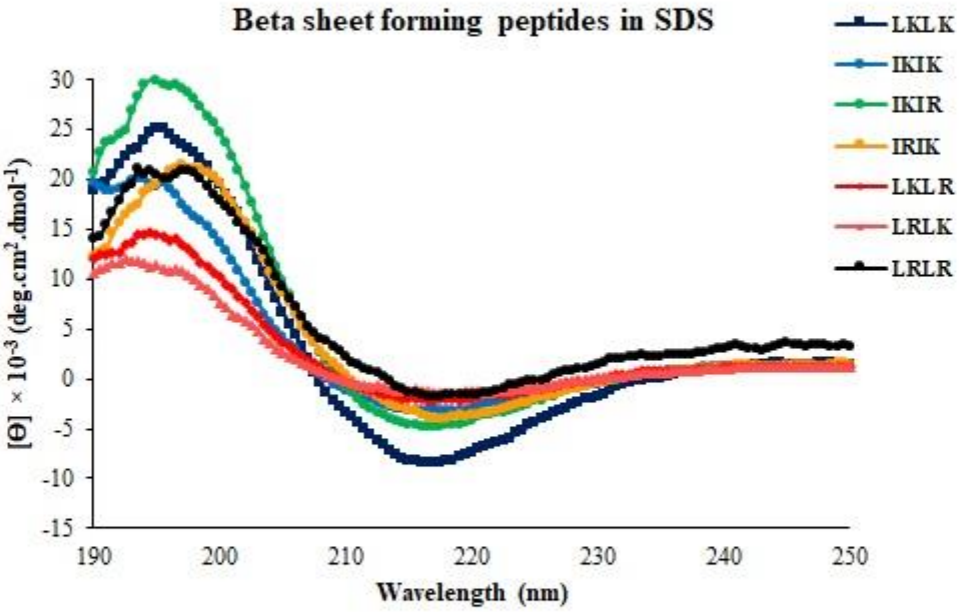

Figure 6.29. CD spectra of the β-sheet forming cationic amphiphilic peptides in SDS micelles. The data are presented as average of three repeats.

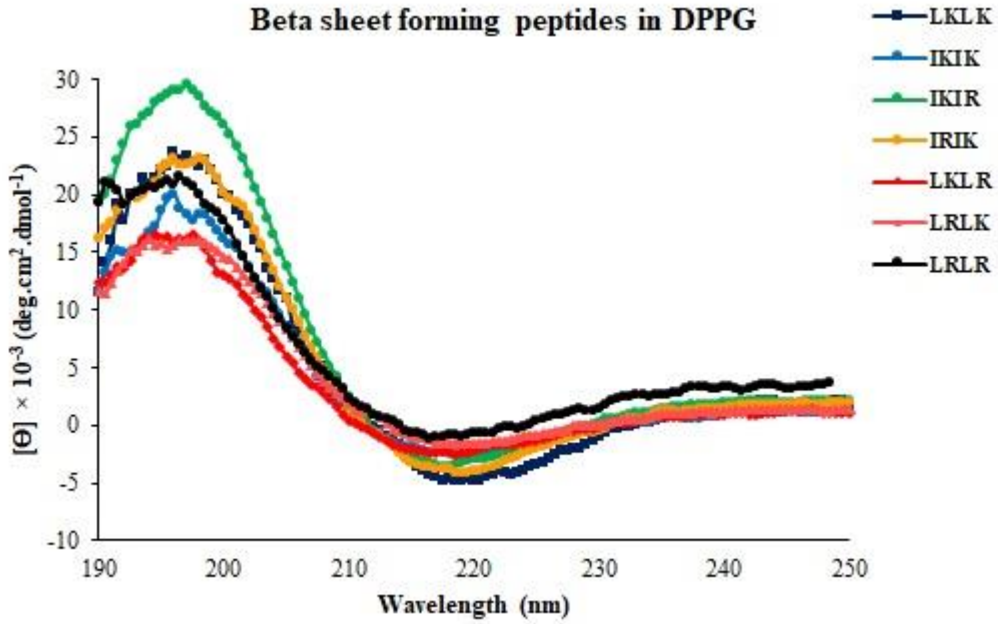

Figure 6.30. CD spectra of the β-sheet forming cationic amphiphilic peptides in DPPG SUVs. The data are presented as average of three repeats.

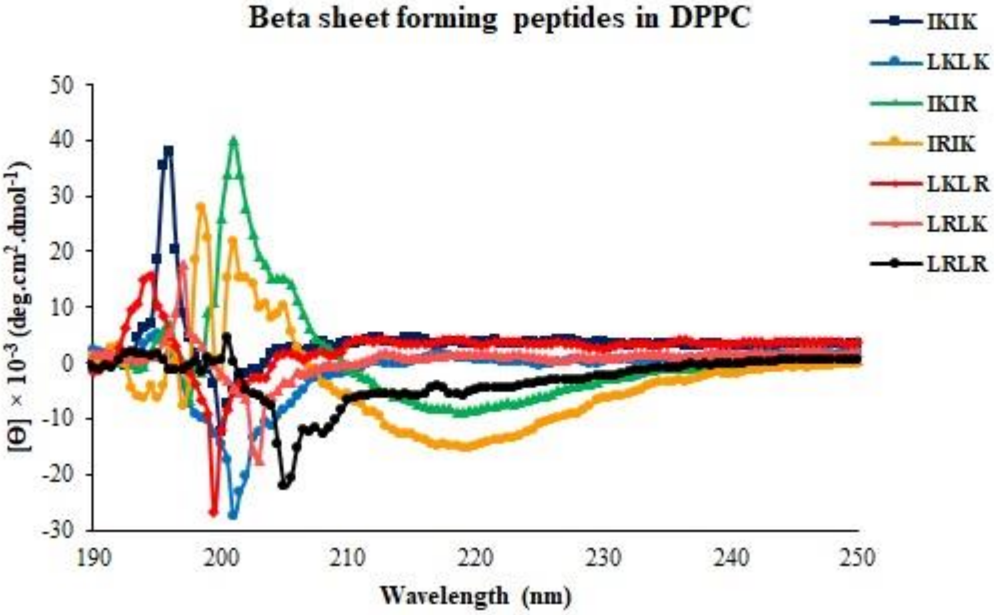

Figure 6.31. CD spectra of the β-sheet forming cationic amphiphilic peptides in DPPC SUVs. The data are presented as average of three repeats.

The relationship between the β-sheet content of the peptides in DPPG and DPPC SUVs and their anticancer activity/toxicity are depicted in Figures 6.32-6.33. As it could be observed, there was a good correlation between the β-sheet content of the peptides in DPPG and their anticancer activity. Hence, the peptides with stronger β-sheet conformation in DPPG SUVs exhibited higher anticancer activity than the peptides with lower β-sheet content. The only exception to the general trend was LKLK which had lower β-sheet content than IKIR an IRIK but exhibited higher anticancer activity. On the other hand, although for most of the peptides their β-sheet content in DPPC SUVs was proportional to their cytotoxicity in human dermal fibroblasts, IKIR and IRIK did not follow this general trend and despite their high β-sheet content in DPPC SUVs, exhibited low toxicity in fibroblasts. This suggests that unlike toxicity against cancer cells which is strongly influenced by the β-sheet content of the cationic amphiphilic peptides, cytotoxicity against normal cells is influenced by an interplay between the β-sheet conformation and other factors.

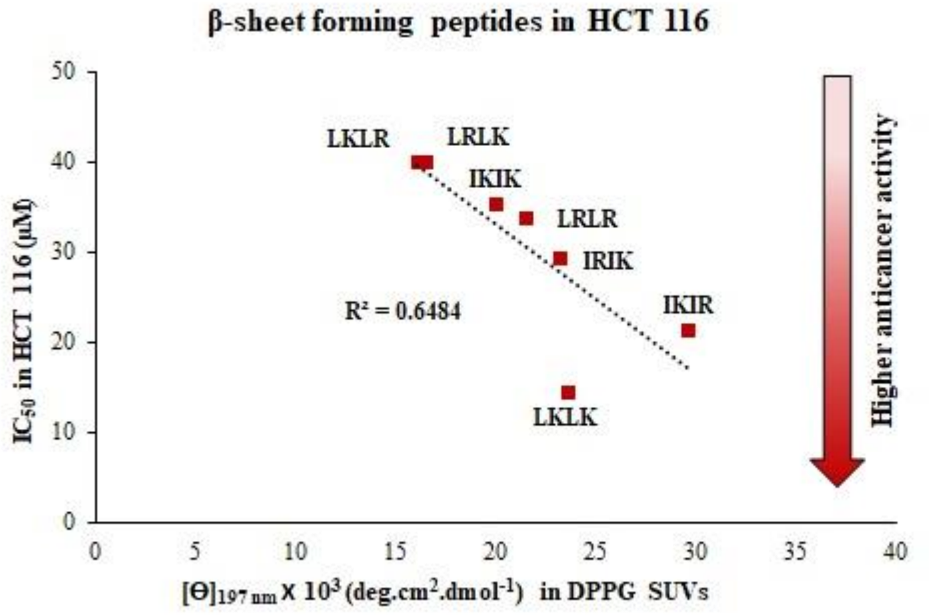

Figure 6.32. Relationship between the β-sheet content of the cationic amphiphilic peptides in DPPG SUVs and their anticancer activity in HCT 116 colorectal cancer cells. (R^2 : correlation coefficient)

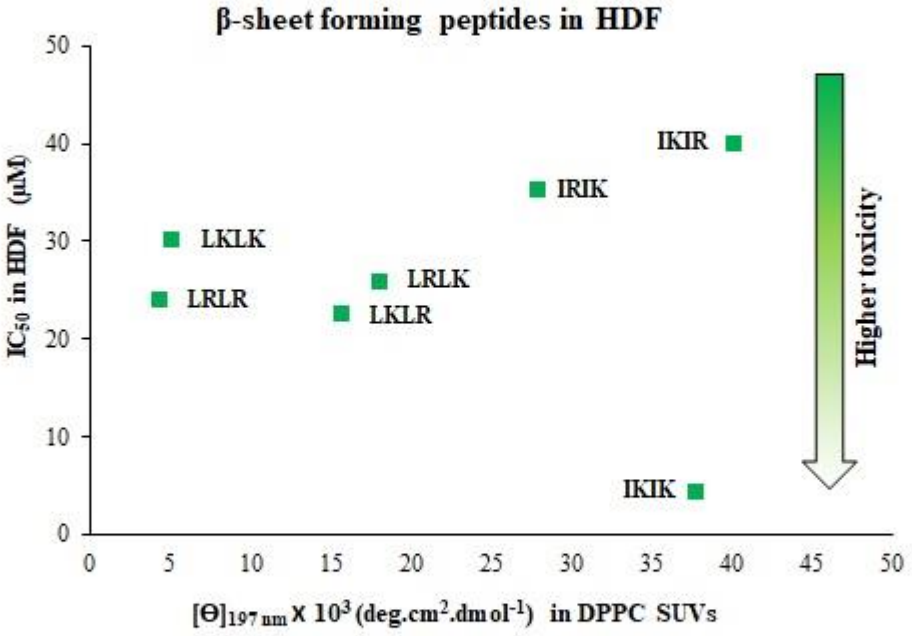

Figure 6.33. Relationship between the β-sheet content of the cationic amphiphilic peptides in DPPC SUVs and their toxicity in normal cells (HDFs).

The CD spectra of the surfactant-like peptides (SLP)s in different experimental conditions are presented in Figures 6.34-6.38. As it could be observed the peptides had a β-sheet structure in aqueous solution (DI and PB) and also in anionic SDS micelles and DPPC SUVs as indicated by presence of a positive peak at 197-200 nm and a negative peak at 217-218 nm [14-16]. However, their β-sheet content in water and buffer was very low compared to their β-sheet content in SDS micelles and DPPG SUVs (based on the mean residue molar ellipticity at 197-2900 nm). In zwitter ionic DPPC also the peptides adopted a weak β-sheet conformation. The stronger beta-sheet structure in negatively charged membranes, could be resulting from forming clusters or nanostructures. According to the literature data on other short surfactant-like peptides with β-sheet structures, it is possible that the peptides self-assemble into nanorods or nanofibers [22]. It is also possible that in aqueous solution the peptides exist more as monomers than nanostructures but upon contact with negatively charged membranes they self-assemble into supramolecular structures within the lipid membrane which increases their β-sheet content [22]. The peptides are supposed to insert into the lipid bilayers through electrostatic interaction of the positively charged lysine residues with the polar heads of the phospholipids followed by insertion of the hydrophobic peptide tails into the lipid bilayer. However, since no experiments have been performed to provide evidence for peptide self-assembly it cannot be known for sure if the peptides form nanostructures and what is the shape and size of the nanostructures. If it is confirmed by further studies that these peptides can form nanostructures, it is possible to study the effect of changing the peptide structure on the shape and size of the self-assembled nanostructures and its impact on the biological activity of the peptides which could be employed for rational design of surfactant-like peptides with improved anticancer activity or higher gene delivery efficiency.

There was no significant difference in the β-sheet content between the two peptides in aqueous solution and DPPC SUVs. On the other hand, in DPPG SUVs and SDS micelles, $(IG)_4K$ had considerably higher β-sheet content than $(IA)_4K$ which suggests the Glycine residues favour the β-sheet formation more than the Alanine residues in this group of peptides. The higher β-sheet content of these peptides in DPPG SUVs compared to DPPC SUVs could be the reason for higher transfection efficiency of these peptides in cancer cells compared to fibroblasts as it indicates stronger interaction with the negatively charged lipid membranes than neutral lipid membranes.

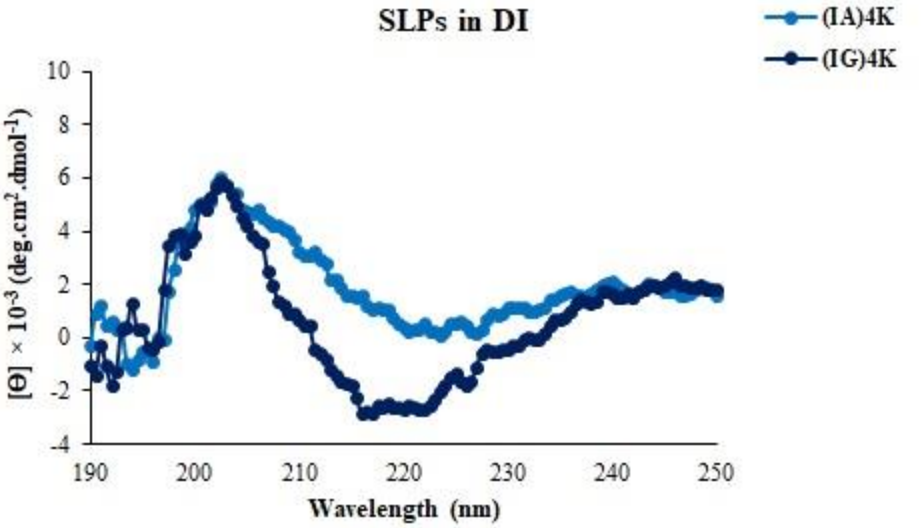

Figure 6.34. CD spectra of the surfactant-like peptides in DI water. The data are presented as average of three repeats.

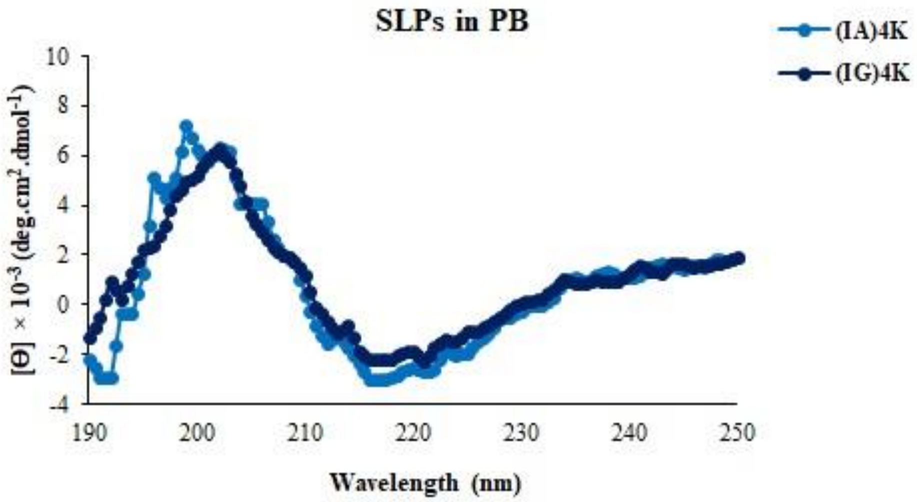

Figure 6.35. CD spectra of the surfactant-like peptides in Phosphate buffer (PB). The data are presented as average of three repeats.

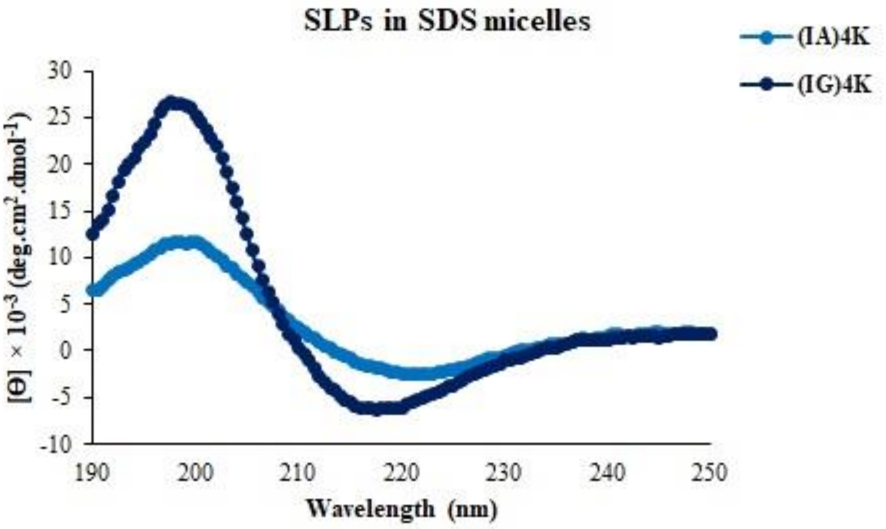

Figure 6.36. CD spectra of the surfactant-like peptides in SDS micelles. The data are presented as average of three repeats.

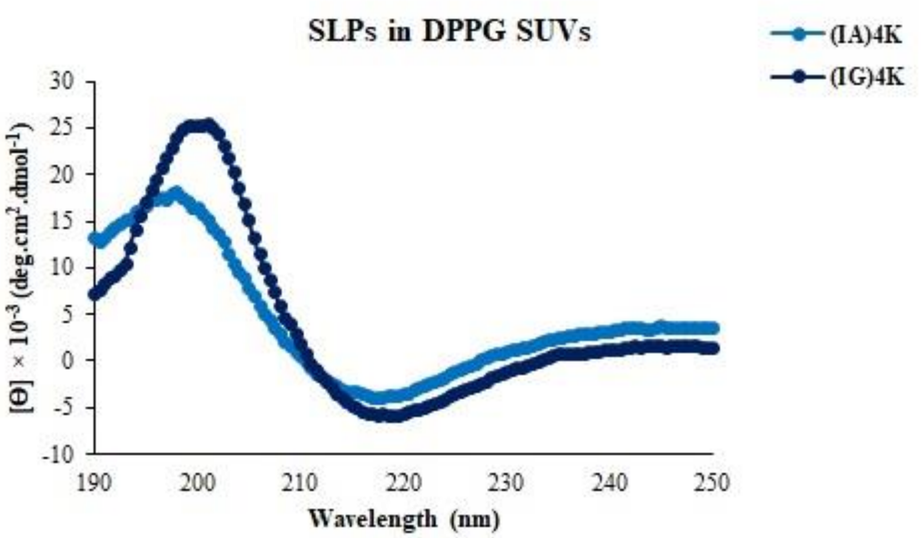

Figure 6.37. CD spectra of the surfactant-like peptides in DPPG SUVs. The data are presented as average of three repeats.

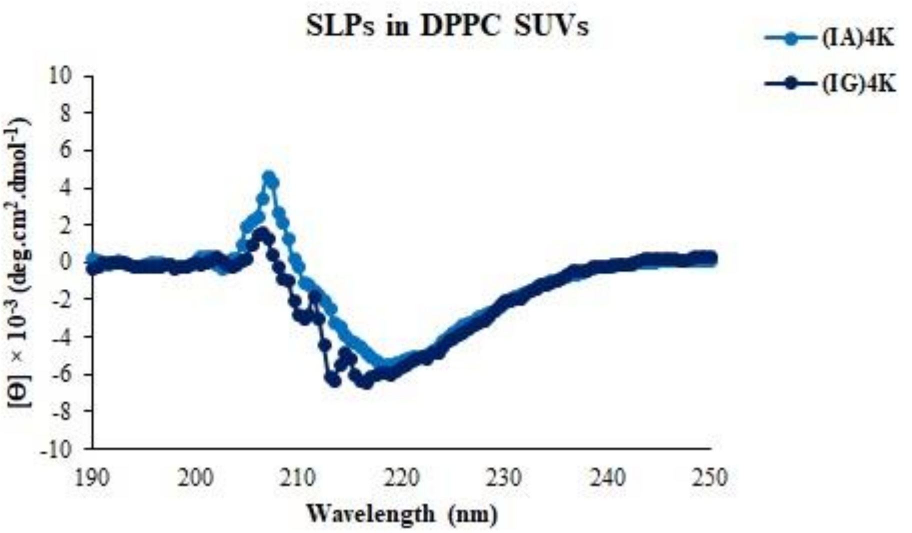

Figure 6.38. CD spectra of the surfactant-like peptides in DPPC SUVs. The data are presented as average of three repeats.

6.3.4 Changes to the surface pressure at the air/water interface

The amphiphilic activities of the cationic amphiphilic peptides were measured by their surface adsorption at the air/water interface. Adsorption of the peptides at the air/water interface, results in a decrease in the surface tension from that of pure water/buffer. The difference between the initial and final surface tension is defined as the surface pressure [2] which is indicative of the surface activity of the amphiphilic peptides. Since the value recorded for the surface tension of water is negative, setting it as the start point (zero) results positive values for surface pressure showing an increase in the surface pressure from that of pure water. The surface activity experiments were only performed on the peptides with high anticancer activity and more selectivity for cancer cells. Nevertheless, one peptide from each group with poor anticancer activity (IIRR and LRLK) was tested as a negative control for comparison. The pressure-time isotherms of the cationic amphiphilic α-helical peptides are demonstrated in Figures 6.39-6.43. The isotherms display a rapid initial rise in the pressure over the first few mins followed by a slower equilibration phase. Increasing the concentration of the cationic amphiphilic peptides in the subphase results in higher surface pressure which indicates the interfacial adsorption of the peptides is concentration dependent.

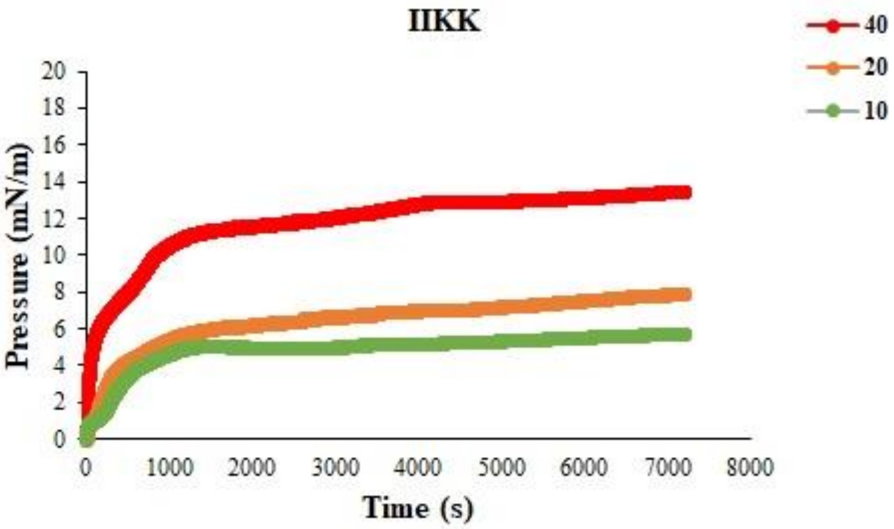

Figure 6.39. Surface pressure (Pi) as a function of time following adsorption of IIKK at the air/water interface at different peptide concentrations (10-40 µM) in the subphase.

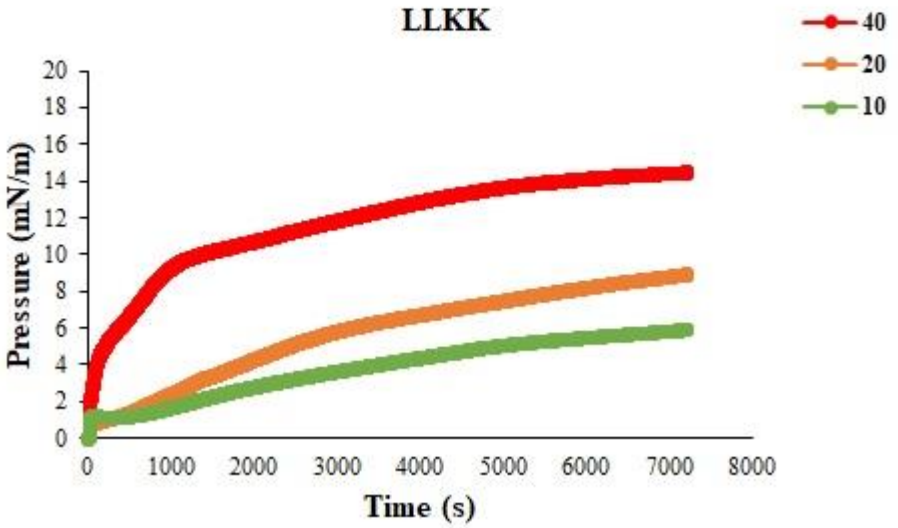

Figure 6.40. Surface pressure (Pi) as a function of time following adsorption of LLKK at the air/water interface at different peptide concentrations (10-40 µM) in the subphase.

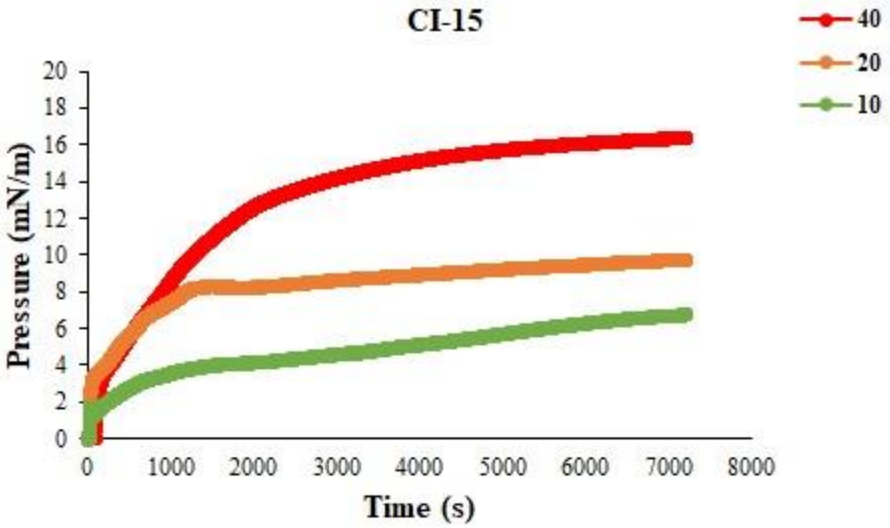

Figure 6.41. Surface pressure as a function of time following adsorption of CI-15 at the air/water interface at different peptide concentrations (10-40 µM) in the subphase.

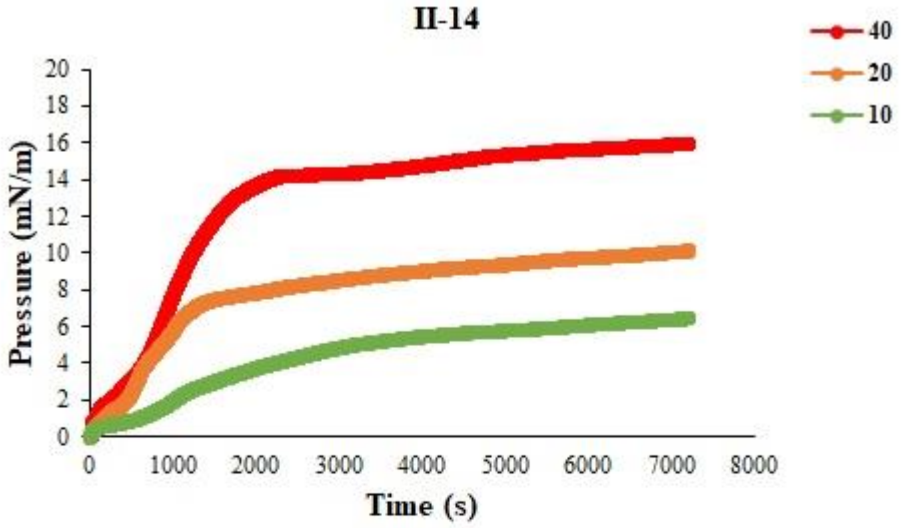

Figure 6.42. Surface pressure as a function of time following adsorption of II-14 at the air/water interface at different peptide concentrations (10-40 µM) in the subphase.

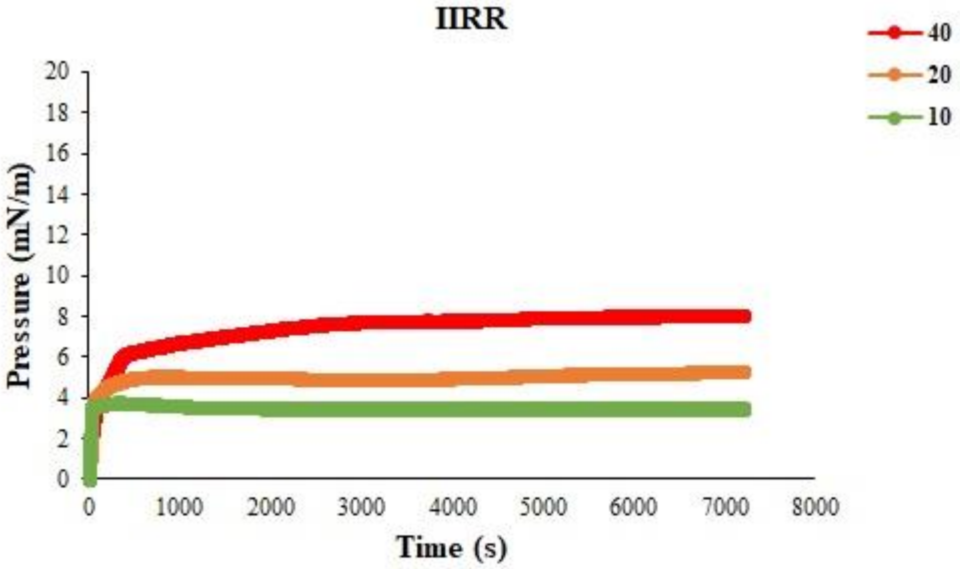

Figure 6.43. Surface pressure as a function of time following adsorption of IIRR at the air/water interface at different peptide concentrations (10-40 µM) in the subphase.

Comparing the surface pressure of different cationic amphiphilic α-helical peptides at the air/water interface (Figure 6.44) shows that except IIRR which has considerably lower surface pressure at all of the peptide concentrations, for the rest of the peptides at low peptide concentrations (10µM) there is no significant difference between the different peptides whereas at higher peptide concentrations (20-40 µM) this difference becomes more considerable.

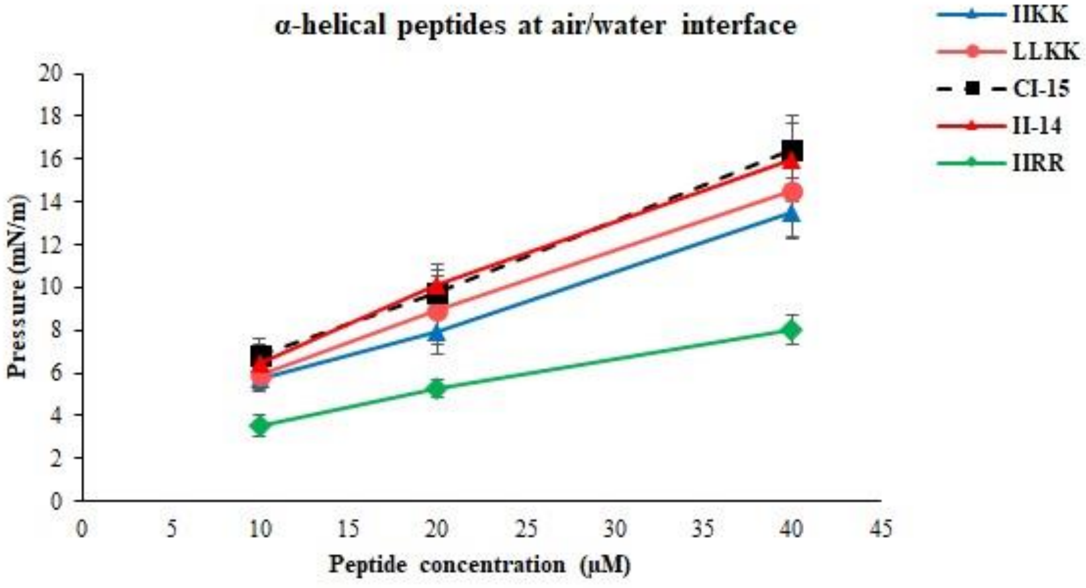

Figure 6.44. Surface pressure as a function of peptide concentration following adsorption of the cationic amphiphilic α-helical peptides at the air/water interface.

There was a very strong correlation between the surface pressure of the cationic amphiphilic peptides in water and their anticancer activity as depicted in Figure 6.45. The peptides with strongest anticancer activity (CI-15 and II-14) had the highest increase in the surface pressure in water whereas IIRR which has poor anticancer activity gave rise to the lowest surface pressure. Furthermore, the order of increase in surface pressure of the peptides was consistent with the order of increase in peptide helicity in SDS micelles, as depicted in Figure 6.46, which suggest conformational changes upon adsorption of the peptides at the air/water interface. It is suggested that the same conformational changes that occur at the curved oil/water interface of the SDS micelles and DPPG SUVs may occur at the air/water interface to allow for orientation of the hydrophilic surface of the α-helix in the aqueous subphase and projection of the hydrophobic surface of the α-helix outside the water in the air [3, 8]. However, since the secondary structures of the peptides at the air/water interface were not measured in this study there is no evidence to show the conformational change of the peptides at the air/water interface. IIRR which was used as a negative control induces considerably lower increase in the surface pressure than the other peptides in this group which is consistent with its low helical content in SDS micelles and its poor of anticancer activity.

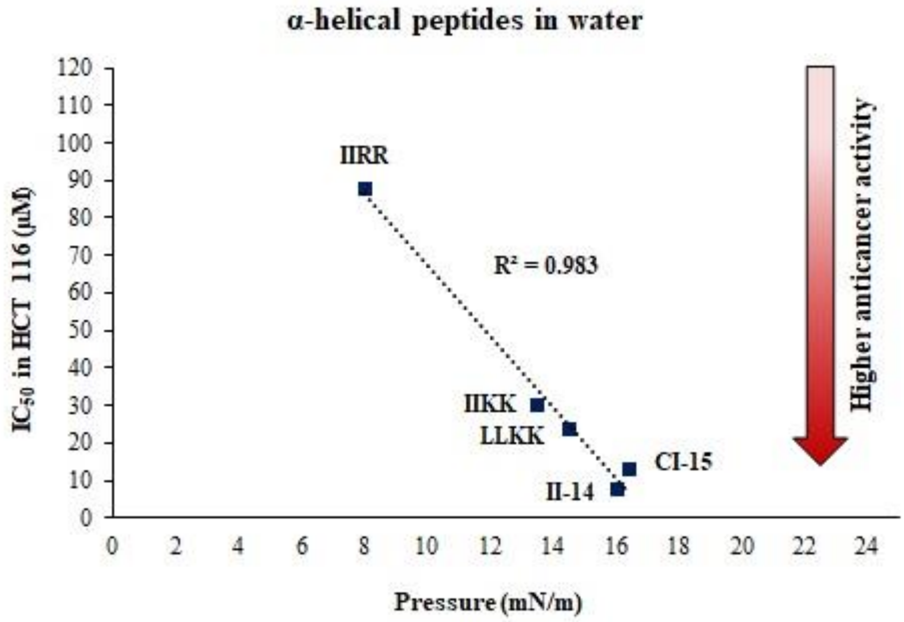

Figure 6.45. Relationship between the anticancer activity of the peptides in HCT 116 colorectal cancer cells and the surface pressure following adsorption of the α-helical cationic amphiphilic peptides (at a concentration of 40 µM) at the air/water interface. (R^2 : correlation coefficient)

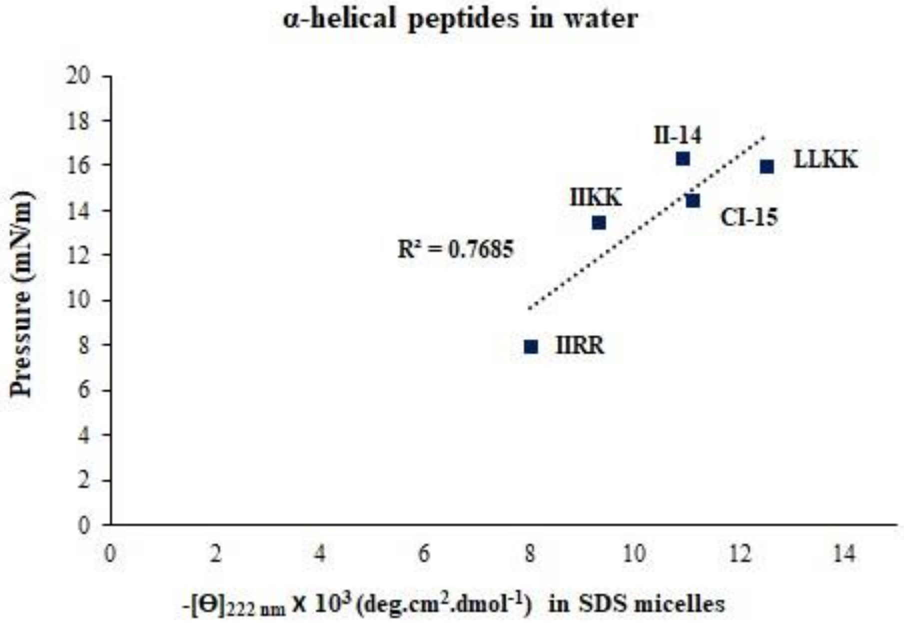

Figure 6.46. Relationship between the helical content of the cationic amphiphilic peptides and the surface pressure following adsorption of the α-helical cationic amphiphilic peptides (at a concentration of 40 µM) at the air/water interface. (R^2 : correlation coefficient)

The surface pressure of the α-helical cationic amphiphilic peptides at the air/water interface was also proportional to their hydrophobicity. As it could be inferred from Figure 6.47, the more hydrophobic peptides increased the surface pressure more than the less hydrophobic peptides. An exception to the general trend was IIRR which was less hydrophobic than IIKK but had higher surface pressure. This is supposed to be due to the lower helicity of IIRR than IIKK. IIRR has the lowest α-helical content in the anionic hydrophobic environments (SDS and DPPG) among all of the peptides therefore it is likely to also form weaker α-helical structure at the air/water interface leading to lower surface pressure. Hence, the surface pressure of the α-helical peptides at the air water interface is governed by an interplay between their hydrophobicity and their helical content. Nevertheless, since the purity of the peptide samples was not very high and they appeared to contain other types of molecules, as discussed in Section 6.3.1, it is possible that some of these molecules also interact with the lipid monolayers thus affecting the apparent surface pressure and since the nature of these impurities is not the same in different peptide samples (based on their molecular masses) this could lead to some inconsistencies in the observed trend from what expected based on the hydrophobicity.

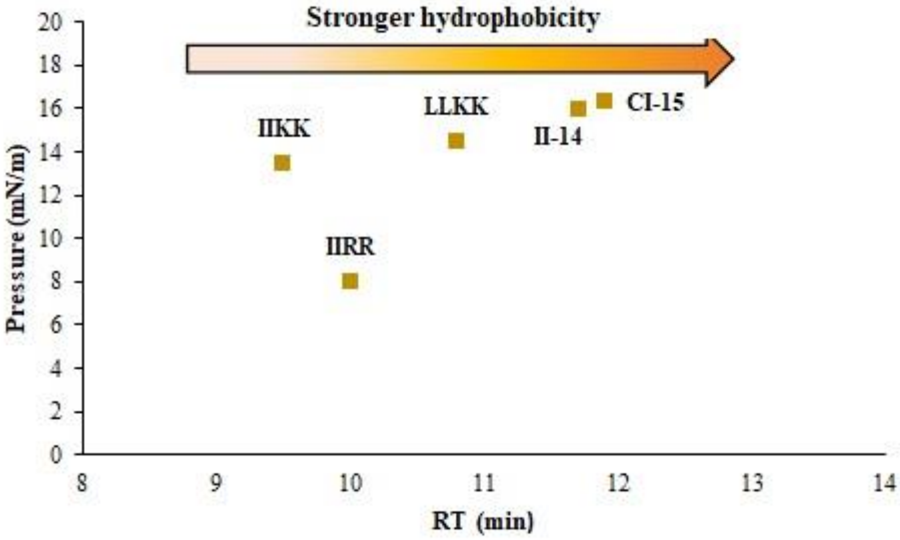

Figure 6.47. Relationship between the surface pressure following adsorption of the cationic amphiphilic α-helical peptides (at a concentration of 40 µM) at the air/water interface and the hydrophobicity of the peptides as measured by their RP-HPLC retention time (RT).

The pressure-time isotherms of the cationic amphiphilic β-sheet forming peptides are demonstrated in Figures 6.48-6.51. Similar to the trend observed for α-helical peptides, the isotherms display a rapid initial rise in the pressure over the first few mins followed by a slower equilibration phase. Increasing the concentration of the cationic amphiphilic peptides in the subphase results in higher surface pressure suggesting the concentration dependent interfacial adsorption of the peptides.

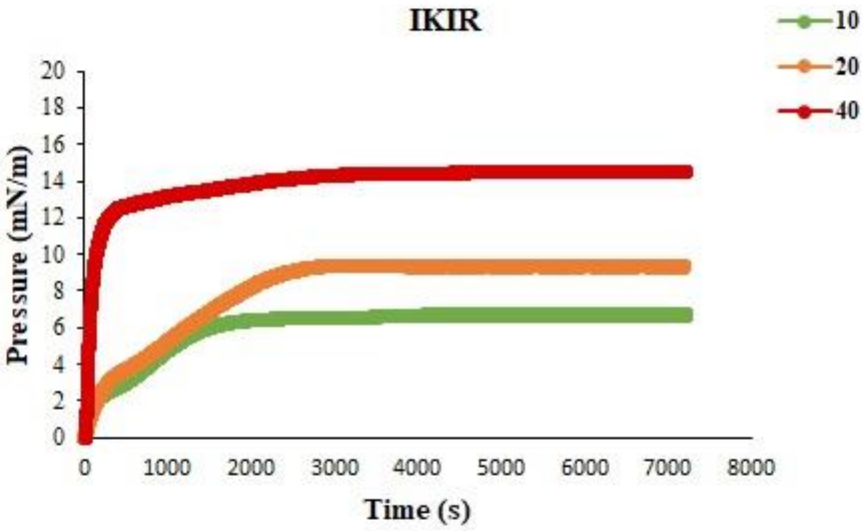

Figure 6.48. Surface pressure as a function of time following adsorption of IKIR at the air/water interface at different peptide concentrations (10-40 µM) in the subphase.

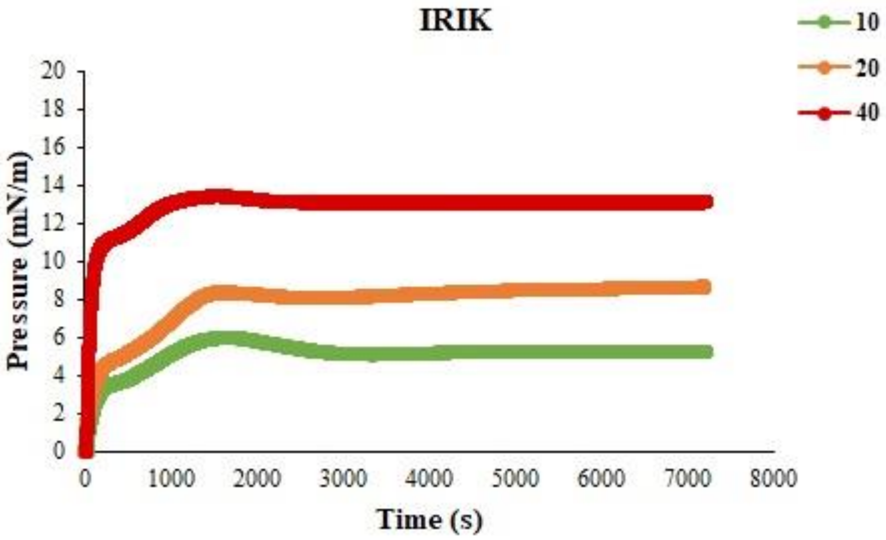

Figure 6.49. Surface pressure as a function of time following adsorption of IRIK at the air/water interface at different peptide concentrations (10-40 µM) in the subphase.

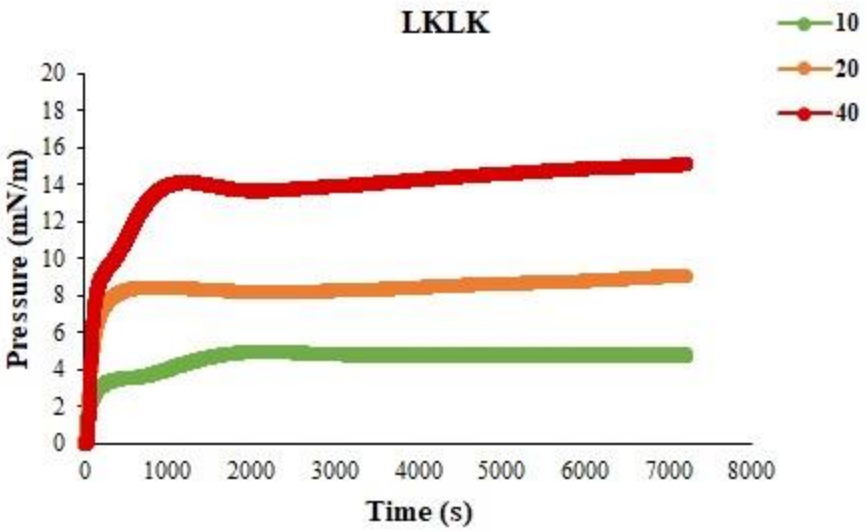

Figure 6.50. Surface pressure as a function of time following adsorption of LKLK at the air/water interface at different peptide concentrations (10-40 µM) in the subphase.

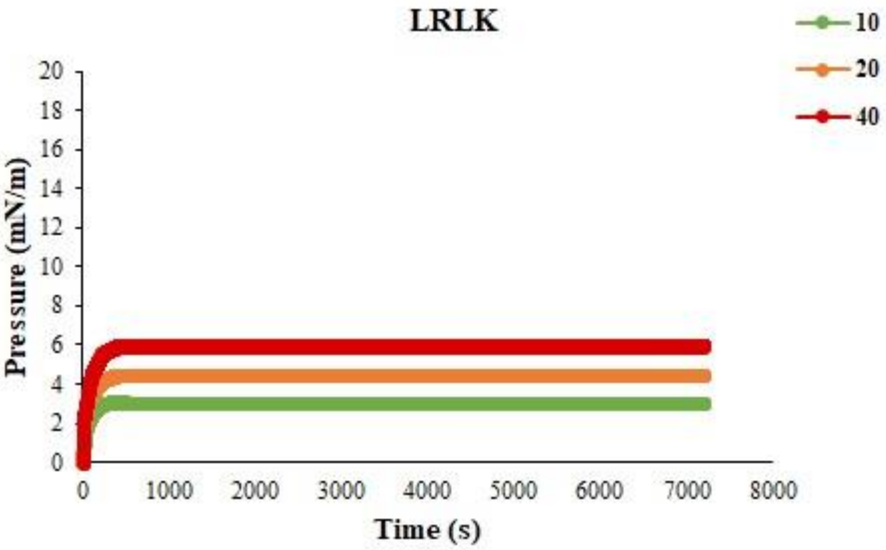

Figure 6.51. Surface pressure as a function of time following adsorption of LRLK at the air/water interface at different peptide concentrations (10-40 µM) in the subphase.

A comparison between the surface pressure of different cationic amphiphilic β-sheet peptides at the air/water interface (Figure 6.52) demonstrates that except LRLK which has considerably lower surface pressure, for the rest of the peptides there was no significant difference between the values of pressure at lower peptide concentration (10-20 µM) while at high peptide concentration (40 µM) this difference becomes more significant.

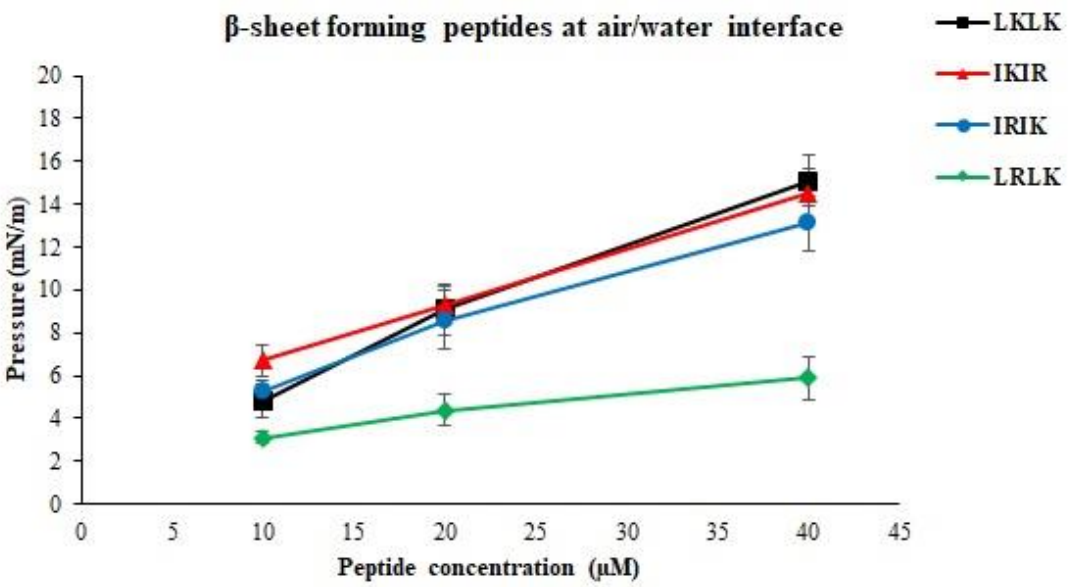

Figure 6.52. Increase in surface pressure at the air/water interface following adsorption of the cationic amphiphilic peptides at different concentrations (10-40 µM).

The order of increase in the surface pressure of the cationic amphiphilic peptides is in similar to the order of increase in their anticancer activity. As it is depicted in Figure 6.53, there is a good correlation between the IC_{50} values of the peptides in HCT 116 colorectal cancer cells and their surface pressure in water ($R^2 = 0.68$). The peptides with higher anticancer activity (LKLK and IKIR) have higher surface pressure and the peptides with weak anticancer activity (LRLK and IKIK) have lower surface pressure.

The increase in the surface pressure achieved by the cationic amphiphilic peptides was directly proportional to their β-sheet content in SDS micelles and there is a strong correlation between the two physical properties ($R^2 = 0.83$), as demonstrated in Figure 6.54. This observation suggests conformational changes to the peptide molecules upon adsorption at the air/water interface to allow for insertion of the polar surface of the β-sheet into the subphase and projection of the nonpolar/hydrophobic surface outside the water in the air to achieve the most stable (lowest energy) status. A conformational change from random coil to β-sheet structure has been reported elsewhere for a cationic amphiphilic peptide consisting of Leucine and Lysine residues, (LK)50, upon forming a peptide monolayer on the surface of water [8]. The surface pressure of the β-sheet forming peptides was inversely proportional to their hydrophobicity (Figure 6.55). LRLK which was more hydrophobic than the other peptides exhibited lower surface pressure at the air/water interface. The other peptides did not have any significant difference in their hydrophobicity and the difference between their surface pressures was also not great.

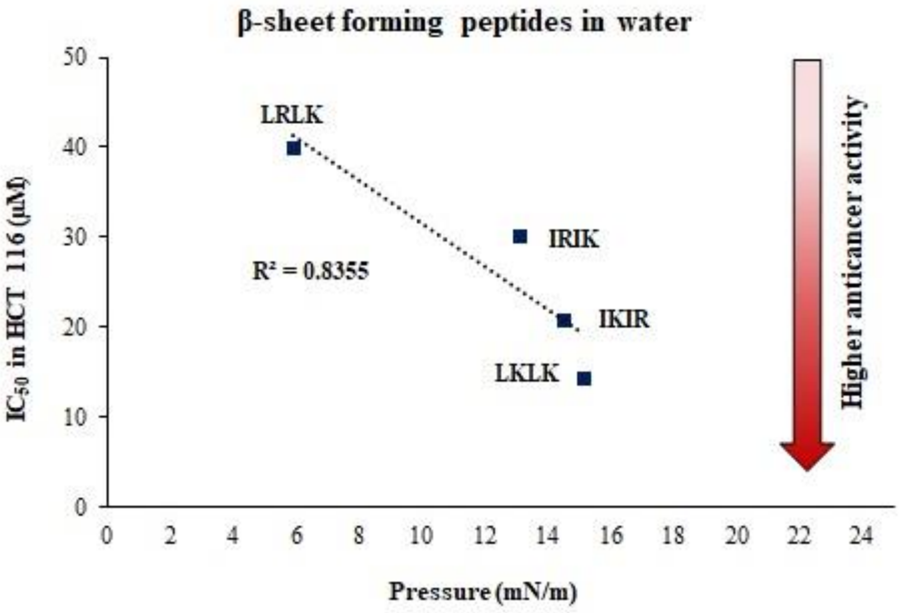

Figure 6.53. Relationship between the anticancer activity of the peptides against HCT 116 colorectal cancer cells and the increase in surface pressure following adsorption of the cationic amphiphilic α-helical peptides (at a concentration of 40 µM) at the air/water interface. R^2: correlation efficient.

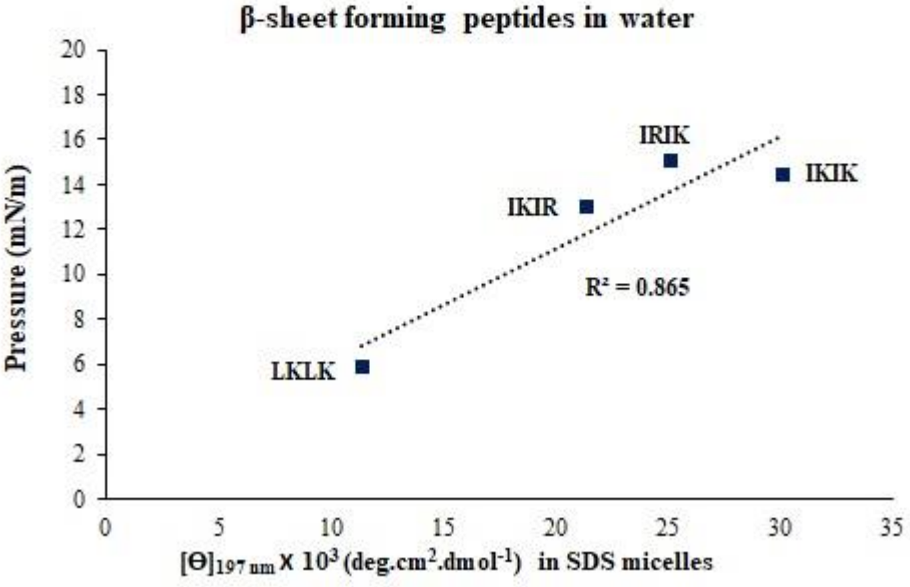

Figure 6.54. Relationship between the β-sheet content of the cationic amphiphilic peptides and the increase in surface pressure following adsorption of the peptides (at the concentration of 40 µM) at the air water interface. R^2 : Correlation coefficient)

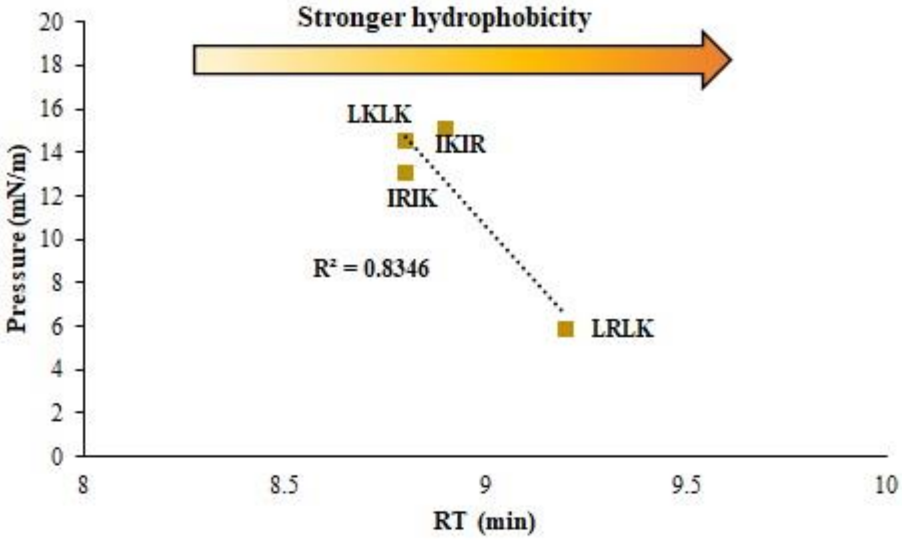

Figure 6.55. Relationship between the surface pressure following adsorption of the cationic amphiphilic β-sheet forming peptides (at a concentration of 40 µM) at the air/water interface and the hydrophobicity of the peptides as measured by their RP-HPLC retention time (RT).

6.3.5 Interaction of the peptides with phospholipid monolayers

To unravel the interaction between the different classes of the designed cationic amphiphilic peptides and the cancer cell/normal cell membranes, two types of phospholipid monolayers were used as in vitro models of the outer leaflet of the cell membrane [5, 6]. The negatively charged DPPG was used as a mimic of cancer cell membrane and the zwitter ionic DPPC was used as a mimic of the normal mammalian cell membrane [5]. The interaction between the cationic amphiphilic peptides and the lipid monolayers was studied by monitoring the changes to the surface pressure over time following injection of the peptide solution under the lipid monolayer at a constant surface area. Changes to the surface pressure is a function of peptide insertion into the lipid monolayer. The experiments were performed at an initial surface pressure of 28 mN/m which is close to the resting pressure of the mammalian cell membrane [3-5]. The binding of the short cationic amphiphilic peptides to the lipid monolayers involves two processes; the electrostatic interaction between the positively charged amino acid residues of the cationic peptide and the negatively charged headgroups of the phospholipid which provides initial binding/adsorption of the peptide to the lipid monolayer and subsequent hydrophobic interaction between the hydrophobic amino acid residues of the peptide and the acyl chains of the phospholipid which disturbs the acyl chain ordering and results in increased surface pressure [7, 8].

The changes to the surface pressure following injection of the of the cationic amphiphilic α-helical peptides under DPPG and DPPC monolayers are presented in Figures 6.56-6.57. As it could be observed all peptides exhibited a greater tendency to interact with the anionic DPPG monolayer than the zwitter ionic DPPC monolayer except IIRR which showed preference for DPPC over DPPG. The higher increase in pressure in DPPC monolayers by IIRR could be due to the monolayer disruption related to improper peptide spreading under the monolayer. The fast initial rising in surface pressure supports such speculation.

The increase in the surface pressure of the DPPG lipid monolayers was consistent with he observed cytotoxicities of this group of peptides in cancer cells as confirmed by the good correlation between the values of IC_{50} for the peptides in HCT 116 colorectal cells and the increase in pressure following injection of the peptides under DPPG monolayers ($R^2 = 0.8$) as depicted in Figure 6.58. In a similar manner, a good correlation was found between the toxicity of this group of peptides in human dermal fibroblasts and the increase in the surface pressure upon injection of these peptides under DPPC lipid monolayers ($R^2 = 0.78$), as presented in Figure 6.59.

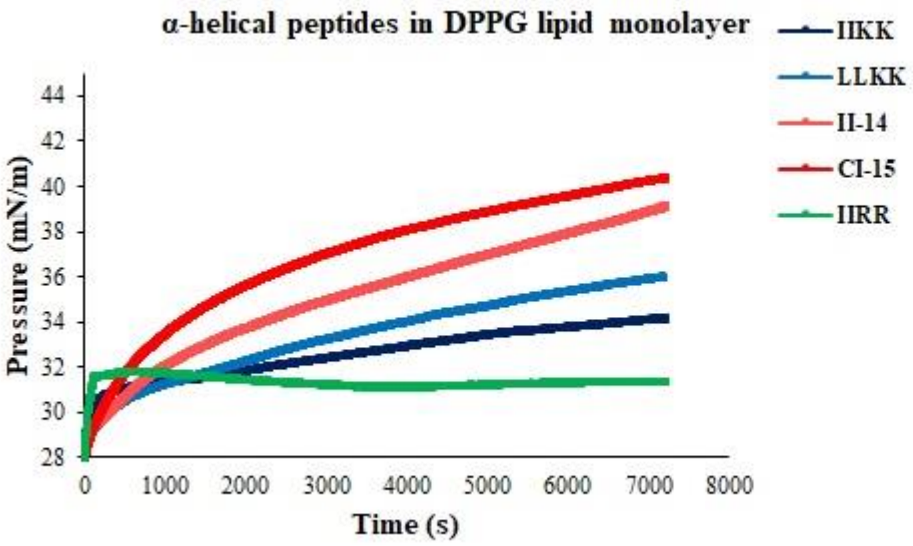

Figure 6.56. Changes to the surface pressure of the lipid monolayers as a function of time upon injection of the cationic amphiphilic α-helical peptides at the concentration of 20 µM under DPPG lipid monolayer. The data are reported as the average of three replicates.

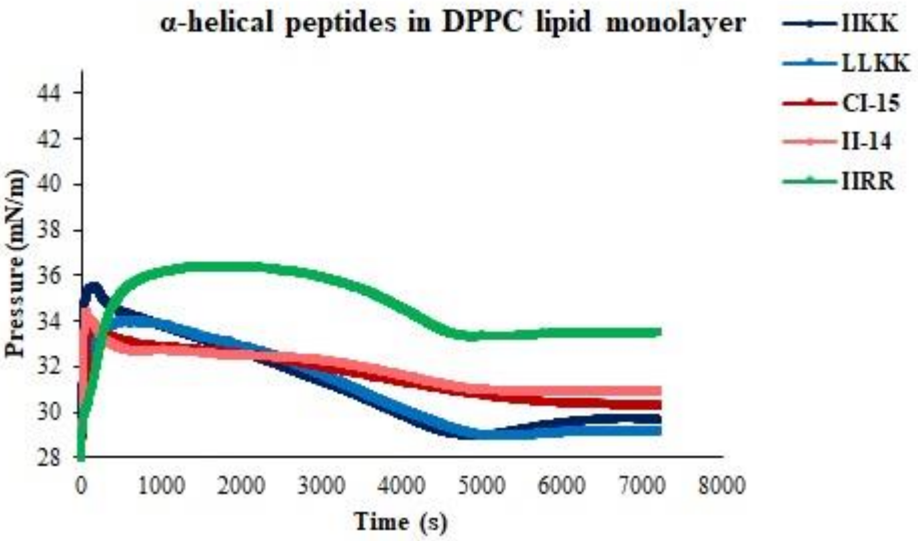

Figure 6.57. Changes to the surface pressure of the lipid monolayers as a function of time upon injection of the cationic amphiphilic α-helical peptides at the concentration of 20 µM under DPPC lipid monolayer. The data are reported as the average of three replicates.

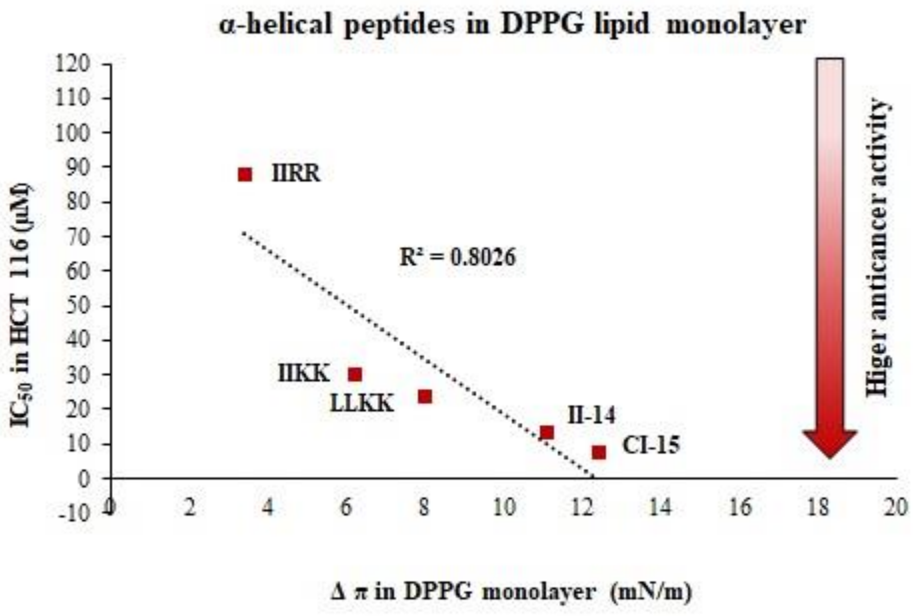

Figure 6.58. Relationship between increase in the surface pressure following injection of the cationic amphiphilic α-helical peptides at the concentration of 20 µM under the DPPG lipid monolayers and anticancer activity of the peptides in HCT 116 colorectal cancer cells. (R^2: Correlation coefficient).

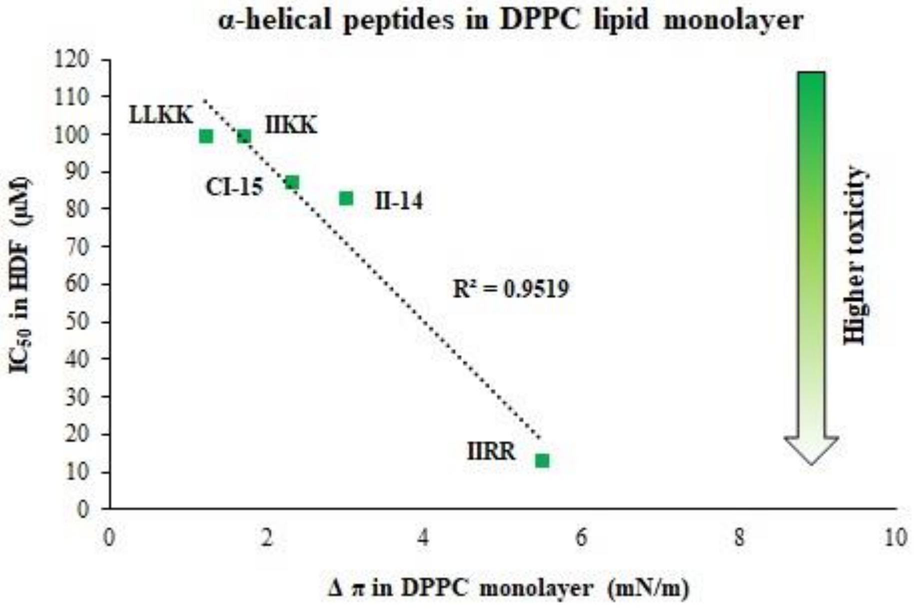

Figure 6.59. Relationship between increase in the surface pressure following injection of the cationic amphiphilic α-helical peptides at the concentration of 20 µM under the DPPC lipid monolayers and toxicity of the peptides in human dermal fibroblasts. The values of IC_{50} for IIKK and LLKK were more than 100 µM and were considered as 100 for clarity. (R^2: Correlation coefficient).

As it could be observed in Figure 6.60, the order of increase in the surface pressure following interaction of the cationic amphiphilic α-helical peptides with DPPG monolayer is consistent with the helicity of the peptides in DPPG SUVs which suggests similar conformational changes that occur upon interaction of the peptides with the DPPG bilayers at the curved oil/water interface of the lipid vesicles may also take place at the water/lipid monolayer resulting in greater penetration of the peptides into the lipid monolayer. However, since the secondary structure of the peptides at the water/lipid interface was not measured in this study, there is no supporting evidence to prove this.

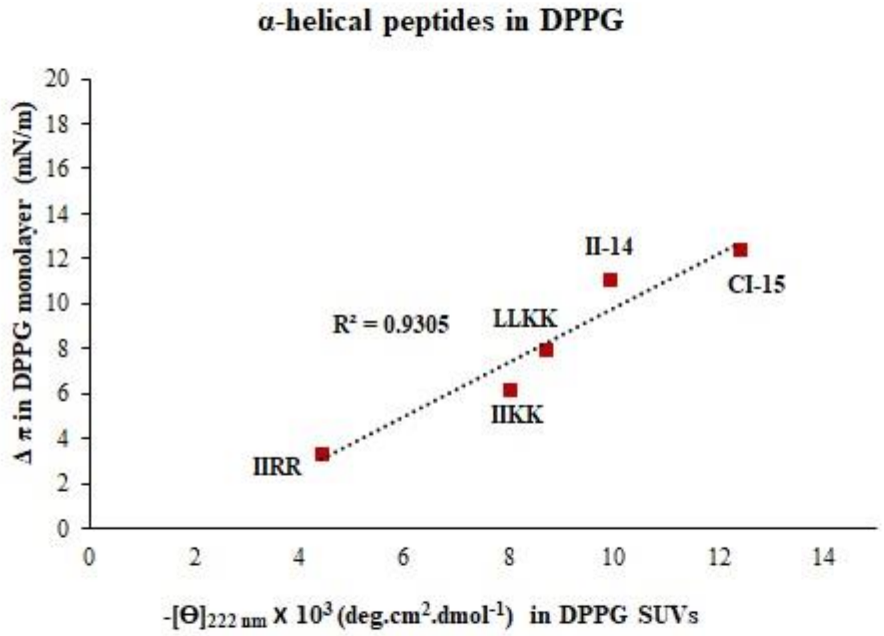

Figure 6.60. Relationship between the increase in surface pressure at the lipid/water interface upon injection of the cationic amphiphilic peptides at the concentration of 20 µM under DPPG lipid monolayers and their helical content in DPPG SUVs. (R^2 : Correlation coefficient).

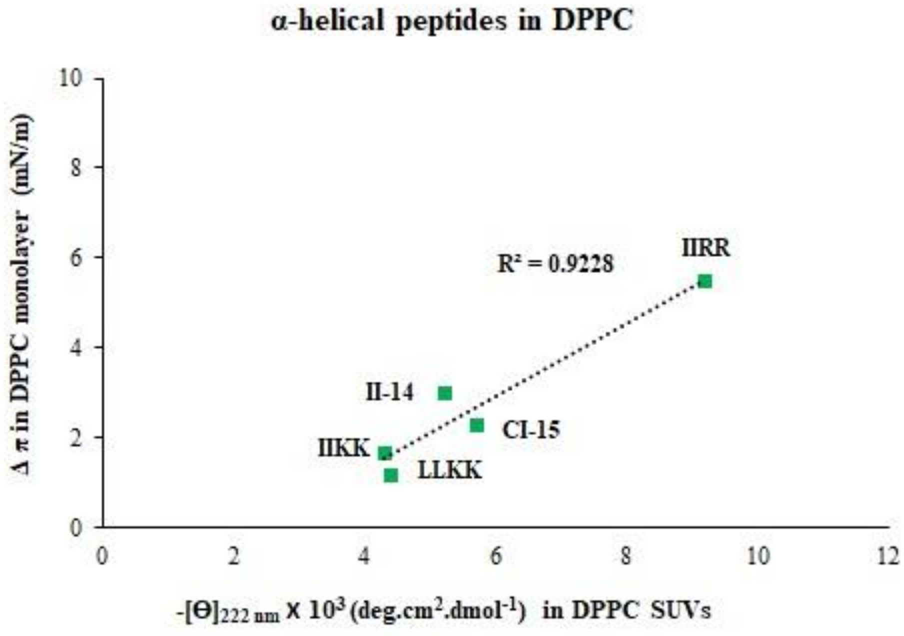

Figure 6.61. Relationship between the increase in surface pressure at the lipid/water interface upon injection of the cationic amphiphilic peptides (at the concentration of 20 µM) under DPPC lipid monolayers and their helical content in DPPC SUVs. (R^2 : Correlation coefficient).

The order of increase in the surface pressure upon interaction of the α-helical cationic amphiphilic peptides with DPPC lipid monolayers was directly proportional to their helical content in DPPC SUVs as it could be observed in Figure 6.61, suggesting the possibility of conformational changes upon interaction of the peptides with the DPPC monolayers. Nevertheless, the lower values of pressure in DPPC monolayers compared to DPPG monolayers indicates weaker interactions and less conformational changes.

The changes to the surface pressure following injection of the of the cationic amphiphilic β-sheet forming peptides under DPPG and DPPC monolayers are presented in Figures 6.62-6.63. Similar to the α-helical peptides, most of the β-sheet forming peptides showed a greater tendency to interact with the anionic DPPG lipid monolayers than the zwitter ionic DPPC lipid monolayers and increased the surface pressure to a higher extent upon injection under DPPG monolayers than DPPC monolayers. Nevertheless, IKIK and LRLK showed similar affinity for both types of lipid monolayers which is consistent with the observed cytotoxicities of these peptides as unlike the rest of the peptides IKIK and LRLK have higher toxicity against fibroblasts than cancer cells. There was a very good correlation between the values of IC_{50} in HCT 116 and the increase in surface pressure of the DPPG monolayers (R^2 = 0.98). The increase in the surface pressure of DPPC lipid monolayers was also directly proportional to the toxicity in HDF (R^2 = 0.71) (Figures 6.64-6.65).

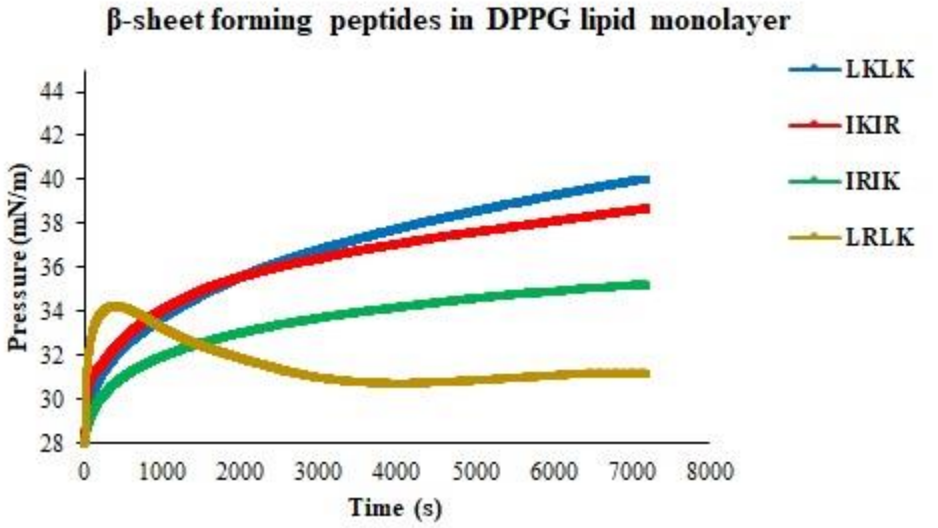

Figure 6.62. Changes to the surface pressure of the lipid monolayers as a function of time upon injection of the cationic amphiphilic α-helical peptides at the concentration of 20 μM under DPPG lipid monolayer. The data are reported as the average of three replicates.

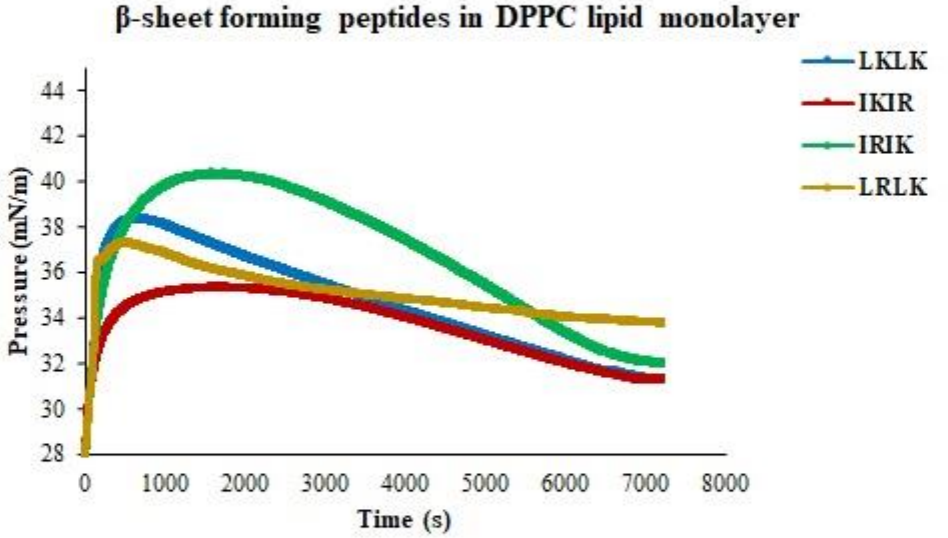

Figure 6.63. Changes to the surface pressure of the lipid monolayers as a function of time upon injection of the cationic amphiphilic α-helical peptides at the concentration of 20 μM under DPPC lipid monolayer. The data are reported as the average of three replicates.

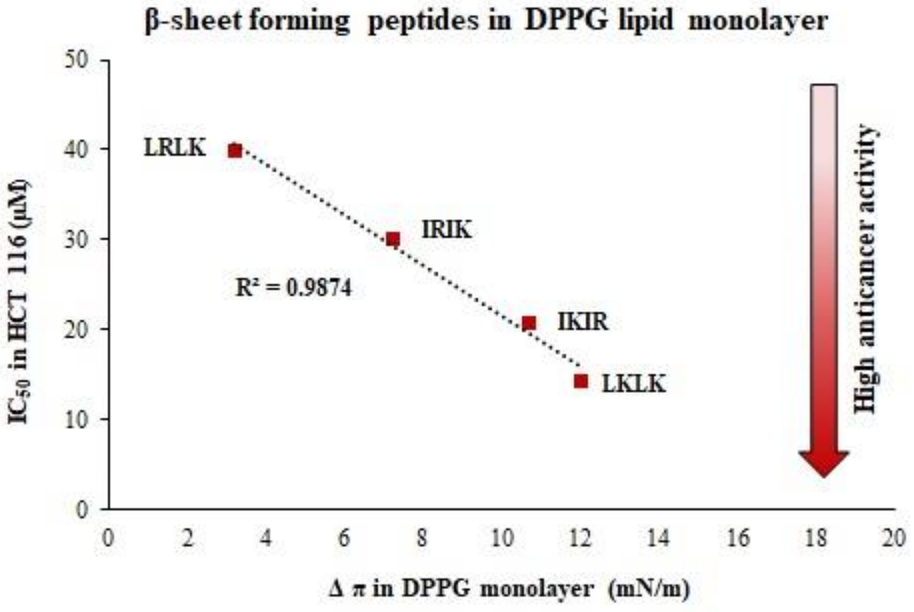

Figure 6.64. Relationship between the increase in surface pressure at the lipid/water interface upon injection of the cationic amphiphilic β-sheet forming peptides at the concentration of 20 µM under DPPG lipid monolayers and the IC_{50} values of the peptides in HCT 116 colorectal cancer cells. The value of IC_{50} for LRLK was more than 40 µM and was considered as 40 for clarity. (R^2: Correlation coefficient).

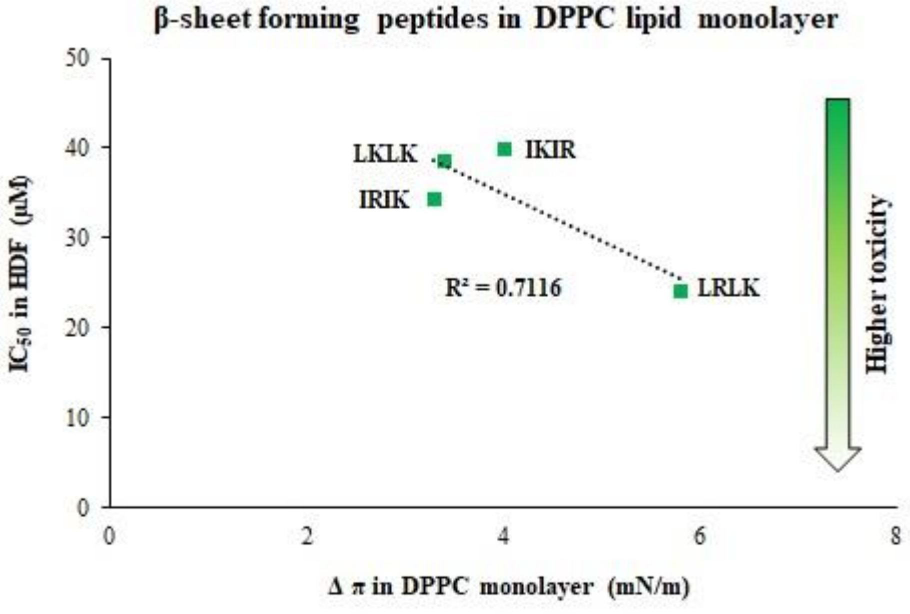

Figure 6.65. Relationship between the increase in surface pressure at the lipid/water interface upon injection of the cationic amphiphilic β-sheet forming peptides at the concentration of 20 µM under DPPC lipid monolayers and the IC50 values of the peptides in Human dermal fibroblasts. The value of IC50 for LKLK was more than 40 µM and was considered as 40 for clarity. (R2: Correlation coefficient).

As it could be observed in Figure 6.66, the order of increase in the surface pressure upon injection of the β-sheet forming peptides under DPPG monolayers was similar to the order of increase in the β-sheet content of the peptides in DPPG SUVs, with the exception of LKLK which had lower β-sheet content than IKIR and IRIK but gave rise to higher pressure in DPPG monolayers. This suggests the same conformational changes that occur at the curved oil/water interface of the DPPG SUVs may occur at the oil/water interface of the DPPG lipid monolayers. On the other hand, the extent of increase in the surface pressure upon injection of the cationic amphiphilic peptides under DPPC monolayers was not consistent with their β-sheet content in DPPC SUVs. As it could be observed in Figure 6.67, for IKIK, LKLK, and LRLK the increase in the surface pressure in DPPG monolayers was consistent with their β-sheet content in DPPC SUVs. IKIR and IRIK on the contrary, showed smaller increase in the surface pressure upon injection under DPPC monolayers than the rest of the peptides despite having higher β-sheet content in DPPC SUVs. Hence, the interaction of the cationic amphiphilic β-sheet forming peptides with DPPC lipid monolayers is not only directed by their conformation, but also other factors may be involved.

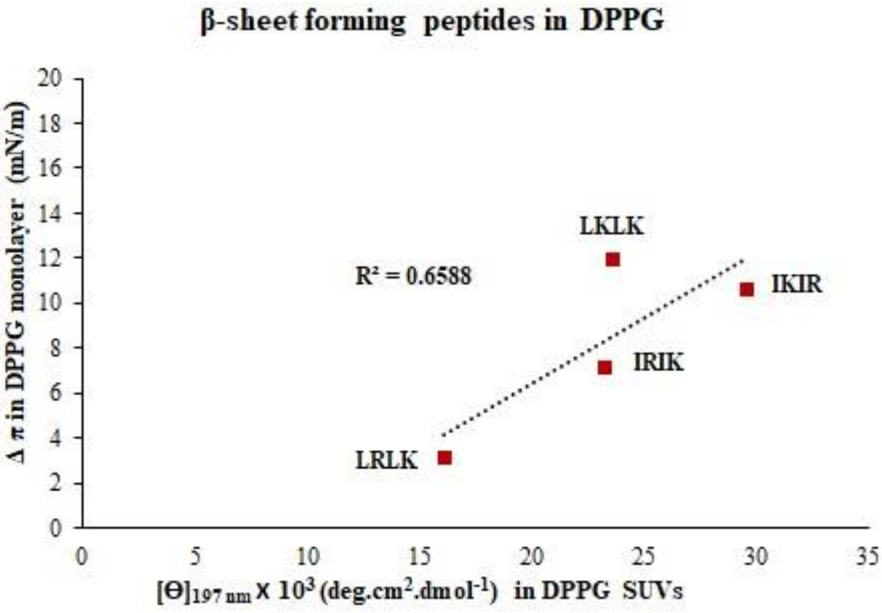

Figure 6.66. Relationship between the increase in surface pressure at the lipid/water interface upon injection of the cationic amphiphilic peptides at the concentration of 20 µM under DPPG lipid monolayers and the β-sheet content of the peptides in DPPG SUVs. (R^2 : Correlation coefficient).

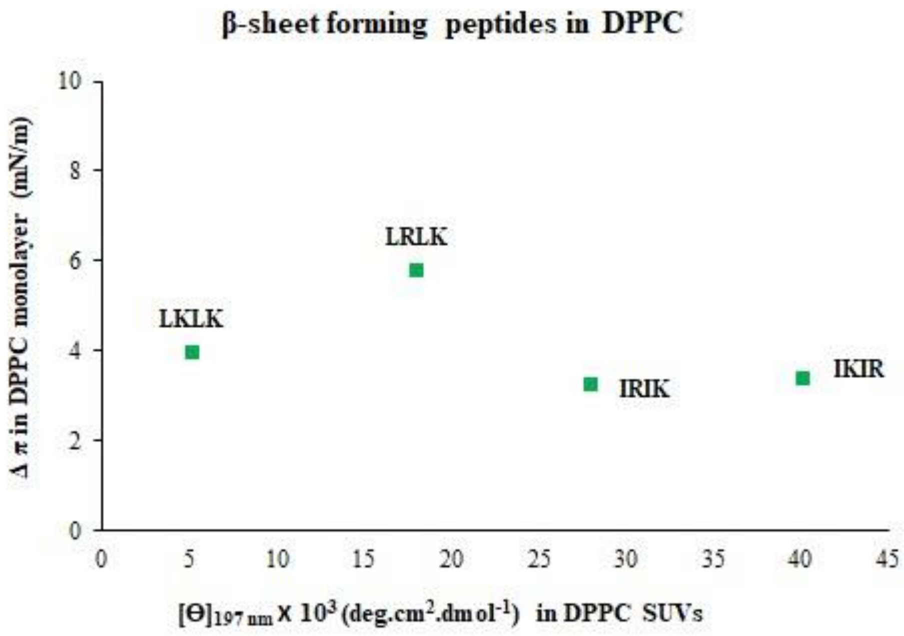

Figure 6.67. Relationship between the increase in surface pressure at the lipid/water interface upon injection of the cationic amphiphilic peptides at the concentration of 20 µM under DPPC lipid monolayers and the β-sheet content of the peptides in DPPC SUVs.

6.4 Conclusion

The three groups of cationic amphiphilic peptides which were designed and tested for their biological activity in the previous chapters, were tested for their sequence, their purity and their secondary structure. The designed sequences were found in the LC-MS spectra of all the peptides except IIKK and LLKK which showed ions corresponding to the dimer molecules suggesting that these two peptides may exist as dimers in the solution. Nevertheless, in all cases the spectra showed presence of other ions which could be attributed to either the peptide degradation products or the impurities in the peptide sample. The RP-HPLC chromatograms also showed the presence of impurities in all peptide samples which was consistent with LC-MS results. Overall, the purity of β-sheet forming peptides and the surfactant-like peptides was considerably less than the α-helical peptides which casts doubt on the validity of the biological data obtained from these peptides. The values of RP-HPLC retention times were used as a measure of the peptide hydrophobicity and it was found that replacing isoleucine with leucine and replacing lysine with arginine makes the peptides more hydrophobic. Nevertheless, these structural changes had stronger effect on the hydrophobicity of α-helical peptides than β-sheet forming peptides. The anticancer activity of the α-helical peptides was directly proportional to their hydrophobicity whereas for β-sheet forming peptides there was no direct link between the hydrophobicity and the anticancer activity.

The α-helical peptides had random coil structure in the aqueous solution (DI water and PB), however, they formed α-helices in SDS micelles and DPPG SUVs which were used as a mimic of cancer cell membranes indicative of conformational changes upon interaction with negatively charged curved surfactant/phospholipid bilayers. In DPPC SUVs which were used as a mimic of normal cell membrane on the other hand, only partial helical structure was observed suggesting weaker interaction of the peptides with zwitter ionic phospholipid bilayers. The degree of helicity of the different peptides in DPPC and DPPG SUVs was consistent with their cytotoxicity against normal cells and cancer cells respectively. Similar to the α-helical peptides, most of the β-sheet forming peptides were in random coil structure in aqueous solution (DI and PB) except IRIK and IKIR which showed strong β-sheet conformation. In DPPC SUVs IRIK and IKIR peptides adopted a weak β-sheet conformation whereas the other peptides in this group showed a mixture of random coil and partial β-sheet structure. In DPPG SUVs and SDS micelles on the other hand, all of the peptides adopted strong β-sheet conformations the extent of which was proportional to their anticancer activity. The surfactant-like peptides had weak β-sheet structures in aqueous solution and partial β-sheet structure in DPPC SUVs but adopted stronger β-sheet structures in anionic environment (DPPG SUVs and SDS micelles). This explains the higher transfection efficiency of these peptides in cancer cells than normal cells.

The α-helical peptides and the β-sheet forming peptides increased the surface pressure at the air-water interface the extent of which was proportional to the strength of their anticancer activity and their α-helical/β-sheet content in SDS micelles suggesting the same conformational changes that occur in SDS micelles may occur at the air/water interface. The rise in the surface pressure at the air/water interface was directly proportional to the peptide hydrophobicity in the case of α-helical peptides and inversely proportional to the peptide hydrophobicity in the case of β-sheet forming peptides. In a similar manner, both the α-helical peptides and the β-sheet forming peptides increased the surface pressure upon injection under DPPC and DPPG lipid monolayers which were used as a model of the outer leaflet of the normal and cancer cell membrane respectively, in a pattern consistent with the strength of their cytotoxicity against normal and cancer cells in order. Furthermore, the order of increase in the surface pressure of the DPPG and DPPC monolayers was directly proportional to the α-helical/β-sheet content of the peptides in DPPG and DPPC SUVs respectively suggesting the same conformational changes that take place upon interaction of the cationic amphiphilic peptides with curved phospholipid bilayers may also occur upon interaction of the cationic amphiphilic peptides with the phospholipid monolayers.

Overall, these data provide supporting evidence for the interaction of the cationic amphiphilic peptides with different types of cell membranes (zwitter ionic membrane of normal cells and anionic membrane of cancer cells) which explains the observed differences in the anticancer activity of each group of the cationic amphiphilic peptides and their toxicities against human dermal fibroblasts. However, the quality of the data from the alpha-helix group was better than the other two beta-sheet peptide groups. One possible reason for this could be the lower purity of these two groups of peptides compared to α-helical peptides. The impurities in the peptide samples could affect the biophysical measurements and cause deviations from the expected patterns or change the readouts of the measurements.

6.5 References

1. H. Gong, J. Zhang, X. Hu, et al. Hydrophobic control of the bioactivity and cytotoxicity of de novo-designed antimicrobial peptides. *ACS Appl. Mater. Interfaces*, 11 (2019): 34609-34620.
2. C. Chen, C. Yang, Y. Chen, et al. Surface physical activity and hydrophobicity of designed helical peptide amphiphiles control their bioactivity and cell selectivity. *ACS Appl. Mater. Interfaces*, 8 (2016): 26501-26510.
3. C. Chen, Y. Chen, C. Yang, et al. High selective performance of designed antibacterial and anticancer peptide amphiphiles. *ACS Appl. Mater. Interfaces*, *7* (2015): 17346-17355.
4. D. Ciumac, R.A. Campbell, L. A. Clifton, et al. Influence of acyl chain saturation on the membrane-binding activity of a short antimicrobial peptide. *ACS Omega*, 2 (2017): 7482-7492.
5. C. Chen, J. Hu, P. Zeng, et al. Molecular mechanisms of anticancer action and cell selectivity of short α-helical peptides. *Biomaterials*, 35 (2014): 1552-1561.
6. D. Ciumac, R.A. Campbell, H. Xu, et al. Implications of lipid monolayer charge characteristics on their selective interactions with a short antimicrobial peptide. *Colloids Surf. B*, 150 (2017): 308-316.
7. Hädicke and A. Blume. Binding of the cationic peptide (KL)4K to lipid monolayers at the air–water interface: effect of lipid headgroup charge, acyl chain length, and acyl chain saturation. *J. Phys. Chem. B*, 120 (2016): 3880-3887.

8. R. Maget-Dana, A. Brack, D. Lelievre. Amphiphilic peptides as models for protein-membrane interactions: interfacial behaviour of sequential Lys- and Leu-based peptides and their penetration into lipid monolayers. *Supramol. Sci.,*4 (1997): 365-368.
9. J. Hu, C. Chen, S. Zhang, et al. Designed antimicrobial and antitumor peptides with high selectivity. *Biomacromolecules,* 12 (2011): 3839-3843.
10. N. Wiradharma, U. Khoe, C.A.E. Hauser, et al. Synthetic cationic amphiphilic α-helical peptides as antimicrobial agents. *Biomaterials*, 32 (2011): 2204-2212.
11. Eiríksdóttir, K. Konate, Ü. Langel, G. Divita, and S. Deshayes. Secondary structure of cell-penetrating peptides controls membrane interaction and insertion. *BBA-Biomembranes,*1798 (2010): 1119-1128.
12. M. Majerowicz, A.J. Waring, S. Wen, and F. Bringezu. Interaction of the antimicrobial peptide Dicynthaurin with membrane phospholipids at the air−liquid interface. *J. Phys. Chem. B,* 111 (2007): 3813-3821
13. Imranpasha and B. Kumar. Kinetics of interaction between antimicrobial peptide nisin and Langmuir monolayers of DPPC and DPPG molecules. *Phys. Rev. E,* 100 (2019): 032404-1-032404-7
14. Z.Y. Ong, S.J. Gao, and Y.Y. Yang. Short synthetic β-sheet forming peptide amphiphiles as broad spectrum antimicrobials with antibiofilm and endotoxin neutralizing capabilities. Adv. Funct. Mater., 23 (2013): 3682-3692.
15. Z.Y. Ong, J. Cheng, Y. Huang, et al. Effect of stereochemistry, chain length and sequence pattern on antimicrobial properties of short synthetic β-sheet forming peptide amphiphiles. *Biomaterials,* 35 (2014): 1315-1325.
16. O. G. Travkova, H. Moehwald, G. Brezesinski. The interaction of antimicrobial peptides with membranes. *Adv. Colloid Interface Sci.,*247 (2017): 521-532.
17. F. Schweizer. Cationic amphiphilic peptides with cancer-selective toxicity. *Eur. J. Pharmacol.,* 625 (2009): 190-194.
18. D.W. Hoskin, A. Ramamoorthy. Studies on anticancer activities of antimicrobial peptides. *BBA-Biomembranes,* 1778 (2008): 357-375.
19. S. Kim, S. S. Kim, B. J. Lee. Correlation between the activities of α-helical antimicrobial peptides and hydrophobicities represented as RP HPLC retention times. *Peptides,* 26 (2005): 2050-2056.
20. Y. Huang, X. Wang, H. Wang, Y. Liu, and Y. Chen. Studies on mechanism of action of anticancer peptides by modulation of hydrophobicity within a defined structural framework. *Mol. Cancer Ther.,* 10 (2011): 416-426.

21. Y. Chen, M. T. Guarnieri, A. I. Vasil, et al. Role of peptide hydrophobicity in the mechanism of action of α-helical antimicrobial peptides. *Antimicrob. Agents Chemother.*, 51 (2007): 1398-1406.
22. C. Chen, J. Hu, S. Zhang, et al. Molecular mechanisms of antibacterial and antitumor actions of designed surfactant-like peptides. *Biomaterials*, 33 (2012): 592-603.

Chapter 7: Conclusion and future work

In this project three different classes of short cationic amphiphilic peptides with different primary and secondary structures (α-helical peptides, β-sheet forming peptides and surfactant-like peptides) were designed based on the key structural features of the naturally occurring or synthetic antimicrobial/anticancer peptides and the structural features required for complexation with nucleic acids according to the available literature. The peptides consist of cationic amino acid residues (arginine and lysine) which are protonated at the physiological/near physiological pH and are capable of complexation with nucleic acids based on electrostatic interactions. Also, it has been widely reported in the literature that the majority of naturally occurring peptides with antimicrobial/anticancer activity are cationic which enables them to bind to and interact with the negatively charged microbial/cancer cell outer membranes. Incorporation of hydrophobic amino acid residues (isoleucine, leucine, glycine, alanine) was supposed to allow for hydrophobic interaction between these hydrophobic regions of the peptide molecules and the phospholipids in the cell membrane and cell penetration.

The biological activity of these peptides in terms of their anticancer activity/cytotoxicity and their ability to deliver different types of nucleic acids (AONs and siRNA) to the cancer cells and normal cells were assessed in an attempt to develop peptides with selective anticancer activity and selective gene delivery to cancer cells to serve as efficient and safe anticancer treatments. The AONs and siRNA are two different strategies for gene silencing which are used to knock down particular genes which are overexpressed in cancer cells and are crucial for their growth, proliferation, immortality, or metabolic activity in order to stop the proliferation or induce apoptosis in the cancer cells. In this study fluorescently labelled anti-cMYC AONs and siGLO™ red fluorescently labelled siRNA were used as transfection indicators and three types of functional siRNA targeting ECT2, UBB, and PLK1 were used for gene silencing. These three genes play a key role in the cell proliferation and are overexpressed in the cancer cells thus making them good targets for anticancer gene therapy.

The peptides had different degrees of anticancer activity and selectivity for cancer cells which was a function of their amino acid combination, their hydrophobicity, and their conformation upon interaction with the lipid membranes. The α-helical peptides consisting of lysine residues were more toxic towards cancer cells than normal fibroblast cells whereas the α-helical peptides consisting of arginine residues were very toxic to fibroblasts and had reduced anticancer activity. Increasing the peptide chain length by addition of extra isoleucine residues to the C-terminal also resulted in increased anticancer activity. There was a strong relationship between the anticancer activity of the α-helical peptides and their hydrophobicity, as well as their helical content in SDS micelles and DPPG lipid vesicles indicating the key role of the hydrophobicity and the secondary structure in governing the anticancer activity of the α-helical peptides.

In the case of the β-sheet forming peptides, the peptides consisting of isoleucine residues had stronger anticancer activity than the peptides consisting of leucine residues. Nevertheless, combination of leucine with lysine residues also bestowed strong and selective anticancer activity upon the peptide whereas introduction of arginine residues in the leucine containing peptides diminished their anticancer activity and instead increased their toxicity against normal cells. Similar to the α-helical peptides, the anticancer activity of the β-sheet forming peptides was strongly affected by their secondary structure. Nevertheless, there was not a big difference in the hydrophobicity of the different peptides in this group and hydrophobicity did not appear to play as important role in determining their anticancer activity as it did for α-helical peptides. The importance of the secondary structure for the anticancer activity of the peptides was further reflected by the difference in the anticancer activity of the cationic amphiphilic peptides with the same combination of amino acids but different repeat patterns which resulted in different secondary structures such as IIKK vs IKIK, LLKK vs LKLK, and LLRR vs LRLR.

In both groups of peptides, the peptides with strong and selective anticancer activity were found to interact more strongly with the negatively charged phospholipid monolayers and bilayers (DPPG) than zwitter ionic/ neutral phospholipid monolayers and bilayers (DPPC) which reflects stronger interaction of these peptides with the negatively charged cancer cell membranes than the charge neutral normal cell membranes. Also, there was an increase in the surface pressure upon injection of the α-helical and the β-sheet forming peptides with anticancer activity at the air/water interface the extent of which was directly proportional to the anticancer activity of the peptides.

The peptides were found to exert their anticancer activity mainly through damaging the mitochondria and reducing the metabolic activity of the cells apart from disturbing the cell membrane as evidenced by changes to the morphology of the mitochondria compared to the healthy cells and depolarization of the mitochondrial membranes which is an indicator of mitochondrial damage. The α-helical peptides were found to have antiproliferative and cytocidal effect whereas the β-sheet forming peptides were found to mainly exert cytostatic effect.

Apart from the difference between the cytotoxicity of the cationic amphiphilic peptides against cancer cells and normal cells, the different cancer cell lines also responded differently to the treatment with the peptides. Some peptides (IIKK, LLKK, LLRR, and LRLR) had higher cytotoxicity against HCT 116 than the other cell lines, some peptides (IKIK, IKIR, IRIK) had stronger cytotoxicity in HeLa, and some (LKLR, LRLK) were more toxic in MDA-MB-231. In general, MDA-MB-231 were more resistant and less responsive to the peptides than the other cancer cell lines as all of the α-helical peptides and most of the β-sheet forming exhibited poor anticancer activity in this cell line.

Although all of the α-helical peptides were capable of more selective delivery of cMyc AONs to the cancer cells, only the peptides consisting of isoleucine residues (IIKK, IIRR, and CI-15) were able to induce gene silencing in the cells upon transfection with and ECT2 siRNA and the peptides containing leucine residues (LLKK and LLRR) were unable to release their associated siRNA inside the cells due to strong complexation. In the case of β-sheet peptides, only the peptides consisting of isoleucine residues (IKIK, IKIR, and IRIK) were able to form complexes with the nucleic acids and to deliver them to the cells whereas the peptides consisting of leucine residues were unable to do so. Unlike the α-helical peptides the β-sheet forming peptides did not show any preference for cancer cells over normal cells and transfected both types of cells to the same extent which is not favourable for a gene carrier. Nevertheless, due to higher expression of the selected ECT2 gene in cancer cells compared to normal cells, they still induced higher death rate in the cancer cells than normal cells.

The surfactant-like peptides ($(IA)_4K$ and $(IG)_4K$) exhibited β-sheet conformation both in aqueous solution and in anionic lipid vesicles (DPPG SUVs and SDS micelles) and partial β-sheet structure in zwitter ionic DPPC SUVs. This is consistent with the biological activity of these peptides as both peptides had higher transfection efficiency for AONs and siRNA in HCT 116 colorectal cancer cells than fibroblasts. However, these peptides, though capable of selective delivery of nucleic acids to the cancer cells, were unable to induce any gene silencing when they were used for delivery of PLK-1 siRNA to the cancer cells due to strong complexation which prevented them from releasing their associated cargo inside the cells. Unlike the other two groups of peptides, these peptides did not show any cytotoxicities in either cancer cells or fibroblasts.

Overall, this research project provided an insight into the structure-activity relationship of the short cationic amphiphilic peptides and the favourable combination and repeat pattern of the amino acids for selective anticancer activity or efficient gene delivery. The cationic amphiphilic peptides consisting of scattered arginine and lysine residues exhibited more favourable biological activity than the surfactant-like peptides which had only one lysine residue per molecule. Also, the peptides with the α-helical conformation showed advantage over their β-sheet forming counterparts in terms of selective anticancer activity and selective gene delivery to cancer cells. These data provide a basis for designing new cationic amphiphilic peptides with enhanced anticancer activity, reduced toxicity, and improved gene delivery efficiency through selecting he best combination of amino acids and the best repeat patterns. However, there are still areas which could not be covered due to the time limit of the project. Further research is required to fill in the gaps within the current data and provide information about the other aspects of the biological activity of the peptides in order to move them from proof of concept to potential anticancer treatments. Future research could be directed towards the following areas:

1. Assessing the long-term physicochemical stability of the peptide solutions and the peptide-siRNA complexes and the changes to their biological activity over time in different storage conditions (i.e., room temperature or fridge) in order to determine their shelf-life.
2. Further investigation of siRNA-induced gene silencing through real-time quantification of the target proteins or the mRNA by western blot or q-RT-PCR respectively to provide compelling evidence that the observed cell death following treatment with peptide-siRNA complexes is due to on gene silencing and no other causes. Also, using other types of siRNA which would give rise to scorable phenotypes instead of inducing cell death could serve as a proof of gene silencing.
3. Studying the peptide self-assembly in solution using relevant techniques such as atomic force microscopy (AFM) or scanning electron microscopy (SEM) to find out if the peptides exist in solution as single molecules or self-assemble into supramolecular structures. This information will shed more light on the observed differences in the physicochemical properties and biological activities of each group of peptides.
4. Studying the interaction of the peptides with the cell membranes using scanning electron microscopy (SEM) to find out any morphological changes or damages to the cell membrane following interaction with the peptides as the in vitro models of cell membranes which were studied in this project only provide evidence of interaction of the peptides with the cell membranes but do not provide any information on the nature of such interactions (i.e., do the peptides only disturb the cell membranes and penetrate into them or they perforate/disrupt the cell membranes).
5. Unravelling the cellular entry pathways of different classes of the cationic amphiphilic peptides by knocking down specific genes which encode the proteins involved in endocytosis (such as myosin, clathrin and caveolin) or genes which encode receptors

which are supposed to be involved in the cellular uptake of the peptides based on the literature data on peptides with closely related structures (such as scavenger receptors).

6. Studying the intracellular trafficking of the peptides, their sites of accumulation within the cells when administered alone or in combination with nucleic acids, and their final fate within the cells. This information could be used to develop strategies for enhancing the availability of the peptides at their intracellular sites of action and reducing the peptide loss within the cells due to entrapment in off-target sites which is important for increasing the potency of the peptides.
7. Studying the physiological and structural differences of the different cancer cell lines used for screening in this project such as the difference in the cell membrane potential, the cell membrane composition, or the expression level of the different types of proteins and/or receptors which might be involved in cellular uptake of the peptides in order to find an explanation for the observed differences in the response of different cancer cell lines to the cationic amphiphilic peptides.
8. Assessing the cytotoxicity of the cationic amphiphilic peptides which had low toxicity against fibroblasts in other types of normal cells such as erythrocytes and THP-1 monocytes to provide more evidence on their safety upon systemic administration.
9. *In vivo* tests in animal models such as tumour bearing mice or zebrafish to study the anticancer activity and safety of the cationic amphiphilic peptides which exhibited selective anticancer activity *in vitro* in a whole organism and to determine the pharmacokinetics of the peptides following systemic administration to the animals. This information is crucial for determining the elimination half-life of the peptides, their stability against protease enzymes in the blood, and any general or organ specific toxicities or immunological reactions which may occur upon systemic/parenteral administration of these peptides.
10. *In vivo* gene delivery using the cationic amphiphilic peptides which showed greater promise for gene delivery *in vitro* to assess their gene delivery efficiency and their stability against nuclease enzymes in the blood. Furthermore, the pharmacokinetics of the peptide-siRNA complexes following systemic administration should be studied in terms of circulation time/elimination half-life, accumulation in any organs other than the intended site of action, and any general or organ specific toxicities caused by the off-target gene silencing in other organs/tissues.

Chapter 8: Supplemental data

Figures S1-S6 depict the concentration-response curves of the α-helical cationic amphiphilic peptides in HCT 116 colorectal cancer cells as measured by MTT assay. Each experiment was repeated 6 times, the replicates were plotted separately and the regression equation for each plot was used to calculate the value of IC_{50} for that replicate.

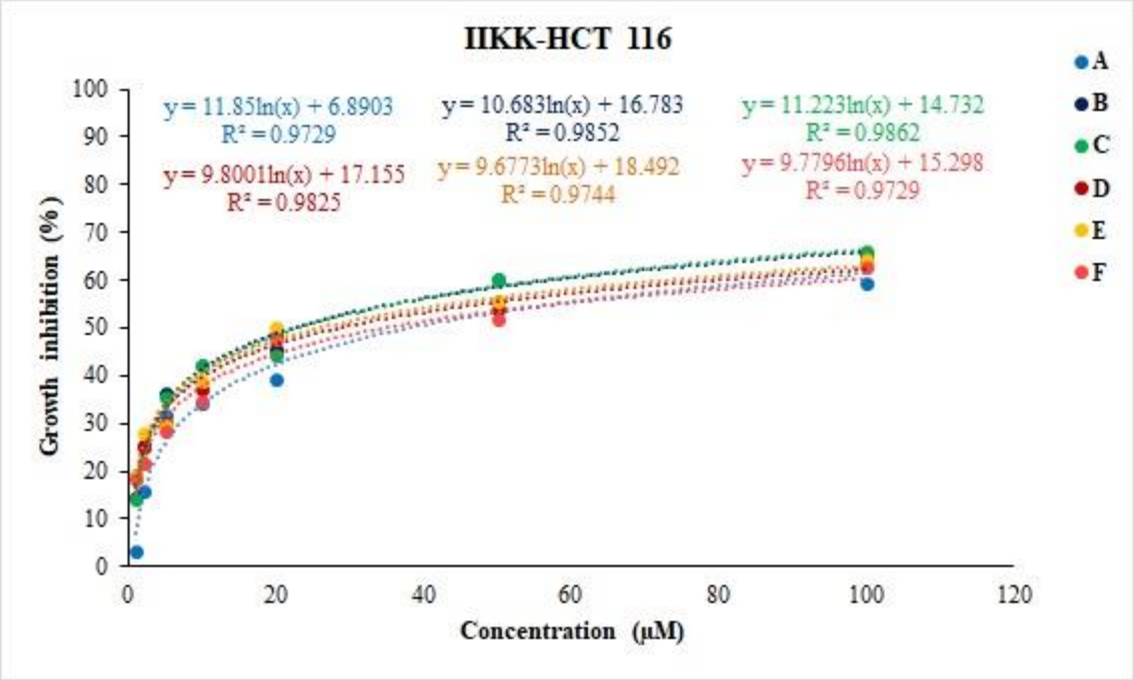

Figure S1. Concentration-response curves of IIKK in HCT 116 colorectal cancer cells. A-F represents the 6 replicates.

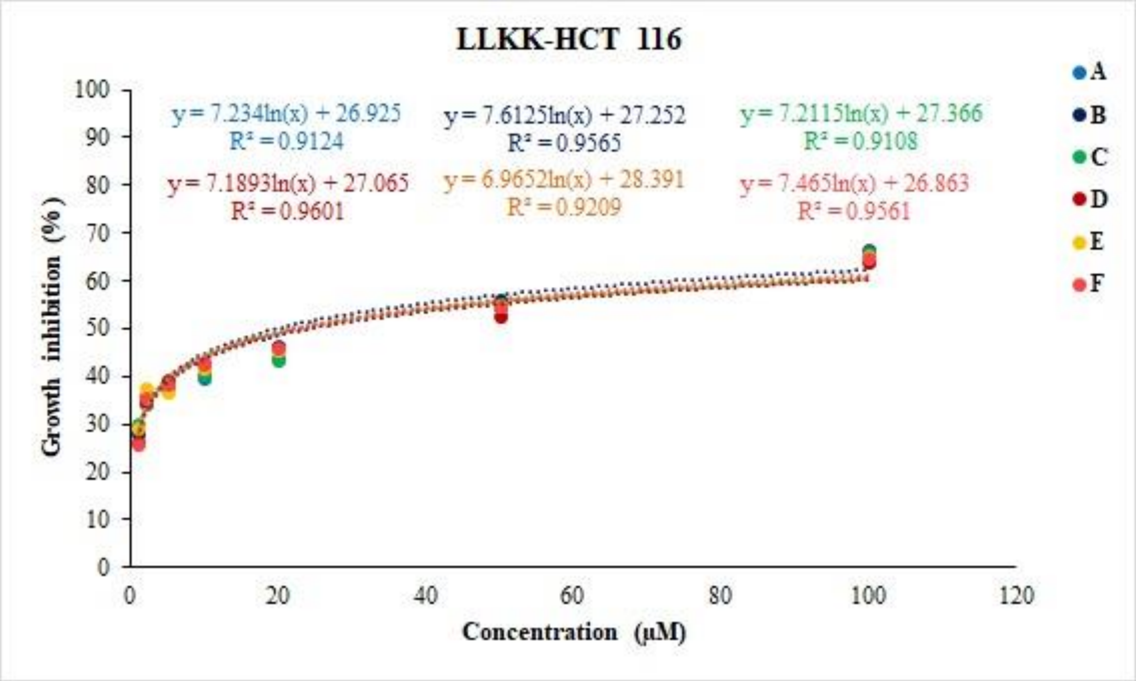

Figure S2. Concentration-response curves of LLKK in HCT 116 colorectal cancer cells. A-F represents the 6 replicates.

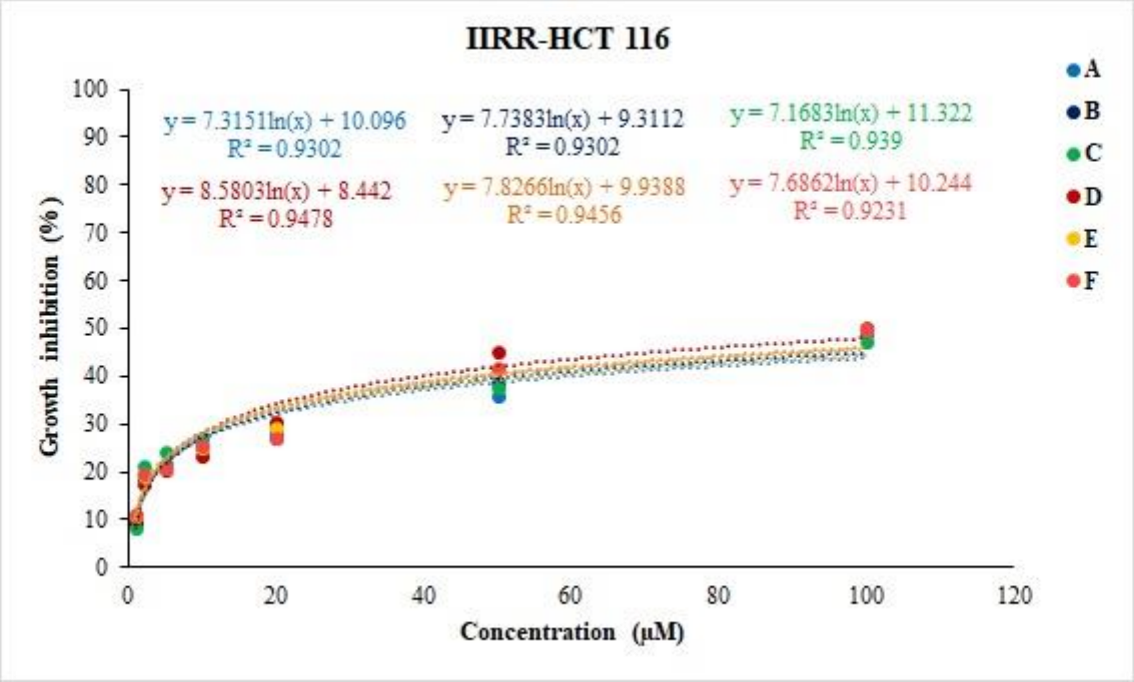

Figure S3. Concentration-response curves of IIRR in HCT 116 colorectal cancer cells. A-F represents the 6 replicates.

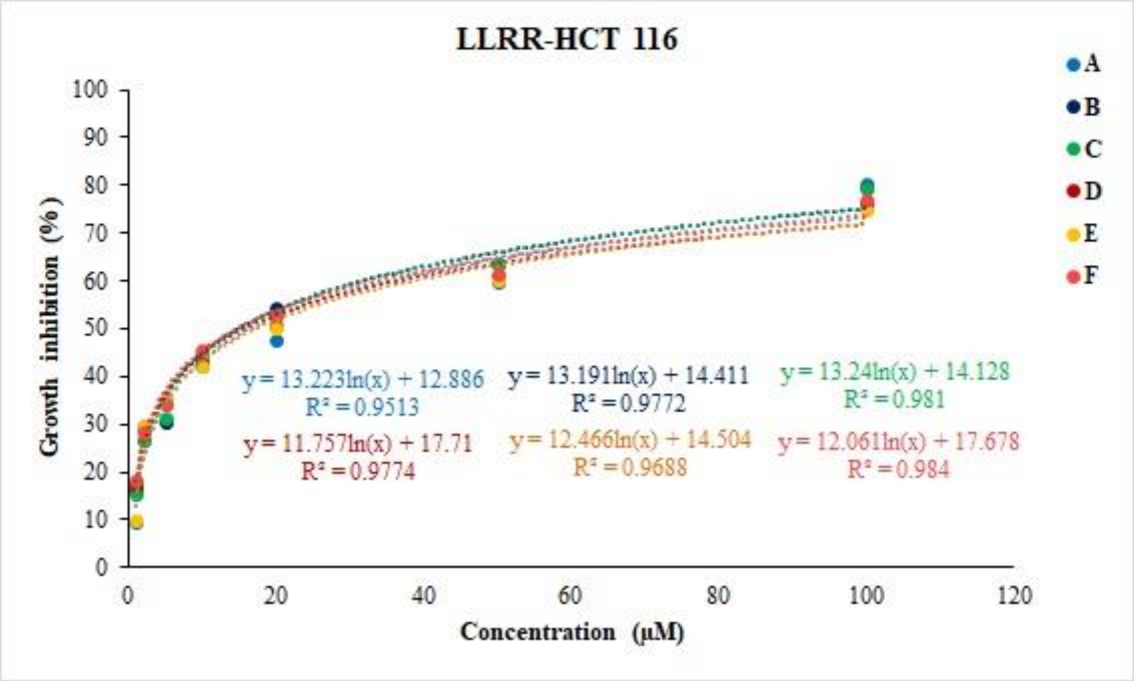

Figure S4. Concentration-response curves of LLRR in HCT 116 colorectal cancer cells. A-F represents the 6 replicates.

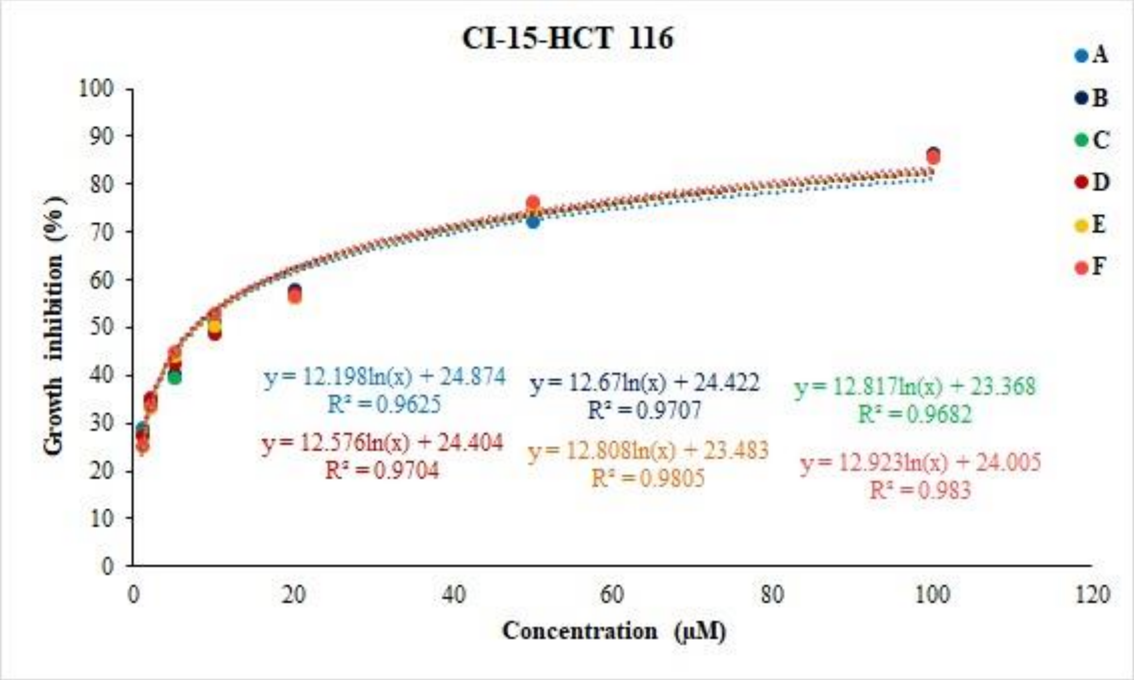

Figure S5. Concentration-response curves of CI-15 in HCT 116 colorectal cancer cells. A-F represents the 6 replicates.

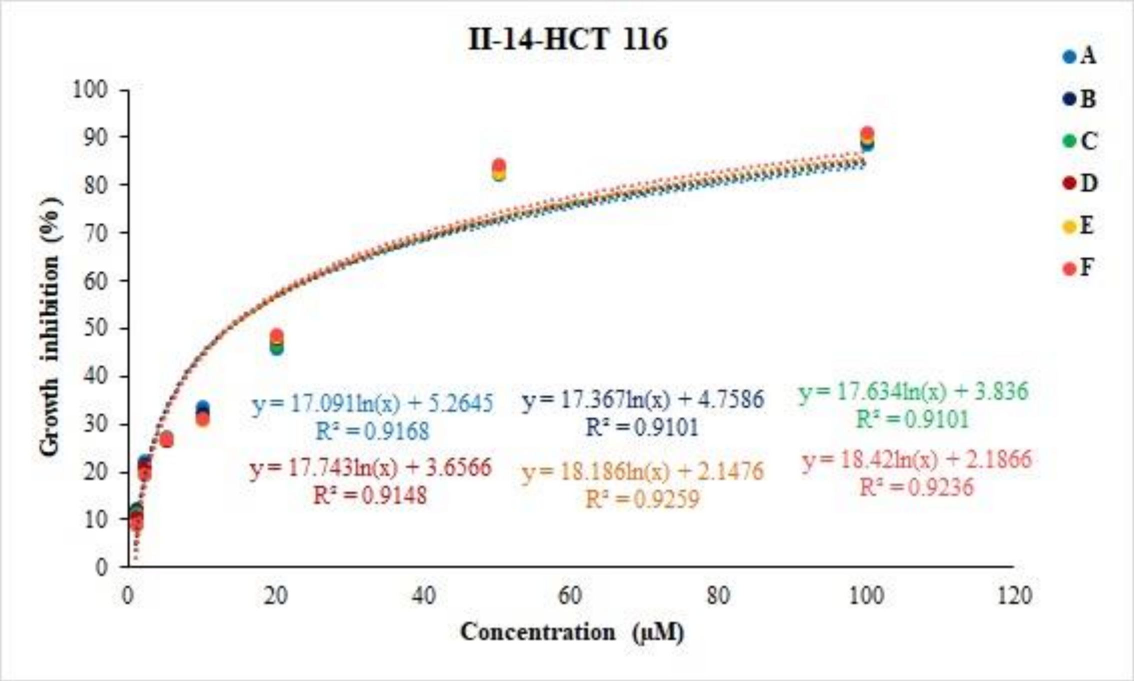

Figure S6. Concentration-response curves of II-14 in HCT 116 colorectal cancer cells. A-F represents the 6 replicates.

Figures S7-S12 depict the concentration-response curves of the α-helical cationic amphiphilic peptides in Hela cervical cancer cells as measured by MTT assay.

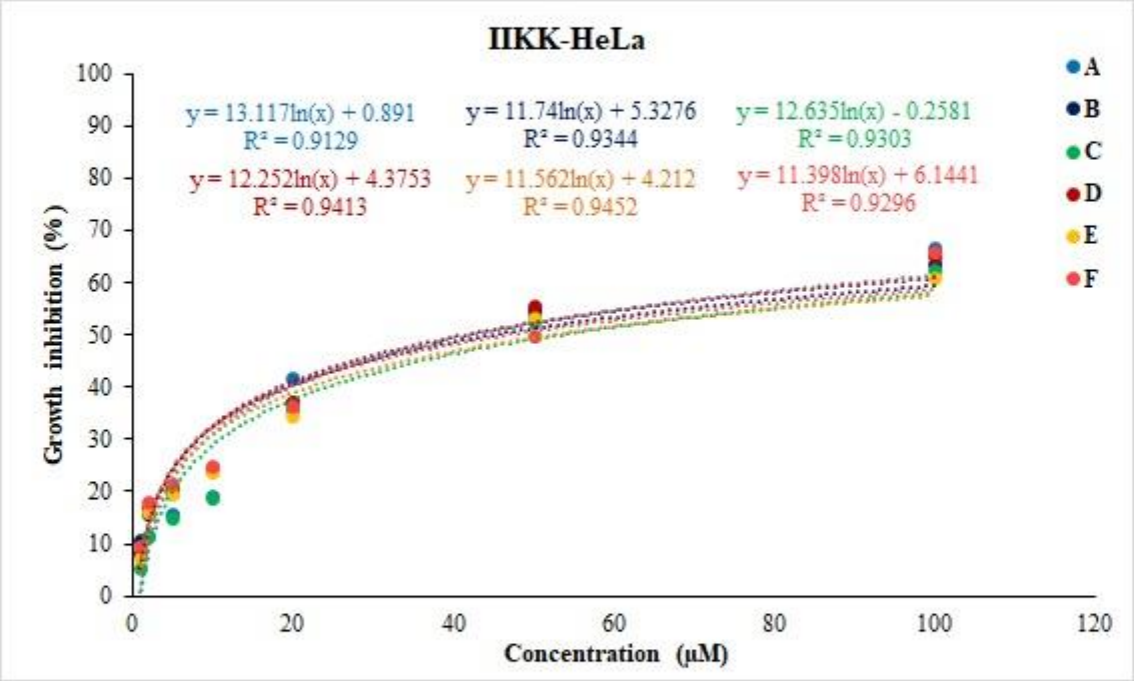

Figure S7. Concentration-response curves of IIKK in HeLa cervical cancer cells. A-F represents the 6 replicates.

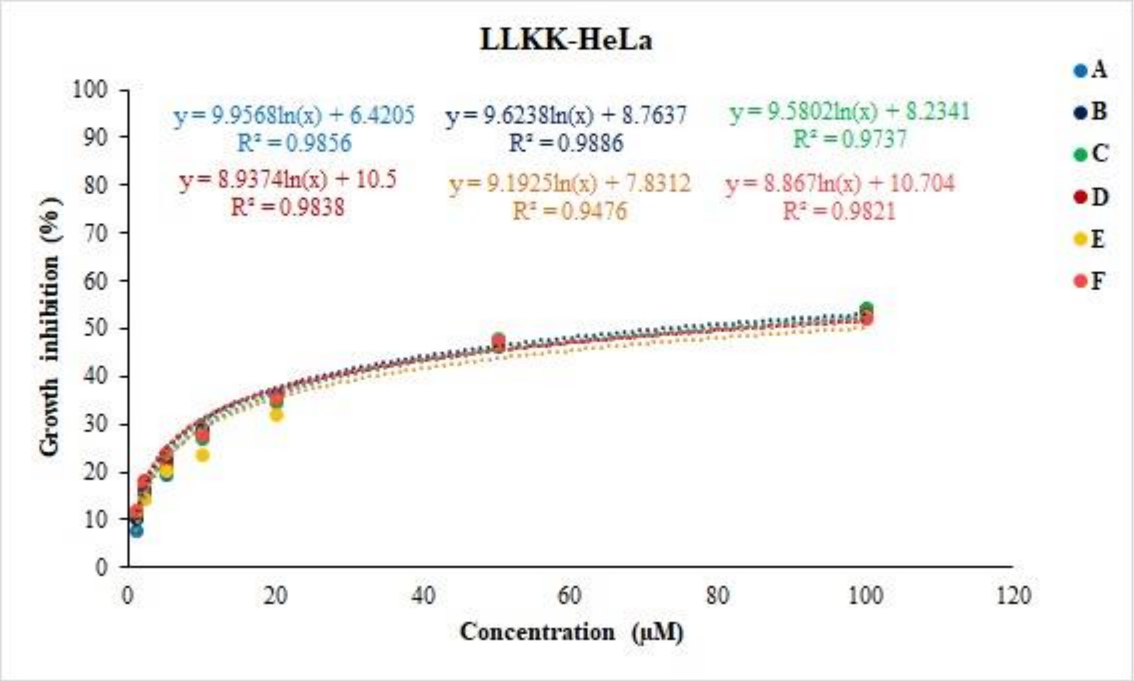

Figure S8. Concentration-response curves of LLKK in HeLa cervical cancer cells. A-F represents the 6 replicates.

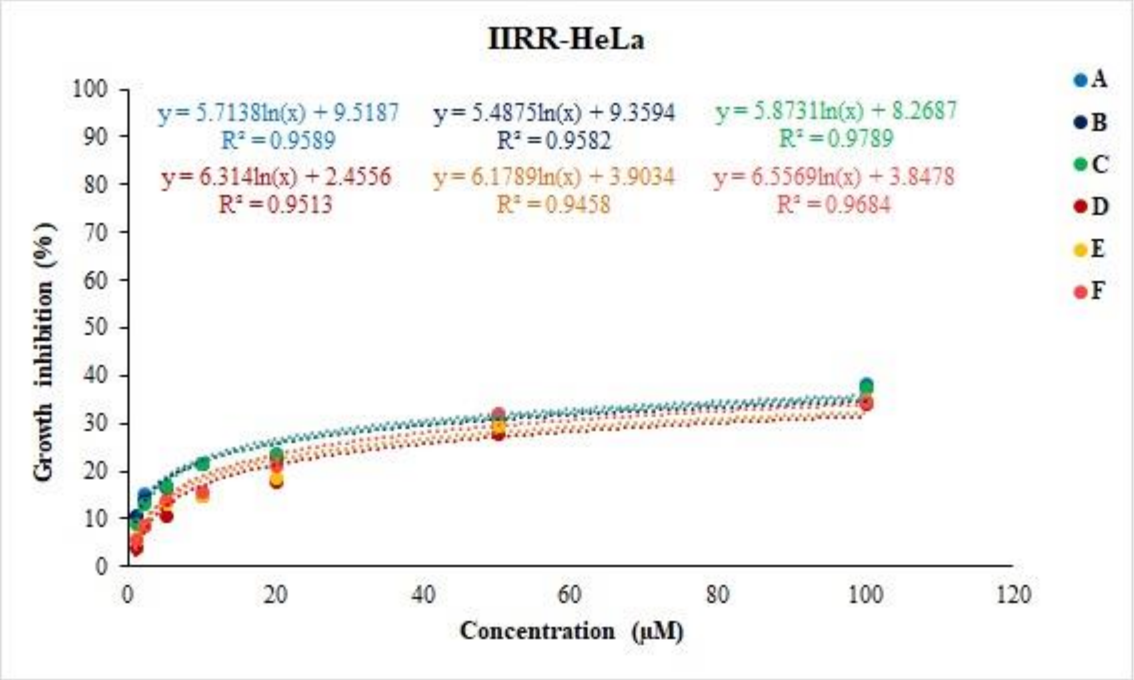

Figure S9. Concentration-response curves of IIRR in HeLa cervical cancer cells. A-F represents the 6 replicates.

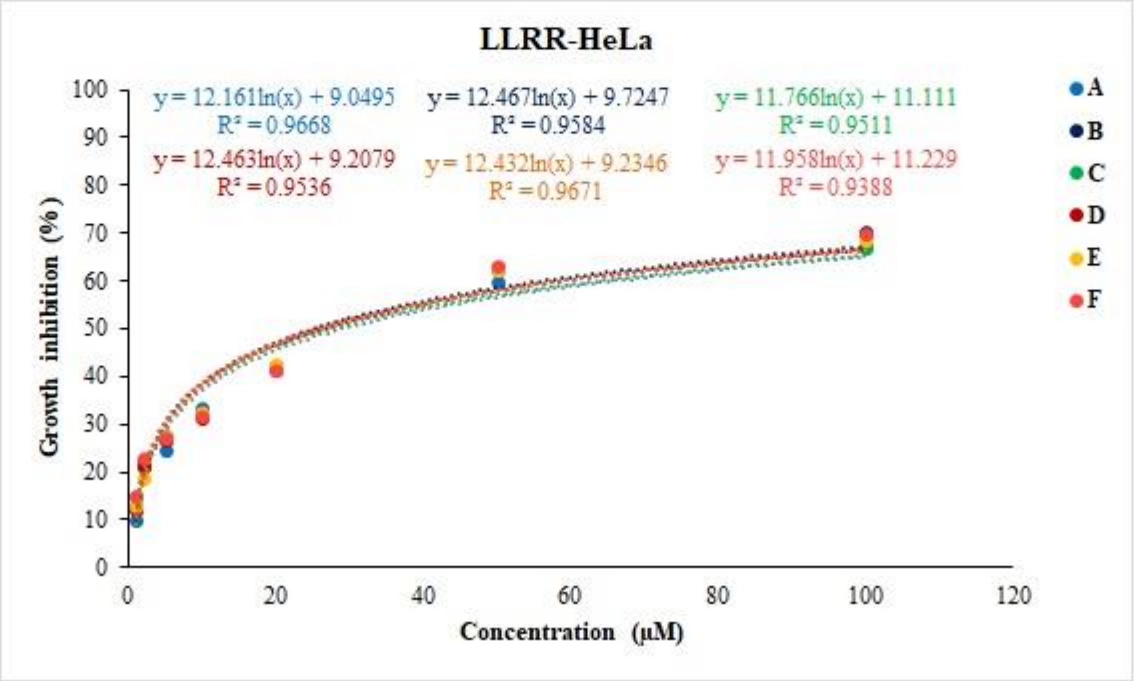

Figure S10. Concentration-response curves of LLRR in HeLa cervical cancer cells. A-F represents the 6 replicates.

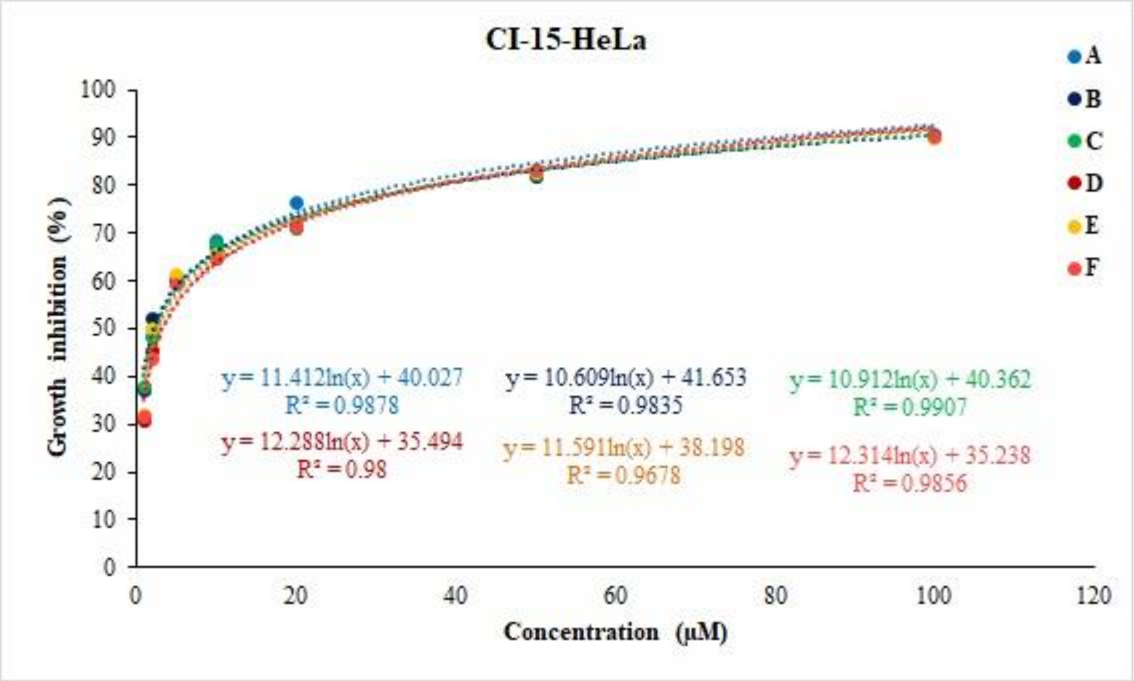

Figure S11. Concentration-response curves of CI-15 in HeLa cervical cancer cells. A-F represents the 6 replicates.

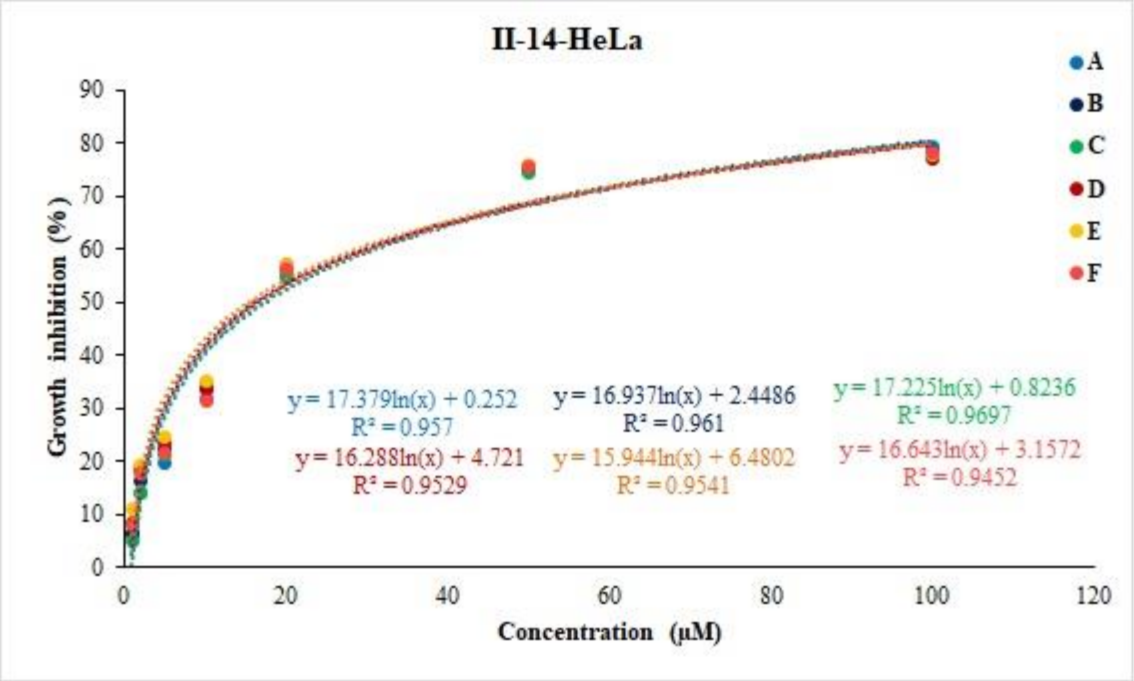

Figure S12. Concentration-response curves of II-14 in HeLa cancer cells. A-F represents the 6 replicates.

Figures S13-S18 depict the concentration-response curves of the α-helical cationic amphiphilic peptides in MDA-MB-231 cervical cancer cells as measured by MTT assay.

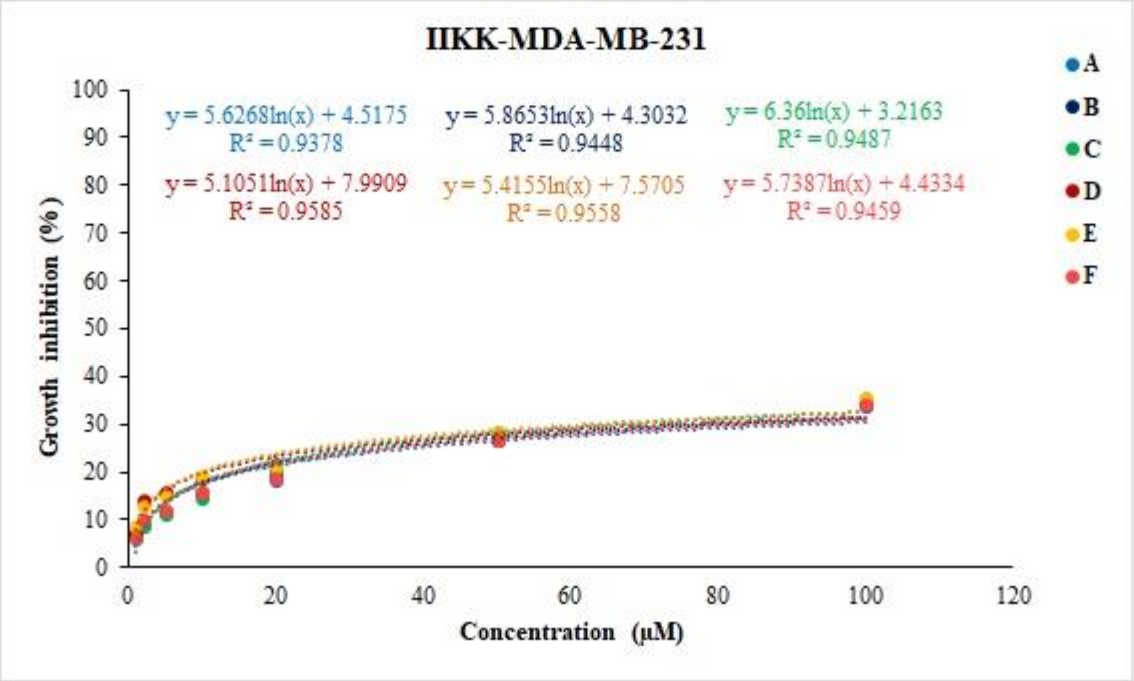

Figure S13. Concentration-response curves of IIKK in MDA-MB-231 breast cancer cells. A-F represents the 6 replicates.

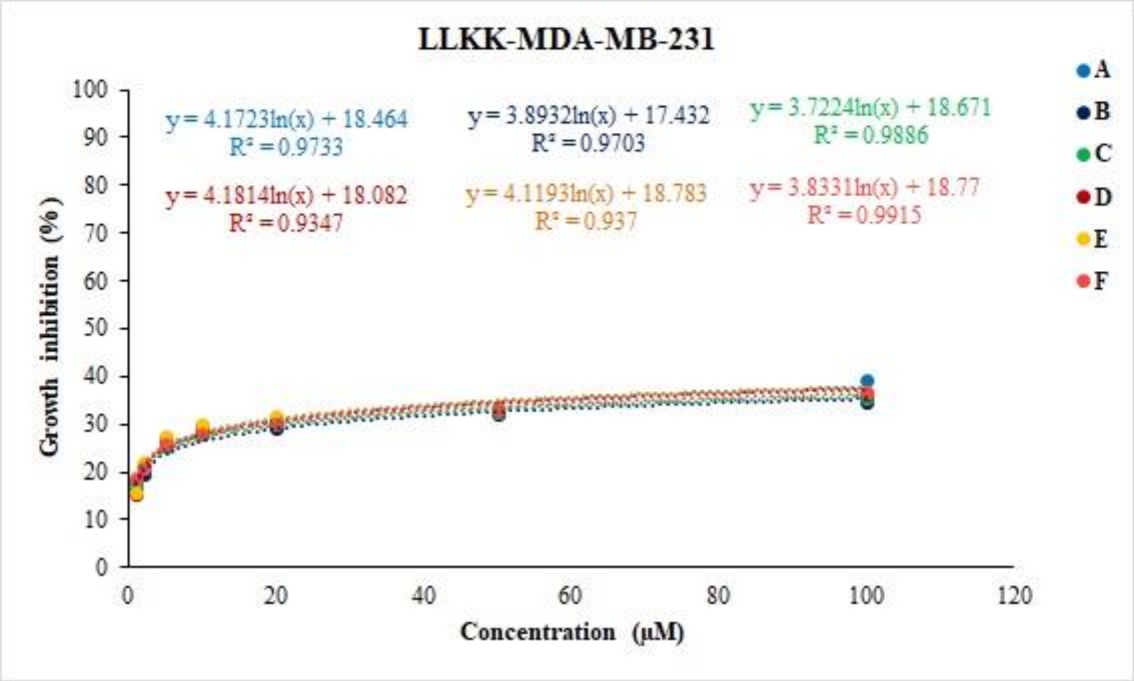

Figure S14. Concentration-response curves of LLKK in MDA-MB-231 breast cancer cells. A-F represents the 6 replicates.

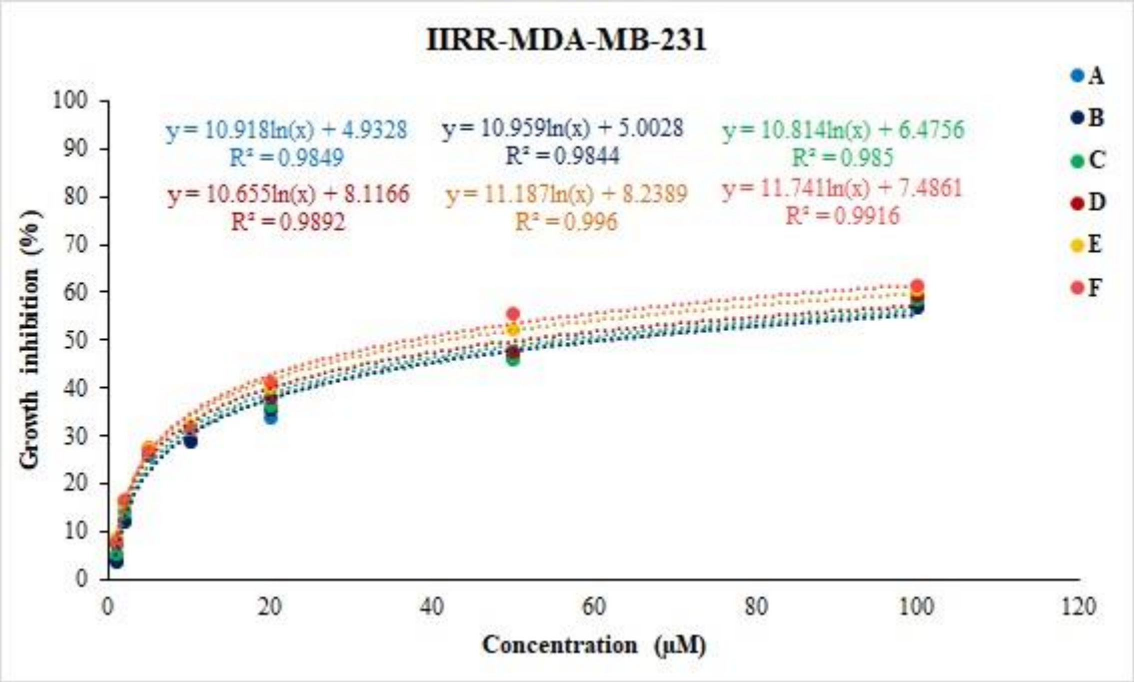

Figure S15. Concentration-response curves of IIRR in MDA-MB-231 breast cancer cells. A-F represents the 6 replicates.

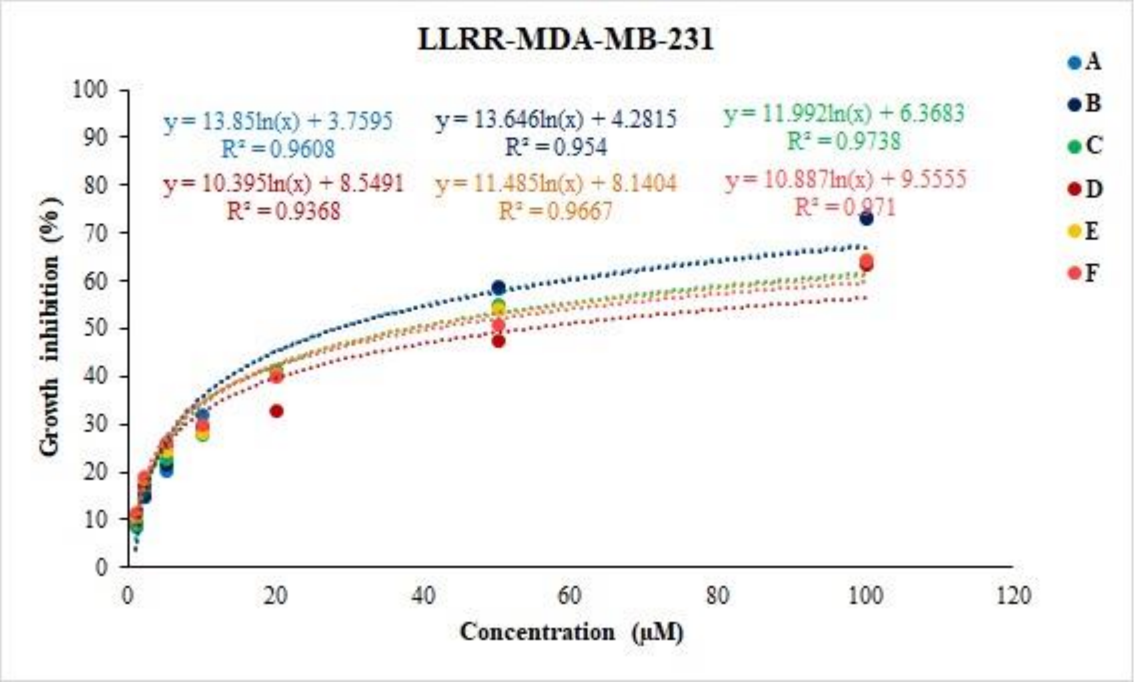

Figure S16. Concentration-response curves of LLRR in MDA-MB-231 breast cancer cells. A-F represents the 6 replicates.

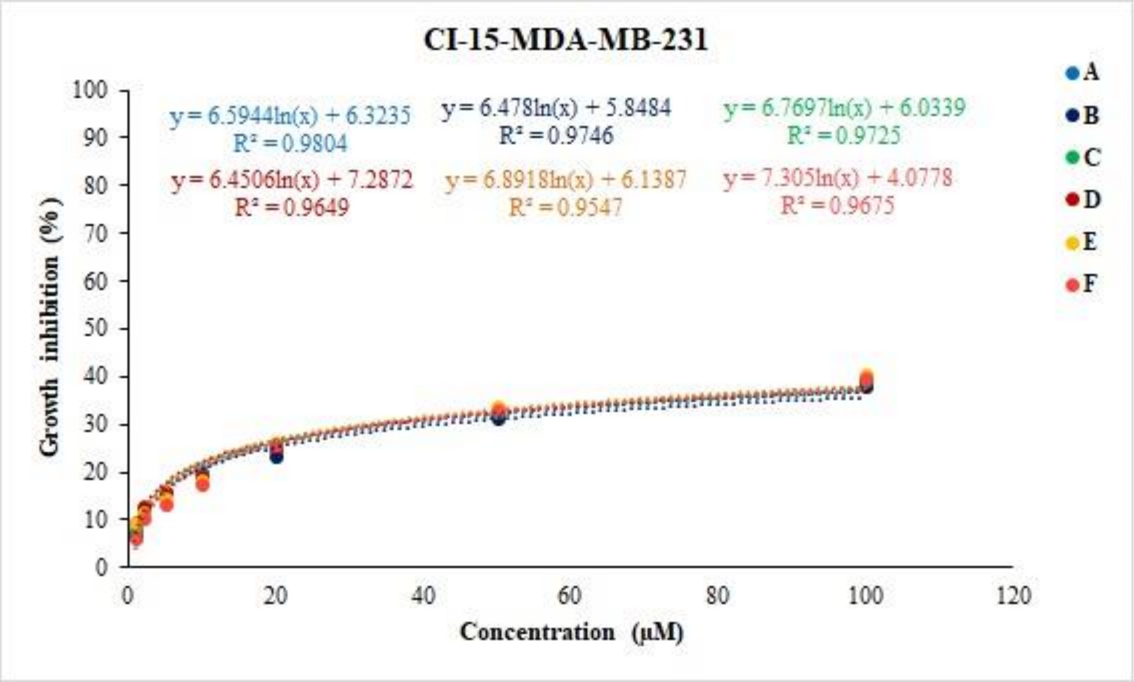

Figure S17. Concentration-response curves of CI-15 in MDA-MB-231 breast cancer cells. A-F represents the 6 replicates.

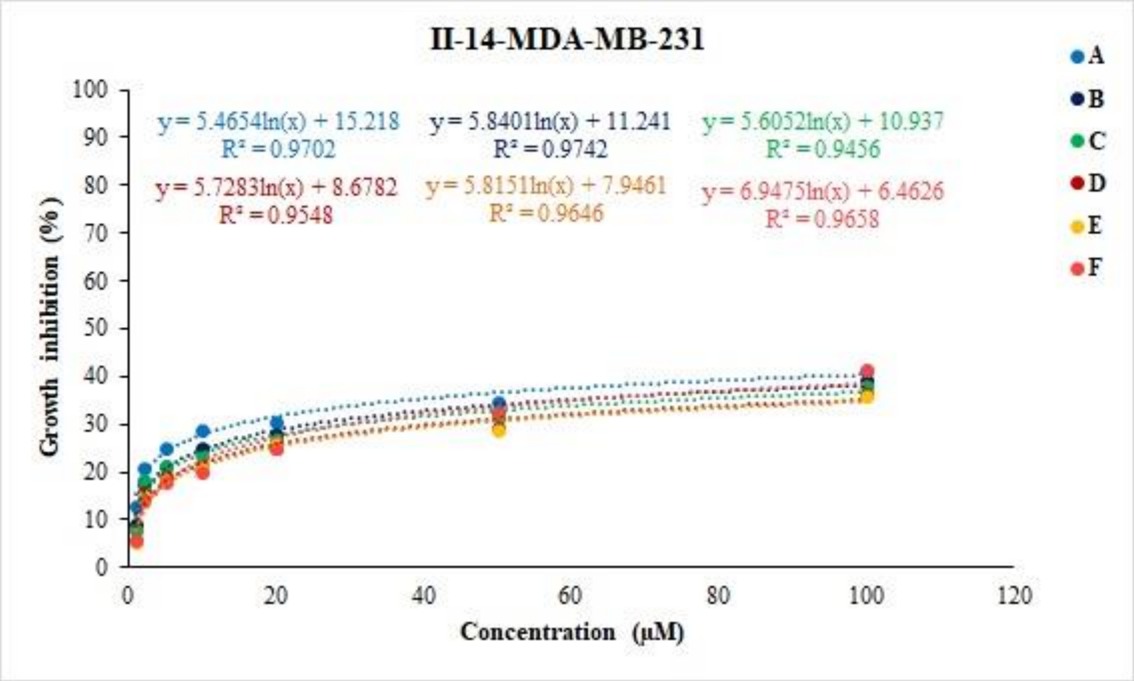

Figure S18. Concentration-response curves of II-14 in MDA-MB-231 breast cancer cells. A-F represents the 6 replicates.

Figures S19-S24 depict the concentration-response curves of the α-helical cationic amphiphilic peptides in human dermal fibroblast (HDF) cells as measured by MTT assay.

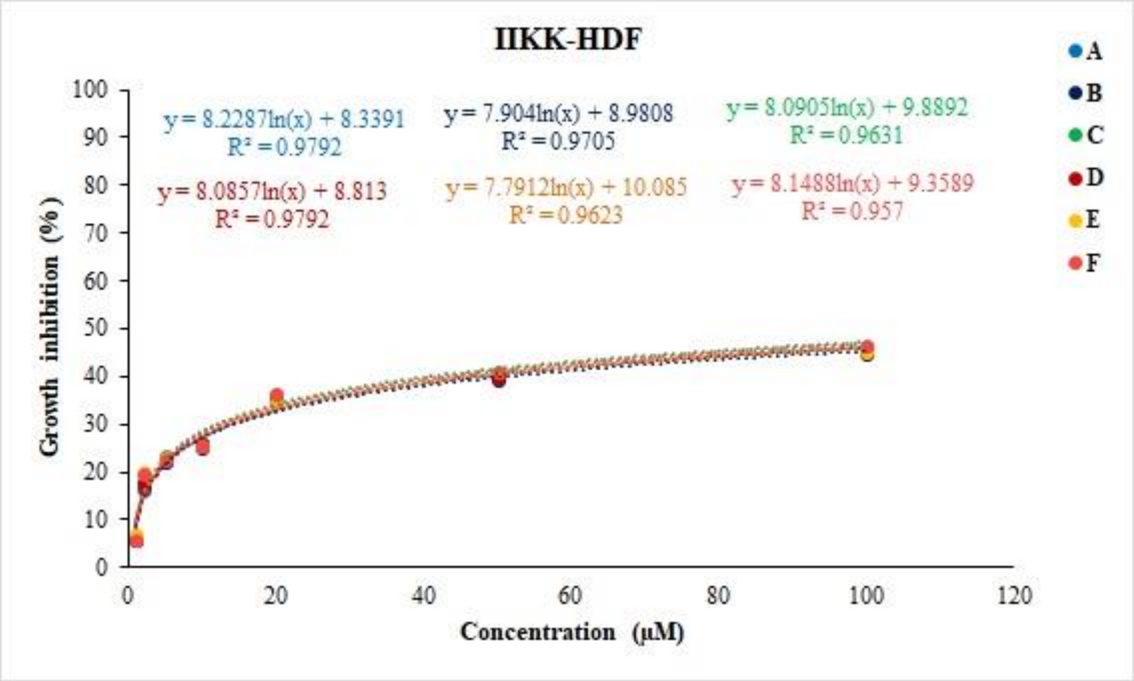

Figure S19. Concentration-response curves of IIKK in human dermal fibroblast (HDF) cells. A-F represents the 6 replicates.

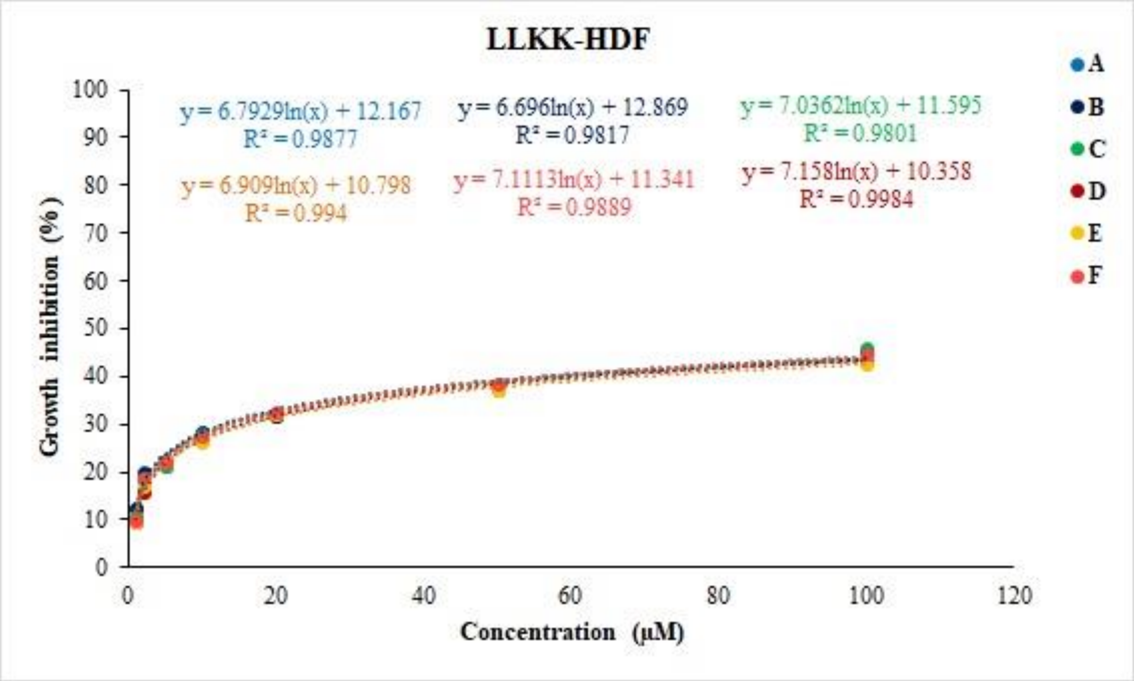

Figure S20. Concentration-response curves of LLKK in human dermal fibroblast (HDF) cells. A-F represents the 6 replicates.

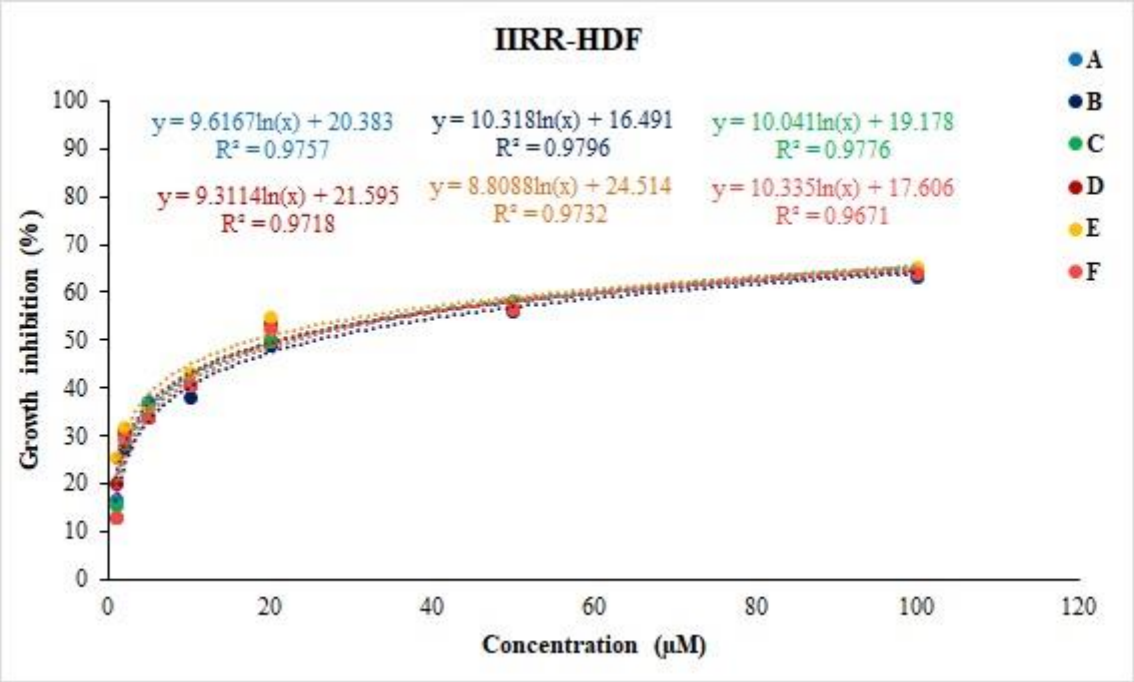

Figure S21. Concentration-response curves of IIRR in human dermal fibroblast (HDF) cells. A-F represents the 6 replicates.

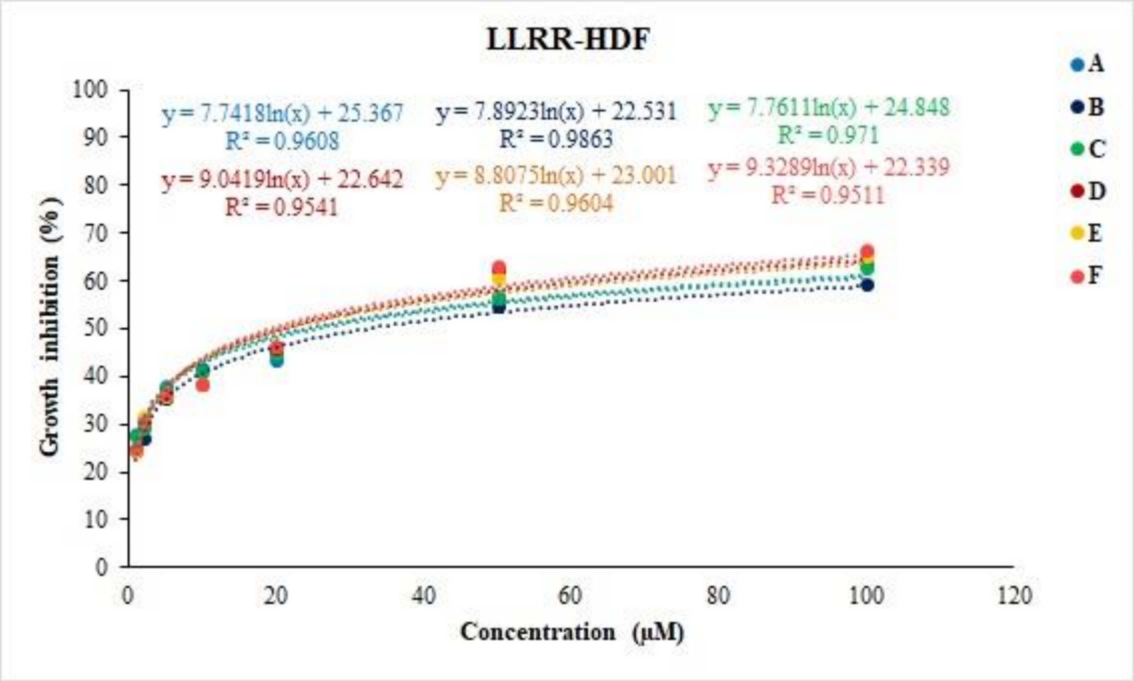

Figure S22. Concentration-response curves of LLRR in human dermal fibroblast (HDF) cells. A-F represents the 6 replicates.

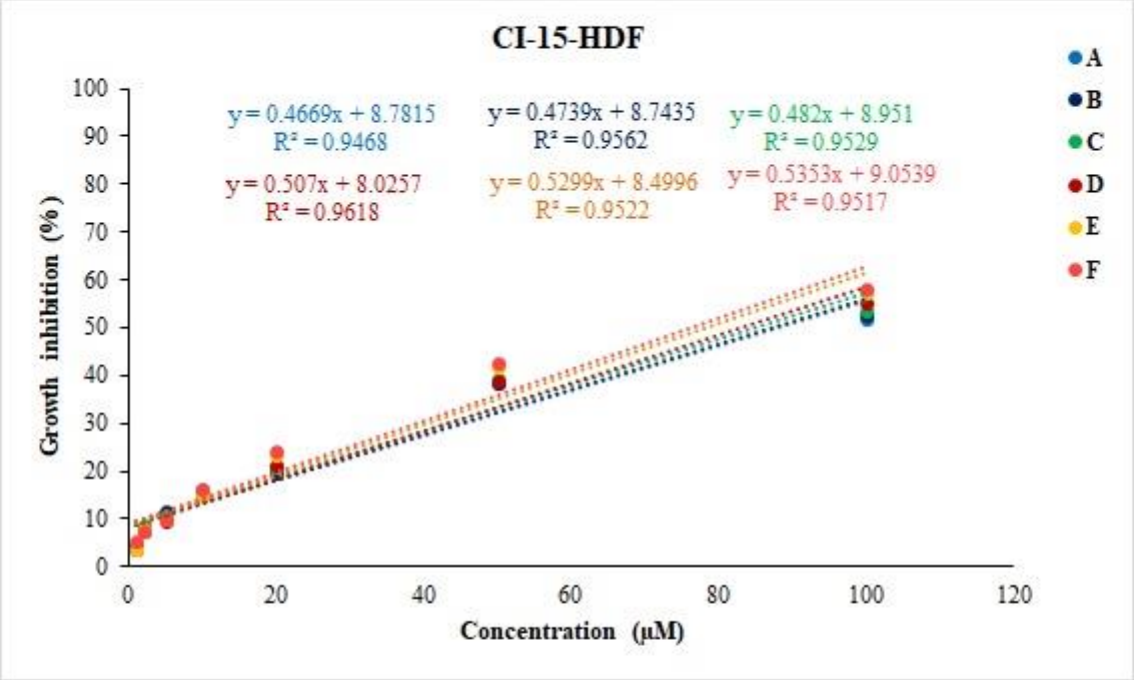

Figure S23. Concentration-response curves of CI-15 in human dermal fibroblast (HDF) cells. A-F represents the 6 replicates.

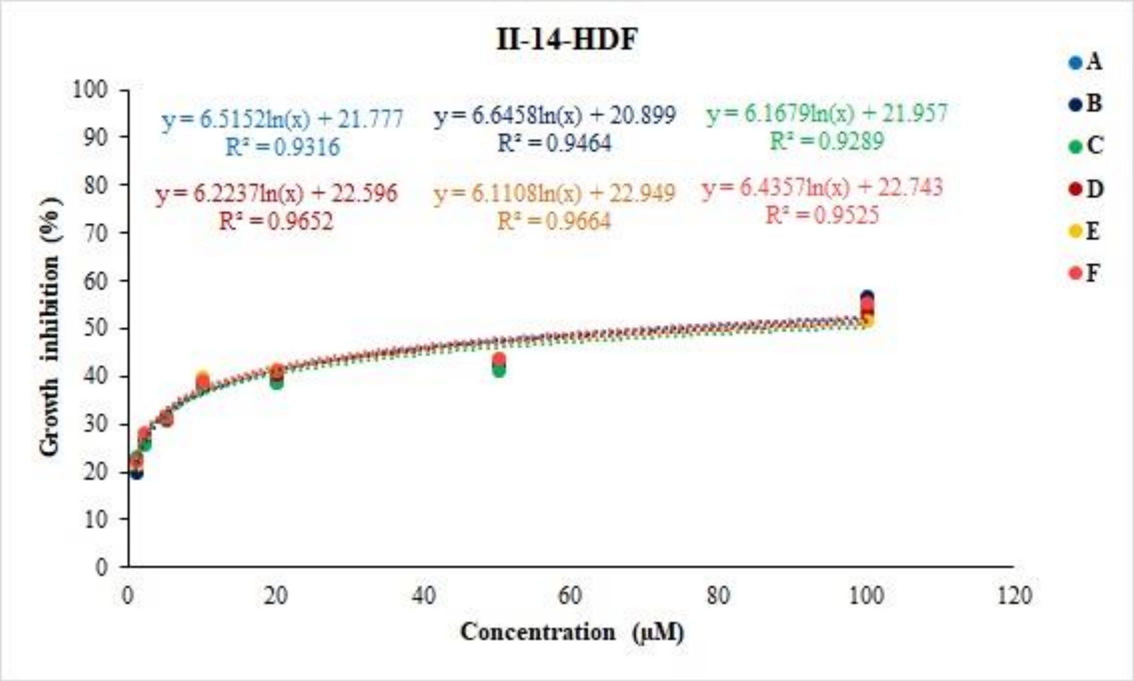

Figure S24. Concentration-response curves of II-14 in human dermal fibroblast (HDF) cells. A-F represents the 6 replicates.

Figures S25-S31 depict the concentration-response curves of the β-sheet forming cationic amphiphilic peptides in HCT 116 colorectal cancer cells as measured by MTT assay.

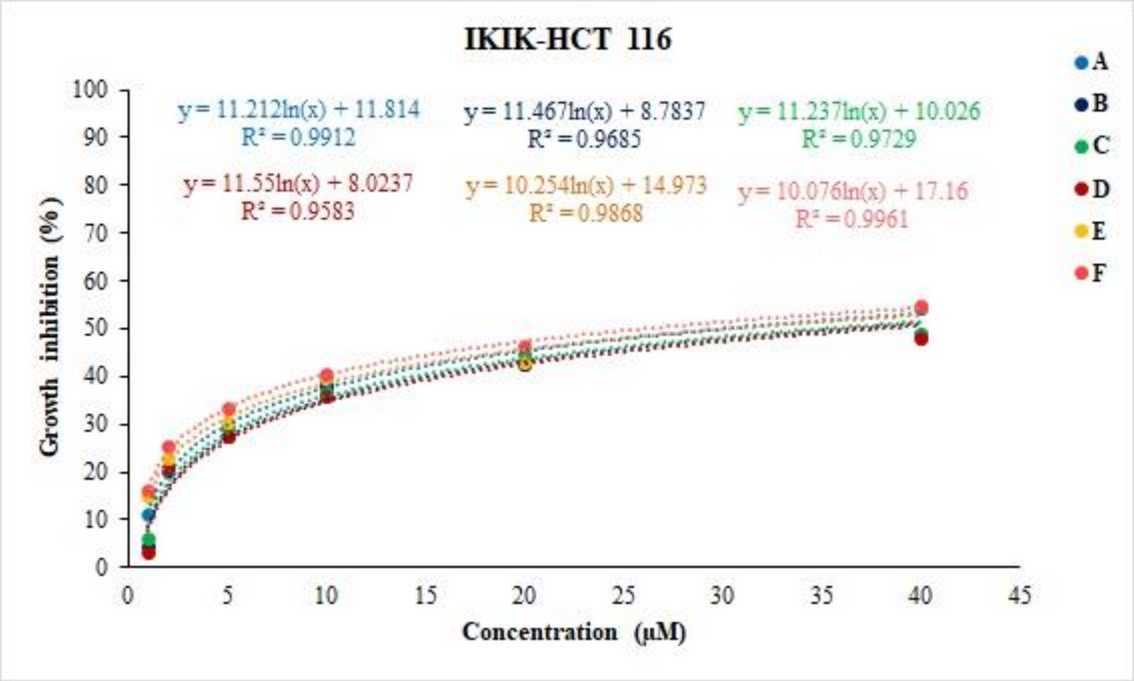

Figure S25. Concentration-response curves of IKIK in HCT 116 colorectal cancer cells. A-F represents the 6 replicates.

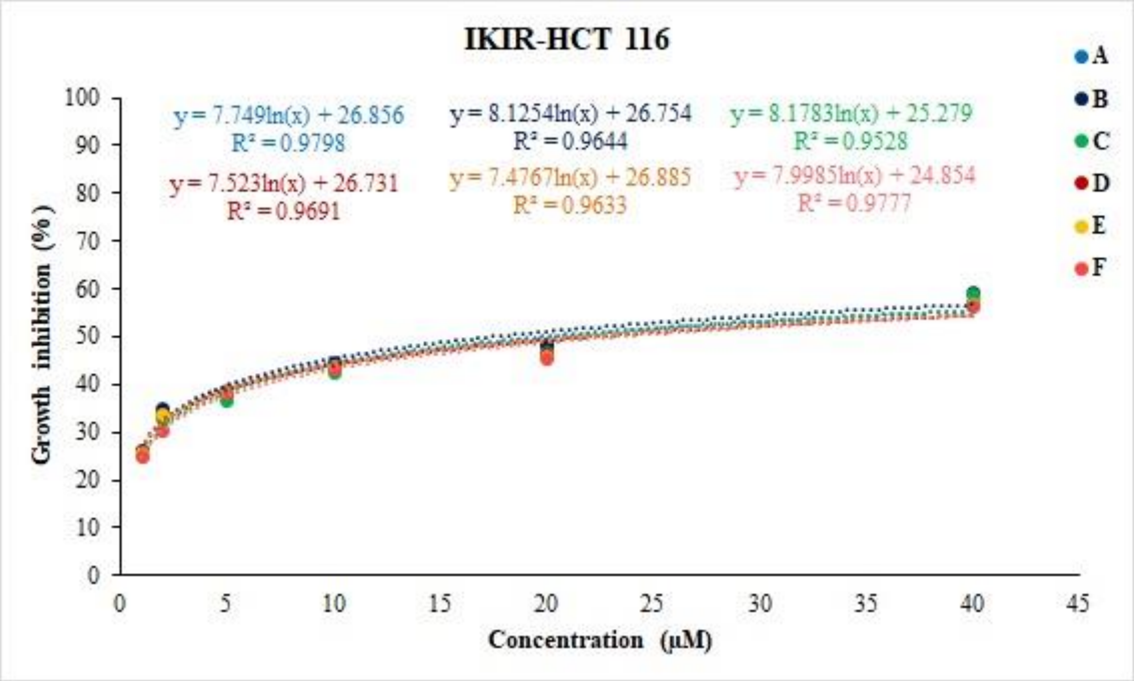

Figure S26. Concentration-response curves of IKIR in HCT 116 colorectal cancer cells. A-F represents the 6 replicates.

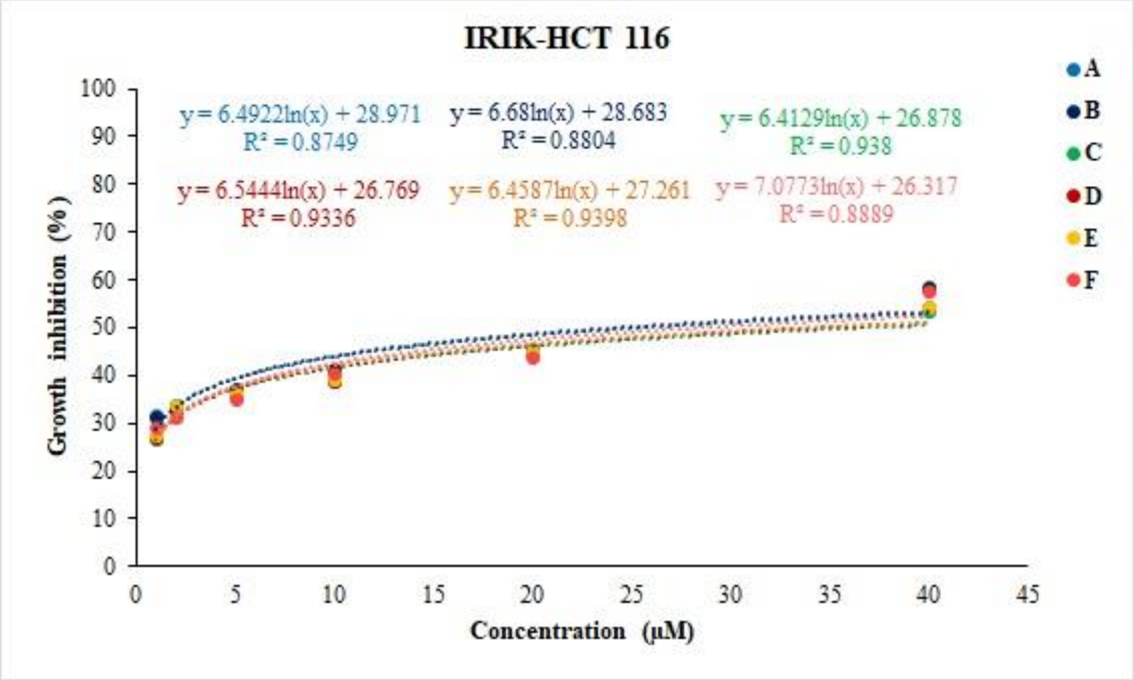

Figure S27. Concentration-response curves of IRIK in HCT 116 colorectal cancer cells. A-F represents the 6 replicates.

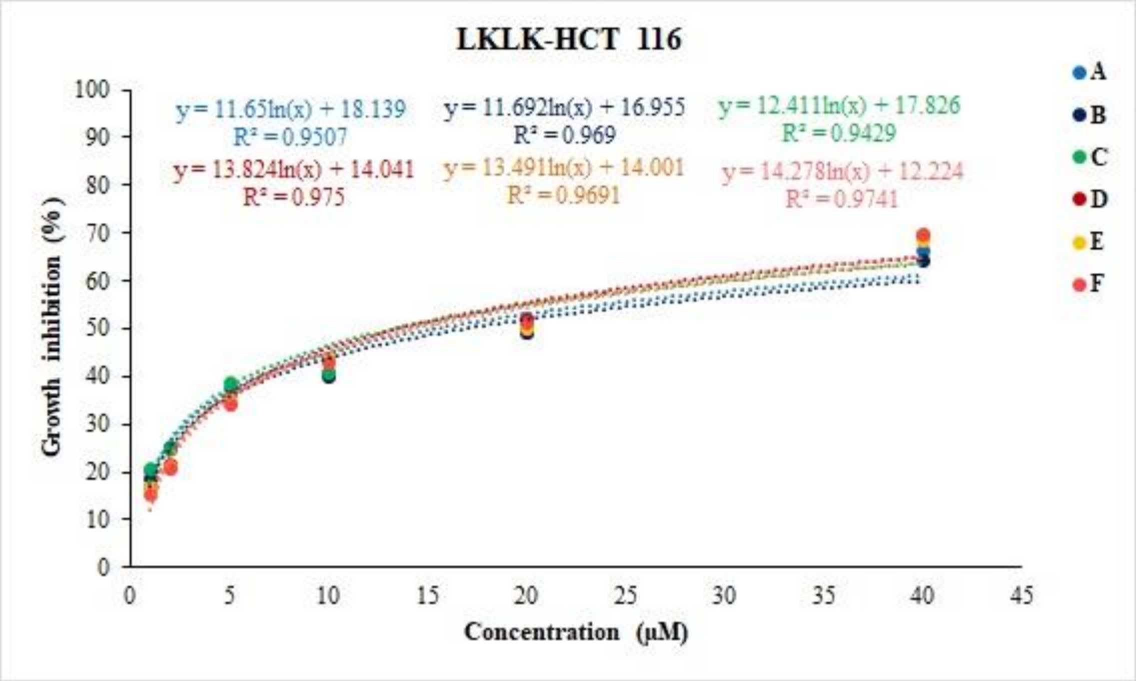

Figure S28. Concentration-response curves of LKLK in HCT 116 colorectal cancer cells. A-F represents the 6 replicates.

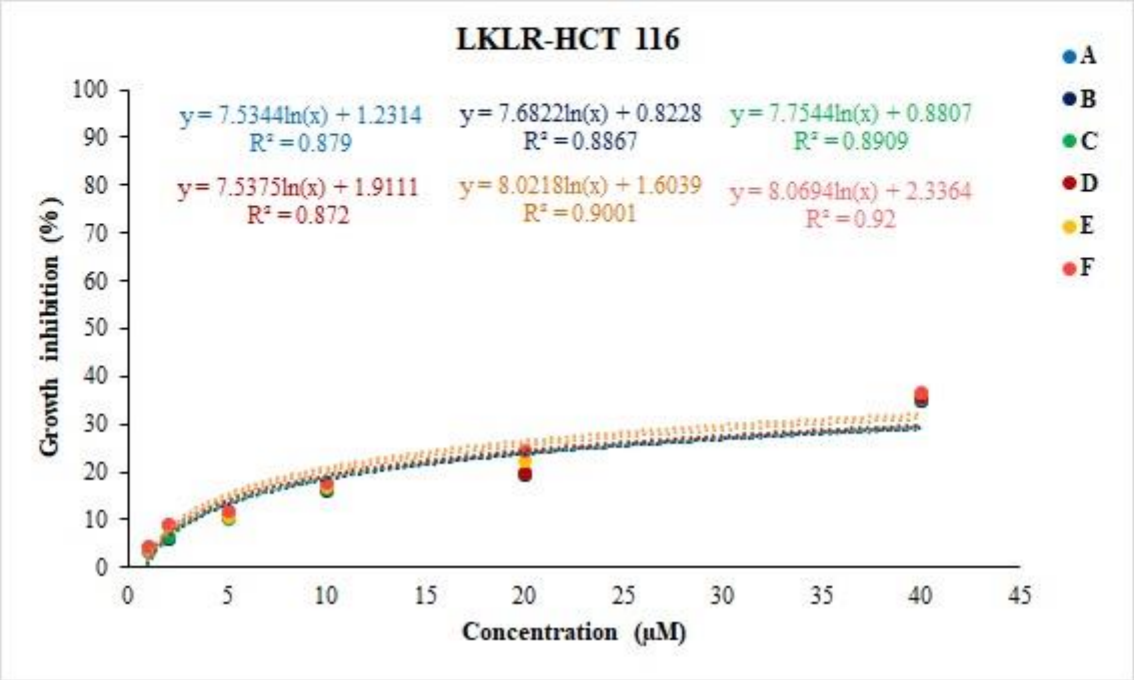

Figure S29. Concentration-response curves of LKLR in HCT 116 colorectal cancer cells. A-F represents the 6 replicates.

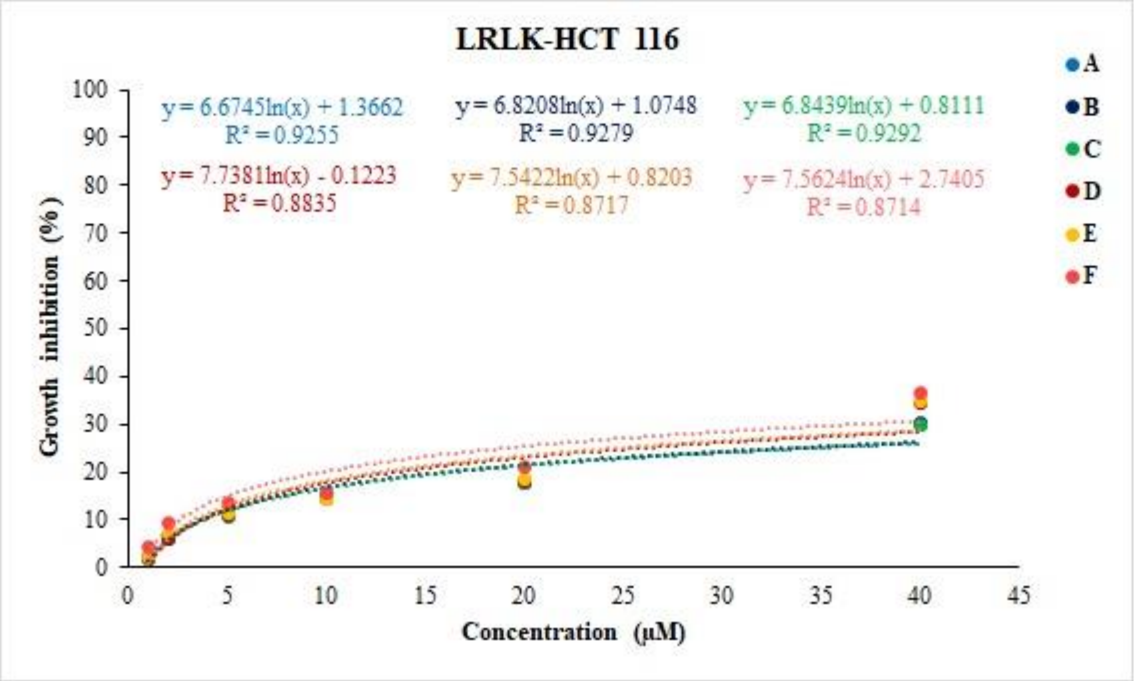

Figure S30. Concentration-response curves of LRLK in HCT 116 colorectal cancer cells. A-F represents the 6 replicates.

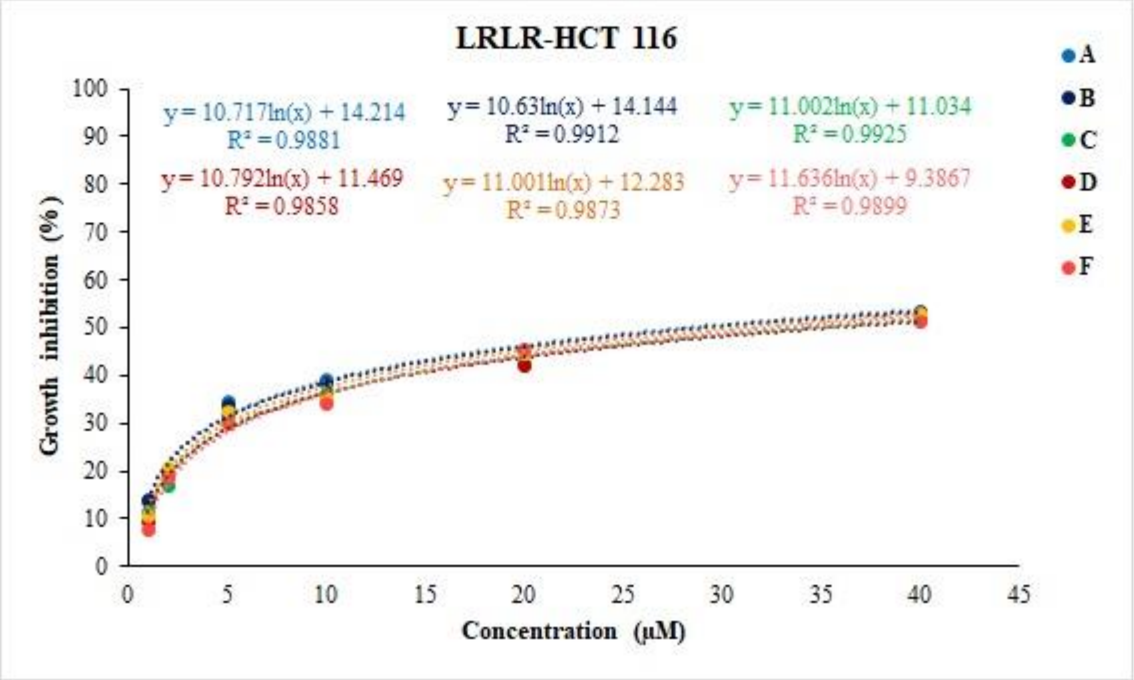

Figure S31. Concentration-response curves of LRLR in HCT 116 colorectal cancer cells. A-F represents the 6 replicates.

Figures S32-S38 depict the concentration-response curves of the β-sheet forming cationic amphiphilic peptides in HeLa cervical cancer cells as measured by MTT assay.

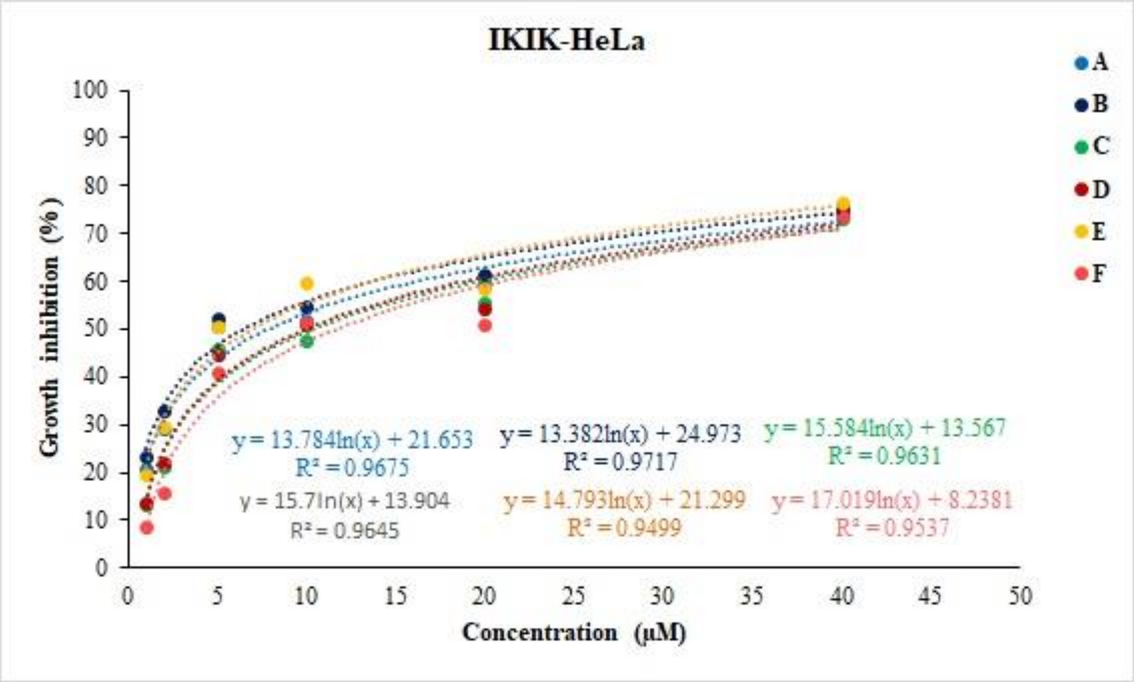

Figure S32. Concentration-response curves of IKIK in HeLa cervical cancer cells. A-F represents the 6 replicates.

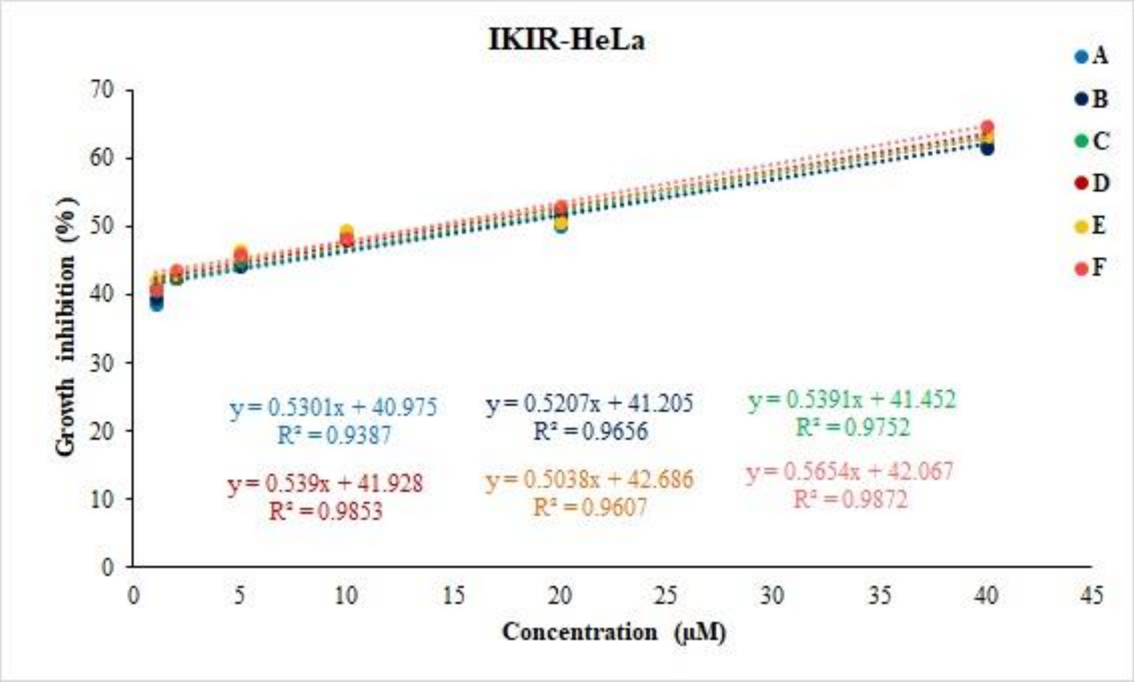

Figure S33. Concentration-response curves of IKIR in HeLa cervical cancer cells. A-F represents the 6 replicates.

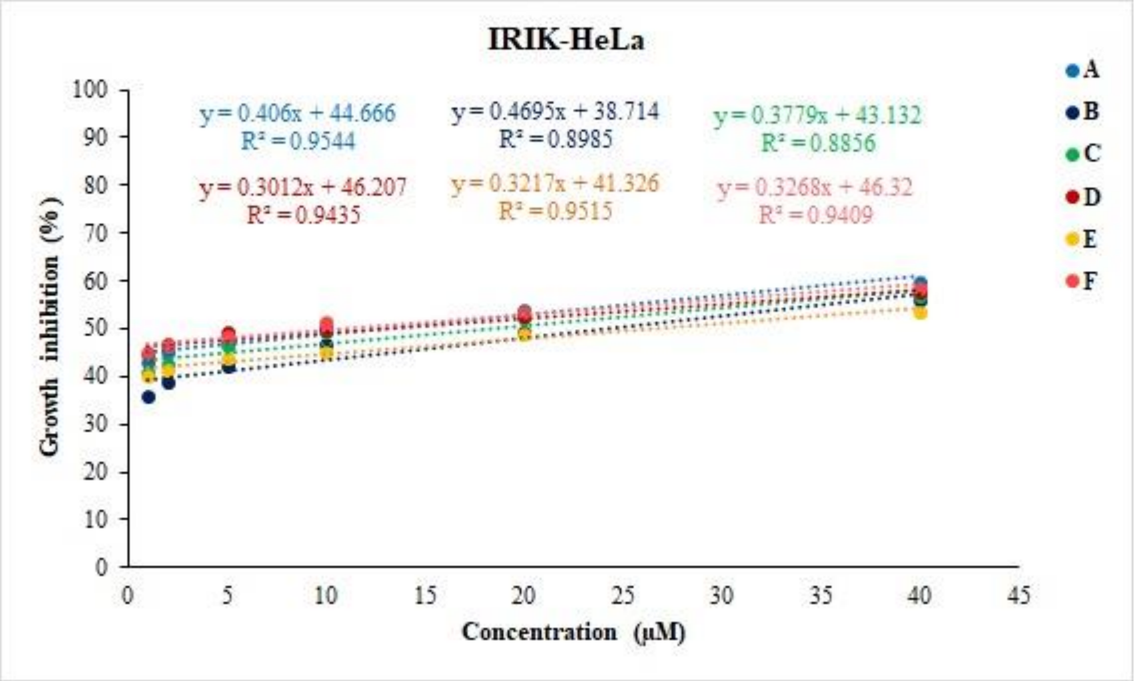

Figure S34. Concentration-response curves of IRIK in HeLa cervical cancer cells. A-F represents the 6 replicates.

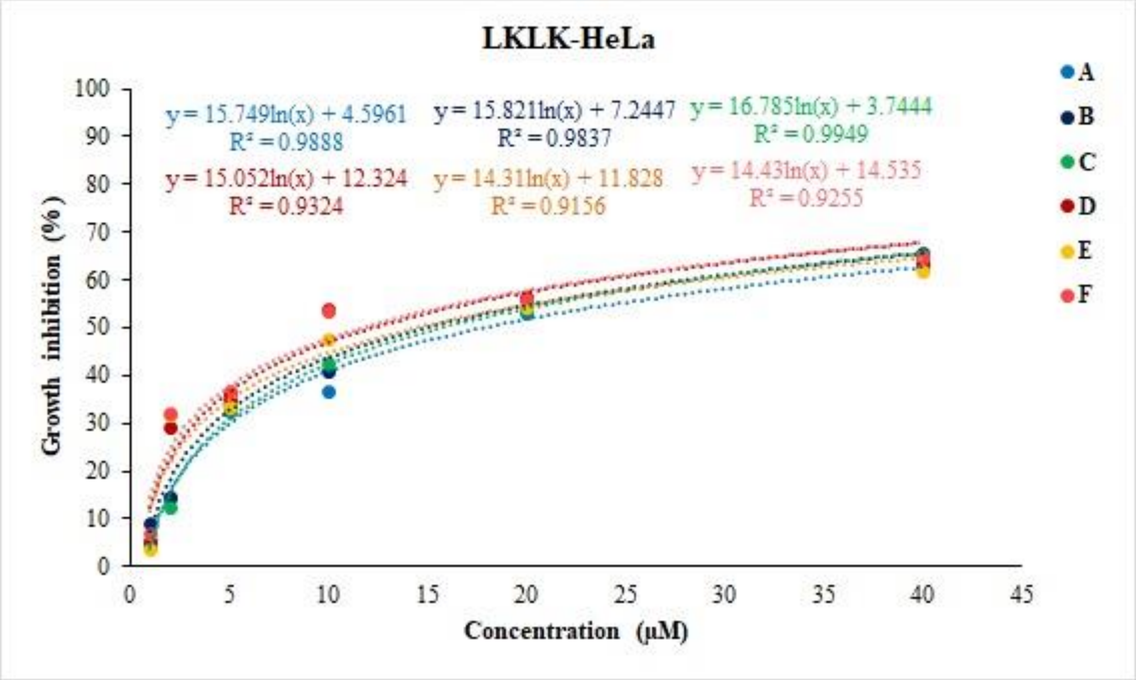

Figure S35. Concentration-response curves of LKLK in HeLa cervical cancer cells. A-F represents the 6 replicates.

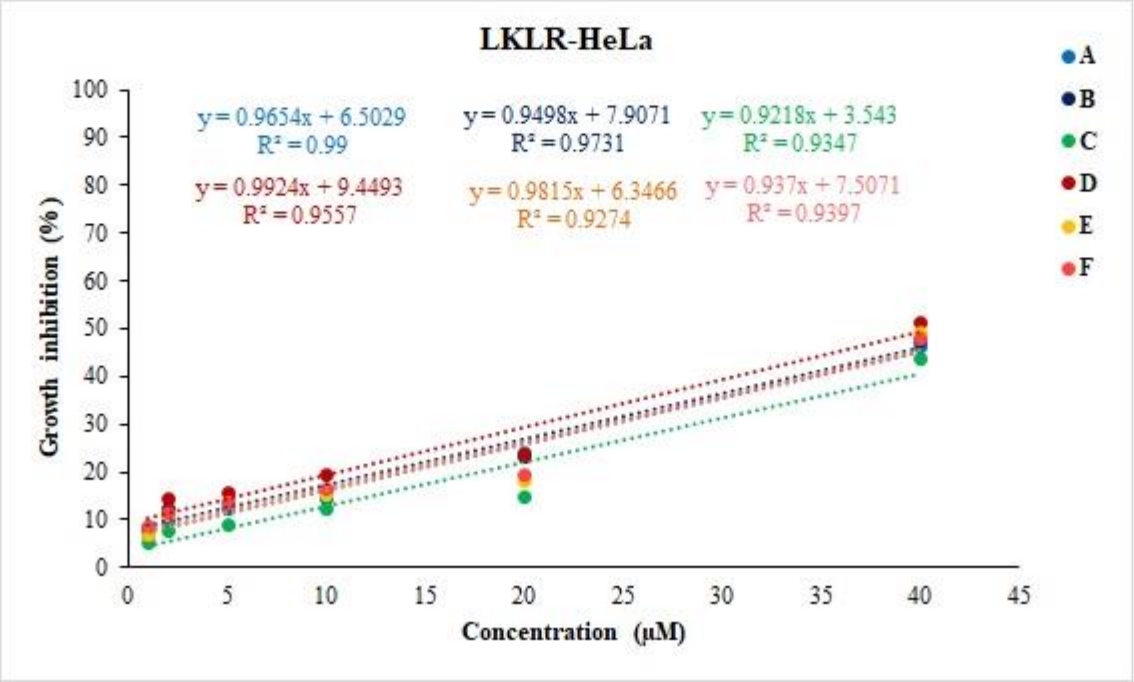

Figure S36. Concentration-response curves of IKIK in HeLa cervical cancer cells. A-F represents the 6 replicates.

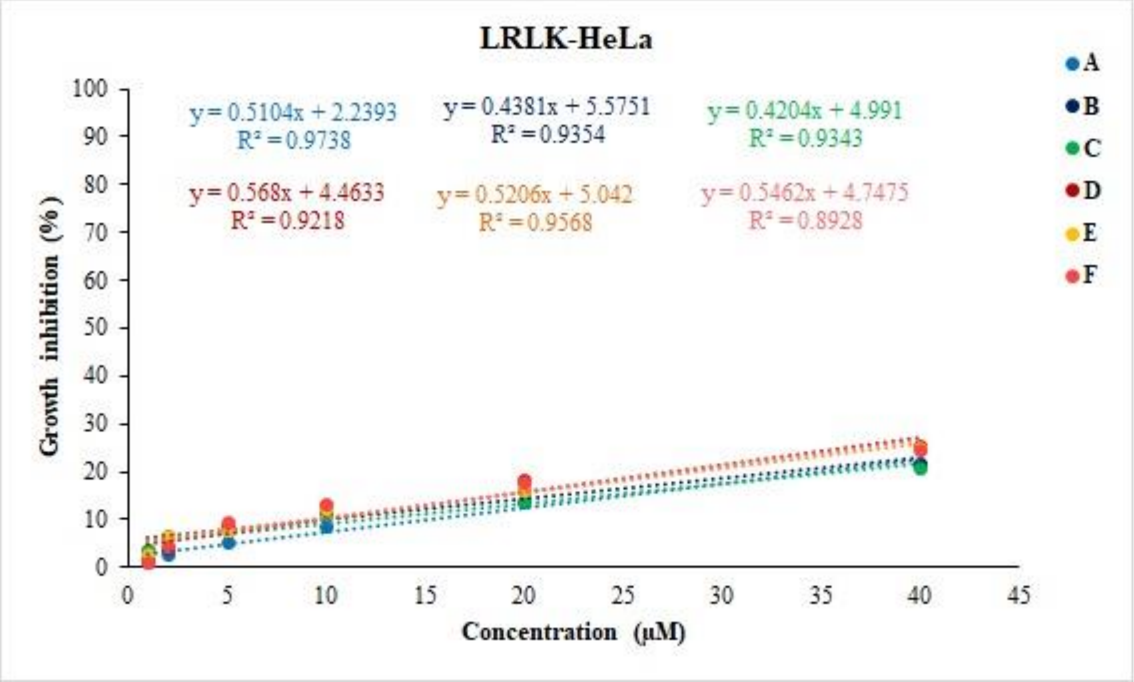

Figure S37. Concentration-response curves of IKIK in HeLa cervical cancer cells. A-F represents the 6 replicates.

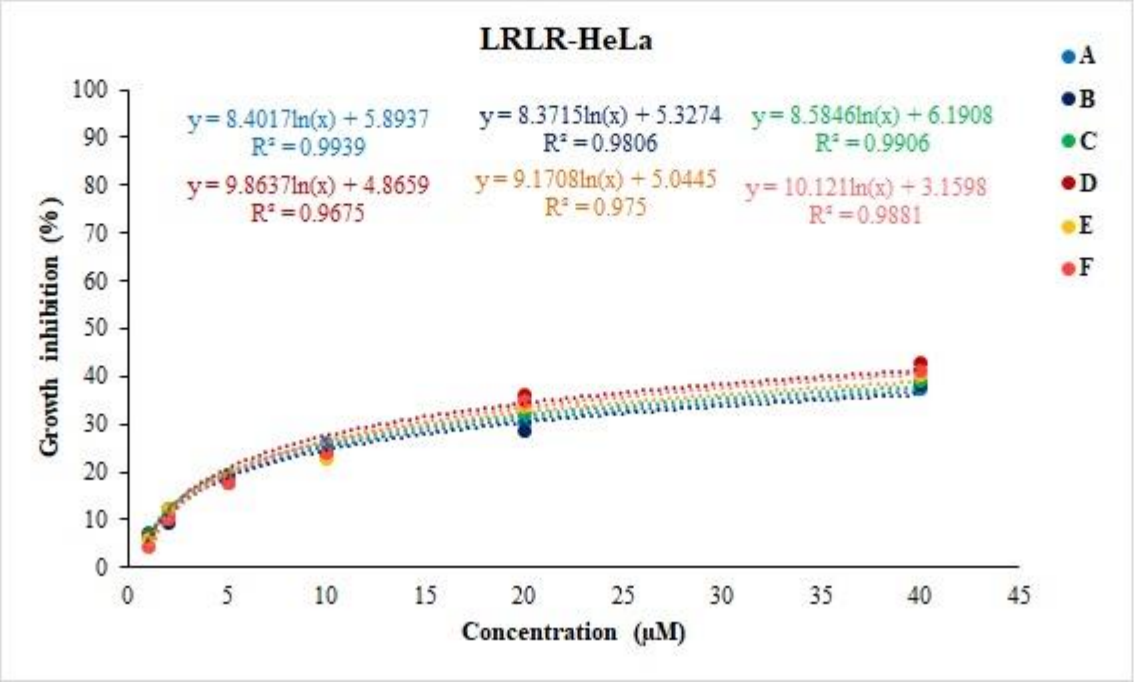

Figure S38. Concentration-response curves of LRLR in HeLa cervical cancer cells. A-F represents the 6 replicates.

Figures S39-S45 depict the concentration-response curves of the β-sheet forming cationic amphiphilic peptides in MDA-MB-231 breast cancer cells as measured by MTT assay.

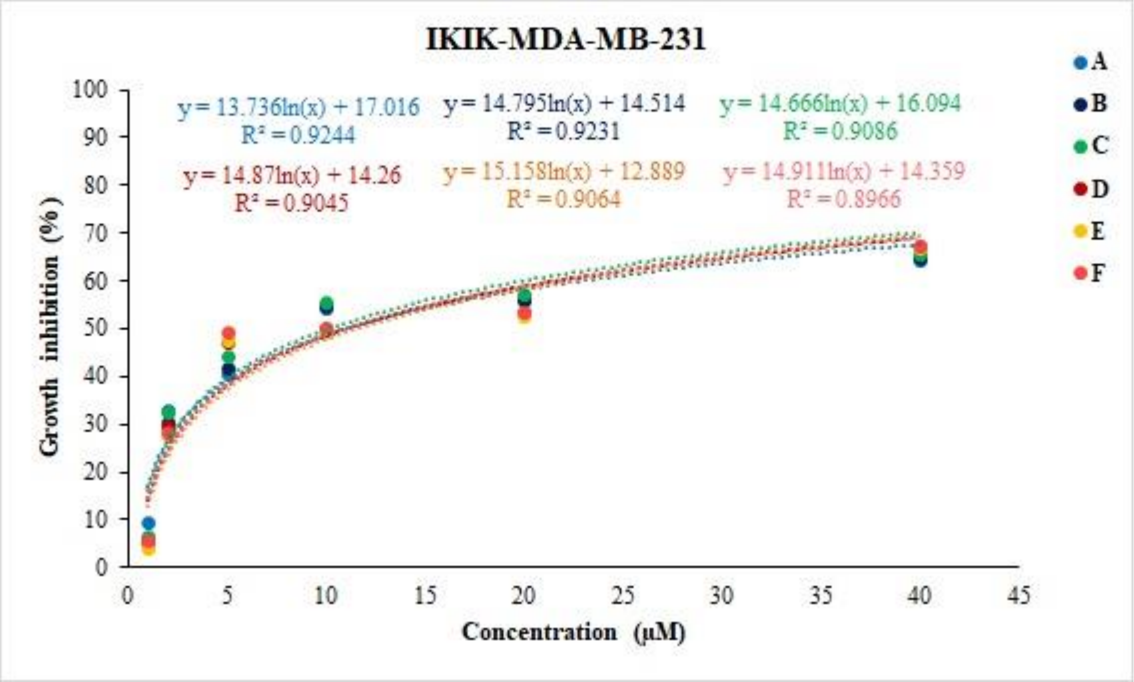

Figure S39. Concentration-response curves of IKIK in MDA-MB-231 breast cancer cells. A-F represents the 6 replicates.

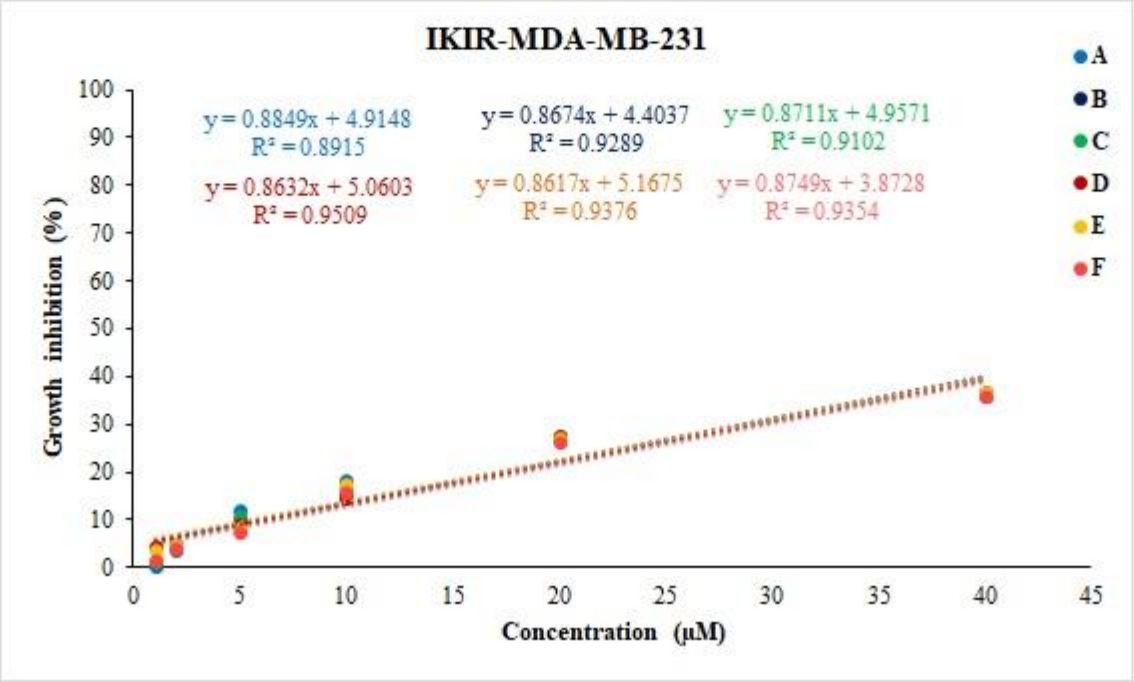

Figure S40. Concentration-response curves of IKIR in MDA-MB-231 breast cancer cells. A-F represents the 6 replicates.

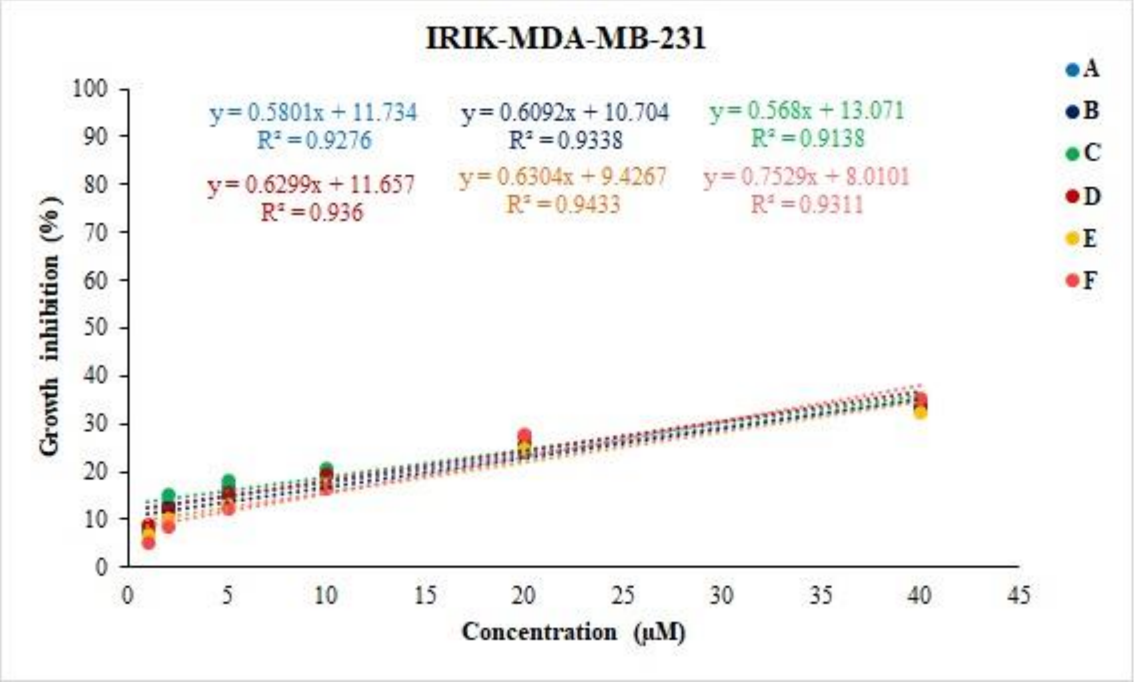

Figure S41. Concentration-response curves of IRIK in MDA-MB-231 breast cancer cells. A-F represents the 6 replicates.

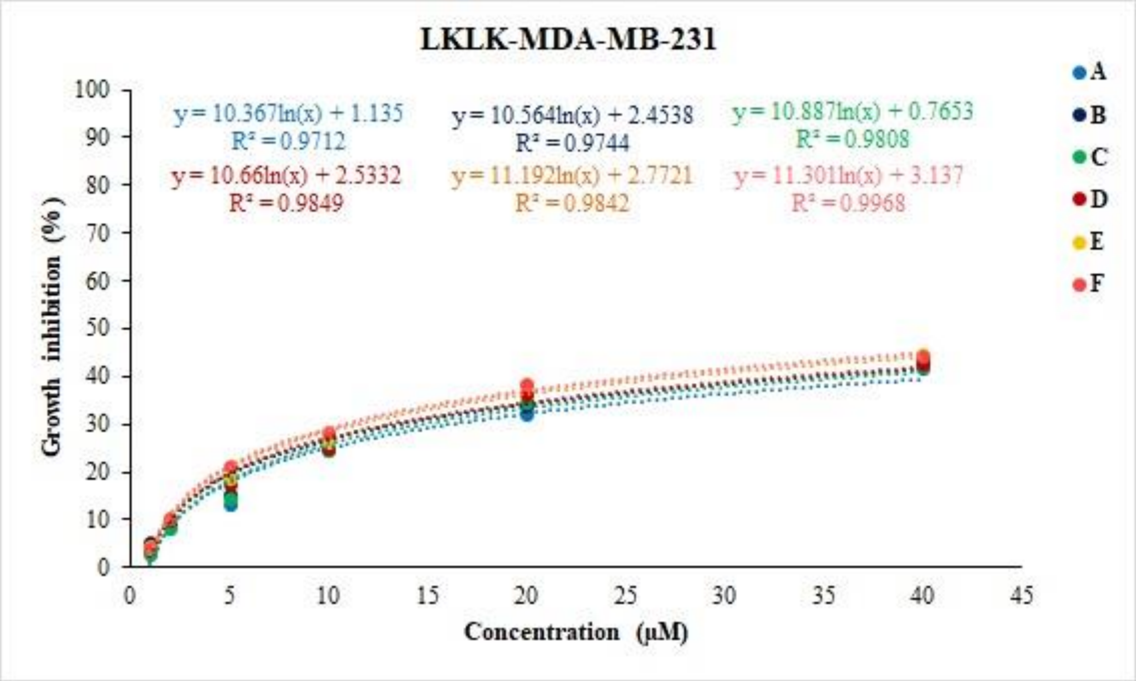

Figure S42. Concentration-response curves of LKLK in MDA-MB-231 breast cancer cells. A-F represents the 6 replicates.

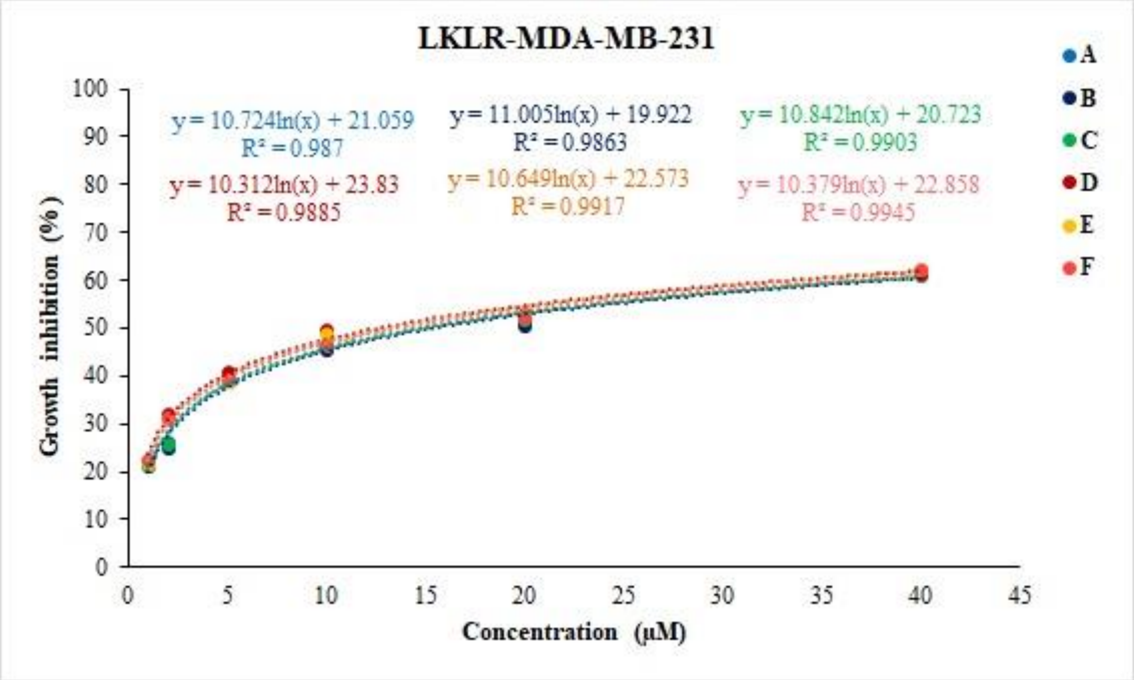

Figure S43. Concentration-response curves of LKLR in MDA-MB-231 breast cancer cells. A-F represents the 6 replicates.

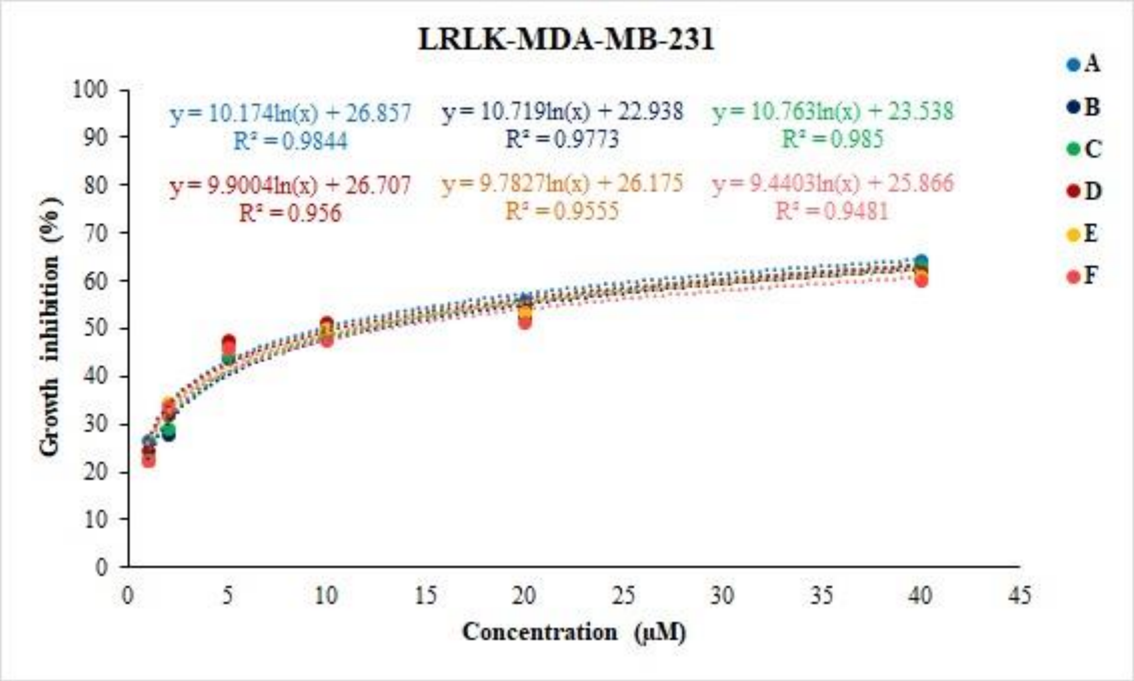

Figure S44. Concentration-response curves of LRLK in MDA-MB-231 breast cancer cells. A-F represents the 6 replicates.

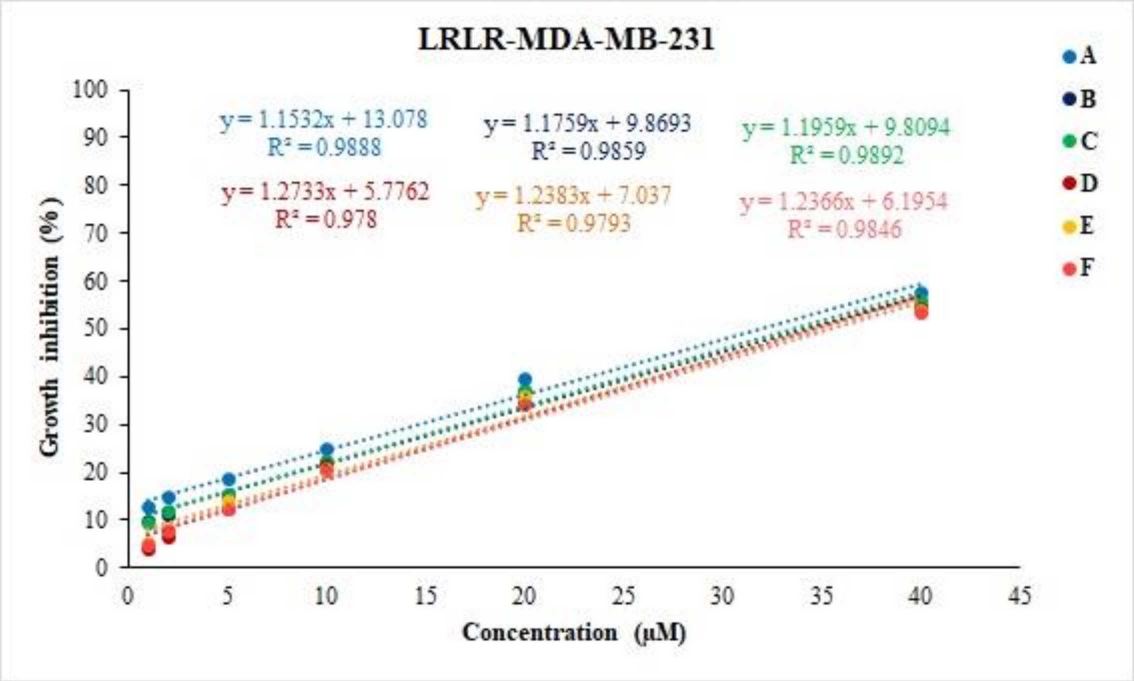

Figure S45. Concentration-response curves of LRLR in MDA-MB-231 breast cancer cells. A-F represents the 6 replicates.

Figures S46-S52 depict the concentration-response curves of the β-sheet forming cationic amphiphilic peptides in Human dermal fibroblast (HDF) cells as measured by MTT assay.

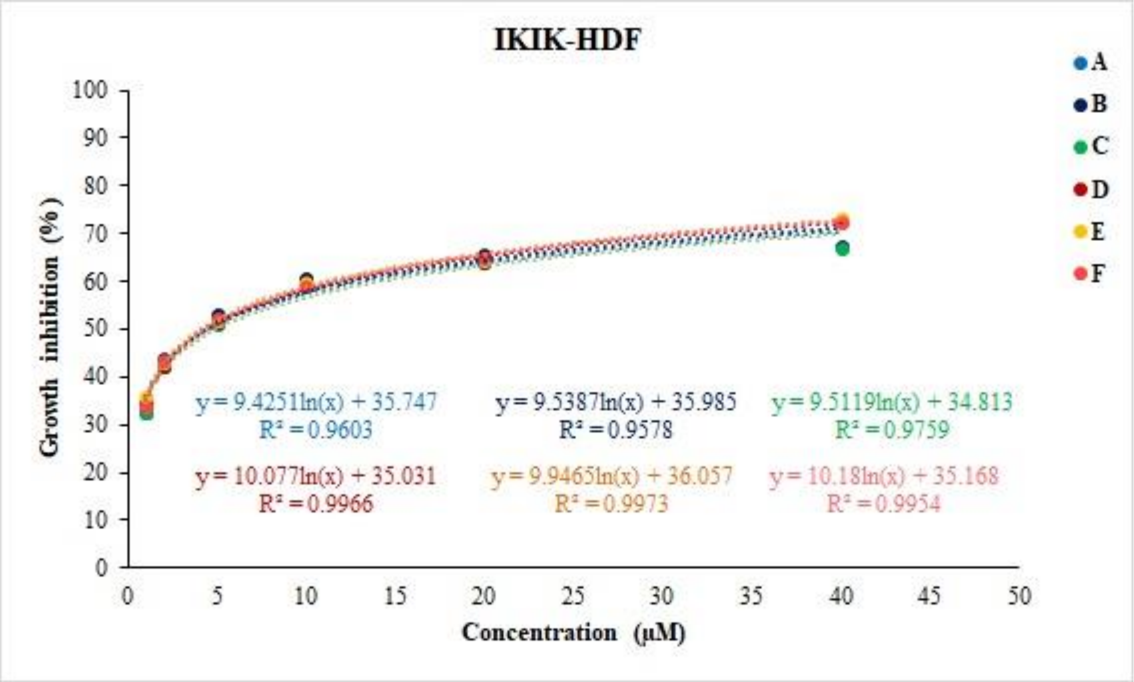

Figure S46. Concentration-response curves of IKIK in human dermal fibroblast (HDF) cells. A-F represents the 6 replicates.

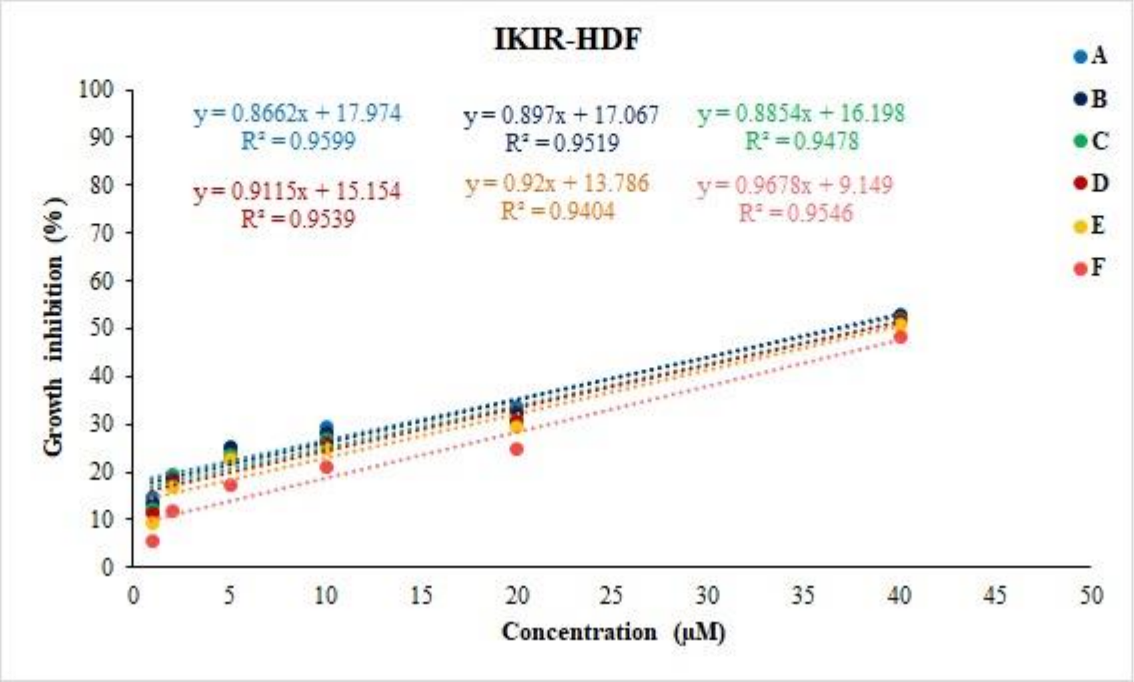

Figure S47. Concentration-response curves of IKIR in human dermal fibroblast (HDF) cells. A-F represents the 6 replicates.

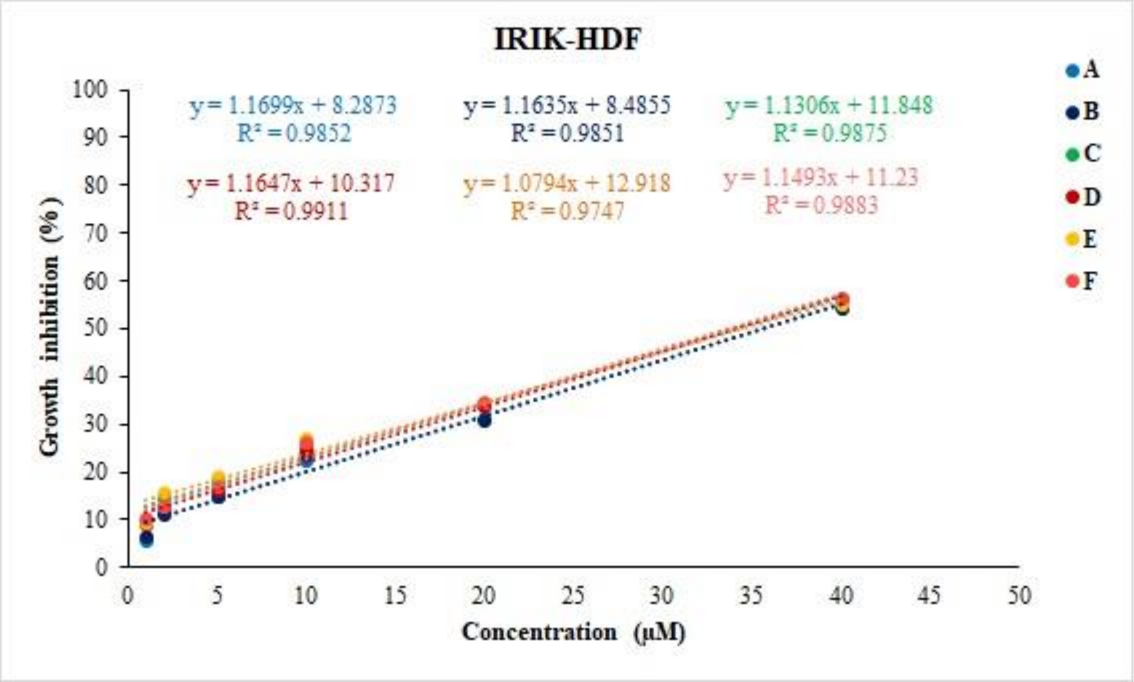

Figure S48. Concentration-response curves of IRIK in human dermal fibroblast (HDF) cells. A-F represents the 6 replicates.

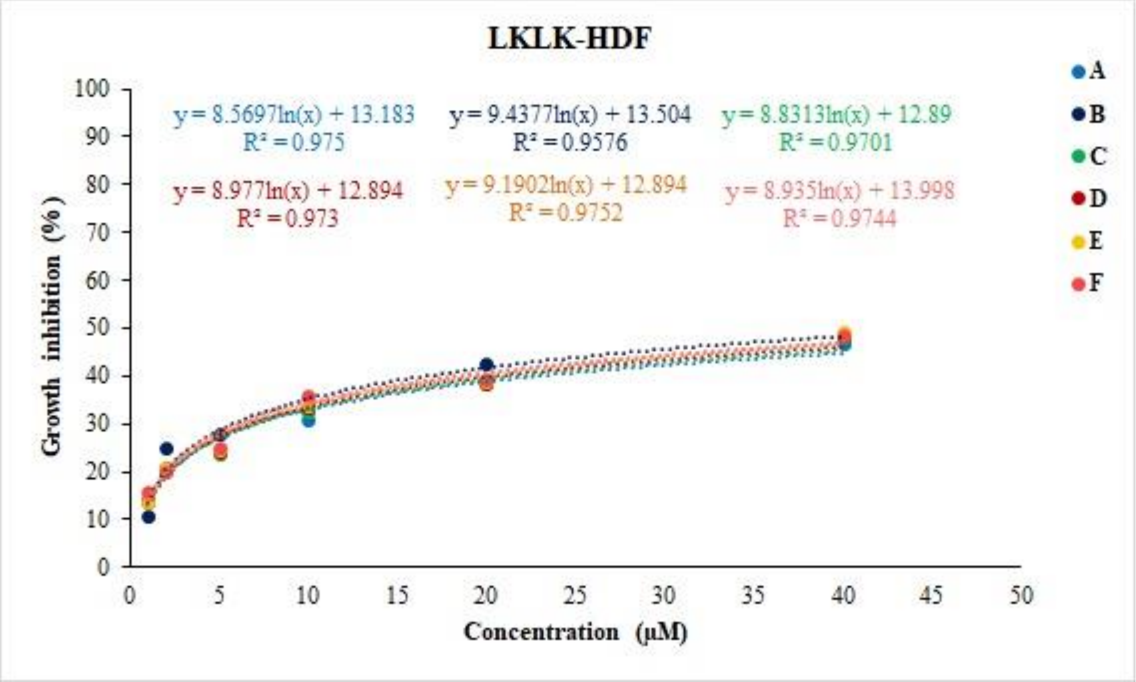

Figure S49. Concentration-response curves of LKLK in human dermal fibroblast (HDF) cells. A-F represents the 6 replicates.

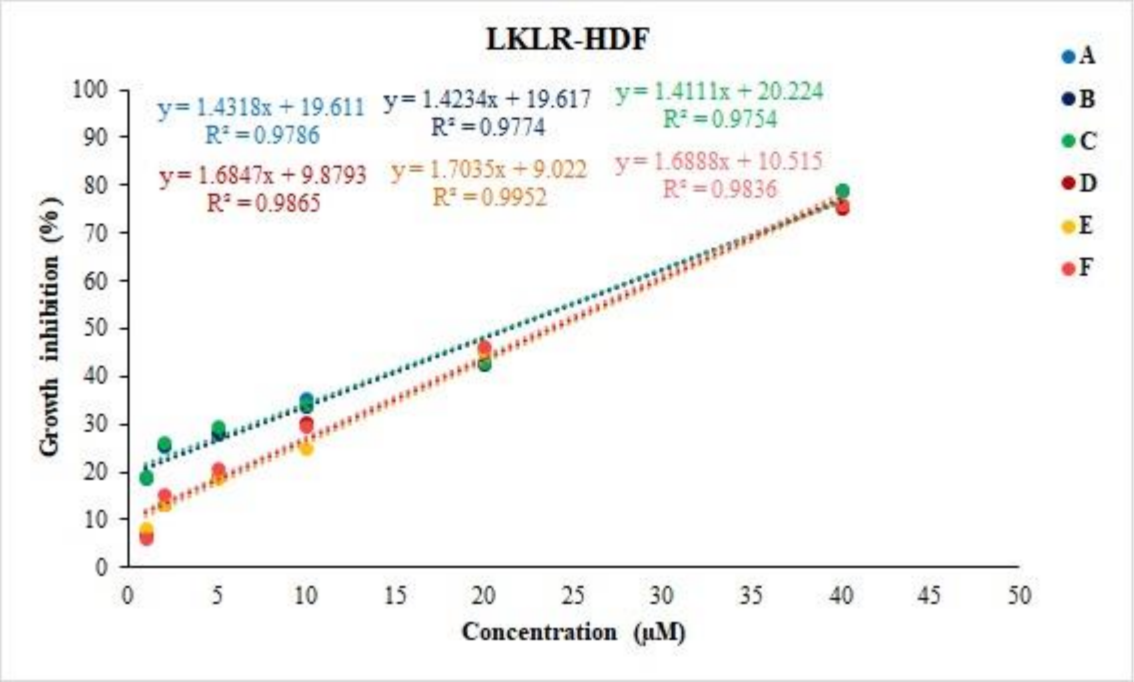

Figure S50. Concentration-response curves of LKLR in human dermal fibroblast (HDF) cells. A-F represents the 6 replicates.

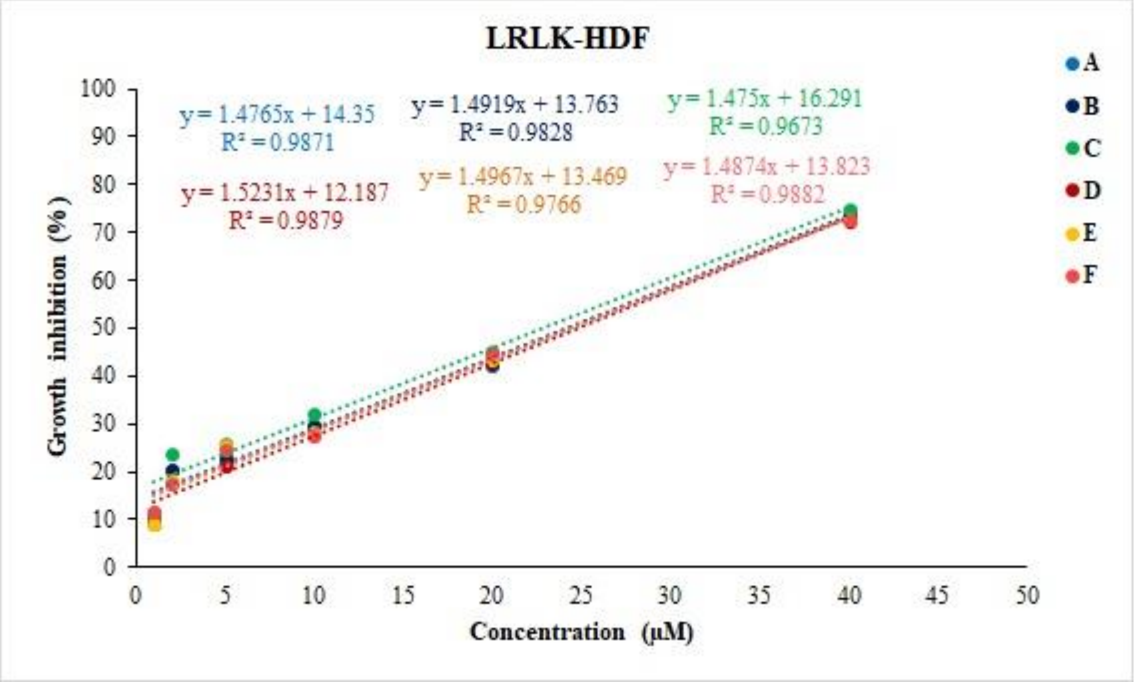

Figure S51. Concentration-response curves of LRLK in human dermal fibroblast (HDF) cells. A-F represents the 6 replicates.

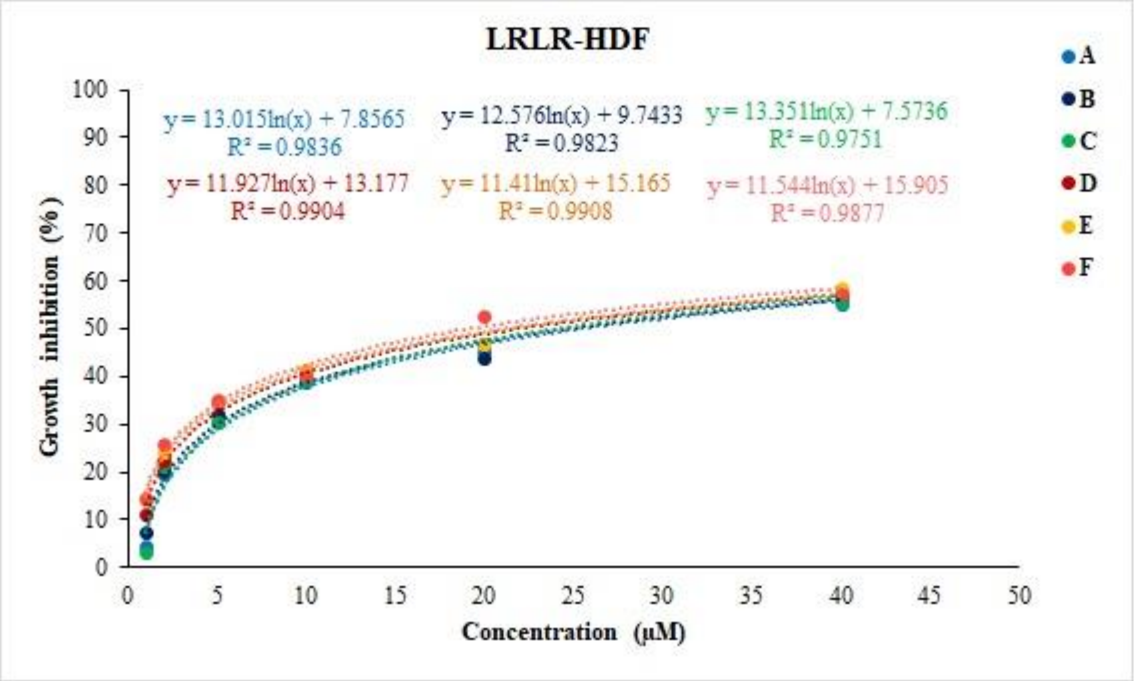

Figure S52. Concentration-response curves of LRLR in human dermal fibroblast (HDF) cells. A-F represents the 6 replicates.

The RP-HPLC peak heights, peak areas and retention times of the α-helical cationic amphiphilic peptides are provided in Tables S1-S6.

Table S1. RP-HPLC peak data for IIKK.

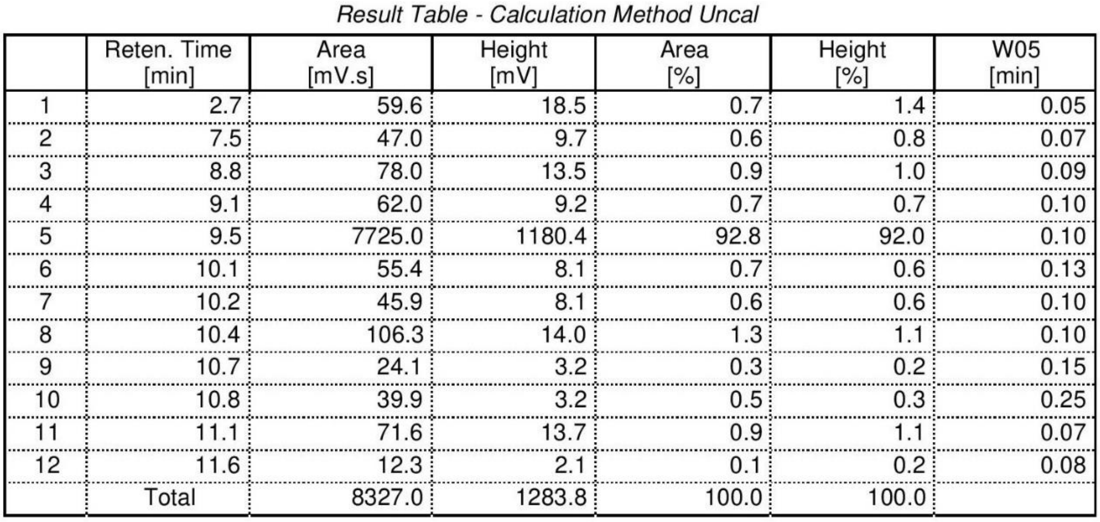

Result Table - Calculation Method Uncal

	Reten. Time [min]	Area [mV.s]	Height [mV]	Area [%]	Height [%]	W05 [min]
1	2.7	59.6	18.5	0.7	1.4	0.05
2	7.5	47.0	9.7	0.6	0.8	0.07
3	8.8	78.0	13.5	0.9	1.0	0.09
4	9.1	62.0	9.2	0.7	0.7	0.10
5	9.5	7725.0	1180.4	92.8	92.0	0.10
6	10.1	55.4	8.1	0.7	0.6	0.13
7	10.2	45.9	8.1	0.6	0.6	0.10
8	10.4	106.3	14.0	1.3	1.1	0.10
9	10.7	24.1	3.2	0.3	0.2	0.15
10	10.8	39.9	3.2	0.5	0.3	0.25
11	11.1	71.6	13.7	0.9	1.1	0.07
12	11.6	12.3	2.1	0.1	0.2	0.08
	Total	8327.0	1283.8	100.0	100.0	

Table S2. RP-HPLC peak data for LLKK.

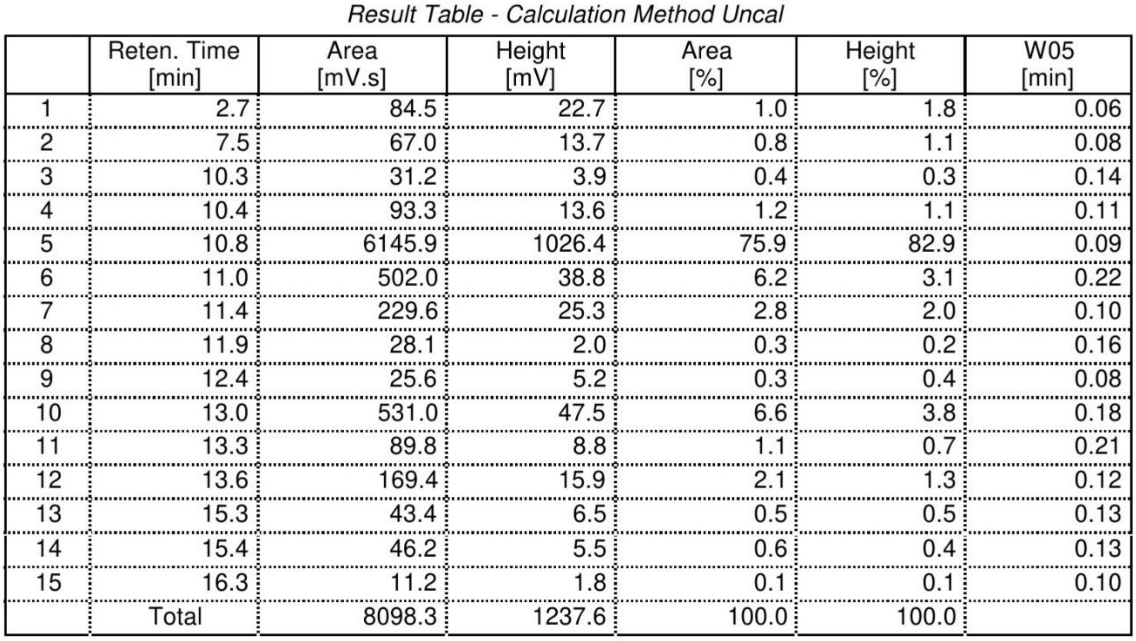

Result Table - Calculation Method Uncal

	Reten. Time [min]	Area [mV.s]	Height [mV]	Area [%]	Height [%]	W05 [min]
1	2.7	84.5	22.7	1.0	1.8	0.06
2	7.5	67.0	13.7	0.8	1.1	0.08
3	10.3	31.2	3.9	0.4	0.3	0.14
4	10.4	93.3	13.6	1.2	1.1	0.11
5	10.8	6145.9	1026.4	75.9	82.9	0.09
6	11.0	502.0	38.8	6.2	3.1	0.22
7	11.4	229.6	25.3	2.8	2.0	0.10
8	11.9	28.1	2.0	0.3	0.2	0.16
9	12.4	25.6	5.2	0.3	0.4	0.08
10	13.0	531.0	47.5	6.6	3.8	0.18
11	13.3	89.8	8.8	1.1	0.7	0.21
12	13.6	169.4	15.9	2.1	1.3	0.12
13	15.3	43.4	6.5	0.5	0.5	0.13
14	15.4	46.2	5.5	0.6	0.4	0.13
15	16.3	11.2	1.8	0.1	0.1	0.10
	Total	8098.3	1237.6	100.0	100.0	

Table S3. RP-HPLC peak data for IIRR.

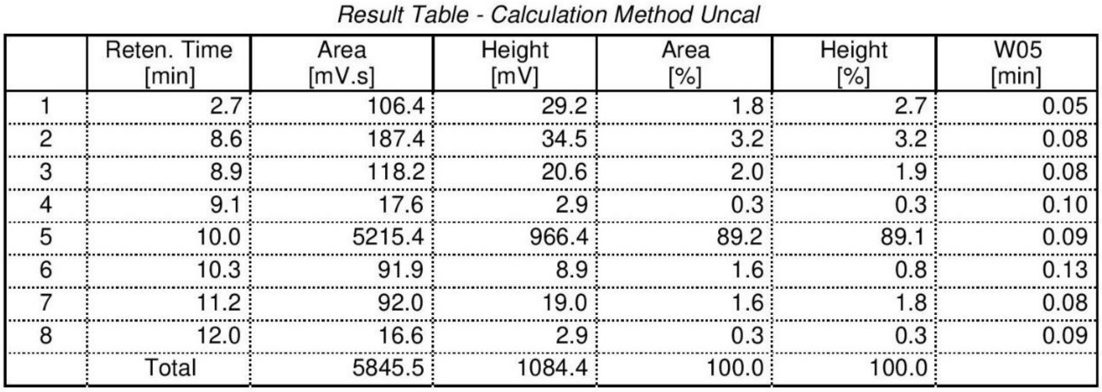

Result Table - Calculation Method Uncal

	Reten. Time [min]	Area [mV.s]	Height [mV]	Area [%]	Height [%]	W05 [min]
1	2.7	106.4	29.2	1.8	2.7	0.05
2	8.6	187.4	34.5	3.2	3.2	0.08
3	8.9	118.2	20.6	2.0	1.9	0.08
4	9.1	17.6	2.9	0.3	0.3	0.10
5	10.0	5215.4	966.4	89.2	89.1	0.09
6	10.3	91.9	8.9	1.6	0.8	0.13
7	11.2	92.0	19.0	1.6	1.8	0.08
8	12.0	16.6	2.9	0.3	0.3	0.09
	Total	5845.5	1084.4	100.0	100.0	

Table S4. RP-HPLC peak data for LLRR.

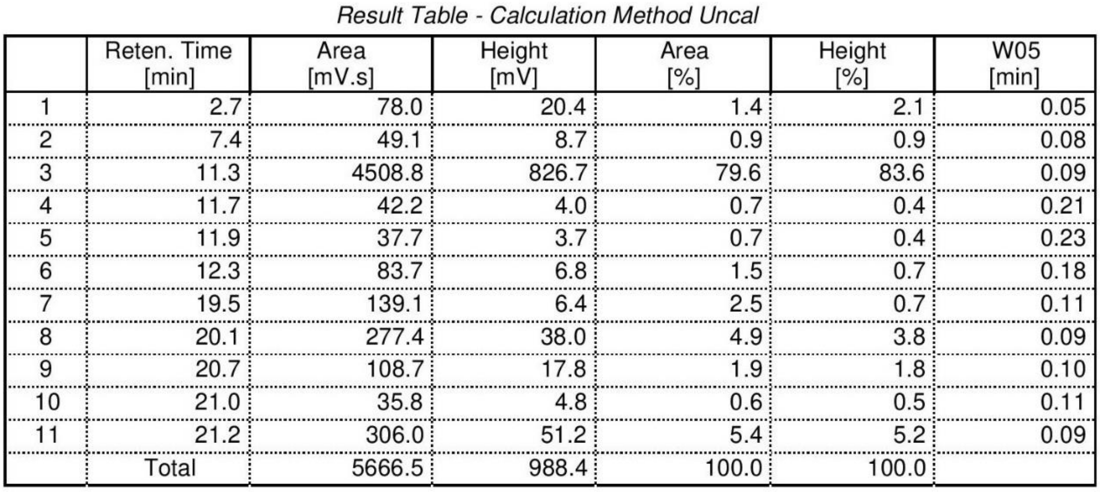

Result Table - Calculation Method Uncal

	Reten. Time [min]	Area [mV.s]	Height [mV]	Area [%]	Height [%]	W05 [min]
1	2.7	78.0	20.4	1.4	2.1	0.05
2	7.4	49.1	8.7	0.9	0.9	0.08
3	11.3	4508.8	826.7	79.6	83.6	0.09
4	11.7	42.2	4.0	0.7	0.4	0.21
5	11.9	37.7	3.7	0.7	0.4	0.23
6	12.3	83.7	6.8	1.5	0.7	0.18
7	19.5	139.1	6.4	2.5	0.7	0.11
8	20.1	277.4	38.0	4.9	3.8	0.09
9	20.7	108.7	17.8	1.9	1.8	0.10
10	21.0	35.8	4.8	0.6	0.5	0.11
11	21.2	306.0	51.2	5.4	5.2	0.09
	Total	5666.5	988.4	100.0	100.0	

Table S5. RP-HPLC peak data for CI-15.

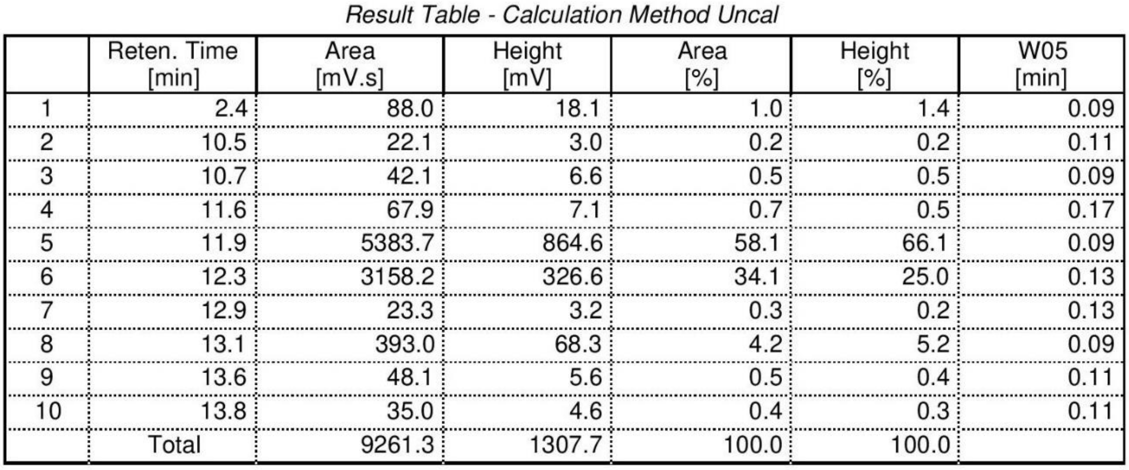

Result Table - Calculation Method Uncal

	Reten. Time [min]	Area [mV.s]	Height [mV]	Area [%]	Height [%]	W05 [min]
1	2.4	88.0	18.1	1.0	1.4	0.09
2	10.5	22.1	3.0	0.2	0.2	0.11
3	10.7	42.1	6.6	0.5	0.5	0.09
4	11.6	67.9	7.1	0.7	0.5	0.17
5	11.9	5383.7	864.6	58.1	66.1	0.09
6	12.3	3158.2	326.6	34.1	25.0	0.13
7	12.9	23.3	3.2	0.3	0.2	0.13
8	13.1	393.0	68.3	4.2	5.2	0.09
9	13.6	48.1	5.6	0.5	0.4	0.11
10	13.8	35.0	4.6	0.4	0.3	0.11
	Total	9261.3	1307.7	100.0	100.0	

Table S6. RP-HPLC peak data for II-14.

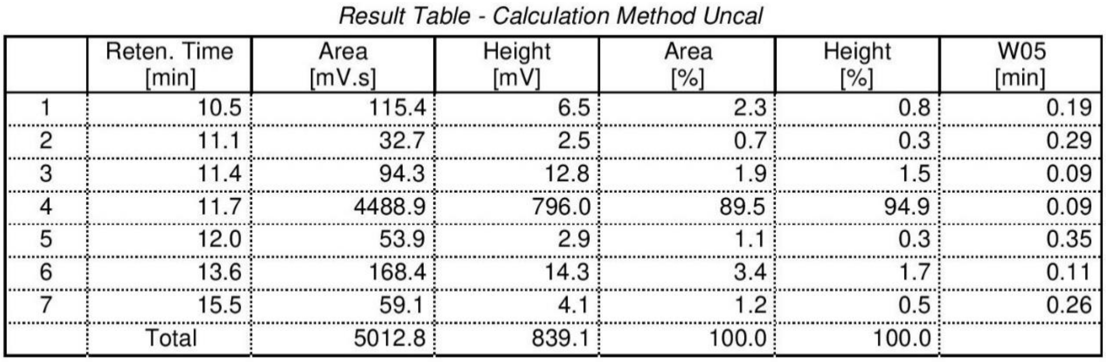

Result Table - Calculation Method Uncal

	Reten. Time [min]	Area [mV.s]	Height [mV]	Area [%]	Height [%]	W05 [min]
1	10.5	115.4	6.5	2.3	0.8	0.19
2	11.1	32.7	2.5	0.7	0.3	0.29
3	11.4	94.3	12.8	1.9	1.5	0.09
4	11.7	4488.9	796.0	89.5	94.9	0.09
5	12.0	53.9	2.9	1.1	0.3	0.35
6	13.6	168.4	14.3	3.4	1.7	0.11
7	15.5	59.1	4.1	1.2	0.5	0.26
	Total	5012.8	839.1	100.0	100.0	

The RP-HPLC peak heights, peak areas and retention times of the β-sheet forming cationic amphiphilic peptides are provided in Tables S7-S13.

Table S7. RP-HPLC peak data for IKIK.

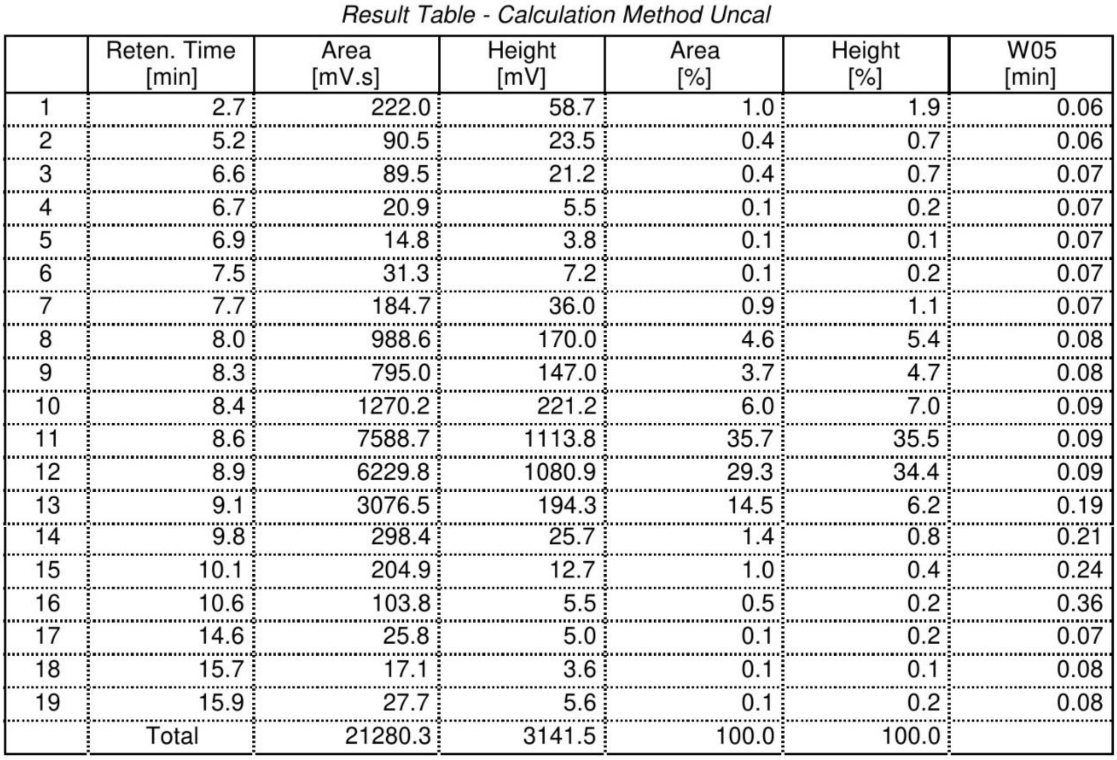

Result Table - Calculation Method Uncal

	Reten. Time [min]	Area [mV.s]	Height [mV]	Area [%]	Height [%]	W05 [min]
1	2.7	222.0	58.7	1.0	1.9	0.06
2	5.2	90.5	23.5	0.4	0.7	0.06
3	6.6	89.5	21.2	0.4	0.7	0.07
4	6.7	20.9	5.5	0.1	0.2	0.07
5	6.9	14.8	3.8	0.1	0.1	0.07
6	7.5	31.3	7.2	0.1	0.2	0.07
7	7.7	184.7	36.0	0.9	1.1	0.07
8	8.0	988.6	170.0	4.6	5.4	0.08
9	8.3	795.0	147.0	3.7	4.7	0.08
10	8.4	1270.2	221.2	6.0	7.0	0.09
11	8.6	7588.7	1113.8	35.7	35.5	0.09
12	8.9	6229.8	1080.9	29.3	34.4	0.09
13	9.1	3076.5	194.3	14.5	6.2	0.19
14	9.8	298.4	25.7	1.4	0.8	0.21
15	10.1	204.9	12.7	1.0	0.4	0.24
16	10.6	103.8	5.5	0.5	0.2	0.36
17	14.6	25.8	5.0	0.1	0.2	0.07
18	15.7	17.1	3.6	0.1	0.1	0.08
19	15.9	27.7	5.6	0.1	0.2	0.08
	Total	21280.3	3141.5	100.0	100.0	

Table S8. RP-HPLC peak data for IKIR.

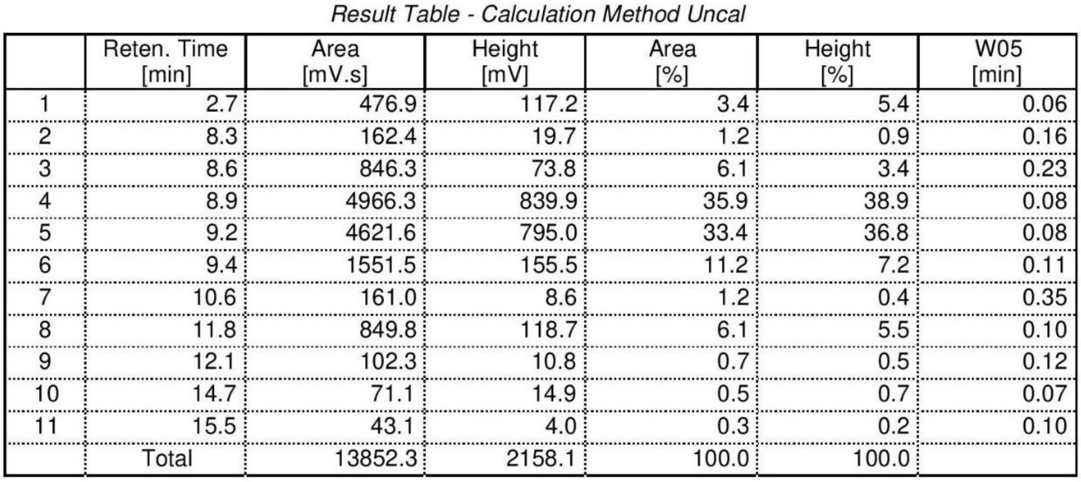

Result Table - Calculation Method Uncal

	Reten. Time [min]	Area [mV.s]	Height [mV]	Area [%]	Height [%]	W05 [min]
1	2.7	476.9	117.2	3.4	5.4	0.06
2	8.3	162.4	19.7	1.2	0.9	0.16
3	8.6	846.3	73.8	6.1	3.4	0.23
4	8.9	4966.3	839.9	35.9	38.9	0.08
5	9.2	4621.6	795.0	33.4	36.8	0.08
6	9.4	1551.5	155.5	11.2	7.2	0.11
7	10.6	161.0	8.6	1.2	0.4	0.35
8	11.8	849.8	118.7	6.1	5.5	0.10
9	12.1	102.3	10.8	0.7	0.5	0.12
10	14.7	71.1	14.9	0.5	0.7	0.07
11	15.5	43.1	4.0	0.3	0.2	0.10
	Total	13852.3	2158.1	100.0	100.0	

Table S9. RP-HPLC peak data for IRIK.

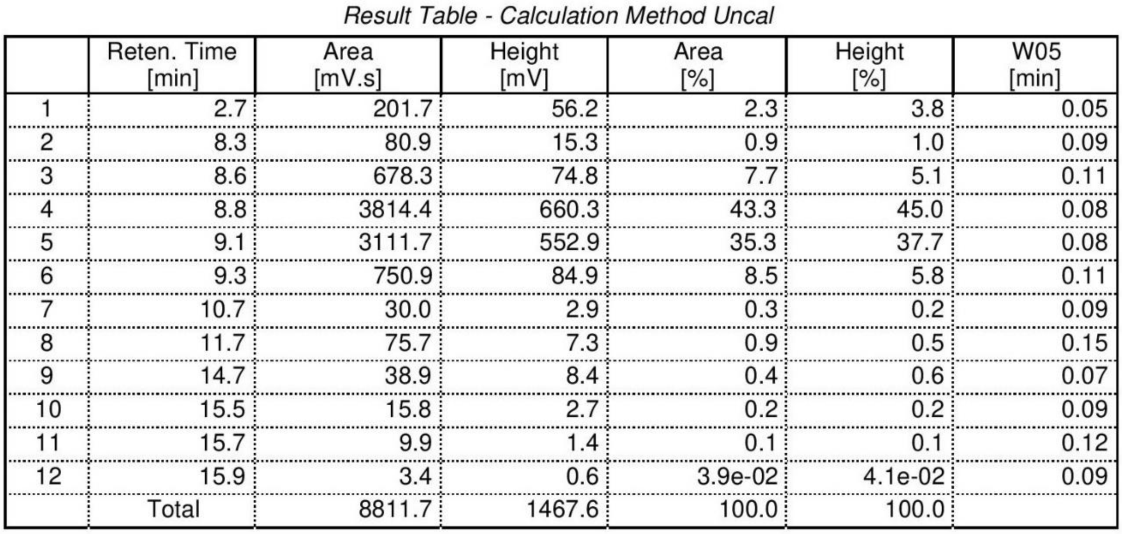

Result Table - Calculation Method Uncal

	Reten. Time [min]	Area [mV.s]	Height [mV]	Area [%]	Height [%]	W05 [min]
1	2.7	201.7	56.2	2.3	3.8	0.05
2	8.3	80.9	15.3	0.9	1.0	0.09
3	8.6	678.3	74.8	7.7	5.1	0.11
4	8.8	3814.4	660.3	43.3	45.0	0.08
5	9.1	3111.7	552.9	35.3	37.7	0.08
6	9.3	750.9	84.9	8.5	5.8	0.11
7	10.7	30.0	2.9	0.3	0.2	0.09
8	11.7	75.7	7.3	0.9	0.5	0.15
9	14.7	38.9	8.4	0.4	0.6	0.07
10	15.5	15.8	2.7	0.2	0.2	0.09
11	15.7	9.9	1.4	0.1	0.1	0.12
12	15.9	3.4	0.6	3.9e-02	4.1e-02	0.09
	Total	8811.7	1467.6	100.0	100.0	

Table S10. RP-HPLC peak data for LKLR.

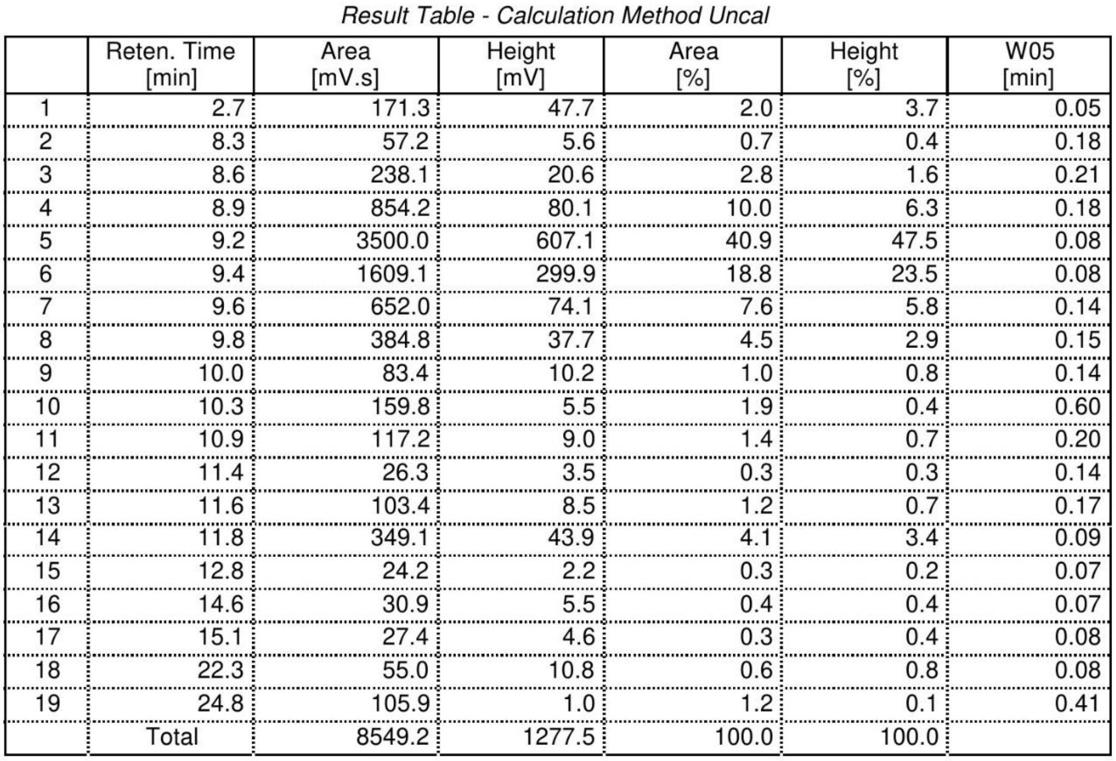

Result Table - Calculation Method Uncal

	Reten. Time [min]	Area [mV.s]	Height [mV]	Area [%]	Height [%]	W05 [min]
1	2.7	171.3	47.7	2.0	3.7	0.05
2	8.3	57.2	5.6	0.7	0.4	0.18
3	8.6	238.1	20.6	2.8	1.6	0.21
4	8.9	854.2	80.1	10.0	6.3	0.18
5	9.2	3500.0	607.1	40.9	47.5	0.08
6	9.4	1609.1	299.9	18.8	23.5	0.08
7	9.6	652.0	74.1	7.6	5.8	0.14
8	9.8	384.8	37.7	4.5	2.9	0.15
9	10.0	83.4	10.2	1.0	0.8	0.14
10	10.3	159.8	5.5	1.9	0.4	0.60
11	10.9	117.2	9.0	1.4	0.7	0.20
12	11.4	26.3	3.5	0.3	0.3	0.14
13	11.6	103.4	8.5	1.2	0.7	0.17
14	11.8	349.1	43.9	4.1	3.4	0.09
15	12.8	24.2	2.2	0.3	0.2	0.07
16	14.6	30.9	5.5	0.4	0.4	0.07
17	15.1	27.4	4.6	0.3	0.4	0.08
18	22.3	55.0	10.8	0.6	0.8	0.08
19	24.8	105.9	1.0	1.2	0.1	0.41
	Total	8549.2	1277.5	100.0	100.0	

Table S11. RP-HPLC peak data for LRLK.

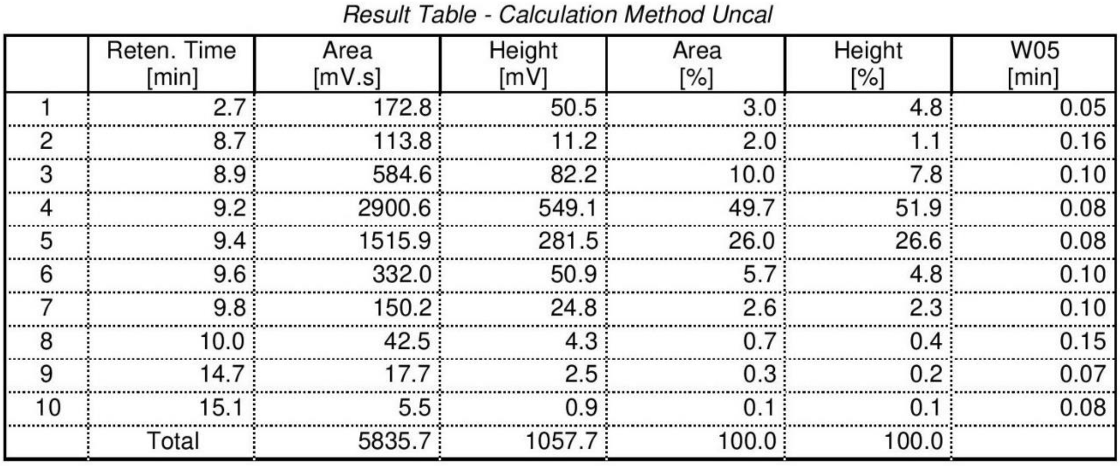

Result Table - Calculation Method Uncal

	Reten. Time [min]	Area [mV.s]	Height [mV]	Area [%]	Height [%]	W05 [min]
1	2.7	172.8	50.5	3.0	4.8	0.05
2	8.7	113.8	11.2	2.0	1.1	0.16
3	8.9	584.6	82.2	10.0	7.8	0.10
4	9.2	2900.6	549.1	49.7	51.9	0.08
5	9.4	1515.9	281.5	26.0	26.6	0.08
6	9.6	332.0	50.9	5.7	4.8	0.10
7	9.8	150.2	24.8	2.6	2.3	0.10
8	10.0	42.5	4.3	0.7	0.4	0.15
9	14.7	17.7	2.5	0.3	0.2	0.07
10	15.1	5.5	0.9	0.1	0.1	0.08
	Total	5835.7	1057.7	100.0	100.0	

Table S12. RP-HPLC peak data for LRLR.

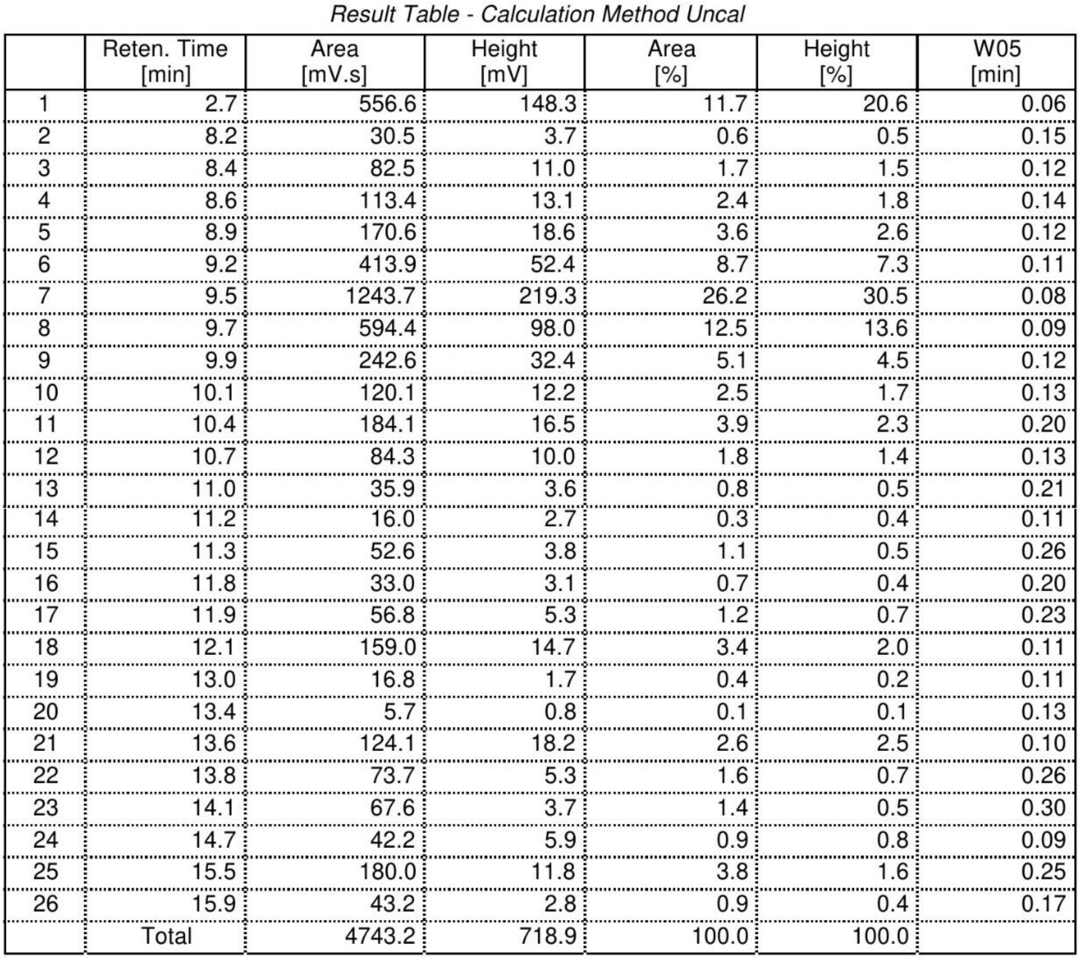

Result Table - Calculation Method Uncal

	Reten. Time [min]	Area [mV.s]	Height [mV]	Area [%]	Height [%]	W05 [min]
1	2.7	556.6	148.3	11.7	20.6	0.06
2	8.2	30.5	3.7	0.6	0.5	0.15
3	8.4	82.5	11.0	1.7	1.5	0.12
4	8.6	113.4	13.1	2.4	1.8	0.14
5	8.9	170.6	18.6	3.6	2.6	0.12
6	9.2	413.9	52.4	8.7	7.3	0.11
7	9.5	1243.7	219.3	26.2	30.5	0.08
8	9.7	594.4	98.0	12.5	13.6	0.09
9	9.9	242.6	32.4	5.1	4.5	0.12
10	10.1	120.1	12.2	2.5	1.7	0.13
11	10.4	184.1	16.5	3.9	2.3	0.20
12	10.7	84.3	10.0	1.8	1.4	0.13
13	11.0	35.9	3.6	0.8	0.5	0.21
14	11.2	16.0	2.7	0.3	0.4	0.11
15	11.3	52.6	3.8	1.1	0.5	0.26
16	11.8	33.0	3.1	0.7	0.4	0.20
17	11.9	56.8	5.3	1.2	0.7	0.23
18	12.1	159.0	14.7	3.4	2.0	0.11
19	13.0	16.8	1.7	0.4	0.2	0.11
20	13.4	5.7	0.8	0.1	0.1	0.13
21	13.6	124.1	18.2	2.6	2.5	0.10
22	13.8	73.7	5.3	1.6	0.7	0.26
23	14.1	67.6	3.7	1.4	0.5	0.30
24	14.7	42.2	5.9	0.9	0.8	0.09
25	15.5	180.0	11.8	3.8	1.6	0.25
26	15.9	43.2	2.8	0.9	0.4	0.17
	Total	4743.2	718.9	100.0	100.0	

Table S13. RP-HPLC peak data for LKLK.

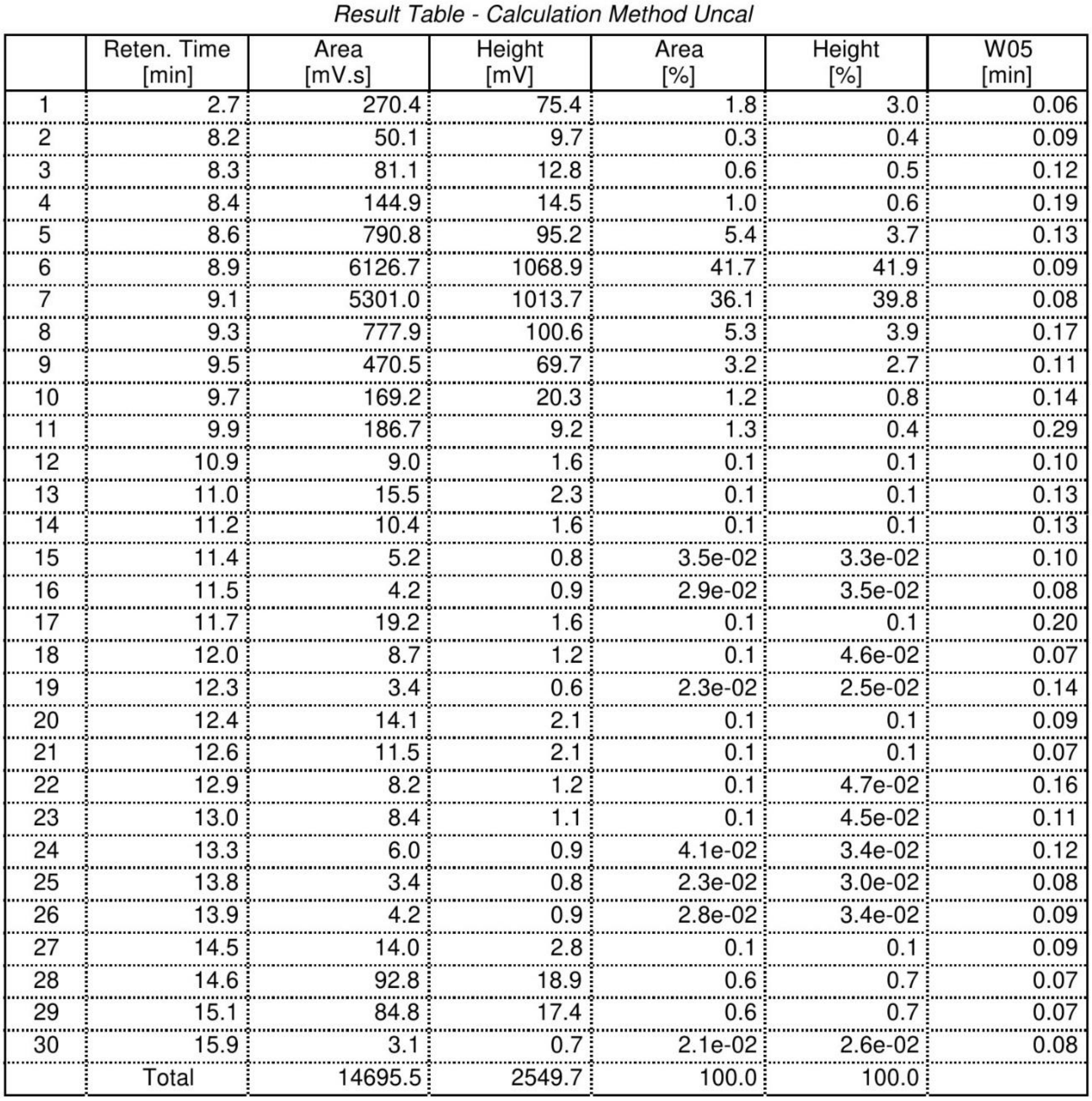

Result Table - Calculation Method Uncal

	Reten. Time [min]	Area [mV.s]	Height [mV]	Area [%]	Height [%]	W05 [min]
1	2.7	270.4	75.4	1.8	3.0	0.06
2	8.2	50.1	9.7	0.3	0.4	0.09
3	8.3	81.1	12.8	0.6	0.5	0.12
4	8.4	144.9	14.5	1.0	0.6	0.19
5	8.6	790.8	95.2	5.4	3.7	0.13
6	8.9	6126.7	1068.9	41.7	41.9	0.09
7	9.1	5301.0	1013.7	36.1	39.8	0.08
8	9.3	777.9	100.6	5.3	3.9	0.17
9	9.5	470.5	69.7	3.2	2.7	0.11
10	9.7	169.2	20.3	1.2	0.8	0.14
11	9.9	186.7	9.2	1.3	0.4	0.29
12	10.9	9.0	1.6	0.1	0.1	0.10
13	11.0	15.5	2.3	0.1	0.1	0.13
14	11.2	10.4	1.6	0.1	0.1	0.13
15	11.4	5.2	0.8	3.5e-02	3.3e-02	0.10
16	11.5	4.2	0.9	2.9e-02	3.5e-02	0.08
17	11.7	19.2	1.6	0.1	0.1	0.20
18	12.0	8.7	1.2	0.1	4.6e-02	0.07
19	12.3	3.4	0.6	2.3e-02	2.5e-02	0.14
20	12.4	14.1	2.1	0.1	0.1	0.09
21	12.6	11.5	2.1	0.1	0.1	0.07
22	12.9	8.2	1.2	0.1	4.7e-02	0.16
23	13.0	8.4	1.1	0.1	4.5e-02	0.11
24	13.3	6.0	0.9	4.1e-02	3.4e-02	0.12
25	13.8	3.4	0.8	2.3e-02	3.0e-02	0.08
26	13.9	4.2	0.9	2.8e-02	3.4e-02	0.09
27	14.5	14.0	2.8	0.1	0.1	0.09
28	14.6	92.8	18.9	0.6	0.7	0.07
29	15.1	84.8	17.4	0.6	0.7	0.07
30	15.9	3.1	0.7	2.1e-02	2.6e-02	0.08
	Total	14695.5	2549.7	100.0	100.0	

The RP-HPLC peak heights, peak areas and retention times of the surfactant-like peptides are provided in Tables S14-S15.

Table S14. RP-HPLC peak data for $(IA)_4K$.

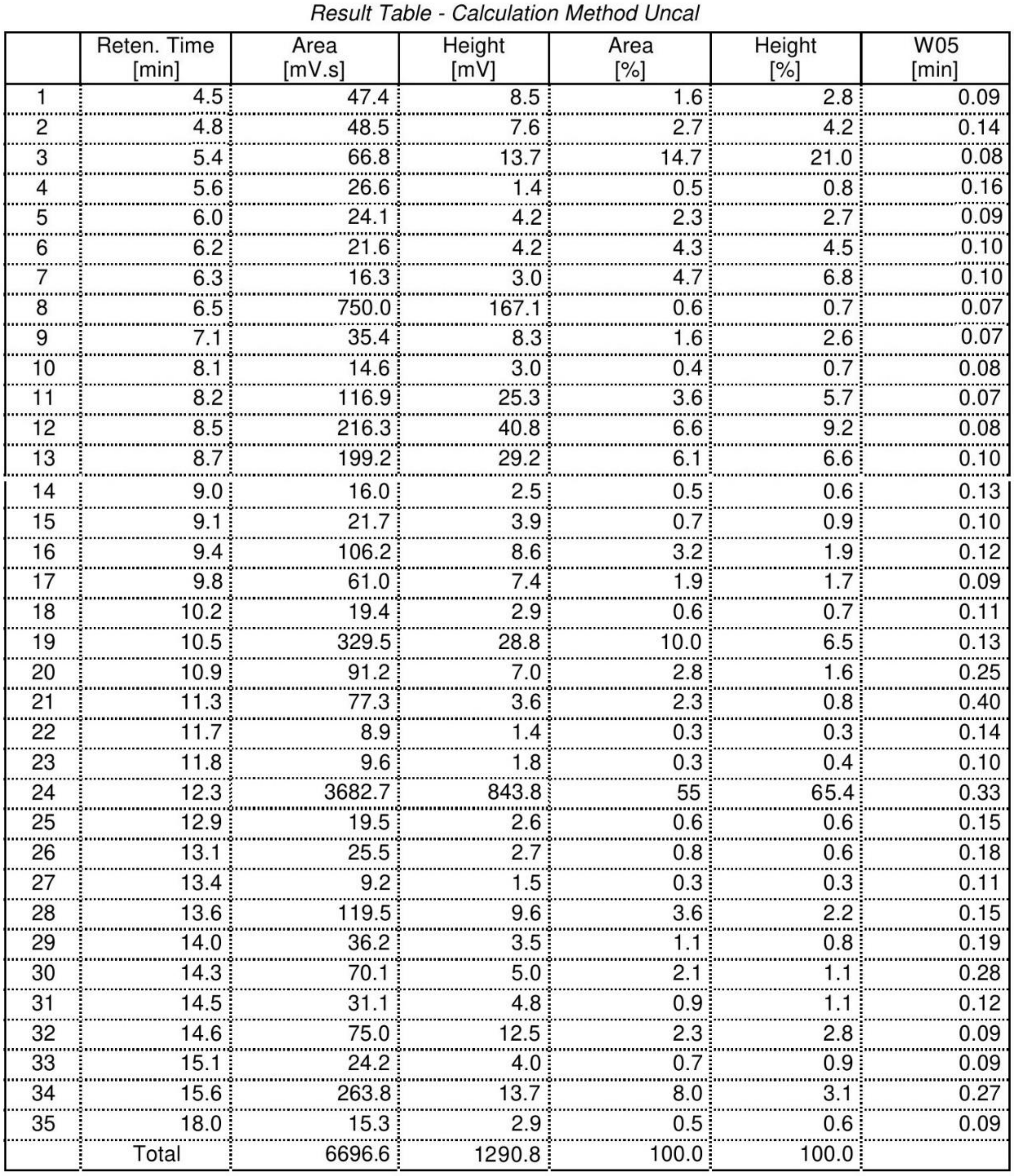

Result Table - Calculation Method Uncal

	Reten. Time [min]	Area [mV.s]	Height [mV]	Area [%]	Height [%]	W05 [min]
1	4.5	47.4	8.5	1.6	2.8	0.09
2	4.8	48.5	7.6	2.7	4.2	0.14
3	5.4	66.8	13.7	14.7	21.0	0.08
4	5.6	26.6	1.4	0.5	0.8	0.16
5	6.0	24.1	4.2	2.3	2.7	0.09
6	6.2	21.6	4.2	4.3	4.5	0.10
7	6.3	16.3	3.0	4.7	6.8	0.10
8	6.5	750.0	167.1	0.6	0.7	0.07
9	7.1	35.4	8.3	1.6	2.6	0.07
10	8.1	14.6	3.0	0.4	0.7	0.08
11	8.2	116.9	25.3	3.6	5.7	0.07
12	8.5	216.3	40.8	6.6	9.2	0.08
13	8.7	199.2	29.2	6.1	6.6	0.10
14	9.0	16.0	2.5	0.5	0.6	0.13
15	9.1	21.7	3.9	0.7	0.9	0.10
16	9.4	106.2	8.6	3.2	1.9	0.12
17	9.8	61.0	7.4	1.9	1.7	0.09
18	10.2	19.4	2.9	0.6	0.7	0.11
19	10.5	329.5	28.8	10.0	6.5	0.13
20	10.9	91.2	7.0	2.8	1.6	0.25
21	11.3	77.3	3.6	2.3	0.8	0.40
22	11.7	8.9	1.4	0.3	0.3	0.14
23	11.8	9.6	1.8	0.3	0.4	0.10
24	12.3	3682.7	843.8	55	65.4	0.33
25	12.9	19.5	2.6	0.6	0.6	0.15
26	13.1	25.5	2.7	0.8	0.6	0.18
27	13.4	9.2	1.5	0.3	0.3	0.11
28	13.6	119.5	9.6	3.6	2.2	0.15
29	14.0	36.2	3.5	1.1	0.8	0.19
30	14.3	70.1	5.0	2.1	1.1	0.28
31	14.5	31.1	4.8	0.9	1.1	0.12
32	14.6	75.0	12.5	2.3	2.8	0.09
33	15.1	24.2	4.0	0.7	0.9	0.09
34	15.6	263.8	13.7	8.0	3.1	0.27
35	18.0	15.3	2.9	0.5	0.6	0.09
	Total	6696.6	1290.8	100.0	100.0	

Table S15. RP-HPLC peak data for $(IG)_4K$.

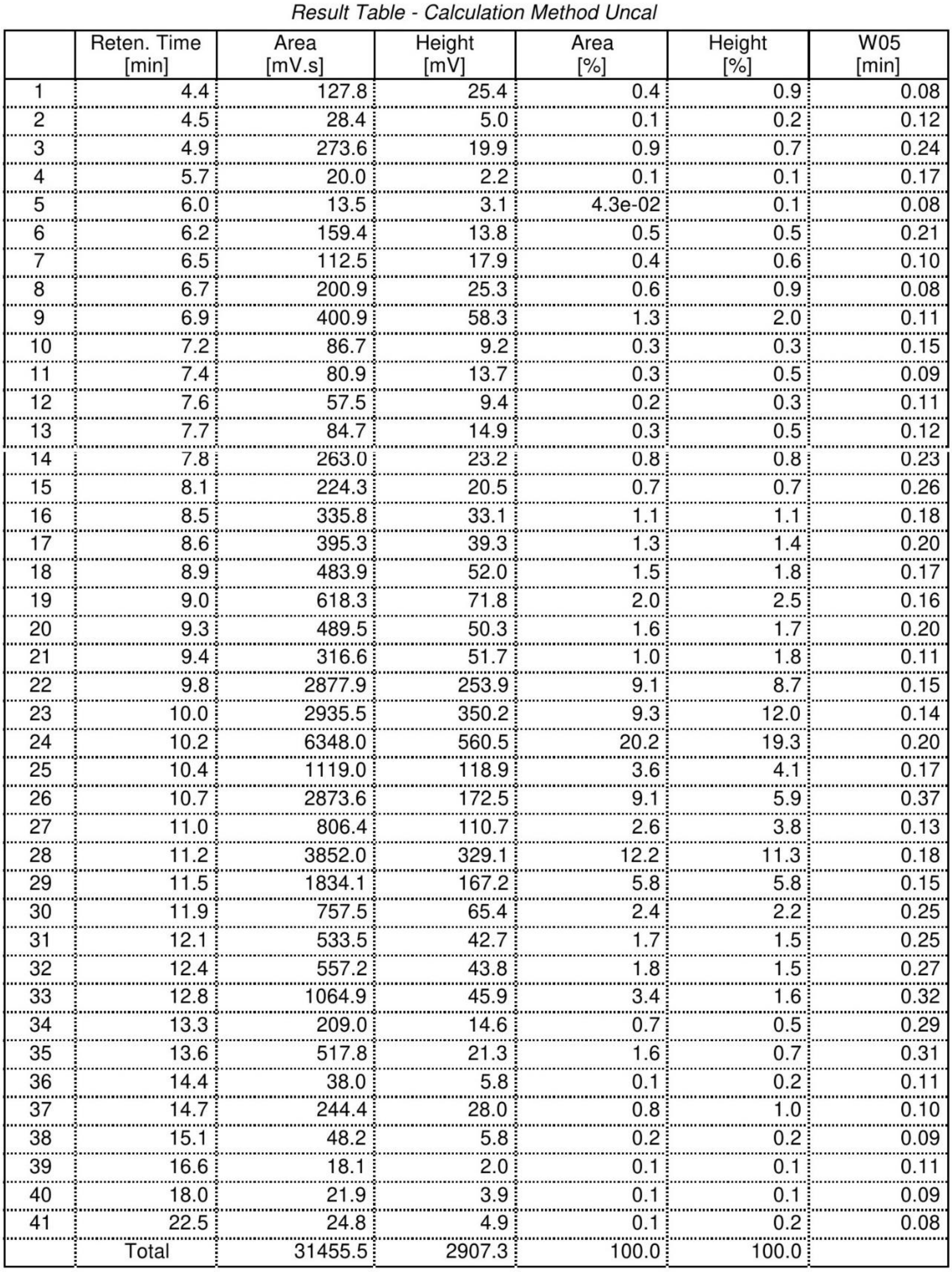

Result Table - Calculation Method Uncal

	Reten. Time [min]	Area [mV.s]	Height [mV]	Area [%]	Height [%]	W05 [min]
1	4.4	127.8	25.4	0.4	0.9	0.08
2	4.5	28.4	5.0	0.1	0.2	0.12
3	4.9	273.6	19.9	0.9	0.7	0.24
4	5.7	20.0	2.2	0.1	0.1	0.17
5	6.0	13.5	3.1	4.3e-02	0.1	0.08
6	6.2	159.4	13.8	0.5	0.5	0.21
7	6.5	112.5	17.9	0.4	0.6	0.10
8	6.7	200.9	25.3	0.6	0.9	0.08
9	6.9	400.9	58.3	1.3	2.0	0.11
10	7.2	86.7	9.2	0.3	0.3	0.15
11	7.4	80.9	13.7	0.3	0.5	0.09
12	7.6	57.5	9.4	0.2	0.3	0.11
13	7.7	84.7	14.9	0.3	0.5	0.12
14	7.8	263.0	23.2	0.8	0.8	0.23
15	8.1	224.3	20.5	0.7	0.7	0.26
16	8.5	335.8	33.1	1.1	1.1	0.18
17	8.6	395.3	39.3	1.3	1.4	0.20
18	8.9	483.9	52.0	1.5	1.8	0.17
19	9.0	618.3	71.8	2.0	2.5	0.16
20	9.3	489.5	50.3	1.6	1.7	0.20
21	9.4	316.6	51.7	1.0	1.8	0.11
22	9.8	2877.9	253.9	9.1	8.7	0.15
23	10.0	2935.5	350.2	9.3	12.0	0.14
24	10.2	6348.0	560.5	20.2	19.3	0.20
25	10.4	1119.0	118.9	3.6	4.1	0.17
26	10.7	2873.6	172.5	9.1	5.9	0.37
27	11.0	806.4	110.7	2.6	3.8	0.13
28	11.2	3852.0	329.1	12.2	11.3	0.18
29	11.5	1834.1	167.2	5.8	5.8	0.15
30	11.9	757.5	65.4	2.4	2.2	0.25
31	12.1	533.5	42.7	1.7	1.5	0.25
32	12.4	557.2	43.8	1.8	1.5	0.27
33	12.8	1064.9	45.9	3.4	1.6	0.32
34	13.3	209.0	14.6	0.7	0.5	0.29
35	13.6	517.8	21.3	1.6	0.7	0.31
36	14.4	38.0	5.8	0.1	0.2	0.11
37	14.7	244.4	28.0	0.8	1.0	0.10
38	15.1	48.2	5.8	0.2	0.2	0.09
39	16.6	18.1	2.0	0.1	0.1	0.11
40	18.0	21.9	3.9	0.1	0.1	0.09
41	22.5	24.8	4.9	0.1	0.2	0.08
	Total	31455.5	2907.3	100.0	100.0	